HOST-PATHOGEN INTERACTION IN CENTRAL NERVOUS SYSTEM INFECTION

EDITED BY: Federico Iovino and Tatiana Barichello
PUBLISHED IN: Frontiers in Cellular and Infection Microbiology

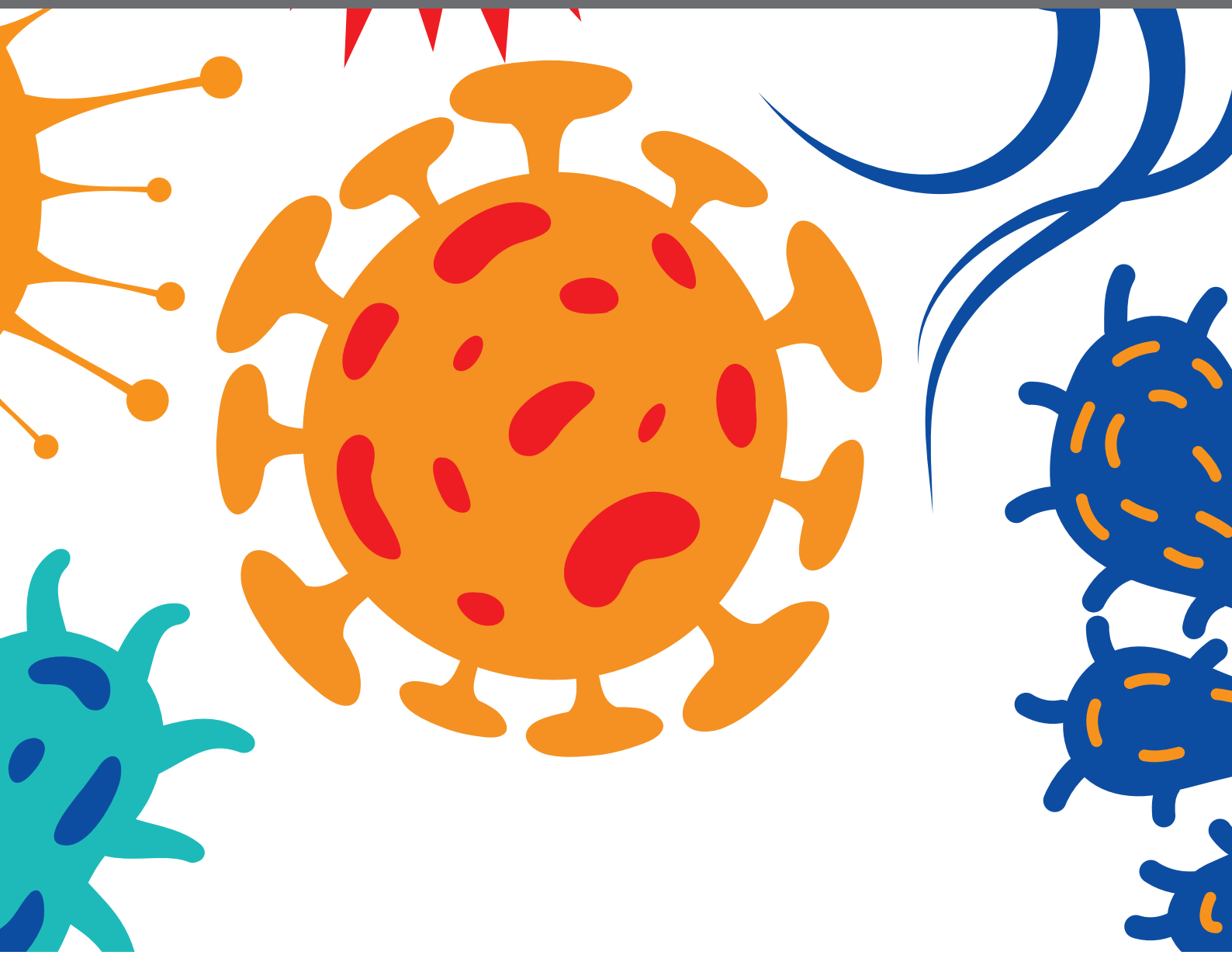

frontiers Research Topics

ISSN 1664-8714
ISBN 978-2-88974-327-8
DOI 10.3389/978-2-88974-327-8

About Frontiers

Frontiers is more than just an open-access publisher of scholarly articles: it is a pioneering approach to the world of academia, radically improving the way scholarly research is managed. The grand vision of Frontiers is a world where all people have an equal opportunity to seek, share and generate knowledge. Frontiers provides immediate and permanent online open access to all its publications, but this alone is not enough to realize our grand goals.

Frontiers Journal Series

The Frontiers Journal Series is a multi-tier and interdisciplinary set of open-access, online journals, promising a paradigm shift from the current review, selection and dissemination processes in academic publishing. All Frontiers journals are driven by researchers for researchers; therefore, they constitute a service to the scholarly community. At the same time, the Frontiers Journal Series operates on a revolutionary invention, the tiered publishing system, initially addressing specific communities of scholars, and gradually climbing up to broader public understanding, thus serving the interests of the lay society, too.

Dedication to Quality

Each Frontiers article is a landmark of the highest quality, thanks to genuinely collaborative interactions between authors and review editors, who include some of the world's best academicians. Research must be certified by peers before entering a stream of knowledge that may eventually reach the public - and shape society; therefore, Frontiers only applies the most rigorous and unbiased reviews.
Frontiers revolutionizes research publishing by freely delivering the most outstanding research, evaluated with no bias from both the academic and social point of view. By applying the most advanced information technologies, Frontiers is catapulting scholarly publishing into a new generation.

What are Frontiers Research Topics?

Frontiers Research Topics are very popular trademarks of the Frontiers Journals Series: they are collections of at least ten articles, all centered on a particular subject. With their unique mix of varied contributions from Original Research to Review Articles, Frontiers Research Topics unify the most influential researchers, the latest key findings and historical advances in a hot research area! Find out more on how to host your own Frontiers Research Topic or contribute to one as an author by contacting the Frontiers Editorial Office: frontiersin.org/about/contact

HOST-PATHOGEN INTERACTION IN CENTRAL NERVOUS SYSTEM INFECTION

Topic Editors:
Federico Iovino, Karolinska Institutet (KI), Sweden
Tatiana Barichello, University of Texas Health Science Center at Houston, United States

Citation: Iovino, F., Barichello, T., eds. (2022). Host-pathogen Interaction in Central Nervous System Infection. Lausanne: Frontiers Media SA.
doi: 10.3389/978-2-88974-327-8

Table of Contents

frontiers in Cellular and Infection Microbiology

EDITORIAL
published: 24 December 2021
doi: 10.3389/fcimb.2021.790761

Editorial: Host-Pathogen Interaction in the Central Nervous System

Tatiana Barichello[1,2] *and Federico Iovino*[3]*

[1] Department of Psychiatry and Behavioral Sciences, University of Texas Health Science Center at Houston, TX, United States, [2] Graduate Program in Health Sciences, University of Southern Santa Catarina (UNESC), Santa Catarina, Brazil, [3] Department of Neuroscience, Karolinska Institutet, Stockholm, Sweden

Keywords: Host-pathogen interaction, Central Nervous System, bacteria, viruses, parasites

Editorial on the Research Topic

Host-Pathogen Interaction in the Central Nervous System

Meningitis is an inflammation of the meninges that cover and protect the brain and the spinal cord. This inflammation occurs upon an infection of the Central Nervous System (CNS), and etiological causes of infection can be bacteria, viruses, and in rare cases parasites. Pathogens in the brain encounter different types of cells, such as microglia, the resident macrophages of the brain, neurons, the fundamental cellular units responsible for electrical and chemical signaling, astrocytes, cells in close contact with the blood-brain barrier that participate in immune responses, and other infiltrating immune cells. The scope of this Research Topic was to shed light on all various types of interaction that the different etiological agents of meningitis (bacteria, viruses, parasites) take with the different cell types of the brain during the pathogenesis process.

OPEN ACCESS

Edited and reviewed by:
Thomas Rudel,
Julius Maximilian University of Würzburg, Germany

***Correspondence:**
Federico Iovino
federico.iovino@ki.se

Specialty section:
This article was submitted to Bacteria and Host, a section of the journal Frontiers in Cellular and Infection Microbiology

Received: *07 October 2021*
Accepted: *25 November 2021*
Published: *24 December 2021*

Citation:
Barichello T and Iovino F (2021) Editorial: Host-Pathogen Interaction in the Central Nervous System. Front. Cell. Infect. Microbiol. 11:790761. doi: 10.3389/fcimb.2021.790761

PARASITIC MENINGITIS

Meningitis caused by parasites does not always obtain enough attention from the scientific community. Parasites like *Toxoplasma gondii* can be resilient and have the capacity to cause lifelong chronic infections requiring continuous immune responses by the host. Bergersen et al. have provided a comprehensive study of how targeted transcriptomic analysis using mouse models of chronic *T. gondii* infection can reveal differences in the host and parasite gene expression, giving tremendous insights into how further understanding the neuropathology aspects of chronic *T. gondii*-CNS infection (Bergersen et al., 2021).

Angiostrongylus cantonensis is another parasite that can cause meningitis, in particular the so-called eosinophilic meningitis. Yet, the pathogenesis of meningitis caused by *A. cantonensis* remains poorly understood. Zhang et al. have shown that upregulation of C-X3-C Motif Chemokine Ligand 1 (CX3CL1) in the brain tissue leads to the recruitment of natural killer (NK) cells into the CNS which of course should help the host in fighting the infection; however, this infiltration into the brain causes a worsening of the host CNS conditions (Zhang et al., 2021). Interestingly, Zhang et al. have observed that by neutralizing CX3CL1 and depleting NK cells, brain injury was alleviated,

therefore proposing a new therapeutic intervention to protect the CNS against *A. cantonensis* infections (Zhang et al., 2021).

VIRAL MENINGITIS

Meningitis can also be caused by certain viruses. Dengue virus (DENV) is transmitted by Aedes mosquitoes to humans and is a serious threat worldwide. The main clinical problem is that, up to today, there is not an effective drug against dengue infections. Shen et al. have observed that metoclopramide (MCP), an antagonist of the dopamine 2 receptor (D2R) promotes an impairment of DENV-double-stranded RNA replication and provided promising results regarding the use of MCP as therapy to reduce DENV-induced neuronal damage (Shen et al., 2021).

The Japanese encephalitis virus (JEV) can cause meningitis with permanent neurological sequelae and yet, the mechanism employed by JEV for brain invasion from the systemic circulation remained unknown. Zou et al. finally elucidated the mechanism of entering the brain by blood-borne JAV (Zou et al., 2021). The virus uses monocytes to spread in the brain tissue and expand the infection in the CNS (Zou et al., 2021). Furthermore, the extracellular High mobility group box protein 1 (HMGB1) facilitates the immune cell migration across the vascular endothelium of the BBB, which further accelerates the onset of JEV-induced meningitis (Zou et al., 2021).

Viral meningitis represents a significant burden in tropical countries of South America, and Arboviruses, such as Chikungunya, Mayaro, Oropouche, and Zika viruses, are major etiological agents of this disease. Arbovirus-caused meningitis is also frequently associated with severe neurological outcomes. The comprehensive genome-wide transcriptome analysis of human primary astrocytes infected with Chikungunya, Mayaro, Oropouche, and Zika viruses described by Viana Geddes et al, has revealed a common pattern in downregulation of the host innate immune response, antiviral response, and expression levels of inflammatory cytokines associated with interferon stimulation for all the arboviruses tested (Viana Geddes et al., 2021). These findings point towards a co-evolution that all these arboviruses have engaged in developing mechanisms to escape the antiviral response induced by interferon (IFN) (Viana Geddes et al., 2021). Altogether, this expands the knowledge on how the antiviral-IFN pathway can be experimentally modified in order to be effective against Arbovirus-caused meningitis, opening avenues for novel clinical approaches (Viana Geddes et al., 2021).

BACTERIAL MENINGITIS

Streptococcus pneumoniae (the pneumococcus) is the leading etiological cause of bacterial meningitis globally (Iovino et al., 2016). Despite access to antibiotics and the introduction of pneumococcal conjugate vaccine programs, mortality from pneumococcal meningitis exceeds 50% in sub-Saharan African countries with high HIV prevalence, and the causes of such high mortality are poorly understood. Wall et al. have interestingly reported that excessive *S. pneumoniae* elongation factor thermal unstable (EF-Tu) protein in the cerebrospinal fluid (CSF) was frequently associated with impaired survival in meningitis in a high HIV prevalence population (Wall et al., 2020). Moreover, EF-Tu can inhibit neutrophil-mediated killing of *S. pneumoniae* in the CSF (Wall et al., 2020). The findings by Wall et al. provide novel important knowledge on how pneumococci avoid essential host innate responses during meningitis pathogenesis (Wall et al., 2020).

Microglia, the resident macrophages of the brain, initiate and drive the inflammatory process during pneumococcal meningitis pathogenesis. Pan et al. have reported that JWH-133, an agonist of G-protein cannabinoid receptor type 2 (CB2) impairs microglial activation and downregulates pro-inflammatory signaling (Pan et al., 2020). Therefore, this important finding suggests that inhibition of microglial activation using CB2 agonists may represent a novel therapy for neuroinflammation modulation (Pan et al., 2020).

Another major etiological agent of bacterial meningitis is *Listeria monocytogenes*. *L. monocytogenes* meningoencephalitis has a mortality rate of up to 50%, and severe neurofunctional sequelae are prevalent. Zbinden et al. have identified that *L. monocytogenes* expressing multiple sequence recognition (hsdS) A causes less damage than when other hsdS genes (B, C or D) are present (Zbinden et al., 2020). On the other hand, the expression of hsdSC and D worsened the disease onset in *L. monocytogenes* meningitis (Zbinden et al., 2020). This observation shows important phenotypical switching that has crucial role in regulating the virulence of CNS infections by *L. monocytogenes* (Zbinden et al., 2020). Nevertheless, further studies are necessary to investigate how this therapy can also be effective in reducing brain injury.

Streptococcus suis (*S. suis*) is an important opportunistic pathogen, which can cause septicemia and meningitis in pigs, but also in humans. In the study by Lauer et al, using Gene Set Enrichment Analysis (GSEA), 18, 28, and 21 enriched hallmark gene sets (GSs) were identified for infected human choroid plexus (CP) epithelial papilloma (HIBCPP) cells, primary porcine CP epithelial cells (PCPEC), and in the CP of pigs affected by *S. suis* ST2 meningitis, respectively of which 8 GSs overlapped among the three different sample sets (Lauer et al., 2021). Most of these GSs were reported to be involved in cellular signaling, host immune and inflammatory response (Lauer et al., 2021). This finding clearly suggests that *S. suis*-infected human and porcine CP epithelial cells share similar cellular processes in the context of host inflammatory response (Lauer et al., 2021).

The pathogens covered in the study subject "Host-pathogen interaction in the Central Nervous System" are summarized in **Figure 1**.

CONCLUDING REMARKS

The Research Topic "Host-pathogen interaction in the Central Nervous System" also contains important review articles focused on i) the trans-endothelial trafficking of *S. pneumoniae* across the BBB endothelium (Anil and Banerjee, 2020), ii) the molecular details of a broad array of CNS responses to the bacterial cell

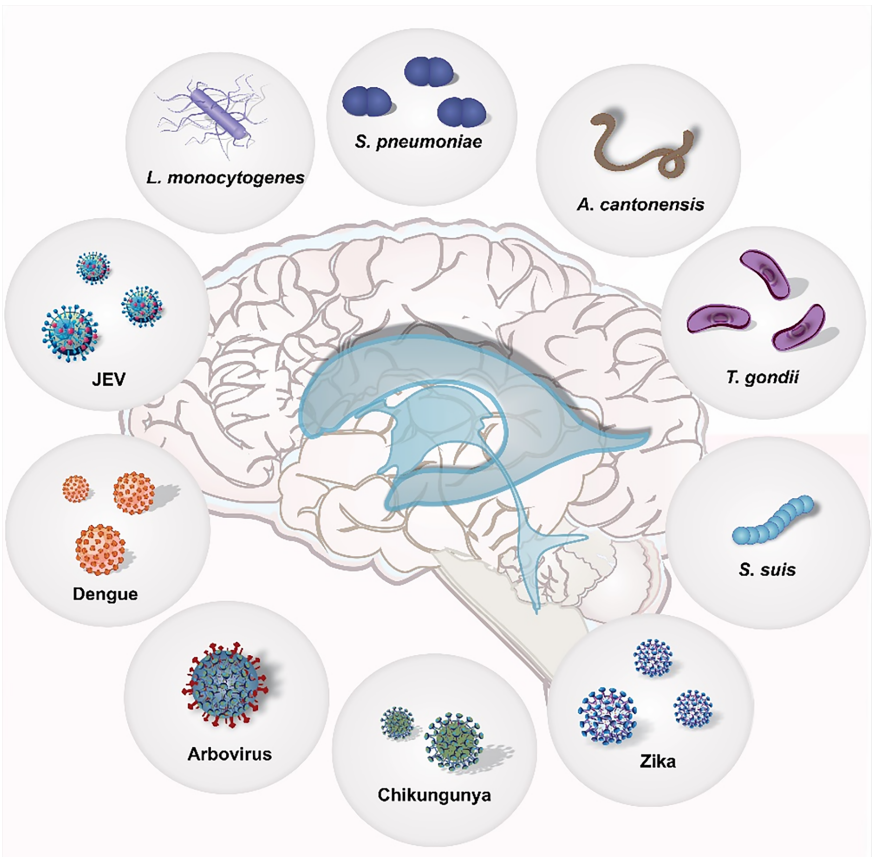

FIGURE 1 | The host-pathogen interaction in the Central Nervous System.

envelope and novel approaches to improve clinical outcome (Maccain and Tuomanen, 2020), iii) the benefits and harms of the use of adjunctive steroid therapy to reduce neuroinflammation in meningitis patients (Gundamraj and Hasbun, 2020), iv) the beneficial or detrimental role of DNA sensors in viral CNS infections (Jeffries and Marriott, 2020).

AUTHOR CONTRIBUTIONS

TB and FI equally contributed to this editorial article. All authors contributed to the article and approved the submitted version.

FUNDING

This work was supported by The University of Texas Health Science Center at Houston. TB has received a grant from the Alzheimer's Association (AARGDNTF-19-619645) and the National Institutes of Health/National Institute on Aging (NIH/NIA grant 1RF1AG072491). FI is funded by Karolinska Institutet Faculty Board, the Swedish Research Council (grant nr. 2020-0261), Bjarne Ahlström Foundation for Research in Clinical Neurology, Magnus Bergvall Foundation, Tore Nilson Foundation, Clas Groschinsky Foundation, and HKH Crown Princess Lovisa's Association for Pediatric Research.

REFERENCES

Anil, A., and Banerjee, A. (2020). Pneumococcal Encounter With the Blood-Brain Barrier Endothelium. *Front. Cell Infect. Microbiol.* 10, 590682. doi: 10.3389/fcimb.2020.590682

Bergersen, K., Barnes, A., Worth, D., David, C., and Wilson, E. H. (2021). Targeted Transcriptomic Analysis of C57BL/6 and BALB/c Mice During Progressive Chronic *Toxoplasma gondii* Infection Reveals Changes in Host and Parasite Gene Expression Relating to Neuropathology and Resolution. *Front. Cell Infect. Microbiol.* 11, 645778. doi: 10.3389/fcimb.2021.645778

Gundamraj, S., and Hasbun, R. (2020). The Use of Adjunctive Steroids in Central Nervous Infections. *Front. Cell Infect. Microbiol.* 10, 592017. doi: 10.3389/fcimb.2020.592017

Iovino, F., Seinen, J., Henriques-Normark, B., and van Dijl, J. M. (2016). How Does Streptococcus Pneumoniae Invade the Brain? *Trends Microbiol.* 24, 307–315. doi: 10.1016/j.tim.2015.12.012

Jeffries, A. M., and Marriott, I. (2020). Cytosolic DNA Sensors and CNS Responses to Viral Pathogens. *Front. Cell Infect. Microbiol.* 10, 576263. doi: 10.3389/fcimb.2020.576263

Lauer, A. N., Scholtysik, R., Beineke, A., Baums, C. G., Klose, K., Valentin-Weigand, P., et al. (2021). A Comparative Transcriptome Analysis of Human and Porcine Choroid Plexus Cells in Response to Streptococcus Suis Serotype 2

Infection Points to a Role of Hypoxia. *Front. Cell Infect. Microbiol.* 11, 639620. doi: 10.3389/fcimb.2021.639620

Maccain, W. J., and Tuomanen, E. I. (2020). Mini-Review: Bioactivities of Bacterial Cell Envelopes in the Central Nervous System. *Front. Cell Infect. Microbiol.* 10, 588378. doi: 10.3389/fcimb.2020.588378

Pan, S. D., Grandgirard, D., and Leib, S. L. (2020). Adjuvant Cannabinoid Receptor Type 2 Agonist Modulate the Polarization of Microglia Towards a Non-Inflammatory Phenotype in Experimental Pneumococcal Meningitis. *Front. Cell Infect. Microbiol.* 10, 588195. doi: 10.3389/fcimb.2020.588195

Shen, T. J., Hanh, V. T., Nguyen, T. Q., Jhan, M. K., Ho, M. R., and Lin, C. F. (2021). Repurposing the Antiemetic Metoclopramide as an Antiviral Against Dengue Virus Infection in Neuronal Cells. *Front. Cell Infect. Microbiol.* 10, 606743. doi: 10.3389/fcimb.2020.606743

Geddes, V. E. V., Brustolini, O. J. B., Cavalcante, L. T. F., Moreira, F. R. R., de Castro, F. L., Guimarães, A. P. C., et al. (2021). Common Dysregulation of Innate Immunity Pathways in Human Primary Astrocytes Infected With Chikungunya, Mayaro, Oropouche, and Zika Viruses. *Front. Cell Infect. Microbiol.* 11, 641261. doi: 10.3389/fcimb.2021.641261

Wall, E. C., Brownridge, P., Laing, G., Terra, V. S., Mlozowa, V., Denis, B., et al. (2020). CSF Levels of Elongation Factor Tu Is Associated With Increased Mortality in Malawian Adults With Streptococcus Pneumoniae Meningitis. *Front. Cell Infect. Microbiol.* 10, 603623. doi: 10.3389/fcimb.2020.603623

Zbinden, F. R., De Ste Croix, M., Grandgirard, D., Haigh, R. D., Vacca, I., Zamudio, R., et al. (2020). Pathogenic Differences of Type 1 Restriction-Modification Allele Variants in Experimental Listeria Monocytogenes Meningitis. *Front. Cell Infect. Microbiol.* 10, 590657. doi: 10.3389/fcimb.2020.590657

Zhang, R., Miao, T., Qin, M., Zhao, C., Wang, W., Zhang, C., et al. (2021). CX_3 CL1 Recruits NK Cells Into the Central Nervous System and Aggravates Brain Injury of Mice Caused by Angiostrongylus Cantonensis Infection. *Front. Cell Infect. Microbiol.* 11, 672720. doi: 10.3389/fcimb.2021.672720

Zou, S. S., Zou, Q. C., Xiong, W. J., Cui, N. Y., Wang, K., Liu, H. X., et al. (2021). Brain Microvascular Endothelial Cell-Derived HMGB1 Facilitates Monocyte Adhesion and Transmigration to Promote JEV Neuroinvasion. *Front. Cell Infect. Microbiol.* 11, 701820. doi: 10.3389/fcimb.2021.701820

Conflict of Interest: The authors declare that the research was conducted in the absence of any commercial or financial relationships that could be construed as a potential conflict of interest.

Publisher's Note: All claims expressed in this article are solely those of the authors and do not necessarily represent those of their affiliated organizations, or those of the publisher, the editors and the reviewers. Any product that may be evaluated in this article, or claim that may be made by its manufacturer, is not guaranteed or endorsed by the publisher.

frontiers in Cellular and Infection Microbiology

REVIEW
published: 16 September 2020
doi: 10.3389/fcimb.2020.576263

Cytosolic DNA Sensors and CNS Responses to Viral Pathogens

*Austin M. Jeffries and Ian Marriott**

Department of Biological Sciences, The University of North Carolina at Charlotte, Charlotte, NC, United States

Viral central nervous system (CNS) infections can lead to life threatening encephalitis and long-term neurological deficits in survivors. Resident CNS cell types, such as astrocytes and microglia, are known to produce key inflammatory and antiviral mediators following infection with neurotropic DNA viruses. However, the mechanisms by which glia mediate such responses remain poorly understood. Recently, a class of intracellular pattern recognition receptors (PRRs), collectively known as DNA sensors, have been identified in both leukocytic and non-leukocytic cell types. The ability of such DNA sensors to initiate immune mediator production and contribute to infection resolution in the periphery is increasingly recognized, but our understanding of their role in the CNS remains limited at best. In this review, we describe the evidence for the expression and functionality of DNA sensors in resident brain cells, with a focus on their role in neurotropic virus infections. The available data indicate that glia and neurons can constitutively express, and/or can be induced to express, various disparate DNA sensing molecules previously described in peripheral cell types. Furthermore, multiple lines of investigation suggest that these sensors are functional in resident CNS cells and are required for innate immune responses to viral infections. However, it is less clear whether DNA sensormediated glial responses are beneficial or detrimental, and the answer to this question appears to dependent on the context of the infection with regard to the identity of the pathogen, host cell type, and host species. Defining such parameters will be essential if we are to successfully target these molecules to limit damaging inflammation while allowing beneficial host responses to improve patient outcomes.

Keywords: DNA sensors, astrocytes, microglia, neuroinflammation, viral encephalitis

OPEN ACCESS

Edited by:
Federico Iovino,
Karolinska Institutet (KI), Sweden

Reviewed by:
Maria Kalamvoki,
University of Kansas Medical Center, United States
Raphael Gaudin,
UMR9004 Institut de Recherche en Infectiologie de Montpellier (IRIM), France

****Correspondence:***
Ian Marriott
imarriot@uncc.edu

Specialty section:
This article was submitted to Virus and Host, a section of the journal Frontiers in Cellular and Infection Microbiology

Received: *25 June 2020*
Accepted: *12 August 2020*
Published: *16 September 2020*

Citation:
Jeffries AM and Marriott I (2020) Cytosolic DNA Sensors and CNS Responses to Viral Pathogens. Front. Cell. Infect. Microbiol. 10:576263. doi: 10.3389/fcimb.2020.576263

INTRODUCTION

Infection of the central nervous system (CNS) can result in encephalitis, a condition that is characterized by severe neuroinflammation resulting in fever, headaches, altered consciousness, seizures, and even death (Roos, 1999). Between 2000 and 2010 there were 7.3 encephalitis cases per 100,000, with most identified etiologies (48.2%) being attributable to viral infections (George et al., 2014). Since the mechanisms that lead to CNS inflammation following infection are poorly understood, current treatment strategies include general immune suppression, and/or antiviral therapy (Chaudhuri and Kennedy, 2002; George et al., 2014; Venkatesan and Geocadin, 2014). Traditionally, it was thought that infiltrating peripheral monocytes and leukocytes were the major contributors of pro-inflammatory mediator production in encephalitis as most resident CNS cells were assumed to lack immune functions. However, it is now appreciated that glial cells, most notably microglia and astrocytes, play a critical role in immune surveillance in the CNS and are

important contributors to both protective and detrimental host responses to infectious agents (Aloisi, 2000, 2001; Bsibsi et al., 2002, 2006; Bowman et al., 2003; Furr et al., 2008, 2011; Chauhan et al., 2009; Liu et al., 2010; Serramía et al., 2015).

Glial cells can produce an array of proinflammatory and antiviral mediators following infection (Chauhan et al., 2009; Furr and Marriott, 2012) and it is now known that they accomplish this via members of multiple families of pattern recognition receptors (PRRs). These PRRs recognize numerous pathogen-associated molecular patterns (PAMPs) and/or damage associated molecular patterns (DAMPs) and trigger transcription factor activation that, in turn, elicits proinflammatory and antiviral mediator production. Of these, the most widely and best studied glial PRRs are the cell surface and endosomal Toll-like receptors (TLRs) and the cytosolic nucleotide-binding and oligomerization domain (NOD)-like receptors (NLRs) (Sterka et al., 2006; Chauhan et al., 2009; Rebsamen et al., 2009; Liu et al., 2010; Dai et al., 2014; Reinert et al., 2016; Su and Zheng, 2017). More recently, multiple classes of cytosolic nucleic acid sensors have been discovered that are likely have an important function during active viral infections due to their intracellular location. These include RNA sensors, such as the retinoic acid-inducible gene-I (RIG-I)-like receptor (RLR) family, and the possible roles and importance of these molecules in glial immune responses have been discussed in depth elsewhere (Furr et al., 2008; Furr and Marriott, 2012; Carty et al., 2014; Nair and Diamond, 2015; Zohaib et al., 2016). However, the importance of DNA sensors, including cyclic guanosine monophosphate-adenosine monophosphate (cGAMP) synthase (cGAS), in viral CNS infections and the initiation of glial immune functions remains more controversial, despite evidence for their antiviral function in peripheral lymphoid and myeloid cells (Unterholzner, 2013; Cai et al., 2014; Dhanwani et al., 2018; Lugrin and Martinon, 2018). In this review article, we will discuss the evidence for the expression and function of DNA sensors in resident CNS cells, their role during viral infections, and their potential as targets for therapeutic intervention.

cGAS/STING

Perhaps the most well-known and best studied cytosolic DNA sensor is cGAS. This molecule directly binds to double stranded DNA and then catalyzes the production of the secondary messenger, 2′3′cyclic GMP-AMP (cGAMP) (Gao P. et al., 2013; Sun et al., 2013; Zhang X. et al., 2013). This secondary messenger subsequently binds to the downstream adaptor protein stimulator of interferon genes (STING), which initiates the phosphorylation of tank binding kinase 1 (TBK1), and interferon regulatory factor 3 (IRF3), and activates nuclear factor kappalight-chain-enhancer of activated B cells (NF-kB). Such transcription factor activation precipitates the expression of interferon-beta (IFN-β) and other antiviral and/or pro-inflammatory cytokines (Ishikawa et al., 2009; Li et al., 2013; Abe and Barber, 2014; Fang et al., 2017; Sun et al., 2017; Aarreberg et al., 2019). Since its discovery in 2013, cGAS has been demonstrated to play a critical role in recognizing and eliminating a diverse array of pathogens, either through direct recognition of microbial DNA or indirect recognition of retroviral DNA intermediates or damage associate molecular patterns (DAMPS), such as released mitochondrial DNA (Gao D. et al., 2013; Abe and Barber, 2014; Dai et al., 2014; Herzner et al., 2015; Paijo et al., 2016; Fang et al., 2017; Sun et al., 2017; Cheng et al., 2018; Wong et al., 2019). As discussed elsewhere (Cai et al., 2014; Chen et al., 2016; Dhanwani et al., 2018; Ablasser and Chen, 2019), numerous studies have demonstrated the expression and function of cGAS in peripheral leukocytic and non-leukocytic cell types, such as human plasmacytoid dendritic cells, macrophages, monocytes, helper T-lymphocytes, and endothelial cells (as summarized in **Table 1**). However, less attention has been given to the role of this sensor in the CNS and the immune responses of glial cells (Lahaye et al., 2013; Li et al., 2013; Dai et al., 2014; Ma Z. et al., 2015; West et al., 2015; Bode et al., 2016; Paijo et al., 2016; Vermeire et al., 2016; Luecke et al., 2017; Su and Zheng, 2017; Sun et al., 2017; Swanson et al., 2017).

The first description of cGAS expression in resident CNS cell types came from Cox et al. (2015), who established the constitutive and inducible expression of mRNA encoding cGAS in murine microglia. Interestingly, while they observed neither constitutive nor IFN-β-inducible expression of cGAS in murine astrocytes, siRNA-mediated cGAS knockdown decreased IFN-β activity in both microglia and astrocytes following exposure to exogenous dsDNA (Cox et al., 2015). Further support for the presence of cGAS in glia has since been provided by our demonstration that primary human microglia and astrocytes both constitutively express cGAS protein and its downstream adaptor molecule STING (Jeffries and Marriott, 2017).

Circumstantial evidence for the functional importance of cGAS in the brain lays in the recognized ability of many important CNS pathogens to interfere with this sensor and/or it's signaling pathway (as summarized in **Table 2**). For example, herpes simplex virus 1 (HSV-1), the dsDNA virus that is the most common cause of fatal sporadic encephalitis, has multiple gene products that can interfere with the cGAS-STING signaling pathway (Bradshaw and Venkatesan, 2016). The HSV-1 encoded protein UL37 attenuates the enzymatic activity of cGAS and lowers cGAMP production in human monocytes and fibroblasts, thereby decreasing antiviral gene expression (Zhang et al., 2018). Mutations in UL37 that interfere with its deamidase activity prevent this protein from inhibiting cGAS and lead to lower HSV-1 titers in the brain following infection (Zhang et al., 2018). Interestingly, such an inhibitory activity appears to show species specificity as UL37 molecule does not appear to be important in infections in some non-human primate species (Zhang et al., 2018). Another HSV-1 product, UL41 (virion host shutoff protein), has been shown to decrease IFN-β production in a human epithelial cell line expression system by reducing cGAS protein expression (Su and Zheng, 2017), and its importance in disrupting cGAS-mediated antiviral responses has been illustrated by the ability of cGAS knockdown to increase viral production of a UL41 null mutant HSV-1 strain, but not a wild type strain (Su and Zheng, 2017). Furthermore, additional HSV-1 products have been demonstrated to target down-stream signaling molecules in the cGAS STING pathway. For instance,

TABLE 1 | Expression and antiviral activity of intracellular DNA sensors in peripheral cell types.

Sensor	Cell type	Ligand	Antiviral activity	Recognized pathogens	References
ZBP1	Mouse primary fibroblast, liver macrophages, BMDM Mouse cell lines, L929, SVEC4-10, NIH3T3, 3T3-SA Human cell lines HT-29, A549, HepG2	dsDNA or RNA	IFN expression NF-κB activation, cell death	HSV-1, IAV, CMV, vaccinia virus, ZIKV, WNV	Upton et al., 2012; Pham et al., 2013; Kuriakose et al., 2016; Lin et al., 2016; Maelfait et al., 2017; Guo et al., 2018; Daniels et al., 2019; Ingram et al., 2019; Rothan et al., 2019; Yang et al., 2020
cGAS	Mouse primary lung fibroblasts, GM-CSF DC, FLt3L DC, BMDM Murine cell lines, L929, RAW 264.7 Hamster cell line BHK Primary human PBMCs, MDM, MDDC, plasmacytoid dendritic cells, PBMCs, CD4+ T cells Human cell lines, THP1, HFFs, A549, HUVEC, EA.hy926	dsDNA	IFN expression, inflammasome priming	HIV, HSV, MLV, SIV, HCMV, DENV, ectromelia virus	Gao D. et al., 2013; Li et al., 2013; Sun et al., 2013; Herzner et al., 2015; Ma F. et al., 2015; Bode et al., 2016; Vermeire et al., 2016
IFI16	Mouse primary corneal epithelium Mouse cell line RAW 264.7 Primary human MDM, keratinocytes, PBMCs, CD4+ T cells, hepatocytes Human cell lines, THP1, hTCEpi, HFFs, BJAB, HMVEC, BCBL1, 184B5, HCC1937, TIME, HELF, U2OS, HUVEC, Akata cells, MUTU1, huh7, HepG2, HeLa, HepaRG cells, C666-1, Raji, LCL	dsDNA	Inflammasome activation, IFN-β production, transcriptional regulation	HSV-1, KSHV, HIV, EBV, HBV	Unterholzner et al., 2010; Conrady et al., 2012; Orzalli et al., 2012; Ansari et al., 2013; Cuchet-Lourenco et al., 2013; Jakobsen et al., 2013; Dell'Oste et al., 2014; Diner et al., 2015; Dutta et al., 2015; Iqbal et al., 2016; Pisano et al., 2017; Lum et al., 2019; Roy et al., 2019; Yang et al., 2020
AIM2	Primary mouse BMDM, BMDC, MEF, alveolar macrophages, peritoneal macrophages Mouse cell lines NR9456, B6-MCL Primary human dermal fibroblasts, keratinocytes Human cell lines, THP1, ATII	dsDNA	Inflammasome activation	HPV, HBV, HCMV	Fernandes-Alnemri et al., 2009; Hornung et al., 2009; Rathinam et al., 2010; Reinholz et al., 2013; Sagulenko et al., 2013; Ekchariyawat et al., 2015; Corrales et al., 2016; Gray et al., 2016; Huang et al., 2017; Nakaya et al., 2017; Zhang et al., 2017; Chen et al., 2018
DDX41	Primary mouse BMDC, peritoneal macrophages, MEF Mouse cell lines, D2SC, L929 Primary human PBMCs Human cell line THP1	dsDNA or DNA:RNA hybrid	IFN and ISG expression	HSV-1, adenovirus, MLV, IAV (mitochondrial DNA)	Zhang Z. et al., 2011, 2013; Lee et al., 2015; Stavrou et al., 2015; Moriyama et al., 2019
DNA-PK	Primary mouse MEF Primary human monocytes, MDDC Human cell lines, HEK293, HeLa, THP1, SK-hep-1, HepG2.2.15, U937s, HFFs	dsDNA	IFN expression	HSV-2, HTLV, HBV, vaccinia virus	Zhang X. et al., 2011; Ferguson et al., 2012; Peters et al., 2013; Li et al., 2016; Wang et al., 2017; Scutts et al., 2018
RNA-pol III	Primary mouse MEF, dendritic cells Mouse cell line RAW264.7 Primary human PBMCs, MDDC Human cell line HEK293	RNA	IFN expression NF-κB activation	adenovirus, HSV-1, EBV	Ablasser et al., 2009; Chiu et al., 2009

UL36 can prevent NF-κB activation by cleaving IκBa poly ubiquitin chains while UL46 and ICP27 interact with STING and TBK1 to prevent the activation of IRF3 and interferon stimulated gene (ISG) expression (Christensen et al., 2016; Deschamps and Kalamvoki, 2017; Ye et al., 2017; You et al., 2019). Since all members of the family Herpesviridae appear to target cGAS [**Table 2** and as reviewed in Chan and Gack (2016) and Phelan et al. (2020)], and such viruses can cause latent infections, it is tempting to speculate that the inhibition of this sensor may play a critical role in establishing viral latency. Such a mechanism could be of particular importance for HSV encephalitis as the reactivation of a latent infection is thought to be a key contributor to the development of this condition (Menendez and Carr, 2017).

In addition to DNA viruses, other neurotropic viruses, such as positive stranded RNA viruses from the family Flaviviridae, can also hamper cGAS activity (**Table 2**). For instance, Dengue virus (DENV) that can cause encephalitis has been shown to target cGAS for degradation and prevent it from detecting released mitochondrial DNA in human monocyte-derived dendritic cells and monocytic and fibroblastic cell lines (Aguirre et al., 2017; Sun et al., 2017).

Specifically, the DENV protein NS2B3 has been shown to directly interact with cGAS and target it for lysosomal degradation (Aguirre et al., 2017). In addition, this viral product can also cleave the downstream signaling molecule STING, further disrupting cGAS-mediated antiviral signaling.

TABLE 2 | Viral inhibitors of DNA sensing pathways.

Sensor	Virus	Viral product	Inhibition mechanisms	References
STING	Coronavirus	Papain-like proteases	Blocks dimerization and signaling	Sun et al., 2012
	DENV	NS2B3	Cleavage (human only)	Aguirre et al., 2012
	HCMV	UL122 (IE86)	Facilitated degradation	Kim et al., 2017
		US9	Blocks dimerization and association with TBK-1	Choi et al., 2018
		UL82	Inhibits translocation and impairs TBK1 and IRF3 recruitment	Fu et al., 2017
	HCV	NS4B	Suppresses accumulation and activation	Yi et al., 2016
	HSV-1	ICP27	Inhibits TBK1/STING signaling	Christensen et al., 2016
		$\gamma_1$34.5	Disrupts translocation	Pan et al., 2018
cGAS	DENV	NS2B3	Autophagosomal cleavage/degradation	Aguirre et al., 2017
	EBV	KSHV ORF52 homolog	Inhibits activity	Wu et al., 2015
	HCMV	pUL83	Reduces cGAMP production	Biolatti et al., 2017
		UL31	Interferes with DNA binding	Huang Z. F. et al., 2018
	HSV-1	UL37	Inhibits cGAMP production (not in NHP)	Zhang et al., 2018
		VP22	Inhibiting enzymatic activity	Huang J. et al., 2018
	KSHV	ORF52	Inhibiting enzymatic activity	Wu et al., 2015
	MHV68	KSHV ORF52 homolog		
	RRV	KSHV ORF52 homolog		
cGAS/STING	HIV-2/SIV	VPX	Blocks cGAS/STING mediated NF-κB activation	Su et al., 2019
	HSV-1	UL41	Unknown	Su and Zheng, 2017
		UL24	Prevents NF-κB translocation	Xu et al., 2017
		UL36	Prevents NF-κB activation by cleaving IkBa polyubiquiting chains	Ye et al., 2017
		UL46	Interacts with TBK1 and STING to reduce ISG expression	Deschamps and Kalamvoki, 2017
		ICP27	Interacts with TBK1 and STING to prevent IRF3 activation	Christensen et al., 2016
	KSHV	ORF36	Unknown	Ma Z. et al., 2015
		ORF73		
		ORF57		
		ORF45		
		ORF55		
		vIRF1	Inhibits STING/TBK1 interactions	
	KSHV	cytoplasmic LANA	Binds cGAS and prevents TBK1 and IRF3 phosphorylation	Zhang G. et al., 2016
cGAS/STING/ RIG-I	HPV	SUV39H1	Represses transcription at their promoter regions	Lo Cigno et al., 2020
IFI16	HCMV	pUL97	Mislocalization	Dell'Oste et al., 2014
	HSV-1	ICP0	Increases degradation	Orzalli et al., 2012; Diner et al., 2015; Li et al., 2016
	KSHV	Unknown	Increases degradation	Roy et al., 2016
IFI16/STING	HSV-1	UL46	Reduces protein expression of each and interferes with STING/TBK1 interaction	Deschamps and Kalamvoki, 2017
ZBP1	HSV-1	ICP6	Blocks human RIP3/MLKL interactions (but activates RIPK3 in mice)	Wang et al., 2014; Huang et al., 2015; Guo et al., 2018
	MCMV	M45	Blocks ZBP1/RIP3 interactions	Upton et al., 2012
AIM2	HCMV	UL83	Prevents IL-1β maturation and may increase IFI16 degradation	Huang et al., 2017
		IE86	Blocks IL-1β secretion	Botto et al., 2019
		IE86	Inhibits NF-κB gene transcription and IL-1β release	
	HSV-1	VP22	Prevents inflammasome oligomerization	Maruzuru et al., 2018
DDX41	HSV-1	miR-H2-3p	Inhibits DDX41 transcription	Duan et al., 2019

Interestingly, this viral product also shows species specificity similar to the HSV-1 product UL37 as NS2B3 targets human STING but does not cleave this molecule in mouse or non-human primate cells (Stabell et al., 2018). Similarly, Zika virus (ZIKV), which came to prominence for its role in CNS and peripheral nerve pathologies including microcephaly and Guillain-Barré syndrome, can cleave STING via its NS2B3 protein and this effect, again, is restricted to human rather than murine cells (Ding et al., 2018). ZIKV can further disrupt cGASSTING signaling by stabilizing caspase-1 protein. This results in cGAS cleavage and reduced expression of type I IFNs and ISGs, and the promotion of inflammasome activation and ZIKV production (Zheng et al., 2018). Importantly, Zheng et al. (2018) demonstrated that cGAS deficiency or caspase-1 inhibition leads to increased cellular levels of ZIKV genetic material. Such findings therefore support the therapeutic potential of augmenting cGAS-STING mediated responses to combat debilitating neurotropic RNA virus infections.

More direct evidence of the importance of cGAS-STING signaling during viral CNS infections comes from the study of HSV-1 infection in STING deficient animals. Parker et al. (2015) demonstrated that STING deficient animals show increased susceptibility to intracerebral HSV-1 infection, with all succumbing within 3–5 days of infection and little mortality in age-matched wildtype animals. Interestingly, it appears that this increased susceptibility is dependent on the route of infection, as STING deficient animals show survival rates comparable to wildtype mice following administration via the cornea, despite the presence of high viral titers in the cornea and trigeminal ganglion (Parker et al., 2015). This phenomenon was subsequently confirmed (Royer and Carr, 2016) and the apparent discrepancy in lethality is likely to be due to difference in the distribution of HSV-1 within the CNS. High viral titers are limited to the trigeminal ganglion following corneal HSV-1 infection, while intracerebral infection results in widely disseminated HSV-1 infection throughout the CNS (Parker et al., 2015). In addition, it should be noted that susceptibility to HSV-1 appears to be strain dependent as STING deficient animals succumb to neuroinvasive strains of HSV-1 following corneal infection more rapidly than wild type animals (Parker et al., 2015). Regardless, it is clear that STING plays a role in HSV-1 neuroinvasion and is critical for protective host responses once the virus has disseminated throughout the CNS (Parker et al., 2015; Royer and Carr, 2016). The increased susceptibility of STING deficient animals to HSV-1 neuroinvasion may be due, at least in part, to a decreased expression of the ISG tetherin [also known as bone marrow stromal antigen 2 (BST2)], as these animals exhibit decreased expression of this ISG (amongst others) during infection (Royer and Carr, 2016), and tetherin depletion has been shown to increase HSV1 titers in the trigeminal ganglion (Royer and Carr, 2016).

Consistent with these studies employing STING deficient animals, treatment with the STING agonist dimethlxanthenone-4-acetic acid (DMXAA) has been demonstrated to increase IFN-β expression by HSV-1 infected mouse fibroblasts and to lower the production of viral particles by these cells (Cerón et al., 2019). Importantly, *in vivo* DMXAA treatment can lower viral titers in the cornea, trigeminal ganglion, and brainstem, of mice infected with the neuroinvasive McKrae strain of HSV-1, and this is reflected by increased survival and improved neurological outcomes in these animals (Cerón et al., 2019). As such, these studies provide a tantalizing glimpse of the potential of targeting the cGAS-STING pathway to treat CNS infections.

While these studies illustrate the importance of cGAS-STING signaling in HSV-1 infections of the CNS, the specific role of this sensor system in glia was established by Reinert et al. (2016) in a mouse model of HSV-1 encephalitis. They demonstrated that cGAS deficiency resulted in a phenotype that matched that observed in STING deficient mice following ocular HSV-1 infection (Reinert et al., 2016). Furthermore, they established that microglia were the primary producers of IFN-β after HSV-1 challenge and showed that only this glial cell type produced higher viral titers *in vitro* following the loss of STING (Reinert et al., 2016). *In vivo*, however, neurons and astrocytes showed greater numbers of HSV-1 viral particles in STING deficient mice (Reinert et al., 2016). This discrepancy was explained by the observation that astrocytes and neurons initiate antiviral programs *in vivo* in response to IFN-β produced by microglia in a TLR3-dependent manner (Reinert et al., 2016). This suggests that microglia represent the first responders to HSV-1 infection in the CNS.

Consistent with these findings in mice, we have shown that cytosolic administration of a dsDNA ligand can phosphorylate IRF3 and induce IFN-β mRNA expression in primary human microglia and astrocytes (Jeffries and Marriott, 2017), and we have demonstrated that such responses are largely dependent on cGAS expression (Jeffries and Marriott, 2017; Jeffries et al., 2020). Furthermore, we showed that ISG expression is lower in cGAS deficient human microglia both at rest and following infection with HSV-1 (Jeffries et al., 2020). However, while cGAS can contribute to antiviral gene expression, the absence of cGAS had no effect on HSV-1 production in infected human microglia (Jeffries et al., 2020). Given the recognized ability of HSV-1 products to abrogate cGAS-STING signaling in peripheral human but not murine cell types, we assessed cGAS protein levels in human glial cells following HSV-1 challenge. We found that the expression of this sensor was markedly reduced in human microglial and astrocytic cells following infection (Jeffries et al., 2020), highlighting the ability of viruses such as HSV-1 to circumvent PRR-mediated immune responses. As such, improving the stability and/or expression of cGAS/STING signaling components might be a viable approach to combat viral infections of the CNS and/or periphery.

IFI16

Interferon gamma inducible protein 16 (IFI16) is a member of the Pyrin and HIN domain (PHYIN) family of proteins that can serve as an intracellular DNA sensing molecule. PHYIN proteins are characterized by the presence of an N-terminal pyrin domain and one or two Cterminal HIN domains (Unterholzner et al., 2010). The HIN domains bind DNA while the pyrin domain is required for protein-protein interactions (Unterholzner et al.,

2010). IFI16, and its mouse ortholog p204, was the first PHYIN family members demonstrated to induce IFN-β in response to transfected DNA (Unterholzner et al., 2010). Additionally, IFI16 has been shown to interact with STING and knockdown of either of these proteins leads to reduced IFN-β production by the human and mouse monocytic cell lines THP-1 and RAW 264.7, respectively (Cridland et al., 2012). Interestingly, similar findings were described in murine astrocytes and microglia where p204 knockdown was shown to reduce IFN-β expression following DNA transfection (Cox et al., 2015), and our own studies indicate that human microglial and astrocytic cells constitutively express robust levels of IFI16 protein (Jeffries et al., 2020).

However, IFI16 does not appear to contribute to IFN-β expression by human foreskin fibroblasts (HFF) stimulated with exogenous DNA (Orzalli et al., 2015). While this finding might be indicative of cell type-specific differences, our studies showing that IFI16 knockdown has no effect on IFN-β protein production by a human microglia cell line following BDNA transfection also indicate that this putative DNA sensor is not required for such responses (Jeffries et al., 2020). Furthermore, Gray et al. (2016) used a mouse model lacking all 13 PHYIN family members to demonstrate that these receptors were dispensable for IFN responses to DNA transfection in bone marrow derived macrophages and mouse embryonic fibroblasts. But despite an apparent lack of involvement in IFN production, this study did identify a requirement for PHYIN family members in inflammasome activation, as characterized by the maturation of the potent pro-inflammatory cytokines IL-1β and IL-18 (Gray et al., 2016). Such a role for IFI16 in linking DNA sensing and inflammasome activation is supported by multiple studies (Ansari et al., 2013, 2015; Johnson et al., 2013; Dutta et al., 2015; Iqbal et al., 2016; Orzalli et al., 2016) and is discussed in depth elsewhere (Dell'Oste et al., 2015), but it is currently unknown whether IFI16-mediated inflammasome activation occurs in CNS cell types.

While there is conflicting evidence for the role of IFI16 in IFN-β responses to foreign DNA challenge, multiple lines of investigation indicate that this DNA sensor contributes to IFN-β and ISG expression following viral infection (Orzalli et al., 2012; Jakobsen et al., 2013; Ansari et al., 2015; Diner et al., 2015; Ma F. et al., 2015; Li et al., 2016; Zhang D. et al., 2016; Jønsson et al., 2017; Lum et al., 2019; Yang et al., 2020). For example, nuclear IRF3 translocation and subsequent IFN production in HSV-1 infected corneal epithelial cells has been shown to be dependent, at least in part, on p204 expression (Conrady et al., 2012), while TBK-1 phosphorylation and subsequent IFN-β expression by HSV-1 infected HFFs was found to require IFI16 and STING (Orzalli et al., 2012).

Interestingly, Orzalli et al. (2012) used attenuated HSV-1 strains to determine that expression of the immediate early viral protein ICP0 leads to IFI16 degradation and reduced nuclear IRF3 translocation, and this degradation was subsequently shown to be dependent on proteasome activity. In addition, another group has shown that HSV-1 can also lead to IFI16 degradation in an ICP0 independent manner, albeit in the U2OS cell line that lacks a functional STING signaling pathway (Cuchet-Lourenco et al., 2013). Moreover, HSV-1 infection markedly lowers IFI16 protein expression in primary human glia and immortalized cells lines, and this observation may explain why knockdown of this DNA sensor fails to alter viral production or IFN-β release by these cells (Jeffries et al., 2020). Such findings are supported in HFFs where IFI16 knockdown does not affect HSV-1 levels in cells infected with wild type HSV-1 but significantly increases viral titers following infection with an ICP0 null mutant virus (Diner et al., 2016). Similarly, IFI16 has been reported to be dispensable for IFN production in mice following HCMV infection (Gray et al., 2016) and this apparent independence may also stem from the reported ability of HCMV to interfere with IFI16 signaling (Dell'Oste et al., 2014). However, it should be noted that the ability of these viruses to reduce IFI16 protein abundance and/or signaling may show cell type specificity as HSV-1 does not elicit such effects in either HeLa cells or U2OS cells, again perhaps due to a lack of a functional STING signaling pathway in the latter (Orzalli et al., 2016; Deschamps and Kalamvoki, 2017).

Since the available evidence indicates that IFI16 has a role in virally-induced IFN signaling and that this is accomplished through via a STING-dependent pathway, it is possible that this molecule could work in concert with cGAS to stimulate antiviral responses. Evidence for this notion comes from the observation that knockdown of either STING, IFI16, or cGAS, in human fibroblasts leads to reduced HSV-1 infection-induced IFN-β expression (Orzalli et al., 2015). Interestingly, in the same study it was noted that cGAS knockdown reduces constitutive IFI16 protein expression and that this effect was dependent on proteasome activity (Orzalli et al., 2015). This suggests that cGAS may stabilize IFI16 protein levels to promote antiviral activity. However, we found no observable difference in IFI16 protein expression in cGAS deficient microglia created with CRISPR/Cas9 approaches (Jeffries et al., 2020) and so it is possible that, like viral ICP0-mediated effects (Orzalli et al., 2016), cGAS-mediated IFI16 stabilization may show cell type specificity.

Additional support for cooperation between IFI16 and cGAS comes from the work of Jønsson et al. (2017) who demonstrated that IFI16 knockdown reduces cGAMP production by THP-1 cells following foreign DNA challenge. Furthermore, they showed that HEK 293T cells stably expressing IFI16 produce higher amounts of cGAMP following intracellular administration of a cGAS expression plasmid than IFI16 deficient cells (Jønsson et al., 2017). Similarly, another study showed that the co-transfection of increasing amounts of an IFI16 expression plasmid with constant levels of STING and cGAS increased IFN-β activity as assessed by IFN promoter driven luciferase activity, and demonstrated the ability of IFI16 and cGAS to interact directly (Almine et al., 2017). It should be noted that these investigators failed to detect significant changes in cGAMP levels in the absence or presence of IFI16 (Almine et al., 2017). Rather, they determined that IFI16 was required for cGAMP to fully activate STING as assessed by CCL5 expression, STING dimerization, and IRF3 nuclear translocation, in response to cGAMP transfection (Almine et al., 2017).

In contrast to such studies that suggest IFI16 acts in concert with cGAS to promote IFN responses, we demonstrated that cGAS knockdown decreased IFN-β production by a human

microglial cell line following DNA transfection but IFI16 knockdown did not (Jeffries et al., 2020). Furthermore, we showed that IFI16 knockdown failed to exacerbate the reduction in IFN-β production by DNA stimulated cGAS deficient microglia, and combined cGAS and IFI16 deficiency failed to significantly alter microglial susceptibility to HSV-1 infection over cGAS deficiency alone (Jeffries et al., 2020). However, an explanation for these results may again stem from the ability of HSV-1 to downregulation IFI16 and cGAS expression and/or inhibit their signaling pathways in human microglia following infection (Jeffries et al., 2020). As such, the development of therapeutics that stabilize the expression of either of these sensor proteins could prove to be an attractive approach to combat the devastating consequences of conditions such as HSV-1 encephalitis.

While cGAS and IFI16 might play redundant roles in STING activation, some evidence suggests that they promote similar responses through different mechanisms. For instance, it was found that IFI16 is not required for cGAS/STING/TBK-1 signaling in HFFs following HSV-1 or HCMV infection, but was for the transcription of IFN-β, ISG54, ISG56, and RANTES (Diner et al., 2016). Interestingly, the same investigators found that IFI16 also reduced the transcription of the HSV-1 genes icp27, icp8, and ul30 (Diner et al., 2016). This suggests that the antiviral functions previously attributed to IFI16 may occur through transcriptional regulation, rather than by direct activation of cGAS-STING signaling. However, our own investigations of the role of IFI16 in HSV-1 transcription in infected human microglial cells showed no discernable effect on icp8 expression (Jeffries et al., 2020). This apparent discrepancy is likely due to differences in the HSV-1 strain employed, as the earlier study used an ICP0 mutant strain that prevents IFI16 degradation, while our studies were performed with the neuroinvasive MacIntyre strain (Diner et al., 2016; Jeffries et al., 2020).

The ability of IFI16 to negatively regulate viral transcription has been reported for other herpesviruses, human papillomavirus (HPV), and hepatitis B virus (HBV) (Gariano et al., 2012; Lo Cigno et al., 2015; Roy et al., 2016, 2019; Pisano et al., 2017; Yang et al., 2020), and the modification of heterochromatin and euchromatin appears to be the primary mechanism by which this is accomplished. For example, U2OS cells or an immortalized human keratinocyte cell line (NIKS) overexpressing IFI16 exhibit elevations in heterochromatin markers, such as H3K9m2, and decreases in euchromatin markers, such as H3K4me2, in early and late HPV promoters as determined by chromatin immunoprecipitation (ChiP) analysis (Lo Cigno et al., 2015). In addition, IFI16 has been demonstrated to directly interact with the histone H3-K9 methyltransferases, SUV39h1 and G9a-like protein (GLP), and knockdown of these proteins in a B cell lymphoma latently infected with KSHV (BCBL1 cells) led to increased viral transcription (Roy et al., 2019). Furthermore, in the same study, IFI16 knockdown reduced the recruitment of both methyltransferases to the KSHV genome (Roy et al., 2019).

In a HBV covalently closed circular DNA (cccDNA) model of infection, overexpression of IFI16 has been shown to increase IFN-β and ISG expression along with decreased euchromatin and increased heterochromatin markers on cccDNA (Yang et al., 2020). Interestingly, knockdown of IFI16 in BCBL1 cells increased the transcription of immediate early, early, and late lytic KSHV genes, indicating reactivation of the lytic cycle, while the reintroduction of IFI16 reduced KSHV genome copy numbers (Roy et al., 2016). This was also found to be true for Akata and MUTU1 cell lines latently infected with Epstein-Barr virus (Pisano et al., 2017). As such, it will be important to determine whether IFI16 similarly contributes to HSV-1 latency in CNS cell types, since reactivation of latent infections is a key event in the onset of HSV-1 encephalitis (Menendez and Carr, 2017). If so, IFI16 could be a promising new therapeutic target, either as an intervention during CNS infection or to prevent reactivation of HSV-1 in at-risk populations.

ZBP1

Z-DNA binding protein 1 [ZBP1; also known as DNA-dependent activator of interferon regulatory factors (DAI) and DLM-1] was the first identified cytosolic DNA sensor, and was shown to directly bind dsDNA in murine L929 fibroblast-like cells (Takaoka et al., 2007). Importantly, this study demonstrated ZBP1 can interact with TBK1 and IRF3 and contribute to IFN-β mRNA expression following DNA transfection or infection with HSV-1 (Takaoka et al., 2007). However, it seems that this cytosolic DNA sensor may function in a cell type and ligand specific manner, as ZBP1 knockdown in mouse embryonic fibroblasts (MEFs) has little or no effect on exogenous DNA-induced IFN-β expression (Wang et al., 2008). Similarly, ZBP1 knockdown was found to significantly reduce IFN-β expression in L929 cells in response to BDNA transfection but had no effect in a similarly challenged human lung epithelial cell line (Lippmann et al., 2008).

In addition to the expression of antiviral cytokines, ZBP1 has also been shown to mediate the expression of the pro-inflammatory cytokine IL-6 (Takaoka et al., 2007; Kaiser et al., 2008) subsequently demonstrated the activation of a NF-kB-driven luciferase promoter in HEK 293T cells overexpressing ZBP1. This group identified three RIP homotypic interaction motif (RHIM)-like repeats and hypothesized that such NF-κB activation occurs via a RHIM-dependent interaction with receptor interacting protein 1 (RIP1) in a similar manner to that seen with TLR3 (Kaiser et al., 2008). This hypothesis was confirmed by the demonstration that ZBP1 can interact with both RIP1 and receptor interacting protein 3 (RIP3) through its first RHIM domain, and by the ability of RIP1 knockdown or mutations in the RHIM domain in RIP1 or ZBP1 to decrease NF-kB promoter activation. The ability of ZBP1 to interact with RIP1 and RIP3, and to activate NF-kB-mediated gene transcription was subsequently confirmed in a similar HEK 293 cell expression system (Rebsamen et al., 2009). In is interesting to note, however, that co-expression of ZBP1 and RIP3 was also reported to elicit NF-kB activation in these studies, an observation that is in contrast to TLR3 signaling where RIP3 blocks RIP1-mediated NF-kB activation (Kaiser et al., 2008).

In agreement with these studies in non-CNS cell types, we have determined that murine microglia and astrocytes express ZBP1 in an inducible manner, and found that this sensor contributes to pro-inflammatory cytokine production by glia following HSV-1 infection (Furr et al., 2011). Furthermore, these studies also showed that HSV-1 infection induces the production of soluble neurotoxic mediators by astrocytes and microglia in a ZBP1-dependent manner (Furr et al., 2011). Surprisingly, combined knockdown of ZBP1 and retinoic acid inducible gene 1 (RIG-I) leads to greater reductions in TNF-a and IL-6 production by HSV-1 infected glia than either alone, suggesting that these dissimilar sensors can act in synergy (Crill et al., 2015). Together, these studies suggest a role for ZBP1 in inflammation and/or antiviral immunity both in the periphery and the CNS.

While the available evidence supports a role for ZBP1 as a DNA sensor capable of inducing cytokine production, some studies suggest that ZBP1 plays a broader role in antiviral immunity. For example, ZBP1 has been reported to work in concert with RIP3 in murine fibroblasts and epithelial cells to induce necroptosis following infection with a mutant murine cytomegalovirus (MCMV) strain (Upton et al., 2012) that lacks the expression of m45, a viral product that limits ZBP1/RIP3 interactions due the presence of a RHIM domain (**Table 1**) (Rebsamen et al., 2009; Upton et al., 2012). Interestingly, a similar immune evasion mechanism has been observed for HSV-1 (**Table 1**), where the viral protein ICP6 also contains a RHIM domain that is capable of inhibiting necroptosis in peripheral human cells (Guo et al., 2015). Necroptotic cell death initiated by simultaneous treatment with TNF-a and the caspase inhibitor zVAD-FMK was blocked following infection with wild type HSV-1, while an ICP6 deficient HSV-1 strain failed to prevent cell death (Guo et al., 2015; Sawai, 2016). This finding is in sharp contrast to studies in mouse cells, where infection with wild type HSV-1 elicits cell death in a RIP3-dependent manner (Wang et al., 2014; Huang et al., 2015). Surprisingly, expression of ICP6 in MEFs was found to be enough to induce RIP3-dependent cell death, while the presence of ICP6 containing mutations in the RHIM domain did not (Wang et al., 2014; Huang et al., 2015), suggesting that ICP6 may be able to directly induce necroptosis in this cell type (Wang et al., 2014). The reason for these apparently contradictory findings was discovered in more recent studies that show ICP6 has species-dependent effects, inducing necroptosis in cells from mice while inhibiting it in human cells, HSV's primary natural host (Huang et al., 2015; Guo et al., 2018).

Importantly, ZBP1 has been found to be a major contributor to necroptosis in both human and mouse fibroblasts following infection with both an ICP6-deficient and an ICP6 RHIM mutant HSV-1 strain (Guo et al., 2018) and our own observations suggest that this cytosolic DNA sensor functions as a mediator of cell death during HSV-1 infection in glia. Our studies indicate that ZBP1 plays a crucial role in triggering necroptosis in murine glia following infection with a strain of HSV-1 that contains mutations in the ICP6 RHIM domain (unpublished observations). The potential importance of this pathway in antiviral immunity within the CNS is underscored by the decreased survival and increased viral burden in the brain of RIP3 deficient mice following HSV-1 infection (Wang et al., 2014; Huang et al., 2015). However, since necroptosis promotes inflammation, it will be important to determine whether this ZBP-mediated response also contributes to CNS pathology during HSV-1 encephalitis, especially in the human host (Dhuriya and Sharma, 2018).

While it is increasingly clear that ZBP1 is a PRR that is capable of initiating cell death pathways, it is less certain what ligands specifically initiate such as response. ZBP1 was initially shown to directly bind BDNA and it has recently been shown to recognize plasmid DNA (Wang et al., 2008; Semenova et al., 2019). However, other studies have shown that ZBP1 is critical for the induction of necroptosis, pyroptosis, and apoptosis, in cells challenged with influenza virus, a segmented negative strand RNA virus (Kuriakose et al., 2016; Thapa et al., 2016), and this role is discussed in depth elsewhere (Dhuriya and Sharma, 2018). By pharmacologically inhibiting various stages of the MCMV life cycle, Sridharan et al. (2017) were able to determine that active transcription was required for ZBP1-mediated cell death, suggesting that RNA serves as the activating ligand in this response. This notion was subsequently supported by two studies describing the ability of ZBP1 to bind endogenous RNA (Maelfait et al., 2017; Jiao et al., 2020).

An ability to sense both RNA and DNA accounts for the protective role of ZBP1 in influenza virus infection and following exposure to other RNA viruses including West Nile virus (WNV) and ZIKV (Daniels et al., 2019; Rothan et al., 2019). Interestingly, however, ZBP1-mediated protection against these neurotropic flaviviruses appears to be independent of cell death in neurons (Daniels et al., 2019; Rothan et al., 2019). Mice genetically deficient in ZBP1 show worse clinical scores, higher viral burdens in the brain, and increased mortality, following WNV infection than wild type mice (Rothan et al., 2019). Similarly, higher viral burdens and mortality have been observed in WNV challenged RIP3 deficient animals, and this effect was independent of cell death pathways (Daniels et al., 2017). Surprisingly, ZBP1 deficient animals demonstrate higher levels of antiviral and inflammatory cytokines/chemokines following WNV infection (Rothan et al., 2019), and this finding is in contrast to similarly infected RIP3 deficient mice, which demonstrate decreased inflammatory cytokine production (Daniels et al., 2017). As such, it is possible these two molecules have independent roles during neuronal infection, especially since peripheral cells undergo cell death in both a ZBP1 and a RIP3-dependent manner (Daniels et al., 2017; Rothan et al., 2019).

A potential mechanism for the antiviral effects of ZBP1 and RIPK3 during neurotropic RNA virus infections comes from the studies of Daniels et al. (2019) that indicate a neuron-specific function for ZBP1. They found that ZBP1-induced antiviral gene expression in neurons following ZIKV infection occurs in a RIP1 and RIP3-dependent manner, and that loss of any of these signaling molecules results in increased viral burden and mortality (Daniels et al., 2019). Surprisingly, RIP3 deficiency in primary microglial cultures did not result in increased ZIKV replication in these studies suggesting that such protection is intrinsic to neurons. Consistent with this notion, upregulation of the antiviral gene *IRG1* was required for protection against both ZIKV and WNV infection in neurons, but this gene was

not upregulated in microglia (Daniels et al., 2019), indicating a cell type specific function for ZBP1. Since we have identified a role for this sensor in glia following HSV-1 infection, it will be interesting to see what role, if any, ZBP1 plays in glial responses to neurotropic RNA viruses (Furr et al., 2011; Crill et al., 2015). Regardless, it is apparent that ZBP1 is an important mediator of CNS innate immune responses to both RNA and DNA viruses.

AIM2

Absent in melanoma 2 (AIM2) is another member of the PHYIN family of interferon inducible proteins that has been found to act as a DNA sensor (Bürckstümmer et al., 2009; Fernandes-Alnemri et al., 2009; Hornung et al., 2009; Adamczak et al., 2014). However, unlike IFI16, recognition of dsDNA by AIM2 has been shown to lead exclusively to inflammasome activation and the induction of pyroptosis, an inflammatory form of cell death (Adamczak et al., 2014). Upon binding to dsDNA, AIM2 associates with the downstream signaling molecule apoptosisassociated speck-like protein containing a CARD domain (ASC), which recruits, and activates caspase-1 (Bürckstümmer et al., 2009; Fernandes-Alnemri et al., 2009; Hornung et al., 2009). Caspase-1 then acts as the effector protein to cleave the immature form of IL-1β and IL-18, leading to the maturation and secretion of these potent inflammatory cytokines (Miao et al., 2011). Additionally, caspase-1 can cleave gasdermin D to initiate pyroptotic cell death, characterized by the formation of pores in the plasma membrane and the release of cellular contents into the extracellular environment (Kayagaki et al., 2015; Shi et al., 2015). The AIM2 inflammasome has been shown to form following infection with either DNA or RNA viruses in peripheral myeloid and lymphoid immune cell-types, such as bone marrow derived dendritic cells (BMDCs), bone marrow derived macrophages (BMDM), monocytes, and fibroblasts (Rathinam et al., 2010; Ekchariyawat et al., 2015; Schattgen et al., 2016; Huang et al., 2017; Zhang et al., 2017), and the role of this and other inflammasomes during viral infection is discussed extensively elsewhere (Chen and Ichinohe, 2015; Lupfer et al., 2015; Man et al., 2016; Shrivastava et al., 2016; Lugrin and Martinon, 2018; Zhu et al., 2019).

While the AIM2 inflammasome is recognized to have an antiviral function in peripheral cell types, relatively little is known about its role in CNS infections despite having been shown to be expressed in neurons and glia (Adamczak et al., 2014; Cox et al., 2015). Furthermore, AIM2 has been shown to function as a DNA sensor in neurons as the cytosolic administration of exogenous DNA induces the association of AIM2 with ASC and leads pyroptosis in these cells (Adamczak et al., 2014). Since neuronal cell death is typically detrimental to the host, it appears likely that the proinflammatory nature of the AIM2 inflammasome can be damaging in the context of viral CNS infections. Circumstantial evidence supporting this notion comes from the effect of deleting ataxia-telangiectasia mutated (ATM), a protein known for its role in activating DNA damage responses, in primary murine microglia (Song et al., 2019). Such a deletion results in cytoplasmic DNA accumulation and cellular activation as demonstrated by the retraction of processes (Song et al., 2019). Moreover, co-culture of microglia and neurons with an ATM inhibitor leads to neuronal cell damage, which is reversed with an IL-1 receptor antagonist consistent with a major role for the inflammasome in this effect (Song et al., 2019). Importantly, this study utilized co-immunoprecipitation approaches to demonstrate that inflammasome activation as a result of ASC association with AIM2 rather than other initiator molecules such as NLR family pyrin domain containing 3 (NLRP3) (Song et al., 2019). A detrimental role for AIM2 in CNS pathologies is further supported by the observation that AIM2 deficient mice show less brain atrophy and cognitive defects following stroke than their wild type counterparts (Kim et al., 2020). Furthermore, caspase-1 inhibition resulted in a similar phenotype in these studies indicating that the improved outcome was due to reduced AIM2 inflammasome activation (Kim et al., 2020).

Despite such evidence, some studies suggest that AIM2 can play a protective role in some infections. For example, the neurotropic RNA viruses, WNV and Chikungunya virus (CHIKV), have been shown to activate the AIM2 inflammasome in peripheral dermal fibroblasts and AIM2 knockdown led to increased CHIKV genome copies in these cells (Ekchariyawat et al., 2015). Furthermore, the higher levels of AIM2, caspase 1, IL-1β, and IL-18, found in brain tissue from still births following ZIKV infection provides circumstantial evidence for a role for this sensor (de Sousa et al., 2018). However, it should be noted that the expression of two other inflammasome activators, NLRP3, and NLRP1, were also elevated in this tissue, and it is not clear whether the upregulation of inflammasome components reflect a protective host response or contribute to disease pathology. Similarly, AIM2 expression is upregulated in neurons following infection with enterovirus A71, the causative agent of hand foot and mouth disease and AIM2 knockdown in a neuronal cell line led to decreased IL-1β cleavage and increased viral copy numbers (Yogarajah et al., 2017). Yet, no mechanism has yet been defined for AIM2mediated sensing of RNA viruses.

With regard to neurotropic DNA viruses, AIM2 was initially demonstrated to be dispensable for inflammasome activation following HSV-1 infection in peritoneal macrophages, but was for necessary for such responses to MCMV challenge (Rathinam et al., 2010). Conversely, another study indicated that IFI16 and NLRP3 were the initiators of inflammasome activation in HFFs following HSV-1 infection (Johnson et al., 2013). This apparent discrepancy may be due to the ability of the HSV-1 product VP22 to block AIM2-mediated inflammasome activation by preventing oligomerization (**Table 2**) (Maruzuru et al., 2018). Intracranial administration of an HSV-1 strain lacking VP22 leads to decreased viral burdens in wildtype mice but not those lacking AIM2, suggesting that this sensor can limit viral replication in the CNS (Maruzuru et al., 2018). Interestingly, the protective functions of AIM2 in the CNS may extend to bacterial pathogens as AIM2 has been shown to contribute to survival following CNS infection with *Staphylococcus aureus* (Hanamsagar et al., 2014).

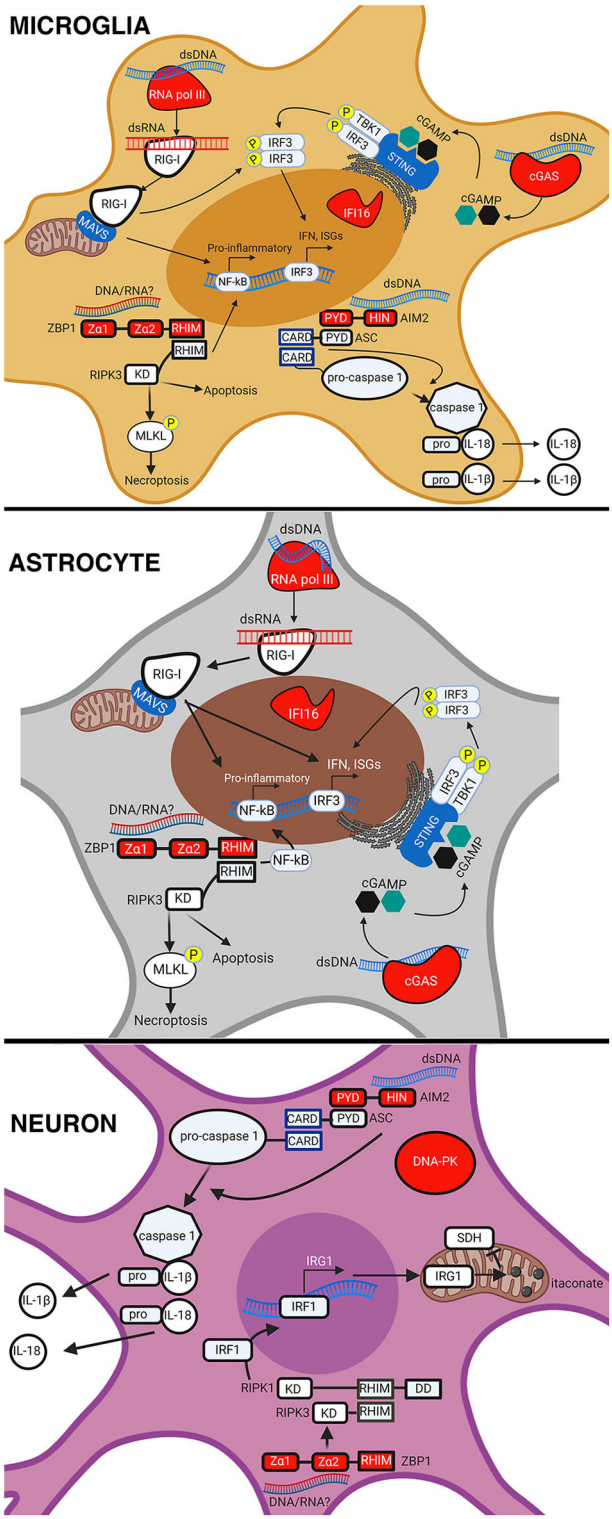

FIGURE 1 | Intracellular DNA sensors in resident CNS cell types. Intracellular nucleic acid sensing by DNA sensors in microglia, astrocytes, and neurons. AIM2 sensing of dsDNA leads to the recruitment of apoptosis-associated speck-like protein containing a CARD (ASC) that then cleaves pro-caspase 1. Active caspase 1 then cleaves the precursor forms of IL18 and IL-1β, causing *(Continued)*

FIGURE 1 | their maturation and release from the cell. ZBP1 sensing of either dsDNA or RNA causes it to associate with RIPK3, activate the transcription factor NF-κB, and phosphorylate mixed lineage kinase domain-like protein (MLKL) in microglia and astrocytes. This results in pro-inflammatory cytokine expression and execution of necroptosis. In neurons, ZBP1 sensing results in the activation of IRF1, expression of IRG1, production of itaconate, and a reduction in succinate dehydrogenase (SDH) activity. Sensing of dsDNA by cGAS leads to the production of cGAMP, which binds to and activates STING causing the phosphorylation and translocation of interferon regulatory factor 3 (IRF3) to the nucleus. This results in the expression of IFN and ISGs in microglia and astrocytes. RNA pol III senses dsDNA and converts it into dsRNA that can then be sensed by RIG-I in microglia and astrocytes. RIG-I sensing of dsRNA causes it to associate with mitochondrial antiviral-signaling protein (MAVS) leading to activation and translocation of IRF3 and NF-κB, resulting in the expression of IFN, ISGs, and pro-inflammatory cytokines. This figure was created with BioRender.com.

It is clear from the available data that out current understanding of the role of AIM2 in the CNS is rudimentary. While some evidence suggests that AIM2 contributes to CNS disease pathology, some indicate protective functions. As such, it may be that AIM2 plays a context-dependent role where this molecule exacerbates sterile inflammation in neurodegenerative diseases when activation tends to be chronic, while acute activation assists in viral or bacterial clearance. Since our understanding of AIM2 in the CNS is based mostly on circumstantial evidence, further study is clearly required to determine the role of this molecule relative to other inflammasome activators, and to determine whether this pathway can be targeted for therapeutic intervention.

DDX41, Ku70/DNA-PK, AND, RNA POLYMERASE III

Several other putative DNA sensors have been identified in peripheral cell types but their role as PRRs in the CNS remains more controversial. DEAD-Box Helicase 41 (DDX41) was first identified as a cytosolic DNA sensor in a murine dendritic cell-like line with the demonstration that this molecule can directly bind dsDNA and interact with the common DNA sensing and antiviral signaling components STING and TBK1 (Zhang Z. et al., 2011). Importantly, DDX41 knockdown was shown to decrease IFN-α production in these cells in response to dsDNA transfection or infection with either HSV-1 or adenovirus (Zhang Z. et al., 2011). Interestingly, DDX41 has also been shown to directly bind cyclic dinucleotides such as cyclic dimeric guanosine monophosphate (c-di-GMP) and cyclic dimeric adenosine monophosphate (c-diAMP), and knockdown of DDX41 prevents STING association with TBK1 or IRF3 and reduces antiviral signaling in response to these molecules (Parvatiyar et al., 2012). As such, it is possible that DDX41 bolsters cGAS-STING signaling by promoting cGAMP-STING interactions. Evidence for such a suggestion comes from the demonstration that DDX41 knockdown further reduces murine leukemia virus (MLV)-induced IFN expression by cGAS deficient macrophages and dendritic cells (Stavrou et al., 2015).

Furthermore, IFN-β expression could be rescued in macrophage-like cells following cGAS knockdown with the administration of exogenous cGAMP prior to MLV infection, but this procedure failed to rescue such responses in cells following DDX41 knockdown (Stavrou et al., 2018). Together, these studies suggest that DDX41 can act in a cooperative manner with cGAS to induce STING activation following viral challenge.

To date, it is not known whether DDX41 is expressed in the mammalian CNS. However, the drosophila DDX41 homolog, Abstrakt, has been shown to be involved in visual and CNS system development (Irion and Leptin, 1999; Schmucker et al., 2000). Furthermore, DDX41 is highly expressed in the zebrafish brain and this gene product performs similar antiviral functions to mammalian DDX41 when expressed in a HEK 293 expression system (Ma et al., 2018). Finally, circumstantial evidence of a role for DDX41 in the human CNS lays in the observation that HSV-1 has evolved an evasion mechanism targeting DDX41 (**Table 2**), suggesting that this molecule can act as a restriction factor for this neurotropic virus (Duan et al., 2019).

DNA protein kinase (DNA-PK) is a protein complex made up of a DNA protein kinase catalytic subunit (DNA-PKcs), ku70, and ku80, and is best known for its role in DNA double stranded break repair. However, several studies have shown that it can bind to transfected DNA and elicit the expression of IFN-β and other ISGs, independent of kinase activity (Ferguson et al., 2012; Harnor et al., 2017; Burleigh et al., 2020). In addition, the Ku70 subunit has also been identified as a possible DNA sensor in studies where plasmid transfected HEK 293 cells produce the type three IFN, IFN-λ1, that can limit HIV replication (Zhang X. et al., 2011). In this work, Ku70 and Ku80 were both found to bind transfected DNA, but only the loss of Ku70 decreased IFN-λ1 expression in these cells (Zhang X. et al., 2011). This finding was confirmed in splenocytes derived from ku70 deficient mice (Zhang X. et al., 2011), and it was later determined that Ku70mediated IFN-λ1 expression requires the expression of STING (Sui et al., 2017). However, it should be noted that these results are in contrast to a more recent report in which signaling through DNA-PK was found to be independent of the presence of STING (Burleigh et al., 2020). While it is presently unclear whether Ku70 functions alone or in concert with Ku80 and the DNA-PKcs to elicit antiviral activity, Ku70/DNA PK has been demonstrated to induce cytokine responses following infection of hepatocyte carcinoma and monocytic cell lines with HBV and human T-cell leukemia virus type 1, respectively (Li et al., 2016; Wang et al., 2017).

Furthermore, vaccinia virus and adenovirus have both been shown to antagonize Ku70/DNA-PK signaling (Peters et al., 2013; Scutts et al., 2018; Burleigh et al., 2020). Together, these studies suggest that ku70/DNA-PK acts as a viral PRR in addition to its DNA repair functions.

Despite evidence for antiviral functions of ku70/DNA-PK in peripheral cell types such as monocytes and fibroblasts, little exists for such a role in the CNS (Li et al., 2016; Burleigh et al., 2020). Expression of DNA-PK in the CNS and its role in DNA repair has been established from the study of mutations in severe combined immunodeficiency (SCID) mice that result in a truncated kinase domain in DNA-PK (Chechlacz et al., 2001; Vemuri et al., 2001). This has been shown to cause increased neuronal cell death *in vitro* and *in vivo*, presumably as a consequence of accumulated dsDNA breaks (Chechlacz et al., 2001; Vemuri et al., 2001). Since the DNA repair functions of DNA-PK are found in CNS cell types, the DNA sensing abilities of this molecule seen in peripheral cells may also be retained in the brain and this possibility requires further investigation.

Finally, RNA polymerase III was simultaneously identified as a DNA sensor by two groups as they investigated the mechanisms responsible for RIG-I mediated DNA sensing (Ablasser et al., 2009; Chiu et al., 2009). They demonstrated that poly (dA:dT) was reverse transcribed to RNA that then served as a ligand to activate RIG-I and induce IFN-β production in monocytes, fibroblasts, and dendritic cells (Ablasser et al., 2009; Chiu et al., 2009). Our own work subsequently showed that RNA polymerase

TABLE 3 | Expression and antiviral activity of intracellular DNA sensors in CNS cell types.

Sensor	CNS cell type	Antiviral activity	References
ZBP1	Primary mouse whole brain tissue, cortical neurons, microglia, and astrocytes	Neuronal immunometabolism regulation, antiviral, and proinflammatory cytokine production	Furr et al., 2011; Daniels et al., 2019; Rothan et al., 2019
cGAS	Primary murine neurons, astrocytes, and microglia Primary human astrocytes and microglia Human cell lines U87-MG and hμglia	IFN and ISG expression	Cox et al., 2015; Reinert et al., 2016; Jeffries and Marriott, 2017
IFI16	Primary mouse epithelial cells Primary human astrocytes Human cell lines, corneal epithelial, astrocytes, microglia	Inflammasome activation	Conrady et al., 2012; Coulon et al., 2019; Jeffries et al., 2020
AIM2	Primary mouse astrocytes and microglia Human cell line, SK-N-SH	Inflammasome activation	Cox et al., 2015; Yogarajah et al., 2017; Song et al., 2019
DDX41	Zebrafish whole brain	IFN expression	Ma et al., 2018
DNA PK	Primary mouse cerebral cortex and neurons	Unknown	Chechlacz et al., 2001; Vemuri et al., 2001
RNA pol III	Primary mouse astrocytes and microglia Mouse cell line, EOC13.31 Human cell line, hμglia	IFN expression and NF-κB activation via RIG-I	Crill et al., 2015; Johnson et al., 2020

III is functionally expressed in murine glia and a human microglial cell line (Crill et al., 2015; Johnson et al., 2020), and that its inhibition reduces HSV-1-induced IRF3 activation and TNF-a production in murine microglia cells and astrocytes (Crill et al., 2015). In addition to HSV-1, evidence suggests that RNA polymerase III also has a role in recognizing varicella-zoster virus (VZV) (Carter-Timofte et al., 2018, 2019). A RNA polymerase III mutation was identified in twins suffering from recurrent VZV CNS vasculitis and PBMCs isolated from them showed reduced antiviral and/or inflammatory cytokine responses to poly(dA:dT) and VZV challenge (Carter-Timofte et al., 2018). Furthermore, additional RNA polymerase III mutations were identified in adult VZV encephalitis patients and PBMCs from these patients similarly showed reduced IFN-β and CXCL10 expression in response to poly(dA:dT). Interestingly, while PBMC cytokine response were unchanged following VZV challenge, patients with these RNA polymerase III mutations showed higher viral gene expression (Carter-Timofte et al., 2019). Together, these studies support a role for RNA polymerase III in combating viral CNS infections.

CONCLUDING REMARKS

It is now appreciated that resident CNS cells are important contributors to innate immunity and, due to their location, are likely the first responders to viral CNS infections. Resident CNS cells, especially astrocytes and microglia, are known to express an array of PRRs including TLRs, RLRs, NLRs, and now intracellular DNA sensors. In addition to their expression, multiple studies have demonstrated the functional nature of these sensors in various CNS cell types (as summarized in **Figure 1** and **Table 3**). For example, we have shown that cGAS is required, at least in part, for microglial IFN responses to foreign DNA (Jeffries et al., 2020). However, our understanding of the role of DNA sensors in viral infections is limited and, in some cases, contradictory. It is currently unclear whether DNA sensors are beneficial or detrimental to the host during CNS infections, and it appears likely that outcomes following activation are pathogen, host cell-type, and even species, specific. This is exemplified by the finding that the HSV-1 product ICP6 blocks ZBP1-mediated responses in human cells but activates ZBP1 in murine cells (Guo et al., 2018). Because of this, future research on the role and therapeutic potential of DNA sensors must be cognizant of such variables.

Lastly, it is important to note that DNA sensors may contribute to other CNS pathologies, such as neurodegenerative diseases, which may be initiated or exacerbated by viral infection. For instance, three prime repair exonuclease 1 (TREX1) deficiency can cause accumulation of mislocalized DNA and lead to Aicardi Goutieres syndrome. This condition is characterized by permanent and often severe neurological damage due to IFN overproduction, and the loss of cGAS has been shown to rescue TREX1 deficient mice from disease pathology (Gray et al., 2016). Similarly, neurodegenerative diseases are associated with chronic overproduction of proinflammatory mediators and neuroinflammation in diseases such as Alzheimer's disease could result from the chronic activation of DNA sensors by released DAMPS and/or viral infection. Regardless, it is clear that our understanding of these DNA sensors in the CNS remains rudimentary and further research is needed to define the cell type, species, and pathogen specificity of each. In doing so, it might be possible to target these molecules judiciously to limit damaging inflammation while allowing beneficial host responses to improve patient outcomes.

AUTHOR CONTRIBUTIONS

AJ and IM co-wrote this literature review article. Both authors contributed to the article and approved the submitted version.

FUNDING

This work was supported by the NINDS research grant R03 NS097840 awarded to IM.

REFERENCES

Aarreberg, L. D., Esser-Nobis, K., Driscoll, C., Shuvarikov, A., Roby, J. A., and Gale, M. (2019). Interleukin-1β Induces mtDNA release to activate innate immune signaling via cGAS-STING. *Mol. Cell* 74, 801–815.e6. doi: 10.1016/j.molcel.2019.02.038

Abe, T., and Barber, G. N. (2014). Cytosolic-DNA-Mediated, STING-Dependent Proinflammatory gene induction necessitates canonical nf- b activation through TBK1. *J. Virol.* 88, 5328–5341. doi: 10.1128/JVI.00037-14

Ablasser, A., Bauernfeind, F., Hartmann, G., Latz, E., Fitzgerald, K. A., and Hornung, V. (2009). RIG-I-dependent sensing of poly(dA:dT) through the induction of an RNA polymerase III transcribed RNA intermediate. *Nat. Immunol.* 10, 1065–1072. doi: 10.1038/ni.1779

Ablasser, A., and Chen, Z. J. (2019). CGAS in action: Expanding roles in immunity and inflammation. *Science* 80:363. doi: 10.1126/science.aat8657

Adamczak, S. E., De Rivero Vaccari, J. P., Dale, G., Brand, F. J., Nonner, D., Bullock, M., et al. (2014). Pyroptotic neuronal cell death mediated by the AIM2 inflammasome. *J. Cereb. Blood Flow Metab.* 34, 621–629. doi: 10.1038/jcbfm.2013.236

Aguirre, S., Luthra, P., Sanchez-Aparicio, M. T., Maestre, A. M., Patel, J., Lamothe, F., et al. (2017). Dengue virus NS2B protein targets cGAS for degradation and prevents mitochondrial DNA sensing during infection. *Nat. Microbiol.* 2, 1–11. doi: 10.1038/nmicrobiol.2017.37

Aguirre, S., Maestre, A. M., Pagni, S., Patel, J. R., Savage, T., Gutman, D., et al. (2012). DENV inhibits type I IFN production in infected cells by cleaving human STING. *PLoS Pathog.* 8:e1002934. doi: 10.1371/journal.ppat.1002934

Almine, J. F., O'Hare, C. A. J., Dunphy, G., Haga, I. R., Naik, R. J., Atrih, A., et al. (2017). IFI16 and cGAS cooperate in the activation of STING during DNA sensing in human keratinocytes. *Nat. Commun.* 8:14392. doi: 10.1038/ncomms14392

Aloisi, F. (2000). The role of microglia and astrocytes in CNS immune surveillance and immunopathology. *Adv Exp Med Biol*, 123–133. doi: 10.1007/978-1-4615-4685-6_10

Aloisi, F. (2001). Immune function of microglia. *Glia* 36, 165–179. doi: 10.1002/glia.1106

Ansari, M. A., Dutta, S., Veettil, M. V., Dutta, D., Iqbal, J., Kumar, B., et al. (2015). Herpesvirus genome recognition induced acetylation of nuclear IFI16 Is essential for its cytoplasmic translocation, inflammasome and IFN-β responses. *PLoS Pathog.* 11:e10050. doi: 10.1371/journal.ppat.1005019

Ansari, M. A., Singh, V. V., Dutta, S., Veettil, M. V., Dutta, D., Chikoti, L., et al. (2013). Constitutive interferon-inducible protein 16-Inflammasome activation during epstein-barr virus latency i, ii, and iii in b and epithelial cells. *J. Virol.* 87, 8606–8623. doi: 10.1128/JVI.00805-13

Biolatti, M., Dell'Oste, V., Pautasso, S., Gugliesi, F., von Einem, J., Krapp, C., et al. (2017). Human cytomegalovirus tegument protein pp65 (pUL83) dampens type I interferon production by inactivating the DNA sensor cGAS without affecting STING. *J. Virol.* 92, e01774–17. doi: 10.1128/JVI.01774-17

Bode, C., Fox, M., Tewary, P., Steinhagen, A., Ellerkmann, R. K., Klinman, D., et al. (2016). Human plasmacytoid dentritic cells elicit a Type I Interferon response by sensing DNA via the cGAS-STING signaling pathway. *Eur. J. Immunol.* 46, 1615–1621. doi: 10.1002/eji.201546113

Botto, S., Abraham, J., Mizuno, N., Pryke, K., Gall, B., Landais, I., et al. (2019). Human cytomegalovirus immediate early 86-kda protein blocks transcription and induces degradation of the immature interleukin-1β protein during virion-mediated activation of the AIM2 inflammasome. *MBio* 10, e02510–18. doi: 10.1128/mBio.02510-18

Bowman, C. C., Rasley, A., Tranguch, S. L., and Marriott, I. (2003). Cultured astrocytes express toll-like receptors for bacterial products. *Glia* 43, 281–291. doi: 10.1002/glia.10256

Bradshaw, M. J., and Venkatesan, A. (2016). Herpes simplex virus-1 encephalitis in adults: pathophysiology, diagnosis, and management. *Neurotherapeutics* 13, 493–508. doi: 10.1007/s13311-016-0433-7

Bsibsi, M., Ravid, R., Gveric, D., and van Noort, J. M. (2002). Broad expression of toll-like receptors in the human central nervous system. *J. Neuropathol. Exp. Neurol.* 61, 1013–21. doi: 10.1093/jnen/61.11.1013

Bsibsi, M., Persoon-Deen, C., Verwer, R. W. H., Meeuwsen, S., Ravid, R., and Van Noort, J. M. (2006). Toll-like receptor 3 on adult human astrocytes triggers production of neuroprotective mediators. *Glia* 53, 688–695. doi: 10.1002/glia.20328

Bürckstümmer, T., Baumann, C., Blüml, S., Dixit, E., Dürnberger, G., Jahn, H., et al. (2009). An orthogonal proteomic-genomic screen identifies AIM2 as a cytoplasmic DNA sensor for the inflammasome. *Nat. Immunol.* 10, 266–272. doi: 10.1038/ni.1702

Burleigh, K., Maltbaek, J. H., Cambier, S., Green, R., Gale, M., James, R. C., et al. (2020). Human DNA-PK activates a STING-independent DNA sensing pathway. *Sci. Immunol.* 5:aba4219. doi: 10.1126/sciimmunol.aba4219

Cai, X., Chiu, Y. H., and Chen, Z. J. (2014). The cGAS-cGAMP-STING pathway of cytosolic DNA sensing and signaling. *Mol. Cell* 54, 289–296. doi: 10.1016/j.molcel.2014.03.040

Carter-Timofte, M. E., Hansen, A. F., Christiansen, M., Paludan, S. R., and Mogensen, T. H. (2019). Mutations in RNA Polymerase III genes and defective DNA sensing in adults with varicella-zoster virus CNS infection. *Genes Immun.* 20, 214–223. doi: 10.1038/s41435-018-0027-y

Carter-Timofte, M. E., Hansen, A. F., Mardahl, M., Fribourg, S., Rapaport, F., Zhang, S. Y., et al. (2018). Varicella-zoster virus CNS vasculitis and RNA polymerase III gene mutation in identical twins. *Neurol. Neuroimmunol. NeuroInflammation* 5:e500. doi: 10.1101/244848

Carty, M., Reinert, L., Paludan, S. R., and Bowie, A. G. (2014). Innate antiviral signaling in the central nervous system. *Trends Immunol.* 35, 79–87. doi: 10.1016/j.it.2013.10.012

Cerón, S., North, B. J., Taylor, S. A., and Leib, D. A. (2019). The STING agonist 5,6-dimethylxanthenone-4-acetic acid (DMXAA) stimulates an antiviral state and protects mice against herpes simplex virus-induced neurological disease. *Virology* 529, 23–28. doi: 10.1016/j.virol.2019.01.006

Chan, Y. K., and Gack, M. U. (2016). Viral evasion of intracellular DNA and RNA sensing. *Nat. Rev. Microbiol.* 14, 360–373. doi: 10.1038/nrmicro.2016.45

Chaudhuri, A., and Kennedy, P. G. E. (2002). Diagnosis and treatment of viral encephalitis. *Postgrad. Med. J.* 78, 575–583. doi: 10.1136/pmj.78.924.575

Chauhan, V. S., Sterka, D. G., Furr, S. R., Young, A. B., and Marriott, I. (2009). NOD2 plays an important role in the inflammatory responses of microglia and astrocytes to bacterial CNS pathogens. *Glia* 57, 414–423. doi: 10.1002/glia.20770

Chechlacz, M., Vemuri, M. C., and Naegele, J. R. (2001). Role of DNA-dependent protein kinase in neuronal survival. *J. Neurochem.* 78, 141–154. doi: 10.1046/j.1471-4159.2001.00380.x

Chen, H., He, G., Chen, Y., Zhang, X., and Wu, S. (2018). Differential activation of NLRP3, AIM2, and IFI16 inflammasomes in humans with acute and chronic hepatitis B. *Viral Immunol.* 31, 639–645. doi: 10.1089/vim.2018.0058

Chen, I. Y., and Ichinohe, T. (2015). Response of host inflammasomes to viral infection. *Trends Microbiol.* 23, 55–63. doi: 10.1016/j.tim.2014.09.007

Chen, Q., Sun, L., and Chen, Z. J. (2016). Regulation and function of the cGAS-STING pathway of cytosolic DNA sensing. *Nat. Immunol.* 17, 1142–1149. doi: 10.1038/ni.3558

Cheng, W. Y., He, X. B., Jia, H. J., Chen, G. H., Jin, Q. W., Long, Z. L., et al. (2018). The cGassting signaling pathway is required for the innate immune response against ectromelia virus. *Front. Immunol.* 9:1297. doi: 10.3389/fimmu.2018.01297

Chiu, Y. H., MacMillan, J. B., and Chen, Z. J. (2009). RNA Polymerase III detects cytosolic DNA and induces type i interferons through the rig-i pathway. *Cell* 138, 576–591. doi: 10.1016/j.cell.2009.06.015

Choi, H. J., Park, A., Kang, S., Lee, E., Lee, T. A., Ra, E. A., et al. (2018). Human cytomegalovirus-encoded US9 targets MAVS and STING signaling to evade type i interferon immune responses. *Nat. Commun.* 9:125. doi: 10.1038/s41467-017-02624-8

Christensen, M. H., Jensen, S. B., Miettinen, J. J., Luecke, S., Prabakaran, T., Reinert, L. S., et al. (2016). HSV−1 ICP 27 targets the TBK 1-activated STING signalsome to inhibit virus-induced type I IFN expression. *EMBO J.* 35, 1385–1399. doi: 10.15252/embj.201593458

Conrady, C. D., Zheng, M., Fitzgerald, K. A., Liu, C., and Carr, D. J. J. (2012). Resistance to HSV-1 infection in the epithelium resides with the novel innate sensor, IFI-16. *Mucosal Immunol.* 5, 173–183. doi: 10.1038/mi.2011.63

Corrales, L., Woo, S.-R., Williams, J. B., McWhirter, S. M., Dubensky, T. W., and Gajewski, T. F. (2016). Antagonism of the STING pathway via activation of the AIM2 inflammasome by intracellular DNA. *J. Immunol.* 196, 3191–3198. doi: 10.4049/jimmunol.1502538

Coulon, P. G., Dhanushkodi, N., Prakash, S., Srivastava, R., Roy, S., Alomari, N. I., et al. (2019). NLRP3, NLRP12, and IFI16 inflammasomes induction and caspase-1 activation triggered by virulent HSV-1 strains are associated with severe corneal inflammatory herpetic disease. *Front. Immunol.* 10:1631. doi: 10.3389/fimmu.2019.01631

Cox, D. J., Field, R. H., Williams, D. G., Baran, M., Bowie, A. G., Cunningham, C., et al. (2015). DNA sensors are expressed in astrocytes and microglia *in vitro* and are upregulated during gliosis in neurodegenerative disease. *Glia* 63, 812–825. doi: 10.1002/glia.22786

Cridland, J. A., Curley, E. Z., Wykes, M. N., Schroder, K., Sweet, M. J., Roberts, T. L., et al. (2012). The mammalian PYHIN gene family: Phylogeny, evolution and expression. *BMC Evol. Biol.* 12:140. doi: 10.1186/1471-2148-12-140

Crill, E. K., Furr-Rogers, S. R., and Marriott, I. (2015). RIG-I is required for VSV-induced cytokine production by murine glia and acts in combination with DAI to initiate responses to HSV-1. *Glia* 63, 2168–2180. doi: 10.1002/glia.22883

Cuchet-Lourenco, D., Anderson, G., Sloan, E., Orr, A., and Everett, R. D. (2013). The Viral Ubiquitin ligase icp0 is neither sufficient nor necessary for degradation of the cellular dna sensor ifi16 during herpes simplex virus 1 infection. *J. Virol.* 87, 13422–13432. doi: 10.1128/JVI.02474-13

Dai, P., Wang, W., Cao, H., Avogadri, F., Dai, L., Drexler, I., et al. (2014). Modified Vaccinia Virus ankara triggers type i ifn production in murine conventional dendritic cells via a cGAS/STING-mediated cytosolic DNA-sensing pathway. *PLoS Pathog.* 10:e1003989. doi: 10.1371/journal.ppat.1003989

Daniels, B. P., Kofman, S. B., Smith, J. R., Norris, G. T., Snyder, A. G., Kolb, J. P., et al. (2019). The nucleotide sensor zbp1 and kinase RIPK3 induce the enzyme irg1 to promote an antiviral metabolic state in neurons. *Immunity* 50, 64–76.e4. doi: 10.1016/j.immuni.2018.11.017

Daniels, B. P., Snyder, A. G., Olsen, T. M., Orozco, S., Oguin, T. H., Tait, S. W. G., et al. (2017). RIPK3 restricts viral pathogenesis via cell Death-Independent Neuroinflammation. *Cell* 169, 301–313.e11. doi: 10.1016/j.cell.2017.03.011

de Sousa, J. R., da Silva Azevedo, R. D. S., Martins Filho, A. J., de Araujo, M. T. F., Cruz, E. D. R. M., Vasconcelos, B. C. B., et al. (2018). *In situ* inflammasome activation results in severe damage to the central nervous system in fatal Zika virus microcephaly cases. *Cytokine* 111, 255–264. doi: 10.1016/j.cyto.2018.08.008

Dell'Oste, V., Gatti, D., Giorgio, A. G., Gariglio, M., Landolfo, S., and De Andrea, M. (2015). The interferon-inducible DNA-sensor protein IFI16: A key player in the antiviral response. *New Microbiol.* 38, 5–20.

Dell'Oste, V., Gatti, D., Gugliesi, F., De Andrea, M., Bawadekar, M., Lo Cigno, I., et al. (2014). Innate nuclear sensor ifi16 translocates into the cytoplasm during the early stage of *in vitro* human cytomegalovirus infection and is entrapped in the egressing virions during the late stage. *J. Virol.* 88, 6970–6982. doi: 10.1128/JVI.00384-14

Deschamps, T., and Kalamvoki, M. (2017). Evasion of the STING DNA-sensing pathway by VP11/12 of herpes simplex virus 1. *J. Virol.* 91:e00535–17. doi: 10.1128/JVI.00535-17

Dhanwani, R., Takahashi, M., and Sharma, S. (2018). Cytosolic sensing of immuno-stimulatory DNA, the enemy within. *Curr. Opin. Immunol.* 50, 82–87. doi: 10.1016/j.coi.2017.11.004

Dhuriya, Y. K., and Sharma, D. (2018). Necroptosis: a regulated inflammatory mode of cell death. *J. Neuroinflammation* 15:199. doi: 10.1186/s12974-018-1235-0

Diner, B. A., Lum, K. K., Javitt, A., and Cristea, I. M. (2015). Interactions of the antiviral factor interferon gamma-inducible protein 16 (IFI16) mediate immune signaling and herpes simplex virus-1 immunosuppression. *Mol. Cell. Proteomics* 14, 2341–2356. doi: 10.1074/mcp.M114.047068

Diner, B. A., Lum, K. K., Toettcher, J. E., and Cristea, I. M. (2016). Viral DNA sensors IFI16 and cyclic GMP-AMP synthase possess distinct functions in regulating viral gene expression, immune defenses, and apoptotic responses during herpesvirus infection. *MBio* 7, e01553–16. doi: 10.1128/mBio.01553-16

Ding, Q., Gaska, J. M., Douam, F., Wei, L., Kim, D., Balev, M., et al. (2018). Species-specific disruption of STING-dependent antiviral cellular defenses by the Zika virus NS2B3 protease. *Proc. Natl. Acad. Sci. U.S.A.* 115, E6310–E6318. doi: 10.1073/pnas.1803406115

Duan, Y., Zeng, J., Fan, S., Liao, Y., Feng, M., Wang, L., et al. (2019). Herpes simplex virus type 1-encoded miR-H2-3p manipulates cytosolic DNA-stimulated antiviral innate immune response by targeting DDX41. *Viruses* 11:756. doi: 10.3390/v11080756

Dutta, D., Dutta, S., Veettil, M. V., Roy, A., Ansari, M. A., Iqbal, J., et al. (2015). BRCA1 Regulates IFI16 mediated nuclear innate sensing of herpes viral dna and subsequent induction of the innate inflammasome and interferon-β responses. *PLOS Pathog.* 11:e1005030. doi: 10.1371/journal.ppat.1005030

Ekchariyawat, P., Hamel, R., Bernard, E., Wichit, S., Surasombatpattana, P., Talignani, L., et al. (2015). Inflammasome signaling pathways exert antiviral effect against chikungunya virus in human dermal fibroblasts. *Infect. Genet. Evol.* 32, 401–408. doi: 10.1016/j.meegid.2015.03.025

Fang, R., Wang, C., Jiang, Q., Lv, M., Gao, P., Yu, X., et al. (2017). NEMO–IKKβ are essential for IRF3 and NF-κB activation in the cGAS–STING pathway. *J. Immunol.* 199, 3222–3233. doi: 10.4049/jimmunol.1700699

Ferguson, B. J., Mansur, D. S., Peters, N. E., Ren, H., and Smith, G. L. (2012). DNA-PK is a DNA sensor for IRF-3-dependent innate immunity. *Elife* 2012:e00047. doi: 10.7554/eLife.00047.012

Fernandes-Alnemri, T., Yu, J. W., Datta, P., Wu, J., and Alnemri, E. S. (2009). AIM2 activates the inflammasome and cell death in response to cytoplasmic DNA. *Nature* 458, 509–513. doi: 10.1038/nature07710

Fu, Y. Z., Su, S., Gao, Y. Q., Wang, P. P., Huang, Z. F., Hu, M. M., et al. (2017). Human cytomegalovirus tegument protein UL82 inhibits STING-mediated signaling to evade antiviral immunity. *Cell Host Microbe* 21, 231–243. doi: 10.1016/j.chom.2017.01.001

Furr, S. R., Chauhan, V. S., Moerdyk-Schauwecker, M. J., and Marriott, I. (2011). A role for DNA-dependent activator of interferon regulatory factor in the recognition of herpes simplex virus type 1 by glial cells. *J. Neuroinflammation* 8:99. doi: 10.1186/1742-2094-8-99

Furr, S. R., Chauhan, V. S., Sterka, D., Grdzelishvili, V., and Marriott, I. (2008). Characterization of retinoic acid–inducible gene-I expression in primary murine glia following exposure to vesicular stomatitis virus. *J. Neurovirol.* 14, 503–513. doi: 10.1080/13550280802337217

Furr, S. R., and Marriott, I. (2012). Viral CNS infection: role of glial pattern recognition receptors in neuroinflammation. *Front. Microbiol.* 3:201. doi: 10.3389/fmicb.2012.00201

Gao, D., Wu, J., Wu, Y. T., Du, F., and Aroh, C., Yan, N., et al. (2013). Cycilc GMP-AMP Synthase is and innate immune sensor of HIV and other retroviruses. *Science* 341, 903–906. doi: 10.1126/science.1240933

Gao, P., Ascano, M., Wu, Y., Barchet, W., Gaffney, B. L., Zillinger, T., et al. (2013). Cyclic [G(2′,5′)pA(3′,5′)p]is the metazoan second messenger produced by DNA-activated cyclic GMP-AMP synthase. *Cell* 153, 1094–1107. doi: 10.1016/j.cell.2013.04.046

Gariano, G. R., Dell'Oste, V., Bronzini, M., Gatti, D., Luganini, A., de Andrea, M., et al. (2012). The intracellular DNA sensor IFI16 gene acts as restriction factor for human Cytomegalovirus replication. *PLoS Pathog.* 8:e1002498. doi: 10.1371/journal.ppat.1002498

George, B. P., Schneider, E. B., and Venkatesan, A. (2014). Encephalitis hospitalization rates and inpatient mortality in the United States, 2000-2010. *PLoS ONE* 9:e0104169. doi: 10.1371/journal.pone.0104169

Gray, E. E., Winship, D., Snyder, J. M., Child, S. J., Geballe, A. P., and Stetson, D. B. (2016). The AIM2-like receptors are dispensable for the interferon response to intracellular DNA. *Immunity* 45, 255–266. doi: 10.1016/j.immuni.2016.06.015

Guo, H., Gilley, R. P., Fisher, A., Lane, R., Landsteiner, V. J., Ragan, K. B., et al. (2018). Species-independent contribution of ZBP1/DAI/DLM-1-triggered necroptosis in host defense against HSV1. *Cell Death Dis.* 9:816. doi: 10.1038/s41419-018-0868-3

Guo, H., Omoto, S., Harris, P. A., Finger, J. N., Bertin, J., Gough, P. J., et al. (2015). Herpes simplex virus suppresses necroptosis in human cells. *Cell Host Microbe* 17, 243–251. doi: 10.1016/j.chom.2015.01.003

Hanamsagar, R., Aldrich, A., and Kielian, T. (2014). Critical role for the AIM2 inflammasome during acute CNS bacterial infection. *J. Neurochem.* 129, 704–711. doi: 10.1111/jnc.12669

Harnor, S. J., Brennan, A., and Cano, C. (2017). Targeting DNA-dependent protein kinase for cancer therapy. *ChemMedChem* 12, 895–900. doi: 10.1002/cmdc.201700143

Herzner, A. M., Hagmann, C. A., Goldeck, M., Wolter, S., Kübler, K., Wittmann, S., et al. (2015). Sequence-specific activation of the DNA sensor cGAS by Y-form DNA structures as found in primary HIV-1 cDNA. *Nat. Immunol.* 16, 1025–1033. doi: 10.1038/ni.3267

Hornung, V., Ablasser, A., Charrel-Dennis, M., Bauernfeind, F., Horvath, G., Caffrey, D. R., et al. (2009). AIM2 recognizes cytosolic dsDNA and forms a caspase-1-activating inflammasome with ASC. *Nature* 458, 514–518. doi: 10.1038/nature07725

Huang, J., You, H., Su, C., Li, Y., Chen, S., and Zheng, C. (2018). Herpes simplex virus 1 tegument protein VP22 abrogates cGAS/STING-mediated antiviral innate immunity. *J. Virol.* 92, e00841–18. doi: 10.1128/JVI.00841-18

Huang, Y., Liu, L., Ma, D., Liao, Y., Lu, Y., Huang, H., et al. (2017). Human cytomegalovirus triggers the assembly of AIM2 inflammasome in THP-1-derived macrophages. *J. Med. Virol.* 89, 2188–2195. doi: 10.1002/jmv.24846

Huang, Z., Wu, S. Q., Liang, Y., Zhou, X., Chen, W., Li, L., et al. (2015). RIP1/RIP3 binding to HSV-1 ICP6 initiates necroptosis to restrict virus propagation in mice. *Cell Host Microbe.* 17, 229–242. doi: 10.1016/j.chom.2015.01.002

Huang, Z. F., Zou, H. M., Liao, B. W., Zhang, H. Y., Yang, Y., Fu, Y. Z., et al. (2018). Human cytomegalovirus protein UL31 inhibits DNA sensing of cGAS to mediate immune evasion. *Cell Host Microbe* 24, 69–80.e4. doi: 10.1016/j.chom.2018.05.007

Ingram, J. P., Thapa, R. J., Fisher, A., Tummers, B., Zhang, T., Yin, C., et al. (2019). ZBP1/DAI drives RIPK3-mediated cell death induced by IFNs in the absence of RIPK1. *J. Immunol.* 203, 1348–1355. doi: 10.4049/jimmunol.1900216

Iqbal, J., Ansari, M. A., Kumar, B., Dutta, D., Roy, A., Chikoti, L., et al. (2016). Histone H2BIFI16 recognition of nuclear herpesviral genome induces cytoplasmic interferon-β responses. *PLOS Pathog.* 12:e1005967. doi: 10.1371/journal.ppat.1005967

Irion, U., and Leptin, M. (1999). Developmental and cell biological functions of the drosophila DEAD-box protein abstrakt. *Curr. Biol.* 9, 1373–1381. doi: 10.1016/S0960-9822(00)80082-2

Ishikawa, H., Ma, Z., and Barber, G. N. (2009). STING regulates intracellular DNA-mediated, type i interferon-dependent innate immunity. *Nature* 461, 788–792. doi: 10.1038/nature08476

Jakobsen, M. R., Bak, R. O., Andersen, A., Berg, R. K., Jensen, S. B., Jin, T., et al. (2013). IFI16 senses DNA forms of the lentiviral replication cycle and controls HIV-1 replication. *Proc. Natl. Acad. Sci. U.S.A.* 110:E4571–80. doi: 10.1073/pnas.1311669110

Jeffries, A. M., and Marriott, I. (2017). Human microglia and astrocytes express cGAS-STING viral sensing components. *Neurosci. Lett.* 658, 53–56. doi: 10.1016/j.neulet.2017.08.039

Jeffries, A. M., Nitika, T. A. W., and Marriott, I. (2020). The intracellular DNA sensors cGAS and IFI16 do not mediate effective antiviral immune responses to HSV-1 in human microglial cells. *J. Neurovirol.* 26, 544–555. doi: 10.1007/s13365-020-00852-1

Jiao, H., Wachsmuth, L., Kumari, S., Schwarzer, R., Lin, J., Eren, R. O., et al. (2020). Z-nucleicacid sensing triggers ZBP1-dependent necroptosis and inflammation. *Nature* 580, 391–395. doi: 10.1038/s41586-020-2129-8

Johnson, K. E., Chikoti, L., and Chandran, B. (2013). Herpes simplex virus 1 infection induces activation and subsequent inhibition of the IFI16 and NLRP3 Inflammasomes. *J. Virol.* 87, 5005–5018. doi: 10.1128/JVI.00082-13

Johnson, M. B., Halman, J. R., Burmeister, A. R., Currin, S., Khisamutdinov, E. F., Afonin, K. A., et al. (2020). Retinoic acid inducible gene-I mediated detection of bacterial nucleic acids in human microglial cells. *J. Neuroinflammation* 17:139. doi: 10.1186/s12974-020-01817-1

Jønsson, K. L., Laustsen, A., Krapp, C., Skipper, K. A., Thavachelvam, K., Hotter, D., et al. (2017). IFI16 is required for DNA sensing in human macrophages by promoting production and function of cGAMP. *Nat. Commun.* 8:14391. doi: 10.1038/ncomms14391

Kaiser, W. J., Upton, J. W., and Mocarski, E. S. (2008). Receptor-interacting protein homotypic interaction motif-dependent control of NF-κB activation via the DNA-dependent activator of IFN regulatory factors. *J. Immunol.* 181, 6427–6434. doi: 10.4049/jimmunol.181.9.6427

Kayagaki, N., Stowe, I. B., Lee, B. L., O'Rourke, K., Anderson, K., Warming, S., et al. (2015). Caspase-11 cleaves gasdermin D for non-canonical inflammasome signalling. *Nature* 526, 666–671. doi: 10.1038/nature15541

Kim, H., Seo, J. S., Lee, S. Y., Ha, K. T., Choi, B. T., Shin, Y., et al. (2020). AIM2 inflammasome contributes to brain injury and chronic post-stroke cognitive impairment in mice. *Brain. Behav. Immun.* 87, 765–776. doi: 10.1016/j.bbi.2020.03.011

Kim, J. E., Kim, Y. E., Stinski, M. F., Ahn, J. H., and Song, Y. J. (2017). Human cytomegalovirus IE2 86 kDa protein induces STING degradation and inhibits cGAMP-mediated IFN-β induction. *Front. Microbiol.* 8:1854. doi: 10.3389/fmicb.2017.01854

Kuriakose, T., Man, S. M., Subbarao Malireddi, R. K., Karki, R., Kesavardhana, S., Place, D. E., et al. (2016). ZBP1/DAI is an innate sensor of influenza virus triggering the NLRP3 inflammasome and programmed cell death pathways. *Sci. Immunol.* 1:aag2045. doi: 10.1126/sciimmunol.aag2045

Lahaye, X., Satoh, T., Gentili, M., Cerboni, S., Conrad, C., Hurbain, I., et al. (2013). The Capsids of HIV-1 and HIV-2 determine immune detection of the viral cdna by the innate sensor cgas in dendritic cells. *Immunity* 39, 1132–1142. doi: 10.1016/j.immuni.2013.11.002

Lee, K. G., Kim, S. S. Y., Kui, L., Voon, D. C. C., Mauduit, M., Bist, P., et al. (2015). Bruton's tyrosine kinase phosphorylates DDX41 and activates its binding of dsDNA and STING to initiate type 1 interferon response. *Cell Rep.* 10, 1055–1065. doi: 10.1016/j.celrep.2015.01.039

Li, X. D., Wu, J., Gao, D., Wang, H., Sun, L., and Chen, Z. J. (2013). Pivotal roles of cGAScGAMP signaling in antiviral defense and immune adjuvant effects. *Science* 341, 1390–1394. doi: 10.1126/science.1244040

Li, Y., Wu, Y., Zheng, X., Cong, J., Liu, Y., Li, J., et al. (2016). Cytoplasm-translocated Ku70/80 complex sensing of HBV DNA induces hepatitis-associated chemokine secretion. *Front. Immunol.* 7:569. doi: 10.3389/fimmu.2016.00569

Lin, J., Kumari, S., Kim, C., Van, T. M., Wachsmuth, L., Polykratis, A., et al. (2016). RIPK1 counteracts ZBP1-mediated necroptosis to inhibit inflammation. *Nature* 540, 124–128. doi: 10.1038/nature20558

Lippmann, J., Rothenburg, S., Deigendesch, N., Eitel, J., Meixenberger, K., van Laak, V., et al. (2008). IFNβ responses induced by intracellular bacteria or cytosolic DNA in different human cells do not require ZBP1 (DLM-1/DAI). *Cell. Microbiol.* 10, 2579–2588. doi: 10.1111/j.1462-5822.2008.01232.x

Liu, X., Chauhan, V. S., Young, A. B., and Marriott, I. (2010). NOD2 mediates inflammatory responses of primary murine glia to *Streptococcus pneumoniae*. *Glia* 58, 839–847. doi: 10.1002/glia.20968

Lo Cigno, I., Calati, F., Borgogna, C., Zevini, A., Albertini, S., Martuscelli, L., et al. (2020). Human papillomavirus E7 oncoprotein subverts host innate immunity via SUV39H1-mediated epigenetic silencing of immune sensor genes. *J. Virol.* 94:19. doi: 10.1128/JVI.01812-19

Lo Cigno, I., De Andrea, M., Borgogna, C., Albertini, S., Landini, M. M., Peretti, A., et al. (2015). The Nuclear DNA Sensor IFI16 acts as a restriction factor for human papillomavirus replication through epigenetic modifications of the viral promoters. *J. Virol.* 89, 7506–7520. doi: 10.1128/JVI.00013-15

Luecke, S., Holleufer, A., Christensen, M. H., Jønsson, K. L., Boni, G. A., Sørensen, L. K., et al. (2017). cGAS is activated by DNA in a length-dependent manner. *EMBO Rep.* 18, 1707–1715. doi: 10.15252/embr.201744017

Lugrin, J., and Martinon, F. (2018). The AIM2 inflammasome: Sensor of pathogens and cellular perturbations. *Immunol. Rev.* 281, 99–114. doi: 10.1111/imr.12618

Lum, K. K., Howard, T. R., Pan, C., and Cristea, I. M. (2019). Charge-mediated pyrin oligomerization nucleates antiviral IFI16 sensing of herpesvirus DNA. *MBio* 10, e01428–19. doi: 10.1128/mBio.01428-19

Lupfer, C., Malik, A., and Kanneganti, T. D. (2015). Inflammasome control of viral infection. *Curr. Opin. Virol.* 12, 38–46. doi: 10.1016/j.coviro.2015.02.007

Ma, F., Li, B., Liu, S., Iyer, S. S., Yu, Y., Wu, A., et al. (2015). Positive feedback regulation of type I IFN production by the IFN-inducible DNA sensor cGAS. *J. Immunol.* 194, 1545–1554. doi: 10.4049/jimmunol.1402066

Ma, J. X., Li, J. Y., Fan, D. D., Feng, W., Lin, A. F., Xiang, L. X., et al. (2018). Identification of DEAD-Box RNA helicase DDX41 as a trafficking protein that involves in multiple innate immune signaling pathways in a zebrafish model. *Front. Immunol.* 9:1327. doi: 10.3389/fimmu.2018.01327

Ma, Z., Jacobs, S. R., West, J. A., Stopford, C., Zhang, Z., Davis, Z., et al. (2015). Modulation of the cGAS-STING DNA sensing pathway by gammaherpesviruses. *Proc. Natl. Acad. Sci. U.S.A.* 112, E4306–E4315. doi: 10.1073/pnas.1503831112

Maelfait, J., Liverpool, L., Bridgeman, A., Ragan, K. B., Upton, J. W., and Rehwinkel, J. (2017). Sensing of viral and endogenous RNA by ZBP 1/ DAI induces necroptosis. *EMBO J.* 36, 2529–2543. doi: 10.15252/embj.201796476

Man, S. M., Karki, R., and Kanneganti, T. D. (2016). AIM2 inflammasome in infection, cancer, and autoimmunity: role in DNA sensing, inflammation, and innate immunity. *Eur. J. Immunol.* 46, 269–280. doi: 10.1002/eji.201545839

Maruzuru, Y., Ichinohe, T., Sato, R., Miyake, K., Okano, T., Suzuki, T., et al. (2018). Herpes Simplex Virus 1 VP22 Inhibits AIM2-dependent inflammasome activation to enable efficient viral replication. *Cell Host Microbe* 23, 254–265.e7. doi: 10.1016/j.chom.2017.12.014

Menendez, C. M., and Carr, D. J. J. (2017). Defining nervous system susceptibility during acute and latent herpes simplex virus-1 infection. *J. Neuroimmunol.* 308, 43–49. doi: 10.1016/j.jneuroim.2017.02.020

Miao, E. A., Rajan, J. V., and Aderem, A. (2011). Caspase-1-induced pyroptotic cell *death*. *Immunol. Rev.* 243, 206–214. doi: 10.1111/j.1600-065X.2011.01044.x

Moriyama, M., Koshiba, T., and Ichinohe, T. (2019). Influenza A virus M2 protein triggers mitochondrial DNA-mediated antiviral immune responses. *Nat. Commun.* 10:4624. doi: 10.1038/s41467-019-12632-5

Nair, S., and Diamond, M. S. (2015). Innate immune interactions within the central nervous system modulate pathogenesis of viral infections. *Curr. Opin. Immunol.* 36, 47–53. doi: 10.1016/j.coi.2015.06.011

Nakaya, Y., Lilue, J., Stavrou, S., Moran, E. A., and Ross, S. R. (2017). AIM2-like receptors positively and negatively regulate the interferon response induced by cytosolic DNA. *MBio* 8:17. doi: 10.1128/mBio.00944-17

Orzalli, M. H., Broekema, N. M., Diner, B. A., Hancks, D. C., Elde, N. C., Cristea, I. M., et al. (2015). CGAS-mediated stabilization of IFI16 promotes innate signaling during herpes simplex virus infection. *Proc. Natl. Acad. Sci. U.S.A.* 112, E1773–E1781. doi: 10.1073/pnas.1424637112

Orzalli, M. H., Broekema, N. M., and Knipe, D. M. (2016). Relative contributions of herpes simplex virus 1 ICP0 and vhs to loss of cellular IFI16 vary in different human cell types. *J. Virol.* 90, 8351–8359. doi: 10.1128/JVI.00939-16

Orzalli, M. H., DeLuca, N. A., and Knipe, D. M. (2012). Nuclear IFI16 induction of IRF-3 signaling during herpesviral infection and degradation of IFI16 by the viral ICP0 protein. *Proc. Natl. Acad. Sci. U.S.A.* 109, E3008–E3017. doi: 10.1073/pnas.1211302109

Paijo, J., Döring, M., Spanier, J., Grabski, E., Nooruzzaman, M., Schmidt, T., et al. (2016). cGAS senses human cytomegalovirus and induces type i interferon responses in human monocyte-derived cells. *PLoS Pathog.* 12:e1005546. doi: 10.1371/journal.ppat.1005546

Pan, S., Liu, X., Ma, Y., Cao, Y., and He, B. (2018). Herpes simplex virus 1 γ 1 34.5 protein inhibits STING activation that restricts viral replication. *J. Virol.* 92, e01015–18. doi: 10.1128/JVI.01015-18

Parker, Z. M., Murphy, A. A., and Leib, D. A. (2015). Role of the DNA sensor STING in protection from lethal infection following corneal and intracerebral challenge with herpes simplex virus 1. *J. Virol.* 89, 11080–11091. doi: 10.1128/JVI.00954-15

Parvatiyar, K., Zhang, Z., Teles, R. M., Ouyang, S., Jiang, Y., Iyer, S. S., et al. (2012). The helicase DDX41 recognizes the bacterial secondary messengers cyclic di-GMP and cyclic di-AMP to activate a type i interferon immune response. *Nat. Immunol.* 13, 1155–1161. doi: 10.1038/ni.2460

Peters, N. E., Ferguson, B. J., Mazzon, M., Fahy, A. S., Krysztofinska, E., Arribas-Bosacoma, R., et al. (2013). A Mechanism for the inhibition of DNA-PK-mediated DNA sensing by a Virus. *PLoS Pathog.* 9:1003649. doi: 10.1371/journal.ppat.1003649

Pham, T. H., Kwon, K. M., Kim, Y. E., Kim, K. K., and Ahn, J. H. (2013). DNA sensing-independent inhibition of herpes simplex virus 1 replication by DAI/ZBP1. *J. Virol.* 87, 3076–3086. doi: 10.1128/JVI.02860-12

Phelan, T., Little, M. A., and Brady, G. (2020). Targeting of the cGAS-STING system by DNA viruses. *Biochem. Pharmacol.* 174:113831. doi: 10.1016/j.bcp.2020.113831

Pisano, G., Roy, A., Ahmed Ansari, M., Kumar, B., Chikoti, L., and Chandran, B. (2017). Interferon-γ-inducible protein 16 (IFI16) is required for the maintenance of Epstein-Barr virus latency. *Virol. J.* 14:221. doi: 10.1186/s12985-017-0891-5

Rathinam, V. A. K., Jiang, Z., Waggoner, S. N., Sharma, S., Cole, L. E., Waggoner, L., et al. (2010). The AIM2 inflammasome is essential for host defense against cytosolic bacteria and DNA viruses. *Nat. Immunol.* 11, 395–402. doi: 10.1038/ni.1864

Rebsamen, M., Heinz, L. X., Meylan, E., Michallet, M. C., Schroder, K., Hofmann, K., et al. (2009). DAI/ZBP1 recruits RIP1 and RIP3 through RIP homotypic interaction motifs to activate NF-κB. *EMBO Rep.* 10, 916–922. doi: 10.1038/embor.2009.109

Reinert, L. S., Lopušná, K., Winther, H., Sun, C., Thomsen, M. K., Nandakumar, R., et al. (2016). Sensing of HSV-1 by the cGAS-STING pathway in microglia orchestrates antiviral defence in the CNS. *Nat. Commun.* 7:13348. doi: 10.1038/ncomms13348

Reinholz, M., Kawakami, Y., Salzer, S., Kreuter, A., Dombrowski, Y., Koglin, S., et al. (2013). HPV16 activates the AIM2 inflammasome in keratinocytes. *Arch. Dermatol. Res.* 305, 723–732. doi: 10.1007/s00403-013-1375-0

Roos, K. L. (1999). Encephalitis. *Neurol. Clin.* 17, 813–833. doi: 10.1016/S0733-8619(05)70168-7

Rothan, H. A., Arora, K., Natekar, J. P., Strate, P. G., Brinton, M. A., and Kumar, M. (2019). ZDNA-binding protein 1 is critical for controlling virus replication and survival in west nile virus encephalitis. *Front. Microbiol.* 10:89. doi: 10.3389/fmicb.2019.02089

Roy, A., Dutta, D., Iqbal, J., Pisano, G., Gjyshi, O., Ansari, M. A., et al. (2016). Nuclear innate immune DNA sensor IFI16 Is degraded during lytic reactivation of kaposi's sarcomaassociated herpesvirus (KSHV): role of ifi16 in maintenance of kshv latency. *J. Virol.* 90, 8822–8841. doi: 10.1128/JVI.01003-16

Roy, A., Ghosh, A., Kumar, B., and Chandran, B. (2019). IfI16, a nuclear innate immune DNA sensor, mediates epigenetic silencing of herpesvirus genomes by its association with H3K9 methyltransferases SUV39H1 and GLP. *Elife* 8:e49500. doi: 10.7554/eLife.49500

Royer, D. J., and Carr, D. J. J. (2016). A STING-dependent innate-sensing pathway mediates resistance to corneal HSV-1 infection via upregulation of the antiviral effector tetherin. *Mucosal Immunol.* 9, 1065–1075. doi: 10.1038/mi.2015.124

Sagulenko, V., Thygesen, S. J., Sester, D. P., Idris, A., Cridland, J. A., Vajjhala, P. R., et al. (2013). AIM2 and NLRP3 inflammasomes activate both apoptotic and pyroptotic death pathways via ASC. *Cell Death Differ.* 20, 1149–1160. doi: 10.1038/cdd.2013.37

Sawai, H. (2016). Induction of apoptosis in TNF-Treated L929 cells in the presence of necrostatin-1. *Int. J. Mol. Sci.* 17:1678. doi: 10.3390/ijms17101678

Schattgen, S. A., Gao, G., Kurt-Jones, E. A., and Fitzgerald, K. A. (2016). Cutting edge: dna in the lung microenvironment during influenza virus infection tempers inflammation by engaging the DNA Sensor AIM2. *J. Immunol.* 196, 29–33. doi: 10.4049/jimmunol.1501048

Schmucker, D., Vorbrüggen, G., Yeghiayan, P., Fan, H. Q., Jäckle, H., and Gaul, U. (2000). The Drosophila gene abstrakt, required for visual system development, encodes a putative RNA helicase of the DEAD box protein family. *Mech. Dev.* 91, 189–196. doi: 10.1016/S0925-4773(99)00298-1

Scutts, S. R., Ember, S. W., Ren, H., Ye, C., Lovejoy, C. A., Mazzon, M., et al. (2018). DNA-PK is targeted by multiple vaccinia virus proteins to inhibit DNA sensing. *Cell Rep.* 25, 1953–1965.e4. doi: 10.1016/j.celrep.2018.10.034

Semenova, N., Bosnjak, M., Markelc, B., Znidar, K., Cemazar, M., and Heller, L. (2019). Multiple cytosolic DNA sensors bind plasmid DNA after transfection. *Nucleic Acids Res.* 47, 10235–10246. doi: 10.1093/nar/gkz768

Serramía, M. J., Muñoz-Fernández, M. Á., and Álvarez, S. (2015). HIV-1 increases TLR responses in human primary astrocytes. *Sci. Rep.* 5:17887. doi: 10.1038/srep17887

Shi, J., Zhao, Y., Wang, K., Shi, X., Wang, Y., Huang, H., et al. (2015). Cleavage of GSDMD by inflammatory caspases determines pyroptotic cell death. *Nature* 526, 660–665. doi: 10.1038/nature15514

Shrivastava, G., León-Juárez, M., García-Cordero, J., Meza-Sánchez, D. E., and Cedillo-Barrón, L. (2016). Inflammasomes and its importance in viral infections. *Immunol. Res.* 64, 1101–1117. doi: 10.1007/s12026-016-8873-z

Song, X., Ma, F., and Herrup, K. (2019). Accumulation of cytoplasmic DNA Due to ATM deficiency activates the microglial viral response system with neurotoxic consequences. *J. Neurosci.* 39, 6378–6394. doi: 10.1523/JNEUROSCI.0774-19.2019

Sridharan, H., Ragan, K. B., Guo, H., Gilley, R. P., Landsteiner, V. J., Kaiser, W. J., et al. (2017). Murine cytomegalovirus IE 3-dependent transcription is required for DAI/ZBP 1mediated necroptosis. *EMBO Rep.* 18, 1429–1441. doi: 10.15252/embr.201743947

Stabell, A. C., Meyerson, N. R., Gullberg, R. C., Gilchrist, A. R., Webb, K. J., Old, W. M., et al. (2018). Dengue viruses cleave STING in humans but not in nonhuman primates, their presumed natural reservoir. *Elife* 7:e31919. doi: 10.7554/eLife.31919

Stavrou, S., Aguilera, A. N., Blouch, K., and Ross, S. R. (2018). DDX41 recognizes RNA/DNA retroviral reverse transcripts and is critical for *in vivo* control of murine leukemia virus infection. *MBio* 9, e00923–18. doi: 10.1128/mBio.00923-18

Stavrou, S., Blouch, K., Kotla, S., Bass, A., and Ross, S. R. (2015). Nucleic acid recognition orchestrates the anti-viral response to retroviruses. *Cell Host Microbe* 17, 478–488. doi: 10.1016/j.chom.2015.02.021

Sterka, D., Rati, D. M., and Marriott, I. (2006). Functional expression of NOD2, a novel pattern recognition receptor for bacterial motifs, in primary murine astrocytes. *Glia* 53, 322–330. doi: 10.1002/glia.20286

Su, C., and Zheng, C. (2017). Herpes simplex virus 1 abrogates the cGAS/STING-mediated cytosolic DNA-sensing pathway via its virion host shutoff protein, UL41. *J. Virol.* 91, e02414–16. doi: 10.1128/JVI.02414-16

Su, J., Rui, Y., Lou, M., Yin, L., Xiong, H., Zhou, Z., et al. (2019). HIV-2/SIV Vpx targets a novel functional domain of STING to selectively inhibit cGAS–STING-mediated NF-κB signalling. *Nat. Microbiol.* 4, 2552–2564. doi: 10.1038/s41564-019-0585-4

Sui, H., Zhou, M., Imamichi, H., Jiao, X., Sherman, B. T., Clifford Lane, H., et al. (2017). STING is an essential mediator of the Ku70-mediated production of IFN-γ1 in response to exogenous DNA. *Sci. Signal.* 10:aah5054. doi: 10.1126/scisignal.aah5054

Sun, B., Sundström, K. B., Chew, J. J., Bist, P., Gan, E. S., Tan, H. C., et al. (2017). Dengue virus activates cGAS through the release of mitochondrial DNA. *Sci. Rep.* 7:3594. doi: 10.1038/s41598-017-03932-1

Sun, L., Wu, J., Du, F., Chen, X., and Chen, Z. J. (2013). Cyclic GMP-AMP synthase is a cytosolic DNA sensor that activates the type I interferon pathway. *Science* 39, 786–91. doi: 10.1126/science.1232458

Sun, L., Xing, Y., Chen, X., Zheng, Y., Yang, Y., Nichols, D. B., et al. (2012). Coronavirus papain-like proteases negatively regulate antiviral innate immune response through disruption of STING-mediated signaling. *PLoS ONE* 7:30802. doi: 10.1371/journal.pone.0030802

Swanson, K. V., Junkins, R. D., Kurkjian, C. J., Holley-Guthrie, E., Pendse, A. A., Morabiti, R., et al. (2017). A noncanonical function of cGAMP in inflammasome priming and activation. *J. Exp. Med.* 214, 3611–3262. doi: 10.1084/jem.20171749

Takaoka, A., Wang, Z., Choi, M. K., Yanai, H., Negishi, H., Ban, T., et al. (2007). DAI (DLM1/ZBP1) is a cytosolic DNA sensor and an activator of innate immune response. *Nature* 448, 501–505. doi: 10.1038/nature06013

Thapa, R. J., Ingram, J. P., Ragan, K. B., Nogusa, S., Boyd, D. F., Benitez, A. A., et al. (2016). DAI senses influenza a virus genomic RNA and

activates RIPK3-dependent cell death. *Cell Host Microbe* 20, 674–681. doi: 10.1016/j.chom.2016.09.014

Unterholzner, L. (2013). The interferon response to intracellular DNA: why so many receptors? *Immunobiology* 218, 1312–1321. doi: 10.1016/j.imbio.2013.07.007

Unterholzner, L., Keating, S. E., Baran, M., Horan, K. A., Jensen, S. B., Sharma, S., et al. (2010). IFI16 is an innate immune sensor for intracellular DNA. *Nat. Immunol.* 11, 997–1004. doi: 10.1038/ni.1932

Upton, J. W., Kaiser, W. J., and Mocarski, E. S. (2012). DAI/ZBP1/DLM-1 Complexes with RIP3 to mediate virus-induced programmed necrosis that is targeted by murine cytomegalovirus vIRA. *Cell Host Microbe* 11, 290–297. doi: 10.1016/j.chom.2012.01.016

Vemuri, M. C., Schiller, E., and Naegele, J. R. (2001). Elevated DNA double strand breaks and apoptosis in the CNS of scid mutant mice. *Cell Death Differ.* 8, 245–255. doi: 10.1038/sj.cdd.4400806

Venkatesan, A., and Geocadin, R. G. (2014). Diagnosis and management of acute encephalitis: a practical approach. *Neurol. Clin. Pract.* 4, 206–215. doi: 10.1212/CPJ.0000000000000036

Vermeire, J., Roesch, F., Sauter, D., Rua, R., Hotter, D., Van Nuffel, A., et al. (2016). HIV Triggers a cGAS-dependent, Vpu- and Vpr-regulated type i interferon response in CD4+ T Cells. *Cell Rep.* 17, 413–424. doi: 10.1016/j.celrep.2016.09.023

Wang, J., Kang, L., Song, D., Liu, L., Yang, S., Ma, L., et al. (2017). Ku70 Senses HTLV-1 DNA and modulates HTLV-1 replication. *J. Immunol.* 199, 2475–2482. doi: 10.4049/jimmunol.1700111

Wang, X., Li, Y., Liu, S., Yu, X., Li, L., Shi, C., et al. (2014). Direct activation of RIP3/MLKLdependent necrosis by herpes simplex virus 1 (HSV-1) protein ICP6 triggers host antiviral defense. *Proc. Natl. Acad. Sci. U.S.A.* 111, 15438–15443. doi: 10.1073/pnas.1412767111

Wang, Z. C., Choi, M. K., Ban, T., Yanai, H., Negishi, H., Lu, Y., et al. (2008). Regulation of innate immune responses by DAI (DLM-1/ZBP1) and other DNA-sensing molecules. *Proc. Natl. Acad. Sci. U.S.A.* 105, 5477–5482. doi: 10.1073/pnas.0801295105

West, A. P., Khoury-Hanold, W., Staron, M., Tal, M. C., Pineda, C. M., Lang, S. M., et al. (2015). Mitochondrial DNA stress primes the antiviral innate immune response. *Nature* 520, 553–557. doi: 10.1038/nature14156

Wong, E. B., Montoya, B., Ferez, M., Stotesbury, C., and Sigal, L. J. (2019). Resistance to ectromelia virus infection requires cGAS in bone marrow-derived cells which can be bypassed with cGAMP therapy. *PLoS Pathog.* 15:e1008239. doi: 10.1371/journal.ppat.1008239

Wu, J. J., Li, W., Shao, Y., Avey, D., Fu, B., Gillen, J., et al. (2015). Inhibition of cGAS DNA sensing by a herpesvirus virion protein. *Cell Host Microbe* 18, 333–344. doi: 10.1016/j.chom.2015.07.015

Xu, H., Su, C., Pearson, A., Mody, C. H., and Zheng, C. (2017). Herpes simplex virus 1 UL24 abrogates the DNA sensing signal pathway by inhibiting NF-κB activation. *J. Virol.* 91, e00025–17. doi: 10.1128/JVI.00025-17

Yang, Y., Zhao, X., Wang, Z., Shu, W., Li, L., Li, Y., et al. (2020). Nuclear sensor interferon-inducible protein 16 inhibits the function of hepatitis b virus covalently closed circular DNA by integrating innate immune activation and epigenetic suppression. *Hepatology* 71, 1154–1169. doi: 10.1002/hep.30897

Ye, R., Su, C., Xu, H., and Zheng, C. (2017). Herpes simplex virus 1 ubiquitin-specific protease ul36 abrogates nf-κb activation in dna sensing signal pathway. *J. Virol.* 91:e02417–16. doi: 10.1128/JVI.02417-16

Yi, G., Wen, Y., Shu, C., Han, Q., Konan, K. V., Li, P., et al. (2016). Hepatitis C virus NS4B can suppress STING accumulation to evade innate immune responses. *J. Virol.* 90, 254–265. doi: 10.1128/JVI.01720-15

Yogarajah, T., Ong, K. C., Perera, D., and Wong, K. T. (2017). AIM2 Inflammasome-mediated pyroptosis in enterovirus A71-infected neuronal cells restricts viral replication. *Sci. Rep.* 7:5845. doi: 10.1038/s41598-017-05589-2

You, H., Zheng, S., Huang, Z., Lin, Y., Shen, Q., and Zheng, C. (2019). Herpes simplex virus 1 tegument protein ul46 inhibits tank-binding kinase 1-mediated signaling. *MBio* 10, 919–938. doi: 10.1128/mBio.00919-19

Zhang, D., Su, C., and Zheng, C. (2016). Herpes simplex virus 1 serine protease VP24 blocks the dna-sensing signal pathway by abrogating activation of interferon regulatory factor 3. *J. Virol.* 90, 5824–5829. doi: 10.1128/JVI.00186-16

Zhang, G., Chan, B., Samarina, N., Abere, B., Weidner-Glunde, M., Buch, A., et al. (2016). Cytoplasmic isoforms of Kaposi sarcoma herpesvirus LANA recruit and antagonize the innate immune DNA sensor cGAS. *Proc. Natl. Acad. Sci. U.S.A.* 113, E1034–E1043. doi: 10.1073/pnas.1516812113

Zhang, H., Luo, J., Alcorn, J. F., Chen, K., Fan, S., Pilewski, J., et al. (2017). AIM2 inflammasome is critical for influenza-induced lung injury and mortality. *J. Immunol.* 198, 4383–4393. doi: 10.4049/jimmunol.1600714

Zhang, J., Zhao, J., Xu, S., Li, J., He, S., Zeng, Y., et al. (2018). Species-specific deamidation of cGAS by herpes simplex virus UL37 protein facilitates viral replication. *Cell Host Microbe* 24, 234–248.e5. doi: 10.1016/j.chom.2018.07.004

Zhang, X., Brann, T. W., Zhou, M., Yang, J., Oguariri, R. M., Lidie, K. B., et al. (2011). Cutting Edge: Ku70 is a novel cytosolic DNA sensor that induces type III rather than type I IFN. *J. Immunol.* 186, 4541–4545. doi: 10.4049/jimmunol.1003389

Zhang, X., Shi, H., Wu, J., Zhang, X., Sun, L., Chen, C., et al. (2013). Cyclic GMP-AMP containing mixed phosphodiester linkages is an endogenous high-affinity ligand for STING. *Mol. Cell* 51, 226–235. doi: 10.1016/j.molcel.2013.05.022

Zhang, Z., Bao, M., Lu, N., Weng, L., Yuan, B., and Liu, Y. J. (2013). The E3 ubiquitin ligase TRIM21 negatively regulates the innate immune response to intracellular double-stranded DNA. *Nat. Immunol.* 14, 172–178. doi: 10.1038/ni.2492

Zhang, Z., Yuan, B., Bao, M., Lu, N., Kim, T., and Liu, Y. J. (2011). The helicase DDX41 senses intracellular DNA mediated by the adaptor STING in dendritic cells. *Nat. Immunol.* 12, 959–965. doi: 10.1038/ni.2091

Zheng, Y., Liu, Q., Wu, Y., Ma, L., Zhang, Z., Liu, T., et al. (2018). Zika virus elicits inflammation to evade antiviral response by cleaving cGAS via NS1-caspase-1 axis. *EMBO J.* 37:e99347. doi: 10.15252/embj.201899347

Zhu, W., Zu, X., Liu, S., and Zhang, H. (2019). The absent in melanoma 2 (AIM2) inflammasome in microbial infection. *Clin. Chim. Acta* 495, 100–108. doi: 10.1016/j.cca.2019.04.052

Zohaib, A., Sarfraz, A., Kaleem, Q. M., Ye, J., Mughal, M. N., Navid, M. T., et al. (2016). The Yin and Yang of antiviral innate immunity in central nervous system. *Curr. Pharm. Des.* 22, 648–655. doi: 10.2174/1381612822666151204001550

Conflict of Interest: The authors declare that the research was conducted in the absence of any commercial or financial relationships that could be construed as a potential conflict of interest.

frontiers in Cellular and Infection Microbiology

MINI REVIEW
published: 26 October 2020
doi: 10.3389/fcimb.2020.588378

Mini-Review: Bioactivities of Bacterial Cell Envelopes in the Central Nervous System

*William J. MacCain and Elaine I. Tuomanen**

Department of Infectious Diseases, St. Jude Children's Research Hospital, Memphis, TN, United States

During acute bacterial meningitis, recognition of the bacterial envelope by immune cells of the central nervous system (CNS) generates a robust response that is essential to clear bacteria. This response is further amplified during treatment when lytic antibiotics, required for cure, also generate a burst of highly inflammatory cell envelope debris. Different peptidoglycan (PG) subcomponents interact with neurons, glia, and the blood brain barrier resulting in the entire symptom complex of meningitis. Recently, this CNS-cell envelope signaling axis has been extended to non-inflammatory recognition of cell wall components circulating from endogenous bacteria to the brain resulting in both benefit and chronic damage. This review will describe the molecular details of a broad array of cell envelope-induced responses in the CNS and what current strategies can be implemented to improve clinical outcome.

Keywords: meningitis, PAMP, pattern recognition receptor, peptidoglycan, neurodevelopment

OPEN ACCESS

Edited by:
Federico Iovino,
Karolinska Institutet (KI), Sweden

Reviewed by:
Lars-Ove Brandenburg,
University Hospital RWTH Aachen, Germany
Anbarasu Kumarasamy,
Bharathidasan University, India

****Correspondence:***
Elaine I. Tuomanen
elaine.tuomanen@stjude.org

Specialty section:
This article was submitted to Bacteria and Host, a section of the journal Frontiers in Cellular and Infection Microbiology

Received: *28 July 2020*
Accepted: *16 September 2020*
Published: *26 October 2020*

Citation:
MacCain WJ and Tuomanen EI (2020) Mini-Review: Bioactivities of Bacterial Cell Envelopes in the Central Nervous System. Front. Cell. Infect. Microbiol. 10:588378. doi: 10.3389/fcimb.2020.588378

INTRODUCTION

The bacterial cell envelope is one of the most powerful pathogen associated molecular patterns (PAMP) recognized by pattern recognition receptors (PRR) of the human immune system. In the central nervous system (CNS), detection of the cell envelope is critical to the course of bacterial meningitis, one of the most dreaded infectious diseases. *Streptococcus pneumoniae*, *Neisseria meningitidis*, and *Hemophilus influenzae* are the three classical pathogens associated with bacterial meningitis (McGill et al., 2016). PG from the cell envelopes elicit signs and symptoms ranging from drowsiness, fever, headache and neck stiffness to severe intracranial pressure and widespread neuronal death with permanent sequelae and an overall fatality rate between 20 and 30% (van de Beek et al., 2002; Christie et al., 2011). Patients are treated with bacteriolytic antibiotics that are required for cure but also cause the rapid release of highly reactive bacterial debris (Tuomanen et al., 1985a). These PG fragments and cell envelope polymers persist and continue to elicit the influx of leukocytes, brain edema, inflammatory cytokines, and neuronal death, causing further neurological damage.

Interactions between cell wall-PAMPs and PRRs go beyond acute infection. Throughout life, PG fragments are released from the microbiome and circulate in serum (Clarke et al., 2010; Molinaro et al., 2019). Upon access to the CNS these fragments can influence neuronal development (Humann et al., 2016) or contribute to neurodegeneration (Laman et al., 2020). Here, we will describe the molecular interactions between a broad array of cell envelope fragments with specific receptors in the CNS that contribute to a spectrum of responses from CNS homeostasis to acute or chronic inflammation.

BACTERIAL ENVELOPE PAMPs

For both Gram positive and negative bacteria, the network of PG is most notable for protecting bacteria against osmotic forces (Silhavy et al., 2010) and maintaining cell shape (Young, 2006). The PG is a highly conserved repeating disaccharide of N-acetylglucosamine (GlcNac) and N-acetylmuramic acid (MurNac) that forms long chains interconnected by cross-linked peptides of varied length (**Figure 1**). In Gram-positive bacteria, the entirety of the cell wall is composed of a thick ≈20-80 nm layer of PG that is covalently linked to wall teichoic acids (TA) and interlaced with membrane-bound lipoteichoic acids (LTA) (Skov Sorensen et al., 1988; Tomasz, 2000). The cell envelope of Gram-negative bacteria is composed of a thin 5–10 nm layer of PG covalently linked to lipoproteins and commonly co-mingled with outer membrane-bound lipopolysaccharide (LPS) (Matias and Beveridge, 2007). The bioactivities of PG, LTA, and LPS are unique for each pathogen as they are affected by small molecular adducts to the glycan backbone, variations in TAs and LPS, and by the detailed variability of the cross-links between invariant stem peptides. For this review, we will focus on the PG, LTA, and LPS as the main sources of bacteria-associated inflammation, and going forward, refer to these three structures as components of the cell envelope. When we refer to the PG, TA, or muropeptides, we will use the term cell wall.

Within the cell wall structure, LTA and LPS, the innate immune system recognizes PAMPs through PRRs that can signal downstream events to combat infection. The highly conserved PG presents PAMPs derived from fragments of muropeptides that are variations of GlcNac-MurNac- pentapeptides (**Figure 1**). PRRs distinguish between variations of the third residue of the pentapeptide: meso-diaminopmelic acid (m-DAP) for Gram-negatives and lysine for Gram-positives. The diversity of muropeptide structures is further generated by autolysins, such as peptidases, amidases, and glycosylases. There can be as many as 80 different muropeptides in a bacteria's PG network (Glauner, 1988; Burroughs et al., 1993b; Bui et al., 2012), each with variable ability to invoke a host immune response.

In addition to muropeptides, LPS, LTA and TA are recognized by PRRs (**Figure 1**). LPS has a tripartite structure: a lipid A anchor, core oligosaccharide, and O-antigen polysaccharide. Different bacteria produce structurally different LPSs that vary in immunostimulatory potency based on phosphorylation, length of oligosaccharides, and composition (Pridmore et al., 2003; Albiger et al., 2007). TAs are linked to the PG MurNac residue and are formed by repeats of ribitol phosphate or glycerol phosphate further decorated by D-alanine and/or sugar residues (Tomasz, 2000; Kang et al., 2016). Most Gram-positive organisms have starkly distinct LTA and TA. However, *S. pneumoniae* is unique because TA and LTA are not only identical, but also both are decorated with phosphorylcholine (ChoP) (Briles and Tomasz, 1973). The ChoP adduct, a decoration shared by the three common meningeal pathogens on their surfaces, mimics the chemokine platelet-activating factor (PAF) and thereby mediates binding of bacteria to the PAF receptor. This actively promotes trafficking of bacteria and cell surface fragments across epithelia and endothelia, including the blood brain barrier (BBB) (Cundell et al., 1995; Clark and Weiser, 2013). Localizing ChoP to TA makes the pneumococcal cell wall a unique PAF receptor ligand and adds to its distribution during infection and its bioactivities (Cundell et al., 1995).

PRRs FOR CELL ENVELOPE COMPONENTS

There is a wide range of PRR pathways that can be triggered by bacterial envelope components to induce a proinflammatory response within the CNS. The families of PRRs are broken down into Toll-Like receptors (TLRs), NOD-like receptors (NLRs), PG recognition proteins (PGLYRPs), and accessory co-receptors such as lipopolysaccharide-binding proteins (LBP, MD-2, and CD-14). While each PRR recognizes a subset of PAMPs, there is considerable plasticity in ligand recognition, which varies by body site and by the presence of various co-receptors (Li et al., 2013). Extracellular TLRs 1,2, 4, and 6 signal when ligands induce the formation of homo- or heterodimers. TLR2 generally recognizes Gram-positive components such as LTA, di- and tri-acylated lipoproteins and PG fragments. Discrimination of subtle differences in lipids of lipoproteins is conferred by dimerization with TLR1 or TLR6 and the transfer of ligands from the co-receptors CD14, CD36, or LBP (Yoshimura et al., 1999; Han et al., 2003; Hoebe et al., 2005; Akira et al., 2006; Jin et al., 2007). The crystal structures of TLR2/1 and 2/6 indicate direct binding to their preferred lipopeptide ligands (Jin et al., 2007). In contrast to TLR2, TLR4 is a homodimer that recognizes Gram-negative components such as LPS, usually in the presence of the co-receptors CD14, MD-2, and LBP (Medzhitov et al., 1997). This division between TLR2 and 4 is not absolute as Gram-negative muropeptides have been reported to bind TLR2 (Asong et al., 2009) and TLR4 co-receptors have been implicated in binding PG fragments and LTA, thereby expanding classical TLR2 ligands to TLR4 and vice versa (Dziarski et al., 1998; Weber et al., 2003a). The final result of TLR2 or 4 signaling is activation of NF-κB and production of inflammatory cytokines.

The cytoplasmic NOD receptors recognize muropeptides within the host cell. NOD1 recognizes the m-DAP portion of Gram-negative muropeptides (Girardin et al., 2003a), and NOD2 recognizes muropeptides with both m-DAP and lysine. The MurNac residue is dispensable for NOD1 activation, but is required for NOD2 activation and can be linked to either a dipeptide or tripeptide moiety (Girardin et al., 2003b). Unlike the TLRs, NLRs can trigger the expression of inflammatory and antimicrobial genes through the NF-κB and MAPK pathways (Mukherjee et al., 2019).

There are four PGLYRPs in human serum, and they each have a different high affinity for LPS, LTA, and PG muropeptides (Royet and Dziarski, 2007). Similar to the NODs, the PGLYRPs differentiate between muropeptides based on the third amino residue being m-DAP or lysine (Kumar et al., 2005). Interestingly, PGLYRP2 is the only PGLYRP with amidase activity that cleaves PG (Wang et al., 2003).

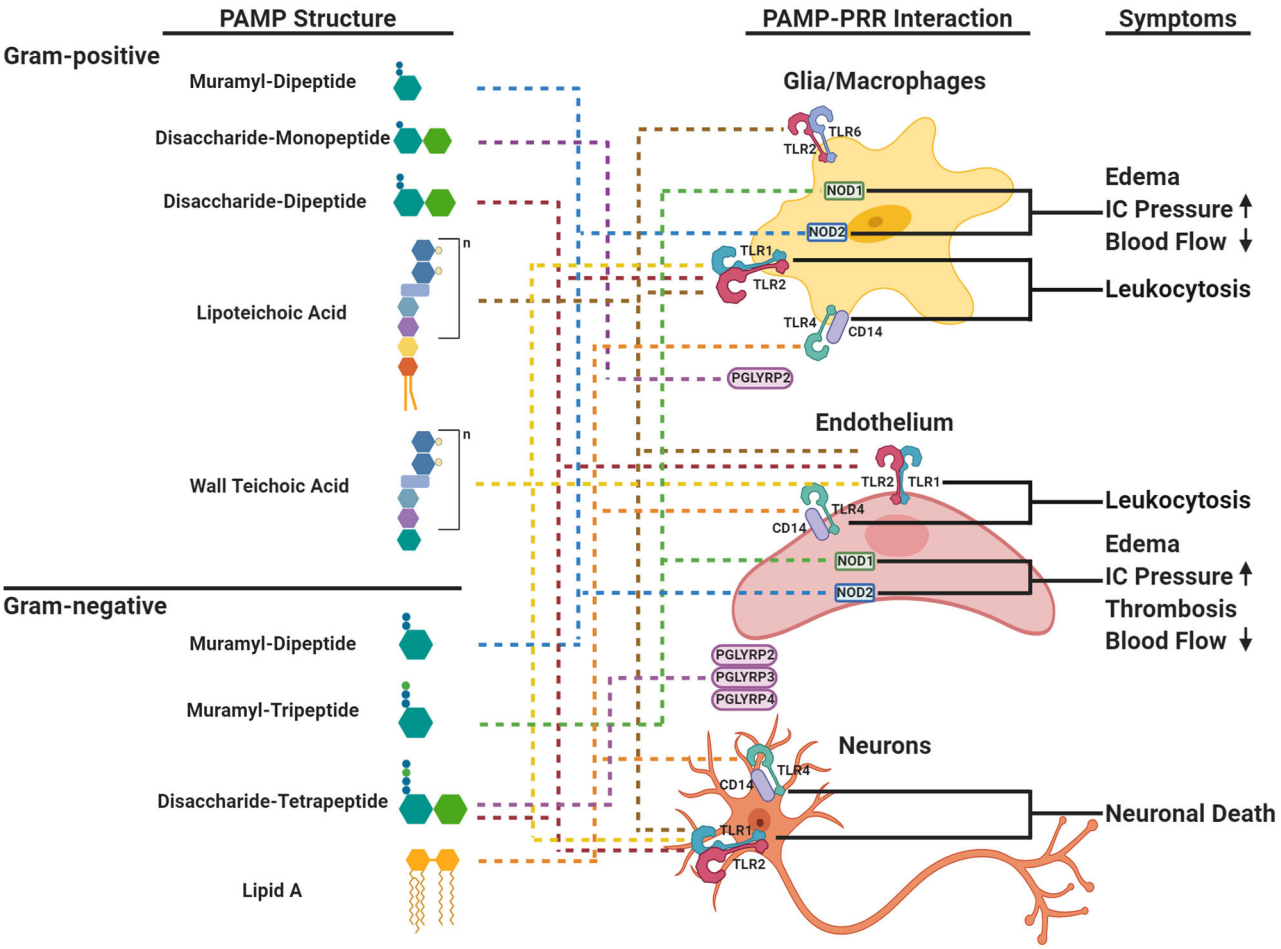

FIGURE 1 | Schematic representation of cell envelope bioactivities during acute bacterial meningitis. The cell envelope is composed of a peptidoglycan (PG) backbone that is decorated and intertwined with wall teichoic acid (TA) or lipoteichoic acid (LTA) in Gram-positive (top panel) and PG and the lipid A components of lipopolysaccharide (LPS) in Gram-negative bacteria (bottom panel), respectively. PAMPs within PG, LTA, or LPS are ligands to PRRs (TLRs, NODs, PGLYRPs shown on cells in right panel) in the brain that elicit distinct major symptoms (right panel) during acute bacterial meningitis. Each component is linked to its cognate PRR by dotted lines. TLR, Toll-like Receptor; NOD, Nucleotide-binding Oligomerization Domain-like Receptor; PGLYRP, Peptidoglycan Recognition Proteins; IC, Intracranial.

CELL ENVELOPE MODIFICATION TO AVOID PRR DETECTION

Pathogenic and commensal bacteria modify their PG to evade detection by the innate immune system. There are two strategies: modification of the glycan backbone (N-deacetylation, N-glycosylation, and acetylation) and modification to the stem peptides. For example, *S. pneumoniae* encodes Adr, O-acetyl transferase, and PgdA, acetylglucosamine deacetylase, that modify the C-6 position of the MurNac and the C-2 position of GlcNac, respectively (Vollmer and Tomasz, 2000; Crisostomo et al., 2006). These modifications prevent degradation by lysozyme and reduce recognition by NOD1 (Boneca et al., 2007). Certain bacteria contain L-ornithine instead of m-DAP in their stem peptides to avoid detection by the NLR family (Girardin et al., 2003b).

Modifications to the LPS, TA, and LTA contribute to immune dampening and avoidance. Meningococcus and *H. influenzae* shorten their O-antigens in LPS to dampen reactivity. To decrease susceptibility to antimicrobial peptides, ethanolamine, and aminoarabinose can be added to LPS (Guo et al., 1998) and D-alanyl can be added to TAs (Collins et al., 2002).

CELL ENVELOPE RELEASE: ANTIBIOTICS VS. NORMAL GROWTH

Cell envelope components are released into the cerebrospinal fluid (CSF) gradually during growth or rapidly during antibiotic-induced autolysis (Tuomanen et al., 1985a; Arditi et al., 1989; Woodhams et al., 2013; Gonzalez-Santana and Diaz Heijtz, 2020). All three meningeal pathogens are autolytic and therefore undergo rapid cell envelope release during stationary phase and during antibiotic therapy. β-lactam antibiotics, the first line of therapy for meningitis, inhibit PG synthetic enzymes and activate

autolysins that destabilize the cell wall network. The result is the release of an array of constituent muropeptides, TA, LTA, and LPS, each with different inflammatory bioactivities (Tuomanen et al., 1985b; Arditi et al., 1989; Burroughs et al., 1993a; Eng et al., 1993; Schneider et al., 1999; Woodhams et al., 2013). It is well-recognized that higher concentrations of PG and LPS in the CSF correlate with poor clinical outcome during meningitis (Arditi et al., 1989; Brandtzaeg et al., 1992; Schneider et al., 1999; Grandgirard et al., 2010).

Given that bactericidal antibiotics are required for curing meningitis and these drugs necessarily release a burst of cell envelope during autolysis, efforts to decrease the resultant neurological damage has focused on dampening the rapid increase in inflammation during the initial doses of antibiotics. In animal models and clinical trials, dexamethasone or non-steroidals, co-administered with the first dose of antibiotics, decrease inflammation and improve outcome (Tuomanen et al., 1987; Odio et al., 1991). Specifically, these measures reduce hearing loss, neurological sequelae and significantly reduce overall mortality (Brouwer et al., 2015; Rayanakorn et al., 2020).

RELATIVE SPECIFIC ACTIVITIES OF CELL ENVELOPE COMPONENTS

The cardinal signs of meningitis in the CSF are a high neutrophil count, protein accumulation associated with BBB permeability, increased intracranial pressure due to brain edema within the closed space of the skull, and low glucose as cerebral metabolism is compromised. Except for low glucose, all of these clinical signs can be recapitulated by infusion of specific cell envelope components into the CSF in animal models indicating that the cell envelope can be considered a library of bioactive PAMPs that together add up to the constellation of pathophysiology of meningitis (**Figure 1**). The specific activity of key bacterial surface components for inciting CSF inflammatory changes can be calculated (**Table 1**). The onset of bacterial seeding of the CSF from blood occurs at ∼10e5 bacteria/ml and rises to 10e7 bacteria/ml at symptomatic disease (Arditi et al., 1989). The cardinal signs of meningitis can be induced by intact *Hemophilus* or pneumococcus at ∼10e5 bacteria which represents 1 ng of LPS/PG or 10 ng LTA/PG-TA: protein influx at 2 h, leukocytosis at 4 h, and brain edema at 6 h post intracisternal injection (Tuomanen et al., 1985b; Burroughs et al., 1993a). More complex components sustain equal or greater activity at 24 h. Yet, each surface component exhibits a different dose response relationship depending on the pathophysiological sign (**Table 1**). For *Hemophilus*, LPS strongly invokes leukocytosis (threshold 10 ng/ml) while PG powerfully induces brain edema (threshold 1 ng/ml). The activity of PG is not affected by the presence of proteins, increases 10 fold if solubilized (autolysis product), and can vary by 2 fold depending on the stem peptide composition (Burroughs et al., 1992, 1993a). In contrast, for pneumococcus, LTA and TA specifically invoke leukocytosis (threshold 500 ng/ml) while multimeric disaccharide stem peptides (autolysis product) powerfully induce both leukocytosis and brain edema (threshold 100 ng/ml) (Tuomanen et al., 1985b; Tomasz and Saukkonen, 1989; Weber et al., 2003b). The disaccharide tetrapeptide, the most common PG building block, is most active for brain edema rather than leukocytosis. The high specific activity of free stem peptides for brain edema (threshold 1 ng/ml) is not due to any one super peptide. Specific bioactivities of the 1,6-anhydromuramyl peptide found at the end of glycan chains includes induction of slow-wave sleep (Krueger et al., 1984) and mitochondrial toxicity in ciliated cells, such as in the choroid plexus (Cookson et al., 1989). In summary, many subcomponents of cell envelopes are bioactive in the range of 10e5–10e7 bacterial equivalents, values found routinely in CSF during meningitis.

TABLE 1 | Threshold (ng/ml) for CNS bioactivity of bacterial components.

Component	Leukocytosis	Edema
Gram negative		
LPS + PG	5	5
LPS	10	100
PG	100	1
Gram positive		
LTA + PG	100	10
LTA	500	–
PG-TA w/stems	20	100
PG	100	–
Stem peptides	10,000	1
TA free	500	10,000

Compiled from: (Tuomanen et al., 1985a,b; Tomasz and Saukkonen, 1989; Burroughs et al., 1992, 1993a,b; Weber et al., 2003a,b).

PATHOPHYSIOLOGICAL HOST-CELL ENVELOPE MEDIATED INFLAMMATORY RESPONSES

PAMPs are detected and interpreted by PRRs on key CNS cells: cerebral capillary endothelial cells of the BBB, glia (microglia, astrocytes, and oligodendrocyte cells) as the resident equivalent of leukocytes, neurons, and incoming peripheral blood neutrophils. All of these cells express the full array of PRRs: TLRs, NODs, PGRPs, but the results of their activation are cell specific and ligand specific (Bsibsi et al., 2002).

Glia serve as sentinels and are essential in the early innate immune recognition of LPS, LTA, and muramyl-peptides via their cognate receptors: TLR4, TLR2, and NODs, respectively (Bsibsi et al., 2002; Olson and Miller, 2004; Liu et al., 2010). The TLR signaling pathways act through MyD88 to activate NF-κB resulting in production of proinflammatory cytokines such as TNF-α, IL-1, IL-6, and IL-8. IL-1 and TNF-α contribute to the production of vasoactive nitric oxide, which in turn increases intracranial pressure and reduces oxygen uptake (Suschek et al., 1993; Tureen, 1995). It is also important to recognize that TLRs are not always proinflammatory. In fact, cell wall induced TLR2-NOD2-RIPK2 signaling leads to the production of the

anti-inflammatory cytokine IL-10, which serves to shut down inflammation as infection resolves (Moreira et al., 2008).

Cerebral endothelial cells form tight junctional complexes that seal the BBB as a barrier from blood. Some small PG fragments, such as dipeptide D-Glu-mDAP and muramyl-dipeptide, are internalized and activate NF-κB through the NLR pathway amplifying the production of proinflammatory cytokines, chemokines (CCL2/3, CXCL1/8, and MIP-2), and prostaglandins (PGE2). These signaling molecules lead to the disruption of the BBB in conjunction with the recruitment of peripheral white blood cells. In bacterial meningitis, neutrophils comprise >90% of infiltrating leukocytes, and cause vasculitis, hemorrhage, and edema (Polfliet et al., 2001; Koedel et al., 2009). Prolonged leukocytosis increases the release of matrix metalloproteinases that degrade collagen IV and fibronectin, which are crucial components of the subendothelial basal lamina furthering the breakdown of the BBB (Lukes et al., 1999). Endothelial-derived tissue type plasminogen activator (tPA) leaks into the CSF, triggering thrombosis and a decrease in blood flow (Winkler et al., 2002). The presence of thrombin activates endothelial cells to produce PAF causing edema (Zimmerman et al., 1985).

Human neurons express TLR1, TLR2, TLR4, and CD14 for the recognition of LTA and the Lipid A portion of LPS (Acosta and Davies, 2008; Dzamko et al., 2017). Neuronal death through caspase-3 dependent apoptosis is driven by PG, LTA and LPS through proinflammatory cytokines (Mitchell et al., 2004). Neurons in the hippocampus, prefrontal cortex, and cerebellum highly express PGLYRP2 and NOD1 for the recognition and distinction of muropeptides from both Gram-positive and Gram-negative bacteria (Arentsen et al., 2017). PGLYRP2 binds to the bacterial cell wall to cleave the stem peptide, and activation of NOD1 causes the production of proinflammatory cytokines (IL-1β, TNF-α, IL-6) (Acarin et al., 2000).

HOST-CELL ENVELOPE INTERACTIONS IN CNS DEVELOPMENT AND NEURODEGENERATION

Although cell envelope PAMPs classically stimulate an acute inflammatory response, there is increasing recognition of their roles in modulating an array of non-inflammatory outcomes in the CNS, ranging from embryonic development to neurodegeneration. Muropeptides from the gut microbiome normally circulate constantly in serum (Clarke et al., 2010). Thus, there is ample opportunity for muropeptide/PRR interactions to occur without frank infection of the CNS. Furthermore, the gut microbiota communicates directly with the brain through the vagus nerve (Fulling et al., 2019), modulating the formation of the BBB (Braniste et al., 2014), and maturation of microglia (Erny et al., 2015).

Evidence implicates interactions of PRRs and cell envelope components in chronic neuroinflammation associated with neurodegeneration and behavioral abnormalities (Laman et al., 2020). Chronic, tonic signals from the microbiome are sensed by neurons and may exacerbate neurodegeneration. LPS can be found at high concentrations in the hippocampus and superior temporal lobe neocortex during Alzheimer's disease (Zhao et al., 2017). Loss of *nod1* and *nod2* severely decreases serotonin levels in the hippocampus and brainstem, which is associated with cognitive impairment and depressive-like behaviors (Pusceddu et al., 2019). Thus, bioactivities encoded in cell envelope components may incite a greater array of pathological processes than just simply acute inflammation during infection.

PRRs are expressed early in fetal development and are found on virtually all CNS cell types throughout life (Okun et al., 2010). Some PG-TA components generated during treatment of maternal infection are capable of crossing the placenta and entering the fetal brain where they alter neurodevelopment (Humann et al., 2016). Early in fetal development, interactions of PG-TA with neuronal TLRs silently induce overproliferation of neuronal progenitors leading to an abnormal increase in cell number in the neocortex in murine models (Humann et al., 2016). This aberrant architecture is permanent and associated with behavioral abnormalities after birth. Absence of PGLYRP2 is associated with altered expression of the brain-derived neurotrophic factor altering formation and regulation of neural circuits (Park and Poo, 2013; Arentsen et al., 2017; Eagleson et al., 2017). Thus, both the presence of excess PG-TA during early windows of development or the absence of PG sensors can lead to abnormal CNS development.

CONCLUSION

The bacterial cell envelope is a highly bioactive library of molecules driving the course of acute and chronic inflammation and perhaps emerging as modifiers of normal development. Each pathogen presents its own array of PRR ligands and thus builds its own pattern of disease. The CNS has a complete and diverse array of innate sensors to engage cell envelope subcomponents and respond with induction of signaling. It appears that timing is key to damage or benefit to outcome. Bursts of PRR-induced signaling are generally damaging while the low level, constant signaling produced by microbiome components, may serve as an ever present source of communication from peripheral organs to the CNS.

AUTHOR CONTRIBUTIONS

WM wrote the initial draft and ET reviewed the draft and wrote the final manuscript.

FUNDING

ET is supported by NIAID R01-128756 and ALSAC.

REFERENCES

Acarin, L., Gonzalez, B., and Castellano, B. (2000). Neuronal, astroglial and microglial cytokine expression after an excitotoxic lesion in the immature rat brain. *Eur. J. Neurosci.* 12, 3505–3520. doi: 10.1046/j.1460-9568.2000.00226.x

Acosta, C., and Davies, A. (2008). Bacterial lipopolysaccharide regulates nociceptin expression in sensory neurons. *J. Neurosci. Res.* 86, 1077–1086. doi: 10.1002/jnr.21565

Akira, S., Uematsu, S., and Takeuchi, O. (2006). Pathogen recognition and innate immunity. *Cell* 124, 783–801. doi: 10.1016/j.cell.2006.02.015

Albiger, B., Dahlberg, S., Henriques-Normark, B., and Normark, S. (2007). Role of the innate immune system in host defence against bacterial infections: focus on the toll-like receptors. *J. Intern. Med.* 261, 511–528. doi: 10.1111/j.1365-2796.2007.01821.x

Arditi, M., Ables, L., and Yogev, R. (1989). Cerebrospinal fluid endotoxin levels in children with H. *influenzae meningitis before and after administration of intravenous ceftrixone. J. Infect. Dis.* 160, 1005–1011. doi: 10.1093/infdis/160.6.1005

Arentsen, T., Qian, Y., Gkotzis, S., Femenia, T., Wang, T., Udekwu, K., et al. (2017). The bacterial peptidoglycan-sensing molecule Pglyrp2 modulates brain development and behavior. *Mol. Psychiatry* 22, 257–266. doi: 10.1038/mp.2016.182

Asong, J., Wolfert, M. A., Maiti, K. K., Miller, D., and Boons, G. J. (2009). Binding and cellular activation studies Rreveal that toll-like receptor 2 can differentially recognize peptidoglycan from gram-positive and gram-negative bacteria. *J. Biol. Chem.* 284, 8643–8653. doi: 10.1074/jbc.M806633200

Boneca, I. G., Dussurget, O., Cabanes, D., Nahori, M. A., Sousa, S., Lecuit, M., et al. (2007). A critical role for peptidoglycan N-deacetylation in *Listeria* evasion from the host innate immune system. *Proc. Natl. Acad. Sci. U.S.A.* 104, 997–1002. doi: 10.1073/pnas.0609672104

Brandtzaeg, P., Ovsteboo, R., and Kierulf, P. (1992). Compartmentalization of lipopolysaccharide production correlates with clinical presentation in meningococcal disease. *J Infect Dis.* 166, 650–652. doi: 10.1093/infdis/166.3.650

Braniste, V., Al-Asmakh, M., Kowal, C., Anuar, F., Abbaspour, A., Toth, M., et al. (2014). The gut microbiota influences blood-brain barrier permeability in mice. *Sci. Transl. Med.* 6:263ra158. doi: 10.1126/scitranslmed.3009759

Briles, E. B., and Tomasz, A. (1973). Pneumococcal Forssman antigen: a choline-containing lipoteichoic acid. *J. Biol. Chem.* 248, 6394–6397.

Brouwer, M. C., McIntyre, P., Prasad, K., and van de Beek, D. (2015). Corticosteroids for acute bacterial meningitis. *Cochrane Database Syst. Rev.* 2015:CD004405. doi: 10.1002/14651858.CD004405.pub5

Bsibsi, M., Ravid, R., Gveric, D., and van Noort, J. M. (2002). Broad expression of toll-like receptors in the human central nervous system. *J. Neuropathol. Exp. Neurol.* 61, 1013–1021. doi: 10.1093/jnen/61.11.1013

Bui, N. K., Eberhardt, A., Vollmer, D., Kern, T., Bougault, C., Tomasz, A., et al. (2012). Isolation and analysis of cell wall components from *Streptococcus pneumoniae*. *Anal. Biochem.* 421, 657–666. doi: 10.1016/j.ab.2011.11.026

Burroughs, M., Cabellos, C., Prasad, S., and Tuomanen, E. (1992). Bacterial components and the pathophysiology of injury to the blood-brain barrier: does cell wall add to the effects of endotoxin in gram-negative meningitis? *J. Infect. Dis.* 165 (Suppl. 1), S82–85. doi: 10.1093/infdis/165-Supplement_1-S82

Burroughs, M., Prasad, S., Cabellos, C., Mendelman, P. M., and Tuomanen, E. (1993a). The biologic activities of peptidoglycan in experimental *Haemophilus influenzae* meningitis. *J. Infect. Dis.* 167, 464–468. doi: 10.1093/infdis/167.2.464

Burroughs, M., Rozdzinski, E., Geelen, S., and Tuomanen, E. (1993b). A structure-activity relationship for induction of meningeal inflammation by muramyl peptides. *J. Clin. Invest.* 92, 297–302. doi: 10.1172/JCI116565

Christie, D., Viner, R. M., Knox, K., Coen, P. G., Wang, H., El Bashir, H., et al. (2011). Long-term outcomes of pneumococcal meningitis in childhood and adolescence. *Eur. J. Pediatr.* 170, 997–1006. doi: 10.1007/s00431-010-1390-5

Clark, S. E., and Weiser, J. N. (2013). Microbial modulation of host immunity with the small molecule phosphorylcholine. *Infect. Immun.* 81, 392–401. doi: 10.1128/IAI.01168-12

Clarke, T. B., Davis, K. M., Lysenko, E. S., Zhou, A. Y., Yu, Y., and Weiser, J. N. (2010). Recognition of peptidoglycan from the microbiota by Nod1 enhances systemic innate immunity. *Nat. Med.* 16, 228–231. doi: 10.1038/nm.2087

Collins, L. V., Kristian, S. A., Weidenmaier, C., Faigle, M., Van Kessel, K. P., Van Strijp, J. A., et al. (2002). *Staphylococcus aureus* strains lacking D-alanine modifications of teichoic acids are highly susceptible to human neutrophil killing and are virulence attenuated in mice. *J. Infect. Dis.* 186, 214–219. doi: 10.1086/341454

Cookson, B. T., Cho, H. L., Herwaldt, L. A., and Goldman, W. E. (1989). Biological activities and chemical composition of purified tracheal cytotoxin from *Bordetella pertussis*. *Infect. Immun.* 57, 2223–2229. doi: 10.1128/IAI.57.7.2223-2229.1989

Crisostomo, M. I., Vollmer, W., Kharat, A. S., Inhulsen, S., Gehre, F., Buckenmaier, S., et al. (2006). Attenuation of penicillin resistance in a peptidoglycan O-acetyl transferase mutant of *Streptococcus pneumoniae*. *Mol. Microbiol.* 61, 1497–1509. doi: 10.1111/j.1365-2958.2006.05340.x

Cundell, D. R., Gerard, N. P., Gerard, C., Idanpaan-Heikkila, I., and Tuomanen, E. I. (1995). *Streptococcus pneumoniae* anchor to activated human cells by the receptor for platelet-activating factor. *Nature* 377, 435–438. doi: 10.1038/377435a0

Dzamko, N., Gysbers, A., Perera, G., Bahar, A., Shankar, A., Gao, J., et al. (2017). Toll-like receptor 2 is increased in neurons in Parkinson's disease brain and may contribute to alpha-synuclein pathology. *Acta Neuropathol.* 133, 303–319. doi: 10.1007/s00401-016-1648-8

Dziarski, R., Tapping, R. I., and Tobias, P. S. (1998). Binding of bacterial peptidoglycan to CD14. *J. Biol. Chem.* 273, 8680–8690. doi: 10.1074/jbc.273.15.8680

Eagleson, K. L., Xie, Z., and Levitt, P. (2017). The pleiotropic MET receptor network: circuit development and the neural-medical interface of autism. *Biol. Psychiatry* 81, 424–433. doi: 10.1016/j.biopsych.2016.08.035

Eng, R. H., Smith, S. M., Fan-Havard, P., and Ogbara, T. (1993). Effect of antibiotics on endotoxin release from gram-negative bacteria. *Diagn. Microbiol. Infect. Dis.* 16, 185–189. doi: 10.1016/0732-8893(93)90109-K

Erny, D., Hrabe de Angelis, A. L., Jaitin, D., Wieghofer, P., Staszewski, O., David, E., et al. (2015). Host microbiota constantly control maturation and function of microglia in the CNS. *Nat. Neurosci.* 18, 965–977. doi: 10.1038/nn.4030

Fulling, C., Dinan, T. G., and Cryan, J. F. (2019). Gut microbe to brain signaling: what happens in vagus. *Neuron* 101, 998–1002. doi: 10.1016/j.neuron.2019.02.008

Girardin, S. E., Boneca, I. G., Carneiro, L. A., Antignac, A., Jehanno, M., Viala, J., et al. (2003a). Nod1 detects a unique muropeptide from gram-negative bacterial peptidoglycan. *Science* 300, 1584–1587. doi: 10.1126/science.1084677

Girardin, S. E., Travassos, L. H., Herve, M., Blanot, D., Boneca, I. G., Philpott, D. J., et al. (2003b). Peptidoglycan molecular requirements allowing detection by Nod1 and Nod2. *J. Biol. Chem.* 278, 41702–41708. doi: 10.1074/jbc.M307198200

Glauner, B. (1988). Separation and quantification of muropeptides with high-performance liquid chromatography. *Anal. Biochem.* 172, 451–464. doi: 10.1016/0003-2697(88)90468-X

Gonzalez-Santana, A., and Diaz Heijtz, R. (2020). Bacterial peptidoglycans from microbiota in neurodevelopment and behavior. *Trends Mol. Med.* 26, 729–743. doi: 10.1016/j.molmed.2020.05.003

Grandgirard, D., Oberson, K., Buhlmann, A., Gaumann, R., and Leib, S. L. (2010). Attenuation of cerebrospinal fluid inflammation by the nonbacteriolytic antibiotic daptomycin versus that by ceftriaxone in experimental pneumococcal meningitis. *Antimicrob. Agents Chemother.* 54, 1323–1326. doi: 10.1128/AAC.00812-09

Guo, L., Lim, K. B., Poduje, C. M., Daniel, M., Gunn, J. S., Hackett, M., et al. (1998). Lipid A acylation and bacterial resistance against vertebrate antimicrobial peptides. *Cell* 95, 189–198. doi: 10.1016/S0092-8674(00)81750-X

Han, S. H., Kim, J. H., Martin, M., Michalek, S., and Nahm, M. H. (2003). Pneumococcal lipoteichoic acid (LTA) is not as potent as staphylococcal LTA in stimulating toll-like receptor 2. *Infect. Immun.* 71, 5541–5548. doi: 10.1128/IAI.71.10.5541-5548.2003

Hoebe, K., Georgel, P., Rutschmann, S., Du, X., Mudd, S., Crozat, K., et al. (2005). CD36 is a sensor for diacylglycerides. *Nature* 433, 523–527. doi: 10.1038/nature03253

Humann, J., Mann, B., Gao, G., Moresco, P., Ramahi, J., Loh, L. N., et al. (2016). Bacterial peptidoglycan traverses the placenta to induce fetal neuroproliferation and aberrant postnatal behavior. *Cell Host Microbe* 19, 388–399. doi: 10.1016/j.chom.2016.05.017

Jin, M. S., Kim, S. E., Heo, J. Y., Lee, M. E., Kim, H. M., Paik, S.-G., et al. (2007). Crystal structure of the TLR1-TLR2 heterodimer induced by binding tri-acylated lipopeptide. *Cell* 130, 1071–1082. doi: 10.1016/j.cell.2007.09.008

Kang, S.-S., Sim, J.-R., Yun, C.-H., and Han, S. H. (2016). Lipoteichoic acids as a major virulence factor causing inflammatory responses via toll-like receptor 2. *Arch. Pharm. Res.* 39, 1519–1529. doi: 10.1007/s12272-016-0804-y

Koedel, U., Frankenberg, T., Kirschnek, S., Obermaier, B., Hacker, H., Paul, R., et al. (2009). Apoptosis is essential for neutrophil functional shutdown and determines tissue damage in experimental pneumococcal meningitis. *PLoS Pathog* 5:e1000461. doi: 10.1371/journal.ppat.1000461

Krueger, J. M., Walter, J., Karnovsky, M. L., Chedid, L., Choay, J. P., Lefrancier, P., et al. (1984). Muramyl peptides. *Variation of somnogenic activity with structure. J. Exp. Med.* 159, 68–76. doi: 10.1084/jem.159.1.68

Kumar, S., Roychowdhury, A., Ember, B., Wang, Q., Guan, R., Mariuzza, R. A., et al. (2005). Selective recognition of synthetic lysine and meso-diaminopimelic acid-type peptidoglycan fragments by human peptidoglycan recognition proteins I{alpha} and S. *J. Biol. Chem.* 280, 37005–37012. doi: 10.1074/jbc.M506385200

Laman, J. D., t'Hart, B. A., Power, C., and Dziarski, R. (2020). Bacterial peptidoglycan as a driver of chronic brain inflammation. *Trends Mol. Med.* 26, 670–682. doi: 10.1016/j.molmed.2019.11.006

Li, J., Lee, D. S., and Madrenas, J. (2013). Evolving bacterial envelopes and plasticity of TLR2-dependent responses: basic research and translational opportunities. *Front. Immunol.* 4:347. doi: 10.3389/fimmu.2013.00347

Liu, X., Chauhan, V. S., Young, A. B., and Marriott, I. (2010). NOD2 mediates inflammatory responses of primary murine glia to Streptococcus pneumoniae. *Glia* 58, 839–847. doi: 10.1002/glia.20968

Lukes, A., Mun-Bryce, S., Lukes, M., and Rosenberg, G.A. (1999). Extracellular matrix degradation by metalloproteinases and central nervous system diseases. *Mol Neurobiol.* 19, 267–284. doi: 10.1007/BF02821717

Matias, V. R., and Beveridge, T. J. (2007). Cryo-electron microscopy of cell division in *Staphylococcus aureus* reveals a mid-zone between nascent cross walls. *Mol. Microbiol.* 64, 195–206. doi: 10.1111/j.1365-2958.2007.05634.x

McGill, F., Heyderman, R. S., Michael, B. D., Defres, S., Beeching, N. J., Borrow, R., et al. (2016). The UK joint specialist societies guideline on the diagnosis and management of acute meningitis and meningococcal sepsis in immunocompetent adults. *J. Infect.* 72, 405–438. doi: 10.1016/j.jinf.2016.01.007

Medzhitov, R., Preston-Hurlburt, P., and Janeway, C. A. Jr. (1997). A human homologue of the drosophila toll protein signals activation of adaptive immunity. *Nature* 388, 394–397. doi: 10.1038/41131

Mitchell, L., Smith, S. H., Braun, J. S., Herzog, K. H., Weber, J. R., and Tuomanen, E. I. (2004). Dual phases of apoptosis in pneumococcal meningitis. *J. Infect. Dis.* 190, 2039–2046. doi: 10.1086/425520

Molinaro, R., Mukherjee, T., Flick, R., Philpott, D. J., and Girardin, S. E. (2019). Trace levels of peptidoglycan in serum underlie the NOD-dependent cytokine response to endoplasmic reticulum stress. *J. Biol. Chem.* 294, 9007–9015. doi: 10.1074/jbc.RA119.007997

Moreira, L. O., El Kasmi, K. C., Smith, A. M., Finkestein, D., Fillon, S., Kim, Y.-G., et al. (2008). The TLR2-HyD-88-Nod2-RipK2 signalling axis regulates a balanced proinflammatory and IL-10 mediated antiinflammatory cytokine response to gram positive cell walls. *Cell. Microbiol.* 10, 2067–2077. doi: 10.1111/j.1462-5822.2008.01189.x

Mukherjee, T., Hovingh, E. S., Foerster, E. G., Abdel-Nour, M., Philpott, D. J., and Girardin, S. E. (2019). NOD1 and NOD2 in inflammation, immunity and disease. *Arch. Biochem. Biophys.* 670, 69–81. doi: 10.1016/j.abb.2018.12.022

Odio, C. M., Faingezicht, I., Paris, M., Nassar, M., Baltodano, A., Rogers, J., et al. (1991). The beneficail effects of early dexamethasone administration in infants and children with bacterial meningitis. *N. Engl. J. Med.* 324, 1525–1531. doi: 10.1056/NEJM199105303242201

Okun, E., Griffioen, K. J., Son, T. G., Lee, J. H., Roberts, N. J., Mughal, M. R., et al. (2010). TLR2 activation inhibits embryonic neural progenitor cell proliferation. *J. Neurochem.* 114, 462–474. doi: 10.1111/j.1471-4159.2010.06778.x

Olson, J. K., and Miller, S. D. (2004). Microglia initiate central nervous system innate and adaptive immune responses through multiple TLRs. *J. Immunol.* 173, 3916–3924. doi: 10.4049/jimmunol.173.6.3916

Park, H., and Poo, M. M. (2013). Neurotrophin regulation of neural circuit development and function. *Nat. Rev. Neurosci.* 14, 7–23. doi: 10.1038/nrn3379

Polfliet, M. M., Zwijnenburg, P. J., van Furth, A. M., van der Poll, T., Dopp, E. A., Renardel de Lavalette, C., et al. (2001). Meningeal and perivascular macrophages of the central nervous system play a protective role during bacterial meningitis. *J. Immunol.* 167, 4644–4650. doi: 10.4049/jimmunol.167.8.4644

Pridmore, A. C., Jarvis, G. A., John, C. M., Jack, D. L., Dower, S. K., and Read, R. C. (2003). Activation of toll-like receptor 2 (TLR2) and TLR4/MD2 by *Neisseria* is independent of capsule and lipooligosaccharide (LOS) sialylation but varies widely among LOS from different strains. *Infect. Immun.* 71, 3901–3908. doi: 10.1128/IAI.71.7.3901-3908.2003

Pusceddu, M. M., Barboza, M., Keogh, C. E., Schneider, M., Stokes, P., Sladek, J. A., et al. (2019). Nod-like receptors are critical for gut-brain axis signaling in mice. *J. Physiol.* 597, 5777–5797. doi: 10.1113/JP278640

Rayanakorn, A., Ser, H. L., Pusparajah, P., Chan, K. G., Goh, B. H., Khan, T. M., et al. (2020). Comparative efficacy of antibiotic(s) alone or in combination of corticosteroids in adults with acute bacterial meningitis: a systematic review and network meta-analysis. *PLoS ONE* 15:e0232947. doi: 10.1371/journal.pone.0232947

Royet, J., and Dziarski, R. (2007). Peptidoglycan recognition proteins: pleiotropic sensors and effectors of antimicrobial defences. *Nat. Rev. Microbiol.* 5, 264–277. doi: 10.1038/nrmicro1620

Schneider, O., Michel, U., Zysk, G., Dubuis, O., and Nau, R. (1999). Clinical outcome in pneumococcal meningitis correlates with CSF lipoteichoic acid concentrations. *Neurology* 53, 1584–1587. doi: 10.1212/WNL.53.7.1584

Silhavy, T. J., Kahne, D., and Walker, S. (2010). The bacterial cell envelope. *Cold Spring Harb. Perspect. Biol.* 2:a000414. doi: 10.1101/cshperspect.a000414

Skov Sorensen, U. B., Blom, J., Birch-Andersen, A., and Henrichsen, J. (1988). Ultrastructural localization of capsules, cell wall polysaccharide, cell wall proteins, and F antigen in pneumococci. *Infect. Immun.* 56, 1890–1896. doi: 10.1128/IAI.56.8.1890-1896.1988

Suschek, C., Rothe, H., Fehsel, K., Enczmann, J., and Kolb-Bachofen, V. (1993). Induction of a macrophage-like nitric oxide synthase in cultured rat aortic endothelial cells. IL-1 beta-mediated induction regulated by tumor necrosis factor-alpha and IFN-gamma. *J. Immunol.* 151, 3283–3291.

Tomasz, A. (2000). "Streptococcus pneumoniae: functional anatomy," in *Streptococcus Pneumoniae: Molecular Biology and Mechanisms of Disease*, ed. *A. Tomasz. (New York, NY: Mary Ann Liebert, Inc.)*, 9–21.

Tomasz, A., and Saukkonen, K. (1989). The nature of cell wall-derived inflammatory components of pneumococci. *Ped. Infect. Dis. J.* 8, 902–903. doi: 10.1097/00006454-198912000-00034

Tuomanen, E., Hengstler, B., Rich, R., Bray, M. A., Zak, O., and Tomasz, A. (1987). Nonsteroidal antiinflammatory agents in the therapy for experimental pneumococcal meningitis. *J. Infect. Dis.* 155, 985–990. doi: 10.1093/infdis/155.5.985

Tuomanen, E., Liu, H., Hengstler, B., Zak, O., and Tomasz, A. (1985a). The induction of meningeal inflammation by components of the pneumococcal cell wall. *J. Infect. Dis.* 151, 859–868. doi: 10.1093/infdis/151.5.859

Tuomanen, E., Tomasz, A., Hengstler, B., and Zak, O. (1985b). The relative role of bacterial cell wall and capsule in the induction of inflammation in pneumococcal meningitis. *J. Infect. Dis.* 151, 535–540. doi: 10.1093/infdis/151.3.535

Tureen, J. (1995). Effect of recombinant human tumor necrosis factor-alpha on cerebral oxygen uptake, cerebrospinal fluid lactate, and cerebral blood flow in the rabbit: role of nitric oxide. *J. Clin. Invest.* 95, 1086–1091. doi: 10.1172/JCI117755

van de Beek, D., Schmand, B., de Gans, J., Weisfelt, M., Vaessen, H., Dankert, J., et al. (2002). Cognitive impairment in adults with good recovery after bacterial meningitis. *J. Infect. Dis.* 186, 1047–1052. doi: 10.1086/344229

Vollmer, W., and Tomasz, A. (2000). The *pgdA* gene encodes for a peptidoglycan N-acetylglucosamine deacetylase in *Streptococcus pneumoniae*. *J. Biol. Chem.* 275, 20496–20501. doi: 10.1074/jbc.M910189199

Wang, Z. M., Li, X., Cocklin, R. R., Wang, M., Wang, M., Fukase, K., et al. (2003). Human peptidoglycan recognition protein-L is an N-acetylmuramoyl-L-alanine amidase. *J. Biol. Chem.* 278, 49044–49052. doi: 10.1074/jbc.M307758200

Weber, J. R., Freyer, D., Alexander, C., Schroder, N. W., Reiss, A., Kuster, C., et al. (2003a). Recognition of pneumococcal peptidoglycan: an

expanded, pivotal role for LPS binding protein. *Immunity* 19, 269–279. doi: 10.1016/S1074-7613(03)00205-X

Weber, J. R., Moreillon, P., and Tuomanen, E. I. (2003b). Innate sensors for gram-positive bacteria. *Curr. Op. Immunol.* 15, 408–415. doi: 10.1016/S0952-7915(03)00078-5

Winkler, F., Kastenbauer, S., Koedel, U., and Pfister, H. W. (2002). Increased serum concentrations of tissue plasminogen activator correlate with an adverse clinical outcome in patients with bacterial meningitis. *J. Neurol. Neurosurg. Psychiatry* 73:456. doi: 10.1136/jnnp.73.4.456

Woodhams, K. L., Chan, J. M., Lenz, J. D., Hackett, K. T., and Dillard, J. P. (2013). Peptidoglycan fragment release from *Neisseria meningitidis*. *Infect. Immun.* 81, 3490–3498. doi: 10.1128/IAI.00279-13

Yoshimura, A., Lien, E., Ingalls, R. R., Tuomanen, E., Dziarski, R., and Golenbock, D. (1999). Cutting edge: recognition of Gram-positive bacterial cell wall components by the innate immune system occurs via toll-like receptor 2. *J. Immunol.* 163, 1–5.

Young, K. D. (2006). The selective value of bacterial shape. *Microbio.l Mol. Biol. Rev.* 70, 660–703. doi: 10.1128/MMBR.00001-06

Zhao, Y., Jaber, V., and Lukiw, W. J. (2017). Secretory products of the human GI tract microbiome and their potential impact on Alzheimer's disease (AD): detection of Llpopolysaccharide (LPS) in AD hippocampus. *Front. Cell. Infect. Microbiol.* 7:318. doi: 10.3389/fcimb.2017.00318

Zimmerman, G. A., McIntyre, T. M., and Prescott, S. M. (1985). Thrombin stimulates the adherence of neutrophils to human endothelial cells *in vitro*. *J. Clin. Invest.* 76, 2235–2246. doi: 10.1172/JCI1 12232

Disclaimer: The content is solely the responsibility of the authors and does not necessarily represent the official views of the National Institutes of Health.

Conflict of Interest: The authors declare that the research was conducted in the absence of any commercial or financial relationships that could be construed as a potential conflict of interest.

frontiers in Cellular and Infection Microbiology

ORIGINAL RESEARCH
published: 30 October 2020
doi: 10.3389/fcimb.2020.590657

Pathogenic Differences of Type 1 Restriction-Modification Allele Variants in Experimental *Listeria monocytogenes* Meningitis

Florian R. Zbinden[1‡], Megan De Ste Croix[2‡], Denis Grandgirard[1], Richard D. Haigh[2], Irene Vacca[2], Roxana Zamudio[2], Emily C. A. Goodall[2], Roger Stephan[3], Marco R. Oggioni[2†] and Stephen L. Leib[1†]*

[1] Neuroinfection Laboratory, Institute for Infectious Diseases, University of Bern, Bern, Switzerland, [2] Department of Genetics and Genome Biology, University of Leicester, Leicester, United Kingdom, [3] Institute for Food Safety and Hygiene, Vetsuisse Faculty, University of Zurich, Zurich, Switzerland

OPEN ACCESS

Edited by:
Federico Iovino,
Karolinska Institutet (KI), Sweden

Reviewed by:
Vijayasree V. Giridharan,
University of Texas Health Science Center at Houston, United States
Matthijs Brouwer,
Amsterdam University Medical Center, Netherlands

***Correspondence:**
Stephen L. Leib
stephen.leib@ifik.unibe.ch

[†] These authors have contributed equally to this work

[‡] These authors share first authorship

Specialty section:
This article was submitted to Bacteria and Host, a section of the journal Frontiers in Cellular and Infection Microbiology

Received: 02 August 2020
Accepted: 25 September 2020
Published: 30 October 2020

Citation:
Zbinden FR, De Ste Croix M, Grandgirard D, Haigh RD, Vacca I, Zamudio R, Goodall ECA, Stephan R, Oggioni MR and Leib SL (2020) Pathogenic Differences of Type 1 Restriction-Modification Allele Variants in Experimental Listeria monocytogenes Meningitis. Front. Cell. Infect. Microbiol. 10:590657. doi: 10.3389/fcimb.2020.590657

Background: *L. monocytogenes* meningoencephalitis has a mortality rate of up to 50% and neurofunctional sequelae are common. Type I restriction-modification systems (RMS) are capable of adding methyl groups to the host genome. Some contain multiple sequence recognition (*hsdS*) genes that recombine, resulting in distinct DNA methylation patterns and patterns of gene expression. These phenotypic switches have been linked to virulence and have recently been discovered in multiple clonal complexes of *L. monocytogenes*. In the present study, we investigated the significant of RMS on *L. monocytogenes* virulence during the acute phase of experimental meningitis.

Methods: *L. monocytogenes* strains containing RMS systems were identified, and purified clones enriched for single *hsdS* alleles were isolated. *In vivo*, 11-day old Wistar rats were infected with an inoculum containing (a) one of 4 single RMS allele variants (A, B, C, D) treated with amoxicillin (AMX 50 mg/kg/dosis, q8h), (b) a mixture of all 4 variants with or without AMX treatment, or (c) different mixtures of 2 RMS allele variants. At selected time points after infection, clinical and inflammatory parameters, bacterial titers and brain damage were determined. Changes in the relative frequency of the occurring RMS alleles in the inoculum and in CSF or cerebellum of infected animals were analyzed by capillary electrophoresis.

Results: We have identified a phase variable RMS locus within *L. monocytogenes* CC4 and generated stocks that stably expressed each of the possible *hsdS* genes within that loci. Generation of these allele variants (A, B, C, D) allowed us to determine the methylation pattern associated with each *hsdS* through SMRT sequencing. *In vivo* infections with these single allele variants revealed differences in disease severity in that C induced the worst clinical outcome and more pronounced hippocampal apoptosis; D showed the most pronounced weight loss and the highest bacterial titer in the cerebellum. A caused the least severe disease.

Conclusion: We identified that *L. monocytogenes* expressing *hsdS* (A) causes less damage than when other *hsdS* genes are expressed. While expression of *hsdSC* and

D worsened the outcome in *L. monocytogenes* meningitis. We also demonstrate a competitive advantage of variants C and B over variant A in this model. Phenotypical switching may therefore represent a mechanism of virulence regulation during the acute phase of CNS infections with *L. monocytogenes*.

Keywords: listeria monocytogenes (*L. monocytogenes*), meningoencephalitis, restriction modification systems, pathogenesis, inflammation, brain damage, neurolisteriosis

INTRODUCTION

Listeria monocytogenes, a gram-positive facultative intracellular bacterium is a ubiquitous pathogen able to cause infections of the central nervous system (CNS), bacteremia involving the spleen and the liver, and localized gastrointestinal symptoms (Disson and Lecuit, 2012). Listeriosis primarily affects immunocompromised adults, the elderly and pregnant women via a foodborne infection route with high mortality rates of up to 50% (Yildiz et al., 2007; de Noordhout et al., 2014; Koopmans et al., 2017). In around 30% of the cases, listeriosis develops into bacterial meningitis and meningoencephalitis (Charlier et al., 2017). After *Streptococcus pneumoniae* and *Neisseria meningitidis*, *Listeria monocytogenes is* the third most common causative pathogen in meningitis/meningoencephalitis in around 5% of all cases (Koopmans et al., 2013).

Infections of the CNS by *L. monocytogenes* cause neurological sequela like epilepsy, hydrocephalus, strokes, severe intellectual disability and motor impairment (Kasanmoentalib et al., 2010; de Noordhout et al., 2014). In up to 18% of the patients, sequelae are still present 3 months after infection (Pelegrin et al., 2014). In neonates with a CNS infection, 44% developed neurological sequelae (de Noordhout et al., 2014). Complications like hydrocephalus occur in 28% percent of the cases (Hsieh et al., 2009) and is a risk factor for higher mortality (Pelegrin et al., 2014). Children are especially affected by long term disabilities. After 5 years 44% of all cases of neonatal neurolisteriosis still showed sequelae (Bedford et al., 2001).

The overshooting immunoreaction of the central nervous system (CNS) is an important driver in the pathophysiology of bacterial meningitis/meningoencephalitis and leads to poor outcome (Agyeman et al., 2014). Adults show a severe meningeal inflammation with a monocytic and granulocytic infiltration. Ventriculitis is frequently encountered and, often the periventricular tissue is being invaded. Commonly, *L. monocytogenes* meningitis leads to micro-abscesses. Those occur in proximity of the ventricles or perivascular spaces. Further the infection with *L. monocytogenes* leads to subendothelial inflammation of the meningeal arteries. Small vessel in the parenchyma show thrombosis and parenchymal bleedings (Engelen-Lee et al., 2018). The hippocampal formation of patients dying in association with bacterial meningitis show neuronal apoptosis of the granular layer in the dentate gyrus (Nau et al., 1999). This is also true in experimental models (Leib et al., 1996; Bifrare et al., 2003; Grandgirard et al., 2007b). The hippocampus is important for spatial and verbal learning and memory and damage within it leads to learning and memory impairment consecutive to bacterial meningitis (Nau et al., 1999; Wellmer et al., 2000; Loeffler et al., 2001; Leib et al., 2003).

The current therapy for listeria meningitis consists of amoxicillin, ampicillin or penicillin G. A duration of 21 days or longer is recommended, however there is no empiric data on an optimal treatment duration (Tunkel et al., 2004; van de Beek et al., 2016; Pagliano et al., 2017).

Phase-variation (PV), a rapid and reversible process, allows bacteria to diversify within populations and quickly adapt to changing environmental conditions. This is a mechanism with the potential to explain the ability of certain species, lineages or clones of pathogenic bacteria to be more successful in causing disease (Srikhanta et al., 2005; De Ste Croix et al., 2017, 2020a). PV DNA methylation systems have been proposed as one mechanism which could allow global gene expression changes through alternate methylation of the genome (Srikhanta et al., 2005; Manso et al., 2014). PV type I restriction modification systems (RMS) have been implicated in species such as *S. pneumoniae* (Manso et al., 2014; Li et al., 2016; Kwun et al., 2018; De Ste Croix et al., 2019, 2020b), *Streptococcus suis* (Atack et al., 2018), *Mycoplasma pulmonis* (Sitaraman et al., 2002) and *L. monocytogenes* (Fagerlund et al., 2016) as potential epigenetic regulators of bacterial virulence. In *L. monocytogenes*, as in many other bacterial species, RMS tend to be specific to the accessory genome of single phylogenetic units such as sequence type or clonal complex (Chen et al., 2017; De Ste Croix et al., 2017; Lee et al., 2019; Zamudio et al., 2020). Previously a PV type I RMS was described in *L. monocytogenes* lineage II sequence type 8 (ST8) isolates of food and human origin (Fagerlund et al., 2016). We identified a related phase variable type I RMS in *L. monocytogenes* lineage I ST4.

The aim of this work was to isolate strains stably expressing each of the PV *hsdS* genes of this type I RMS and characterize the associated methylome changes and their potential effects on disease associated phenotypes in an established infant rat model of experimental meningitis/neurolisteriosis.

MATERIALS AND METHODS

Bacterial Strains, Growth Conditions, and Growth Curves

L. monocytogenes isolates of sequence type 4 (ST4) were clinical isolates from the Institute of Infectious Diseases in Bern and blood culture isolates collected by the National Reference Laboratory for Enteropathogenic Bacteria and Listeria (NENT)

TABLE 1 | *L. monocytogenes* strains used in this study.

Strain	Origin	Source	Type	ST	Accession	
2250248	Bern	CSF	4b	4	JACBGT000000000	This work
N12-0320	Zurich	Blood	4b	4	NZ_QYGX00000000.1	Althaus et al., 2014
N12-0794	Zurich	Blood	4b	4	NZ_QYGH00000000.1	Althaus et al., 2014
N13-0772	Zurich	Blood	4b	4	NZ_QYEK00000000.1	Althaus et al., 2014

in Zürich (**Table 1**). Bacterial strains were grown at 37°C on brain heat infusion (BHI) agar plates or in BHI broth (Thermo Fisher Scientific, UK). Wildtype (wt) clones of *L. monocytogenes* N12-320 stably expressing a single RMS *hsdS* allele were generated. These clones were generated through the passaging of single colony isolates on BHI agar at 37°C, followed by PCR analysis of the *hsdS* locus using primers WRT3 and WRT4 as described below. For each *hsdS* allele 3 clones were independently generated and named A1-3, B1-3, C1-3, and D1-3. Each of these clones is a wt isolate capable of recombination within the RM system locus, however it is significantly enriched (>90%) for a single *hsdS* allele. Stable *hsdS* expressing clones were also generated in the CC4 strains 2250248 and N12-0794.

Clones enriched for a single *hsdS* allele, from strain N12-0320, were used to confirm that all strains showed a similar growth rate *in vitro*. Strains were plated on BHI agar (Oxoid, UK) and incubated overnight at 37°C. For each strain a sweep of colonies was resuspended in BHI broth to an OD600 of ∼0.4. An additional 25% mix containing A1, B1, C1, and D1 was generated by pooling strains in equal proportions by OD. Each sweep was then diluted 1:100 in fresh BHI broth. 200 ul per strain per replicate was aliquoted into a sterile, flat-bottomed, 96 well-plate (Thermo Fisher Scientific, UK) and sealed with a Breathe-Easy membrane (SigmaAldrich, UK). Growth was measured for 24 h in an Eon Biotek plate reader (Biotek, UK) at 37°C. Growth curve data was plotted using ggplot2 in R/4.0.2. Data from independent strains (e.g. A1, A2, A3) were used to generate error bars.

Molecular Analysis

SMRT Sequencing

We determined the complete genome of *L. monocytogenes* N12-0794 *hsdSA* and N12-0794 *hsdSC* using single-molecule, real-time (SMRT) sequencing. In short DNA was prepared from exponential phase (OD0.4) cultures using the Zymo Clean & Concentrator DNA kit (Cambio, UK) and the manufacturers protocol. Sequencing libraries were prepared according to the manufacturer's instructions and sequenced on the PacBio Sequel II instrument. Genomes were assembled *de novo* and reads were analyzed for methylation patterns using SMRT analysis software (available from Pacific Biosciences). Analysis was conducted on CLIMB (Cloud Infrastructure for Microbial Bioinformatics) (Connor et al., 2016).

GeneScan of *hsdS* Alleles in Recovered Samples

Bacterial colonies obtained from intra-cisternal infections of Wistar Rat pups were analyzed for *hsdS* expression and compared to the initial inoculating dose. To ensure only live bacteria were analyzed all samples were plated on BHI agar and incubated at 37°C overnight. All bacterial growth was collected and used for PCR amplification of the phase variable region of interest with a FAM labeled primer (WRT4 5′-[6FAM]CCAGTAATCCGGTTT AAAGGC) and primer WRT3 (5′-CCAAGCGAATCTGTA GCCC) (Sigma, UK). Following successful PCR amplification of the phase variable region of interest, samples were digested using EcoRV (NEB, UK), giving a unique fragment size for each variant when in the active *hsdS* position (allele A 780, B 727, C 705, and D 756 bp). Fragment size analysis of FAM labeled, digested PCR products was done on an ABI Prism DNA sequencer using the LIZ1200 size standard (Thermo Fischer Scientific, UK). Size analysis of each labeled fragment was run in Peak Scanner v1.0 (Thermo Fisher, UK). For homogenized organs 20 ul was plated and for CSF samples (due to the small sample volume) 10 ul was plated. A minimum of 10 colonies were required for analysis to ensure samples were representative, samples with < 10 colonies were not analyzed further. The initial inoculum for each experiment was also analyzed by plating and PCR of the recovered colonies. If two attempts to PCR amplify the locus of interest failed the sample was excluded from further study.

Phylogenetic Analysis

As we previously described, the core-genome phylogenetic tree for our Swiss isolates was build based on 1,596 core genes, which represent 93.8% of the well-defined cgMLST scheme (Zamudio et al., 2020). Gene markers for phase variable Modification Restriction systems (pv-MRS) were identified in our 160 Swiss isolates by using BLASTn with 100% coverage and 98% identity. The gene presence/absence matrix was mapped into the phylogenetic tree using the ggtree R package v1.15 (Yu et al., 2017).

Bacteria Preparation for *in vivo* Infections

Clones enriched for a single *hsdS* allele, isolated from the strain N12-0320, were used in all *in vivo* experiments. The bacteria stored at −80°C on ceramic beads were stroked on Columbia sheep blood agar and incubated overnight at 30°C. Single colonies were picked up and grown at 30°C in prewarmed brain heart infusion broth (BHI) for 18 h, under static conditions. After that, bacteria were pelleted at 1,560 rcf (Heraeus Biofuge Fresco, Thermo Fischer Scientific, Waltham, Massachusetts, US) for 10 min at 4°C. The pellet was resuspended in sterile NaCl 0.85%. This procedure was repeated twice. The resuspended bacterial preparation was diluted in sterile NaCl 0.85% and adjusted to the desired concentration by measuring the optical density at 570 nm. Inoculum size accuracy was checked by quantitative culture on blood agar plates. For *in vivo* experiments, 10 μl of the suspension were injected intracisternally.

Experimental Model of Neurolisteriosis

All animal studies were approved by the Animal Care and Experimentation Committee of the Canton of Bern, Switzerland (license no. BE 1/18). The model used in the present study was previously established in our group (Michelet et al., 1999; Remer et al., 2001). Per experiment 14 eleven-day old rat pups of mixed sex and one dam were purchased from Charles Rivers (Sulzfeld,

Germany). The dams were provided with tap water and pellet diet *ad libitum*. Litters were kept in rooms at a controlled temperature of 22 ± 2°C. The average weight of the animals upon start of the experiments was 22.0 ± 2.7 g. Our experimental model with 11-day old rats, corresponds to term infants or very young children <1 year old in term of brain development (Semple et al., 2013). This model is therefore well-suited to investigate both the acute phase of the disease and later neurofunctional deficits.

Via a 30-gauge needle (Becton Dickinson Microlance™, Allschwil, Switzerland) 10 µl of the bacteria suspension was injected into the cisterna magna of infant rats. The animals were weighted, clinically scored according to this scheme (1 = coma, 2 = does not turn upright, 3 = turns upright in >5 s, 4 = turns upright in <5 s, 5 = normal) and CSF was gained by puncturing the cisterna magna at different times points (18, 24, and 42 h post infection, hpi). These time points correspond to (a) a time preceding the symptoms appearance, when we begin to monitor the animals (18 hpi), (b) initiation of antibiotic therapy, with a significant worsening of clinical symptoms (24 hpi), and (c) to the time of sacrifice, when we investigate the development of acute brain damage by histology. Depending on the experiment (see next paragraph), animals were treated with either Amoxicillin (AMX 50 mg/kg/dosis, q8h) or saline, starting at 24 hpi. Animals were checked regularly to evaluate their health status by determining their clinical score. When reaching a clinical score <2, animals were euthanized for ethical reasons. At 42 h after infection, surviving animals were sacrificed with an overdose of the anesthetic pentobarbital (Esconarkon, Streuli Pharma AG, Uznach, Switzerland 200 mg/kg body weight, i.p.,). Animals were perfused through the left ventricle with ice-cold phosphate buffered saline (PBS). Brains were removed for later histological processing. The cerebellar samples were frozen on dry ice and stored at −80°C for later homogenization.

Experimental Design

Infections With Single RMS Allele Variants

Animals ($n = 36$) received an inoculum prepared from a clone enriched for a single *hsdS* allele as described above. Inoculum sizes were 2.03 ± 0.55 × 10^7 cfu/ml for variant A ($n = 3$), 1.70 ± 0.60 × 10^7 cfu/ml for B ($n = 3$), 2.19 ± 1.52 × 10^7 cfu/ml for C ($n = 3$), and 2.46 ± 1.65 × 10^7 cfu/ml for D ($n = 3$). The assignment of the animals for infection with one of the variants was randomized with 9 animals infected per variants. All animals were treated starting at 24 hpi with Amoxicillin (AMX 50 mg/kg/dosis, q8h). Two animals had to be sacrificed early, due to traumatic puncture injuries (B: $n = 1$; D: $n = 1$) and two animals died spontaneously from infection (A: $n = 1$ and C: $n = 1$). Thirty-two animals reached the endpoint of the experiment at 42 hpi (A: $n = 8$, B: $n = 8$, C: $n = 8$, D: $n = 8$).

Infections With a Mixture of the 4 RMS Allele Variants (A:B:C:D)

Animals ($n = 28$) received an inoculum prepared from a mix of 4 clones enriched for the different *hsdS* alleles. The inoculum size was 1.80 ± 0.35 × 10^7 cfu/ml ($n = 3$). The animals were randomly assigned to a treatment with AMX (50 mg/kg/dosis, q8h) or saline starting at 24 hpi. The assignment to the treatment group was randomized (AMX $n = 14$, saline $n = 14$). Three animals spontaneously died in the control group and one animal of the AMX group had to be sacrificed early due to a traumatic puncture injury, so that a total of 24 animals reached the endpoint of the experiment at 42 hpi and were further included in the analysis data (AMX = 13, control = 11). Apart from clinical, histological and inflammatory parameters, the *hsdS* expression (A:B:C:D) within the bacterial colonies recovered from the CSF and cerebellum was compared to the original inoculum by analysis of PCR fragments (GeneScan).

Infections With a Mixture of 2 RMS Allele Variants (A:B, A:C, B:C)

Animals received an inoculum prepared from a mix of 2 clones enriched for *hsdS* alleles A and B (A:B, $n = 36$), alleles A and C (A:C, $n = 24$) or alleles B and C (B:C, $n = 24$). The inoculum size was 1.46 ± 0.32 × 10^7 cfu/ml for A:B ($n = 3$), 1.03 ± 0.11 × 10^7 cfu/ml for A:C ($n = 4$) and 1.16 ± 0.37 × 10^7 cfu/ml for B:C ($n = 4$). No treatment was applied for these experiments. Twenty-five animals reached the endpoint of the experiment at 42 hpi for A:B, 16 for A:C and 15 for B:C. The *hsdS* expression of the different alleles (A, B, C, and D) within the bacterial colonies recovered from the CSF and cerebellum was compared to the original inoculum by analysis of PCR fragments (GeneScan).

Quantitative cfu Determination

CSF samples were serially diluted in sterile NaCl 0.85% and plated on CSBA plates. To prepare cerebellar homogenates, 1 ml of NaCl 0.85% was added per gram of tissue and mechanically processed in a glass homogenizer. The homogenate was serially diluted and plated on CSBA plates. All plates were cultured at 37°C overnight. Results were expressed as cfu/ml for CSF samples, respectively, cfu/g for homogenized tissue.

Analysis of Cytokine Expression in Cerebellar Homogenates

Cytokines known to be upregulated during *L. monocytogenes* meningitis (IL-1β, IL-6, IL-10, IL-18, TNF-α, and VEGF) (Koopmans et al., 2014, 2018) were assessed using magnetic multiplex assay (Rat Magnetic Luminex® Assay, Rat Premixed Multi-Analyte Kit, R&D Systems, Bio-Techne) on a Bio-Plex 200 station (Bio-Rad Laboratories) as described previously (Perny et al., 2016; Muri et al., 2018). Cerebellum homogenates were centrifuged (16,000 × g, 10 min, 4°C) and protein concentration determined using Pierce™ BCA Protein Assay kit (ThermoFischer Scientific). 100–150 µg proteins were diluted to a final volume of 50 µl. For each sample, a minimum of 50 beads was measured. If the concentration of the sample was below the detection limit, a value corresponding to the lower limit of detection provided by the manufacturer was used. The detection limits for undiluted samples were 2.93 pg/ml for IL-1β, 23.2 pg/ml for IL-6, 8.95 pg/ml for IL-10, 3.32 pg/ml for IL-18,11.5 pg/ml for TNF-α, and 15.6 pg/ml for VEGF.

Histopathology

Brain harvested at sacrifice were fixed for 4 h in 4% PFA and cryo-preserved in a 18% sucrose in PBS at 4°C for 24 h.

After freezing the brains in methyl-butane at −80°, forty-five μm slices were cut and every 15th cut was mounted on a gelatin coated glass slide. The slides were stained with cresyl violet (Merck, Zug, Switzerland) for Nissl bodies and mounted with DPX mounting medium for Histology (Sigma-Aldrich, Buchs, Switzerland). The sections were analyzed for hippocampal apoptosis as described previously (Grandgirard et al., 2007a). Hydrocephalus was assessed by determining the volume of the lateral and third ventricles normalized to the respective total cortical volume. All volumes were determined using the Cavalieri principle (Grandgirard et al., 2007a) using Image J for the analysis (V. 1.45, National Institutes of Health, Bethesda, Maryland, US). In our hand, a 15th cutting frequency allows enough resolution to determine volumes using histology, with negligible variation compared to water displacement method. Histologic assessment was performed and evaluated by investigators blinded to treatment modalities of the individual animals. Digital pictures of the dentate gyrus were taken using an AxioImager M1 microscope equipped with an AxioCam MRc CDD camera (Carl Zeiss Microscopy, Göttingen, Germany) at a magnification of 40x. Entire histological slices were scanned using a Path Enabler IV scanner (Meyer Instruments Inc., Houston, TX, US) at a resolution of 3,600 dpi.

Statistical Analyses

Statistical analyses were performed using GraphPad Prism (Prism 8; GraphPad Software Inc., San Diego, USA). Results are presented as mean values ± standard deviation if not stated otherwise. Survival was calculated using a log rank (Mantel-Cox) test. To compare differences between two groups, an unpaired Student *t*-test or a non-parametric Mann-Whitney test were used. When comparing multiple groups, we performed either one-way ANOVA with Tukey multiple comparison or a Kruskal-Wallis with Dunn's multiple comparison test depending on the normal distribution of the groups. For data available for different time points we performed a mixed-effects model of a 2-way ANOVA with repeated measures (because of missing values for animals that died spontaneously) and Tukey multiple comparison. The active *hsdS* allele composition of each sample was compared to the initial inoculum using a Kruskal-Wallis test. Normal distribution was tested using the D'Agostino & Pearson test. A $p < 0.05$ was considered statistically significant with $p < 0.05$ (*), $p < 0.01$ (**), $p < 0.001$ (***), and $p < 0.0001$ (****).

RESULTS

Genetic, Genomic, and Phenotypic Analysis of the Phase Variable Type I RMS

For the genetic and genomic analysis of the phase variable type I RMS Lmo0320I in *L. monocytogenes* lineage I ST4 (sequence type 4, clonal complex 4 CC4) isolate N13-0320, we aligned the RMS system loci of four ST4 genomes (**Figure 1A**). The 8,446 bp phase variable RMS locus was found to be inserted into a hairpin in the intergenic between lmo020 and lmo0521 in the reference strain EGD-e (between GeneID 985284 and 985300) creating a deletion of 32 bp. The structure of the locus was maintained between all CC4 isolates with an *hsdR* gene coding for the restriction subunit, an *hsdM* gene encoding for the methyltransferase, and one active and one inactive *hsdS* gene encoding for the specificity subunit, interspaced by the gene for a site-specific recombinase with a 99% nucleotide identity spanning the whole locus. As already shown for other phase variable type I RMS loci (Manso et al., 2014; Fagerlund et al., 2016), shuffling of the single target recognition domains (TRD) of the *hsdS* genes is readily evident from the aligned genome sequences (**Figure 1A**). Testing our collection of 160 Swiss *L. monocytogenes* isolates of food and clinical origin (Althaus et al., 2014) shows presence of the phase variable RMS Lmo0320I in all eight CC4 isolates and the related isolates of ST54 and ST1286 (**Figure 1B**). Further interrogation of our set of genomes with the sequences of the Lmo0320I *hsdR* genes detected orthologous systems in CC5 and CC8 with sequence identity, respectively, of 3063/3063 (100%) (Lineage I CC5 isolate N13-0402, accession RDSW00000000) and 3015/3063 (98%) (Lineage II CC8 isolate N11-2036 accession QYHX00000000) (**Figure 1B**). The *hsdM* genes shared a similar level of sequence identity. Three of the Lmo0320I target recognition domains were present in CC5, namely TRD 1.2, 2.1, and 2.2 (nucleotide identity 99–100%). In the more distantly related lineage II CC8 RMS (Fagerlund et al., 2016), only one of the four TRDs was partially conserved (TRD1.1, identity 642/695 92%).

Analysis of *hsdS* allele prevalence in single colonies of N12-0320, N12-0794, and 2250248 showed that it was possible to isolate colonies, and stocks derived thereof, which expressed prevalently different *hsdS* alleles. Allele quantification showed that over 95% of cells in overnight grown colonies (16 generations) had the same active *hsdS* allele (data not shown), indicating that in this condition recombination in the locus was a rare event. These enriched stocks were used for SMRT sequencing. Methylome analysis identified four different methylation targets for the four different *hsdS* alleles (**Figure 1C**). In strain N12-0320, there are a total of 620 *hsdSA*, 531 *hsdSB*, 597 *hsdSC,* and 484 *hsdSD* methylation sites, representing a huge range of genes potentially regulated by a single type I RMS.

The growth rates of the N12-030 strains expressing different alleles, used for all *in vivo* work in this study, were analyzed *in vitro*. All strains showed a similar growth rate (**Supplementary Figure 1A**).

Infections With Single RMS Allele Variants

All results presented in this paragraph are also summarized in **Supplementary Table 1.**

Clinical Parameters

All animals developed meningoencephalitis, as demonstrated by a worsening of clinical score and weight loss over time and growth of bacteria in the cerebellum (**Figures 2A–C**).

Animals infected with the different variants didn't significantly differ in mortality (**Supplementary Figure 1B**). Significant differences in clinical scores were observed between animals infected with the different strains at 18, 24 h, and 42 hpi, with those infected with variant A having consistently better clinical outcome scores at all time points and C significantly worse (**Figure 2A** and **Supplementary Table 2** for detailed

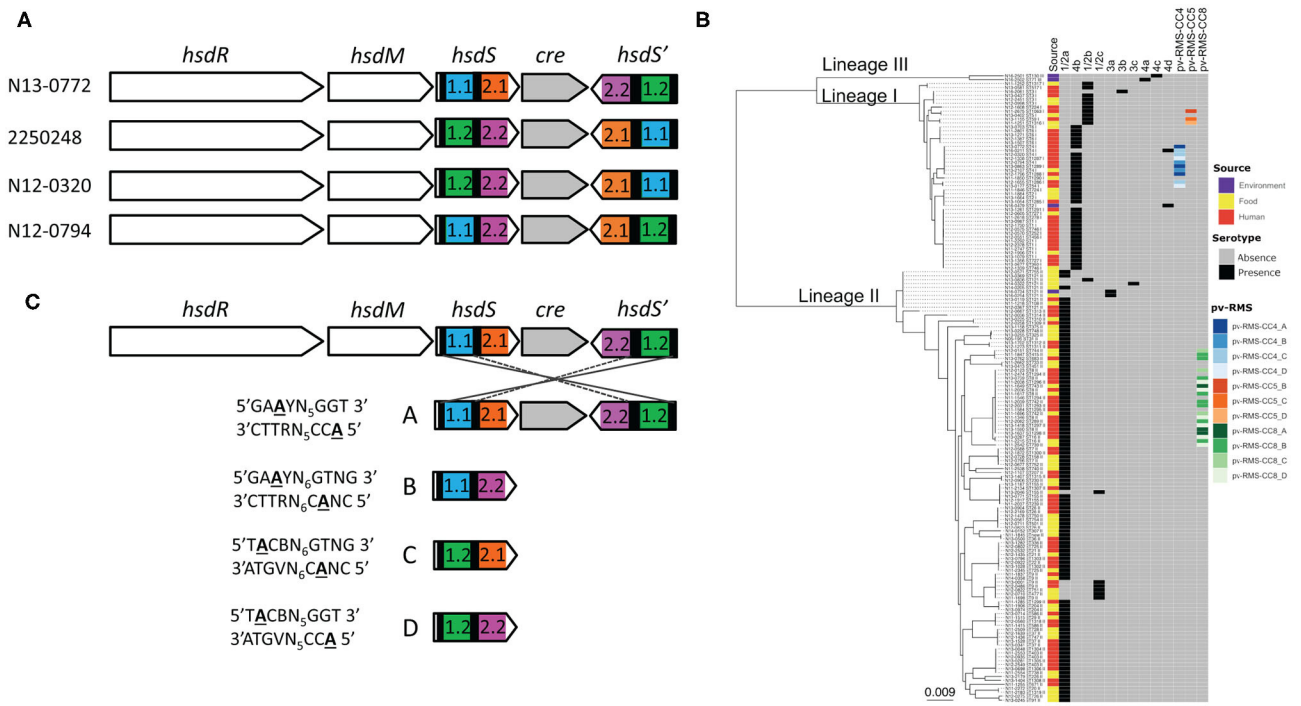

FIGURE 1 | The phase variable Lmo0320I RMS in *L. monocytogenes* CC4. The locus of the Lmo0772I RMS is composed of an operon containing the co-transcribed *hsdR* (restriction subunit), *hsdM* (methylation subunit) and *hsdS* (specificity subunit) genes, a site-specific recombinase (gray), and a further inactive *hsdS* gene without a proper start codon and no promoter. The alignment of the locus for the phase variable RMS from four Swiss ST4 CC4 isolates indicates how recombination on the inverted repeats within the *hsdS* genes (black bars) is able to shuffle the target recognition domains TRD1.1 (blue), 1.2 (green), 2.1 (orange), and 2.2 (pink) **(A)**. To investigate the phylogenetic context all *L. monocytogenes* phase variable RMSs were mapped on a core-genome phylogenetic tree of 160 Swiss *L. monocytogenes* isolates (Zamudio et al., 2020). The color of the squares in the heat map are linked to the source (human in red, food in yellow and environment in purple), serotype (presence in black and absence in gray) and phase variable RMS (pv-RMS-CC4 in blue, pv-RMS-CC5 in orange and pv-RMS-CC8 in green. The active variant (A, B, C, or D) of each pv-RMS is indicated by a different shading. **(B)** Rearrangements within the locus generate the four possible hsdS alleles, A–D by creating different combinations of TRDs 1.1 (blue), 1.2 (green), 2.1 (orange) and 2.2 (pink). Each TRD combination results in an alternative methylation pattern of the genome. These methylation patterns were determined by SMRT sequencing and are shown to the left of each hsdS allele **(C)**.

statistical analysis). After the application of AMX, there was an improvement of clinical signs for all variants.

Animals infected with all variants showed pronounced weight loss over time. In contrast to its effect on clinical score, AMX treatment didn't attenuate weight loss over time. By comparing the different strains, infection with variant A and B caused the smallest weight change at all time points whereas variant D caused the most pronounced weight loss over the duration of the experiment (**Figure 2B** and **Supplementary Table 3** for detailed statistical analysis).

Cerebellum homogenates at 42 hpi showed significantly higher bacterial titers for animals infected with variants B, C, and D compared to variant A, and variant D showed the highest titer overall (p value for the comparison allele A vs. B, pAvsB = 0.0263, pAvsC = 0.0018, pAvsD < 0.0001, Tukey multiple comparison test) (**Figure 2C**).

No differences (p = 0.2886, one-way ANOVA) in bacterial titers could be observed in the CSF harvested at 24 hpi, before initiation of antibiotic therapy. However, CSF could be harvested only in a subset of the animals (**Figure 2D**) (variant A 1.555 ± 0.0707 × 105 cfu/ml n = 2, B 4.896 ± 5.287 × 105 cfu/ml n = 3, C 2.335 ± 3.062 × 105 cfu/ml n = 6, D 3.582 ± 1.265 × 105 cfu/ml n = 5).

Inflammatory Parameters

The levels of different cytokines were investigated in cerebellar homogenates at 42 hpi (**Figures 3A–C**). A significant lower level of IL-1β concentration was observed in animals infected with variant A compared to those infected with D (p = 0.0488, Tukey's multiple comparison test). No further difference between the groups could be reported. No difference in IL-18 concentration was observed in animals treated with the different variants. Animals infected with variant C and D resulted in lower VEGF expression than A or B (pAvsC = 0.0319, pBvsC < 0.0001; pBvsD < 0.0001, Tukey's multiple comparison test). Further infection with variant B resulted in higher VEGF level than variant A (pAvsB = 0.0028). The level of matrix-metalloproteinase 9 (MMP9) was not different in animals infected with the different strains (**Supplementary Figure 2**).

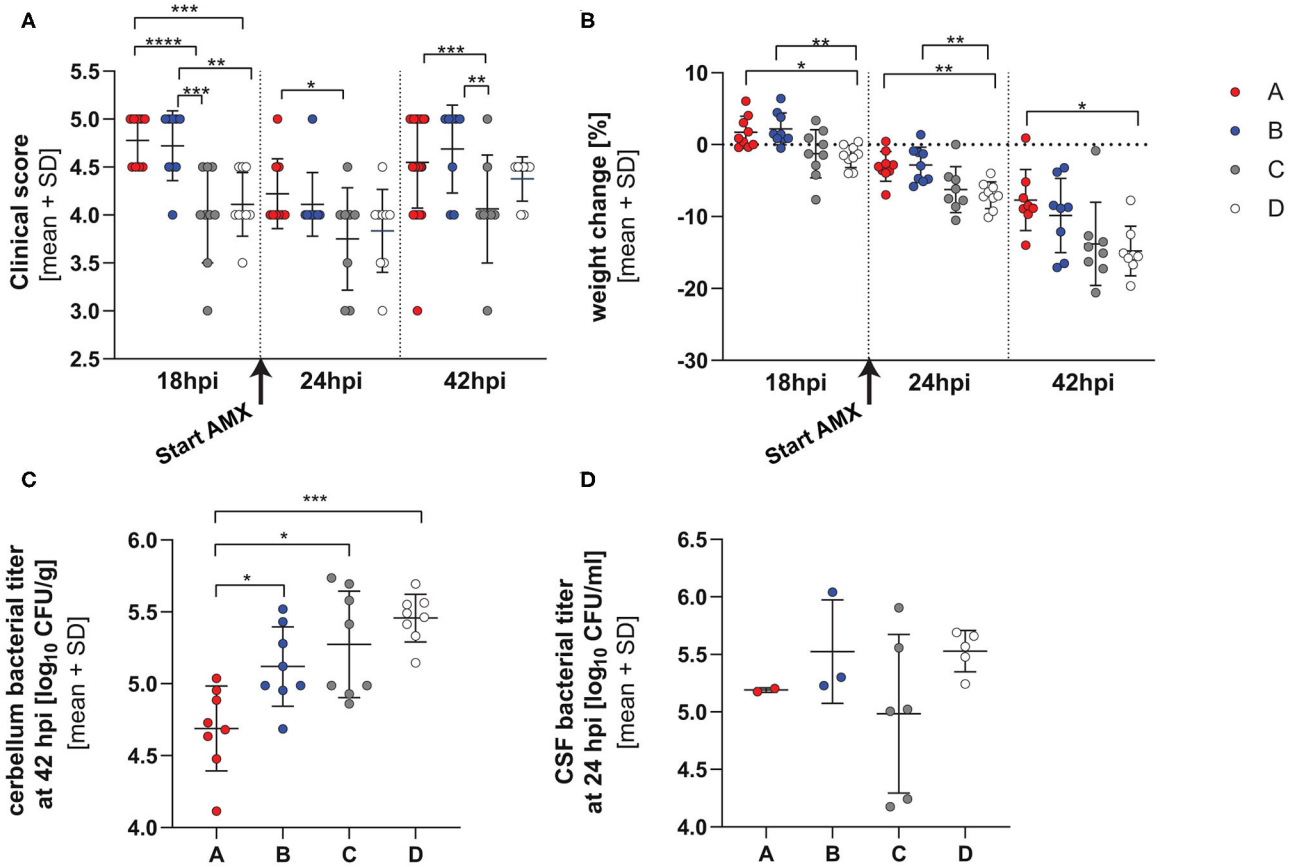

FIGURE 2 | Clinical parameters in infection with single RMS allele variant. Clinical score **(A)**, weight change **(B)** and bacterial titers in cerebellum at 42 hpi **(C)** and CSF at 24 hpi **(D)** in animals infected with the 4 different *hsdS* allele variants (A: $n = 8$, B: $n = 8$, C: $n = 8$, D: $n = 8$). The vertical dotted lines represent separation between the different time points and the initiation of the amoxicillin treatment is indicated by an arrow under the x-axis. The variants show altered virulence measured by the clinical score, weight change and cerebellum titer. The detailed statistical analyses are provided in **Supplementary Tables 1**, **2**. $^{*}p < 0.05$; $^{**}p < 0.01$; $^{***}p < 0.001$; $^{****}p < 0.0001$.

Histology

Animals infected with variant A show less apoptotic cells in the hippocampus compared to animals infected with variant C. A trend for less severe apoptotic damage was also found for variant A compared to variant D (pAvsC = 0.0500, pAvsD = 0.0792, Dunn's multiple comparison test, **Figure 3D** and **Supplementary Figure 3**).

All animals showed enlarged ventricles. However, we did not find any significant difference in hydrocephalus for animals infected with the different variants ($p = 0.6670$, one- way ANOVA, **Figure 3E** and **Supplementary Figure 3**).

Infections With a Mixture of the 4 RMS Allele Variants (A:B:C:D)

All results presented in this paragraph are also summarized in **Supplementary Table 1.**

Clinical Parameters

Although 3 animals died prematurely in the saline-treated group, the treatment did not alter survival over 42 hpi ($p = 0.0826$, Mantel-Cox, **Figure 4A**). The infection induced an initial worsening of the clinical score up to 24 h post infection (hpi) and of weight loss up to 42 hpi. The treatment with AMX administered after 24 hpi significantly improved clinical score compared to saline at 42 hpi ($p = 0.0317$, unpaired *t*-test), but did not significantly attenuate weight loss (**Figures 4B,C**).

Bacterial titers investigated in cerebellum homogenates at 42 hpi showed a significantly lower bacterial titers for animals treated with AMX ($p < 0.0001$, unpaired *t*-test, **Figure 4D**).

Analysis of the colonies recovered from the CSF and brains of rat pups infected with the inoculum containing all four *hsdS* clones in relatively equal proportions allowed us to determine if any had a phenotypic advantage within a host meningitis model. To account for the variations in inoculum composition between the independent experiments, we calculated the change in proportion for each allele between the inoculum and the

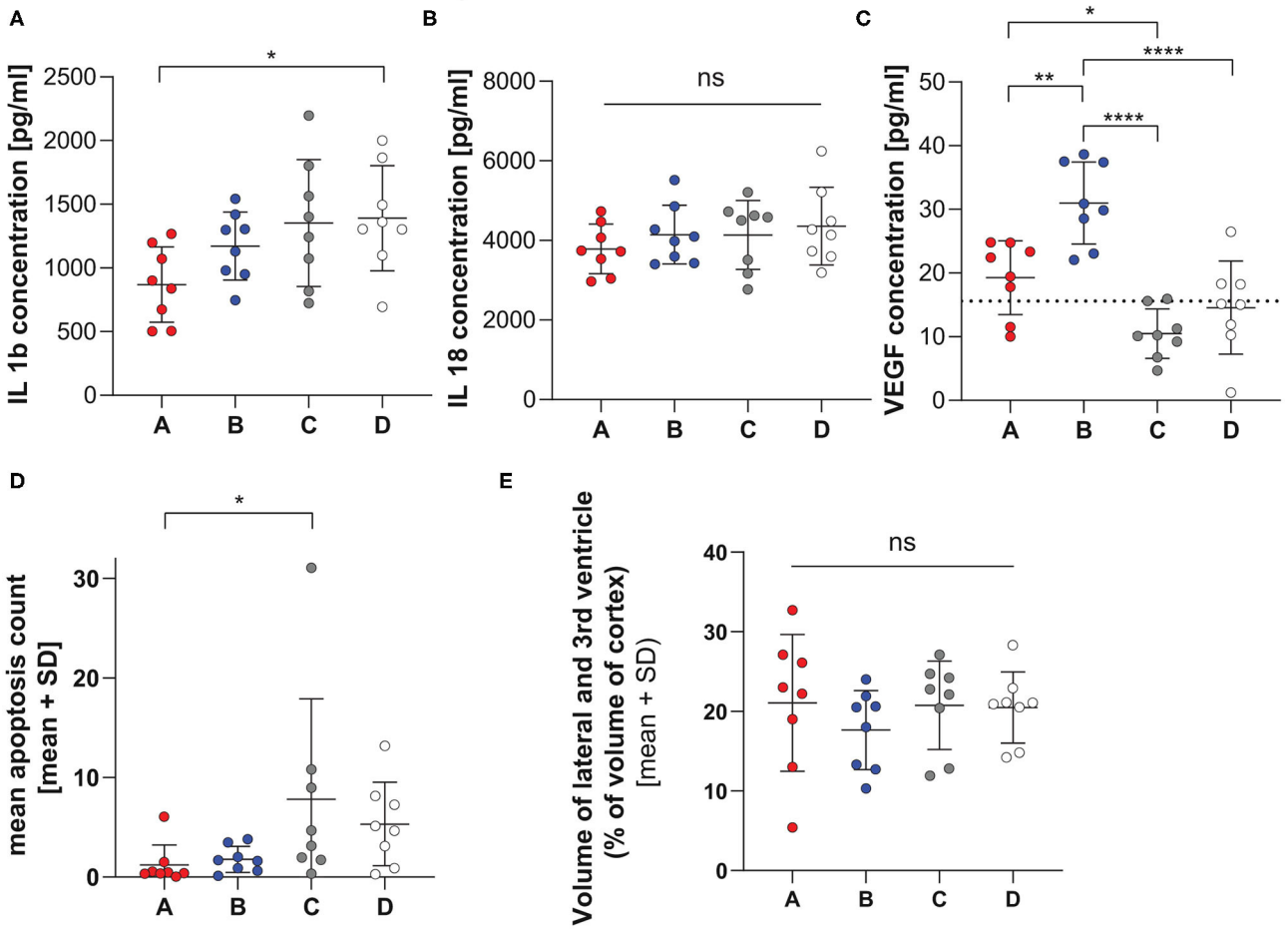

FIGURE 3 | Inflammatory and histological parameters in infection with single RMS allele variant. Cytokine levels of IL-1β **(A)**, IL-18 **(B)**, and VEGF **(C)** measured in cerebellum homogenate at 42 hpi in infant rats infected with the 4 different *hsdS* allele variants (A: $n = 8$, B: $n = 8$, C: $n = 8$, D: $n = 8$). The horizontal dotted line represents the lower limit of detection, data points under the line are extrapolated measurements. The variants show different concentrations for IL-1β and VEGF. Variant D leads to higher IL-1β level, whereas variant B shows elevated VEGF levels. No significance was found for IL-18 levels. Significant difference in the level of apoptosis **(D)** was only found for the comparison between infection with variants A and C, while hydrocephalus **(E)** was not different between infection with the 4 variants. *$p < 0.05$; **$p < 0.01$; ****$p < 0.0001$.

different *in vivo* samples, as determined by PCR. All CSF samples were collected prior to antibiotic treatment with amoxicillin, and brain samples were analyzed by separating the treatment groups. In this experimental paradigm, we did not observe any difference between the alleles, either in homogenized brain tissue or in the CSF (**Figure 5**).

Inflammatory Parameters

Except for VEGF, cytokines levels in cerebellum homogenates were significantly more elevated in saline treated animals compared to AMX treatment (IL-1β, $p < 0.0001$; IL-6, $p = 0.0065$; IL-10, $p = 0.0095$; TNF-α, $p = 0.0033$) (**Supplementary Figure 4**).

Histology

Animals who received AMX treatment suffered less hippocampal damage compared to animals who were treated with saline ($p = 0.0107$, Mann Whitney test, **Figures 6A,C,D**). Unexpectedly, animals treated with AMX had significantly more severe hydrocephalus than animals treated with saline ($p = 0.0163$, unpaired *t*-test) (**Figures 6B,E,F**).

Infections With a Mixture of 2 RMS Allele Variants (A:B, A:C, and B:C)

The competition assay was repeated, but by reducing the mix to only two variants, A:B, A:C, or B:C. The animals were left untreated. All animals developed meningoencephalitis, proven by growth of bacteria in the cerebellum at 42 hpi and a worsening of clinical symptoms (not shown).

Similar to the experiment with the mix of 4 variants, we determined the changes in the proportion of different alleles between the inoculum and the different *in vivo* samples. Analysis of the recovered colonies, when compared to the inoculum,

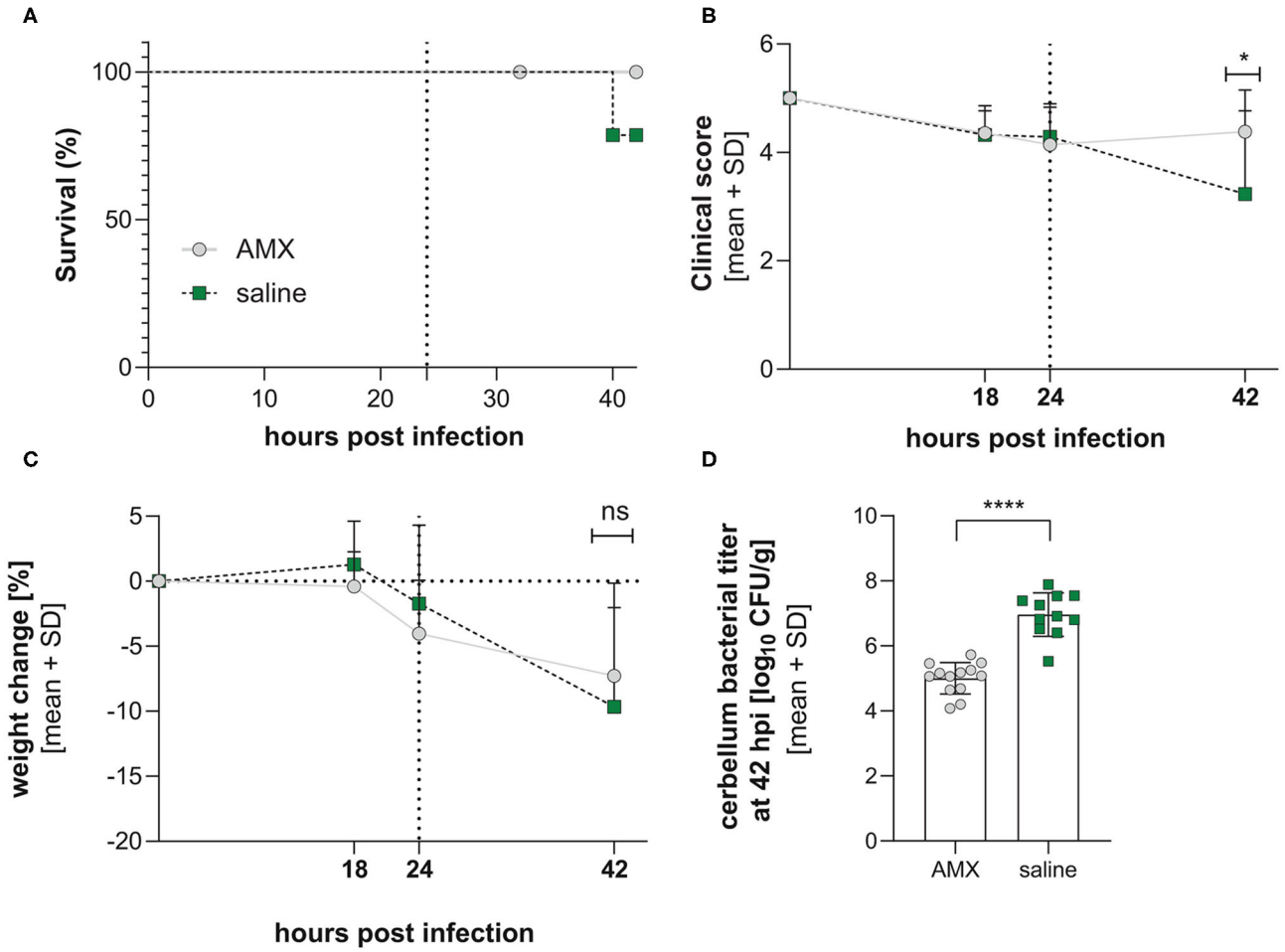

FIGURE 4 | Clinical parameters in infection with a mixture of the 4 RMS allele variants. Comparison between AMX-treated and saline-treated animals didn't reveal changes in survival **(A)** (AMX = 14, control = 14). In contrast, clinical score **(B)**, weight change **(C)**, and bacterial titer in the cerebellum **(D)** were significantly improved by AMX treatment with amoxicillin improves outcome (AMX = 13, control = 11). Statistical significance was reached for clinical score and cerebellum titers. The vertical dotted line represents the initiation of the amoxicillin treatment. *$p < 0.05$; ****$p < 0.0001$; ns: not significant.

revealed that in both the brain tissue and in the CSF, variant A was significantly less represented when compared to the inoculum (**Figure 7**). This decrease was not observed with the other variants. Due to the nature of analysis a decrease in one variant is accompanied by an increase in an alternative variant. In both the brain and CSF, the observed reduction in variant A is accompanied by an increase in variant C ($p < 0.0001$ and $p = 0.0166$, respectively). In addition, the grouped comparison reveals that within the cerebellum the increase in the variant C is also at the expense of the variant B ($p = 0.0226$) while B appears to outcompete A ($p = 0.008$) (**Figure 7**). While no specific assay was conducted with the variant D, inoculums contained up to 10% D due to the wildtype nature of the strains. The results obtained are in line with those of the single variant infection experiments, showing significantly lower cerebellar titer for variant A in comparison to B and C (**Figure 2C**).

DISCUSSION

In the present study, we identified a phase-variable RMS system in a collection of clinical isolates of *Listeria monocytogenes* strains. While not as ubiquitous as some PV RMS (Manso et al., 2014), there appears to be a clear, clonal complex specific, distribution of PV RMS in *L. monocytogenes*. Analysis of the 160 genomes recently published by Zamudio et al. (2020) showed that all CC4 strains contain different orientations of the same loci (**Figure 1B**). Isolation of clones expressing a single *hsdS* variant in strains N12-0320, N12-0794, and 225078 allowed us to confirm that changes in *hsdS* expression are on-going and relatively stable at 37°C. Long read sequencing of N12-0320 allowed us to identify different methylation patterns associated with each *hsdS* (**Figure 1C**).

We tested clones enriched in one of the four allelic variants derived from a CC4 serotype 4b clinical isolate that displays

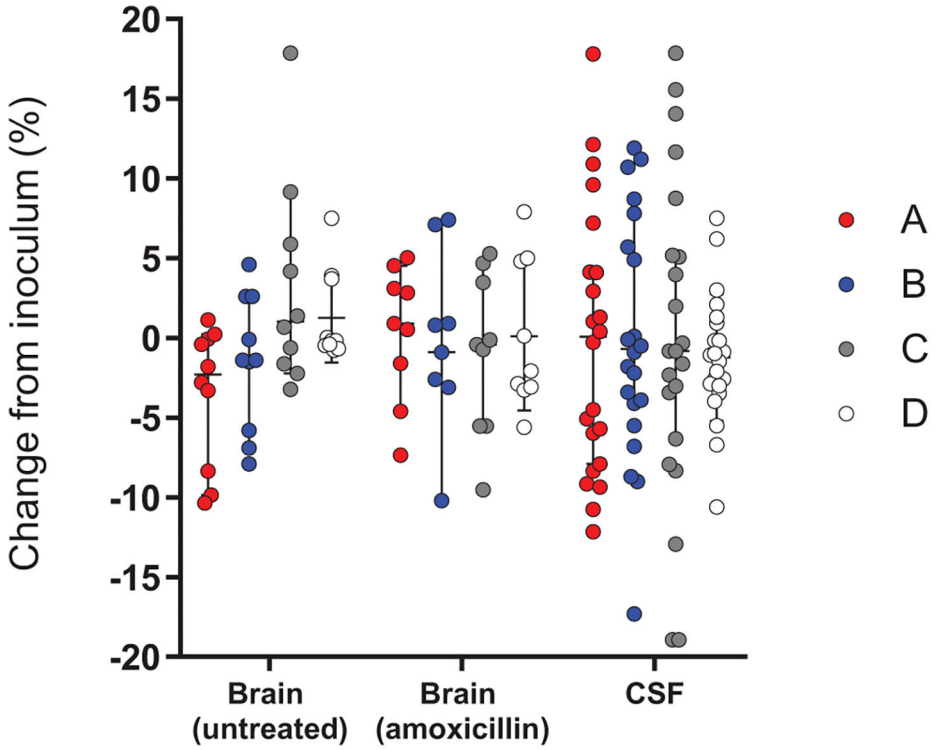

FIGURE 5 | Change in frequency of the expressed RMS allele between the inoculum and different *in vivo* samples in infection with a mixture of the 4 RMS allele variants. The relative proportions of *hsdS* variants A (red), B (blue), C (gray) and D (white) between the inoculum and the bacteria harvested in the different *in vivo* samples, including the brains of untreated animals ($n = 10$) or AMX-treated animals ($n = 9$) and CSF samples ($n = 22$), were not significantly different between the alleles. A Kruskal-Wallis test found no significant differences between variant proportions in the inoculums and *in vivo* samples.

this phase variable RMS in a neonatal rat model. Such phase variation mechanisms have been described in *S. pneumoniae* and are shown to be important in virulence in pneumococcal invasive diseases (Manso et al., 2014). While in *Hemophilus influenzae* a PV type III RMS has been linked to virulence phenotypes such as antibiotic resistance, biofilm formation and evasion of the immune system (Atack et al., 2015). Here we show that phase variation in type I RMS in *L. monocytogenes* leads to an altered outcome in our animal model of listeria meningitis.

When comparing animals infected with the single RMS allele variants, infection with variant A show the mildest clinical disease phenotype on different parameters, including clinical score, weight loss, bacterial titer in the cerebellum, cytokines in cerebellum homogenate and hippocampal apoptosis. Mortality was however not significantly different between all groups up to 42 h after infection. Further cerebellar titers were lower in comparison to other strains.

For variant B, the phenotype mostly resembled that of variant A with defined differences, including more elevated cerebellar bacterial titers. Elevated VEGF levels were found in animals infected with this allele. Vascular endothelial growth factor VEGF is secreted in the process of efferocytosis (Golpon et al., 2004; Vandivier et al., 2006). Elevated VEGF levels in the cerebrospinal fluid in cases of listeria meningitis is shown to be associated with poor outcome (Koopmans et al., 2014). However, this was not observed in our experimental model, neither on mortality rates nor in the level of brain damage.

Variant C presented with the worst clinical disease phenotype at 24 hpi and the most pronounced hippocampal damage assessed by quantification of apoptotic cells in the dentate gyrus of the hippocampus. Further variant C had significantly higher cerebellum titers compared to variant A. For variant D, we describe the most pronounced weight loss of all the variants and the highest bacterial titer in the cerebellum.

These observed differences when animals were infected with single variants demonstrate that changes in diseases severity are caused by the phase variable epigenetic modifications. These findings are in accordance to those observed by Manso et al. (2014) where RMS mutants showed differences in virulence in an intravenous mouse model of infection with *S. pneumoniae*. To permit a more detailed investigation into the interaction of bacteria expressing different *hsdS* alleles, we conducted competition experiments where either two or four *hsdS* variants were combined to create an inoculum.

Lees et al. (2017) were unable to detect observable selective advantages of *hsdS* variants in clinical blood and CSF samples, however analysis of these samples was complicated by the lack of known infecting strain. In contrast, a model infection as presented here, and in De Ste Croix et al. (2020b), with a starting inoculum of defined bacterial composition, allows for results

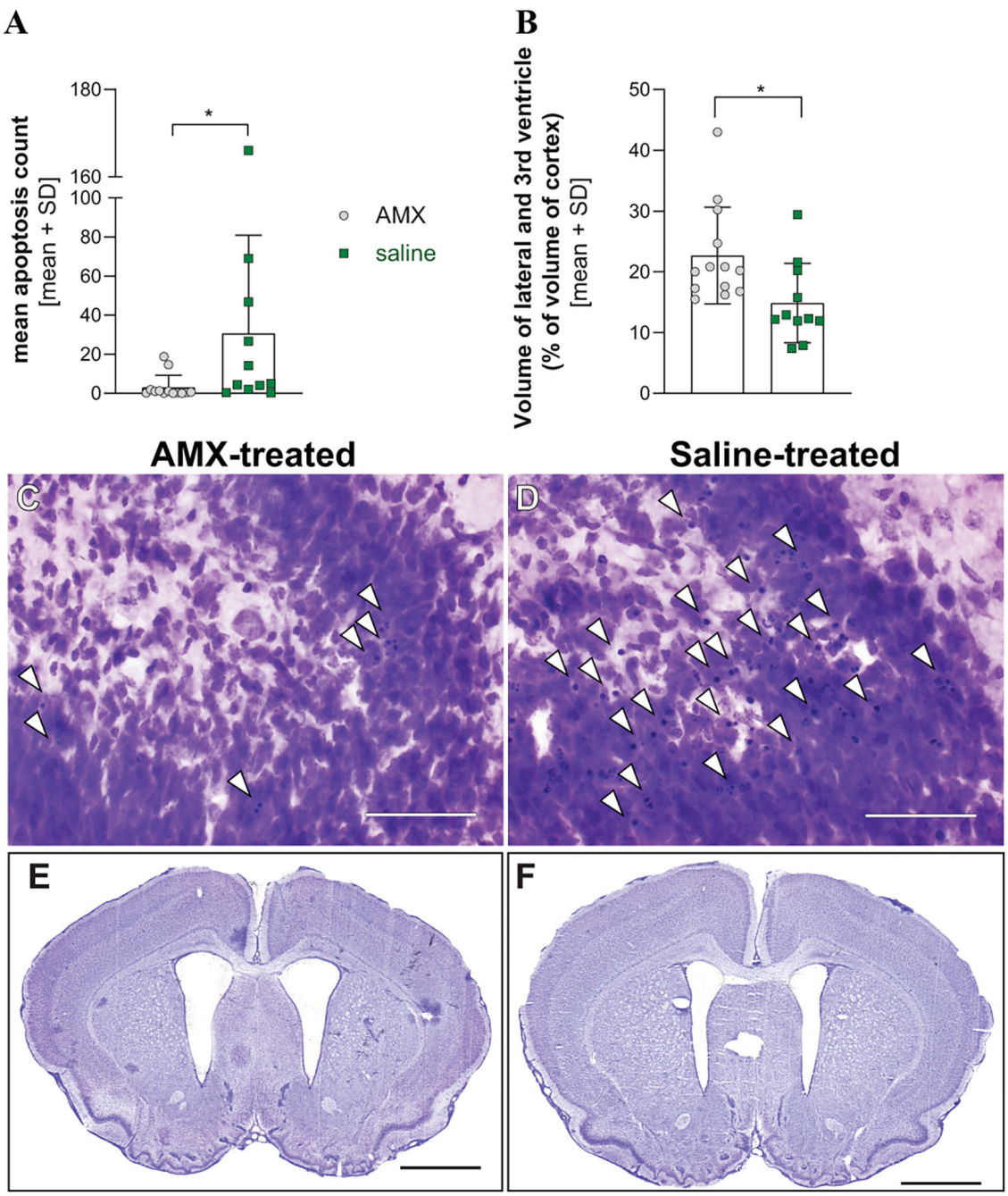

FIGURE 6 | Histological parameters in infection with a mixture of the 4 RMS allele variants. Treatment of infected animals with AMX ($n = 13$) attenuated hippocampal apoptosis in comparison to saline-treated animals ($n = 11$) **(A)** but was associated with enlarged ventricle size **(B)**. Representative pictures of cresy violet-stained sections of the apex of the dentate gyrus (**C,D**, bar size 50 μm), with examples of apoptotic cells indicated with white arrowheads, or from entire sections with enlarged lateral ventricles (**E,F**, bar size 2 mm). *$p < 0.05$.

to be analyzed in comparison to the inoculating dose and can therefore account for differences in the input population.

In PV RM systems there is likely to be continuous, stochastic variation at the loci. This results in a continuous re-generation of diversity within the bacterial population (De Ste Croix et al., 2020a). When a bacterial species enters a host there is a high probability of bottlenecking i.e., a significant reduction within the population is observed. Non-selective bottlenecks will frequently lead to high levels of divergence within the bacterial population of biological replicates, while an *in vivo* fitness advantage is

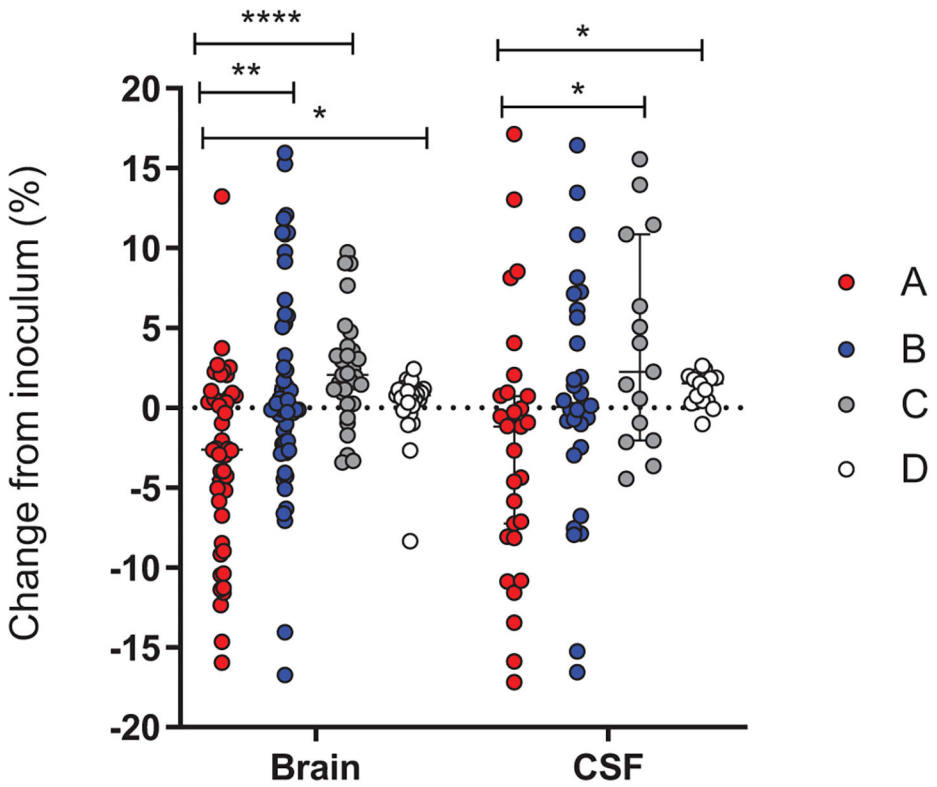

FIGURE 7 | Change in the proportion of PV RMS alleles between the 2 variants inoculums and *in vivo* samples. Results were pooled from seven independent experiments and each variant is independently calculated as a percentage change from the initial inoculum for that experiment. The relative proportions of *hsdS* variants A (red), B (blue), C (gray) and D (white) between the inoculum and the bacteria harvested in *In vivo* CSF and cerebellum samples. A Kruskal-Wallis test showed that the proportion of the A variant is repeatedly reduced in comparison to the starting inoculum, while the C (CSF and brain) and B (brain) variants increase. $p < 0.05$ (*), $p < 0.01$ (**), and $p < 0.0001$ (****).

indicated by a population continuously driven in a single direction (Aidley et al., 2017). The small but subtle differences we have observed in *hsdS* profiles when animals are infected with mixed inoculums suggests a potential competitive advantage. It should also be considered that strains which induce a greater level of damage may be selected against, and as a result be underrepresented within animals which survive until the end point of the experiment.

As there is little recombination of the RMS loci at higher temperatures (>30°C), we conducted mixed competition studies of different allelic combinations to look for selective advantages. When animals were infected with a mixture of 4 allelic variants, we did not identify any variant as having a selective advantage in either the CSF or the brain. To further explore the competition between populations expressing alternate *hsdS* alleles we infected animals with inoculums containing only two variants. This approach allows us to have a larger starting proportion to analyze against. Across multiple experiments we have observed a reduction in the proportion of the variant A when compared to the starting inoculum, in agreement with the clinical observations in our single variant experiments where animals infected with the variant A showed significantly better clinical scores at all time points. The loss of the variant A is accompanied by an increase in the variant C, further confirming the clinical score data of the single variant infections.

In the case of the infections with the inoculum composed of the 4 alleles, we designed 2 experimental groups that received antibiotic treatment or only saline, to determine whether antibiotic treatment could reveal a further selective advantage of one of the alleles. Such an advantage was not detected. However, we observed several differences between the two treatment groups. AMX treatment improve clinical parameters and decreased bacterial titers in the cerebellum. Survival was lower in saline-treated animals, without reaching statistical significance. In both groups, the observed mortality was in the range (0–25%) from what has been reported for neonates affected with neurolisteriosis (Mclauchlin, 1990; Mylonakis et al., 2002; Koopmans et al., 2017). Hippocampal apoptosis was also reduced. In contrast, treatment with amoxicillin worsens the size of the hydrocephalus. In a clinical setting, hydrocephali occur in 28% percent of neonatal cases (Hsieh et al., 2009). Bacterial lysis under antibiotic treatment could lead to an elevated release of bacterial components and therefore aggravated inflammation, as it is

proposed for pneumococcal meningitis (Agyeman et al., 2014). However, in the present model, AMX treatment lead to a diminished expression of all analyzed pro-inflammatory and anti-inflammatory cytokines, so that inflammation couldn't account for the observed finding of increased hydrocephalus in AMX-treated animals.

Our model has certain limitations and displays differences when compared to human disease. For example, we did not find any pathognomic abscesses (Engelen-Lee et al., 2018) in the histological analysis, however, hydrocephalus occurred in all animals. Further, we use Wistar rats which express a wild type murine E-Cadherin which has been shown not to interact with the cell invasion factor internalin InlA (Lecuit et al., 1999, 2001). Our model does bypass the different physiological barriers the bacteria must cross in a natural food-borne infection by injecting the pathogen into the cisterna magna. In doing so, we have consistent CNS infection, but we remove the initial step of bacterial invasion. In this model, we therefore couldn't investigate on the role of this phase variable loci early in the disease process, but only when CNS invasion has been established.

This study allowed us to gain a better insight on bacterial determinants that influence virulence in neonates affected by listeria meningitis, in particular the development of brain damage. This will be important to understand how the damage translates into neurofunctional deficits, in order to develop specific therapeutic strategies.

Work is on-going to fully understand the phenotypic attributes of this PV RMS of *Listeria monocytogenes* CC4 serotype 4b, however we observe differences in virulence in an acute meningitis/meningoencephalitis model. We now shall investigate long-term outcomes and further look into the biochemical mechanics of this altered virulence.

DATA AVAILABILITY STATEMENT

The original contributions presented in the study are included in the article/**Supplementary Material**, further inquiries can be directed to the corresponding author/s.

ETHICS STATEMENT

The animal study was reviewed and approved by the Animal Care and Experimentation Committee of the Canton of Bern, Switzerland (license no. BE 01/18).

AUTHOR CONTRIBUTIONS

FZ designed the studies, performed animal experiments, analyzed the results, and contributed to manuscript preparation. DG designed the study, analyzed the results, co-supervised the studies, and contributed to manuscript preparation. SL designed the study, co-supervised the studies, and contributed to manuscript preparation. MD conducted GeneScan analysis of the inoculum, CSF and cerebellum samples, conducted statistical analysis, and contributed to the manuscript. RH conducted WGS of Listeria strains and developed the GeneScan protocol. RZ analyzed WGS data. IV isolated *hsdS* strains and developed the GeneScan protocol. EG isolated *hsdS* strains. MO analyzed WGS data, provided supervision, and contributed to the manuscript. All authors contributed to the article and approved the submitted version.

FUNDING

This work was in part supported by BBSRC grant BB/N002903/1 to MO and Swiss National Science Foundation grant (189136) to SL.

ACKNOWLEDGMENTS

We thank the ESCMID study group on infection of the brain (ESGIB) for stimulating discussions and suggestions. We thank Robert Lukesch and Franziska Simon for excellent technical assistance. The contribution of William R. Thomas to the set-up of the allele quantification assay is acknowledged.

SUPPLEMENTARY MATERIAL

The Supplementary Material for this article can be found online at: https://www.frontiersin.org/articles/10.3389/fcimb.2020.590657/full#supplementary-material

REFERENCES

Agyeman, P., Grandgirard, D., and Leib, S. L. (2014). "Pathogenesis and pathophysiology of bacterial infections," in *Infections of the Central Nervous System, 4th Edn,* eds M. W. Scheld, R. J. Whitley and C. M. Marra. (Philadelphia, PA: Lippincott Williams & Wilkins).

Aidley, J., Rajopadhye, S., Akinyemi, N. M., Lango-Scholey, L., Jones, M. A., and Bayliss, C. D. (2017). Nonselective bottlenecks control the divergence and diversification of phase-variable bacterial populations. *mBio* 8:16. doi: 10.1128/mBio.02311-16

Althaus, D., Lehner, A., Brisse, S., Maury, M., Tasara, T., and Stephan, R. (2014). Characterization of Listeria monocytogenes strains isolated during 2011-2013 from human infections in Switzerland. *Foodborne Pathog. Dis.* 11, 753–758. doi: 10.1089/fpd.2014.1747

Atack, J. M., Srikhanta, Y. N., Fox, K. L., Jurcisek, J. A., Brockman, K. L., Clark, T. A., et al. (2015). A biphasic epigenetic switch controls immunoevasion, virulence and niche adaptation in non-typeable Haemophilus influenzae. *Nat. Commun.* 6:7828. doi: 10.1038/ncomms8828

Atack, J. M., Weinert, L. A., Tucker, A. W., Husna, A. U., Wileman, T. M., Hadjirin, N. F., et al. (2018). Streptococcus suis contains multiple phase-variable methyltransferases that show a discrete lineage distribution. *Nucleic Acids Res.* 46, 11466–11476. doi: 10.1093/nar/gky913

Bedford, H., De Louvois, J., Halket, S., Peckham, C., Hurley, R., and Harvey, D. (2001). Meningitis in infancy in England and Wales: follow up at age 5 years. *BMJ* 323, 533–536. doi: 10.1136/bmj.323.7312.533

Bifrare, Y. D., Gianinazzi, C., Imboden, H., Leib, S. L., and Täuber, M. G. (2003). Bacterial meningitis causes two distinct forms of cellular damage in the hippocampal dentate gyrus in infant rats. *Hippocampus* 13, 481–488. doi: 10.1002/hipo.10142

Charlier, C., Perrodeau, E., Leclercq, A., Cazenave, B., Pilmis, B., Henry, B., et al. (2017). Clinical features and prognostic factors of listeriosis: the MONALISA national prospective cohort study. *Lancet Infect. Dis.* 17, 510–519. doi: 10.1016/S1473-3099(16)30521-7

Chen, P., Den Bakker, H. C., Korlach, J., Kong, N., Storey, D. B., Paxinos, E. E., et al. (2017). Comparative genomics reveals the diversity of restriction-modification systems and dna methylation sites in listeria monocytogenes. *Appl. Environ. Microbiol.* 83, e02091–16. doi: 10.1128/AEM.02091-16

Connor, T. R., Loman, N. J., Thompson, S., Smith, A., Southgate, J., Poplawski, R., et al. (2016). CLIMB (the Cloud Infrastructure for Microbial Bioinformatics): an online resource for the medical microbiology community. *Microb. Genom.* 2:e000086. doi: 10.1099/mgen.0.000086

de Noordhout, C. M., Devleesschauwer, B., Angulo, F. J., Verbeke, G., Haagsma, J., Kirk, M., et al. (2014). The global burden of listeriosis: a systematic review and meta-analysis. *Lancet Infect. Dis.* 14, 1073–1082. doi: 10.1016/S1473-3099(14)70870-9

De Ste Croix, M., Holmes, J., Wanford, J. J., Moxon, E. R., Oggioni, M. R., and Bayliss, C. D. (2020a). Selective and non-selective bottlenecks as drivers of the evolution of hypermutable bacterial loci. *Mol. Microbiol.* 113, 672–681. doi: 10.1111/mmi.14453

De Ste Croix, M., Mitsi, E., Morozov, A., Glenn, S., Andrew, P. W., Ferreira, D. M., et al. (2020b). Phase variation in pneumococcal populations during carriage in the human nasopharynx. *Sci. Rep.* 10:1803. doi: 10.1038/s41598-020-58684-2

De Ste Croix, M., Vacca, I., Kwun, M. J., Ralph, J. D., Bentley, S. D., Haigh, R., et al. (2017). Phase-variable methylation and epigenetic regulation by type I restriction-modification systems. *FEMS Microbiol. Rev.* 41, S3–S15. doi: 10.1093/femsre/fux025

De Ste Croix, M., Chen, K. Y., Vacca, I., Manso, A. S., Johnston, C., Polard, P., et al. (2019). Recombination of the phase-variable spnIII locus is independent of all known pneumococcal site-specific recombinases. *J. Bacteriol.* 201:e00233–00219. doi: 10.1128/JB.00233-19

Disson, O., and Lecuit, M. (2012). Targeting of the central nervous system by Listeria monocytogenes. *Virulence* 3, 213–221. doi: 10.4161/viru.19586

Engelen-Lee, J. Y., Koopmans, M. M., Brouwer, M. C., Aronica, E., and Van De Beek, D. (2018). Histopathology of listeria meningitis. *J. Neuropathol. Exp. Neurol.* 77, 950–957. doi: 10.1093/jnen/nly077

Fagerlund, A., Langsrud, S., Schirmer, B. C., Moretro, T., and Heir, E. (2016). Genome analysis of listeria monocytogenes sequence type 8 strains persisting in salmon and poultry processing environments and comparison with related strains. *PLoS ONE* 11:e0151117. doi: 10.1371/journal.pone.0151117

Golpon, H. A., Fadok, V. A., Taraseviciene-Stewart, L., Scerbavicius, R., Sauer, C., Welte, T., et al. (2004). Life after corpse engulfment: phagocytosis of apoptotic cells leads to VEGF secretion and cell growth. *FASEB J.* 18, 1716–1718. doi: 10.1096/fj.04-1853fje

Grandgirard, D., Schurch, C., Cottagnoud, P., and Leib, S. L. (2007a). Prevention of brain injury by the nonbacteriolytic antibiotic daptomycin in experimental pneumococcal meningitis. *Antimicrob Agents Chemother* 51, 2173–2178. doi: 10.1128/AAC.01014-06

Grandgirard, D., Steiner, O., Täuber, M. G., and Leib, S. L. (2007b). An infant mouse model of brain damage in pneumococcal meningitis. *Acta Neuropathol.* 114, 609–617. doi: 10.1007/s00401-007-0304-8

Hsieh, W. S., Tsai, L. Y., Jeng, S. F., Hsu, C. H., Lin, H. C., Hsueh, P. R., et al. (2009). Neonatal listeriosis in Taiwan, 1990-2007. *Int. J. Infect. Dis.* 113, 193–195. doi: 10.1016/j.ijid.2008.06.006

Kasanmoentalib, E. S., Brouwer, M. C., Van Der Ende, A., and Van De Beek, D. (2010). Hydrocephalus in adults with community-acquired bacterial meningitis. *Neurology* 75, 918–923. doi: 10.1212/WNL.0b013e3181f11e10

Koopmans, M. M., Bijlsma, M. W., Brouwer, M. C., Van De Beek, D., and Van Der Ende, A. (2017). Listeria monocytogenes meningitis in the Netherlands, 1985-2014: a nationwide surveillance study. *J. Infect.* 75, 12–19. doi: 10.1016/j.jinf.2017.04.004

Koopmans, M. M., Brouwer, M. C., Bijlsma, M. W., Bovenkerk, S., Keijzers, W., Van Der Ende, A., et al. (2013). Listeria monocytogenes sequence type 6 and increased rate of unfavorable outcome in meningitis: epidemiologic cohort study. *Clin. Infect. Dis.* 57, 247–253. doi: 10.1093/cid/cit250

Koopmans, M. M., Brouwer, M. C., Geldhoff, M., Seron, M. V., Houben, J., Van Der Ende, A., et al. (2014). Cerebrospinal fluid inflammatory markers in patients with Listeria monocytogenes meningitis. *BBA Clin.* 1, 44–51. doi: 10.1016/j.bbacli.2014.06.001

Koopmans, M. M., Engelen-Lee, J., Brouwer, M. C., Jaspers, V., Man, W. K., Vall Seron, M., et al. (2018). Characterization of a Listeria monocytogenes meningitis mouse model. *J. Neuroinflammation.* 15:257. doi: 10.1186/s12974-018-1293-3

Kwun, M. J., Oggioni, M. R., De Ste Croix, M., Bentley, S. D., and Croucher, N. J. (2018). Excision-reintegration at a pneumococcal phase-variable restriction-modification locus drives within- and between-strain epigenetic differentiation and inhibits gene acquisition. *Nucleic Acids Res.* 46, 11438–11453. doi: 10.1093/nar/gky906

Lecuit, M., Dramsi, S., Gottardi, C., Fedor-Chaiken, M., Gumbiner, B., and Cossart, P. (1999). A single amino acid in E-cadherin responsible for host specificity towards the human pathogen Listeria monocytogenes. *EMBO J.* 18, 3956–3963. doi: 10.1093/emboj/18.14.3956

Lecuit, M., Vandormael-Pournin, S., Lefort, J., Huerre, M., Gounon, P., Dupuy, C., et al. (2001). A transgenic model for listeriosis: role of internalin in crossing the intestinal barrier. *Science* 292, 1722–1725. doi: 10.1126/science.1059852

Lee, J. Y. H., Carter, G. P., Pidot, S. J., Guerillot, R., Seemann, T., Goncalves Da Silva, A., et al. (2019). mining the methylome reveals extensive diversity in staphylococcus epidermidis restriction modification. *mBio* 10:19. doi: 10.1128/mBio.02451-19

Lees, J. A., Kremer, P. H. C., Manso, A. S., Croucher, N. J., Ferwerda, B., Seron, M. V., et al. (2017). Large scale genomic analysis shows no evidence for pathogen adaptation between the blood and cerebrospinal fluid niches during bacterial meningitis. *Microb. Genom.* 3:e000103. doi: 10.1099/mgen.0.000103

Leib, S. L., Heimgartner, C., Bifrare, Y. D., Loeffler, J. M., and Täuber, M. G. (2003). Dexamethasone aggravates hippocampal apoptosis and learning deficiency in pneumococcal meningitis in infant rats. *Pediatr. Res.* 54, 353–357. doi: 10.1203/01.PDR.0000079185.67878.72

Leib, S. L., Kim, Y. S., Chow, L. L., Sheldon, R. A., and Täuber, M. G. (1996). Reactive oxygen intermediates contribute to necrotic and apoptotic neuronal injury in an infant rat model of bacterial meningitis due to group B streptococci. *J. Clin. Invest.* 98, 2632–2639. doi: 10.1172/JCI119084

Li, J., Li, J. W., Feng, Z., Wang, J., An, H., Liu, Y., et al. (2016). Epigenetic Switch Driven by DNA Inversions Dictates Phase Variation in Streptococcus pneumoniae. *PLoS Pathog.* 12:e1005762. doi: 10.1371/journal.ppat.1005762

Loeffler, J. M., Ringer, R., Hablutzel, M., Täuber, M. G., and Leib, S. L. (2001). The free radical scavenger alpha-phenyl-tert-butyl nitrone aggravates hippocampal apoptosis and learning deficits in experimental pneumococcal meningitis. *J. Infect. Dis.* 183, 247–252. doi: 10.1086/317921

Manso, A. S., Chai, M. H., Atack, J. M., Furi, L., De Ste Croix, M., Haigh, R., et al. (2014). A random six-phase switch regulates pneumococcal virulence via global epigenetic changes. *Nat. Commun.* 5:5055. doi: 10.1038/ncomms6055

Mclauchlin, J. (1990). Human listeriosis in Britain, 1967-85, a summary of 722 cases. 1. Listeriosis during pregnancy and in the newborn. *Epidemiol Infect* 104, 181–189. doi: 10.1017/S0950268800059343

Michelet, C., Leib, S. L., Bentue-Ferrer, D., and Täuber, M. G. (1999). Comparative efficacies of antibiotics in a rat model of meningoencephalitis due to *Listeria monocytogenes*. *Antimicrob Agents Chemother.* 43, 1651–1656. doi: 10.1128/AAC.43.7.1651

Muri, L., Grandgirard, D., Buri, M., Perny, M., and Leib, S. L. (2018). Combined effect of non-bacteriolytic antibiotic and inhibition of matrix metalloproteinases prevents brain injury and preserves learning, memory and hearing function in experimental paediatric pneumococcal meningitis. *J. Neuroinflam.* 15:233. doi: 10.1186/s12974-018-1272-8

Mylonakis, E., Paliou, M., Hohmann, E. L., Calderwood, S. B., and Wing, E. J. (2002). Listeriosis during pregnancy: a case series and review of 222 cases. *Medicine* 81, 260–269. doi: 10.1097/00005792-200207000-00002

Nau, R., Soto, A., and Bruck, W. (1999). Apoptosis of neurons in the dentate gyrus in humans suffering from bacterial meningitis. *J. Neuropathol. Exp. Neurol.* 58, 265–274. doi: 10.1097/00005072-199903000-00006

Pagliano, P., Arslan, F., and Ascione, T. (2017). Epidemiology and treatment of the commonest form of listeriosis: meningitis and bacteraemia. *Infez. Med.* 25, 210–216.

Pelegrin, I., Moragas, M., Suarez, C., Ribera, A., Verdaguer, R., Martinez-Yelamos, S., et al. (2014). Listeria monocytogenes meningoencephalitis in

adults: analysis of factors related to unfavourable outcome. *Infection* 42, 817–827. doi: 10.1007/s15010-014-0636-y

Perny, M., Roccio, M., Grandgirard, D., Solyga, M., Senn, P., and Leib, S. L. (2016). The severity of infection determines the localization of damage and extent of sensorineural hearing loss in experimental pneumococcal meningitis. *J. Neurosci.* 36, 7740–7749. doi: 10.1523/JNEUROSCI.0554-16.2016

Remer, K. A., Jungi, T. W., Fatzer, R., Täuber, M. G., and Leib, S. L. (2001). Nitric oxide is protective in listeric meningoencephalitis of rats. *Infect. Immun.* 69, 4086–4093. doi: 10.1128/IAI.69.6.4086-4093.2001

Semple, B. D., Blomgren, K., Gimlin, K., Ferriero, D. M., and Noble-Haeusslein, L. J. (2013). Brain development in rodents and humans: Identifying benchmarks of maturation and vulnerability to injury across species. *Prog. Neurobiol.* 106–107, 1–16. doi: 10.1016/j.pneurobio.2013.04.001

Sitaraman, R., Denison, A. M., and Dybvig, K. (2002). A unique, bifunctional site-specific DNA recombinase from Mycoplasma pulmonis. *Mol. Microbiol.* 46, 1033–1040. doi: 10.1046/j.1365-2958.2002.03206.x

Srikhanta, Y. N., Maguire, T. L., Stacey, K. J., Grimmond, S. M., and Jennings, M. P. (2005). The phasevarion: a genetic system controlling coordinated, random switching of expression of multiple genes. *Proc. Natl. Acad. Sci. U.S.A.* 102, 5547–5551. doi: 10.1073/pnas.0501169102

Tunkel, A. R., Hartman, B. J., Kaplan, S. L., Kaufman, B. A., Roos, K. L., Scheld, W. M., et al. (2004). Practice guidelines for the management of bacterial meningitis. *Clin. Infect. Dis.* 39, 1267–1284. doi: 10.1086/425368

van de Beek, D., Cabellos, C., Dzupova, O., Esposito, S., Klein, M., Kloek, A. T., et al. (2016). ESCMID guideline: diagnosis and treatment of acute bacterial meningitis. *Clin. Microbiol. Infect.* 22(Suppl 3), S37–S62. doi: 10.1016/j.cmi.2016.01.007

Vandivier, R. W., Henson, P. M., and Douglas, I. S. (2006). Burying the dead: the impact of failed apoptotic cell removal (efferocytosis) on chronic inflammatory lung disease. *Chest* 129, 1673–1682. doi: 10.1378/chest.129.6.1673

Wellmer, A., Noeske, C., Gerber, J., Munzel, U., and Nau, R. (2000). Spatial memory and learning deficits after experimental pneumococcal meningitis in mice. *Neurosci. Lett.* 296, 137–140. doi: 10.1016/S0304-3940(00)01645-1

Yildiz, O., Aygen, B., Esel, D., Kayabas, U., Alp, E., Sumerkan, B., et al. (2007). Sepsis and meningitis due to Listeria monocytogenes. *Yonsei. Med. J.* 48, 433–439. doi: 10.3349/ymj.2007.48.3.433

Yu, G. C., Smith, D. K., Zhu, H. C., Guan, Y., and Lam, T. T. Y. (2017). GGTREE: an R package for visualization and annotation of phylogenetic trees with their covariates and other associated data. *Methods Ecol. Evol.* 8, 28–36. doi: 10.1111/2041-210X.12628

Zamudio, R., Haigh, R. D., Ralph, J. D., De Ste Croix, M., Tasara, T., Zurfluh, K., et al. (2020). Lineage-specific evolution and gene flow in Listeria monocytogenes are independent of bacteriophages. *Environ. Microbiol.* doi: 10.1111/1462-2920.15111. [Epub ahead of print].

Conflict of Interest: The authors declare that the research was conducted in the absence of any commercial or financial relationships that could be construed as a potential conflict of interest.

frontiers in Cellular and Infection Microbiology

MINI REVIEW
published: 03 November 2020
doi: 10.3389/fcimb.2020.590682

Pneumococcal Encounter With the Blood–Brain Barrier Endothelium

*Anjali Anil and Anirban Banerjee**

Department of Biosciences and Bioengineering, Indian Institute of Technology Bombay, Mumbai, India

Meningitis, the inflammation of the protective membrane surrounding the brain and spinal cord (known as meninges), is a condition associated with high mortality rates and permanent neurological sequelae in a significant proportion of survivors. The opportunistic pathogen *Streptococcus pneumoniae* (SPN/pneumococcus) is the leading cause of bacterial meningitis in adults and older children. Following infection of the lower respiratory tract and subsequent bloodstream invasion, SPN breaches the blood–brain barrier endothelium for invasion of the central nervous system. Transcytosis, a mode of passage through the endothelial cells has been identified as the predominant route of pneumococcal blood–brain barrier trafficking. Herein, we review the interactions enabling SPN invasion into the brain endothelial cells, events involved in the tug-of-war between pneumococcal virulence factors and host intracellular defense machineries and pneumococcal strategies for evasion of host defenses and successful transendothelial trafficking.

Keywords: meningitis, *Streptococcus pneumoniae*, blood-brain barrier, brain microvascular endothelial cells, transcytosis, autophagy, ubiquitin-proteasome machinery

OPEN ACCESS

Edited by:
Federico Iovino,
Karolinska Institutet (KI), Sweden

Reviewed by:
Marco Rinaldo Oggioni,
University of Leicester,
United Kingdom
Mathieu Coureuil,
Institut National de la Santé et de la Recherche Médicale (INSERM), France

****Correspondence:***
Anirban Banerjee
abanerjee@iitb.ac.in

Specialty section:
This article was submitted to Bacteria and Host, a section of the journal Frontiers in Cellular and Infection Microbiology

Received: *02 August 2020*
Accepted: *22 September 2020*
Published: *03 November 2020*

Citation:
Anil A and Banerjee A (2020) Pneumococcal Encounter With the Blood–Brain Barrier Endothelium. Front. Cell. Infect. Microbiol. 10:590682. doi: 10.3389/fcimb.2020.590682

INTRODUCTION

The central nervous system (CNS) consists primarily of the brain, the control center of the body, and the spinal cord, enveloped in meninges and protected by the skull and vertebrae, respectively. The meninges is a membranous covering of connective tissue whose primary function is to shield the brain and spinal cord from trauma. It is composed of 3 layers: outermost dura matter, arachnoid, and the inner pia matter. The space between the arachnoid and pia matter is called the subarachnoid space and houses the cerebrospinal fluid and major vasculature. Acute inflammation of the meninges, a condition known as meningitis, is triggered by certain infections, autoimmune disorders, cancer, and drugs and is associated with a high mortality rate and long-term neurological sequelae in survivors (Collaborators, 2018). *Streptococcus pneumoniae*, *Neisseria meningitidis*, and *Hemophilus influenzae* are the major etiological agents of bacterial meningitis in adults and older children, and group B streptococcus is responsible for most cases in neonates (Oordt-Speets et al., 2018). *Streptococcus pneumoniae* (SPN/pneumococcus), a commensal resident of the human nasopharynx and an opportunistic pathogen, causes meningitis following bloodstream invasion from the lower respiratory tract and high-grade bacteremia (Mook-Kanamori et al., 2011). Although a spread of infection directly from the middle ear (following otitis media) to the brain has been reported (Marra and Brigham, 2001), SPN predominantly adopts the hematogenous route and breaches the blood–brain barrier (BBB) for invasion of the CNS.

The BBB is constituted by brain microvascular endothelial cells (BMECs), which form the wall of the blood capillaries, maintained by support from the basement membrane, astrocytes, and pericytes and helps to maintain homeostasis of the CNS. The BBB endothelium is characterized

by the presence of tight junctions and low pinocytosis/transcytosis ability. The tight junctions composed of claudins (specifically, claudin-3, −5, and −12), occludins and junction adhesion molecules are present toward the apical (luminal) side of the barrier and, along with the adherens junctions, contributes to the high transendothelial electrical resistance and dictates polarity to the BBB endothelium (Sandoval and Witt, 2008; Luissint et al., 2012). These features, along with the asymmetric distribution of efflux and nutrient transporters across the polarized endothelial membrane, enable it to strictly control the transport of blood-borne molecules into the brain and guard the latter from harmful materials present in the circulatory system (Daneman and Prat, 2015). Meningeal pathogens, however, have been shown to breach the BBB by (a) paracytosis: traversal via the intercellular space, (b) transcytosis: intracellular trafficking through the endothelial cells, or (c) Trojan horse mechanism: utilizing infected phagocytes as vehicles (Doran et al., 2013). Apart from these strategies, recognition of pathogen-associated molecular patterns (PAMPs) by host pattern recognition receptors (PRRs) following microbial invasion and replication in the brain elicits an overwhelming inflammatory response. Ensuing leukocyte recruitment along with the combined cytotoxicity of microbial toxins and reactive oxygen/nitrogen species generated by the immune cells lead to BBB disruption, which additionally fosters pathogen infiltration into the brain.

Events involved in the interaction of SPN with the BBB leading to meningitis is studied in detail by Iovino et al. (2013) using a clinical meningitis isolate TIGR4 (serotype 4) in a mouse model of bacteremia-derived meningitis. Subarachnoid vessels were identified as the primary contact site of SPN with the brain (at 1 h post-infection), which later spread to the cerebral cortex, septum, and eventually, to choroid plexus (by 8 h post-infection). Early in the course of infection, SPN were found tightly attached to the BBB endothelium; however, these numbers reduce with time with a concomitant increase in the number of SPN present in the brain tissue, suggesting pneumococcal translocation across the BBB. Interestingly, the junctions between the endothelial cells in the subarachnoid space and choroid plexus were found to be intact during the course of infection, suggesting that SPN predominantly adopts the transcytosis route for crossing the BBB, especially in the early stages of infection. Indeed, a follow-up study confirmed the presence of SPN inside the BMECs *in vivo* (Iovino et al., 2014). In this review, we summarize the molecular events involved in pneumococcal interaction with the BMECs, facilitating its trafficking across the BBB.

Adherence and Invasion

The first step in the interaction of blood-borne SPN with brain endothelium is adherence/attachment to BMECs. Multiple interactions between pneumococcal surface proteins and the brain endothelial cell receptors are known to facilitate this (**Figure 1**); some of these interactions are common across different cell types. Additionally, some of the receptors can bind to multiple ligands on the SPN surface and vice versa. The laminin receptor on the BMECs serve as a common receptor for the attachment of a wide array of meningeal/neurotropic agents (Orihuela et al., 2009). SPN interacts with the laminin receptor via PspC (also called CbpA), a member of the family of choline-binding proteins, which anchor to phosphoryl choline on the SPN cell wall (Orihuela et al., 2009). PspC additionally facilitates SPN adhesion to brain endothelium via its interaction with the human polymeric immunoglobulin receptor (hpIgR) (Iovino et al., 2017). hpIgR, along with the platelet endothelial cell adhesion molecule (PECAM-1), facilitate binding of SPN via the pneumococcal pilus-1 adhesin RrgA (Iovino et al., 2017). Enolase, the pneumococcal glycolytic enzyme is a moonlighting protein that gets secreted via an unknown mechanism (Bergmann et al., 2001). The surface-displayed enolase acts as a receptor to host cell surface-bound plasminogen, promoting SPN adherence to BMECs (Bergmann et al., 2013). A recent study that utilized a proteomics-bioinformatics approach to identify SPN cell wall ligands that mediate adherence to BMECs revealed 5 putative candidates: adhesion lipoprotein, pneumococcal histidine triad protein A (PhtA), endo-β-N-acetylglucosaminidase, and two hypothetical proteins: Spr0777 and Spr1730 (Jimenez-Munguia et al., 2018). Their respective interacting partners on the endothelium, however, remains to be investigated.

Following adherence, SPN internalize into (invade) endothelial cells via the endocytic pathway. Endocytosis is a eukaryotic cellular process designed for uptake of nutrients from the extracellular milieu but is exploited by microbes to gain entry into host cells (Cossart and Helenius, 2014). SPN have been shown to enter the BMECs via multiple endocytic routes, specifically clathrin- and caveolae-mediated pathways (Gradstedt et al., 2013). The former is characterized by the formation of clathrin coats on the vesicles budding off from the plasma membrane, and the latter is distinguished by the presence of caveolin and formation of flask-shaped invagination at cholesterol-rich domains of the plasma membrane (lipid rafts). Both of these are classified under dynamin-dependent pathways, which utilize the GTPase dynamin for the scission of vesicles from the plasma membrane. Recent findings from our lab additionally demonstrate a role of dynamin-independent pathways in facilitating SPN entry into BMECs (Surve et al., 2020).

One of the earliest identified SPN–host cell interactions is the binding of phosphoryl choline (PCho) present on SPN cell walls to the platelet-activating factor receptor (PAFR) on epithelial and endothelial cells (Cundell et al., 1995). This molecular mimicry of platelet-activating factor by PCho for binding to PAFR is also demonstrated by other respiratory/meningeal pathogens, such as *Neisseria meningitidis* and *Hemophilus influenzae* (Swords et al., 2001; Jen et al., 2013). PCho-PAFR interaction not only fosters SPN adherence to host cells, but also internalization via the clathrin-dependent endocytosis involving the adapter molecule β-arrestin 1 (Radin et al., 2005). Inflammatory activation of BMECs upon treatment with tumor necrosis factor (TNF-α) is demonstrated to remarkably improve SPN invasion via upregulation of PAFR expression (Cundell et al., 1995). Additionally, the transparent phase variants of SPN that harbor more PCho on the surface invades BMECs significantly better than the opaque phase variants (Ring et al., 1998). Neuraminidase

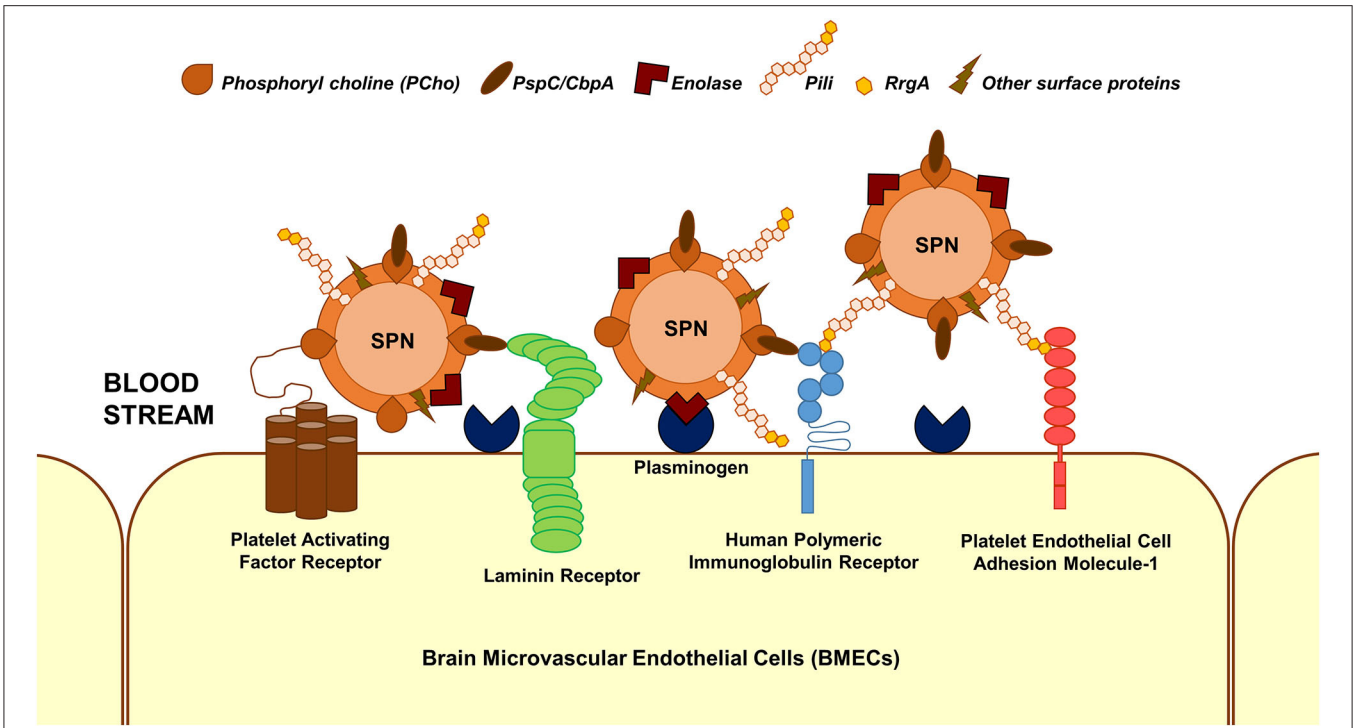

FIGURE 1 | Major interactions facilitating SPN adhesion to BMECs. Major interactions between SPN ligands and host cell receptors that enable adhesion of blood-borne SPN to BMECs are depicted. These involve but are not limited to phosphoryl choline–platelet activating factor receptor, PspC (CbpA)–laminin receptor, PspC–human polymeric immunoglobulin receptor, RrgA (component of pneumococcal pili)–human polymeric immunoglobulin receptor, RrgA–platelet endothelial cell adhesion molecule 1, and enolase–plasminogen interactions.

A (NanA) is a surface-attached exoglycosidase that removes terminal sialic acid from glycoconjugates, in turn, serving diverse purposes, such as nutrient acquisition, unmasking host receptors for attachment, disabling host components involved in bacterial clearance, etc. (King et al., 2006). Additionally, NanA has been demonstrated to induce inflammatory activation of BMECs in a sialidase-independent, laminin G–like lectin binding domain-dependent manner, enabling improved invasion of BMECs (Banerjee et al., 2010). Although ligand-receptor interaction facilitating SPN uptake into BMECs via a caveolae-dependent pathway has not been identified, the PspC-hpIgR interaction is shown to mediate SPN internalization via both clathrin- and caveolae-dependent endocytosis in epithelial cells (Asmat et al., 2014).

The polysaccharide capsule of SPN is an antiphagocytic factor that provides an advantage during bloodstream invasion by enabling it to escape complement-mediated opsonophagocytosis (Hyams et al., 2010). Presence of the capsule, however, poses a problem during SPN interaction with non-phagocytic cells and is shown to impede invasion of BMECs (Ring et al., 1998). To overcome this, SPN downregulate expression of the capsule during interaction with epithelial cells both *in vitro* and *in vivo*, enabled by the controlled activity of cell wall amidase LytA (Hammerschmidt et al., 2005; Kietzman et al., 2016). However, preliminary studies that compare the association of SPN with BBB endothelium using antipneumococcal serum and an antibody against the polysaccharide capsule reveal no difference, suggesting that the capsule is likely maintained during pneumococcal interaction with BMECs (Iovino et al., 2013).

Candidate combox site 4 (ccs4) is a competence-induced protein that has been implicated in facilitating SPN association and invasion of BMECs although the details of this interaction remain to be investigated (Hirose et al., 2018). With a plethora of SPN factors working in concert to aid SPN invasion of the CNS, a member of the family of paralogous zinc metalloproteases, ZmpC, has been demonstrated to impede BMEC invasion (Yamaguchi et al., 2017). This counterintuitive function of ZmpC is thought to be an evolutionary adaptation in SPN, aimed at attenuating virulence in order to minimize host mortality, in turn, enabling prolonged infection and replication within the host (Yamaguchi et al., 2017).

Intracellular Fate

Transmission electron microscopy analysis of infected BMECs reveals that SPN resides within intracellular vacuoles (Ring et al., 1998). The endocytic vacuole formed following fission of the plasma membrane undergoes a maturation process (from early to late endosome), acquiring different protein (Rab GTPases and effectors) and lipid markers (phosphoinositides) and eventually fuses with lysosomes resulting in the degradation of the cargo that they carry (Huotari and Helenius, 2011). Endosomal maturation is also accompanied by progressive acidification of the vacuolar

lumen, which is critical for the optimum activity of lysosomal hydrolases. A major fraction of SPN internalized into BMECs following PCho-PAFR interaction associated initially with Rab5 or EEA1 (markers of the early endosome) and later with Rab7 or LAMP-1 (markers of late endosome or lysosome), suggesting that they proceed toward lysosomal degradation (Radin et al., 2005). Indeed, treatment of BMECs with ammonium chloride (NH_4Cl) or chloroquine, which inhibit lysosome acidification, results in improved intracellular survival of SPN (Gradstedt et al., 2013). Inhibition of lysosomes also correlates with improved ability of SPN to transcytose across the BMECs in an *in vitro* transcytosis assay (Gradstedt et al., 2013). On the other hand, overexpression of β-arrestin 1, the protein involved in PAFR-mediated uptake of SPN, is found to reduce colocalization of SPN containing vacuoles with Rab7, suggesting its role in shunting of the vacuoles away from lysosomal degradation (Radin et al., 2005). The recently identified dynamin-independent pathway of pneumococcal internalization is also found to prevent targeting of SPN containing vacuoles to lysosomes (Surve et al., 2020).

Apart from the endocytic pathway, few other cellular homeostasis pathways also function as defense machineries against intracellular microbes; examples of these include autophagy and ubiquitin-proteasome machineries, which normally function to degrade aged organelles and damaged/misfolded proteins. A recent study reveals that SPN interacts with these pathways inside BMECs in a manner dependent on the expression of its pore-forming toxin pneumolysin (Surve et al., 2018). Pneumolysin (Ply) belongs to the family of cholesterol-dependent cytolysins (CDCs) and forms pores on eukaryotic membranes by a 3-step process consisting of (a) monomer binding to membrane cholesterol, (b) oligomerization to form a pre-pore structure, and (c) pre-pore to pore transition (Tilley et al., 2005). Surve et al. (2018) demonstrate that Ply expressed by SPN within BMEC vacuoles creates pores and ruptures the vacuolar membrane. This damage is sensed by the host cytosolic "eat me" signal galectin-8 (Gal8), which then binds to exposed glycans on the luminal side of ruptured vacuoles and interacts with the adapter molecule NDP52 to trigger antibacterial autophagy (xenophagy). Induction of autophagy results in enveloping of damaged SPN containing vacuoles in double membrane bound structures (autophagosomes) decorated with LC3B for fusion with lysosomes. Treatment with 3-methyl adenine, an autophagy inhibitor, improved the intracellular survival of SPN confirming the role of autophagy in SPN killing within BMECs (Surve et al., 2018). Interestingly, a subset of SPN is observed to reside within non-acidified autophagosomes for a prolonged period of time; however, the factors governing this phenotype remain elusive (Surve et al., 2018). In this context, CbpC (a choline-binding protein) released by SPN is shown to interact with and direct Atg14 (an autophagy-related protein) toward autophagic degradation in epithelial cells and fibroblasts, thus utilizing Atg14 depletion as a strategy to subvert xenophagic killing of intracellular SPN (Shizukuishi et al., 2020). Furthermore, excessive damage to the vacuolar membrane by Ply pores allows exit of SPN from the vacuole into the cytosol. Although cytosolic escape is advantageous for certain pathogens, such as *Listeria monocytogenes*, and facilitates cell-to-cell spread (Schnupf and Portnoy, 2007), cytosolic SPN is found to be recognized and tagged by host ubiquitin (Ubq) machinery for degradation either via autophagy or an autophagy-independent, proteasome-dependent pathway (Surve et al., 2018). Recent studies exploring the molecular details of SPN ubiquitination inside epithelial cells reveals that cytosolic SPN and vacuolar membrane remnants are tagged with the K48-type Ubq chains for autophagic degradation while SPN-containing autophagosomes harbor the K63-type Ubq chains, formed by the action of Nedd4-1 E3 ligase (Ogawa et al., 2018). Additionally, SPN is also shown to associate with the proteasome inside BMECs *in vivo* (Iovino et al., 2014), and proteasome inhibition by treatment with MG132 improves SPN intracellular survival (Iovino et al., 2014; Surve et al., 2018).

Studies by Surve et al. (2018) further illustrate the simultaneous existence of 6 different subsets of SPN within BMECs, each characterized by their association with a different combination of degradative pathway markers (Gal8, Ubq, and LC3). These intracellular subsets are found to arise as a consequence of heterogeneous expression of Ply among the individual cells of an isogenic SPN population (Surve et al., 2018). SPN expressing a low amount of Ply (SPN:Ply-low) are found to be predominantly confined to the vacuole while those expressing a high amount of Ply (SPN:Ply-high) are mostly cytosolic with the former demonstrating improved intracellular survival compared to the latter (Surve et al., 2018). SPN:Ply-high, owing to extensive damage to vacuolar membrane became cytosol exposed where they were detected by host ubiquitin machinery and subjected to clearance (Surve et al., 2018). SPN:Ply-low also occupied a unique vacuole, devoid of Gal8 and Ubq but positive for LC3. These $Gal8^{-}Ubq^{-}LC3^{+}$ vacuoles are speculated to originate as a result of formation of small ion-channel-sized pores on the vacuolar membrane (by action of low amount of Ply), causing osmotic imbalance and, in turn, recruiting LC3 independent of conventional autophagy markers (a form of non-canonical autophagy) (Florey et al., 2015; Surve et al., 2018). A similar, Ply-dependent formation of non-canonical, LC3-associated phagosome (LAP)-like vacuoles harboring SPN has also been observed in epithelial cells and were found to serve as a precursor to the formation of canonical SPN containing autophagosomes (Ogawa et al., 2020). The improved ability of SPN:Ply-low to survive inside BMECs are also reflected in their ability to transcytose across the BBB and invade the brain in a mouse model of meningitis (Surve et al., 2018). Consistent with these findings, clinical meningitis isolates TIGR4 (serotype 4) and Tupelo (serotype 14) were found to consist of low numbers of Ply producers in comparison to a sepsis strain D39 (serotype 2) or a colonizer strain A60 (serotype 19F) (Surve et al., 2018).

Recycling and Transcytosis

Although a major fraction of SPN get killed by the machineries inside the host cell, a subset successfully evade the intracellular defenses and transcytose across the endothelium for invasion of the brain, resulting in uncontrolled bacterial replication and development of meningitis. Another fraction was found to recycle out of apical side of the endothelium in vacuoles

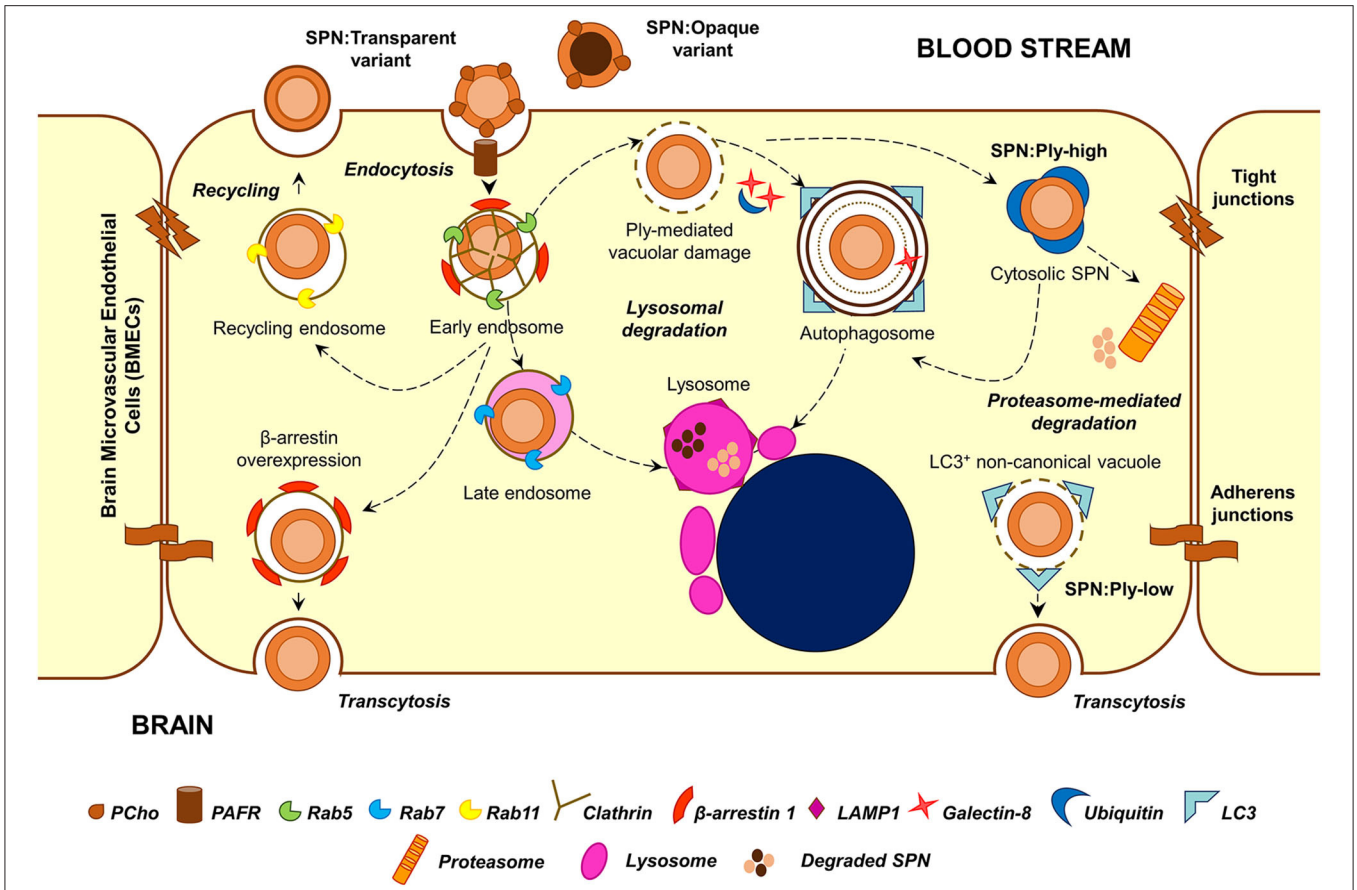

FIGURE 2 | Major stages in the intracellular stint of SPN within BMECs. Following PCho-PAFR interaction, SPN is internalized into BMECs via clathrin-dependent endocytosis, in vacuoles decorated with β-arrestin 1. A major fraction of these vacuoles undergoes maturation and fusion with lysosomes; overexpression of β-arrestin 1 shunts these vacuoles away from lysosomal killing for improved transcytosis. A minor subset of these vacuoles recycles back to the apical side. Ply-mediated damage to SPN containing vacuoles trigger recruitment of cytosolic "eat me" signals, such as galectin-8 and ubiquitin, which target these vacuoles toward autophagic (xenophagic) degradation. Excessive damage to the vacuolar membrane enable SPN to escape into the cytosol, where it is tagged by ubiquitin for degradation by autophagy or proteasome-mediated pathway. Expression of low amounts of Ply also give rise to a unique Gal8^{-}Ubq^{-}LC3^{+} non-canonical autophagic vacuoles, which has been speculated to have improved transcytosis ability. The transparent phase variants of SPN, owing to higher amounts of surface-exposed PCho, demonstrate improved invasive, and transcytosis capability. On the other hand, a majority of the opaque phase variants are degraded within lysosomes.

decorated with Rab11 (marker of recycling endosome) (Radin et al., 2005). This population, which recycles back into the bloodstream, is thought to serve as a reservoir for infection, temporarily hidden from the host intracellular defenses (Ring et al., 1998).

The opaque and transparent phase variants demonstrate a clear distinction in their intracellular fates. The opaque variants are mostly killed within the BMECs while the transparent variants undergo transcytosis (Ring et al., 1998). A fraction of transparent variants also recycle back to the apical surface (Ring et al., 1998). PAFR-mediated invasion and association of β-arrestin 1 with SPN containing vacuoles is suggested to play a role in this by reducing its association with Rab7 and skewing SPN fate toward transcytosis away from lysosomal killing or recycling (Ring et al., 1998; Radin et al., 2005). There exists another school of thought according to which transcytosis across endothelial cells is mediated by caveolae-dependent endocytosis (Simionescu et al., 2009). Whether the PspC-hpIgR interaction leads to caveolae-dependent invasion in endothelial cells and whether this pathway supports SPN transcytosis is yet to be explored.

The low Ply expressing SPN subset demonstrates improved transcytosis ability both *in vitro* and *in vivo* (Surve et al., 2018). Pore-forming toxin mediates release of Ca^{2+} from bacteria-containing vacuoles into the host cytosol has been speculated to facilitate exocytosis-like exit of *Serratia marcescens* from the host cell (Di Venanzio et al., 2017); a similar mechanism might explain the improved transcytosis of SPN:Ply-low. Apart from these, the chain size also plays a role in dictating the fate in internalized SPN. Work by Iovino et al. (2016) demonstrates that, off the SPN, which exists mostly as chains in the bloodstream, a small fraction (<5%) of piliated, RrgA-expressing single-cocci are the ones that successfully cross the BBB. Although the identity and role of pneumococcal factors that enable evasion

of BMEC intracellular defenses are becoming clearer, transit of the lysosome-evaded SPN-containing vacuole to the basal side of the polarized endothelium would require additional steps, probably involving manipulation of host cytoskeleton and motor molecules; this might be an interesting avenue for future research.

CONCLUSION

Pneumococcal encounter with the BBB endothelium is a critical event in meningitis involving an interplay of several pneumococcal and host factors. Initial events of adhesion and invasion are driven by SPN surface proteins and involve usurping of diverse endothelial cell receptors for gaining entry into the cell (**Figure 1**). In spite of being an extracellular pathogen, SPN own impressive strategies to invade and evade the degradative machineries of the BBB endothelium for successful transcytosis (**Figure 2**). This involves utilizing specialized endocytic pathways that confer a survival advantage, maintenance of phenotypic variants in virulence factors, such as capsule and pneumolysin, which influences its intracellular fate, etc. Transcytosis across the capillary endothelium into the brain presents a niche for unrestricted pneumococcal replication, in turn, eliciting an overwhelming host inflammatory response, which significantly contributes to the tissue injury associated with meningitis. Current treatment for pneumococcal meningitis includes antibiotics and adjunctive therapy with corticosteroids, such as dexamethasone to manage the inflammation (Hoffman and Weber, 2009). Immunization with pneumococcal vaccines is an effective prevention strategy to reduce incidences of invasive pneumococcal diseases, including meningitis, but is complicated due to emergence and rise of non-vaccine serotypes (Hsu et al., 2009). Detailed understanding of the events involved in pneumococcal interaction with the BBB endothelium is hoped to enable better management of pneumococcal meningitis.

AUTHOR CONTRIBUTIONS

AA and AB wrote the manuscript and prepared the figures.

REFERENCES

Asmat, T. M., Agarwal, V., Saleh, M., and Hammerschmidt, S. (2014). Endocytosis of *Streptococcus pneumoniae* via the polymeric immunoglobulin receptor of epithelial cells relies on clathrin and caveolin dependent mechanisms. *Int. J. Med. Microbiol.* 304, 1233–1246. doi: 10.1016/j.ijmm.2014.10.001

Banerjee, A., Van Sorge, N. M., Sheen, T. R., Uchiyama, S., Mitchell, T. J., and Doran, K. S. (2010). Activation of brain endothelium by pneumococcal neuraminidase NanA promotes bacterial internalization. *Cell. Microbiol.* 12, 1576–1588. doi: 10.1111/j.1462-5822.2010.01490.x

Bergmann, S., Rohde, M., Chhatwal, G. S., and Hammerschmidt, S. (2001) α-Enolase of *Streptococcus pneumoniae* is a plasmin(ogen)-binding protein displayed on the bacterial cell surface. *Mol. Microbiol.* 40, 1273–1287. doi: 10.1046/j.1365-2958.2001.02448.x

Bergmann, S., Schoenen, H., and Hammerschmidt, S. (2013). The interaction between bacterial enolase and plasminogen promotes adherence of *Streptococcus pneumoniae* to epithelial and endothelial cells. *Int. J. Med. Microbiol.* 303, 452–462. doi: 10.1016/j.ijmm.2013.06.002

Collaborators, G. B. D. M. (2018). Global, regional, and national burden of meningitis, 1990-2016: a systematic analysis for the global burden of disease study 2016. *Lancet Neurol.* 17, 1061–1082. doi: 10.1016/S1474-4422(18)30387-9

Cossart, P., and Helenius, A. (2014). Endocytosis of viruses and bacteria. *Cold Spring Harb. Perspect. Biol.* 6:a016972. doi: 10.1101/cshperspect.a016972

Cundell, D. R., Gerard, N. P., Gerard, C., Idanpaan-Heikkila, I., and Tuomanen, E. I. (1995). *Streptococcus pneumoniae* anchor to activated human cells by the receptor for platelet-activating factor. *Nature* 377, 435–438. doi: 10.1038/377435a0

Daneman, R., and Prat, A. (2015). The blood-brain barrier. *Cold Spring Harb. Perspect. Biol.* 7:a020412. doi: 10.1101/cshperspect.a020412

Di Venanzio, G., Lazzaro, M., Morales, E. S., Krapf, D., and Garcia Vescovi, E. (2017). A pore-forming toxin enables serratia a nonlytic egress from host cells. *Cell. Microbiol.* 19:e12656. doi: 10.1111/cmi.12656

Doran, K. S., Banerjee, A., Disson, O., and Lecuit, M. (2013). Concepts and mechanisms: crossing host barriers. *Cold Spring Harb. Perspect. Med.* 3:a010090. doi: 10.1101/cshperspect.a010090

Florey, O., Gammoh, N., Kim, S. E., Jiang, X., and Overholtzer, M. (2015). V-ATPase and osmotic imbalances activate endolysosomal LC3 lipidation. *Autophagy* 11, 88–99. doi: 10.4161/15548627.2014.984277

Gradstedt, H., Iovino, F., and Bijlsma, J. J. (2013). *Streptococcus pneumoniae* invades endothelial host cells via multiple pathways and is killed in a lysosome dependent manner. *PLoS ONE* 8:e65626. doi: 10.1371/journal.pone.0065626

Hammerschmidt, S., Wolff, S., Hocke, A., Rosseau, S., Muller, E., and Rohde, M. (2005). Illustration of pneumococcal polysaccharide capsule during adherence and invasion of epithelial cells. *Infect. Immun.* 73, 4653–4667. doi: 10.1128/IAI.73.8.4653-4667.2005

Hirose, Y., Yamaguchi, M., Goto, K., Sumitomo, T., Nakata, M., and Kawabata, S. (2018). Competence-induced protein Ccs4 facilitates pneumococcal invasion into brain tissue and virulence in meningitis. *Virulence* 9, 1576–1587. doi: 10.1080/21505594.2018.1526530

Hoffman, O., and Weber, R. J. (2009). Pathophysiology and treatment of bacterial meningitis. *Ther. Adv. Neurol. Disord.* 2, 1–7. doi: 10.1177/1756285609337975

Hsu, H. E., Shutt, K. A., Moore, M. R., Beall, B. W., Bennett, N. M., Craig, A. S., et al. (2009). Effect of pneumococcal conjugate vaccine on pneumococcal meningitis. *N. Engl. J. Med.* 360, 244–256. doi: 10.1056/NEJMoa0800836

Huotari, J., and Helenius, A. (2011). Endosome maturation. *EMBO J.* 30, 3481–3500. doi: 10.1038/emboj.2011.286

Hyams, C., Camberlein, E., Cohen, J. M., Bax, K., and Brown, J. S. (2010). The *Streptococcus pneumoniae* capsule inhibits complement activity and neutrophil phagocytosis by multiple mechanisms. *Infect. Immun.* 78, 704–715. doi: 10.1128/IAI.00881-09

Iovino, F., Engelen-Lee, J. Y., Brouwer, M., van de Beek, D., van der Ende, A., Valls Seron, M., et al. (2017). pIgR and PECAM-1 bind to pneumococcal adhesins RrgA and PspC mediating bacterial brain invasion. *J. Exp. Med.* 214, 1619–1630. doi: 10.1084/jem.20161668

Iovino, F., Gradstedt, H., and Bijlsma, J. J. (2014). The proteasome-ubiquitin system is required for efficient killing of intracellular *Streptococcus pneumoniae* by brain endothelial cells. *MBio* 5, e00984–e00914. doi: 10.1128/mBio.00984-14

Iovino, F., Hammarlof, D. L., Garriss, G., Brovall, S., Nannapaneni, P., and Henriques-Normark, B. (2016). Pneumococcal meningitis is promoted by single cocci expressing pilus adhesin RrgA. *J. Clin. Invest.* 126, 2821–2826. doi: 10.1172/JCI84705

Iovino, F., Orihuela, C. J., Moorlag, H. E., Molema, G., and Bijlsma, J. J. (2013). Interactions between blood-borne *Streptococcus pneumoniae* and the blood-brain barrier preceding meningitis. *PLoS ONE* 8:e68408. doi: 10.1371/journal.pone.0068408

Jen, F. E., Warren, M. J., Schulz, B. L., Power, P. M., Swords, W. E., Weiser, J. N., et al. (2013). Dual pili post-translational modifications synergize to mediate meningococcal adherence to platelet activating factor receptor on human airway cells. *PLoS Pathog.* 9:e1003377. doi: 10.1371/journal.ppat.1003377

Jimenez-Munguia, I., Pulzova, L., Kanova, E., Tomeckova, Z., Majerova, P., Bhide, K., et al. (2018). Proteomic and bioinformatic pipeline to screen the ligands of

S. pneumoniae interacting with human brain microvascular endothelial cells. *Sci. Rep*. 8:5231. doi: 10.1038/s41598-018-23485-1

Kietzman, C. C., Gao, G., Mann, B., Myers, L., and Tuomanen, E. I. (2016). Dynamic capsule restructuring by the main pneumococcal autolysin LytA in response to the epithelium. *Nat. Commun*. 7:10859. doi: 10.1038/ncomms10859

King, S. J., Hippe, K. R., and Weiser, J. N. (2006). Deglycosylation of human glycoconjugates by the sequential activities of exoglycosidases expressed by *Streptococcus pneumoniae*. *Mol. Microbiol*. 59, 961–974. doi: 10.1111/j.1365-2958.2005.04984.x

Luissint, A. C., Artus, C., Glacial, F., Ganeshamoorthy, K., and Couraud, P. O. (2012). Tight junctions at the blood brain barrier: physiological architecture and disease-associated dysregulation. *Fluids Barriers CNS*. 9:23. doi: 10.1186/2045-8118-9-23

Marra, A., and Brigham, D. (2001). *Streptococcus pneumoniae* causes experimental meningitis following intranasal and otitis media infections via a nonhematogenous route. *Infect. Immun*. 69, 7318–7325. doi: 10.1128/IAI.69.12.7318-7325.2001

Mook-Kanamori, B. B., Geldhoff, M., van der Poll, T., and van de Beek, D. (2011). Pathogenesis and pathophysiology of pneumococcal meningitis. *Clin. Microbiol. Rev*. 24, 557–591. doi: 10.1128/CMR.00008-11

Ogawa, M., Matsuda, R., Takada, N., Tomokiyo, M., Yamamoto, S., Shizukuishi, S., et al. (2018). Molecular mechanisms of *Streptococcus pneumoniae*-targeted autophagy via pneumolysin, golgi-resident Rab41, and Nedd4-1-mediated K63-linked ubiquitination. *Cell. Microbiol*. 20:e12846. doi: 10.1111/cmi.12846

Ogawa, M., Takada, N., Shizukuishi, S., Tomokiyo, M., Chang, B., Yoshida, M., et al. (2020). *Streptococcus pneumoniae* triggers hierarchical autophagy through reprogramming of LAPosome-like vesicles via NDP52-delocalization. *Commun. Biol*. 3:25. doi: 10.1038/s42003-020-0753-3

Oordt-Speets, A. M., Bolijn, R., van Hoorn, R. C., Bhavsar, A., and Kyaw, M. H. (2018). Global etiology of bacterial meningitis: a systematic review and meta-analysis. *PLoS ONE* 13:e0198772. doi: 10.1371/journal.pone.0198772

Orihuela, C. J., Mahdavi, J., Thornton, J., Mann, B., Wooldridge, K. G., Abouseada, N., et al. (2009). Laminin receptor initiates bacterial contact with the blood brain barrier in experimental meningitis models. *J. Clin. Invest*. 119, 1638–1646. doi: 10.1172/JCI36759

Radin, J. N., Orihuela, C. J., Murti, G., Guglielmo, C., Murray, P. J., and Tuomanen, E. I. (2005). β-Arrestin 1 participates in platelet-activating factor receptor-mediated endocytosis of *Streptococcus pneumoniae*. *Infect. Immun*. 73, 7827–7835. doi: 10.1128/IAI.73.12.7827-7835.2005

Ring, A., Weiser, J. N., and Tuomanen, E. I. (1998). Pneumococcal trafficking across the blood-brain barrier. Molecular analysis of a novel bidirectional pathway. *J. Clin. Invest*. 102, 347–360. doi: 10.1172/JCI2406

Sandoval, K. E., and Witt, K. A. (2008). Blood-brain barrier tight junction permeability and ischemic stroke. *Neurobiol. Dis*. 32, 200–219. doi: 10.1016/j.nbd.2008.08.005

Schnupf, P., and Portnoy, D. A. (2007). Listeriolysin O: a phagosome-specific lysin. *Microbes Infect*. 9, 1176–1187. doi: 10.1016/j.micinf.2007.05.005

Shizukuishi, S., Ogawa, M., Matsunaga, S., Tomokiyo, M., Ikebe, T., Fushinobu, S., et al. (2020). *Streptococcus pneumoniae* hijacks host autophagy by deploying CbpC as a decoy for Atg14 depletion. *EMBO Rep*. 21:e49232. doi: 10.15252/embr.201949232

Simionescu, M., Popov, D., and Sima, A. (2009). Endothelial transcytosis in health and disease. *Cell. Tissue Res*. 335, 27–40. doi: 10.1007/s00441-008-0688-3

Surve, M. V., Apte, S., Bhutda, S., Kamath, K. G., Kim, K. S., and Banerjee, A. (2020). *Streptococcus pneumoniae* utilizes a novel dynamin independent pathway for entry and persistence in brain endothelium. *Curr. Res. Microbial Sci*. 1, 62–68. doi: 10.1016/j.crmicr.2020.08.001

Surve, M. V., Bhutda, S., Datey, A., Anil, A., Rawat, S., Pushpakaran, A., et al. (2018). Heterogeneity in pneumolysin expression governs the fate of *Streptococcus pneumoniae* during blood-brain barrier trafficking. *PLoS Pathog*. 14:e1007168. doi: 10.1371/journal.ppat.1007168

Swords, W. E., Ketterer, M. R., Shao, J., Campbell, C. A., Weiser, J. N., and Apicella, M. A. (2001). Binding of the non-typeable haemophilus influenzae lipooligosaccharide to the PAF receptor initiates host cell signalling. *Cell. Microbiol*. 3, 525–536. doi: 10.1046/j.1462-5822.2001.00132.x

Tilley, S. J., Orlova, E. V., Gilbert, R. J., Andrew, P. W., and Saibil, H. R. (2005). Structural basis of pore formation by the bacterial toxin pneumolysin. *Cell* 121, 247–256. doi: 10.1016/j.cell.2005.02.033

Yamaguchi, M., Nakata, M., Sumioka, R., Hirose, Y., Wada, S., Akeda, Y., et al. (2017). Zinc metalloproteinase ZmpC suppresses experimental pneumococcal meningitis by inhibiting bacterial invasion of central nervous systems. *Virulence* 8, 1516–1524. doi: 10.1080/21505594.2017.1328333

Conflict of Interest: The authors declare that the research was conducted in the absence of any commercial or financial relationships that could be construed as a potential conflict of interest.

frontiers in Cellular and Infection Microbiology

ORIGINAL RESEARCH
published: 05 November 2020
doi: 10.3389/fcimb.2020.588195

Adjuvant Cannabinoid Receptor Type 2 Agonist Modulates the Polarization of Microglia Towards a Non-Inflammatory Phenotype in Experimental Pneumococcal Meningitis

Steven D. Pan, Denis Grandgirard† and Stephen L. Leib†*

Neuroinfection Laboratory, Institute for Infectious Diseases, University of Bern, Bern, Switzerland

OPEN ACCESS

Edited by:
Federico Iovino, Karolinska Institutet (KI), Sweden

Reviewed by:
Lars-Ove Brandenburg, University Hospital RWTH Aachen, Germany
Elisabetta Blasi, University of Modena and Reggio Emilia, Italy

***Correspondence:**
Stephen L. Leib
stephen.leib@ifik.unibe.ch

†These authors have contributed equally to this work

Specialty section:
This article was submitted to Bacteria and Host, a section of the journal Frontiers in Cellular and Infection Microbiology

Received: *28 July 2020*
Accepted: *14 October 2020*
Published: *05 November 2020*

Citation:
Pan SD, Grandgirard D and Leib SL (2020) Adjuvant Cannabinoid Receptor Type 2 Agonist Modulates the Polarization of Microglia Towards a Non-Inflammatory Phenotype in Experimental Pneumococcal Meningitis. Front. Cell. Infect. Microbiol. 10:588195. doi: 10.3389/fcimb.2020.588195

Background: Microglia initiates and sustains the inflammatory reaction that drives the pathogenesis of pneumococcal meningitis. The expression of the G-protein cannabinoid receptor type 2 (CB2) in the brain is low, but is upregulated in glial cells during infection. Its activation down-regulates pro-inflammatory processes, driving microglia towards an anti-inflammatory phenotype. CB2 agonists are therefore therapeutic candidates in inflammatory conditions like pneumococcal meningitis. We evaluated the effects of JWH-133, a specific CB2 agonist on microglial cells, inflammation, and damage driven by *S. pneumoniae in vitro* and in experimental pneumococcal meningitis.

Materials/methods: Primary mixed glial cultures were stimulated with live or heat-inactivated *S. pneumoniae*, or lipopolysaccharide and treated with JWH-133 or vehicle. Nitric oxide and cytokines levels were measured in the supernatant. *In vivo*, pneumococcal meningitis was induced by intracisternal injection of live *S. pneumoniae* in 11 days old Wistar rats. Animals were treated with antibiotics (Ceftriaxone, 100 mg/kg, s.c. bid) and JWH-133 (1 mg/kg, i.p. daily) or vehicle (10% Ethanol in saline, 100 µl/25g body weight) at 18 h after infection. Brains were harvested at 24 and 42 h post infection (hpi) for histological assessment of hippocampal apoptosis and cortical damage and determination of cyto/chemokines in tissue homogenates. Microglia were characterized using Iba-1 immunostaining. Inflammation in brain homogenates was determined using membrane-based antibody arrays.

Results: *In vitro*, nitric oxide and cytokines levels were significantly lowered by JWH-133 treatment. *In vivo*, clinical parameters were not affected by the treatment. JWH-133 significantly lowered microglia activation assessed by quantification of cell process length and endpoints per microglia. Animals treated with JWH-133 demonstrated significantly lower parenchymal levels of chemokines (CINC-1, CINC-2α/β, and MIP-3α), TIMP-1, and IL-6 at 24 hpi, and CINC-1, MIP-1α, and IL-1α at 42 hpi. Quantitative analysis of brain damage did not reveal an effect of JWH-133.

Conclusions: JWH-133 attenuates microglial activation and downregulates the concentrations of pro-inflammatory mediators in pneumococcal infection *in vitro* and *in vivo*. However, we didn't observe a reduction in cortical or hippocampal injury. This data provides evidence that inhibition of microglia by adjuvant CB2 agonists therapy effectively downmodulates neuroinflammation but does not reduce brain damage in experimental pneumococcal meningitis

Keywords: bacterial meningitis, microglia, endocannabinoid system, neuro-inflammation, brain damage

INTRODUCTION

In bacterial meningitis an overshooting inflammatory reaction in the central nervous system contributes to the pathophysiology of the disease including the development of brain damage. Specifically, pneumococcal meningitis is characterized by a high rate of mortality and morbidity, even when patients are treated with efficient antibiotic therapy. Survivors, in particular children, are left with several long-lasting disabilities, the most frequent being hearing loss, but also cognitive impairments, including learning and memory deficits, as well as focal neurological deficits (Edmond et al., 2010; Agyeman et al., 2014; Lucas et al., 2016; Muri et al., 2019a). The causes of these different sequelae have been deduced from the histological analyses of tissues of deceased patients or from experimental models. Hearing loss has been related to damage in the inner ear, including loss of hair cells or spiral ganglion neurons and from cochlear ossification (Klein et al., 2003; Perny et al., 2016). Focal neurological deficits are mostly caused by cerebrovascular events or intracerebral bleeding and characterized by the occurrence of cerebral infarcts due to localized hypoxia/ischemia or hemorrhages, respectively (Ment et al., 1986; Auer et al., 2000; Vergouwen et al., 2010). Finally, the development of cognitive impairments was linked to the detection of hippocampal damage, including apoptosis in the dentate gyrus (Nau et al., 1999; Wellmer et al., 2000; Loeffler et al., 2001; Leib et al., 2003; Grandgirard et al., 2007a).

On the pathophysiological level, these damages are the consequence of an intensive inflammatory reaction initiated by the recognition of bacterial compounds by endothelial cells, microglia and perivascular macrophages. The further recruitment of neutrophils in the cerebrospinal fluid contributes to the over-production of pro-inflammatory mediators, including cytokines, chemokines, matrix-metalloproteinases, and nitric oxide. Together with the release of bacterial toxins, they contribute directly or indirectly to the development of the different forms of damage described above (Mook-Kanamori et al., 2011; Agyeman et al., 2014).

Limiting this detrimental inflammatory reaction has therefore been extensively investigated (Van Der Flier et al., 2003; Grandgirard and Leib, 2006; Bewersdorf et al., 2018), but to date, adjuvant corticosteroids is the only recommended therapeutic option (Van De Beek et al., 2016). It has been proven beneficial, in specific patient populations, especially in high income countries, for the prevention of hearing loss (Brouwer et al., 2015). However, detrimental effects of dexamethasone therapy has been observed in a number of experimental models (Leib et al., 2003; Spreer et al., 2006; Bally et al., 2016) and dexamethasone may predispose patients to delayed cerebral thrombosis (Lucas et al., 2013).

Thus, alternative anti-inflammatory approaches for the adjuvant therapy of BM are being evaluated. Recently, the endocannabinoid system has received considerable attention for its potential to modulate inflammation and pain disorders. Immune cells, regardless of their lineage, express cannabinoid receptors (CB). These receptors are divided into multiple subtypes, the most common being central cannabinoid receptor type 1 (CB1) and peripheral cannabinoid receptor type 2 (CB2) (Facci et al., 1995; Mccoy, 2016). CB1 is primarily expressed in the CNS and various peripheral tissues. On the other hand, CB2 is prevalent within all lineage of the immune system. In the healthy brain, CB2 expression is limited (Svizenska et al., 2008; Turcotte et al., 2016). However, during neurological diseases, glial cells express high levels of CB2 (Ashton and Glass, 2007; Stella, 2010). *In vitro* experiments demonstrated that activation of CB2 by its endogenous ligands, the endocannabinoids, led to contrasting results. While activation with 2-arachidonoyl-glycerol (2-AG) mostly up-regulated functions related to leukocytes recruitment, *N*-Arachidonoyl-ethanolamide (AEA) down-regulated leukocyte functions, such as pro-inflammatory cytokine release and nitric oxide production (Turcotte et al., 2016). In contrast to endocannabinoids, exogenous CB2 receptor agonists exert exclusively anti-inflammatory activity. It has been for example demonstrated that JWH-015 repressed LPS-induced TNF-α production and migration in microglial cells (Romero-Sandoval et al., 2009). It also suppressed TNF-α and nitric oxide production induced by IFN-γ or Aβ peptide (Ehrhart et al., 2005). Furthermore, *in vivo* studies demonstrated that CB2 knockout mice were characterized by the development of an exacerbated inflammatory response, including increased leukocyte recruitment and pro-inflammatory cytokine production, which often caused tissue damage. In particular, CB2 -/- mice with traumatic brain injury displayed an increased gene expression of TNF-α, iNOS and ICAM, accompanied by an elevated blood brain barrier permeability (Amenta et al., 2014).

JWH-133 is a potent and selective CB2 agonist, with no activity on CB1 receptor, in both human and mouse. It has therefore been recommended as one of the most suitable CB2 agonist for preclinical target validation (Soethoudt et al., 2017).

It has already been shown to have beneficial effects, including downregulation of the inflammation and the improvement in neurofunctional outcome in different experimental models of brain injury, including okadaic-induced neurodegeneration (Cakir et al., 2019), subarachnoid hemorrhages (Fujii et al., 2014a; Fujii et al., 2014b), stroke (Zarruk et al., 2012; Li et al., 2015; Bravo-Ferrer et al., 2017), endotoxemia (Gamal et al., 2015), traumatic brain injury (Amenta et al., 2014) or Parkinson's disease (Chung et al., 2016).

Since pneumococcal meningitis shares pathophysiological mechanisms with some of the brain diseases successfully targeted by JWH-133, we hypothesized that its application as adjuvant therapy may prevent the excessive neuroinflammation by reducing pro-inflammatory glial activity during the acute phase of the disease and attenuate brain damage.

MATERIALS AND METHODS

Infecting Organism

A clinical isolate of *Streptococcus pneumoniae* (serotype 3) from a patient with bacterial meningitis was cultured overnight in Brain Heart Infusion (BHI) medium, diluted tenfold in pre-warmed BHI, and grown for 5 h to reach logarithmic growth phase. Bacteria were then centrifuged for 10 min at 3,100 × g and resuspended in 0.85% saline (NaCl). After a second wash in saline, bacteria were further diluted with saline to the desired optical density at 570 nm, so to obtain a mean concentration of approx. 1×10^7 CFU/ml. Inoculum concentration was determined using serial dilution and plating on Columbia sheep blood agar (CSBA) plates.

In Vitro Mixed Glia Stimulation

Mixed glial cultures consisting of microglial and astroglial cells were isolated from infant rat brains at postnatal day 3 (P3) as previously described (Muri et al., 2019b). Cortex was mechanically homogenized in PBS by pipetting up and down, and resuspended in DMEM (Sigma-Aldrich, Merk Switzerland) containing 5% FCS (Biochrom, Germany), 1% GlutaMAX™ (ThermoFisher, Switzerland) and antibiotic-antimycotic solution (100 units/ml penicillin and streptomycin, 0,25 µg/ml Amphotericin B, Thermofisher, Switzerland) and plated in a poly-L-ornithine-coated T75 flask. On day 11, cells were seeded at a density of 200,000 cells/well onto a poly-o-ornithine coated 24-well plate. Mixed glial cells were challenged with 1 µg/ml of lipopolysaccharide (*Escherichia coli*, L2654, Sigma-Aldrich), live *S. pneumoniae* serotype 3 (9.1×10^8 CFU/ml) in presence of Ceftriaxone (CRO, 12 mg/ml, Rocephine, Roche) or PBS as a control. Each group was treated with 1.0 µM of JWH-133 (Tocris Bioscience) compared to untreated cells. Three independent experiments were performed with all conditions in triplicates.

Quantification of Nitric Oxide Production From Mixed Glial Cell Stimulation

After 42 h challenge, 100 µl of cell culture supernatant was mixed with 100 µl of Griess reagent (Sigma-Aldrich) in a 96-well plate. NO_2- concentration, serving as an indicator of NO release, was determined by measuring absorbance at 550 nm with a microplate reader (Molecular Devices, THERMO max). A serial dilution of $NaNO_2$ from 100–1.625 µM was used to generate a standard curve. All measures were performed in triplicate and a mean value was calculated

Quantification of Cyto/Chemokines in the Supernatants of Stimulated Mixed Glial Cells

Cytokines known to be upregulated during PM (IL-1β, IL-6, TNF-α, IL-10, and IFN-γ) were assessed using magnetic multiplex assay (Rat Magnetic Luminex® Assay, Rat Premixed Multi-Analyte Kit, R&D Systems, Bio-Techne) on a Bio-Plex 200 station (Bio-Rad Laboratories) as described previously (Muri et al., 2019a). Fifty µl of cell culture medium was used undiluted. For each sample, a minimum of 50 beads was measured. If the concentration of the sample was below the detection limit, a value corresponding to the detection limit provided by the manufacturer was used, considering the dilution factor. The detection limits for undiluted samples were 2.93 pg/ml for IL-1β, 23.2 pg/ml for IL-6, 8.95 pg/ml for IL-10, 11.5 pg/ml for TNF-α, and 70.9 pg/ml for IFN-γ.

In Vivo Pneumococcal Meningitis Model

All animal experiments were approved by the Animal Care and Experimentation Committee of the Canton of Bern (BE 1/18). A well characterized *in vivo* model of pneumococcal meningitis was used (Leib et al., 2001; Perny et al., 2016). Eleven-day old mixed gender Wistar rats and their dams were purchased from Charles River (Sulzfeld, Germany), and housed at room temperature (22 ± 2°C) in natural light. The pups were infected intracisternally with 10 µl of live *S. pneumoniae* serotype 3 ($1.14 \times 10^7 \pm 7.5 \times 10^6$ CFU/ml). Control animals were injected with 10 µl of 0.85% NaCl. Meningitis was confirmed through quantification of bacterial titers from cerebrospinal fluid (CSF) harvested from animals at 18 hpi. CSF was harvested through puncture of the cisterna magna with a 30-guage needle and diluted in saline for plating on CSBA plates. Disease symptoms were scored as following: (1) = minimal or no spontaneous motor activity, coma (2) = unable to turn upright (3) = turns upright within 30s (4) = signs of disease in terms of weight loss and/or appearance of fur, (5) = healthy, normal behavior. Spontaneous mortality was documented and animals with a score of 2 or lower were sacrificed.

A total of 84 infant rats were used for this study, representing 7 independent experiments of 12 animals. All animals were sacrificed during the acute phase of pneumococcal meningitis to assess neuroinflammation. Both infected and uninfected animals were randomized for treatment with JWH-133 (1mg/kg, i.p.) and/or CRO (100 mg/kg, i.p). JWH-133 was first dissolved in 100% ethanol and diluted 1:10 in 0.9% saline at a final concentration of 0.25 mg/ml). JWH-133 was administered once at 18 hpi, and CRO was administered at 18 hpi and 24 hpi. Animals not treated with JWH-133 received an equivalent volume (100 µl/25 g) of vehicle. Depending on the endpoints,

animals were sacrificed at 24 hpi and 42 hpi with an overdose of pentobarbital (Eskonarkon, Streuli Pharma AG, Uznach, Switzerland, 150mg/kg b.w. i.p) and perfused via the left ventricle with either 4% paraformeldahype (PFA) in PBS or ice-cold PBS.

Histological Analysis of Cortical Damage and Hippocampus Apoptosis

Brains were harvested at 42 hpi after perfusion of animal with 4% PFA and fixed in 4% PFA for 4 h at 4°C. After 4 h, brains were transferred into 18% sucrose and kept at 4°C overnight. Brain cryosections (45 µM) were stained for Nissl substance with cresyl violet. Cortical damage was quantified using ImageJ software, and apoptosis was measured in the hippocampal dentate gyrus using x 400 magnification.

Iba1 Staining of Microglial Cells

Brains harvested at 42 hpi were sampled into 50 µm free-floating cryosections. Microglia immunostaining was performed with ImmPRESS™ HRP anti-rabbit IgG Peroxidase Polymer Detection Kit (Vector Laboratories, USA) in conjunction with rabbit anti Iba-1 (WAKO, Germany). Free-floating sections were incubated at room temperature for 72 h in 1 ml of primary Iba-1 antibody diluted 1:400. Endogenous peroxidase activity was blocked with 3% hydrogen peroxide, followed by incubation for 20 min in 2.5% normal goat blocking serum. Sections were then incubated in the ImmPRESS™ anti-rabbit peroxidase polymer for 30 min. Microglia were visualized following a 2-minute incubation with Vector© 3,3'-diaminobenzidine (DAB) substrate (Vector Laboratories, USA).

Quantification and Categorical Analysis of Microglia Morphology

Quantification was performed in a subset of the animals, randomly chosen in each experimental group with Iba-1 staining of sufficient good quality. Our method of microglia quantification was adapted from a previously described methodology (Young and Morrison, 2018). Nine separate images of microglia in the cortex and hippocampus of 50 µm brain sections were randomly sampled under x 400 magnification from each animal (3 images per section, 3 sections per animal). Through ImageJ, microglia images were passed through an unsharp mask filter and converted into an 8-bit image, and then a binary image. Incomplete microglia structures around the periphery of the image were cleared. The binary image of microglia was then skeletonized with the AnalyzeSkeleton plugin, which allowed to measurement of cell branching and summed branch length. The summed endpoints and branch length were divided by the number of cell bodies in the visual field to determine the endpoints/cell and branch length/cell of the microglia visualized.

Using a previously described characterizations of microglia activations states (Davis et al., 1994; Davis et al., 2017), cells were classified into three categories: resting = round, oval body with thin, long and radially projecting processes; intermediate = enlarged and darkened cell bodies with thick processes and less branching; active = enlarged, darkened cell bodies with little to no processes observed.

Quantification of Cyto/Chemokines in the Brain Parenchmya

Quantification of neuroinflammation in the parenchyma was performed using a membrane-based immunoassay containing a panel detecting 29 inflammatory parameters (Proteome Profiler Rat Cytokine Array Panel A, R&D Biosystems, Biotechne). Brains were harvested from animals perfused with ice cold PBS at 24 and 42 hpi. The brains were snap frozen on dry ice and stored at -80°C until further processing. For preparation of homogenates, brain samples were thawed on ice, and a portion of the frontal cortex was excised. Samples were homogenized in a 7-ml glass tissue grinder (Kontes Glass Co., USA) with a 7× volume to mass ratio in a buffer consisting of ice-cold PBS, 1% Triton-X-100, and protease inhibitors (cOmplete™, Mini, EDTA-Free, Sigma-Adrich, Merk, Switzerland). The homogenate was cleared by centrifugation at 16000 × g, for 10 min at 4°C. Protein concentration was determined using Pierce™ BCA Protein Assay kit (ThermoFischer Scientific). Each membrane was incubated with 900µg of protein extract and processed according to the manufacturer's instructions. Enhanced chemiluminescent detection (ECL) was performed on a Fusion FX-6 imaging system (Vilber Lourmat, Marne-la-Vallée, France). Spot density was determined on digitalized images using Image J for the analysis (V. 1.45, National Institutes of Health, Bethesda, Maryland, US) and normalized using internal controls integrated on each membrane.

Statistical Analysis

All statistical analyses were performed with GraphPad Prism (Prism 8; GraphPad Software Inc., San Diego, USA). Results are presented as mean values ± standard deviation if not stated otherwise. Survival was calculated using a log rank (Mantel-Cox) test. To compare differences between two groups, an unpaired Student t test or a non-parametric Mann-Whitney test were used. To compared difference between multiple groups, we use one-way ANOVA with Tukey's multiple comparison test. For combined *in vitro* experiments, we performed a repeated measure two-way ANOVA with Sidak multiple comparison for NO and multiple t test with Holm Sidak multiple comparison for cytokines. For clinical scores and weight changes, we used a repeated measure mixed effect model (because of missing values at later time points). A value of $p < 0.05$ was considered as significant.

RESULTS

JWH-133 Reduces Inflammatory Cytokine Levels and Nitric Oxide Production *In Vitro*

Following stimulation of mixed glial cells with LPS, *S. pneumoniae* serotype 3, and heat inactivated *S. pneumoniae*, each stimulation condition was immediately treated with JWH-133. Both NO and cytokine concentrations showed that LPS and live bacteria induced inflammatory responses in the mixed glial cells (**Figures 1A–E**). In cells stimulated with LPS, JWH-133 significantly decreased NO concentration ($p < 0.0001$), as well as

IL-1β concentration ($p = 0.019$). In cells stimulated with live *S. pneumoniae* serotype 3, JWH-133 significantly decreased concentrations of NO ($p = 0.0071$), IL-6 ($p = 0.00034$), IL-1β ($p = 0.014$), and TNF-α ($p = 0.014$). Challenge with LPS didn't efficiently stimulated the production of IL-10, and stimulation with live bacteria wasn't affected by JWH-133 treatment. In cells stimulated with PBS, NO levels were observed in very low concentrations and cytokines levels were under detection limit. No significant difference between treated and untreated cells were observed in cells stimulated with PBS only.

Clinical Parameters of Animals With Pneumococcal Meningitis Are Not Impacted by JWH-133 Administration

A total of 84 infant rats were used in this study, of which 70 were infected with *S. pneumoniae*. The development of productive bacterial meningitis was proven in all 70 animals, with CSF bacterial titers $\geq 10^6$ CFU/ml and clinical scores inferior to 5, both determined at 18 hpi. Of these infected animals, 35 were concomitantly treated with JWH-133 and CRO, while the remaining were treated with CRO only.

Survival, relative weight change, and clinical scores were significantly different in animals infected with PM compared to uninfected animals. However, in infected animals, adjuvant JWH-133 treatment did not alter these clinical parameters when compared to animals treated with CRO only (**Figures 2A–C**).

Microglia Morphology and Distribution Are Affected by JWH-133 Administration

A prominent characteristic of microglia is their different branching and cell body morphology linked to their activation states (Davis et al., 1994; Karperien et al., 2013; Gomez-Nicola and Perry, 2015). To assess how JWH-133 attenuates inflammation through microglia modulation, the morphology and activation of microglia cells were quantified on Iba-1 immuno-stained sections.

Quantitative Assessment of Branching and Cell Process Length

The microglia images were skeletonized on ImageJ software, as previously described in the methods (**Figures 3A–D**). These images were analyzed for the endpoints per cell body, as well as the total summed branch length per cell body. Infected animals treated with CRO exhibited significantly fewer endpoints per cell as well as branch length when compared with every other experimental groups. In particular, the difference between infected animals that received JWH-133 or not was highly significant for endpoints ($p < 0.0001$) and branch length ($p < 0.001$). In contrast, infected animals treated with JWH-133 didn't

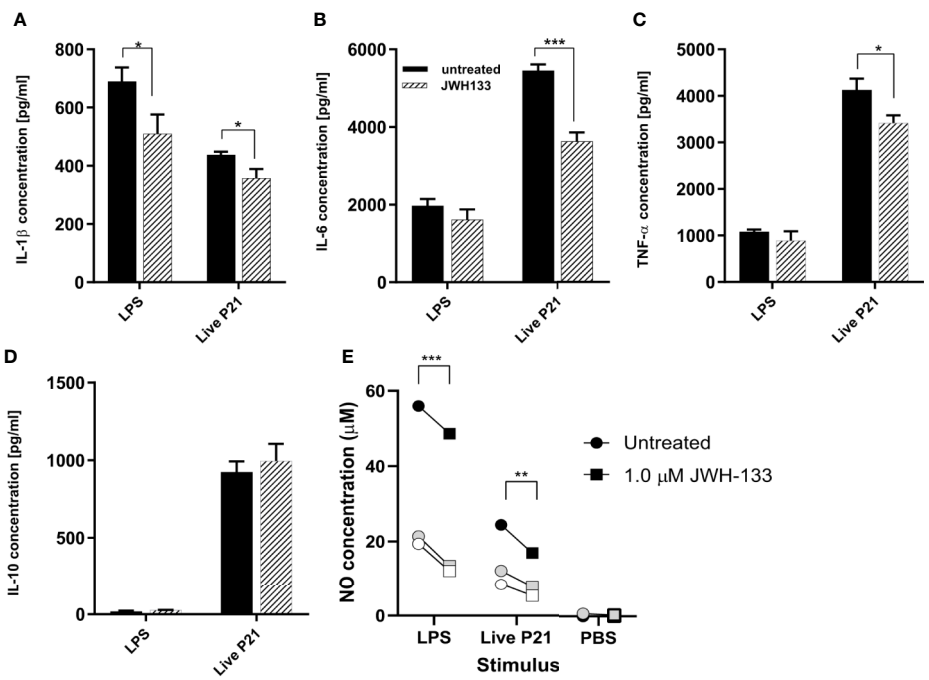

FIGURE 1 | *In vitro*, JWH-133 treatment attenuates LPS or *S. pneumoniae*-induced activation of glial cells. The expression of IL-1β **(A)**, IL-6 **(B)**, and TNF-α **(C)** was reduced by JWH-133 during challenge of astroglial cells by *S. pneumoniae*. JWH-11 also attenuated LPS-induced production of IL-β, but had not effect on IL-10 **(D)**. Nitric oxide production **(E)** upon LPS- and *S. pneumoniae* activation was reduced by JWH-133. (For cytokines, n = 3 for each group; for NO: three independent experiments represented by black, gray, and white symbols; *p < 0.05; **p < 0.01, ***p < 0.001).

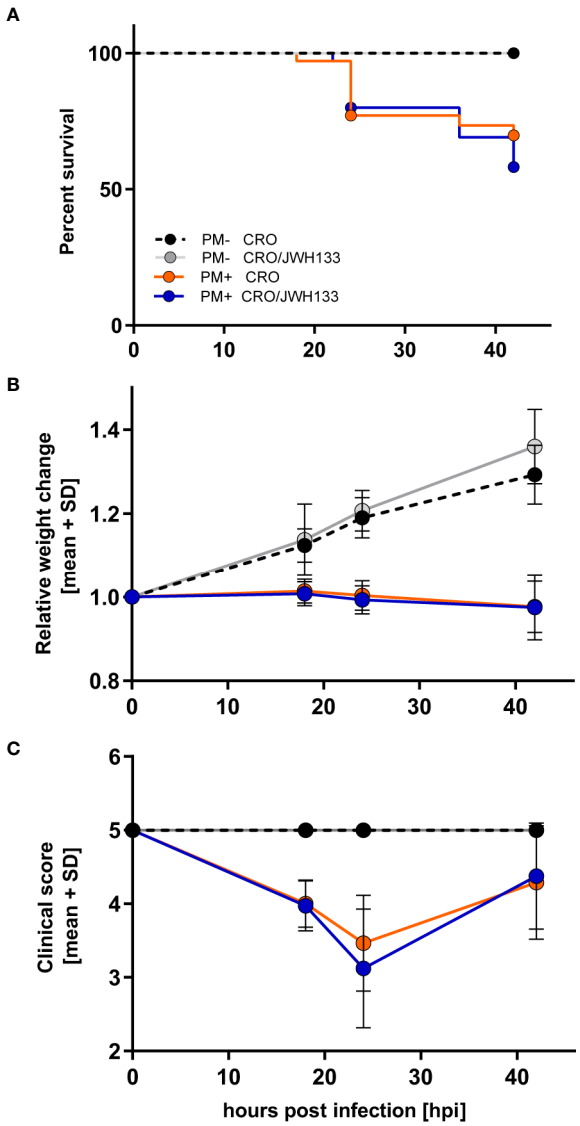

FIGURE 2 | Survival and time-course of clinical parameters during experimental pneumococcal meningitis. No differences could be observed in survival **(A)**, relative weight changes **(B)** or clinical score **(C)** between animals treated with ceftriaxone (CRO) or ceftriaxone combined to adjuvant JWH-133 (CRO/JWH133), neither in uninfected (PM-) nor infected (PM+) animals (PM- CRO and PM- CRO/JHW-133, n = 7; PM+ CRO and PM+ CRO/JWH133, n = 19–35, depending on the time points).

exhibit differences in branch length and endpoints when compared to uninfected animals (**Figures 3E, F**).

Classification of Microglia in Three Categories Based On Morphology

In conjunction with quantitative assessments of microglia morphology, the Iba-1+ cells were also classified in three categories, based on their morphology. In uninfected animals, more microglial cells possessed thin processes with light staining of cell bodies (**Figure 4B**). These characteristics are indicative of "resting" microglia, which patrol the body under physiological conditions (Davis et al., 1994). Interestingly, JHW-133 increased the proportion of this microglial type not only in infected animals, but also in uninfected. In infected animals treated only with CRO, Iba-1 staining showed significantly more cells with little to no processes, with enlarged bodies and an amoeboid shape (**Figure 4D**) compared to animals treated with JHW-133. Between these two phenotypes, microglia can possess thicker processes and larger cell bodies (Davis et al., 1994; Davis et al., 2017). These microglial cells are believed to be an intermediate between ramified and reactive microglia, and have been referred to as "bushy", "hypertrophied", "rod-like" and "bipolar" (Davis et al., 2017). In our study, we characterized these cells as "hypertrophied" (**Figure 4C**). In contrast to the treatment with CRO alone, the brain of infected animals with adjuvant JWH-133 exhibited a majority of Iba-1$^+$ cells possessing the phenotypic characteristics of hypertrophied microglia (**Figure 4A**).

Quantitative Assessment of Microglial Density

The total number of Iba-1+ cells was assessed to determine whether adjuvant JWH-133 influences the density of microglia. No statistically significant difference caused by JWH-133 treatment, neither in uninfected nor in infected animals was observed. Furthermore, when comparing infected and uninfected animals, no significant increase in microglial density was documented (**Supplementary Figure 1**).

JWH-133 Reduces the Expression of Inflammatory Cyto/Chemokines, But Not of MMP-9 in the Parenchyma of Animals With Pneumococcal Meningitis

In order to analyze the inflammation in the parenchyma over the course of acute meningitis, brain homogenates of animals sacrificed at 24 and 42 hpi were used to profile an array of inflammatory cytokines. With the exception of fractalkaline, sICAM-1, and thymus chemokine, inflammatory proteins were not detected in uninfected animals, while animals with PM demonstrated detectable levels of several inflammatory cytokines (**Figures 5A, B**). At 24 hpi, the animals treated with JWH-133 demonstrated significantly decreased levels of several neutrophil chemoattractants, including CINC-1 ($p < 0.001$), CINC-2α/β ($p = 0.0037$), and CINC-3 ($p < 0.001$). At 42 h, the only chemoattractant that was significantly reduced was CINC-1 ($p < 0.001$). Inflammatory interleukin levels were also reduced in the parenchyma after administration of JWH-133 (**Figures 5A, B**). At 24 h, IL-6 was significantly reduced ($p < 0.001$), and at 42 h, IL-1α was significantly reduced compared to animals treated with only CRO ($p < 0.001$). Macrophage inflammatory proteins were also significantly reduced following JWH-133 administration at both 24 and 42 hpi (**Figures 5A, B**). Levels of MIP-3α (CCL20) were significantly reduced at 24 hpi ($p < 0.001$), and levels of MIP-1α (CCL3) were reduced by JWH-133 at 42hpi ($p < 0.001$). While JWH-133 administration reduced levels of inflammatory cytokines, it also reduced the level of metalloproteinase inhibitor TIMP-1 at 24 hpi ($p = 0.0019$). In contrast, we couldn't detect a reduction in MMP-9, neither at 24 hpi, nor 48 hpi (**Supplementary Figure 2**).

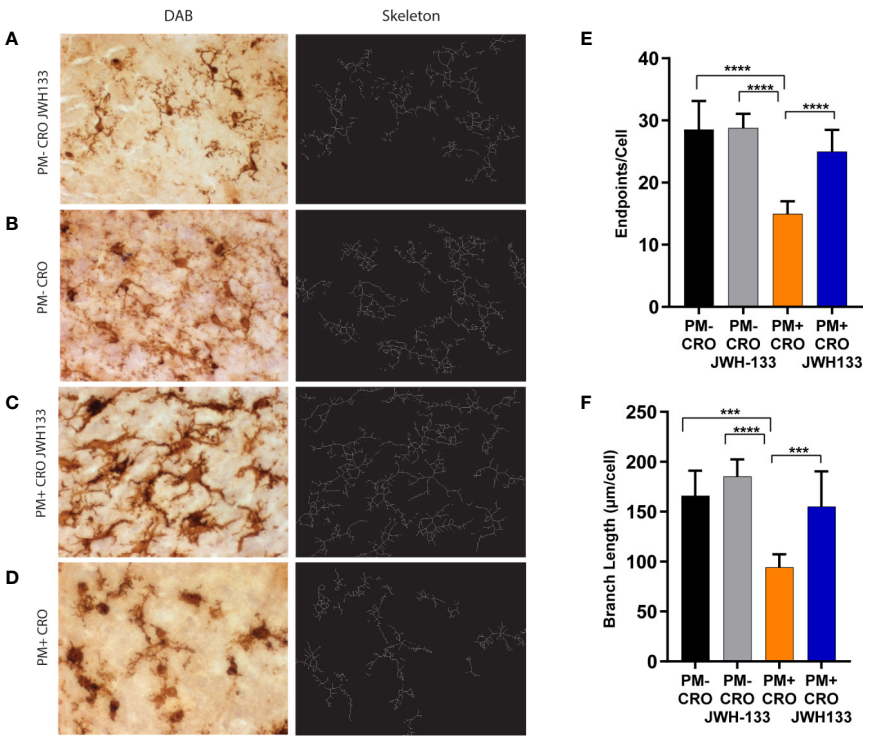

FIGURE 3 | Quantitative phenotypic analysis of microglial activation state on Iba-1 immuno-stained sections. Brain sections of animals from each experimental group, were immuno-stained for microglia using Iba-1 (pictures on the left, **A**–**D**). The digital image was skeletonized (pictures on the right, **(A–D)** and endpoints/cell **(E)** or summed branch length **(F)** were determined. In infected animals with ceftriaxone treatment (PM+ CRO), both parameters were significantly reduced compared to the others groups. In contrast, no differences between infected animals treated with JWH-133 (PM+ CRO/JWH133) and uninfected animals (PM-) could be observed. (PM- CRO, n = 3; PM- CRO/JWH133, n = 5; PM+ CRO, n = 11; PM+ CRO/JWH133, n = 6; one-way ANOVA with Tukey's multiple comparison test: ***$p < 0.001$; ****$p < 0.0001$).

Adjuvant JWH-133 Doesn't Significantly Alter Cortical Damage or Hippocampus Apoptosis

To further assess the effects of JWH-133, cortical damage and hippocampal apoptosis were analyzed. No cortical damage was observed in uninfected animals with CRO or CRO/JWH133 administered. In animals infected with PM, administration of JWH-133 didn't reduce the cortical damage nor hippocampal apoptosis (**Figure 6**).

DISCUSSION

Pneumococcal meningitis induces inflammation in the CNS, that can be exacerbated by bacteriolytic antibiotics such as CRO, leading to long term neurological sequelae (Mook-Kanamori et al., 2011). While dexamethasone is currently used as an adjuvant therapeutic, its long-term neuroprotective properties on hearing loss and memory impairment are limited (Leib et al., 2003; Van De Beek, 2009) and concerns exist about corticosteroids being responsible of delayed cerebral thrombosis after initial good recovery (Schut et al., 2009; Gallegos et al., 2018). Thus, studying the efficacy of alternative therapeutic candidates for PM is important for the improvement of clinical outcome following infection and the identification of new treatment modalities.

In this study, we assessed the anti-inflammatory and neuroprotective effects of JWH-133 administration. Previous studies have shown the protective properties of administering specific endocannabinoid receptor type 2 agonists in various disease models. JWH-133 has a very high affinity and specificity for CB2 (K_i CB2 3.4 nM/K_i CB1 680 nM) (Huffman et al., 1999) when compared to other CB2 agonists, like JWH-015 (K_i CB2: 13.8 nM/K_i CB1: 383 nM) (Pertwee, 1999). Importantly, JWH-015 has been reported to have seven off-target receptors, while JWH-133 had none (Soethoudt et al., 2017). As a consequence, JWH-015 may act independently from CB receptors, for example through the glucocorticoid receptor (Fechtner et al., 2019).

So far, few studies have addressed the use of CB2 agonists in infectious diseases (Hernandez-Cervantes et al., 2017). These studies have mostly used non-selective agonists, including tetrahydrocannabinol (THC), cannabidiol (CBD) or marijuana extracts. For bacterial infection, a model of sepsis using cecal ligation and puncture (CLP) demonstrated that the selective CB2 agonist Gp1, given shortly after CLP induction, decreased neutrophil recruitment, while increasing neutrophil activation

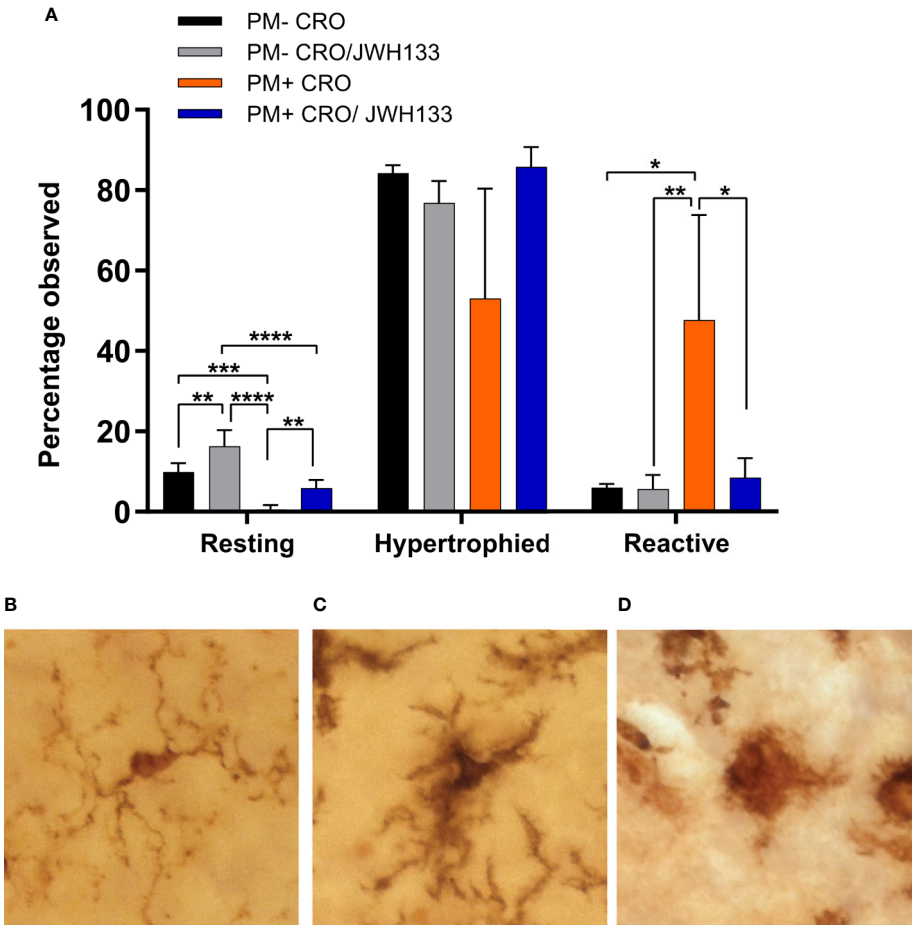

FIGURE 4 | Classification of microglia based on their morphology on Iba-1 immuno-stained sections. Significance differences in the proportion of the microglia classified in the categories "resting" and "reactive" were found between the experimental groups **(A)**. Examples of microglia classified into the three different categories: resting = round, oval body with thin, long, and radially projecting processes **(B)**; hypertrophied = enlarged and darkened cell bodies with thick processes and less branching **(C)**; reactive = enlarged, darkened cell bodies with little to no processes observed **(D)**. PM- CRO, n = 3; PM- CRO/JWH133, n = 4; PM+ CRO, n = 8; PM+ CRO/JWH133, n = 4; one-way ANOVA with Tukey's multiple comparison test: *p < 0.05; **p < 0.01; ***p < 0.001; ****p < 0.0001.

at the site of infection. Further, it decreased pulmonary damage (Tschop et al., 2009). Non-selective inhibitors have also been investigated in paradigms of viral infections. A beneficial effect was found in viral infections where inflammation participates in viral spread and is detrimental. For example, CB2 agonists have the potential to reduced HIV-associated neurocognitive disorders (Purohit et al., 2014). JWH-133 was shown to reduce lung inflammation and damage in experimental respiratory syncytial virus infection in mice (Tahamtan et al., 2018). Very recently, therapy using CB2 agonist has been proposed to control the cytokine storm observed during acute cases of SARS-CoV-2 infection (Rossi et al., 2020)

Since CB2 agonists are generally considered as immunosuppressive, the timing of application is critical. Inactivation of CB2 prior to infection or using knockout models may be detrimental. CB2 deficiency may prolong host exposure to pathogens, decrease viral clearance, and broke down immune cell crosstalk, such as neutrophil migration. This way, treatment with CB2 agonists may render individuals more susceptible to infections (Hussain et al., 2019). Evidence for a role of CB2 deficiency as a risk factor for bacterial infection of the CNS is lacking so far. A review paper by Gowin and colleagues (Gowin and Januszkiewicz-Lewandowska, 2018) inventoried SNPs involved in bacterial meningitis, but CB2-related SNPs were not reported.

Here, the efficacy of a very specific CB2 agonist is evaluated for its ability to reduce neuroinflammation during the acute phase of bacterial meningitis, with a special focus on microglia. Our results indicate that JWH-133 exerts anti-inflammatory effects on glial cells *in vitro* and that its administration as adjuvant therapy *in vivo* modulates microglia activity in the CNS, thus also exerting an anti-inflammatory effect.

Our *in vitro* data with mixed glial cell cultures demonstrate anti-inflammatory properties of JWH-133 in both LPS and live

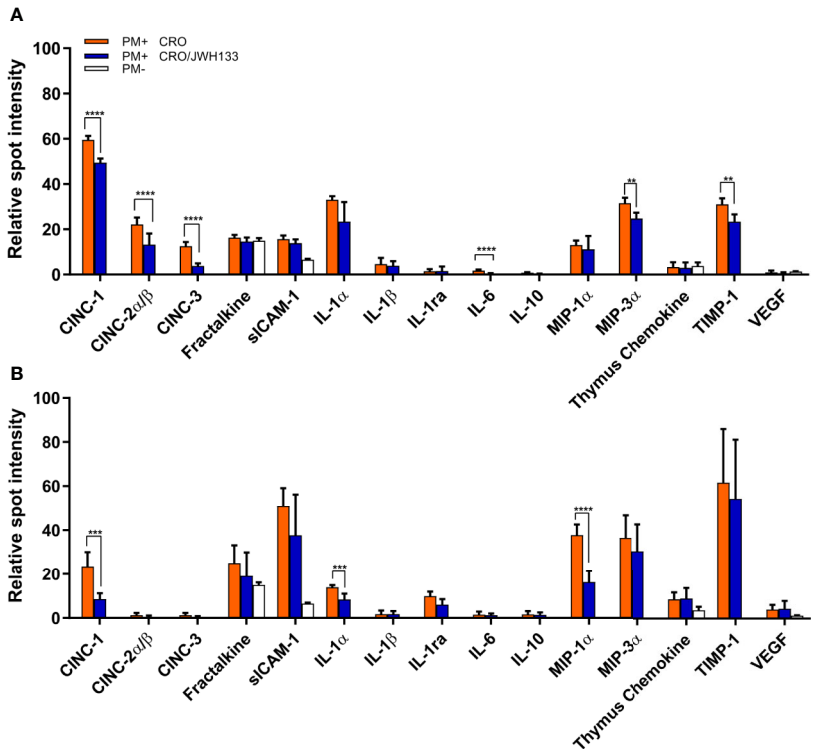

FIGURE 5 | Analysis of inflammatory parameters in the brain parenchyma of infected animals. At 24 hpi **(A)** and 42 hpi **(B)**, the protein levels of several inflammatory parameters were significantly decreased in infected animals treated with CRO/JWH-13 (blue bars) compared to animals treated with CRO only (orange bars). Only few inflammatory parameters could be detected in uninfected animals (white bars). (PM+ CRO, n = 6; PM+ CRO/JWH133, n = 6; PM-, n = 4; Multiple t test with Holm-Sidak correction; **p < 0.01; ***p < 0.001; ****p < 0.0001).

S. pneumoniae serotype 3-stimulated cells. JWH-133 reduced IL-6, IL-1, and TNF-α, all of which have been shown to play an important role in upregulating neuroinflammation in PM (Coutinho et al., 2013). Thus, attenuating the levels of these cytokines may have significant neuroprotective effects in PM, and improve outcomes. We have also shown that NO concentrations were significantly reduced in cultures treated with either LPS or living *S. pneumoniae*. NO is a signaling molecule released by macrophages and is involved in inflammatory processes, including vasodilation (Sharma et al., 2007). During infection, microglial cells are a major source of inflammatory cytokines (Hanisch, 2002), including IL-1β, IL-6-α, and TNF-α (Lee et al., 1993; Hanisch, 2002). Thus, the attenuated production of these cytokines and of NO by mixed glial cell cultures *in vitro* suggests that the agonist JWH-133 drives microglia toward an anti-inflammatory state.

In vivo, we administered a concentration of JWH-133 (1mg/kg) in line with different models of brain injuries (Murikinati et al., 2010; Gamal et al., 2015; Fujii et al., 2016; Cakir et al., 2019). As previously described, microglia serve as the primary immune cells of the brain, releasing various pro-inflammatory cytokines (Hanisch, 2002). We were able to determine differences in microglia morphology by measuring endpoints per cell and branch length per cell. These measurements are relevant because previous studies have shown that activation states of microglia cells are associated with branching (Davis et al., 1994; Karperien et al., 2013; Gomez-Nicola and Perry, 2015). Activated microglia possess a round amoeboid shape, with little to no branching. These characteristics are indicative of "active" microglia, which function as macrophages in response to injury, and secrete several pro-inflammatory cytokines like IL-1, IL-6, and TNF (Davis et al., 1994; Smith et al., 2012; Davis et al., 2017). Pro-inflammatory functions of active microglia have been shown to directly contribute to neuronal death and neurodegeneration (Vezzani et al., 1999; Takeuchi et al., 2006). Thus, upon infection, we expect microglia to have significantly fewer endpoints per cell and smaller branch lengths than in healthy animals. After infection with *S. pneumoniae* and treatment with CRO, Iba-1+ cells indeed possessed significantly fewer endpoints and smaller branch lengths than other experimental groups. Due to the bacteriolytic and pro-inflammatory nature of antibiotics like CRO (Grandgirard et al., 2007b; Muri et al., 2018), the increase in microglia activation could be the result of both bacterial infection and antibiotic treatment. Following adjuvant treatment with JWH-133, the Iba-1+ cells demonstrated significantly increased endpoints and branch lengths, suggesting modulation towards a resting and/or intermediate hypertrophied state. In contrast, JWH-133 was

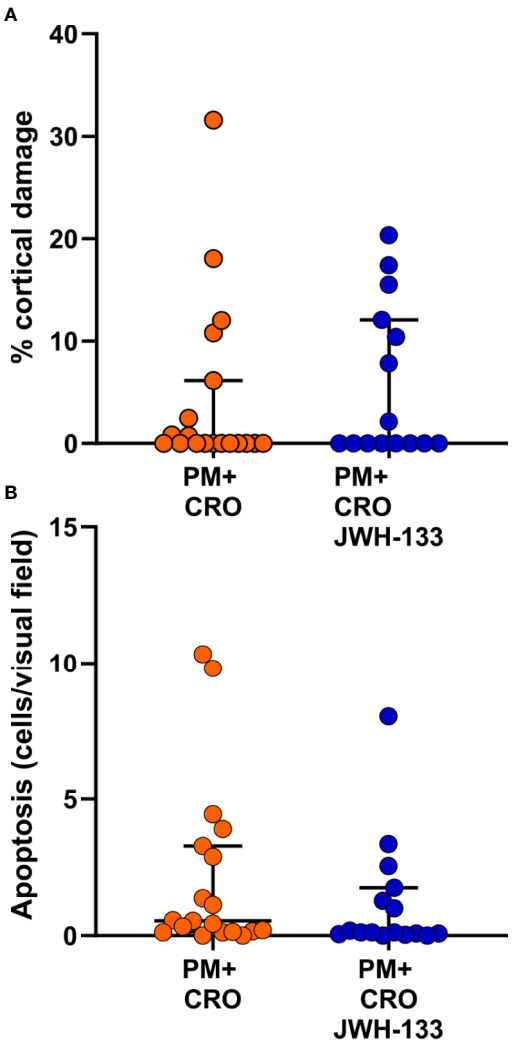

FIGURE 6 | Levels of brain damage. No significant differences for cortical damage **(A)** nor for hippocampal apoptosis **(B)** could be detected between infected animals treated with CRO alone (orange dots) or CRO/JHW133 (blue dots). (PM + CRO, n = 19; PM+ CRO/JWH133, n = 16; Mann-Whitney test: cortical damage, p = 0.62; hippocampal apoptosis, p = 0.13).

not able to influence overall microglial density in the parenchyma. Further, we did not observe differences between uninfected and infected animals. A significant difference upon infection was demonstrated by Dörr and colleagues in an experimental model of pneumococcal meningitis in mice (Dorr et al., 2015). However, their analysis focused on the hippocampal formation, which was not the case in our study. In conjunction with data from *in vitro* glial cells, our analysis suggests that JWH-133 is effective in modulating microglia phenotype away from a reactive state with phagocytotic activity, and through this pathway, reduces neuroinflammation in PM.

The acute phase of PM is characterized by significantly increased levels of inflammatory cytokines released by resident brain immune cells and infiltrating leukocytes (Mook-Kanamori et al., 2011). We measured cytokine levels in the brain parenchyma of infected animals to further understand how adjuvant JWH-133 treatment modulates neuro-inflammation. Our results showed that at 24 and 42 hpi, adjuvant JWH-133 therapy significantly reduced neutrophil chemoattractants CINC-1, CINC-2α/β, and CINC-3. Massive neutrophils infiltration to the CNS is observed in acute PM, forming neutrophil extracellular traps (NETs) in the CSF, which have been shown to trap pneumococcal bacteria and hinder bacterial clearance (Mohanty et al., 2019). Invading leukocytes act also as sources of pro-inflammatory mediators, such as reactive oxygen species and matrix-metalloproteinases (Meli et al., 2003). In these cells, CB2 activation also result in anti-inflammatory effects (Murikinati et al., 2010; Kapellos et al., 2019). The specific involvement of neutrophils was not the primary focus of the present study. The reduction in the production of chemoattractants in brain parenchyma by JWH-133 may attenuate the recruitment of neutrophils. This has been proposed as a mechanism for JWH-133-mediated attenuation of brain damage following ischemia in rats subjected to middle cerebral artery occlusion (MCAO) (Murikinati et al., 2010). This would merit further investigation in our experimental model. In addition, JWH-133 also down-regulates MIP-1a and MIP-3α in our model. Macrophage inflammatory proteins are secreted by brain-resident macrophages, and have been shown to be up-regulated in pneumococcal meningitis, where they are involved in the recruitment of leukocytes into the CNS (Driscoll, 1994; Coutinho et al., 2013). Pro-inflammatory interleukins such as IL-6 and IL-1α were also down-regulated by JWH-133 administration. Microglia function has been described as one of the primary mediators of immune response in the brain following infection (Barichello et al., 2016; Thorsdottir et al., 2019), and the attenuation of inflammatory responses in brain tissue following administration of JWH-133 further corroborates that JWH-133 may be a promising neuro-protective therapy targeting microglial cells.

Acute inflammation in the subarachnoid space and the ensuing vasculitis, as well as cerebral thrombosis, are believed to be the causes of cortical damage in PM (Leib et al., 1996; Nau and Bruck, 2002). Adjuvant JWH-133 therapy didn't reduce brain damage in rats infected with PM. This is in contrast to the neuroprotective effect of JWH-133 observed in experimental models of okadaic acid-induced neuroinflammation and damage (Cakir et al., 2019) or MCAO-induced ischemia (Murikinati et al., 2010). However, in these models, JWH-133 was applied at the time or shortly before surgery. In our model, JWH-133 was given as adjuvant therapy to antibiotics, a paradigm more relevant to clinical application. This may explain the lack of effect observed on brain damage, although the anti-inflammatory effect on microglia is demonstrated. In previous studies from our group, decrease in inflammatory parameters by different adjunctive therapies was associated with improved neuroprotection and attenuation of cortical damage (Grandgirard et al., 2007b; Liechti et al., 2014; Muri et al., 2018). In particular, the attenuation of cortical damage was consistently associated with a reduction of MMP-9 activity

(Liechti et al., 2015). In the present study, the expression of parenchymal MMP-9 was not reduced by JWH-133, in line with its inability to decrease cortical damage.

JWH-133 therapy was shown to improve outcome in term of neurofunctional behavior in different experimental models. In particular, it attenuated the impairment of Morris watermaze performance induced by okadaic acid treatment in rats (Cakir et al., 2019). In the present study, we only focused on the acute phase of the disease and didn't investigate a possible effect of the chronic application of JWH-133 on later neurofunctional parameters. Such a study was performed on adult rats with pneumococcal meningitis using cannabidiol for treatment (Barichello et al., 2012). A reduction in the host immune response and a prevention of cognitive impairments were documented. However, therapy was initiated at the time of infection. Further, in contrast to JWH-133, the effects of CBD are very unspecific, which makes a direct comparison between the two treatments subject to caution. Specific endocannabinoid modulation of microglia drives their polarization toward a phenotype warranting therapeutic functionality, with not only anti-inflammatory and neuroprotective effect, but also tissue-remodeling or regenerative capacity. This is the fundament proposed for the treatment of different neuropathologies by endocannabinoids (Tanaka et al., 2020). Cannabinoids are potent regulators of neural stem cell (NSC) biology (Rodrigues et al., 2019). JWH-133 has been shown to increase NSC proliferation in the subventricular zone (Goncalves et al., 2008), and another CB2 agonist, AM1241, enhanced cell proliferation in the hippocampus of mice displaying deficits in neurogenesis (Avraham et al., 2014). Based on these observations, chronic application of JWH-133 during experimental pneumococcal may hold more potential to support regeneration and improve the neurofunctional outcome of infected animals than influencing the acute reaction, when used in a clinically relevant therapeutic modality.

Our study has several limitations: 1) by using a primary mixed glial culture, the effect of JWH-133 was not specifically investigated on microglia, but more on a general glial population consisting of astrocytes and microglia. Astrocytes are likely to also be regulated by CB2 agonists (Kozela et al., 2017). This could however better reflect the *in vivo* situation in the parenchyma. 2) Neutrophils participate in the hyperinflammatory state during pneumococcal meningitis. Unfortunately, the effect of JWH-133 treatment on the recruitment of these cells in the CSF couldn't be determined, given the limited quantity of CSF that could be harvested from infant rats.

In conclusion, we could demonstrate both *in vitro* and *in vivo* the ability of JWH-133 to modulate microglial behavior to a non-inflammatory phenotype. When applied as adjuvant therapy, this was however not effective in improving clinical outcome and brain damage in the acute phase. Given the proven effect on microglia and its potential to support neuronal regeneration, JWH-133 may hold promise in a chronic application.

DATA AVAILABILITY STATEMENT

The raw data supporting the conclusions of this article will be made available by the authors, without undue reservation.

ETHICS STATEMENT

The animal study was reviewed and approved by Animal Care and Experimentation Committee of the Canton of Bern, Switzerland (license no. BE 1/18).

AUTHOR CONTRIBUTIONS

SDP performed the experiments, analyzed the results, and contributed to study design and manuscript preparation. DG contributed to study design, supervised the experiments, analyzed the results, and contributed to manuscript preparation. SLL supervised the experiments, participated in the study design, and contributed to manuscript preparation. All authors contributed to the article and approved the submitted version.

FUNDING

The work was supported by a grant from the Swiss National Science Foundation (no. 189136) to SLL and a Swiss Government Excellence Scholarship (0532) awarded to SDP.

ACKNOWLEDGMENTS

We thank Robert Lukesch for technical assistance for the animal experiments and Franziska Simon for technical assistance for Luminex determination and MMP gel zymography. We also thank the ESCMID study group on infection of the brain (ESGIB) for stimulating discussions and suggestions.

SUPPLEMENTARY MATERIAL

The Supplementary Material for this article can be found online at: https://www.frontiersin.org/articles/10.3389/fcimb.2020.588195/full#supplementary-material

REFERENCES

Agyeman, P., Grandgirard, D., and Leib, S. L. (2014). "Pathogenesis and pathophysiology of bacterial infections," in *Infections of the Central Nervous System*, Scheld, M. W., Whitley, R. J., and Marra, C. M. 4th ed (Philadelphia, PA, USA: Lippincott Williams & Wilkins), 361–364.

Amenta, P. S., Jallo, J. I., Tuma, R. F., Hooper, D. C., and Elliott, M. B. (2014). Cannabinoid receptor type-2 stimulation, blockade, and deletion alter the

vascular inflammatory responses to traumatic brain injury. *J. Neuroinflamm.* 11, 191. doi: 10.1186/s12974-014-0191-6

Ashton, J. C., and Glass, M. (2007). The cannabinoid CB2 receptor as a target for inflammation-dependent neurodegeneration. *Curr. Neuropharmacol.* 5, 73–80. doi: 10.2174/157015907780866884

Auer, M., Pfister, L. A., Leppert, D., Tauber, M. G., and Leib, S. L. (2000). Effects of clinically used antioxidants in experimental pneumococcal meningitis. *J. Infect. Dis.* 182, 347–350. doi: 10.1086/315658

Avraham, H. K., Jiang, S., Fu, Y., Rockenstein, E., Makriyannis, A., Zvonok, A., et al. (2014). The cannabinoid CB(2) receptor agonist AM1241 enhances neurogenesis in GFAP/Gp120 transgenic mice displaying deficits in neurogenesis. *Br. J. Pharmacol.* 171, 468–479. doi: 10.1111/bph.12478

Bally, L., Grandgirard, D., and Leib, S. L. (2016). Inhibition of Hippocampal Regeneration by Adjuvant Dexamethasone in Experimental Infant Rat Pneumococcal Meningitis. *Antimicrob. Agents Chemother.* 60, 1841–1846. doi: 10.1128/AAC.02429-15

Barichello, T., Ceretta, R. A., Generoso, J. S., Moreira, A. P., Simoes, L. R., Comim, C. M., et al. (2012). Cannabidiol reduces host immune response and prevents cognitive impairments in Wistar rats submitted to pneumococcal meningitis. *Eur. J. Pharmacol.* 697, 158–164. doi: 10.1016/j.ejphar.2012.09.053

Barichello, T., Generoso, J. S., Simoes, L. R., Goularte, J. A., Petronilho, F., Saigal, P., et al. (2016). Role of Microglial Activation in the Pathophysiology of Bacterial Meningitis. *Mol. Neurobiol.* 53, 1770–1781. doi: 10.1007/s12035-015-9107-4

Bewersdorf, J. P., Grandgirard, D., Koedel, U., and Leib, S. L. (2018). Novel and preclinical treatment strategies in pneumococcal meningitis. *Curr. Opin. Infect. Dis.* 31, 85–92. doi: 10.1097/QCO.0000000000000416

Bravo-Ferrer, I., Cuartero, M. I., Zarruk, J. G., Pradillo, J. M., Hurtado, O., Romera, V. G., et al. (2017). Cannabinoid Type-2 Receptor Drives Neurogenesis and Improves Functional Outcome After Stroke. *Stroke* 48, 204–212. doi: 10.1161/STROKEAHA.116.014793

Brouwer, M. C., Mcintyre, P., Prasad, K., and Van De Beek, D. (2015). Corticosteroids for acute bacterial meningitis. *Cochrane Database Syst. Rev.* (9), CD004405. doi: 10.1002/14651858.CD004405.pub5

Cakir, M., Tekin, S., Doganyigit, Z., Erden, Y., Soyturk, M., Cigremis, Y., et al. (2019). Cannabinoid type 2 receptor agonist JWH-133, attenuates Okadaic acid induced spatial memory impairment and neurodegeneration in rats. *Life Sci.* 217, 25–33. doi: 10.1016/j.lfs.2018.11.058

Chung, Y. C., Shin, W. H., Baek, J. Y., Cho, E. J., Baik, H. H., Kim, S. R., et al. (2016). CB2 receptor activation prevents glial-derived neurotoxic mediator production, BBB leakage and peripheral immune cell infiltration and rescues dopamine neurons in the MPTP model of Parkinson's disease. *Exp. Mol. Med.* 48, e205. doi: 10.1038/emm.2015.100

Coutinho, L. G., Grandgirard, D., Leib, S. L., and Agnez-Lima, L. F. (2013). Cerebrospinal-fluid cytokine and chemokine profile in patients with pneumococcal and meningococcal meningitis. *BMC Infect. Dis.* 13:326. doi: 10.1186/1471-2334-13-326

Davis, E. J., Foster, T. D., and Thomas, W. E. (1994). Cellular forms and functions of brain microglia. *Brain Res. Bull.* 34, 73–78. doi: 10.1016/0361-9230(94)90189-9

Davis, B. M., Salinas-Navarro, M., Cordeiro, M. F., Moons, L., and De Groef, L. (2017). Characterizing microglia activation: a spatial statistics approach to maximize information extraction. *Sci. Rep.* 7, 1576. doi: 10.1038/s41598-017-01747-8

Dorr, A., Kress, E., Podschun, R., Pufe, T., Tauber, S. C., and Brandenburg, L. O. (2015). Intrathecal application of the antimicrobial peptide CRAMP reduced mortality and neuroinflammation in an experimental model of pneumococcal meningitis. *J. Infect.* 71, 188–199. doi: 10.1016/j.jinf.2015.04.006

Driscoll, K. E. (1994). Macrophage inflammatory proteins: biology and role in pulmonary inflammation. *Exp. Lung Res.* 20, 473–490. doi: 10.3109/01902149409031733

Edmond, K., Clark, A., Korczak, V. S., Sanderson, C., Griffiths, U. K., and Rudan, I. (2010). Global and regional risk of disabling sequelae from bacterial meningitis: a systematic review and meta-analysis. *Lancet Infect. Dis.* 10, 317–328. doi: 10.1016/S1473-3099(10)70048-7

Ehrhart, J., Obregon, D., Mori, T., Hou, H., Sun, N., Bai, Y., et al. (2005). Stimulation of cannabinoid receptor 2 (CB2) suppresses microglial activation. *J. Neuroinflamm.* 2:29. doi: 10.1186/1742-2094-2-29

Facci, L., Dal Toso, R., Romanello, S., Buriani, A., Skaper, S. D., and Leon, A. (1995). Mast cells express a peripheral cannabinoid receptor with differential sensitivity to anandamide and palmitoylethanolamide. *Proc. Natl. Acad. Sci. U.S.A.* 92, 3376–3380. doi: 10.1073/pnas.92.8.3376

Fechtner, S., Singh, A. K., Srivastava, I., Szlenk, C. T., Muench, T. R., Natesan, S., et al. (2019). Cannabinoid Receptor 2 Agonist JWH-015 Inhibits Interleukin-1beta-Induced Inflammation in Rheumatoid Arthritis Synovial Fibroblasts and in Adjuvant Induced Arthritis Rat via Glucocorticoid Receptor. *Front. Immunol.* 10:1027. doi: 10.3389/fimmu.2019.01027

Fujii, M., Sherchan, P., Krafft, P. R., Rolland, W. B., Soejima, Y., and Zhang, J. H. (2014a). Cannabinoid type 2 receptor stimulation attenuates brain edema by reducing cerebral leukocyte infiltration following subarachnoid hemorrhage in rats. *J. Neurol. Sci.* 342, 101–106. doi: 10.1016/j.jns.2014.04.034

Fujii, M., Sherchan, P., Soejima, Y., Hasegawa, Y., Flores, J., Doycheva, D., et al. (2014b). Cannabinoid receptor type 2 agonist attenuates apoptosis by activation of phosphorylated CREB-Bcl-2 pathway after subarachnoid hemorrhage in rats. *Exp. Neurol.* 261, 396–403. doi: 10.1016/j.expneurol.2014.07.005

Fujii, M., Sherchan, P., Soejima, Y., Doycheva, D., Zhao, D., and Zhang, J. H. (2016). Cannabinoid Receptor Type 2 Agonist Attenuates Acute Neurogenic Pulmonary Edema by Preventing Neutrophil Migration after Subarachnoid Hemorrhage in Rats. *Acta Neurochir. Suppl.* 121, 135–139. doi: 10.1007/978-3-319-18497-5_24

Gallegos, C., Tobolowsky, F., Nigo, M., and Hasbun, R. (2018). Delayed Cerebral Injury in Adults With Bacterial Meningitis: A Novel Complication of Adjunctive Steroids? *Crit. Care Med.* 46, e811–e814. doi: 10.1097/CCM.0000000000003220

Gamal, M., Moawad, J., Rashed, L., El-Eraky, W., Saleh, D., Lehmann, C., et al. (2015). Evaluation of the effects of Eserine and JWH-133 on brain dysfunction associated with experimental endotoxemia. *J. Neuroimmunol.* 281, 9–16. doi: 10.1016/j.jneuroim.2015.02.008

Gomez-Nicola, D., and Perry, V. H. (2015). Microglial dynamics and role in the healthy and diseased brain: a paradigm of functional plasticity. *Neuroscientist* 21, 169–184. doi: 10.1177/1073858414530512

Goncalves, M. B., Suetterlin, P., Yip, P., Molina-Holgado, F., Walker, D. J., Oudin, M. J., et al. (2008). A diacylglycerol lipase-CB2 cannabinoid pathway regulates adult subventricular zone neurogenesis in an age-dependent manner. *Mol. Cell Neurosci.* 38, 526–536. doi: 10.1016/j.mcn.2008.05.001

Gowin, E., and Januszkiewicz-Lewandowska, D. (2018). Genes and their single nucleotide polymorphism involved in innate immune response in central nervous system in bacterial meningitis: review of literature data. *Inflamm. Res.* 67, 655–661. doi: 10.1007/s00011-018-1158-3

Grandgirard, D., and Leib, S. L. (2006). Strategies to prevent neuronal damage in paediatric bacterial meningitis. *Curr. Opin. Pediatr.* 18, 112–118. doi: 10.1097/01.mop.0000193292.09894.b7

Grandgirard, D., Bifrare, Y. D., Pleasure, S. J., Kummer, J., Leib, S. L., and Tauber, M. G. (2007a). Pneumococcal meningitis induces apoptosis in recently postmitotic immature neurons in the dentate gyrus of neonatal rats. *Dev. Neurosci.* 29, 134–142. doi: 10.1159/000096218

Grandgirard, D., Schurch, C., Cottagnoud, P., and Leib, S. L. (2007b). Prevention of brain injury by the nonbacteriolytic antibiotic daptomycin in experimental pneumococcal meningitis. *Antimicrob. Agents Chemother.* 51, 2173–2178. doi: 10.1128/AAC.01014-06

Hanisch, U. K. (2002). Microglia as a source and target of cytokines. *Glia* 40, 140–155. doi: 10.1002/glia.10161

Hernandez-Cervantes, R., Mendez-Diaz, M., Prospero-Garcia, O., and Morales-Montor, J. (2017). Immunoregulatory Role of Cannabinoids during Infectious Disease. *Neuroimmunomodulation* 24, 183–199. doi: 10.1159/000481824

Huffman, J. W., Liddle, J., Yu, S., Aung, M. M., Abood, M. E., Wiley, J. L., et al. (1999). 3-(1 ',1 '-dimethylbutyl)-1-deoxy-Delta(8)-THC and related compounds: Synthesis of selective ligands for the CB2 receptor. *Bioorg. Med. Chem.* 7, 2905–2914. doi: 10.1016/S0968-0896(99)00219-9

Hussain, M. T., Greaves, D. R., and Iqbal, A. J. (2019). The Impact of Cannabinoid Receptor 2 Deficiency on Neutrophil Recruitment and Inflammation. *DNA Cell Biol.* 38, 1025–1029. doi: 10.1089/dna.2019.5024

Kapellos, T. S., Taylor, L., Feuerborn, A., Valaris, S., Hussain, M. T., Rainger, G. E., et al. (2019). Cannabinoid receptor 2 deficiency exacerbates inflammation and neutrophil recruitment. *FASEB J.* 33, 6154–6167. doi: 10.1096/fj.201802524R

Karperien, A., Ahammer, H., and Jelinek, H. (2013). Quantitating the subtleties of microglial morphology with fractal analysis. *Front. Cell. Neurosci.* 7, 3. doi: 10.3389/fncel.2013.00003

Klein, M., Koedel, U., Pfister, H. W., and Kastenbauer, S. (2003). Morphological correlates of acute and permanent hearing loss during experimental pneumococcal meningitis. *Brain Pathol.* 13, 123–132. doi: 10.1111/j.1750-3639.2003.tb00012.x

Kozela, E., Juknat, A., and Vogel, Z. (2017). Modulation of Astrocyte Activity by Cannabidiol, a Nonpsychoactive Cannabinoid. *Int. J. Mol. Sci.* 18, 1669. doi: 10.3390/ijms18081669

Lee, S. C., Liu, W., Dickson, D. W., Brosnan, C. F., and Berman, J. W. (1993). Cytokine production by human fetal microglia and astrocytes. Differential induction by lipopolysaccharide and IL-1 beta. *J. Immunol.* 150, 2659–2667.

Leib, S. L., Kim, Y. S., Chow, L. L., Sheldon, R. A., and Tauber, M. G. (1996). Reactive oxygen intermediates contribute to necrotic and apoptotic neuronal injury in an infant rat model of bacterial meningitis due to group B streptococci. *J. Clin. Invest.* 98, 2632–2639. doi: 10.1172/JCI119084

Leib, S. L., Clements, J. M., Lindberg, R. L., Heimgartner, C., Loeffler, J. M., Pfister, L. A., et al. (2001). Inhibition of matrix metalloproteinases and tumour necrosis factor alpha converting enzyme as adjuvant therapy in pneumococcal meningitis. *Brain* 124, 1734–1742. doi: 10.1093/brain/124.9.1734

Leib, S. L., Heimgartner, C., Bifrare, Y. D., Loeffler, J. M., and Taauber, M. G. (2003). Dexamethasone aggravates hippocampal apoptosis and learning deficiency in pneumococcal meningitis in infant rats. *Pediatr. Res.* 54, 353–357. doi: 10.1203/01.PDR.0000079185.67878.72

Li, L., Tao, Y., Tang, J., Chen, Q., Yang, Y., Feng, Z., et al. (2015). A Cannabinoid Receptor 2 Agonist Prevents Thrombin-Induced Blood-Brain Barrier Damage via the Inhibition of Microglial Activation and Matrix Metalloproteinase Expression in Rats. *Transl. Stroke Res.* 6, 467–477. doi: 10.1007/s12975-015-0425-7

Liechti, F. D., Grandgirard, D., Leppert, D., and Leib, S. L. (2014). Matrix metalloproteinase inhibition lowers mortality and brain injury in experimental pneumococcal meningitis. *Infect. Immun.* 82, 1710–1718. doi: 10.1128/IAI.00073-14

Liechti, F. D., Grandgirard, D., and Leib, S. L. (2015). Bacterial meningitis: insights into pathogenesis and evaluation of new treatment options: a perspective from experimental studies. *Future Microbiol.* 10, 1195–1213. doi: 10.2217/fmb.15.43

Loeffler, J. M., Ringer, R., Hablutzel, M., Tauber, M. G., and Leib, S. L. (2001). The free radical scavenger alpha-phenyl-tert-butyl nitrone aggravates hippocampal apoptosis and learning deficits in experimental pneumococcal meningitis. *J. Infect. Dis.* 183, 247–252. doi: 10.1086/317921

Lucas, M. J., Brouwer, M. C., and Van De Beek, D. (2013). Delayed cerebral thrombosis in bacterial meningitis: a prospective cohort study. *Intensive Care Med.* 39, 866–871. doi: 10.1007/s00134-012-2792-9

Lucas, M. J., Brouwer, M. C., and Van De Beek, D. (2016). Neurological sequelae of bacterial meningitis. *J. Infect.* 73, 18–27. doi: 10.1016/j.jinf.2016.04.009

Mccoy, K. L. (2016). Interaction between Cannabinoid System and Toll-Like Receptors Controls Inflammation. *Mediators Inflammation* 2016, 18. doi: 10.1155/2016/5831315

Meli, D. N., Christen, S., and Leib, S. L. (2003). Matrix metalloproteinase-9 in pneumococcal meningitis: activation via an oxidative pathway. *J. Infect. Dis.* 187, 1411–1415. doi: 10.1086/374644

Ment, L. R., Ehrenkranz, R. A., and Duncan, C. C. (1986). Bacterial meningitis as an etiology of perinatal cerebral infarction. *Pediatr. Neurol.* 2, 276–279. doi: 10.1016/0887-8994(86)90019-6

Mohanty, T., Fisher, J., Bakochi, A., Neumann, A., Cardoso, J. F. P., Karlsson, C., et al. (2019). Neutrophil extracellular traps in the central nervous system hinder bacterial clearance during pneumococcal meningitis. *Nat. Commun.* 10, 1667. doi: 10.1038/s41467-019-09040-0

Mook-Kanamori, B. B., Geldhoff, M., Van Der Poll, T., and Van De Beek, D. (2011). Pathogenesis and pathophysiology of pneumococcal meningitis. *Clin. Microbiol. Rev.* 24, 557–591. doi: 10.1128/CMR.00008-11

Muri, L., Grandgirard, D., Buri, M., Perny, M., and Leib, S. L. (2018). Combined effect of non-bacteriolytic antibiotic and inhibition of matrix metalloproteinases prevents brain injury and preserves learning, memory and hearing function in experimental paediatric pneumococcal meningitis. *J. Neuroinflamm.* 15, 233. doi: 10.1186/s12974-018-1272-8

Muri, L., Le, N. D., Zemp, J., Grandgirard, D., and Leib, S. L. (2019a). Metformin mediates neuroprotection and attenuates hearing loss in experimental pneumococcal meningitis. *J. Neuroinflamm.* 16, 156. doi: 10.1186/s12974-019-1549-6

Muri, L., Perny, M., Zemp, J., Grandgirard, D., and Leib, S. L. (2019b). Combining Ceftriaxone with Doxycycline and Daptomycin Reduces Mortality, Neuroinflammation, Brain Damage, and Hearing Loss in Infant Rat Pneumococcal Meningitis. *Antimicrob. Agents Chemother.* 63, e00220-00219. doi: 10.1128/AAC.00220-19

Murikinati, S., Juttler, E., Keinert, T., Ridder, D. A., Muhammad, S., Waibler, Z., et al. (2010). Activation of cannabinoid 2 receptors protects against cerebral ischemia by inhibiting neutrophil recruitment. *FASEB J.* 24, 788–798. doi: 10.1096/fj.09-141275

Nau, R., and Bruck, W. (2002). Neuronal injury in bacterial meningitis: mechanisms and implications for therapy. *Trends Neurosci.* 25, 38–45. doi: 10.1016/S0166-2236(00)02024-5

Nau, R., Soto, A., and Bruck, W. (1999). Apoptosis of neurons in the dentate gyrus in humans suffering from bacterial meningitis. *J. Neuropathol. Exp. Neurol.* 58, 265–274. doi: 10.1097/00005072-199903000-00006

Perny, M., Roccio, M., Grandgirard, D., Solyga, M., Senn, P., and Leib, S. L. (2016). The Severity of Infection Determines the Localization of Damage and Extent of Sensorineural Hearing Loss in Experimental Pneumococcal Meningitis. *J. Neurosci.* 36, 7740–7749. doi: 10.1523/JNEUROSCI.0554-16.2016

Pertwee, R. G. (1999). Pharmacology of cannabinoid receptor ligands. *Curr. Med. Chem.* 6, 635–664.

Purohit, V., Rapaka, R. S., and Rutter, J. (2014). Cannabinoid receptor-2 and HIV-associated neurocognitive disorders. *J. Neuroimmune Pharmacol.* 9, 447–453. doi: 10.1007/s11481-014-9554-0

Rodrigues, R. S., Lourenco, D. M., Paulo, S. L., Mateus, J. M., Ferreira, M. F., Mouro, F. M., et al. (2019). Cannabinoid Actions on Neural Stem Cells: Implications for Pathophysiology. *Molecules* 24, 1350. doi: 10.3390/molecules24071350

Romero-Sandoval, E. A., Horvath, R., Landry, R. P., and Deleo, J. A. (2009). Cannabinoid receptor type 2 activation induces a microglial anti-inflammatory phenotype and reduces migration via MKP induction and ERK dephosphorylation. *Mol. Pain* 5, 25. doi: 10.1186/1744-8069-5-25

Rossi, F., Tortora, C., Argenziano, M., Di Paola, A., and Punzo, F. (2020). Cannabinoid Receptor Type 2: A Possible Target in SARS-CoV-2 (CoV-19) Infection? *Int. J. Mol. Sci.* 21, 3809. doi: 10.3390/ijms21113809

Schut, E. S., Brouwer, M. C., De Gans, J., Florquin, S., Troost, D., and Van De Beek, D. (2009). Delayed cerebral thrombosis after initial good recovery from pneumococcal meningitis. *Neurology* 73, 1988–1995. doi: 10.1212/WNL.0b013e3181c55d2e

Sharma, J. N., Al-Omran, A., and Parvathy, S. S. (2007). Role of nitric oxide in inflammatory diseases. *Inflammopharmacology* 15, 252–259. doi: 10.1007/s10787-007-0013-x

Smith, J. A., Das, A., Ray, S. K., and Banik, N. L. (2012). Role of pro-inflammatory cytokines released from microglia in neurodegenerative diseases. *Brain Res. Bull.* 87, 10–20. doi: 10.1016/j.brainresbull.2011.10.004

Soethoudt, M., Grether, U., Fingerle, J., Grim, T. W., Fezza, F., De Petrocellis, L., et al. (2017). Cannabinoid CB2 receptor ligand profiling reveals biased signalling and off-target activity. *Nat. Commun.* 8:13958. doi: 10.1038/ncomms13958

Spreer, A., Gerber, J., Hanssen, M., Schindler, S., Hermann, C., Lange, P., et al. (2006). Dexamethasone increases hippocampal neuronal apoptosis in a rabbit model of Escherichia coli meningitis. *Pediatr. Res.* 60, 210–215. doi: 10.1203/01.pdr.0000227553.47378.9f

Stella, N. (2010). Cannabinoid and cannabinoid-like receptors in microglia, astrocytes, and astrocytomas. *Glia* 58, 1017–1030. doi: 10.1002/glia.20983

Svizenska, I., Dubovy, P., and Sulcova, A. (2008). Cannabinoid receptors 1 and 2 (CB1 and CB2), their distribution, ligands and functional involvement in nervous system structures–a short review. *Pharmacol. Biochem. Behav.* 90, 501–511. doi: 10.1016/j.pbb.2008.05.010

Tahamtan, A., Samieipoor, Y., Nayeri, F. S., Rahbarimanesh, A. A., Izadi, A., Rashidi-Nezhad, A., et al. (2018). Effects of cannabinoid receptor type 2 in respiratory syncytial virus infection in human subjects and mice. *Virulence* 9, 217–230. doi: 10.1080/21505594.2017.1389369

Takeuchi, H., Jin, S., Wang, J., Zhang, G., Kawanokuchi, J., Kuno, R., et al. (2006). Tumor necrosis factor-alpha induces neurotoxicity via glutamate release from

hemichannels of activated microglia in an autocrine manner. *J. Biol. Chem.* 281, 21362–21368. doi: 10.1074/jbc.M600504200

Tanaka, M., Sackett, S., and Zhang, Y. (2020). Endocannabinoid Modulation of Microglial Phenotypes in Neuropathology. *Front. Neurol.* 11, 87. doi: 10.3389/fneur.2020.00087

Thorsdottir, S., Henriques-Normark, B., and Iovino, F. (2019). The Role of Microglia in Bacterial Meningitis: Inflammatory Response, Experimental Models and New Neuroprotective Therapeutic Strategies. *Front. Microbiol.* 10:576:576. doi: 10.3389/fmicb.2019.00576

Tschop, J., Kasten, K. R., Nogueiras, R., Goetzman, H. S., Cave, C. M., England, L. G., et al. (2009). The cannabinoid receptor 2 is critical for the host response to sepsis. *J. Immunol.* 183, 499–505. doi: 10.4049/jimmunol.0900203

Turcotte, C., Blanchet, M. R., Laviolette, M., and Flamand, N. (2016). The CB2 receptor and its role as a regulator of inflammation. *Cell Mol. Life Sci.* 73, 4449–4470. doi: 10.1007/s00018-016-2300-4

Van De Beek, D., Cabellos, C., Dzupova, O., Esposito, S., Klein, M., Kloek, A. T., et al. (2016). ESCMID guideline: diagnosis and treatment of acute bacterial meningitis. *Clin. Microbiol. Infect.* 22 Suppl 3, S37–S62. doi: 10.1016/j.cmi.2016.01.007

Van De Beek, D. (2009). Corticosteroids for acute adult bacterial meningitis. *Med. Mal. Infect.* 39, 531–538. doi: 10.1016/j.medmal.2009.02.033

Van Der Flier, M., Geelen, S. P., Kimpen, J. L., Hoepelman, I. M., and Tuomanen, E. I. (2003). Reprogramming the host response in bacterial meningitis: how best to improve outcome? *Clin. Microbiol. Rev.* 16, 415–429. doi: 10.1128/CMR.16.3.415-429.2003

Vergouwen, M. D., Schut, E. S., Troost, D., and Van De Beek, D. (2010). Diffuse cerebral intravascular coagulation and cerebral infarction in pneumococcal meningitis. *Neurocrit. Care* 13, 217–227. doi: 10.1007/s12028-010-9387-5

Vezzani, A., Conti, M., De Luigi, A., Ravizza, T., Moneta, D., Marchesi, F., et al. (1999). Interleukin-1beta immunoreactivity and microglia are enhanced in the rat hippocampus by focal kainate application: functional evidence for enhancement of electrographic seizures. *J. Neurosci.* 19, 5054–5065. doi: 10.1523/JNEUROSCI.19-12-05054.1999

Wellmer, A., Noeske, C., Gerber, J., Munzel, U., and Nau, R. (2000). Spatial memory and learning deficits after experimental pneumococcal meningitis in mice. *Neurosci. Lett.* 296, 137–140. doi: 10.1016/s0304-3940(00)01645-1

Young, K., and Morrison, H. (2018). Quantifying Microglia Morphology from Photomicrographs of Immunohistochemistry Prepared Tissue Using ImageJ. *J. Vis. Exp.* (136), e57648. doi: 10.3791/57648

Zarruk, J. G., Fernandez-Lopez, D., Garcia-Yebenes, I., Garcia-Gutierrez, M. S., Vivancos, J., Nombela, F., et al. (2012). Cannabinoid type 2 receptor activation downregulates stroke-induced classic and alternative brain macrophage/microglial activation concomitant to neuroprotection. *Stroke* 43, 211–219. doi: 10.1161/STROKEAHA.111.631044

Conflict of Interest: The authors declare that the research was conducted in the absence of any commercial or financial relationships that could be construed as a potential conflict of interest

frontiers in Cellular and Infection Microbiology

REVIEW
published: 23 November 2020
doi: 10.3389/fcimb.2020.592017

The Use of Adjunctive Steroids in Central Nervous Infections

Shalini Gundamraj[1] *and Rodrigo Hasbun*[2*]

[1] Cornell University, Ithaca, NY, United States, [2] Department of Internal Medicine, UT Health McGovern Medical School, Houston, TX, United States

Central nervous system (CNS) infections continue to be associated with significant neurological morbidity and mortality despite various existing therapies. Adjunctive steroid therapy has been employed clinically to reduce inflammation in the treatment of CNS infections across various causative pathogens. Steroid therapy can potentially improve clinical outcomes including reducing mortality rates, provide no significant benefit, or cause worsened outcomes, based on the causative agent of infection. The data on benefits or harms of adjunctive steroid therapy is not consistent in outcome or density through CNS infections, and varies based on the disease diagnosis and pathogen. We summarize the existing literature on the effects of adjunctive steroid therapy on outcome for a number of CNS infections, including bacterial meningitis, herpes simplex virus, West Nile virus, tuberculosis meningitis, cryptococcal meningitis, *Angiostrongylus cantonensis*, neurocysticercosis, autoimmune encephalitis, toxoplasmosis, and bacterial brain abscess. We describe that while steroid therapy is beneficial and supported in pathogens such as pneumococcal meningitis and tuberculosis, for other diseases, like *Listeria monocytogenes* and *Cryptococcus neoformans* they are associated with worse outcomes. We highlight areas of consistent and proven findings and those which need more evidence for supported beneficial clinical use of adjunctive steroid therapy.

Keywords: meningitis, encephalitis, steroids, central nervous system infections, brain abscess, cysticercosis

OPEN ACCESS

Edited by:
Federico Iovino, Karolinska Institutet (KI), Sweden

Reviewed by:
Fabricia Petronilho, Universidade do Sul de Santa Catarina, Brazil
Jaqueline Generoso, Universidade do Extremo Sul Catarinense, Brazil

***Correspondence:**
Rodrigo Hasbun
Rodrigo.Hasbun@uth.tmc.edu

Specialty section:
This article was submitted to Bacteria and Host, a section of the journal Frontiers in Cellular and Infection Microbiology

Received: *06 August 2020*
Accepted: *23 October 2020*
Published: *23 November 2020*

Citation:
Gundamraj S and Hasbun R (2020) The Use of Adjunctive Steroids in Central Nervous Infections. Front. Cell. Infect. Microbiol. 10:592017. doi: 10.3389/fcimb.2020.592017

INTRODUCTION

Central nervous system (CNS) infections involve the brain, spine, and associated membranes, and are linked to significant neurological morbidity and mortality, with long term consequences in survivors that affect the quality of life and activity of daily living (ADLS) (Erdem et al., 2017; Sulaiman et al., 2017). CNS infection broadly can be categorized as encephalitis, meningitis, or intracranial suppurative complications (e.g., brain abscess), with a broad range of causal organisms and clinical presentations. CNS infections can either originate by hematogenous spread (e.g., bacteremia, viremia), by retrograde neuronal invasion (e.g., viral infection through axonal transport such as rabies, *Naegleria fowleri*) or by contiguous spread of microorganisms (e.g., post cranial trauma or surgery, implementation of medical hardware into the brain or spine, or by parameningeal spread from a focus such as sinusitis or mastoiditis) (Archibald and Quisling, 2013; Koyuncu et al., 2013). Various bacteria, fungi, viruses, and parasites can be the source of CNS infection, which often presents nonspecifically with headache, fever, altered mental status, and

behavioral changes (Dorsett and Liang, 2016). Precision in diagnosis, however, is essential to treatment, which varies across CNS infection. Despite the use of antimicrobial therapies neurological morbidity and mortality remains high for certain pathogens such as *Streptococcus pneumoniae* (Steel et al., 2013). Of all the adjunctive therapies that have been evaluated to date only adjunctive steroids have shown benefit in some CNS infections. Adjunctive steroids can ameliorate the host's inflammatory response to the infection that account for the neurological morbidity associated with the CNS infection. In contrast, in some CNS infections, the use of steroids has no clear beneficial effects or is detrimental with worse outcomes (Fitch and van de Beek, 2008). In this review, we will review the available data for the use of adjunctive steroids in the most common CNS infections and make clear recommendations for its use or not.

PATHOPHYSIOLOGY FOR USE OF ADJUNCTIVE STEROIDS IN MENINGITIS

Meningitis is characterized by inflammation of the subarachnoid space (space between two membranes (i.e., meninges) that surrounds the brain and spinal cord). Meningitis can be caused by bacteria, viruses, fungus, amebic, parasites, mycobacteria or due to noninfectious causes. Patients typically have abnormalities in the cerebrospinal fluid (CSF) such as elevated white blood cells (WBC), elevated protein (due to alterations in the blood brain barrier), and low glucose in some cases. The presentation of meningitis can be classified as acute (symptoms for less than 5 days), subacute (symptoms 6-30 days), or chronic (symptoms for more than 30 days) (Sulaiman et al., 2017). Presentation clinically varies according to the age of the patient, the causative agents, and the presence of underlying conditions (Hasbun et al., 2018). Once bacteria invades the meninges and disrupts the blood-brain barrier, it rapidly replicates in the subarachnoid space (van de Beek et al., 2016a). In the physiological response to infection, blood vessels become leaky allowing fluid, leukocytes, and other larger particles involved in fighting infection to enter the meninges and the brain (Dando et al., 2014). This process causes severe inflammation, which has been shown to increase the adverse outcomes of the infection. Steroid therapy has been employed to reduce the inflammatory response commonly exhibited in meningitis, although its effects vary by the study population studied and by the pathogen (Hoffman and Weber, 2009). Corticosteroid therapy can reduce inflammation by suppressing multiple activated inflammatory genes (encoding pro-inflammatory cytokines. and chemokines, inflammation mediators, adhesion molecules, inflammatory enzymes, etc.) through primarily reversing histone acetylation, by decreasing cell activation and recruitment and stabilizing lysosomes, by temporarily alleviating the leaky blood brain barrier, and by interacting with DNA recognition sites to activate the transcription of anti-inflammatory genes in higher concentrations in humans (Coyle, 1999; Barnes, 2006). In animal models of bacterial meningitis, studies have shown outcomes to worsen based on the degree of inflammation (Scheld et al., 1980; Tauber et al., 1985; Brouwer et al., 2018). This inflammatory response can be reduced in the CSF by the administration of corticosteroid therapy, resulting in improved outcomes for meningitis in animal models (Scheld et al., 1980; Tauber et al., 1985). Thus, the use of corticosteroids has been investigated and employed in meningitis as adjuvant therapy over the past 30 years but must be further investigated in some infections.

BACTERIAL MENINGITIS BY PATHOGEN

Bacterial meningitis is a severe infection and inflammation of the meninges, the membrane surrounding the brain and spine, due to bacterial invasion into the subarachnoid space (Hoffman and Weber, 2009). The condition is associated with high mortality and neurological morbidity rates, with the most common causal pathogens including *S. pneumoniae (i.e., pneumococcal)*, *Neisseria meningitides (i.e., meningococcal)*, *Haemophilus influenzae*, and *Listeria monocytogenes* (Hoffman and Weber, 2009). Due to the development and implementation of vaccines against *H. influenzae* type b, *S. pneumoniae*, and *N. meningitidis* the incidence of bacterial meningitis has been reduced to 1–2/100,000 in children (Hasbun et al., 2018). In infants from 4–6 weeks, the dominating etiologies are *Streptococcus agalactiae, Escherichia coli*, other Enterobacteriaceae, and *L. monocytogenes.* In children older than 6 weeks up to adults of age 50 years, *S. pneumoniae*, *N. meningitidis*, and *H. influenzae* are the dominating etiologies of infection. In both adults over the age of 50 years and immunocompromised individuals of all ages, *S. pneumoniae*, *N. meningitidis*, *H. influenzae*, and *L. monocytogenes* prevail (Hasbun et al., 2018).

S. pneumoniae

S pneumoniae is the leading cause of bacterial meningitis in the USA (Castelblanco et al., 2014). A review in 2018 of corticosteroid treatment effects in 25 trials across 2,511 children and 1,517 adults showed there was no significant change in mortality found overall with steroid therapy, although an effective mortality reduction was seen for *S. pneumoniae* meningitis from 36% to 29.9%. The reduction in mortality for *S, pneumoniae* meningitis in 16 high-income countries was attributed to the use of adjunctive steroid therapy as compared to patients who did not receive steroid therapy. Patient outcome was not significantly different with the use of adjunctive steroids in low-income countries, which made up 9 of the 25 analyzed studies. Dexamethasone was the specific corticosteroid administered as adjunctive therapy in 22 of the trials, while hydrocortisone and prednisone were administered in the remaining 3 studies (Brouwer et al., 2018). No significant adverse effects were reported in the clinical studies by the use of adjunctive steroid therapy. The lack of effect of corticosteroid use in low-income countries, contrasted with significant reductions in mortality with corticosteroid adjunctive treatment for

S. pneumoniae in high-income countries, is most likely due to the delay in patient presentation and treatment in low-income countries after inflammation in the CNS has already begun and progressed (van de Beek et al., 2016b). A 2002 randomized control trial on the effects of dexamethasone treatment in adults with meningitis similarly found a reduction in mortality and adverse outcomes, seizure incidence, and cardiorespiratory failure in contrast with the placebo group in pneumococcal meningitis (de Gans and van de Beek, 2002) (see **Table 1**). Dexamethasone corticosteroid adjunctive therapy has been shown to reduce mortality in pneumococcal meningitis and is a recommended therapy by the Infectious Diseases Society of America (IDSA), European and United Kingdom guidelines (Tunkel et al., 2004; NICE UK, 2010; McGill et al., 2016; van de Beek et al., 2016b). The implementation of dexamethasone treatment in the Netherlands has shown a decrease of 10% in the mortality rate of pneumococcal meningitis (Brouwer et al., 2010). A study of 26,429 adults from 2011–2014 with a discharge diagnosis of meningitis or encephalitis showed that only patients with pneumococcal meningitis had a significantly reduced mortality with the use of adjunctive intravenous steroids. The study had 572 patients with pneumococcal meningitis and showed a decrease in hospital mortality rate with the use of steroids [(6.67% with and 12.5% without steroids, (P=0.0245)] (Hasbun et al., 2017) (see **Table 1**). Recently, delayed cerebral injury (DCI) in patients with bacterial meningitis has been described in up to 4% of patients and has a possible association with the administration of adjunctive steroid (Gallegos et al., 2018). Pathological studies suggest a cerebral vasculitis, thromboembolism of large arteries, and infectious intracranial aneurysms (Engelen-Lee et al., 2018). Components of the pneumococcal cell wall can be seen weeks after the initial presentation and may be a source of resurging inflammation after the initial immunosuppression by

TABLE 1 | Studies and Significant Findings on Adjunctive Steroid Therapy for Bacterial Meningitis Treatment by Pathogen.

Reference	Pathogen	N	Primary Findings	Type of Study
de Gans and van de Beek, 2002	*S. pneumoniae*	108	Adults treated with dexamethasone compared to placebo. Unfavorable outcome in 26% of the dexamethasone group and 52% of the placebo group (Relative risk, 0.50; 95 percent confidence interval, 0.30 to 0.83; P=0.006). Dexamethasone associated with a reduction in risk of unfavorable outcomes (relative risk, 0.59; 95 percent confidence interval, 0.37 to 0.94; P=0.03) and reduction in mortality (relative risk of death, 0.48; 95 percent confidence interval, 0.24 to 0.96)	RCT
Brouwer et al., 2010	*S. pneumoniae*	709	Cohort of dexamethasone treatment in 84% of episodes (2006–2009) compared to cohort of dexamethasone treatment in 3% (1998–2002). Rates of death (20% vs. 30%; $p = 0.001$) and hearing loss (12% vs. 22%; $p = 0.001$) were lower in 2006–2009 cohort.	Observational study
Castelblanco et al., 2014	*S. pneumoniae*	21,858	Incidence and inpatient Mortality decreased between 2005 (0·049 per 100 000 people) and 2008 (0·024 per 100 000 people) compared with between 2002 (0·073 per 100 000 people) and 2004 (0·063 per 100 000 people; RR 0·5720, 95% CI 0·4303–0·7582). Temporal association of improved outcomes with recommendations of corticosteroids in clinical practice since 2004	Observational study
Glimåker et al., 2016	*S. pneumoniae*	115	Adults treated with corticosteroids compared to those not given corticosteroids showed lower mortality (10.2% vs. 21.3%, p <0.001). Recovery without sequelae observed increased in corticosteroid-treated compared with non-corticosteroid-treated patients (45.2% vs. 35.1%, p <0.05)	Observational study
Hasbun et al., 2017	*S. pneumoniae*	572	Significantly reduced mortality with the use of adjunctive intravenous steroids. [(6.67% with and 12.5% without steroids, (P=0.0245)].	Observational study
Brouwer et al., 2018	*S. pneumoniae*	1,132	Corticosteroid treatment effects in 25 studies showed mortality reduction from 36% to 29.9%. (RR 0.84, 95% CI 0.72 to 0.98).	Meta analysis
Gallegos et al., 2018	*S. pneumoniae*	120	Adjunctive steroids within 4 hours were more likely given to those with delayed cerebral injury (5/5, 100% vs. 43/115, 37.5%; p=0.01). Adverse effect of delayed cerebral injury found in a higher prevalence (4.1%) in patients with pneumococcal meningitis, associated with adjunctive steroid administration.	Observational study
McIntyre et al., 1997	*H. influenzae*	848	Significant reduction in severe hearing loss with dexamethasone treatment in children (combined odds ratio [OR], 0.31; 95% confidence interval [CI], 0.14-0.69).	Meta analysis
Brouwer et al., 2018	*H. influenzae*	825	Corticosteroid treatment of across 25 studies showed significant reduction in the rate of hearing loss overall in children from 12% to 4% after adjunctive corticosteroid therapy. (RR 0.34, 95% CI 0.20 to 0.59) was found.	Meta analysis
Heckenberg et al., 2012	*N. meningitidis*	354	Dexamethasone administered in 17% of patients from 1998-2002 and 90% patients in the 2006-2011 cohort (p<0.001). Rate of arthritis was lower in patients treated with dexamethasone (32 of 258 [12%] vs. 5 of 96 [5%], p = 0.046). Adjunctive dexamethasone not found to improve clinical outcomes significantly.	Observational study
Glimåker et al., 2016	*N. meningitidis*	198	Increased survival and recovery without sequelae in corticosteroid-treated compared with non-corticosteroid-treated patients with N. meningitidis (68.6% vs. 58.1%). Positive trend is observed, but there is no statistically significant change.	Observational study
Glimåker et al., 2016	*Listeria monocytogenes*	77	Adjunctive steroid therapy showed worsened outcome trend compared to non-steroid-treated patients (48.5% vs. 40.0%).	Observational study
Charlier et al., 2017	*Listeria monocytogenes*	818	Higher mortality in patients when given adjunctive dexamethasone (OR 4·58 [1·50-13·98], p=0·008).	Observational study

dexamethasone. The demonstrated benefits of adjunctive steroid therapy in reducing pneumococcal meningitis mortality in high-income countries outweigh the possible risks and should continue to be used (Gallegos et al., 2018).

H. influenzae

The incidence of infection due to *H. influenzae* was reduced significantly in children due to the introduction of the *H. influenzae* type B vaccine. A large 1997 cross-study meta-analysis found a significant reduction in severe hearing loss in *H. influenzae* with dexamethasone treatment in children (McIntyre et al., 1997) (see **Table 1**). More recent data from a meta analysis of corticosteroid use for the treatment of bacterial meningitis found no significant reductions in mortality across 25 studies in *H. influenzae* meningitis cases treated with adjunctive steroid therapy, but similarly did observe a significant reduction in the rate of hearing loss overall in children with *H. influenzae* meningitis from 12% to 4% after adjunctive corticosteroid therapy (Brouwer et al., 2018). Based on the available data, the IDSA guidelines recommend using steroids in children with documented *H. influenzae* meningitis (Tunkel et al., 2004).

N. meningitidis

Vaccination has been available since the 1970s against *N. meningitidis* and used on populations identified as high risk. The incidence of meningococcal meningitis in the US decreased from 1997 to 2010 from 0·721 to 0·123 per 100,000 people (RR 0·1386, 95% CI 0·048–0·4284), which has placed this pathogen close to *H. influenzae* (Castelblanco et al., 2014). Adjunctive dexamethasone does not improve clinical outcomes in meningococcal meningitis but it has been associated with a decrease in arthritis (Heckenberg et al., 2012) (see **Table 1**). In a study from the Swedish quality registry from 1995-2014, there was trend towards decrease mortality with the use of adjunctive steroids in meningococcal meningitis (Glimåker et al., 2016).

Listeria monocytogenes

L. monocytogenes most commonly occurs in neonates, adults above the age of 50 years and in patients with cellular immunodeficiency. In the Swedish study, adjunctive steroids showed a trend towards worse outcomes in patients with Listeria meningitis (48.5% vs. 40.0%) (Glimåker et al., 2016) (see **Table 1**). A large prospective study in France of 818 cases of Listeriosis documented a higher mortality in patients with neurolisteriosis when given adjunctive dexamethasone (OR 4·58 [1·50–13·98], p=0·008) (Charlier et al., 2017). Adjunctive dexamethasone should be discontinued if meningitis is found not to be caused by *S. pneumoniae*, especially if it is caused by *L. monocytogenes* (Hasbun, 2019).

ENCEPHALITIS

Encephalitis is caused by brain tissue inflammation that results in neurological dysfunction from varied etiologies. A nationwide study in the US from 2000–2010, reporting encephalitis hospitalizations, showed unknown etiology in 50% of patients and viral etiologies (48.2%), most commonly herpes simplex virus, *toxoplasma gondii*, and West Nile Virus, with co-morbid HIV present in 7.7% of hospitalizations. Autoimmune encephalitis among other specified causes was reported in 32.5% of cases with known etiology (George et al., 2014). The international consortium of encephalitis diagnostic criteria include 1 major criteria: altered mental status for more than 24 h without alternative diagnosis and several minor criteria: documented fever of >38°C (100.4 F) within 72 h of presentation, seizures not attributed to preexisting seizure disorders, the onset of focal neurological deficits, CSF WBC count >5/cubic mm, new or onset neuroimaging abnormalities consistent with encephalitis presentation, and abnormalities on electroencephalography not due to other causes and consistent with encephalitis presentation (Venkatesan et al., 2013). Possible encephalitis is defined as 1 major criteria with 2 minor criteria; probable encephalitis as 1 major and 3 minor criteria and confirmed if a positive etiology is identified (Encephalitis, Table 3, 2017).

HERPES SIMPLEX VIRUS

Herpes simplex virus (HSV) is the most common cause of sporadic encephalitis and can manifest with temporal lobe abnormalities leading to personality changes, alterations in mental status, decreased consciousness, seizures, and focal neurological deficits (Hasbun et al., 2018). The peak incidence of herpes simplex encephalitis (HSE) occurs in very young children and adults over the age of 50 years with both sexes equally affected and have an incidence of 2–4/1,000,000 persons. HSE is primarily caused by HSV-1, which accounts for 90% of HSE in adults and children, while HSV meningitis is commonly caused by HSV-2 (Bradshaw and Venkatesan, 2016). In about one third of 113 confirmed HSV encephalitis cases, the infection was associated with primary infection of HSV-1. In the remaining cases, the virus was associated with the reactivation of latent virus, demonstrated through serologic assessments (Nahmias et al., 1982). High-dose intravenous acyclovir treatment is recommended for 14–21 days in immunocompetent and immunosuppressed patients, respectively. The benefit of acyclovir treatment has been shown through randomized controlled trials to significantly reduce mortality, establishing it as the standard of care for HSV encephalitis (Bradshaw and Venkatesan, 2016). Furthermore, a delay in starting acyclovir therapy has been associated with worse clinical outcomes (Erdem et al., 2015). The use of adjunctive corticosteroid therapy with acyclovir has shown to be beneficial in mouse and pre-clinical models, showing a reduction in the severity of infection, beneficial long-term effects, and no increase in viral burden (Meyding-Lamade et al., 2003). Despite this evidence, there is very limited clinical data evaluating the use of corticosteroid therapy. Furthermore, there is also the potential concern of potentially increasing viral replication. A small non-randomized retrospective study of 45 patients treated with adjunctive steroids and acyclovir in Japan showed a beneficial

impact on clinical outcome and reduction in the extent of HSE infection, without inhibition of the antiviral action of acyclovir (Kamei et al., 2005) (see **Table 2**). The German trial of Acyclovir and Corticosteroids in Herpes-simplex-virus Encephalitis (GACHE) similarly studied the treatment of dexamethasone adjunctive steroid therapy with acyclovir treatment in 41 patients, with 21 patients receiving steroid treatment and 20 receiving a placebo. The small study was stopped prematurely due to slow recruitment and found no significant differences in primary or secondary outcomes between treatment and placebo groups. The primary measured outcome was the functional outcome after 6 months on a modified Rankin scale, and secondary outcomes were the mortality after 6 and 12 months, functional outcomes after 6 and 12 months on the Glasgow outcome scale (GOS), functional outcome after 12 months measured with mRS, quality of life measurements after 6 and 12 months, cranial magnetic resonance imaging findings after 6 months and seizure incidence. This study reinforces the unclear results of corticosteroid adjunctive therapy on HSE and the necessity for larger scale controlled trials (Meyding-Lamadé et al., 2019). Although corticosteroid adjunctive therapy must be studied further as a treatment for HSE, adjunctive corticosteroids are used in practice for patients with increased intracranial pressure and cerebral edema to reduce inflammation.

WEST NILE VIRUS ENCEPHALITIS

West Nile virus (WNV) is an arthropod-borne infection that is most commonly transmitted by a mosquito bite. The mosquito injects saliva containing the virus into the host dermis with local viral replication in target cells. The virus then migrates to lymph tissue and then disseminates to the CNS *via* viremia (Colpitts et al., 2012; Hasbun et al., 2018). Incubation periods range from 2 days to 14 days, where 80% of cases remain asymptomatic, 20% have a febrile illness presentation, and 1% present with neuro-invasive disease, which may show aseptic meningitis, encephalitis, or acute flaccid paralysis/myelitis, disrupting the spinal cord (Hasbun et al., 2018). If the virus infiltrates the brain, it commonly infects the basal ganglia, thalamus, and brain stem. Neuronal death, necrosis, and inflammation occur on a microscopic level. Patients presenting with West Nile Encephalitis (WNE) also have chorioretinitis in 50% of cases (Hasbun et al., 2016). Other common symptoms include fever, altered mentation, fatigue, myalgia, headache, stiff neck, rash, vomiting, and diarrhea. Patients diagnosed with WNE have a mortality rate of 15%–18.6%. Currently, no FDA approved treatments vaccine or therapy is approved for WNV infections in humans (Hasbun et al., 2018). Although there are no specific treatments for WNV infections, corticosteroid adjunctive treatment has been used in treatment for and shown rapid improvement effects in a case report of high dose corticosteroid treatment resulting in improvement of a patient from stupor to wakefulness over the course of treatment. The patient was a 71-year-old woman with a WNV infection that rapidly progressed to weakness, encephalitis manifesting with dysphagia and dysarthria, persistent delirium, and stupor. After a 5-day course of steroid treatment she made a rapid improvement to wakefulness. This case study provides the observations of only one patient, so the effect may not be due to the anti-inflammatory steroid treatment (Leis and Sinclair, 2019). A study of 228 patients with WNV in Colorado, found no difference in patients with WNE, 17 patients received corticosteroids and 3 died (18%), whereas 9 of 48 patients who did not receive adjunctive corticosteroid treatment died (19%) (Bode et al., 2006) (see **Table 2**). Other case studies and reviews of small cohorts have shown no significant changes for patients treated with adjunctive steroids with WNV infection (Bakri and Kaiser, 2004). Due to paucity of data, the evidence for the use of corticosteroid therapy in the treatment of WNE is still unclear and must be further investigated in large cohorts.

AUTOIMMUNE ENCEPHALITIS

Autoimmune encephalitis is caused by inflammation from the body's own immune system attacking healthy cells in the brain and spinal cord. Primary autoimmune encephalitis is characterized by immune response directed at cell surface proteins, while paraneoplastic autoimmune encephalitis is a subset associated with tumors and may be the by-product of immune responses to cancerous growth (Hasbun et al., 2017; Hasbun et al., 2018). Autoimmune encephalitis requires clinical criteria of rapid progression in less than 3 months, resulting in neurological debilitation and working memory deficits. Other neurological symptoms include altered level of consciousness, lethargy, personality changes, and other diagnostic findings specific to autoantibodies present in infection. The standard

TABLE 2 | Studies on adjunctive steroid therapy for viral encephalitis.

Reference	Diagnosis	N	Primary Findings	Type of Study
Kamei et al., 2005	Herpes Simplex Virus	45	Effects of adjunctive steroids and acyclovir studied. Beneficial impact on clinical outcome and reduction in the extent of HSE infection, without inhibition of the antiviral action of acyclovir.	Observational study
Martinez-Torres et al., 2008	Herpes Simplex Virus	41	Dexamethasone adjunctive steroid therapy with acyclovir versus placebo found no significant differences in primary or secondary outcomes between groups.	RCT
Leis and Sinclair, 2019	West Nile Virus	1	71-year-old woman with weakness, encephalitis, dysphagia and dysarthria, persistent delirium, and stupor improved to wakefulness, after 5-day course of adjunctive steroid treatment.	Case report
Bode et al., 2006	West Nile Virus	228	3/17 patients with corticosteroids died (18%), while 9/48 patients who did not receive adjunctive corticosteroid treatment died (19%).	Observational Study

clinical evaluation of patients for autoimmune encephalitis includes clinical presentation, an MRI of the brain, CSF assessment, and EEG. Autoantibodies detected determine disease pathogenesis and classification within autoimmune encephalitis (Graus et al., 2016; Hasbun et al., 2018). The most frequent clinical syndromes are from anti-N-methyl-D-aspartate receptor (NMDAR) encephalitis, characterized by behavioral and psychiatric differences, seizures, memory deficits, and limbic encephalitis, characterized by confusion, agitation, memory deficits, and seizures (Nosadini et al., 2015) (see **Table 3**). Treatment of acute autoimmune encephalitis includes immunotherapy, addressing underlying detected malignancies, and treatment of associated sequelae. Autoimmune encephalitis, characterized by antibodies attacking cell surface proteins, responds to antibody-directed therapy such as intravenous immunoglobulin and plasmapheresis. This treatment is accompanied by the administration of corticosteroids intravenously, such as methyl prednisone. Second-line therapy in the acute phase is rituximab and cyclophosphamide. In the maintenance phase mycophenolate, azathioprine, rituximab, cyclophosphamide, corticosteroids, and intravenous immunoglobulin are administered (Nosadini et al., 2015; Hasbun et al., 2018). Corticosteroids are incorporated into first and second-line immunotherapy for autoimmune encephalitis in conjunction with intravenous immunoglobulin administration. In a review of studies on the treatment of anti-LG1 autoantibody encephalitis, the addition of corticosteroids was shown to have a significant association with the cessation of faciobrachial dystonic seizures (FBDS) in 30% of patients by the first week, and 60% within 2 months. In second-line immune therapy, the most consistent reductions in seizure frequency and mRS score for neurologic disability improvement were associated with steroid treatment (Shin et al., 2013; Nosadini et al., 2015; Shin et al., 2018). The accepted first-line therapies include adjunctive corticosteroid treatment, intravenous immunoglobin, plasma exchange, and immune-adsorption, which have consistently shown positive results in treatment through case studies and systematic review. Corticosteroid therapy in autoimmune encephalitis is used to broadly inhibit the inflammatory response, but possesses little targeted therapy and is associated with systemic side effects, such as the aggravation of psychiatric symptoms like depression, insomnia, agitation, and psychosis, and neurotoxic effects through the potential to induce neuro-degeneration with chronic exposure, making other lines of treatment more effective in combination (Shin et al., 2018). More research must be conducted to determine the optimization of corticosteroid use in conjunction with alternative therapies to maximize clinical benefits and further research on steroid-sparing agents in second-line therapy and long- term maintenance of autoimmune encephalitis.

TUBERCULOSIS

Initial Therapy

Tuberculosis (TB) is caused by *Mycobacterium tuberculosis* and in 85% of cases it involves the lungs. One of the most common sites of extra pulmonary TB is the CNS (Hasbun et al., 2018). Tuberculosis meningitis is the most common form of CNS tuberculosis and is found in 10%–15% of children <2 years old after untreated TB infection and is often misdiagnosed as bacterial meningitis (Hasbun et al., 2018). Tuberculosis meningitis is postulated to occur in two stages. First, bacterial lesions form in the brain or meninges, from the dispersion of bacteria through the bloodstream in early infection, leading to the development of meningitis upon entry into the subarachnoid space. Second, proteins and chemicals from the organism leak into the CSF, eliciting an immune response and intense inflammation at the brain and meninges (Hasbun et al., 2018). Bacille Calmette-Guerin (BCG) vaccines can prevent up to 50%–80% of TB meningitis cases, but effectiveness varies with available strains of BCG. The vaccination rates do not meet optimal standards in many areas still (Hasbun et al., 2018). The adjunctive treatment of corticosteroids has been employed to reduce inflammation in tuberculosis meningitis. A randomized, double blind, controlled trial in Vietnam of 545 patients with TB meningitis over 14 years of age with and without human immunodeficiency virus (HIV) infection, studied the use of dexamethasone steroid treatments effects. Treatment with dexamethasone was associated with reduced risk of death and significantly fewer adverse events than in placebo groups, which was consistent across various grades of disease severity and HIV status, providing strong evidence for corticosteroid adjunctive therapy to improve survival in patients over age 14 years with TB meningitis (Thwaites et al., 2004) (see **Table 4**). In a meta analysis of published RCTs of corticosteroid treatment used in TB meningitis, six randomized controlled trials totaling 990 patients were identified, one of which included HIV infected patients. In all studies, the use of corticosteroid adjunctive treatment reduced mortality rates. These results were significant in four of the documented studies. Approximately 39%–73% of the patients across the six trials were severely ill with stage 2 disease (drowsy with focal neurologic deficits) and 23%–56% with stage 3 disease (coma). Faster defervescence, fewer complications of tuberculomas, and fewer clinical complications from anti-tuberculosis medications were documented as well (McGee and

TABLE 3 | Studies on Adjunctive Steroid Therapy for Autoimmune Encephalitis.

Reference	Pathogen	N	Primary Findings	Type of Study
Shin et al., 2013	Autoimmune Encephalitis	14	Patients with LG1 antibodies as a target protein treated with steroids alone were more likely to relapse and had less favorable outcomes than those treated with steroids and intravenous immunoglobins (IVIG).	Case Series
Nosadini et al., 2015	Autoimmune Encephalitis	1,390	Corticosteroids treatment associated with cessation of FBDS (faciobrachial dystonic seizures) within 1 week in 30% (3/10) of patients, and within 2 months in 60% (6/10). mRS improvement consistently associated with corticosteroids second-line immune therapy.	Meta analysis

TABLE 4 | Studies and Significant Findings on Adjunctive Steroid Therapy for Tuberculosis Meningitis Treatment.

Reference	Pathogen	N	Primary Findings	Type of Study
Thwaites et al., 2004	*Mycobacterium tuberculosis*	545	Effects of dexamethasone steroid treatments in patients over 14 years of age with and without HIV infection. Dexamethasone treatment was associated with reduced risk of death (relative risk, 0.69; 95 percent confidence interval, 0.52 to 0.92;P=0.01) and significantly fewer adverse events than in placebo groups (26 of 274 patients vs. 45 of 271 patients, P=0.02), consistent across various grades of disease severity and HIV status.	RCT
McGee and Hirschmann, 2008	*Mycobacterium tuberculosis*	990	Across six randomized controlled studies, corticosteroid adjunctive treatment reduced mortality rates and the differences were significant in 4/6 of the trials. Faster defervescence, fewer complications of tuberculomas, and fewer clinical complications from anti-tuberculosis medications documented.	Meta analysis
Murdoch et al., 2007	*Mycobacterium tuberculosis*	-	Adjunctive corticosteroid therapy effective in some cases of TB-IRIS for anti-inflammatory purposes in alleviating symptoms. Corticosteroids effectiveness often anecdotal, requiring larger systematic studies worldwide.	Meta analysis
Meintjes et al., 2010	*Mycobacterium tuberculosis*	110	Patients with TB-IRIS treated with prednisone (1.5mg/kg/day for 2 weeks then 0.75mg/kg/day for 2 weeks) for more rapid improvement in the steroid-treated group arm at 2 weeks (p=0.001) and 4 weeks (p=0.03), and reduced the number of days hospitalized (median cumulative of 0 vs. 3 days; (p=0.009)). Infections occurred in 27 participants in the prednisone arm and 17 in the placebo arm (p=0.05), although the majority of infections were mild.	RCT
Prasad et al., 2016	*Mycobacterium tuberculosis*	1,337	Across nine trials, use of adjunctive steroids in tuberculosis meningitis (with and without HIV) reduced deaths by almost one quarter after an 18-month follow up.(RR 0.75, 95% CI 0.65 to 0.87). Reduction in the risk of death or disabling residual neurological deficit with corticosteroids (RR 0.80, 95% CI 0.72 to 0.89; eight trials, 1314 participants)	Meta analysis

Hirschmann, 2008). A Cochrane study has also demonstrated over nine trials and 1,337 participants that use of adjunctive steroids in tuberculosis meningitis reduced deaths by almost one quarter after an 18 month follow up. While the former meta-analysis does not indicate outcome differences between stages of TB infection, the Cochrane study shows that the effect of corticosteroids is significantly consistent across all stages of the disease. Analysis also did not show differences in outcome based on HIV status, although the analysis was noted as underpowered (Prasad et al., 2016). CDC guidelines on the treatment of Tuberculosis based off of published treatment results, recommend the addition of corticosteroids in treatment for tuberculosis meningitis for all patients, although data is limited for patients with HIV (American Thoracic Society, CDC, & Infectious Disease Society of America, 2003; Lewinsohn et al., 2017). Overall, the research shows benefit in reduction of mortality and adverse effects in the use of corticosteroids as an adjunctive treatment in cases of initial therapy for confirmed tuberculosis meningitis.

PARADOXICAL REACTION

Paradoxical reaction (PR) in tuberculosis is the clinical or radiological worsening of pre-existing TB or the development of new TB lesions in patients who have received treatment against TB and improved in treatment initially. It affects up to 25% of patients and can cause significant morbidity especially in CNS tuberculosis (Bloch et al., 2009). The manifestation of PR in TB patients includes neuroimaging abnormalities, altered CSF pictures, and changes in CSF, including lymphatic pleocytosis, and an increase in CSF protein levels. Corticosteroid treatment has been demonstrated to have beneficial effects through case studies (Teoh et al., 1986; Garcia-Monco et al., 2005; Kim and Kim, 2009; Singh et al., 2016). TB related immune reconstitution inflammatory syndrome (IRIS) can also occur in HIV-positive patients after introducing antiretroviral therapy (ART) and can be life threatening. In a meta-analysis of 8 RCTs it was shown that there was a two-fold increase in TB-IRIS in patients treated with ART. In patients with a new diagnosis of TB and a CD4 count of less than 50/mm^3, ART within 1–4 weeks of diagnosis improved outcomes. Earlier ART, however, may be associated with more frequent TB-IRIS, so ART therapy is recommended only after 4–6 weeks of diagnosis in patients with HIV-1 TB and higher CD4 counts (Davis et al., 2018). TB related IRIS is more common in adults, occurring in 15.7% of TB patients within 2 months of ART therapy, and is a frequent complication of ART in resource-limited countries, with up to a 30% overall mortality rate (Meintjes et al., 2010; Fane et al., 2018; Hasbun et al., 2018). Adjunctive corticosteroid therapy has shown to be effective in some cases of TB-IRIS for anti-inflammatory purposes in alleviating symptoms. The use of corticosteroids has been variable, however, and effectiveness often anecdotal, requiring larger systematic studies worldwide (Murdoch et al., 2007). A randomized double-blind controlled trial of 110 patients in South Africa shows that patients with TB-IRIS were treated with prednisone resulting in more rapid improvement in the steroid-treated group and reduced the number of days hospitalized with no excess of glucocorticoid adverse drug reaction. Glucocorticoid therapy can be effective in treating TB-IRIS in severe cases, however, the diagnoses of paradoxical TB-IRIS must be correct, and alternate diagnoses must be eliminated completely, due to the existing possibility of adverse effects from steroid adjunctive treatment (Meintjes et al., 2010).

CRYPTOCOCCAL MENINGITIS

Initial Infection

Cryptococcal meningitis (CM) is an infection of the meninges due to *Cryptococcus neoformans* or *Cryptococcus gatti*, which is less common and thought to cause disease more often in immunocompetent

patients (Hasbun et al., 2018). CM is the most prevalent cause of meningitis in populations with high HIV prevalence, particularly as seen in studies conducted in countries and populations with high HIV prevalence in sub-Saharan Africa. It is correlated with a lower CD4 + count in HIV patients (Jarvis et al., 2010; Rajasingham et al., 2015). CM associated with HIV infection causes over 600,000 deaths per year worldwide, with little improvement in treatment. A double-blind randomized controlled trial studied the use of adjunctive dexamethasone steroid therapy in combination with antifungal treatments, amphotericin B and fluconazole, for six weeks in 451 adult patients with CM in Vietnam, Thailand, Indonesia, Laos, Uganda, and Malawi. The trial was stopped prior to completion for safety concerns. A mortality rate of 47% with dexamethasone treatment and 41% in the placebo group at 10 weeks was originally observed, but after 6 months of treatment the corticosteroid treatment group had increased mortality of 57% in comparison to the placebo of 47%. The percentage of patients with disability by 10 weeks of treatment was higher in dexamethasone-treated groups and dexamethasone-treated groups showed more clinically adverse outcomes such as the increased prevalence of grade 3 or 4 infection, renal events, and cardiac events (Beardsley et al., 2016) (see **Table 5**). Based on this study, adjunctive steroids should be avoided in Cryptococcal meningitis.

Immune Reconstitution Syndrome (IRIS)

IRIS occurs when immunological recovery after infection contributes to worsening disease in the long term. In HIV patients, after ART and successful immune restoration, inflammatory responses and worsened opportunistic infection has been observed. IRIS is clinically characterized by localized and systemic inflammatory response during invasive fungal infection (Singh and Perfect, 2007). CM-IRIS is seen in HIV patients with CM either as: a) paradoxical IRIS, meaning a relapse of infection after antifungal therapy and initiation of ART or b) as unmasking IRIS, when CM is developed after starting ART and an underlying, previously undiagnosed infection resurfaces. IRIS is developed in 30% HIV and CM co-infected patients who initiate ART. It is increased in individuals with high CSF fungal burdens in initial CM infection and in those who do not clear infection prior to the initiation of antiretroviral treatments (Shelburne et al., 2005; Fane et al., 2018; Hasbun et al., 2018). Systemic corticosteroids

TABLE 5 | Studies and Significant Findings on Adjunctive Steroid Therapy for Fungal and Parasitic CNS Infection.

Reference	Pathogen	N	Primary Findings	Type of Study
Murdoch et al., 2007	*C. neoformans* or *C. gatti*	–	Across small studies and anecdotal benefits, it is reasonable to administer systemic corticosteroids to alleviate unresponsive inflammatory effects.	Meta analysis
Beardsley et al., 2016	*C. neoformans* or *C. gatti*	451	Studied use of adjunctive dexamethasone steroid therapy in combination with antifungal treatments, amphotericin B and fluconazole, for six weeks. Mortality rate of 47% with dexamethasone treatment and 41% in the placebo group (10 weeks) and 57% mortality with dexamethasone treatment in comparison to the placebo of 47% (6 months). Disability and adverse effects higher in dexamethasone-treated groups by 10 weeks of treatment.	RCT
Perfect et al., 2018	*C. neoformans* or *C. gatti*	–	In CM-IRIS major complications, such as CNS inflammation with increased intracranial pressure, corticosteroids (0.5–1.0 mg/kg per day of prednisone equivalent) should be administered and possibly dexamethasone at higher doses for severe CNS signs and symptoms, with a concomitant antifungal regimen.	Meta analysis
Slom et al., 2002	*A. cantonensis*	12	Repeated lumbar punctures and corticosteroid therapy led to improvement of severe headaches and intracranial pressure decrease.	Case series
Maretic et al., 2009	*A. cantonensis*	11	Data supports use of albendazole and mebendazole steroid treatment. Anthelmintic treatment administration not recommended without adjunctive steroid treatment.	Case series
Wang et al., 2012	*A. cantonensis*	–	Small outbreak data supports corticosteroids treatment in combination with anthelmintics	Meta analysis
Pereira-Chioccola et al., 2009	*Toxoplasma gondii*	–	Cases of diffuse encephalitis and expansive lesions with a mass effect in the brain are recommended adjunctive corticosteroid therapy.	Meta analysis
Sonneville et al., 2012	*Toxoplasma gondii*	100	Analyzed patients with HIV and the outcome of adjunctive steroid therapy. With the use of pyrimethamine-sulfadiazine treatment, adjunctive steroids to treat cerebral edema associated with focal lesions are safe but not associated with better neurologic outcomes.	Observational Study
Singhi et al., 2004	*Taenia solium*	133	Disappearance of lesions at 3-month follow up higher (62.9%) in corticosteroid treatment with albendazole group compared to albendazole treatment alone (52.6%). Children in the corticosteroid group had significantly higher seizure recurrence while on AEDs.	RCT
Kishore and Misra, 2007	*Taenia solium*	100	Higher resolution in group that received prednisone alone (68.1%) compared to treatment with antiepileptic monotherapy (60.9%) ($p<0.05$)	RCT
White et al., 2018	*Taenia solium*	–	Guidelines for the treatment of Neurocysticercosis in America. Corticosteroids should be used in viable parenchymal NCC for reduction in seizure frequency.Corticosteroids should be given with antiparasitic with single enhancing lesion NCC. Corticosteroids should be used, while avoiding antiparasitic treatment with cysticercal encephalitis (with diffuse cerebral edema). Corticosteroids should not be routinely used for calcified parenchymal NCC with or without perilesional edema due to the development of calcifications with perilesional edema in some cases	Meta analysis

have been administered to alleviate inflammation and resulted in positive response through case studies (King et al., 2002; Murdoch et al., 2007). The particular role of adjunctive steroid treatment remains unclear in IRIS, although it has been considered reasonable to administer corticosteroids only in severe cases of unresponsive inflammation (Sharma and Soneja, 2011; Fane et al., 2018).

Angiostrongylus cantonensis

Angiostrongylus is a parasitic nematode causing severe CNS diseases in humans. *A. cantonensis* from larval invasion causes eosinophilic meningitis as the primary clinical manifestation of the disease. Infection occurs from consuming infected intermediate hosts or vegetables contaminated by these hosts (Martins et al., 2015). Outbreaks in human angiostrongyliasis have been reported in endemic regions such as the Pacific Islands, Southeast Asia, the Caribbean Islands, and Brazil. Treatment includes corticosteroids in combination with anthelmintics (Wang et al., 2012) (see **Table 5**). In a retrospective cohort study, out of 12 hospitalized adults who had traveled to Jamaica and were diagnosed with eosinophilic meningitis, repeated lumbar punctures and corticosteroid therapy led to the improvement of severe headaches in two out of three patients, and intracranial pressure decrease in all three (Slom et al., 2002). A review of case studies demonstrates data favoring the use of antiparasitic (albendazole or mebendazole) and steroid treatment, although anthelmintic administration was not recommended without steroid treatment (Maretic et al., 2009). Anthelmintic treatment is recommended only in early stages of infection, through demonstrated CNS and pulmonary complications when administered beyond 3 weeks of treatment. When anthelmintic treatment is effective later in infection, it kills viable larvae, suspending them in the CNS with negative clinical consequences. Similar effects of delayed resolution of inflammation and disposal of the worm carcass, causing further damage, is noted with prolonged corticosteroid therapy (Prociv and Turner, 2018). Corticosteroid therapy may be beneficial in early treatment, with recommendations to apply the treatment in severe cases, although data is limited in large clinical trials to demonstrate significance and effectiveness in treatment.

Toxoplasma gondii

Toxoplasma gondii, a single-celled parasite found across the world, causes toxoplasmosis infection. Toxoplasmosis is one of the most common human infections. CNS infection by *T. gondii* causes toxoplasma encephalitis, which is the most common cause of brain mass lesions in HIV infected patients, causing high mortality and morbidity (Vidal, 2019). *T. gondii* causes latent infection in 10%–90% of the world's population, but clinical presentation otherwise often includes brain abscess and diffuse encephalitis or ventriculitis (Marra, 2018). In patients with HIV, single or multiple ring-enhancing lesions on CT or MRI scans suggest toxoplasma encephalitis in the setting of a positive Toxoplasma IGG. Adjunctive corticosteroid therapy should be considered in patients with brain abscesses with significant cerebral edema (Pereira-Chioccola et al., 2009) (see **Table 5**). The most effective treatment for CNS toxoplasmosis is sulfadiazine and pyrimethamine. Steroid treatment is not recommended unless disproportionate cytotoxic edema is displayed and life threatening. In the case of brain abscess, steroids effectively reduce brain edema, but reduce the effectiveness of host defense processes as well (Muzumdar et al., 2011; Patel and Clifford, 2014). There is no large study demonstrating the efficacy of adjunctive steroid therapy in HIV related toxoplasmosis. Steroid administration is recommended only when lesions due to toxoplasmosis have developed significant mass effect or diffuse brain edema is seen, although the significant benefit of adjunctive steroid therapy in mortality, even in the treatment of cerebral edema, has not been demonstrated in a large cohort (Haverkos, 1987; Rothova et al., 1989; Pereira-Chioccola et al., 2009; Sonneville et al., 2012; Vidal, 2019). Corticosteroids can be used in severe abscess related edema or cases of clinically significant mass effect, with early animal studies showing a reduction in the penetration of antimicrobials into the abscess (Patel and Clifford, 2014).

NEUROCYSTICERCOSIS

Neurocysticercosis (NCC) is the most common parasitic disease of the CNS in humans, caused by the larval stage of the *Taenia solium* tapeworm. The parasites, once ingested, reach mature size at 3 months, and are established as larval cysts in the tissue, causing single lesions or several lesions in some cases (Garcia et al., 2010). NCC is the single most common cause of acquired epileptic episodes in the developing world, which is the most common presentation of parenchymal NCC (Singhi et al., 2004; Garcia et al., 2010). The Infectious Disease Society of America (IDSA) strongly recommends adjuvant corticosteroid therapy with antiparasitics for anti-inflammatory purposes in patients with viable parenchymal neurocysticercosis (NCC). Steroid therapy has been associated with fewer seizures, although optimal doses have not yet been defined. For single enhancing lesions due to NCC, corticosteroids concomitant with antiparasitic treatment is also strongly recommended, due to data on worsening symptoms with antiparasitic treatment alone (Singhi et al., 2004; White et al., 2018). In the case of calcified parenchymal NCC with or without perilesional edema, corticosteroid therapy is not routinely recommended. In cysticercal encephalitis with diffuse cerebral edema, the IDSA recommends that corticosteroid treatment is administered, without the use of antiparasitic drugs, because antiparasitic treatment is associated with worsening edema. The guidelines show that evidence from large case series and overall evaluation points to antiparasitic treatment with steroid therapy, over antiparasitic treatment alone, as antiparasitic drugs have been shown to worsen the symptoms of NCC (White et al., 2018). Corticosteroids are the primary treatment for chronic cysticercosis arachnoiditis or encephalitis NCC (Garcia et al., 2010). Due to the varying nature of antiparasitic treatment in combination with adjunctive corticosteroid therapy across different presentations of NCC, treatment of NCC with must be individualized (Singhi et al., 2004).

TABLE 6 | Studies on adjunctive steroids use for the treatment of bacterial brain abscess.

Reference	Pathogen	N	Primary Findings	Type of Study
Muzumdar et al., 2011	Brain Abscess	289	Steroid administration is not recommended unless life-threatening issues of cytotoxic edema. Intravenous were steroids administered for 15 patients, who presented with significant perifocal edema. Steroid therapy was tapered over 2 weeks and edema was markedly reduced with resolution of the abscess cavity after steroid therapy.	Observational Study
Patel and Clifford, 2014	Bacterial Brain Abscess	–	Steroid administration is not recommended unless severe abscess related edema has led to clinically significant mass effect. Corticosteroid therapy may reduce antimicrobial penetration into the abscess.	Meta analysis

BACTERIAL BRAIN ABSCESS

Brain abscess is a focal infection of the brain with localized inflammation of the cerebrum. Bacteria is responsible for over 95% of all brain abscesses, entering the brain through the contiguous spread, hematogenous dissemination, or as a consequence of distant infectious foci in other organs. (Patel and Clifford, 2014; Sonneville et al., 2017). The incidence of bacterial brain abscess is around 0.3–0.9/100,000 inhabitants per year in developed countries (Sonneville et al., 2017). Clinical symptoms of bacterial brain abscess include fever, focal neurological deficits, seizures, and altered consciousness. In addition to antibacterial treatment that is recommended upon identification of the condition, patients with warning signs of brain herniation can be placed on a short course of adjunctive steroids (Sonneville et al., 2017). Steroid administration is not typical to bacterial brain abscess and is not recommended unless life-threatening issues of cytotoxic edema are present and have led to clinical mass effect (Miranda et al., 2013). In these cases, the adjunctive corticosteroid therapy may be effective in reducing antimicrobial penetration into the abscess. Although steroid therapy is effective due to anti-inflammatory properties in the case of brain edema, the host's defense mechanisms may be disrupted. Steroids have also been shown to inhibit collagen capsule formation, which may inhibit a key mechanism for leucocyte travel in the body's defense systems (Muzumdar et al., 2011; Patel and Clifford, 2014) (see **Table 6**).

CONCLUSION

Adjunctive steroids therapy has proven effective to improved outcomes in some cases of CNS infection, although in others administration of steroid therapy can be detrimental. Critical evaluation of the presenting infection and point of administration is necessary for optimal therapeutic use as indicated through the review. Adjunctive steroids are effective in reducing inflammation and improving clinical outcomes in some causes of meningitis such as *S. pneumoniae* (mortality), *H. influenzae* (hearing loss), *N. meningitidis* (arthritis), and *M. tuberculosis* (mortality). Even though the use of adjunctive steroids is an essential therapy of autoimmune encephalitis, its use in viral encephalitis is unclear as there are limited studies. Steroids are also used in *A. cantonensis* meningitis and in brain abscesses caused by bacteria or by toxoplasmosis when associated with significant mass effect or cerebral edema. Adjunctive corticosteroid therapy is also consistently recommended in neurocysticercosis with cerebral edema. Adjunctive corticosteroids are also used in IRIS treatment to alleviate inflammation in severe cases. The use of corticosteroid therapy can also be detrimental as in *L. monocytogenes* or CM so an accurate, prompt diagnosis is key. Overall, data for the use adjunctive steroids in several CNS infections (e.g., HSV, WNV, etc.) are limited and future studies should explore the utility of steroids in larger-scale studies.

AUTHOR CONTRIBUTIONS

RH conceived the general idea and provided critical revision and final approval of the manuscript. SG conducted the literature review and wrote the draft manuscript. All authors contributed to the article and approved the submitted version.

FUNDING

The Grant A Starr Foundation supported this work.

REFERENCES

American Thoracic Society, CDC, & Infectious Disease Society of America (2003). Treatment of Tuberculosis. *Am. J. Respir. Crit. Care Med.* 167, 603–662.

Archibald, L. K., and Quisling, R. G. (2013). Central Nervous System Infections. *Textbook Neurointensive Care* 1, 427–517. doi: 10.1007/978-1-4471-5226-2_22

Bakri, S., and Kaiser, P. (2004). Ocular manifestations of West Nile virus. *Curr. Opin. Ophthamol.* 15, 537–540. doi: 10.1097/01.icu.0000143687.45232.f1

Barnes, P. J. (2006). How corticosteroids control inflammation: Quintiles Prize Lecture 2005. *Br. J. Pharmacol.* 148 (3), 245–254. doi: 10.1038/sj.bjp.0706736

Beardsley, J., Wolbers, M., Kibengo, F. M., Ggayi, A. B. M., Kamali, A., Cuc, N. T. K., et al. (2016). Adjunctive Dexamethasone in HIV-Associated Cryptococcal Meningitis. *N. Engl. J. Med.* 374 (6), 543–554. doi: 10.1056/NEJMoa1509024

Bloch, S., Wickremasinghe, M., Wright, A., Rice, A., Thompson, M., and Kon, O. M. (2009). Paradoxical reactions in non-HIV tuberculosis presenting as endobronchial obstruction. *Eur. Respir. Rev.* 18 (114), 295–298. doi: 10.1183/09059180.00003709

Bode, A. V., Sejvar, J. J., Pape, W. J., Campbell, G. L., and Marfin, A. A. (2006). West Nile Virus Disease: A Descriptive Study of 228 Patients Hospitalized in a 4-County Region of Colorado in 2003. *Clin. Infect. Dis.* 42 (9), 1234–1240. doi: 10.1086/503038

Bradshaw, M. J., and Venkatesan, A. (2016). Herpes Simplex Virus-1 Encephalitis in Adults: Pathophysiology, Diagnosis, and Management. *Neurotherapeutics* 13 (3), 493–508. doi: 10.1007/s13311-016-0433-7

Brouwer, M. C., Heckenberg, S. G. B., de Gans, J., Spanjaard, L., Reitsma, J. B., and van de Beek, D. (2010). Nationwide implementation of adjunctive dexamethasone therapy for pneumococcal meningitis. *Neurology* 75 (17), 1533–1539. doi: 10.1212/WNL.0b013e3181f96297

Brouwer, M., McIntyre, P., Prasad, K., and van de Beek, D. (2018). Corticosteroids for acute bacterial meningitis (Review). *Cochrane Database Syst. Rev.* 9. doi: 10.1002/14651858.CD004405.pub5

Castelblanco, R. L., Lee, M. J., and Hasbun, R. (2014). Epidemiology of bacterial meningitis in the USA from 1997 to 2010: A population-based observational study. *Lancet Infect. Dis.* 14 (9), 813–819. doi: 10.1016/S1473-3099(14)70805-9

Charlier, C., Perrodeau, É, Leclercq, A., Cazenave, B., Pilmis, B., Henry, B., et al. (2017). Clinical features and prognostic factors of listeriosis: the MONALISA national prospective cohort study. *Lancet Infect. Dis.* 17 (5), 10. doi: 10.1016/S1473-3099(16)30521-7

Colpitts, T. M., Conway, M. J., Montgomery, R. R., and Fikrig, E. (2012). West Nile virus: Biology, transmission, and human infection. *Clin. Microbiol. Rev.* 25 (4), 635–648. doi: 10.1128/CMR.00045-12

Coyle, P. K. (1999). Glucocorticoids in Central Nervous System Bacterial Infection. *Arch. Neurol.* 56 (7), 796–801. doi: 10.1001/archneur.56.7.796

Dando, S. J., Mackay-Sim, A., Norton, R., Currie, B. J., St John, J. A., Ekberg, J. A., et al. (2014). Pathogens penetrating the central nervous system: infection pathways and the cellular and molecular mechanisms of invasion. *Clin. Microbiol. Rev.* 27 (4), 691–726. doi: 10.1128/CMR.00118-13

Davis, A., Meintjes, G., and Wilkinson, R. J. (2018). Treatment of Tuberculous Meningitis and Its Complications in Adults. *Curr. Treat Options Neurol.* 20 (3), 5. doi: 10.1007/s11940-018-0490-9

de Gans, J., and van de Beek, D. (2002). Dexamethasone In Adults With Bacterial Meningitis. *N. Engl. J. Med.* 346 (13), 957–966. doi: 10.1056/NEJMoa021334

Dorsett, M., and Liang, S. Y. (2016). Diagnosis and Treatment of Central Nervous System Infections in the Emergency Department. *Emergency Med. Clinics North Am.* 34 (4), 917–942. doi: 10.1016/j.emc.2016.06.013

Encephalitis, Table 3 (2017). *Johns Hopkins ABX Guide* (Johns Hopkins Guide: The Johns Hopkins University). Available at: https://www.hopkinsguides.com/hopkins/view/Johns_Hopkins_ABX_Guide/540639/all/Encephalitis:Table_3. Retrieved October 17, 2020.

Engelen-Lee, J. Y., Brouwer, M. C., Aronica, E., and van de Beek, D. (2018). Delayed cerebral thrombosis complicating pneumococcal meningitis: An autopsy study. *Ann. Intensive Care* 8 (1), 20. doi: 10.1186/s13613-018-0368-8

Erdem, H., Cag, Y., Ozturk-Engin, D., Defres, S., Kaya, S., Larsen, L., et al. (2015). Results of a Multinational Study Suggest the Need for Rapid Diagnosis and Early Antiviral Treatment at the Onset of Herpetic Meningoencephalitis. *Antimicrob. Agents Chemother.* 59 (6), 3084–3089. doi: 10.1128/AAC.05016-14

Erdem, H., Inan, A., Guven, E., Hargreaves, S., Larsen, L., Shehata, G., et al. (2017). The burden and epidemiology of community-acquired central nervous system infections: a multinational study. *Eur. J. Clin. Microbiol. Infect. Dis.* 36 (9), 1595–1611. doi: 10.1007/s10096-017-2973-0

Fane, M., Mustapha, S., Chakib, A., K, M., and Filali, L. (2018). HIV and Immune Reconstitution Inflammatory Syndrome (HIV-IRIS). *J. Infect. Dis. Pathog.* 1 (2), 1–8.

Fitch, M. T., and van de Beek, D. (2008). Drug Insight: steroids in CNS infectious diseases–new indications for an old therapy. *Nat. Clin. Pract. Neurol.* 4 (2), 97–104. doi: 10.1038/ncpneuro0713

Gallegos, C., Tobolowsky, F., Nigo, M., and Hasbun, R. (2018). Delayed Cerebral Injury in Adults With Bacterial Meningitis: A Novel Complication of Adjunctive Steroids? *Crit. Care Med.* 46 (8), e811–e814. doi: 10.1097/CCM.0000000000003220

Garcia-Monco, J., Ferreira, E., and Gomex-Belderrain, M. (2005). The therapeutic paradox in the diagnosis of tuberculous meningitis. *Neurology*. 65 (12), 1991–1992. doi: 10.1212/01.wnl.0000188885.31724.07

García, H. H., Gonzalez, A. E., Rodriguez, S., Tsang, V. C., Pretell, E. J., Gonzales, I., et al. (2010). Neurocysticercosis: unraveling the nature of the single cysticercal granuloma. *Neurology* 75 (7), 654–658. doi: 10.1212/WNL.0b013e3181ed9eae

George, B. P., Schneider, E. B., and Venkatesan, A. (2014). Encephalitis Hospitalization Rates and Inpatient Mortality in the United State-2010. *PLoS One* 9 (9), e104169. doi: 10.1371/journal.pone.0104169

Glimåker, M., Brink, M., Naucler, P., and Sjölin, J. (2016). Betamethasone and dexamethasone in adult community-acquired bacterial meningitis: a quality registry study from 1995 to 2014. *Clin. Microbiol. Infect.* 22 (9), 814.e1–814.e7. doi: 10.1016/j.cmi.2016.06.019

Graus, F., Titulaer, M., Balu, R., and Al, E. (2016). A clinical approach to diagnosis of autoimmune encephalitis.. *Lancet Neurology* 15 (4), 391–404. doi: 10.1016/S1474-4422(15)00401-9

Hasbun, R., Garcia, M. N., Kellaway, J., Baker, L., Salazar, L., Woods, S. P., et al. (2016). West nile virus retinopathy and associations with long term neurological and neurocognitive sequelae. *PLoS One* 11 (3), 1–10. doi: 10.1371/journal.pone.0148898

Hasbun, R., Rosenthal, N., Balada-Llasat, J. M., Chung, J., Duff, S., Bozzette, S., et al. (2017). Epidemiology of Meningitis and Encephalitis in the United State-2014. *Clin. Infect. Dis.* 65 (3), 359–363. doi: 10.1093/cid/cix319

Hasbun, R., Hammadi, A. A., Aurpibul, L., and Al, E. (2018). *Meningitis and encephalitis: Management and Prevention Challenges* (Switzerland AG: Springer Nature). doi: 10.5005/jp/books/14182_10

Hasbun, R. (2019). Update and advances in community acquired bacterial meningitis. *Curr. Opin. Infect. Dis.* 32 (3), 233–238. doi: 10.1097/QCO.0000000000000543

Haverkos, H. (1987). Assessment of therapy for toxoplasma encephalitis. *Am. J. Med.* 82, 907–914. doi: 10.1016/0002-9343(87)90151-3

Heckenberg, S., Brouwer, M., van der Ende, A., and van de Beek, D. (2012). Adjunctive dexamethasone in adults with meningococcal meningitis. *Neurology* 79 (15), 1563–1569. doi: 10.1212/WNL.0b013e31826e2684

Hoffman, O., and Weber, J. R. (2009). Pathophysiology and treatment of bacterial meningitis. *Ther. Adv. Neurol. Disord.* 2 (6), 401–412. doi: 10.1177/1756285609337975

Jarvis, J. N., Meintjes, G., Williams, A., Brown, Y., Crede, T., and Harrison, T. S. (2010). Adult meningitis in a setting of high HIV and TB prevalence: Findings from 4961 suspected cases. *BMC Infect. Dis.* 10 (67). doi: 10.1186/1471-2334-10-67

Kamei, S., Sekizawa, T., Shiota, H., Mizutani, T., Itoyama, Y., Takasu, T., et al. (2005). Evaluation of combination therapy using aciclovir and corticosteroid in adult patients with herpes simplex virus encephalitis. *J. Neurol. Neurosurg. Psychiatry* 76 (11), 1544–1549. doi: 10.1136/jnnp.2004.049676

Kim, S., and Kim, Y. (2009). Immunologic paradox in the diagnosis of tuberculous meningitis. *Clin. Vaccine Immunol.* 16 (12), 1847–1849. doi: 10.1128/CVI.00321-09

King, M., Perlino, C., Cinnamon, J., and Jernigan, J. (2002). Paradoxical recurrent meningitis following therapy of cryptococcal meningitis: an immune reconstitution syndrome after initiation of highly active antiretroviral therapy. *Int. J. STD AIDS* 13 (10), 724–726. doi: 10.1258/095646202760326516

Kishore, D., and Misra, S. (2007). Short course of oral prednisolone on disappearance of lesion and seizure recurrence in patients of solitary cysticercal granuloma with single small enhancing CT lesion: an open label randomized prospective study. *J. Assoc. Phys. India* 55, 419–424.

Koyuncu, O. O., Hogue, I. B., and Enquist, L. W. (2013). Virus infections in the nervous system. *Cell Host Microbe* 13 (4), 379–393. doi: 10.1016/j.chom.2013.03.010

Leis, A. A., and Sinclair, D. J. (2019). Lazarus effect of high dose corticosteroids in a patient with West Nile virus encephalitis: A coincidence or a clue? *Front. Med.* 6:81 (APR). doi: 10.3389/fmed.2019.00081

Lewinsohn, D. M., Leonard, M. K., Lobue, P. A., Cohn, D. L., Daley, C. L., Desmond, E., et al. (2017). Official American Thoracic Society/Infectious Diseases Society of America/Centers for Disease Control and Prevention Clinical Practice Guidelines: Diagnosis of Tuberculosis in Adults and Children. *Clin. Infect. Dis.* 64 (2), e1–e33. doi: 10.1093/cid/ciw694

Maretic, T., Perovic, M., Vince, A., Lukas, D., Dekumyoy, P., and Begovac, J. (2009). Meningitis and Radiculomyelitis Caused by Angiostrongylus cantonensis. *Clin. Infect. Dis.* 15 (6), 996–998. doi: 10.1086/499815

Marra, C. (2018). Central nervous system infection with Toxoplasma gondii. *Handbook of Clin. Neurol.* 152, 117–122. doi: 10.1016/B978-0-444-63849-6.00009-8

Martinez-Torres, F., Menon, S., Pritsch, M., Victor, N., Jenetzky, E., Jensen, K., et al. (2008). Protocol for German trial of Acyclovir and corticosteroids in Herpes-simplex-virus-encephalitis (GACHE): A multicenter, multinational, randomized, double-blind, placebo-controlled German, Austrian and Dutch trial [ISRCTN45122933]. *BMC Neurol.* 8, 1–10. doi: 10.1186/1471-2377-8-40

Martins, Y. C., Tanowitz, H. B., and Kazacos, K. R. (2015). Central nervous system manifestations of Angiostrongylus cantonensis infection. *Acta Tropica* 141 (Pt A), 46–53. doi: 10.1016/j.actatropica.2014.10.002

McGee, S., and Hirschmann, J. (2008). Use of corticosteroids in treating infectious diseases. *Arch. Internal Med.* 168 (10), 1034–1046. doi: 10.1001/archinte.168.10.1034

McGill, F., Heyderman, R. S., Michael, B. D., Defres, S., Beeching, N. J., Borrow, R., et al. (2016). The UK joint specialist societies guideline on the diagnosis and management of acute meningitis and meningococcal sepsis in immunocompetent adults. *J. Infect.* 72 (4), 405–438. doi: 10.1016/j.jinf.2016.01.007

McIntyre, P., Berkey, C., King, S., and Al, E. (1997). Dexamethasone as adjunctive therapy in bacterial meningitis. A meta-analysis of randomized clinical trials since 1988. *JAMA* 278 (11), 925–931. doi: 10.1001/jama.278.11.925

Meintjes, G., Wilkinson, R. J., Morroni, C., Pepper, D. J., Rebe, K., Rangaka, M. X., et al. (2010). Randomized placebo-controlled trial of prednisone for paradoxical TB-associated IRIS. *AIDS* 24 (15), 2381–2390. doi: 10.1097/QAD.0b013e32833dfc68

Meyding-Lamade, U., Oberlinner, C., Rau, P., and Al, E. (2003). Experimental herpes simplex virus encephalitis: a combination therapy of acyclovir and glucocorticoids reduces long-term magnetic resonance imaging abnormalities. *J. Neurovirol.* 9 (1), 118–125. doi: 10.1080/13550280390173373

Meyding-Lamadé, U., Jacobi, C., Martinez-Torres, F., Lenhard, T., Kress, B., Kieser, M., et al. (2019). The German trial on Aciclovir and Corticosteroids in Herpes-simplex-virus-Encephalitis (GACHE): a multicenter, randomized, double-blind, placebo-controlled trial. *Neurol. Res. Pract.* 1 (1), 1–9. doi: 10.1186/s42466-019-0031-3

Miranda, H. A., Castellar-Leones, S. M., Elzain, M. A., and Moscote-Salazar, L. R. (2013). Brain abscess: Current management. *J. Neurosci. Rural Pract.* 4 (Suppl 1), S67–S81. doi: 10.4103/0976-3147.116472

Murdoch, D. M., Venter, W. D. F., Van Rie, A., and Feldman, C. (2007). Immune reconstitution inflammatory syndrome (IRIS): Review of common infectious manifestations and treatment options. *AIDS Res. Ther.* 4 (9), 1–10. doi: 10.1186/1742-6405-4-9

Muzumdar, D., Jhawar, S., and Goel, A. (2011). Brain abscess: An overview. *Int. J. Surg.* 9 (2), 136–144. doi: 10.1016/j.ijsu.2010.11.005

Nahmias, A. J., Whitley, R. J., Visintine, A. N., Takei, Y., Alford, C. A. Jr., and Group, C. A. S. (1982). Herpes Simplex Virus Encephalitis: Laboratory Evaluations and Their Diagnostic Significance. *J. Infect. Dis.* 145 (6), 829–836. doi: 10.1093/infdis/145.6.829

NICE UK (2010). "Meningitis (bacterial) and meningococcal septicaemia in under 16s: recognition, diagnosis and management," in *NICE Clinical Guideline [CG102]*, 1–40. Available at: https://www.nice.org.uk/guidance/CG102/chapter/1-Guidance#pre-hospital-management-of-suspected-bacterial-meningitis-and-meningococcal-septicaemia.

Nosadini, M., Mohammad, S. S., Ramanathan, S., Brilot, F., and Dale, R. C. (2015). Immune therapy in autoimmune encephalitis: A systematic review. *Expert Rev. Neurother.* 15 (12), 1391–1419. doi: 10.1586/14737175.2015.1115720

Patel, K., and Clifford, D. B. (2014). Bacterial Brain Abscess. *Neurohospitalist* 4 (4), 196–204. doi: 10.1177/1941874414540684

Pereira-Chioccola, V., Vidal, J., and Su, C. (2009). Toxoplasma gondii infection and cerebral toxoplasmosis in HIV-infected patients. *Future Microbiol.* 4, 1363–1379. doi: 10.2217/fmb.09.89

Perfect, J. R., Dismukes, W. E., Dromer, F., Goldman, D. L., John, R., Hamill, R. J., et al. (2018). Clinical Practice Guidelines for the Management of Cryptococcal Disease: 2010 Update by the Infectious Diseases Society of America. *Clin. Infect. Dis.* 50 (3), 291–322. doi: 10.1086/649858

Prasad, K., Singh, M., and Ryan, H. (2016). Corticosteroids for managing tuberculous meningitis (Review). *Cochrane Database Syst. Rev.* 4, 2008–2010. doi: 10.1002/14651858.CD002244.pub4.www.cochranelibrary.com

Prociv, P., and Turner, M. (2018). Perspective piece neuroangiostrongyliasis: The "subarachnoid phase" and its implications for anthelminthic therapy. *Am. J. Trop. Med. Hyg.* 98 (2), 353–359. doi: 10.4269/ajtmh.17-0206

Rajasingham, R., Rhein, J., Klammer, K., Musubire, A., Nabeta, H., Akampurira, A., et al. (2015). Epidemiology of meningitis in an HIV-infected Ugandan cohort. *Am. J. Trop. Med. Hyg.* 92 (2), 274–279. doi: 10.4269/ajtmh.14-0452

Rothova, A., Buitenhuis, H. J., Meenken, C., Baarsma, G. S., Boen-Tan, T. N., de Jong, P. T., et al. (1989). Therapy of ocular toxoplasmosis. *Int. Ophthalmol.* 13 (6), 415–419. doi: 10.1007/BF02306491

Scheld, W. M., Dacey, R. G., Winn, H. R., Welsh, J. E., Jane, J. A., and Sande, M. A. (1980). Cerebrospinal fluid Outflow Resistance in Rabbits with Experimental Meningitis: Alterations with Penicillin and Methylprednisolone. *J. Clin. Invest.* 66 (2), 243–253. doi: 10.1172/JCI109850

Sharma, S. K., and Soneja, M. (2011). HIV & immune reconstitution inflammatory syndrome (IRIS). *Indian J. Med. Res.* 134 (6), 866–877. doi: 10.4103/0971-5916.92632

Shelburne, III, S. A., Darcourt, J., White, J. A.C., Greenberg, S. B., Hamill, R. J., Atmar, R. L., et al. (2005). The Role of Immune Reconstitution Inflammatory Syndrome in AIDS-Related Cryptococcus neoformans Disease in the Era of Highly Active Antiretroviral Therapy. *Clin. Infect. Dis.* 40 (7), 1049–1052. doi: 10.1086/428618

Shin, Y., Lee, S., Shin, J., and Al, E. (2013). VGKC-complex/LGI1-antibody encephalitis: clinical manifestations and response to immunotherapy. *J. Neuroimmunol.* 265 (1–2), 75–81. doi: 10.1016/j.jneuroim.2013.10.005

Shin, Y. W., Lee, S. T., Park, K.II, Jung, K. H., Jung, K. Y., Lee, S. K., et al. (2018). Treatment strategies for autoimmune encephalitis. *Ther. Adv. Neurol. Disord.* 11, 1–19. doi: 10.1177/1756285617722347

Singh, N., and Perfect, J. R. (2007). Immune reconstitution syndrome associated with opportunistic mycoses. *Lancet Infect. Dis.* 7 (6), 395–401. doi: 10.1016/S1473-3099(07)70085-3

Singh, A. K., Malhotra, H. S., Garg, R. K., Jain, A., Kumar, N., Kohli, N., et al. (2016). Paradoxical reaction in tuberculous meningitis: Presentation, predictors and impact on prognosis. *BMC Infect. Dis.* 16 (1), 1–11. doi: 10.1186/s12879-016-1625-9

Singhi, P., Jain, V., and Khandelwal, N. (2004). Corticosteroids versus albendazole for treatment of single small enhancing CT lesions in children with NCC. *J. Child Neurol.* 19, 323–327. doi: 10.1177/088307380401900503

Slom, J. T., Cortese, M. M., Gerber, S. I., Jones, R. C., Holtz, T. H., Lopez, A. S., et al. (2002). An outbreak of eosinophilic meningitis caused by Angiostrongylus cantonensis in travelers returning from the Caribbean. *New Engl. J. Med.* 346 (9), 668–675. doi: 10.1056/NEJMoa012462

Sonneville, R., Schmidt, M., Messika, J., and Al, E. (2012). Neurologic outcomes and adjunctive steroids in HIV patients with severe cerebral toxoplasmosis. *Neurology* 79 (17), 1762–1766. doi: 10.1212/WNL.0b013e3182704040

Sonneville, R., Ruimy, R., Benzonana, N., Riffaud, L., Carsin, A., Tadié, J. M., et al. (2017). An update on bacterial brain abscess in immunocompetent patients. *Clin. Microbiol. Infect.* 23 (9), 614–620. doi: 10.1016/j.cmi.2017.05.004

Steel, H. C., Cockeran, R., Anderson, R., and Feldman, C. (2013). Overview of community-acquired pneumonia and the role of inflammatory mechanisms in the immunopathogenesis of severe pneumococcal disease. *Mediators Inflammation* 2013, 490346. doi: 10.1155/2013/490346

Sulaiman, T., Salazar, L., and Hasbun, R. (2017). Acute Versus Subacute Community-Acquired Meningitis: Analysis of 611 Patients. *Open Forum Infect. Dis.* 96 (36), e7984. doi: 10.1093/ofid/ofw172.878

Tauber, M., Khayam-Bakshi, H., and Sande, M. A. (1985). Effects of ampicillin and corticosteroids on brain water content, cerebrospinal fluid pressure, and cerebrospinal fluid lactate levels in experimental pneumococcal meningitis. *J. Infect. Dis. Pathog.* 151 (3), 528–534. doi: 10.1093/infdis/151.3.528

Teoh, R., O'Mahony, G., and Yeung, V. (1986). Polymorphonuclear pleocytosis in the cerebrospinal fluid during chemotherapy for tuberculous meningitis. *J. Neurol. Neurosurg. Psychiatry* 233, 237–241. doi: 10.1007/BF00314027

Thwaites, G. E., Bang, N. D., Dung, N. H., Quy, H. T., Oanh, D. T. T., Thoa, N. T. C., et al. (2004). Dexamethasone for the Treatment of Tuberculous Meningitis in Adolescents and Adults. *New Engl. J. Med.* 351 (17), 1741–1751. doi: 10.1056/NEJMoa040573

Tunkel, A. R., Hartman, B. J., Kaplan, S. L., Kaufman, B. A., Roos, K. L., Scheld, W. M., et al. (2004). Practice Guidelines for the Management of Bacterial Meningitis. *Clin. Infect. Dis.* 39 (9), 1267–1284. doi: 10.1086/425368

van de Beek, D., Cabellos, C., Dzupova, O., Esposito, S., Klein, M., Kloek, A. T., et al. (2016a). ESCMID guideline: diagnosis and treatment of acute bacterial meningitis. *Clin. Microbiol. Infect.* 22, S37–S62. doi: 10.1016/j.cmi.2016.01.007

van de Beek, D., Brouwer, M., Hasbun, R., Koedel, U., Whitney, C. G., and Wijdicks, E. (2016b). Community-acquired bacterial meningitis. *Nat. Rev.: Dis. Primers* 2, 1–21. doi: 10.1038/nrdp.2016.74

Venkatesan, A., Tunkel, A. R., Bloch, K. C., Lauring, A. S., Sejvar, J., Bitnun, A., et al. (2013). Case definitions, diagnostic algorithms, and priorities in encephalitis: consensus statement of the international encephalitis consortium. *Clin. Infect. Dis.* 57 (8), 1114–1128. doi: 10.1093/cid/cit458

Vidal, J. E. (2019). HIV-Related Cerebral Toxoplasmosis Revisited: Current Concepts and Controversies of an Old Disease. *J. Int. Assoc. Providers AIDS Care* 18, 1–20. doi: 10.1177/2325958219867315

Wang, Q., Wu, Z., Wei, J., and Al, E. (2012). Human Angiostrongylus cantonensis: an update. *Eur. J. Clin. Microbiol. Infect. Dis.* 31, 389–395. doi: 10.1007/s10096-011-1328-5

White, A. C., Coyle, C. M., Rajshekhar, V., Singh, G., Hauser, W. A., Mohanty, A., et al. (2018). Diagnosis and Treatment of Neurocysticercosis: 2017 Clinical Practice Guidelines by the Infectious Diseases Society of America (IDSA) and the American Society of Tropical Medicine and Hygiene (ASTMH). *Clin. Infect. Dis.* 66 (8), e49–e75. doi: 10.1093/cid/cix1084

Conflict of Interest: RH has received research support and personal fees from Biofire.

The remaining authors declare that the research was conducted in the absence of any commercial or financial relationships that could be construed as a potential conflict of interest.

frontiers in Cellular and Infection Microbiology

ORIGINAL RESEARCH
published: 11 December 2020
doi: 10.3389/fcimb.2020.603623

CSF Levels of Elongation Factor Tu Is Associated With Increased Mortality in Malawian Adults With *Streptococcus pneumoniae* Meningitis

Emma C. Wall[1,2,3], Philip Brownridge[4], Gavin Laing[5], Vanessa S. Terra[6], Veronica Mlozowa[3], Brigitte Denis[3], Mulinda Nyirenda[7,8], Theresa Allain[8], Elisa Ramos-Sevillano[9], Enitan Carrol[10], Andrea Collins[5,11], Stephen B. Gordon[3,5], David G. Lalloo[5], Brendan Wren[6], Robert Beynon[4], Robert S. Heyderman[2,3] and Jeremy S. Brown[9]*

[1] The Francis Crick Institute, London, United Kingdom, [2] Division of Infection and Immunity, University College London, London, United Kingdom, [3] Malawi-Liverpool-Wellcome Trust Clinical Research Programme, College of Medicine, University of Malawi, Blantyre, Malawi, [4] Centre for Proteomics, Institute of Integrative Biology, University of Liverpool, Liverpool, United Kingdom, [5] Liverpool School of Tropical Medicine, Liverpool, United Kingdom, [6] London School of Hygiene and Tropical Medicine, London, United Kingdom, [7] Adult Emergency Trauma Centre, Queen Elizabeth Central Hospital, Ministry of Health, Blantyre, Malawi, [8] College of Medicine, University of Malawi, Blantyre, Malawi, [9] UCL Respiratory, Division of Medicine, University College London, London, United Kingdom, [10] Institute of Infection and Global Health, University of Liverpool, Liverpool, United Kingdom, [11] Liverpool University Hospital Foundation Trust, Liverpool, United Kingdom

OPEN ACCESS

Edited by:
Federico Iovino, Karolinska Institutet (KI), Sweden

Reviewed by:
Uwe Koedel, Ludwig Maximilian University of Munich, Germany
Lars-Ove Brandenburg, University Hospital RWTH Aachen, Germany

***Correspondence:**
Emma C. Wall
emma.wall@crick.ac.uk

Specialty section:
This article was submitted to Bacteria and Host, a section of the journal Frontiers in Cellular and Infection Microbiology

Received: *07 September 2020*
Accepted: *10 November 2020*
Published: *11 December 2020*

Citation:
Wall EC, Brownridge P, Laing G, Terra VS, Mlozowa V, Denis B, Nyirenda M, Allain T, Ramos-Sevillano E, Carrol E, Collins A, Gordon SB, Lalloo DG, Wren B, Beynon R, Heyderman RS and Brown JS (2020) CSF Levels of Elongation Factor Tu Is Associated With Increased Mortality in Malawian Adults With Streptococcus pneumoniae Meningitis. Front. Cell. Infect. Microbiol. 10:603623. doi: 10.3389/fcimb.2020.603623

Background: Mortality from bacterial meningitis, predominately caused by *Streptococcus pneumoniae*, exceeds 50% in sub-Saharan African countries with high HIV prevalence. Underlying causes of high mortality are poorly understood. We examined the host and pathogen proteome in the CSF of adults with proven pneumococcal meningitis (PM), testing if there was an association between differentially expressed proteins and outcome.

Materials/Methods: CSF proteomes were analyzed by quantitative Mass-Spectrometry. Spectra were identified using the Swissprot human and TIGR4 pneumococcal protein libraries. Proteins were quantitated and analyzed against mortality. Unique proteins in PM were identified against published normal CSF proteome. Random-Forest models were used to test for protein signatures discriminating outcome. Proteins of interest were tested for their effects on growth and neutrophil opsonophagocytic killing of *S. pneumoniae*.

Results: CSF proteomes were available for 57 Adults with PM (median age 32 years, 60% male, 70% HIV-1 co-infected, mortality 63%). Three hundred sixty individual human and 23 pneumococcal proteins were identified. Of the human protein hits, 30% were not expressed in normal CSF, and these were strongly associated with inflammation and primarily related to neutrophil activity. No human protein signature predicted outcome. However, expression of the essential *S. pneumoniae* protein Elongation Factor Tu (EF-Tu) was significantly increased in CSF of non-survivors [False Discovery Rate (q) <0.001]. Expression of EF-Tu was negatively co-correlated against expression of Neutrophil

defensin (r 0.4 p p < 0.002), but not against complement proteins C3 or Factor H. *In vitro*, addition of EF-Tu protein impaired *S. pneumoniae* neutrophil killing in CSF.

Conclusions: Excessive *S. pneumoniae* EF-Tu protein in CSF was associated with reduced survival in meningitis in a high HIV prevalence population. We show EF-Tu may inhibit neutrophil mediated killing of *S. pneumoniae* in CSF. Further mechanistic work is required to better understand how *S. pneumoniae* avoids essential innate immune responses during PM through production of excess EF-Tu.

Keywords: meningitis, HIV—human immunodeficiency virus, mortality, *Streptococcus pneumoniae*, cerebrospinal fluid, proteomics, Elongation factor Tu (EF-Tu)

INTRODUCTION

Acute bacterial meningitis (ABM) is a leading cause of infectious mortality and morbidity worldwide; an estimated 2.8 million incident cases of community-acquired ABM were reported in 2016 occurring predominately in children and young people (Collaborators GBDM, 2018). There is a particularly high toll of meningitis caused by *Streptococcus pneumoniae* (pneumococcal meningitis, PM) in sub-Saharan Africa, where the combination of high HIV prevalence and high burden of nasopharyngeal carriage create a potent environment for PM to flourish in all age groups (Gessner et al., 2010; Heinsbroek et al., 2015; Britz et al., 2016; Swarthout et al., 2020). Ambitious global WHO targets to defeat meningitis by 2030 were published in 2018 (Organisation) WWH, [[NoYear]]). However, progress in Africa is limited by the lack of affordable vaccines and effective adjunctive therapies to antibiotics (Scarborough et al., 2007; Ajdukiewicz et al., 2011; Wall et al., 2017a). In African LMICs mortality from ABM in adults and adolescents exceeds 50% compared to 10–20% in better resourced settings, but causes of excessive mortality from ABM in this setting are not well described (van de Beek et al., 2010; Mourvillier et al., 2013; Wall et al., 2017a; Tenforde et al., 2019).

Prognostic scores for ABM have low sensitivity and specificity (Weisfelt et al., 2008; Wall et al., 2017b), suggesting pathological differences in the CNS leading to poor outcome are not readily detected by clinical parameters. During PM, large numbers of neutrophils rapidly trans-migrate from blood in response to pro-inflammatory mediators in CSF (Potter and Harding, 2001; Koedel et al., 2009; de Oliveira et al., 2016). Neutrophils have a critical role in killing *S. pneumoniae* by phagocytosis (Ramos-Sevillano et al., 2016; Ullah et al., 2017), but also contribute to counter-productive inflammatory responses which may mediate death and disability in pneumococcal meningitis, sepsis and pneumonia (Bewley et al., 2011; Ramos-Sevillano et al., 2016; Ritchie et al., 2018; Domon et al., 2018). This host-pathogen interaction triggers an inflammatory cascade of both cytotoxic effects of host pro-inflammatory mediators (Mook-Kanamori et al., 2011; Wang et al., 2016), and bacterial toxins, that drive tissue damage in non-survivors characterized by apoptotic neuronal cell injury, raised intracranial pressure (ICP), thrombosis, cerebral edema, and ischemia (Wall et al., 2012; Wippel et al., 2013; Wall et al., 2014; Doran et al., 2016).

Proteomics provides an opportunity to dissect this host-pathogen interaction in CSF during disease by both quantitating the relative abundance of multiple inflammatory proteins, and testing for associations between human and bacterial proteins and outcome (Zhang et al., 2015; Bastos et al., 2017). Previously, the CSF proteome in a small number of children with PM from our center showed marked upregulation of multiple inflammatory and bacterial proteins compared to hospital controls, including neutrophil proteins S100A9 and myeloperoxidase in CSF (Gomez-Baena et al., 2017). In an earlier study, using 2D electrophoresis proteomics of adults with PM, demonstrated consumption of complement C3 in non-survivor CSF, we described an exacerbated host response including proteins involved with brain damage (Goonetilleke et al., 2010; Goonetilleke et al., 2012), but did not find major proteomic differences between the outcome groups.

In this study, we utilized label-free quantitative tandem mass-spectrometry proteomics to quantitate the host and pathogen proteome in adults with PM, to determine if a CSF protein signature predicts the outcome from PM. We further tested the effects of a protein associated with poor outcome using an *in vitro* neutrophil killing assay.

METHODS

Patients

CSF was obtained for proteomics from adults and adolescents on admission to hospital with suspected bacterial meningitis at Queen Elizabeth Central Hospital in Blantyre, Malawi between 2011 and 2013 (Wall et al., 2017a). All CSF samples were collected prior to administration of parenteral antibiotics 2 g BD for 10 days (Scarborough et al., 2007; Ajdukiewicz et al., 2011). Clinical data were recorded on admission to hospital, clinical outcome data reported at 6 weeks post-discharge (Wall et al., 2017a).

Procedures

Routine CSF microscopy, cell count, and CSF culture was done at the Malawi-Liverpool-Wellcome Trust Clinical Research Programme laboratory in Blantyre, Malawi as previously described (Wall et al., 2017a). Culture negative samples were

screened using the multiplex real-time polymerase chain reaction for *S. pneumoniae*, *Neisseria. Meningitidis*, and *Haemophilus influenzae type b* (Hib) kit from Fast-Track Diagnostics (FTD Luxemburg) according to the manufacturer's instructions, bacterial loads were estimated from Ct values. Additionally, CSF was screened for Herpes viruses including EBV, CMV, and HSV1. We excluded patients with active viral co-infection in the CSF. We collected 2.0 ml of CSF for proteomics, stored on receipt in the laboratory (within 2 h of LP) at −80 degrees Celsius. In-hospital HIV testing was done on all patients by the clinical teams using point-of care Genie™ HIV1&2 test kits (BioRad, USA).

CSF Protein Extraction and Mass-Spectrometry

Protein concentration in all CSF samples was measured by nanodrop (Thermo Scientific, UK) and normalized to 200 μg/ml. Samples were centrifuged at 13,000 *g* and the pellet stored at −80°C until peptide extraction. Proteins were treated with the surfactant 0.1% (v/v) RapiGest™ (Waters) at 80°C for 10 min followed by reduction with diothiothreitol (DTT) at a final concentration of 3 mM (60°C for 10 min) and alkylation with iodoacetamide (IAA) at a final concentration of 50 mM (room temp, in the dark, 1 h). The enzyme trypsin (sequencing grade, Promega) was added at an enzyme:substrate ratio of 1:50 and incubated overnight with agitation at 37°C. The surfactant was inactivated the following day by treatment with 0.1% trifluoroacetic acid (TFA) (37°C for 1 h) and peptides were recovered following centrifugation at 13,000 *g*.

Resultant CSF peptides were separated by RPLC using a DIONEX UltiMate™ 3000LC chromatography system and MSMS analysis performed on an LTQ Orbitrap Velos using Xcalibur software v2.1 (both Thermo Scientific, UK). Peptides (10 μl = ~500 ng) were injected onto the analytical column (Dionex Acclaim® PepMap RSLC C18, 2 μm, 100 Å, 75 μm i.d. ×15 cm, nanoViper.), which was maintained at 35°C and at a nanoflow rate of 0.3 $\mu l min^{-1}$. Peptides were separated over linear chromatographic gradients composed of buffer A (2.5% ACN: 0.1% FA) and buffer B (90% ACN: 0.1% FA). Two gradients, 60 (3–50% buffer B in 40 min) and 180 min (3–60% buffer B in 140 min), were employed for analysis. Full scan MS spectra were acquired over the *m/z* range of 350–2,000 in positive polarity mode by the Orbitrap at a resolution of 30,000. A data-dependent Top20 collision induced dissociation (CID) data acquisition method was used. The ion-trap operated with CID MSMS on the 20 most intense ions (above the minimum MS signal threshold of 500 counts).

Bio-informatic Quantitative Analysis

Data was initially mass recalibrated using the mzRefiner filter of the Proteowizard msconvert tool. The resulting files were then processed using Progenesis QI (version 2 Nonlinear Dynamics, Newcastle upon Tyne, UK). Samples were aligned according to retention time using a combination of manual and automatic alignment. Default peak picking parameters were applied and features with charges from 1+ to 4+ featuring three or more isotope peaks were retained. Database searching was performed using Mascot (Matrix Science, London, UK). A Mascot Generic File, created by Progenesis QI, was searched against a merged database of the reviewed entries of the Uniprot reference proteome set of *H. sapiens* (09/12/2015, 20,187 sequences) and *S. pneumoniae* (09/12/2015, 2,030 sequences). A fixed carbamidomethyl modification for cysteine and variable oxidation modification for methionine were specified. A precursor mass tolerance of 10 ppm and a fragment ion mass tolerance of 0.6 Da were applied. The results were then filtered to obtain a peptide false discovery rate of 1%. Protein inference and quantification was performed using the "Relative Quantitation using non-conflicting peptides" option in Progenesis. Protein quantification values are determined from all peptides but weighted according to peptide intensity. Proteins were annotated as differentially expressed if they achieved an FDR corrected q value of 0.05. Outcome prediction was performed by random forest using the cforest function of the "party" package in R. Pathways analysis of proteins was done using Innate DB.

Synthesis of Pneumococcal Proteins

E. coli cells containing pEQ30_EF-Tu were kindly donated by Prof. Sven Hammerschmidt. *E. coli* was grown at 25°C in LB supplemented with 100 μg/ml ampicillin (Mohan et al., 2014). When the OD_{595nm} reached 0.5, protein expression was induced by adding 1 mM isopropyl β-d-thiogalactoside (IPTG). EF-Tu was modified to contain a polyhistidine tag to aid purification and detection. EF-tu is insoluble when expressed in *E. coli* and precipitates in inclusion bodies. Firstly, the cells were pelleted by centrifugation at 3,250 × g, then the pellet was resuspended in 10 ml of 50 mM NaH_2PO_4, 300 mM NaCl (pH 8). This was followed firstly by sonication and then by centrifugation at 4,300 × g, for 30 min at 4°C. The pellet containing the inclusion bodies was then washed in 50 mM NaH_2PO_4, 300 mM NaCl (pH 8) and resuspended in 500 μl of 50 mM NaH_2PO_4, 300 mM NaCl, 4 M Urea (pH 8) to solubilize the inclusion bodies. This suspension was then centrifuged at 18,000 × g for 30 min at 4°C. The supernatant that contained EF-Tuf was then mixed with Ni-NTA (Qiagen, Germany) that had been resuspended in the same buffer as the protein. The column was then washed with 10 column volumes (CV) of 50 mM NaH_2PO_4, 300 mM NaCl, 4 M Urea (pH 8). The protein was eluted with 6 CV's using 50 mM NaH_2PO_4, 300 mM NaCl, 4 M Urea, 250 mM immidazole (pH 8). Eluted EF-Tuf was refolded by dialysis in 20 mM Tris-HCl 5 mM MgCl2 pH 7.4. Finally, the protein was recovered, and the buffer exchanged into PBS during concentration. Presence of the protein was confirmed *via* an anti-His western blot. Identity of the protein of choice was confirmed by running an anti-His western blot of the cell lysates prepared in the presence and absence of IPTG. Non-induced cell extracts did not react with anti-his antibody (**Supplementary Figure 1**).

Bacterial Growth Conditions

Strains of *S. pneumoniae* serotype 1 ST5316 (Terra et al., 2020) were grown in Todd-Hewitt broth supplemented with 0.5% yeast extract (THY) to OD 0.5 and stored in 80% glycerol at −80°C as previously described (Ramos-Sevillano et al., 2012). Bacteria

were thawed, washed in PBS twice, and diluted to 1×10^6 CFU/ml in either pooled serum from five healthy laboratory donors (non-PCV vaccinated) or thawed human cerebrospinal fluid (CSF). CSF was obtained from patients who underwent therapeutic lumbar puncture for idiopathic intracranial hypertension, all had biochemically normal, acellular CSF. CSF was kindly donated by Professor Diederik van de Beek (Amsterdam Medical Centre, Netherlands). Four ug of purified EF-Tu, bovine serum albumin (BSA), NanA or PiaA or PBS control were added to five technical replicates.

Growth for 24 h was detected by changes in optical density at 620 nm with shaking in a microplate reader (Tecan® USA) at 37°C.

Opsonophagocytosis Assays

Bacterial killing by purified human neutrophils was done using a previously described opsonophagocytosis assay (Hyams et al., 2010). Briefly, neutrophils were extracted from whole blood of healthy donors by negative selection Maxspress kit (Milteyni biotech, USA) according to the manufacturer's instructions. Bacteria were opsonized in either 10% pooled serum or CSF for 30 min at 37°C then incubated with purified fresh human neutrophils in HBSS with either 4 ug of purified EF-Tu, BSA, or PBS at 37°C for 45 min with shaking in the dark. Cytochalasin D was included in the negative control to stop phagocytosis. Serial dilutions of the reaction mix were plated on Colombia agar supplemented with 5% horse blood, and colony forming units (CFU) counted after 18 h incubation at 37°C.

Statistical Methods

All conventional statistical tests were two tailed, alpha <0.05 determined statistical significance. Ninety-five percent confidence intervals are presented for odds ratios. Logistic regression was used to model associations between clinical outcomes and risk factors while controlling for confounding factors.

Data Deposition

All proteomic data was submitted to the ProteomeXchange: Accession number:

Submission Reference: 1-20200901-167440

Submission Path:/nfs/pride/drop/pride-drop-003/philipjb_20200901_134730

Ethical Approvals

All participants or nominated guardians gave written informed consent for inclusion. Ethical approval for the transcriptomics study was granted by both the College of Medicine Research and Ethics Committee (COMREC), University of Malawi (P.01/10/980, January 2011), and the Liverpool School of Tropical Medicine Research Ethics Committee, UK (P10.70, November 2010) Committee, Liverpool, UK.

RESULTS

Patients

Fifty-seven patients with proven PM, whose CSF was stored within 4 h of presentation to hospital, were included in the study, 33 (57%) of whom had died within 6 weeks (**Table 1**). Median age was 33 years (IQR 26–44), and predominantly HIV co-infected (34/47, 72%). CSF protein and bacterial loads were high, and although raised, the CSF white cell counts (WCC) were substantially lower than those reported in high income settings (Costerus et al., 2016) (**Table 1**). Neither CSF bacterial load, CSF protein, nor CSF WCC differed significantly between survivors and non-survivors in an un-adjusted analysis. Similarly, to our previous reports, Glasgow Coma Score (GCS) was significantly lower in non-survivors (11/15) than survivors (14/15) (OR 0.57, 95% CI 0.35–0.87) on admission (Wall et al., 2017b).

CSF Human Proteome

A total of 336 peptides matching Uniprot identifiers were found in the CSF (**Figure 1**, **Supplementary Data 1**). Albumin was the most abundant CSF protein, followed by sub-classes of immunoglobulins, complement C3, alpha-1 antitrypsin, haptoglobin, hemopexin, and neutrophil proteins S100A8&9 (**Table 2**). Overall, the most abundant protein classes were immunoglobulins, metabolic proteins, and complement, along with antigen-binding proteins, neutrophil-associated and anti-bacterial proteins, inflammatory response, and vasomotor tone. Blood brain barrier (BBB) breakdown was suggested by the identification of hemoglobin, haptoglobin, and fibrinogen in the CSF (**Figure 1**). Pathways analysis of the entire proteome (Innate DB) found 16 pathways enriched with $q < 0.05$, dominated by complement, platelet degranulation, scavenging of heme, and axon guidance pathways (**Table 3**).

Sub-Set of Proteins Unique to PM

When compared to two reports of the proteome in normal CSF (Guldbrandsen et al., 2014; Zhang et al., 2015), we found 130/336 (38%) of proteins in PM were not normally found in CSF (**Figure**

TABLE 1 | Demographic details of included participants.

	Survivors (n = 19)	Non-survivors (n = 33)	OR Survival	p
Bacterial load (log_{10})	4.7×10^6 (7.7×10^5–3.5×10^7)	1.4×10^7 (9.8×10^5–6.8×10^7)	1.1 (0.83 : 1.56)	0.5
Age (years)	30 (26–41)	36 (24–44)	1.02 (0.96 : 1.06)	0.3
Male gender	11 (58%)	21 (63%)	0.78 (0.24 : 2.4)	0.68
GCS	14 (13–15)	12 (8–13)	0.57 (0.35 : 0.85)	0.007
CSF WCC cells/mm^3	52 (2–1760)	27 (2–287)	0.83 (0.43 : 1.5)	0.56
CSF protein (g/dl)	3.02 (2.5–4.0)	2.52 (1.8–5.6)	1.1 (0.7 : 1.7)	0.63
HIV infection	10/16 (62%)	24/31 (77%)	0.48 (0.1 : 1.8)	0.28

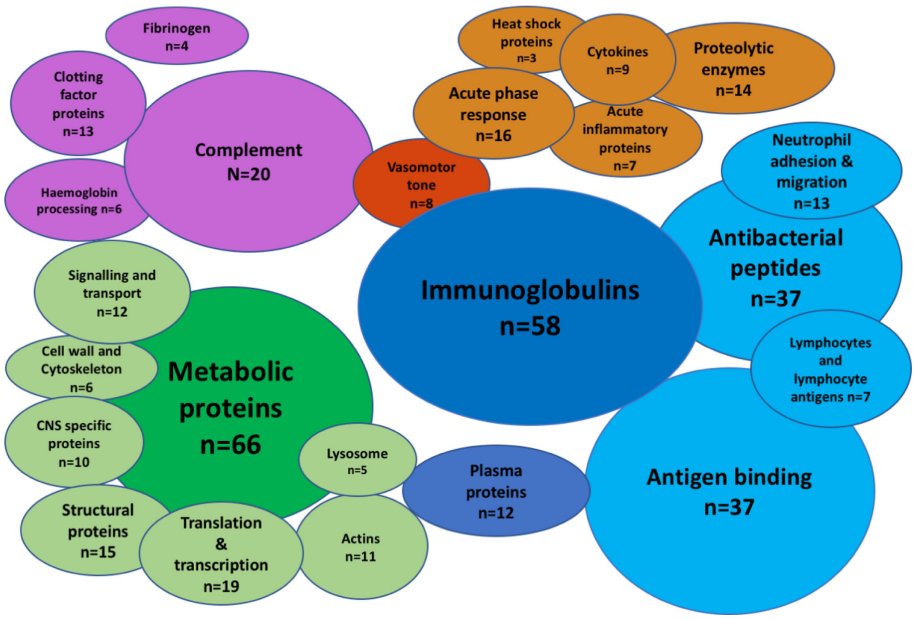

FIGURE 1 | The CSF proteome in pneumococcal meningitis is diverse and highly inflammatory. Bubble plot summary of the CSF proteome in pneumococcal meningitis. Three hundred thirty-six peptides identified by Mass-Spectrometry. Green, cellular functional proteins; blue, proteins synthesized by white and plasma cells; purple, complement and clotting cascades; orange, pro-inflammatory proteins.

TABLE 2 | Estimated abundance (arbitrary quantitative units) of 20 most highly expressed proteins in the CSF of patients with PM.

#	Protein	Median protein abundance (units)	#	Protein	Median protein abundance
1	Serum albumin	2.02E+09	**13**	Hemopexin	4.86E+07
2	Ig gamma-1 chain C region	1.39E+09	**14**	Apolipoprotein A-I	3.24E+07
3	Ig kappa chain C region	6.02E+08	**15**	Fibrinogen gamma chain	2.63E+07
4	Immunoglobulin lambda-like polypeptide 5	2.91E+08	**16**	Protein S100-A9	2.51E+07
5	Alpha-1-acid glycoprotein 1	1.33E+08	**17**	Alpha-2-macroglobulin	2.49E+07
6	Ig lambda-2 chain C	1.25E+08	**18**	Ig heavy chain V-III region BRO	2.46E+07
7	Haptoglobin	1.09E+08	**19**	Neutrophil defensin 1	2.25E+07
8	Alpha-1-antitrypsin	9.06E+07	**20**	Alpha-1-acid glycoprotein	2.11E+07
9	Ig alpha-1 chain C region	9.04E+07	**21**	Complement C3	2.10E+07
10	Serotransferrin	8.65E+07	**22**	Vitamin D-binding protein	2.09E+07
11	Ig gamma-3 chain C region	6.67E+07	**23**	Protein S100-A8	1.91E+07
12	Ig gamma-2 chain C region	6.39E+07	**24**	Ig mu heavy chain disease protein	1.88E+07

TABLE 3 | Enrichment of 10 most highly expressed biological pathways in the CSF of patients with PM.

Pathway number	Pathway name	P-adj value enrichment
1	Innate immune system	3.23E-73
2	Immune system	3.72E-61
3	Complement cascade, Regulation of complement cascade	3.29E-59
4	Hemostasis	7.66E-53
5	Neutrophil degranulation	3.29E-43
6	Scavenging heme from plasma	4.16E-41
7	RHO GTPases activate PKNs (actin dynamics)	1.70E-39
8	Binding and Uptake of Ligands by Scavenger Receptors	2.77E-39
9	Classical antibody-mediated complement activation	1.23E-36
10	Platelet degranulation	7.48E-36

2A). These include the majority of the immunoglobulin sub-classes, neutrophil and inflammatory proteins, CNS proteins, hemoglobin, and some metabolic proteins (**Figure 2B**). Pathways analysis of this protein set unique to PM was strongly enriched for complement activity, hemostasis and heme activation, neutrophil and platelet degranulation, actin dynamics, and scavenger receptor binding (**Table 4**). We also identified 10 proteins with a primary CNS source including *BSAP1*, *APLP1*, *CHL1*, mapping to pathways including Axon guidance and Dorso-ventricular axis.

CSF *Streptococcus pneumoniae* Proteome

Of the 30 pneumococcal proteins detected in CSF, four proteins were structural, ten related to metabolic activity, eight were ribosomal proteins, and nine had primary functions in virulence, or the stress response. These included the virulence factor PspA

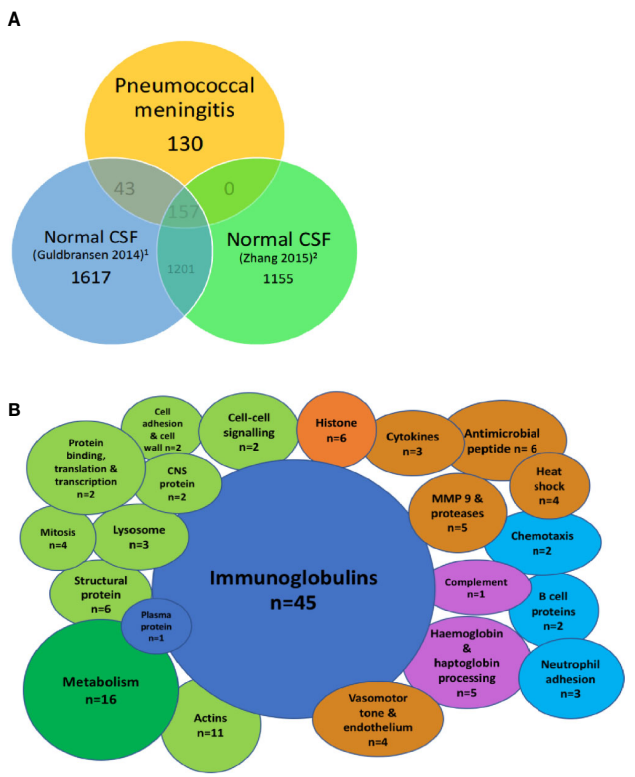

FIGURE 2 | Highly abundant CSF proteins in pneumococcal meningitis are directly involved in the host-pathogen interaction and demonstrate evidence of blood-brain barrier breakdown. Venn diagram showing overlap between the uniport peptide hits from the proteome of patients with PM and two previously published proteomes of normal CSF **(A)**. Bubble plot showing breakdown of proteins found in the subset of proteins unique to PM n = 130 from **Figure 1 (B)**. Green, cellular functional proteins; blue, proteins synthesized by white and plasma cells; purple, complement and clotting cascades; orange, pro-inflammatory proteins.

(involved in avoiding complement mediated immunity), the manganese transporter lipoprotein PsaA (required for protection against oxidative stress), ABC transporter component GalT1 (released during opsonophagocytosis, associated with avoidance of mucosal immunity) (Matthias et al., 2008), and the multi-functional protein Elongation Factor Tu (EF-Tu) (**Table 4**).

The Human Proteome Did Not Predict Outcome

To investigate the hypothesis that lower GCS reflects worsening inflammation in the CNS, we used a Random Forest model to test for a protein signature to predict outcome in CSF. Principal component analysis of the CSF proteome in PM did not show any separation between outcome groups testing either peptides or proteins (**Figure 3A**). We were unable to detect any sub-set or "signature" of proteins that correlated with outcome status (**Figure 3B**). The Random Forest Accuracy was 0.68 (95% CI 0.54–0.88), no information rate (NIR) 0.61, p-value (Accuracy >NIR) = 0.16. We then tested for associations with individual proteins that may be associated with clinical outcome status (**Figure 3C**). A number of host proteins were over-expressed in the CSF of either patient group (**Supplementary Figure 2**) at an individual level, including S100A8 and CD163. However, none were significantly expressed at >1 log fold change from the mean with FDR <0.05.

Poor Outcome Was Associated With Higher Levels of the *Streptococcus pneumoniae* Protein Elongation Factor Tu

Although the human CSF proteome did not correlate with outcome in PM, two *S. pneumoniae* proteins identified in the CSF did exceed adjusted FDR significance threshold in non-survivor CSF on the individual association analysis. These were Q8CWR9 (a ribosomal protein) and Elongation Factor Tu (EF-Tu, P64031) (**Figure 3C**). EF-Tu is an immunogenic surface expressed *S. pneumoniae* protein (Thofte et al., 2018; Nagai et al., 2019), involved in the transport of amino acylated tRNA components to ribosomes and is thought to

TABLE 4 | Abundance and function of pneumococcal proteins in the CSF of patients with PM, in order of abundance.

	Protein	Function	Estimated abundance (units)		Protein	Function	Estimated abundance (units)
1	Elongation factor Tu	Multi-function	9.20E+05	**11**	Thioredoxin	Stress response	4.46E+04
2	Chaperone protein DnaK	Protein folding	2.52E+05	**12**	Enolase	Carbohydrate degradation	4.05E+04
3	Ribosomal proteins (n=8)	Ribosome	1.80E+05	**13**	Acyl carrier protein	Lipid metabolism	3.83E+04
4	Pyruvate oxidase	Metabolism	1.60E+05	**14**	Endo-Peptidase O	Virulence	2.16E+04
5	Ketol-acid reductoisomerase	Metabolism	1.36E+05	**15**	ABC transporter GalT1	Metabolism	1.52E+04
6	Glyceraldehyde-3-phosphate dehydrogenase	Metabolism, immuno-stimulant	1.09E+05	**16**	Phosphoglycerate kinase	Metabolism	1.30E+04
7	Histone-like DNA-binding protein	DNA stabilization	1.08E+05	**17**	Pyruvate kinase	Metabolism	2.96E+03
8	Manganese ABC transporter substrate-binding lipoprotein	Surface antigen	1.03E+05	**18**	Uncharacterized protein	Unknown	2.54E+03
9	Glutamate dehydrogenase	Metabolism	4.78E+04	**19**	General stress protein GSP-781	Stress response	2.23E+03
10	Elongation factor G	Translation and collagen binding	4.64E+04	**20**	Surface protein pspA	Virulence and surface antigen	2.8E+03

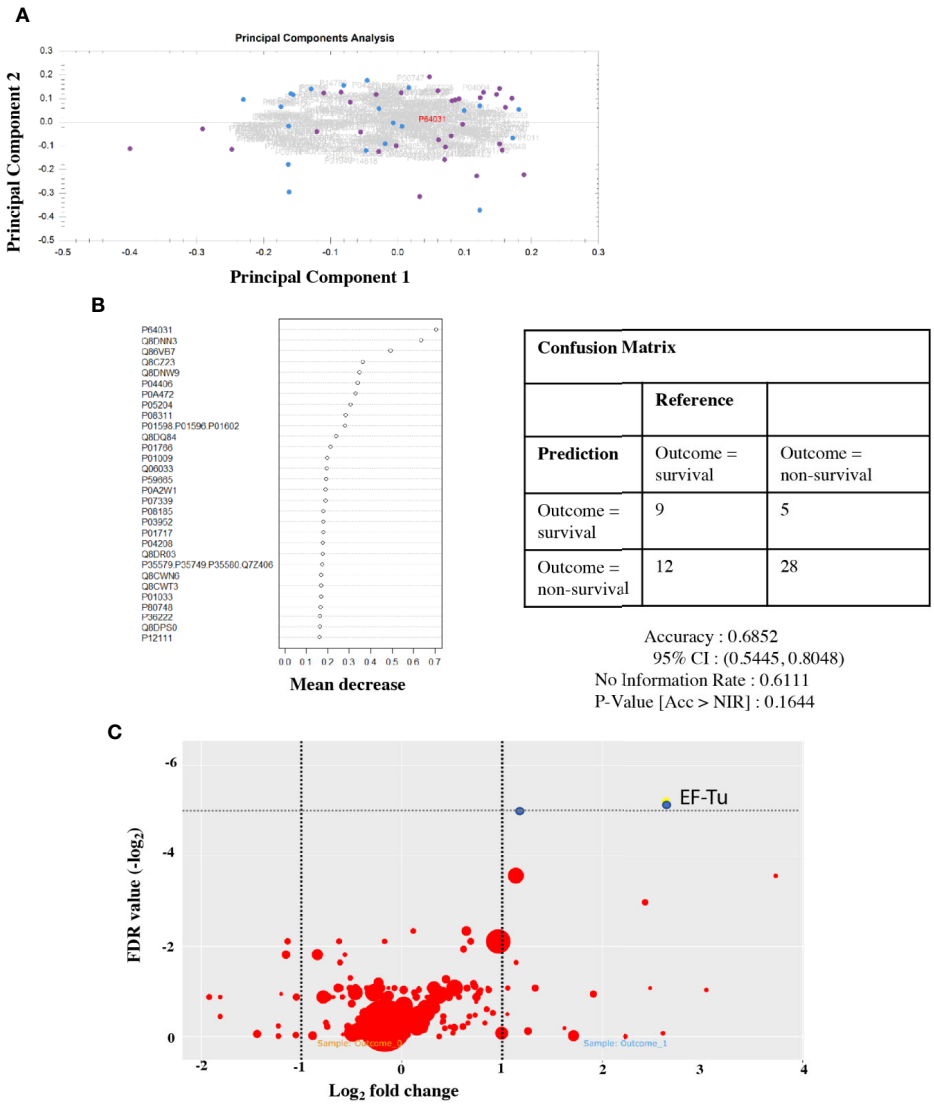

FIGURE 3 | Protein signatures in CSF do not predict outcome from PM, but individual pneumococcal proteins are highly expressed in non-survivors. CSF proteome does not separate by outcome group **(A)**. Principal component analysis of the CSF protein hits. Dot, individual patients; blue, survivor; and purple, non-survivor. Summary plot of Random Forest analysis of highly abundant individual CSF peptide hits **(B)**. Dot per protein shows deviation away from the mean (x axis) toward non-survival. No cluster/signature of abundant proteins accurately predicts outcome in CSF. Quantitative volcano plot of all protein hits **(C)**. Dots represent proteins. Red, non-significantly expressed; blue, significantly expressed (FDR < 0.01). Dot size represents quantitative estimates of abundance.

be essential. Recent data suggests that it may also assist *S. pneumoniae* evasion of complement-mediated immunity (Mohan et al., 2014).

EF-Tu May Inhibit Neutrophil Opsonophagocytosis in Cerebrospinal Fluid

To further investigate the possible effects of EF-Tu on the host-pathogen interaction in PM, we tested for statistical correlations within with host proteins from the 130 unique PM protein dataset. EF-Tu did not positively correlate with any human CSF proteins, but did negatively correlate with levels of neutrophil defensin (r^2 −0.06, $p < 0.01$) (**Figure 4A**). Mean CSF levels of EF-Tu in non-survivors were 2.88 log2-fold higher [1.77×10^6 units/ml (Std 1.38×10^6)] compared to 1.64×10^5 units/ml CSF (Std 3.4×10^5) in survivors (ANOVA p −0.05 × 10^5. In contrast, CSF levels of neutrophil defensin in survivors was 5.76×10^7 (Std 5.61×10^7) compared to 2.4×10^7 (Std 4.2×10^7) in non-survivors (ANOVA p 0.008).

Addition of recombinant EF-Tu did not alter growth of Serotype 1 ST5316 in THY, pooled human serum or hCSF (five technical replicates, three experiments), suggesting no significant effects of EF-Tu on autolysis *in vitro* (Nagai et al.,

2018) (**Figure 4B**). Hence, we tested if EF-Tu had a negative effect on the interaction between *S. pneumoniae* and neutrophils in a human CSF model of neutrophil killing. When *S. pneumoniae* were opsonized with pooled human serum, addition of recombinant EF-Tu to the reaction mix did not impair neutrophil killing. However, when bacteria were opsonized with CSF, addition of EF-Tu caused a reduction in *S. pneumoniae* killing compared to PBS control and resulted in a similar effect to inhibition of phagocytosis by cytochalasin D (**Figure 4C**).

DISCUSSION

The pathogenesis of PM is dominated by a rapid and intense inflammatory response within the CSF compartment driven by an influx of neutrophils reacting to the presence of *S. pneumoniae*. Here, we show the highly inflammatory nature of the proteome in PM on admission to hospital, containing both brain- and blood-derived proteins, but the proteome does not differ between patients who survive and those who subsequently die. Over-expression of bacterial proteins in non-survivors may reflect adaptation of *S. pneumoniae* to the survival in the CSF compartment, that may have negative effects on the innate immune response in PM that requires further investigation.

Human and animal data have shown that the rapid neutrophil influx and the synthesis of antimicrobial peptides triggers the release of highly damaging proteins including tissue proteases (Tuomanen et al., 1985a; Tuomanen et al., 1985b) that in some patients are thought to result in BBB breakdown, cerebral thrombosis, and edema, thereby increasing mortality (Roine et al., 2015; Savonius et al., 2018). We have now replicated our earlier, smaller studies one in children and one in adults of the proteome during PM (Gomez-Baena et al., 2017)[30,31], using high-throughput quantitative proteomics (Bastos et al., 2017). This method enabled us to estimate abundance of individual proteins, thus determining the most abundant proteins in CSF during PM for the first time (Distler et al., 2016). By adjusting for abundance and using high sensitivity acquisition, we were able to detect all spectra present in CSF and confirm definitively that CSF proteins, whilst highly inflammatory, do not differ between survivors and non-survivors of PM.

Patients in our study were typical for PM patients in Africa, young adults and adolescents, the majority co-infected with HIV, with low CSF WCC and high CSF pneumococcal loads on admission to hospital (Tenforde et al., 2019). As we have previously reported (Wall et al., 2014), neither the bacterial load, CSF WCC and protein concentration, or the HIV status were associated with outcome in our patients. The CSF in patients with proven PM is highly inflammatory. We detected both expansion of the anti-infective components of CSF (immunoglobulins and complement) and high levels of expression of neutrophil-associated proteins including S100A8/9, cathepsin, neutrophil defensin, and matrix-metalloproteinases 9 (MMP9) that infection models have suggested are detrimental to the host (Tuomanen et al., 1989; Roine et al., 2014; Mohanty et al., 2019). Severe BBB breakdown has previously been assumed to be a pre-morbid event in PM (Barichello et al., 2011; Prager et al., 2017), and quantifying BBB breakdown in patients is complex (Helms et al., 2016; Prager et al., 2017; Natarajan et al., 2017). In this dataset, which is controlled for protein abundance, the presence of both brain-derived proteins (e.g. axonal proteins), combined with serum components like hemoglobin, haptoglobin, hemopexin, and fibrinogen, strongly suggest breakdown of the BBB is evident on admission to hospital with PM. We hypothesized that lower GCS on admission was related to worsening BBB breakdown and cerebral inflammation, but this was not supported by the CSF proteome. Our previous study on Malawian adults with PM using unadjusted 2D page proteomics suggested C3 and transferrin were reduced in non-survivor CSF (Goonetilleke et al., 2010; Goonetilleke et al., 2012), and data from The Netherlands also suggested that complement activity in CSF was associated with worse clinical outcomes (Mook-Kanamori et al., 2014; Kasanmoentalib et al., 2015; Kasanmoentalib et al., 2017; Kasanmoentalib et al., 2019). Whilst we demonstrated marked expansion of C3 and transferrin in CSF, after adjusting for overall protein abundance and composition these proteins did not correlate with outcome. These earlier reports were tested only for individual associations between proteins and outcome and were not adjusted for abundance, introducing potential confounding. We also tested if other human CSF proteins singly or in combination using Random Forest models predicted outcome but found no statistically significant association with mortality. The lack of any predictive protein signature suggests that measuring static inflammation through proteins does not reveal the complexity of the host-pathogen interactions associated with tissue damage. Clinical outcomes may instead be associated with dysfunctional processes such as ineffective opsonophagocytosis which are not readily identified by the abundance of specific proteins (Andre et al., 2017; Campos et al., 2017; Ullah et al., 2017; Wright et al., 2017; Lowe et al., 2018; Ritchie et al., 2018).

Compared to the abundance of host proteins, the number of pathogenic proteins identified in our study was relatively small; this probably reflects the relative abundance of bacteria and host cells within the infected CNS. The number and range of *S. pneumoniae* proteins identified in the CSF were similar to our earlier study, including PspA, abundant ribosomal proteins and EF-Tu (Gomez-Baena et al., 2017). These proteins differ from those identified in a CSF proteome study in a murine model of PM (Schmidt et al., 2019), in which high CSF levels of the competence regulator ComDE and the AliB oligopeptide transporter in murine meningitis were associated with leukocyte recruitment to the CSF compartment and disease severity (Schmidt et al., 2019). However, we did not detect either expression of ComDE or AliB in patient PM CSF, and we also did not detect other, previously reported virulence proteins in PM including pneumolysin (Wall et al., 2012; Wippel et al., 2013). The very limited number *S. pneumoniae* proteins detected in this study may be because the abundance of most *S. pneumoniae* proteins were below the limit of detection, proteomics is a relatively insensitive method of assessing bacterial activity during human PM.

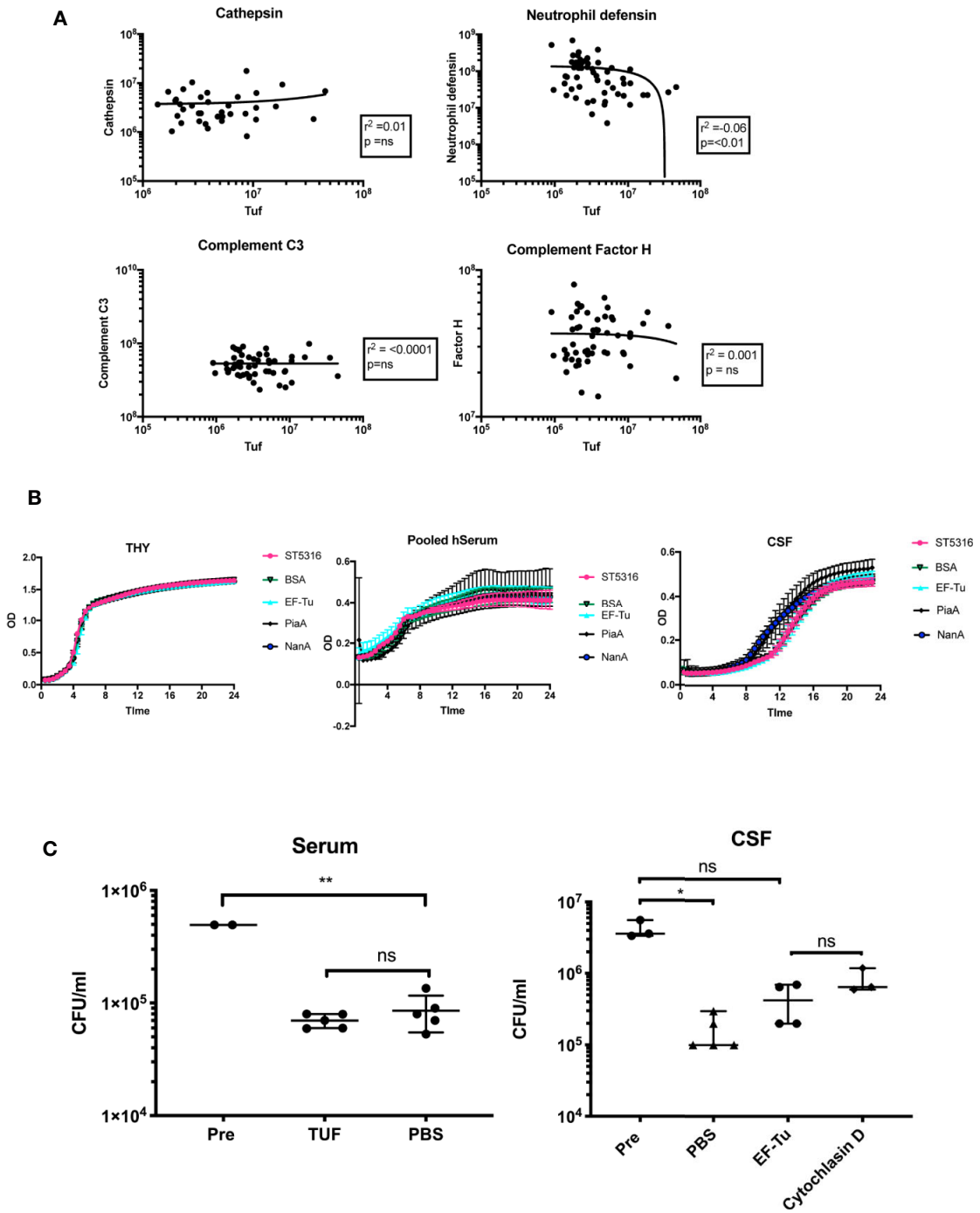

FIGURE 4 | EF-Tu negatively correlates with neutrophil defensin in CSF, and effects on neutrophil-mediated killing in CSF but not serum. **(A)** EF-TU negatively correlates with neutrophil defensin. Estimates of the abundance of Tuf (x axis, $\log_{10}$ scale) plotted against abundance of highly expressed proteins (y axis, $\log_{10}$ scale) known to interact with S. pneumoniae (complement C3, Factor H), and the most highly abundant neutrophil protein, Neutrophil defensin **(A)**. Correlation estimated with Spearman's test. **(B)** EF-Tu does not enhance ST5316 growth in CSF, serum or THY. Growth curves of S. pneumoniae serotype 1 strain ST5316 in Todd-Hewitt broth supplemented with 0.5% yeast extract (THY), pooled human serum and human CSF. Growth plotted over time (x axis) against optical density (y axis) at 620 nm. Growth in normal CSF compared to growth supplemented with 40 ug of recombinant EF-Tu. Additional proteins used as controls, bovine serum albumin (BSA), neuroaminidase A (NanA), and pneumococcal iron acquisition system A (PiaA). **(C)** EF-Tu effects on neutrophil mediated killing of *S. pneumoniae* in CSF but not serum. Viable S. pneumoniae strain ST5316 after 45 min neutrophil opsonophagocytosis assay, supplemented with 400 ug of recombinant Tuf protein. Bacteria opsonized with serum (left panel) and CSF (right panel). Viability measured by colony forming unit (CFU) counts on blood agar after 18 h incubation. Data expressed as medians with range. Statistical significance calculated using the Mann-Whitney U test.

Despite the lack of sensitivity of the *S. pneumoniae* CSF proteomics, we found that higher CSF levels of EF-Tu and the ribosomal protein Q8CWR9 were associated with mortality. The over-expression of these proteins in non-survivor CSF is an important finding, and suggests a pathological role during PM. Both proteins are important for *S. pneumoniae* replication, and perhaps therefore reflect rapid bacterial growth as a driver for poorer outcomes. EF-Tu is an essential, highly abundant, ubiquitous bacterial protein, found in diverse prokaryotic species including enterobacteriaceae, *Pseudomonas*, Staphylococci, and *Hemophilus* spp (Harvey et al., 2019). While the primary function of EF-Tu is transport of amino acylated tRNA components to the ribosome, this protein has also been shown to have a surprisingly varied range of moonlighting functions in different bacterial species, including some that affect virulence. EF-Tu can be anchored to the bacterial cell surface, adhere to extracellular components including complement factors (Mohan et al., 2014), chaperone bacterial virulence proteins to the cell surface in membrane vesicles (Olaya-Abril et al., 2014), promote adhesion and invasion of host cells, and alter bacterial shape *via* post-translational modification of bacterial proteins (Harvey et al., 2019). *S. pneumoniae* EF-Tu can bind complement factors H and related proteins Factor HL1 and CFHR1, and plasminogen, has effects on autolysis even provides potent antigen stimulation in an experimental pneumococcal vaccine (Mohan et al., 2014; Nagai et al., 2018; Thofte et al., 2018; Harvey et al., 2019; Nagai et al., 2019). We investigated whether EF-Tu levels in the CSF correlated with complement proteins, proteins associated with BBB breakdown or neutrophil proteins found in the human CSF proteome. Levels of EF-Tu did not correlate with either complement C3 or Factor H (Kasanmoentalib et al., 2019), but did negatively correlate with neutrophil defensin, suggesting a possible interaction with neutrophil opsonophagocytosis in CSF. No correlation was found with other neutrophil proteins in CSF including neutrophil elastase, collagenase, and lipocalin-1.

Neutrophil defensins are multi-functional immunomodulatory proteins with direct anti-microbial activity (Voglis et al., 2009). We tested the hypothesis that excessive EF-Tu effected on neutrophil killing in CSF, finding that EF-Tu promoted bacterial survival when opsonized with CSF but not with serum. The *Pseudomonas aeruginosa* EF-Tu promotes neutrophil apoptosis both *in vitro* and *in vivo* murine pneumonia models an effect that was thought to be mediated by oxygen sensing prolyl hydroxases recognition of EF-Tu (Dickinson et al., 2017). EF-Tu from *S. pneumoniae* may have a similar effect, leading to reduced neutrophil function, especially in the conditions found within CSF compared to serum. Alternatively, functions of EF-Tu may be more effectively attenuated in serum due to components not present in CSF. However, these hypotheses will need more detailed investigation to confirm the association of EF-Tu with mortality and the underlying mechanism(s) involved.

LIMITATIONS

Patients in our study were predominately HIV co-infected, and we were unable to discriminate which inflammatory CSF proteins were directly related to HIV infection rather than PM due to the small number of HIV-negative participants. Neither control CSF nor validated CSF proteomic libraries from healthy individuals living with HIV were available (Wall et al., 2017a). However, data from our center suggests no differences in the transcriptome of children with PM between HIV negative and children living with HIV (Kulohoma et al., 2017). We were unable to stratify HIV co-infected patients by CSF HIV viral load or CD4 count, but all were classified as WHO AIDS Stage 3 with advanced disease. We actively excluded patients with viral co-infection in CSF; infection with hepatitis viruses is common in our setting, and could also potentially through indirect effects on immune function increase the heterogeneity of our host CSF proteomic data. Although we detected an abundance of inflammatory proteins, including those known to be associated with poor outcomes in other studies of PM, we did not detect any cytokines and chemokines known to be present in CSF (Mai et al., 2009; Bociaga-Jasik et al., 2012; Coutinho et al., 2013; Grandgirard et al., 2013; Wall et al., 2014; Roine et al., 2015; Srinivasan et al., 2016). Cytokines and chemokines may be too rapidly degraded to be assessed using mass-spectrometry compared with more sensitive techniques such as ELISA (Kupcova Skalnikova et al., 2017). Visibly traumatic, blood stained CSF was rejected by the laboratory for analysis, however we cannot exclude microscopic blood contamination as a source of CSF hemoglobin/haptoglobin. After extraction of proteins for this study, insufficient CSF remained to validate our findings by measuring CSF levels of EF-Tu by an alternative method. Supporting the proteome data, our unpublished data on gene expression demonstrated high levels of expression of EF-Tu in both patient CSF and during *S. pneumoniae* culture in CSF *in vitro* (unpublished data). Finally, our data are from a single time point, and we cannot determine if dynamic changes in human or *S. pneumoniae* CSF protein predict outcome.

CONCLUSIONS

The CSF proteome in PM is highly inflammatory with evidence of BBB breakdown, but we did not find a human protein signature correlated with clinical outcome. However, higher levels of the *S. pneumoniae* ribosomal protein and EF-Tu were found in non-survivor CSF, and *in vitro* EF-Tu may inhibit neutrophil killing of *S. pneumoniae* in CSF. To better understand the causes of mortality in PM, the role of EF-Tu requires further investigation, using models that accurately reflect conditions in during acute disease.

DATA AVAILABILITY STATEMENT

The proteomics data presented in this article is publicly available at the PRIDE repository under the accession number PXD021268.

AUTHOR CONTRIBUTIONS

EW, GL, PB, VT, RB, AC, SG, RH, and JB conceived and designed the work. EW, GL, VT, MN, VM, TA, ER-S, and BD collected the data. EW, PB, BW, JB, RH, and VT analyzed and

interpreted the data. EW drafted the article. EW, PB, GL, VT, VM, BD, MN, TA, ER-S, EC, AC, SG, DL, BW, RB, RH, and JB critically revised the article. EW, PB, GL, VT, VM, BD, MN, TA, ER-S, EC, AC, BG, DL, BW, RB, RH, and JB approved the final version to be published. All authors contributed to the article and approved the submitted version.

FUNDING

This study was funded by a Clinical Lecturer Starter Grant from the Academy of Medical Sciences (UK), a UCL-Institutional Strategic Support Fund award to EW from both the Wellcome Trust and the Robin Weiss Foundation and by a PhD Fellowship in Global Health to EW from the Wellcome Trust (089671/B/09/Z). The Malawi-Liverpool-Wellcome Trust Clinical Research Programme is supported by a core grant from the Wellcome Trust (101113/Z/13/Z). The laboratory work was undertaken at LSTM and UCL Respiratory, which received a proportion of funding from the National Institute for Health Research University College London Hospitals Department of Health's NIHR Biomedical Research Centre. JB is supported by the Centre's funding scheme. The funders of the study had no role in study design, data collection, data analysis, data interpretation, or writing of the report. The corresponding author had full access to all the data and the final responsibility to submit for publication. JB, VT and BW acknowledge funding from Medical Research Council (MR/R00/1871/1).

ACKNOWLEDGMENTS

The authors would like to thank the patients and guardians who contributed samples and clinical data to the study through the Bundles for Adult Meningitis (BAM) trial, the BAM study team led by VM, the nurses and clinical staff of the AETC at Queen Elizabeth Central Hospital in Blantyre, and the laboratory and research support staff at the Malawi-Liverpool-Wellcome Trust Clinical Research Programme in Blantyre, Malawi. We also extend our gratitude to Professor Diederik van de Beek and colleagues at the Amsterdam Medical Centre in the Netherlands for the use of normal human CSF, and to Professor Sven Hammerschmidt of the University of Ernst Moritz Arndt University, Greifswald, Germany, for the *Escherichia coli* strain containing EF-Tu plasmid used in this study.

SUPPLEMENTARY MATERIAL

The Supplementary Material for this article can be found online at: https://www.frontiersin.org/articles/10.3389/fcimb.2020.603623/full#supplementary-material

SUPPLEMENTARY FIGURE 1 | Confirmation of expression of recombinant pQE30 EF-Tu from *E. coli* 2 and 24 h after protein induction. **(A)** Image of a Ponceau Western membrane showing the presence of pQE30_EF-Tu. *E. coli* containing an pQE30 tagged EF_Tu plasmid. **(B)** Image of a Coomassie stained Western membrane showing the same. Data show experiments in parallel from induced, and non-induced controls. From left to right Ladder, with 55 and 35 KD points indicated respectively. Lane 1 Non-induced isolates, prior to induction. Lane 2 Induced isolates, prior to induction. Lane 3 non-induced isolates, 2 h post induction, Lane 4 induced isolates, 2 h post induction. Lane 5 non-induced isolates, 24 h post induction, Lane 6 induced isolates, 24 h after induction shows the presence of a large 50 kD protein with the pQE30 tag.

SUPPLEMENTARY FIGURE 2 | Individual proteins are more highly expressed in non-survivor CSF. Distribution (estimates of abundance, y-axis, arbitrary units) of proteins individually more abundant ($p < 0.05$) in non-survivors (purple) compared to survivors (blue), that do not reach significance at the FDR level. Each bar represents an individual patient. Colors represent individual proteins statistically over-expressed in non-survivors. Protein identifiers available in the **supplementary appendix**.

REFERENCES

Ajdukiewicz, K. M., Cartwright, K. E., Scarborough, M., Mwambene, J. B., Goodson, P., Molyneux, M. E., et al. (2011). Glycerol adjuvant therapy in adults with bacterial meningitis in a high HIV seroprevalence setting in Malawi: a double-blind, randomised controlled trial. *Lancet Infect. Dis.* 11 (4), 293–300. doi: 10.1016/S1473-3099(10)70317-0

Andre, G. O., Converso, T. R., Politano, W. R., Ferraz, L. F., Ribeiro, M. L., Leite, L. C., et al. (2017). Role of Streptococcus pneumoniae Proteins in Evasion of Complement-Mediated Immunity. *Front. Microbiol.* 8, 224. doi: 10.3389/fmicb.2017.00224

Barichello, T., Lemos, J. C., Generoso, J. S., Cipriano, A. L., Milioli, G. L., Marcelino, D. M., et al. (2011). Oxidative stress, cytokine/chemokine and disruption of blood-brain barrier in neonate rats after meningitis by Streptococcus agalactiae. *Neurochem. Res.* 36 (10), 1922–1930. doi: 10.1007/s11064-011-0514-2

Bastos, P., Ferreira, R., Manadas, B., Moreira, P. I., and Vitorino, R. (2017). Insights into the human brain proteome: Disclosing the biological meaning of protein networks in cerebrospinal fluid. *Crit. Rev. Clin. Lab. Sci.* 54 (3), 185–204. doi: 10.1080/10408363.2017.1299682

Bewley, M. A., Marriott, H. M., Tulone, C., Francis, S. E., Mitchell, T. J., Read, R. C., et al. (2011). A cardinal role for cathepsin d in co-ordinating the host-mediated apoptosis of macrophages and killing of pneumococci. *PloS Pathog.* 7 (1), e1001262. doi: 10.1371/journal.ppat.1001262

Bociaga-Jasik, M., Garlicki, A., Ciesla, A., Kalinowska-Nowak, A., Sobczyk-Krupiarz, I., and Mach, T. (2012). The diagnostic value of cytokine and nitric oxide concentrations in cerebrospinal fluid for the differential diagnosis of meningitis. *Adv. Med. Sci.* 57 (1), 142–147. doi: 10.2478/v10039-012-0013-y

Britz, E., Perovic, O., von Mollendorf, C., von Gottberg, A., Iyaloo, S., Quan, V., et al. (2016). The Epidemiology of Meningitis among Adults in a South African Province with a High HIV Prevalence, 2009-2012. *PloS One* 11 (9), e0163036. doi: 10.1371/journal.pone.0163036

Campos, I. B., Herd, M., Moffitt, K. L., Lu, Y. J., Darrieux, M., Malley, R., et al. (2017). IL-17A and complement contribute to killing of pneumococci following immunization with a pneumococcal whole cell vaccine. *Vaccine* 35 (9), 1306–1315. doi: 10.1016/j.vaccine.2017.01.030

Collaborators GBDM (2018). Global, regional, and national burden of meningitis, 1990-2016: a systematic analysis for the Global Burden of Disease Study 2016. *Lancet Neurol.* 17 (12), 1061–1082. doi: 10.1016/S1474-4422(18)30499-X

Costerus, J. M., Brouwer, M. C., van der Ende, A., and van de Beek, D. (2016). Repeat lumbar puncture in adults with bacterial meningitis. *Clin. Microbiol. Infect.: Off. Publ. Eur. Soc. Clin. Microbiol. Infect. Dis.* 22 (5), 428–433. doi: 10.1016/j.cmi.2015.12.026

Coutinho, L. G., Grandgirard, D., Leib, S. L., and Agnez-Lima, L. F. (2013). Cerebrospinal-fluid cytokine and chemokine profile in patients with pneumococcal and meningococcal meningitis. *BMC Infect. Dis.* 13 (1), 326. doi: 10.1186/1471-2334-13-326

de Oliveira, S., Rosowski, E. E., and Huttenlocher, A. (2016). Neutrophil migration in infection and wound repair: going forward in reverse. *Nat. Rev. Immunol.* 16 (6), 378–391. doi: 10.1038/nri.2016.49

Dickinson, R. S., Murphy, F., Doherty, C., Williams, S., Mirchandani, A., Willson, J., et al. (2017). Pseudomonas expression of an oxygen sensing prolyl hydroxylase homologue regulates neutrophil host responses *in vitro* and *in vivo*. *Wellcome Open Res.* 2, 104. doi: 10.12688/wellcomeopenres.12871.1

Distler, U., Kuharev, J., Navarro, P., and Tenzer, S. (2016). Label-free quantification in ion mobility-enhanced data-independent acquisition proteomics. *Nat. Protoc.* 11 (4), 795–812. doi: 10.1038/nprot.2016.042

Domon, H., Nagai, K., Maekawa, T., Oda, M., Yonezawa, D., Takeda, W., et al. (2018). Neutrophil Elastase Subverts the Immune Response by Cleaving Toll-Like Receptors and Cytokines in Pneumococcal Pneumonia. *Front. Immunol.* 9, 732. doi: 10.3389/fimmu.2018.00732

Doran, K. S., Fulde, M., Gratz, N., Kim, B. J., Nau, R., Prasadarao, N., et al. (2016). Host-pathogen interactions in bacterial meningitis. *Acta Neuropathol.* 131 (2), 185–209. doi: 10.1007/s00401-015-1531-z

Gessner, B. D., Mueller, J. E., and Yaro, S. (2010). African meningitis belt pneumococcal disease epidemiology indicates a need for an effective serotype 1 containing vaccine, including for older children and adults. *BMC Infect. Dis.* 10, 22. doi: 10.1186/1471-2334-10-22

Gomez-Baena, G., Bennett, R. J., Martinez-Rodriguez, C., Wnek, M., Laing, G., Hickey, G., et al. (2017). Quantitative Proteomics of Cerebrospinal Fluid in Paediatric Pneumococcal Meningitis. *Sci. Rep.* 7 (1), 7042. doi: 10.1038/s41598-017-07127-6

Goonetilleke, U. R., Scarborough, M., Ward, S. A., and Gordon, S. B. (2010). Proteomic analysis of cerebrospinal fluid in pneumococcal meningitis reveals potential biomarkers associated with survival. *J. Infect. Dis.* 202 (4), 542–550. doi: 10.1086/654819

Goonetilleke, U. R., Scarborough, M., Ward, S. A., Hussain, S., Kadioglu, A., and Gordon, S. B. (2012). Death is associated with complement C3 depletion in cerebrospinal fluid of patients with pneumococcal meningitis. *mBio* 3 (2), 1–7. doi: 10.1128/mBio.00272-11

Grandgirard, D., Gaumann, R., Coulibaly, B., Dangy, J. P., Sie, A., Junghanss, T., et al. (2013). The causative pathogen determines the inflammatory profile in cerebrospinal fluid and outcome in patients with bacterial meningitis. *Mediators Inflammation* 2013, 312476. doi: 10.1155/2013/312476

Guldbrandsen, A., Vethe, H., Farag, Y., Oveland, E., Garberg, H., Berle, M., et al. (2014). In-depth characterization of the cerebrospinal fluid (CSF) proteome displayed through the CSF proteome resource (CSF-PR). *Mol. Cell. Proteomics: MCP* 13 (11), 3152–3163. doi: 10.1074/mcp.M114.038554

Harvey, K. L., Jarocki, V. M., Charles, I. G., and Djordjevic, S. P. (2019). The Diverse Functional Roles of Elongation Factor Tu (EF-Tu) in Microbial Pathogenesis. *Front. Microbiol.* 10, 2351. doi: 10.3389/fmicb.2019.02351

Heinsbroek, E., Tafatatha, T., Phiri, A., Ngwira, B., Crampin, A. C., Read, J. M., et al. (2015). Persisting high prevalence of pneumococcal carriage among HIV-infected adults receiving antiretroviral therapy in Malawi: a cohort study. *AIDS* 29 (14), 1837–1844. doi: 10.1097/QAD.0000000000000755

Helms, H. C., Abbott, N. J., Burek, M., Cecchelli, R., Couraud, P. O., Deli, M. A., et al. (2016). In vitro models of the blood-brain barrier: An overview of commonly used brain endothelial cell culture models and guidelines for their use. *J. Cereb. Blood Flow Metab.: Off. J. Int. Soc. Cereb. Blood Flow Metab.* 36 (5), 862–890. doi: 10.1177/0271678X16630991

Hyams, C., Yuste, J., Bax, K., Camberlein, E., Weiser, J. N., and Brown, J. S. (2010). Streptococcus pneumoniae resistance to complement-mediated immunity is dependent on the capsular serotype. *Infect. Immun.* 78 (2), 716–725. doi: 10.1128/IAI.01056-09

Kasanmoentalib, E. S., Valls Seron, M., Morgan, B. P., Brouwer, M. C., and van de Beek, D. (2015). Adjuvant treatment with dexamethasone plus anti-C5 antibodies improves outcome of experimental pneumococcal meningitis: a randomized controlled trial. *J. Neuroinflamm.* 12, 149. doi: 10.1186/s12974-015-0372-y

Kasanmoentalib, E. S., Valls Seron, M., Ferwerda, B., Tanck, M. W., Zwinderman, A. H., Baas, F., et al. (2017). Mannose-binding lectin-associated serine protease 2 (MASP-2) contributes to poor disease outcome in humans and mice with pneumococcal meningitis. *J. Neuroinflamm.* 14 (1), 2. doi: 10.1186/s12974-016-0770-9

Kasanmoentalib, E. S., Valls Seron, M., Engelen-Lee, J. Y., Tanck, M. W., Pouw, R. B., van Mierlo, G., et al. (2019). Complement factor H contributes to mortality in humans and mice with bacterial meningitis. *J. Neuroinflamm.* 16 (1), 279. doi: 10.1186/s12974-019-1675-1

Koedel, U., Frankenberg, T., Kirschnek, S., Obermaier, B., Hacker, H., Paul, R., et al. (2009). Apoptosis is essential for neutrophil functional shutdown and determines tissue damage in experimental pneumococcal meningitis. *PloS Pathog.* 5 (5), e1000461. doi: 10.1371/journal.ppat.1000461

Kulohoma, B. W., Marriage, F., Vasieva, O., Mankhambo, L., Nguyen, K., Molyneux, M. E., et al. (2017). Peripheral blood RNA gene expression in children with pneumococcal meningitis: a prospective case-control study. *BMJ Paediatr. Open* 1 (1), e000092. doi: 10.1136/bmjpo-2017-000092

Kupcova Skalnikova, H., Cizkova, J., Cervenka, J., and Vodicka, P. (2017). Advances in Proteomic Techniques for Cytokine Analysis: Focus on Melanoma Research. *Int. J. Mol. Sci.* 18 (12), 2–32. doi: 10.3390/ijms18122697

Lowe, D. M., Demaret, J., Bangani, N., Nakiwala, J. K., Goliath, R., Wilkinson, K. A., et al. (2018). Differential Effect of Viable Versus Necrotic Neutrophils on Mycobacterium tuberculosis Growth and Cytokine Induction in Whole Blood. *Front. Immunol.* 9, 903. doi: 10.3389/fimmu.2018.00903

Mai, N. T., Tuan, T. V., Wolbers, M., Hoang, D. M., Nga, T. V., Chau, T. T., et al. (2009). Immunological and biochemical correlates of adjunctive dexamethasone in Vietnamese adults with bacterial meningitis. *Clin. Infect. Diseases: an Off. Publ. Infect. Dis. Soc. America* 49 (9), 1387–1392. doi: 10.1086/630207

Matthias, K. A., Roche, A. M., Standish, A. J., Shchepetov, M., and Weiser, J. N. (2008). Neutrophil-toxin interactions promote antigen delivery and mucosal clearance of Streptococcus pneumoniae. *J. Immunol.* 180 (9), 6246–6254. doi: 10.4049/jimmunol.180.9.6246

Mohan, S., Hertweck, C., Dudda, A., Hammerschmidt, S., Skerka, C., Hallstrom, T., et al. (2014). Tuf of Streptococcus pneumoniae is a surface displayed human complement regulator binding protein. *Mol. Immunol.* 62 (1), 249–264. doi: 10.1016/j.molimm.2014.06.029

Mohanty, T., Fisher, J., Bakochi, A., Neumann, A., Cardoso, J. F. P., Karlsson, C. A. Q., et al. (2019). Neutrophil extracellular traps in the central nervous system hinder bacterial clearance during pneumococcal meningitis. *Nat. Commun.* 10 (1), 1667. doi: 10.1038/s41467-019-09040-0

Mook-Kanamori, B. B., Geldhoff, M., van der Poll, T., and van de Beek, D. (2011). Pathogenesis and pathophysiology of pneumococcal meningitis. *Clin. Microbiol. Rev.* 24 (3), 557–591. doi: 10.1128/CMR.00008-11

Mook-Kanamori, B. B., Brouwer, M. C., Geldhoff, M., Ende, A., and van de Beek, D. (2014). Cerebrospinal fluid complement activation in patients with pneumococcal and meningococcal meningitis. *J. Infect.* 68 (6), 542–547. doi: 10.1016/j.jinf.2013.12.016

Mourvillier, B., Tubach, F., van de Beek, D., Garot, D., Pichon, N., Georges, H., et al. (2013). Induced hypothermia in severe bacterial meningitis: a randomized clinical trial. *JAMA: J. Am. Med. Assoc.* 310 (20), 2174–2183. doi: 10.1001/jama.2013.280506

Nagai, K., Domon, H., Maekawa, T., Oda, M., Hiyoshi, T., Tamura, H., et al. (2018). Pneumococcal DNA-binding proteins released through autolysis induce the production of proinflammatory cytokines *via* toll-like receptor 4. *Cell. Immunol.* 325, 14–22. doi: 10.1016/j.cellimm.2018.01.006

Nagai, K., Domon, H., Maekawa, T., Hiyoshi, T., Tamura, H., Yonezawa, D., et al. (2019). Immunization with pneumococcal elongation factor Tu enhances serotype-independent protection against Streptococcus pneumoniae infection. *Vaccine* 37 (1), 160–168. doi: 10.1016/j.vaccine.2018.11.015

Natarajan, R., Northrop, N., and Yamamoto, B. (2017). Fluorescein Isothiocyanate (FITC)-Dextran Extravasation as a Measure of Blood-Brain Barrier Permeability. *Curr. Protoc. Neurosci.* 79, 9 58 1–9 9 15. doi: 10.1002/cpns.25

Olaya-Abril, A., Prados-Rosales, R., McConnell, M. J., Martin-Pena, R., Gonzalez-Reyes, J. A., Jimenez-Munguia, I., et al. (2014). Characterization of protective extracellular membrane-derived vesicles produced by Streptococcus pneumoniae. *J. Proteomics* 106, 46–60. doi: 10.1016/j.jprot.2014.04.023

Organisation) WWH. Defeating meningitis by 2030 WHO2019. https://www.who.int/emergencies/diseases/meningitis/en/.

Potter, N. S., and Harding, C. V. (2001). Neutrophils process exogenous bacteria *via an* alternate class I MHC processing pathway for presentation of peptides to T lymphocytes. *J. Immunol.* 167 (5), 2538–2546. doi: 10.4049/jimmunol.167.5.2538

Prager, O., Friedman, A., and Nebenzahl, Y. M. (2017). Role of neural barriers in the pathogenesis and outcome of Streptococcus pneumoniae meningitis. *Exp. Ther. Med.* 13 (3), 799–809. doi: 10.3892/etm.2017.4082

Ramos-Sevillano, E., Rodriguez-Sosa, C., Diez-Martinez, R., Gimenez, M. J., Olmedillas, E., Garcia, P., et al. (2012). Macrolides and beta-lactam antibiotics enhance C3b deposition on the surface of multidrug-resistant Streptococcus pneumoniae strains by a LytA autolysin-dependent mechanism. *Antimicrob. Agents Chemother.* 56 (11), 5534–5540. doi: 10.1128/AAC.01470-12

Ramos-Sevillano, E., Urzainqui, A., de Andres, B., Gonzalez-Tajuelo, R., Domenech, M., Gonzalez-Camacho, F., et al. (2016). PSGL-1 on Leukocytes is a Critical Component of the Host Immune Response against Invasive Pneumococcal Disease. *PloS Pathog.* 12 (3), e1005500. doi: 10.1371/journal.ppat.1005500

Ritchie, N. D., Ritchie, R., Bayes, H. K., Mitchell, T. J., and Evans, T. J. (2018). IL-17 can be protective or deleterious in murine pneumococcal pneumonia. *PloS Pathog.* 14 (5), e1007099. doi: 10.1371/journal.ppat.1007099

Roine, I., Pelkonen, T., Bernardino, L., Lauhio, A., Tervahartiala, T., Lappalainen, M., et al. (2014). Predictive value of cerebrospinal fluid matrix metalloproteinase-9 and tissue inhibitor of metalloproteinase-1 concentrations in childhood bacterial meningitis. *Pediatr. Infect. Dis. J.* 33 (7), 675–679. doi: 10.1097/INF.0000000000000249

Roine, I., Pelkonen, T., Lauhio, A., Lappalainen, M., Cruzeiro, M. L., Bernardino, L., et al. (2015). Changes in MMP-9 and TIMP-1 Concentrations in Cerebrospinal Fluid after 1 Week of Treatment of Childhood Bacterial Meningitis. *J. Clin. Microbiol.* 53 (7), 2340–2342. doi: 10.1128/JCM.00714-15

Savonius, O., Helve, O., Roine, I., Andersson, S., Saukkoriipi, A., Gonzalez Mata, A., et al. (2018). Cerebrospinal Fluid Cathelicidin Correlates With the Bacterial Load and Outcomes in Childhood Bacterial Meningitis. *Pediatr. Infect. Dis. J.* 37 (2), 182–185. doi: 10.1097/INF.0000000000001744

Scarborough, M., Gordon, S. B., Whitty, C. J., French, N., Njalale, Y., Chitani, A., et al. (2007). Corticosteroids for bacterial meningitis in adults in sub-Saharan Africa. *New Engl. J. Med.* 357 (24), 2441–2450. doi: 10.1056/NEJMoa065711

Schmidt, F., Kakar, N., Meyer, T. C., Depke, M., Masouris, I., Burchhardt, G., et al. (2019). In vivo proteomics identifies the competence regulon and AliB oligopeptide transporter as pathogenic factors in pneumococcal meningitis. *PloS Pathog.* 15 (7), e1007987. doi: 10.1371/journal.ppat.1007987

Srinivasan, L., Kilpatrick, L., Shah, S. S., Abbasi, S., and Harris, M. C. (2016). Cerebrospinal fluid cytokines in the diagnosis of bacterial meningitis in infants. *Pediatr. Res.* 80 (4), 566–572. doi: 10.1038/pr.2016.117

Swarthout, T. D., Fronterre, C., Lourenco, J., Obolski, U., Gori, A., Bar-Zeev, N., et al. (2020). High residual carriage of vaccine-serotype Streptococcus pneumoniae after introduction of pneumococcal conjugate vaccine in Malawi. *Nat. Commun.* 11 (1), 2222. doi: 10.1038/s41467-020-15786-9

Tenforde, M. W., Mokomane, M., Leeme, T. B., Tlhako, N., Tsholo, K., Chebani, T., et al. (2019). Mortality in adult patients with culture-positive and culture-negative meningitis in the Botswana national meningitis survey: a prevalent cohort study. *Lancet Infect. Dis.* 19 (7), 740–749. doi: 10.1016/S1473-3099(19)30066-0

Terra, V. S., Plumptre, C. D., Wall, E. C., Brown, J. S., and Wren, B. W. (2020). Construction of a pneumolysin deficient mutant in streptococcus pneumoniae serotype 1 strain 519/43 and phenotypic characterisation. *Microb. Pathog.* 141, 103999. doi: 10.1016/j.micpath.2020.103999

Thofte, O., Su, Y. C., Brant, M., Littorin, N., Duell, B. L., Alvarado, V., et al. (2018). EF-Tu From Non-typeable Haemophilus influenzae Is an Immunogenic Surface-Exposed Protein Targeted by Bactericidal Antibodies. *Front. Immunol.* 9, 2910. doi: 10.3389/fimmu.2018.02910

Tuomanen, E., Liu, H., Hengstler, B., Zak, O., and Tomasz, A. (1985a). The induction of meningeal inflammation by components of the pneumococcal cell wall. *J. Infect. Dis.* 151 (5), 859–868. doi: 10.1093/infdis/151.5.859

Tuomanen, E., Tomasz, A., Hengstler, B., and Zak, O. (1985b). The relative role of bacterial cell wall and capsule in the induction of inflammation in pneumococcal meningitis. *J. Infect. Dis.* 151 (3), 535–540. doi: 10.1093/infdis/151.3.535

Tuomanen, E. I., Saukkonen, K., Sande, S., Cioffe, C., and Wright, S. D. (1989). Reduction of inflammation, tissue damage, and mortality in bacterial meningitis in rabbits treated with monoclonal antibodies against adhesion-promoting receptors of leukocytes. *J. Exp. Med.* 170 (3), 959–969. doi: 10.1084/jem.170.3.959

Ullah, I., Ritchie, N. D., and Evans, T. J. (2017). The interrelationship between phagocytosis, autophagy and formation of neutrophil extracellular traps following infection of human neutrophils by Streptococcus pneumoniae. *Innate Immun.* 23 (5), 413–423. doi: 10.1177/1753425917704299

van de Beek, D., Farrar, J. J., de Gans, J., Mai, N. T., Molyneux, E. M., Peltola, H., et al. (2010). Adjunctive dexamethasone in bacterial meningitis: a meta-analysis of individual patient data. *Lancet Neurol.* 9 (3), 254–263. doi: 10.1016/S1474-4422(10)70023-5

Voglis, S., Quinn, K., Tullis, E., Liu, M., Henriques, M., Zubrinich, C., et al. (2009). Human neutrophil peptides and phagocytic deficiency in bronchiectatic lungs. *Am. J. Respir. Crit. Care Med.* 180 (2), 159–166. doi: 10.1164/rccm.200808-1250OC

Wall, E. C., Gordon, S. B., Hussain, S., Goonetilleke, U. R., Gritzfeld, J., Scarborough, M., et al. (2012). Persistence of pneumolysin in the cerebrospinal fluid of patients with pneumococcal meningitis is associated with mortality. *Clin. Infect. Diseases: an Off. Publ. Infect. Dis. Soc. America* 54 (5), 701–705. doi: 10.1093/cid/cir926

Wall, E. C., Gritzfeld, J. F., Scarborough, M., Ajdukiewicz, K. M., Mukaka, M., Corless, C., et al. (2014). Genomic pneumococcal load and CSF cytokines are not related to outcome in Malawian adults with meningitis. *J. Infect.* 69 (5), 440–446. doi: 10.1016/j.jinf.2014.06.011

Wall, E. C., Mukaka, M., Denis, B., Mlozowa, V. S., Msukwa, M., Kasambala, K., et al. (2017a). Goal directed therapy for suspected acute bacterial meningitis in adults and adolescents in sub-Saharan Africa. *PloS One* 12 (10), e0186687. doi: 10.1371/journal.pone.0186687

Wall, E. C., Mukaka, M., Scarborough, M., Ajdukiewicz, K. M. A., Cartwright, K. E., Nyirenda, M., et al. (2017b). Prediction of Outcome From Adult Bacterial Meningitis in a High-HIV-Seroprevalence, Resource-Poor Setting Using the Malawi Adult Meningitis Score (MAMS). *Clin. Infect. Diseases: an Off. Publ. Infect. Dis. Soc. America* 64 (4), 413–419. doi: 10.1093/cid/ciw779

Wang, S., Peng, L., Gai, Z., Zhang, L., Jong, A., Cao, H., et al. (2016). Pathogenic Triad in Bacterial Meningitis: Pathogen Invasion, NF-kappaB Activation, and Leukocyte Transmigration that Occur at the Blood-Brain Barrier. *Front. Microbiol.* 7, 148. doi: 10.3389/fmicb.2016.00148

Weisfelt, M., van de Beek, D., Spanjaard, L., Reitsma, J. B., and de Gans, J. (2008). A risk score for unfavorable outcome in adults with bacterial meningitis. *Ann. Neurol.* 63 (1), 90–97. doi: 10.1002/ana.21216

Wippel, C., Maurer, J., Fortsch, C., Hupp, S., Bohl, A., Ma, J., et al. (2013). Bacterial Cytolysin during Meningitis Disrupts the Regulation of Glutamate in the Brain, Leading to Synaptic Damage. *PloS Pathog.* 9 (6), e1003380. doi: 10.1371/journal.ppat.1003380

Wright, H. L., Makki, F. A., Moots, R. J., and Edwards, S. W. (2017). Low-density granulocytes: functionally distinct, immature neutrophils in rheumatoid arthritis with altered properties and defective TNF signalling. *J. Leukocyte Biol.* 101 (2), 599–611. doi: 10.1189/jlb.5A0116-022R

Zhang, Y., Guo, Z., Zou, L., Yang, Y., Zhang, L., Ji, N., et al. (2015). Data for a comprehensive map and functional annotation of the human cerebrospinal fluid proteome. *Data Brief* 3, 103–107. doi: 10.1016/j.dib.2015.02.004

Conflict of Interest: The authors declare that the research was conducted in the absence of any commercial or financial relationships that could be construed as a potential conflict of interest.

frontiers in Cellular and Infection Microbiology

ORIGINAL RESEARCH
published: 02 February 2021
doi: 10.3389/fcimb.2020.606743

Repurposing the Antiemetic Metoclopramide as an Antiviral Against Dengue Virus Infection in Neuronal Cells

Ting-Jing Shen[1,2], *Vu Thi Hanh*[2,3,4], *Thai Quoc Nguyen*[2,3,5], *Ming-Kai Jhan*[1,2], *Min-Ru Ho*[1,2] *and Chiou-Feng Lin*[1,2,6*]

[1] Graduate Institute of Medical Sciences, College of Medicine, Taipei Medical University, Taipei, Taiwan, [2] Department of Microbiology and Immunology, School of Medicine, College of Medicine, Taipei Medical University, Taipei, Taiwan, [3] International Ph.D. Program in Medicine, College of Medicine, Taipei Medical University, Taipei, Taiwan, [4] Centre for Hematology and Blood Transfusion, Bach Mai Hospital, Hanoi, Vietnam, [5] Centre for Tropical Diseases, Bach Mai Hospital, Hanoi, Vietnam, [6] Center of Infectious Diseases and Signaling Research, National Cheng Kung University, Tainan, Taiwan

OPEN ACCESS

Edited by:
Tatiana Barichello,
University of Texas Health Science Center at Houston, United States

Reviewed by:
Jaqueline Generoso,
Universidade do Extremo Sul Catarinense, Brazil
Allan Collodel,
Universidade do Extremo Sul Catarinense—UNESC, Brazil

***Correspondence:**
Chiou-Feng Lin
cflin2014@tmu.edu.tw

Specialty section:
This article was submitted to Virus and Host, a section of the journal Frontiers in Cellular and Infection Microbiology

Received: 15 September 2020
Accepted: 10 December 2020
Published: 02 February 2021

Citation:
Shen T-J, Hanh VT, Nguyen TQ, Jhan M-K, Ho M-R and Lin C-F (2021) Repurposing the Antiemetic Metoclopramide as an Antiviral Against Dengue Virus Infection in Neuronal Cells. Front. Cell. Infect. Microbiol. 10:606743. doi: 10.3389/fcimb.2020.606743

Dengue virus (DENV) is transmitted by Aedes mosquitoes to humans and is a threat worldwide. No effective new drugs have been used for anti-dengue treatment, and repurposing drugs is an alternative approach to treat this condition. Dopamine 2 receptor (D2R) is a host receptor positively associated with DENV infection. Metoclopramide (MCP), a D2R antagonist clinically used to control vomiting and nausea in patients with DENV infection, was putatively examined for inhibition of DENV infection by targeting D2R. In the mouse neural cell line Neuro-2a with D2R expression, a plaque assay demonstrated the antiviral efficacy of MCP treatment. However, in the cell line BHK-21, which did not express D2R, MCP treatment caused no further inhibition of DENV infection. Either MCP treatment or exogenous administration of a neutralizing D2R antibody blocked DENV binding. Treatment with MCP also reduced DENV dsRNA replication and DENV-induced neuronal cell cytotoxicity *in vitro*. An *in vivo* study demonstrated the antiviral effect of MCP against DENV-induced CNS neuropathy and mortality. These results showed that repurposing the D2R-targeting antiemetic MCP is a potential therapeutic strategy against DENV infection.

Keywords: dengue virus, antiemetics, metoclopramide, antiviral, dopamine receptor

INTRODUCTION

Aedes mosquitoes transmit four serotypes of dengue virus (DENV), namely, DENV1, DENV2, DENV3, and DENV4, to cause arthropod-borne viral diseases (Guzman et al., 2016; Ferguson, 2018) in tropical and subtropical countries. An estimated 390 million people are at risk of DENV infection annually (Guzman et al., 2010; Ferguson, 2018). Following receptor binding, the interaction with the viral envelope (E) protein allows the internalization of virus particles *via*

clathrin-dependent and clathrin-independent endocytosis (Acosta et al., 2008; van der Schaar et al., 2008). Within the virus-containing endosomes, the pH value decreases to induce a shape change in the E protein of the virus, leading to fusion with the endosomal membrane. As a result, the viral single-strand positive-sense RNA enters the cytoplasm to induce viral protein translation as well as dsRNA replication (Zaitseva et al., 2010). Then, the virions are transported through the trans-Golgi network and secreted (Yu et al., 2008; Welsch et al., 2009) to generate the next infectious cycle. Targeting the DENV infectious process is speculated to be therapeutic against viral infection.

The symptoms of mild dengue fever include fever, rash, headache, and joint pain (Hadinegoro, 2012). However, other symptoms occurring in dengue fever, such as plasma leakage and abnormal hemostasis, may cause severe disease. In addition to dengue hemorrhagic fever (DHF) and dengue shock syndrome (DSS) (Leong et al., 2007), encephalitis and encephalopathy have been observed in severe dengue disease in clinical studies, which suggests that DENV indirectly affects the CNS to cause encephalopathy in DENV infection (Solomon et al., 2000). DENV can be identified in the cerebrospinal fluid and the brain tissue of encephalitis patients (Verma et al., 2014). It has been suggested that DENV can enter neuronal systems through membrane receptors and contribute to neurological manifestations, including encephalitis, encephalopathy, and dengue-associated neuromuscular complications (Calderon-Pelaez et al., 2019). Appropriate medical interventions are needed to prevent neurological complications and death.

Dopamine receptors, a class of G protein-coupled receptors that are highly expressed in the vertebrate central nervous system (CNS), mediate multiple functions in motivation, pleasure, cognition, memory, learning, and fine motor control (Ito et al., 1999). Additionally, dopamine 2 receptor (D2R) contributes to virus infection, including human immunodeficiency virus infection (Gaskill et al., 2014) as well as Japanese encephalitis virus infection (Simanjuntak et al., 2017), by promoting viral entry into cells at the early stage. Prochlorperazine (PCZ), a D2R antagonist, shows antiviral activity against DENV infection (Simanjuntak et al., 2014). Additionally, targeting D2R by another compound, chlorpromazine (CPZ), blocks DENV infection *in vitro* and *in vivo* (Ho et al., 2017). DENV causes infection in the brain and induces CNS neuropathy in severe dengue patients (Solomon et al., 2000; Verma et al., 2014), and treatment with repurposed dopamine blockers can inhibit DENV infection as an alternative antiviral strategy. Dopamine blockers include two groups, phenothiazines and benzamides. While PCZ and CPZ are phenothiazines, aminobenzamide is a benzamide derivative that can also inhibit viral proteases in the flavivirus DENV and West Nile virus (Aravapalli et al., 2012). Additionally, *N*-(adamantane-1-yl)-4-[(adamantane-1-yl)sulfamoyl]benzamide can inhibit DENV infection (Joubert et al., 2018). The antiemetic metoclopramide (MCP) is also a D2R-blocking benzamide derivative that is clinically used as a common drug for treating nausea and vomiting in dengue patients. In this study, we investigated the approach of repurposing metoclopramide as a D2R antagonist to inhibit DENV infection.

MATERIALS AND METHODS

Chemicals, Cell Culture, Virus, and Reagents

MCP hydrochloride (4-amino-5-chloro-N-[2-(diethylamino) ethyl]-2-methylxo benzamide monohydrochloride; $C_{14}H_{22}ClN_3O_2 \bullet HCl$) (Sigma-Aldrich, St. Louis, MO), a white crystalline, is dissolved in distilled water with a concentration of 100 mM and kept at −20°C. The optimal dose of MCP was evaluated by MTT and LDH assay. Murine neuroblastoma cell line Neuro-2a (ATCC; CCL-131) and baby hamster kidney cell line BHK-21 (ATCC; CCL-10) were maintained and cultured in medium DMEM with 10% fetal bovine serum (FBS) (Biological Industries, Israel), 100 U/ml penicillin, and 100 μg/ml streptomycin at 37°C and 5% CO_2. *Aedes albopictus* C6/36 cells (ATCC; CRL-1660) were cultured in minimal essential medium (MEM) (Invitrogen, California, USA) with 10% FBS, 100 U/ml penicillin, 100 μg/ml streptomycin, 1% sodium pyruvate, 1% non-essential amino acids (Thermo Fisher Scientific) and 1% HEPES at 28°C and 5% CO_2. The propagation of DENV serotype 2 (PL046) in C6/36 cells with multiplicity infection (MOI) of 0.01 was maintained at 28°C and 5% CO_2 for 5 days. The supernatant was harvested and purified by centrifugation. Virus titers were evaluated by plaque assay on BHK-21 cells as described below. The antibodies used in the study are antibodies of DENV dsRNA, NS1, NS2B, NS3, NS4, and NS5 (GeneTex, San Antonio, TX) and Alexa Fluor 488-conjugated goat anti-mouse IgG (Invitrogen, Carlsbad, CA).

Immunocytochemistry

For D2R detection, the cells were stained with primary antibody for 1 h at 4°C followed by incubation with the secondary antibody. The expression of D2R was analyzed using flow cytometry (Attune NxT, Thermo Fisher Scientific, Waltham, MA). For dsRNA detection, the cells were infected with DENV 2 (MOI = 1) for 6 h, the medium was removed, and the cells were washed and fixed with 4% paraformaldehyde. After 15 min, the cells were permeabilized and blocked with permeabilization buffer (PBS + 1% Triton X-100) at room temperature and blocking buffer (PBS + 1% BSA + 0.01% Triton X-100) at 4°C, respectively. Then, cells were stained with mouse anti-dsRNA J2 primary antibody overnight at 4°C followed by incubation with the Alexa Flour 488-conjugated goat anti-mouse secondary antibody (Thermo Fisher Scientific) and DAPI (Sigma-Aldrich) at room temperature for 15 min. The expression of dsRNA was visualized under a fluorescence microscope (EVOS FL cell imaging system, Thermo Fisher Scientific).

DENV Infection and Treatment

The Neuron-2a and BHK-21 cells were infected with DENV 2 (MOI = 1) at 37°C with or without MCP. After 2 h, the virus was removed from wells and cells supplied by the medium with or without MCP. Then, the cells were incubated at 37°C in 5% CO_2. At indicated time points, sampled were collected to conduct further analysis.

Plaque Assay

BHK-21 cells were seeded in 12-well plates at a density of 7×10^4 cells per well and then inoculated with the supernatants for treatment at diluted ratios of 10^{-1}, 10^{-2}, and 10^{-3}. After 2 h, the virus inoculum was discarded and replaced with a new DMEM containing 4% FBS and 0.5% methylcellulose. Five days after infection, the methylcellulose was discarded and washed with PBS twice. The cells were fixed and stained with crystal violet solution containing 1% crystal violet, 0.64% NaCl, and 2% formalin. The next day, the stain was removed by water, and the plates were kept dry at room temperature; the viral plaques were counted by eye observation.

Western Blotting

Treated Neuro-2a and BHK-21 cells were collected and lysed. The protein samples were separated by electrophoresis in 10% SDS-PAGE and transferred to nitrocellulose membrane and analyzed to determine the presence of the NS1, NS3, NS4B, and NS5 proteins according to our previous works (Ho et al., 2017). The use of ImageJ image software quantified the band density of western blot.

Fluorescent DENV

The purified DENV was labeled with fluorescent (Alexa Fluor 549) accordingly (Ho et al., 2017). The infected cells were visualized under a fluorescence microscope (EVOS FL cell imaging system).

Cell Viability and Cytotoxicity Assay

Cell viability and cytotoxicity were determined *in vitro* by using a colorimetric 3-(4,5-Dimethylthiazol-2-yl)-2,5-Diphenyltetrazolium Bromide (MTT) assay (Bio Basic, Toronto, Canada) and a Cytotoxicity Detection kit assay (Roche Diagnostics, Lewes, UK) (Ho et al., 2017), respectively.

Animal Model

As approved by the Institutional Animal Care and User Committee of the National Defense Medical Center (IACUC number: 16-261) and based on the protocol of DENV infection *in vivo* (Tsai et al., 2016; Ho et al., 2017; Shen et al., 2019), seven-day-old Institute of Cancer Research (ICR) strain suckling mice were inoculated intracerebrally with 2.5×10^5 plaque-forming units (PFU) and intraperitoneally with 7.5×10^5 PFU of DENV 2 (PL046). MCP (1 mg/kg) was given concurrently by intracerebral and intraperitoneal injections. The time-kinetic changes in disease progression and survival rate of mice were monitored and recorded daily. The disease severity was scored as follows: 0 for healthy; 1 for minor illness, including weight loss, reduced mobility, and a hunchback body orientation; 2 for limbic seizures; 3 for moving with difficulty and anterior limb or posterior limb weakness; 4 for paralysis; and 5 for death. Organs were harvest homogenized in PBS at day 9 post-infection. The protein expressions and tissue viral load were examined by Western blotting and plaque assay, respectively.

Statistical Analysis

The data were analyzed as the mean ± standard deviation (SD) and compared by the Unpaired *t*-test as well as one-way ANOVA (Tukey's multiple comparisons test) by using GraphPad Prism software. The survival rate followed a log-rank test. Statistical significance was set at $p < 0.05$.

RESULTS

Expression of D2R on the Surface of Neuro-2a and BHK-21 Cells and Its Roles in Mediating DENV Infection

Targeting dopamine receptor D2 (D2R) hinders DENV infection in neuronal cells *in vitro* and in the brain *in vivo* (Simanjuntak et al., 2014; Ho et al., 2017). For the identification of FDA-approved D2R antagonists for anti-dengue treatment, the antiemetic MCP was individually investigated in this study because it has been used not only for D2R antagonism but also for symptomatic medication, including persisting nausea and vomiting, during the onset of dengue fever (Marra et al., 2011). In this study, repurposing anti-nausea/vomiting MCP as an anti-dengue strategy was examined.

D2R-expressing cells are needed to prove the antiviral efficacy of MCP. Based on our previous study showing that DENV infects Neuro-2a and BHK-21 cells (Ho et al., 2017), the expression of D2R was monitored. Nonfixed immunostaining followed by flow cytometric analysis showed that Neuron-2a cells highly expressed D2R at 78.3% (**Figure 1A,** left), while BHK-21 cells displayed a relatively decreased level of D2R expression (19.7%) (**Figure 1A,** right). Based on these results, Neuro-2a cells were subsequently used in this study.

For antiviral treatment, an optimal dose of MCP without lethal effects is necessary. Using MTT and LDH assays, we evaluated serial concentrations of MCP from 1 to 2,000 μM to monitor its potential effects on cell growth and cytotoxicity. The MTT assay showed a significant inhibitory effect of MCP on cell growth at concentrations over 200 μM (**Supplemental Figure S1A**). At concentrations between 800 and 2,000 μM, the LDH assay displayed significant cytotoxic effects of MCP (**Supplemental Figure S1B**). According to the results, 200 μM of MCP was susceptible to use for further examining its antiviral efficacy in Neuro-2a cells.

To measure the antiviral efficacy of MCP, we performed a plaque assay, which showed that the viral titers after MCP treatment of Neuro-2a cells were significantly decreased (**Figure 1B,** left). However, MCP did not cause effects on BHK-21 cells, probably due to the lower expression of D2R in BHK-21 cells (**Figure 1B,** right). Based on these data, MCP can impede DENV infection in D2R-positive Neuro-2a cells.

MCP Treatment as an Antiviral Strategy Against Viral Protein Expression and dsRNA Replication

To investigate the possible antiviral actions of MCP, we explored the cellular responses and infectious processes during DENV infection. The Western blot results showing the inhibition of DENV NS1, NS3, NS4B, and NS5 protein expression in the presence of MCP confirmed the antiviral effect of MCP in the DENV-infected Neuro-2a cells (**Supplemental Figure S2A**) but

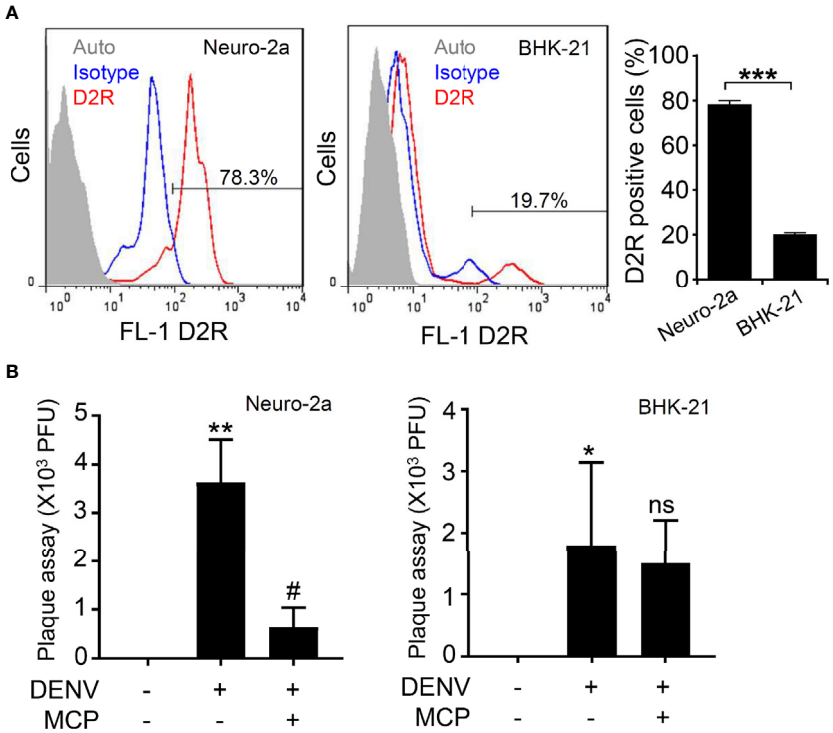

FIGURE 1 | Expression of dopamine receptor D2 (D2R) and its roles in mediating dengue virus (DENV) infection in the murine neural cell line Neuro-2a. **(A)** Representative histograms and statistical results of D2R expression, as measured by flow cytometry, show the percentages of D2R expression in the Neuro-2a and BHK-21 cells used in this study. Auto, autofluorescence. Isotype, isotype control of IgG. **(B)** In the presence of the D2R antagonist MCP, plaque assays showed the level of viral replication 24 h post-infection in the Neuro-2a and BHK-21 cells. The quantitative data are depicted as the mean ± SD of three independent experiments. $^{*}p < 0.05$, $^{**}p < 0.01$, and $^{***}p < 0.001$, compared with the untreated cells. $^{\#}p < 0.05$, compared with DENV. ns, not significant compared with DENV.

not in the DENV-infected BHK-21 cells **(Supplemental Figure S2B)**. Immunocytochemistry followed by fluorescent microscopic observation **(Figure 2A)** showed the expression of dsRNA in the DENV-infected Neuro-2a cells, while MCP treatment significantly reduced its expression **(Figure 2B)**. These results confirm the antiviral efficacy of MCP against DENV protein synthesis as well as dsRNA replication.

MCP Treatment as an Antiviral Strategy Against D2R-Mediated Viral Binding/Entry Does Not Affect the Antiviral IFN Response

Viral binding/entry is an early step for DENV infection (Cruz-Oliveira et al., 2015). D2R is highly expressed in Neuro-2a cells; therefore, we next evaluated the MCP-mediated blockade of DENV binding/entry. Fluorescent DENV was prepared according to our previous works (Ho et al., 2017). Microscopic observation **(Figure 3A)**, as well as quantification analysis **(Figure 3B)**, showed viral binding/entry at 2 h post-inoculation, which was significantly impeded by MCP treatment. To further validate the requirement of D2R in facilitating DENV binding/entry in Neuro-2a cells, we exogenously administered neutralizing antibodies against D2R. The results demonstrated a significant inhibitory effect of D2R neutralization on DENV entry/binding **(Figure 3C)**. Our findings demonstrate the MCP-mediated blocking of D2R-mediated viral entry/binding at the early stage of DENV infection.

To confirm the target of MCP underlying its antiviral capacity through interference with viral binding/entry, we monitored the off-target effect of MCP on the type I IFN response to assess its potent antiviral activity. The results of ELISA showed a significant increase in IFN-β production in the DENV-infected Neuro-2a cells; however, MCP did not increase IFN-β production **(Supplemental Figure S3)**. These data indicate that MCP directly blocked D2R-mediated viral binding/entry independent of the antiviral type I IFN response.

MCP Treatment Reduces the *In Vitro* Neurotoxicity Induced by DENV Infection

Infection with DENV causes neuronal cell apoptosis, particular 72 h post-infection (Ho et al., 2017). To analyze the roles of the D2R pathways involved in DENV infection in neuronal cells, we showed that pretreatment with MCP effectively abolished the DENV-induced changes in cell morphology **(Figure 4A)**, cell growth inhibition **(Figure 4B)**, and cytotoxicity **(Figure 4C)**.

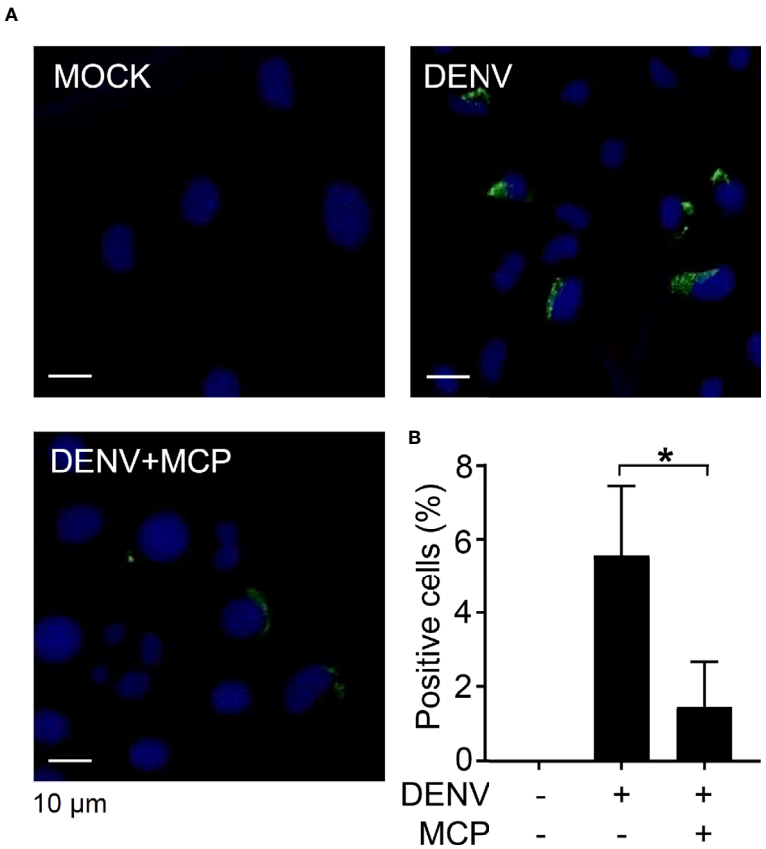

FIGURE 2 | Metoclopramide (MCP) treatment abolishes dengue virus 2 (DENV2) dsRNA replication. Neuro-2a cells were inoculated with DENV2 (MOI = 1) for 6 h in the presence of MCP. **(A)** Immunocytochemistry and **(B)** the percentages of viral dsRNA (*green*) were shown. DAPI (*blue*) was used for nuclear staining. The quantitative data are depicted as the mean ± SD of three independent experiments. $^{*}p < 0.05$.

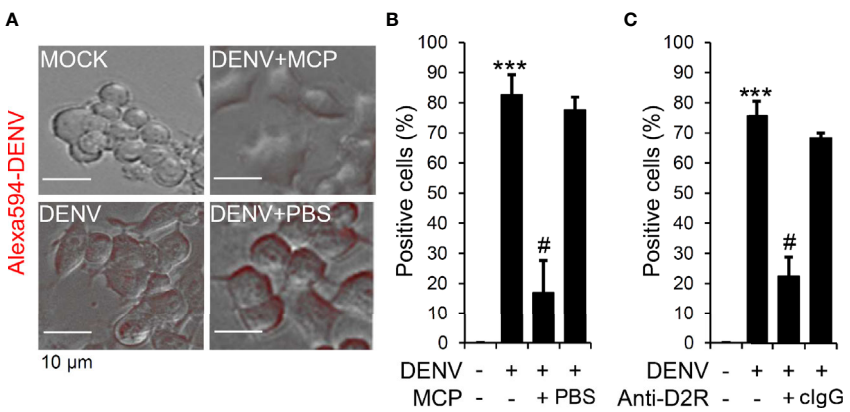

FIGURE 3 | Metoclopramide (MCP) or neutralizing anti-D2R treatment hinders dengue virus (DENV) entry. **(A)** Fluorescence microscopy measured the positive Neuro-2a cells carrying Alexa-594-labeled (*red*) DENV 2 (MOI = 1) 2 h post-infection in the presence of MCP or the neutralizing anti-D2R IgG. **(B** & **C)** represented the counts of Alexa-594-labeled (*red*) DENV 2-positive cells. PBS and isotype control IgG (cIgG) were used as controls. The quantitative data are depicted as the mean ± SD of three independent experiments. $^{***}p < 0.001$, compared with the untreated cells. $^{\#}p < 0.05$, compared with DENV.

These results indicate the cytoprotective effects of MCP, which targets D2R-mediated DENV binding/entry on DENV-induced neurotoxicity *in vitro*.

MCP Treatment Abolishes DENV Infection and Acute Viral Encephalitis-Like Disease Progression *In Vivo*

We next verified the *in vivo* antiviral effects of MCP against viral replication, viral encephalitis, and mortality in DENV-infected ICR suckling mice (Ho et al., 2017; Shen et al., 2019). For this animal study, we inoculated seven-day-old ICR suckling mice by intracerebrally and intraperitoneally given with 2.5×10^5 PFU and 7.5×10^5 PFU of DENV 2, respectively. Mice were concurrently intracranially and intraperitoneally treated with MCP (dissolved in PBS) in a dose of 1 mg/kg body weight. A significant increase in the clinical scores **(Figure 5A)** occurred in the DENV-infected mice compared to the mock-infected mice by day 7 post-infection. The survival rate of DENV-infected mice decreased by day 9 post-infection, and all of the mice died by day 10 post-infection **(Figure 5B)**. Cotreatment with MCP significantly reduced DENV-induced disease progression and mortality. According to the Western blot analysis of the NS4B viral protein **(Figure 5C)** and the plaque assays for detecting the production of infectious particles **(Figure 5D)**, DENV caused significant infection and replication in the mouse brains at day 9 post-infection, and MCP inhibited viral protein expression and replication. These data indicate that a single-dose treatment of MCP partly abolished encephalitic DENV infection in our model, which leads to neural impairment following viral replication.

DISCUSSION

The number of cases of DENV infection is continuously increasing in several areas of the world (Guzman et al., 2010; Tuiskunen Bäck and Lundkvist, 2013). The identification of antiviral drugs is still urgently needed. To date, there have been no effective drugs for the treatment of DENV infection. Drug repurposing has been widely studied to find new effects of existing drugs that contribute to inhibiting DENV infection (Botta et al., 2018). This study showed the antiviral activity observed through repurposing an antiemetic medication.

Pharmacologically targeting D2R by using selective antagonists, including PCZ and CPZ, decreases DENV infection and viral replication in neuronal cells *in vitro* and in the brain *in vivo* (Simanjuntak et al., 2014; Ho et al., 2017). Notably, during the onset of dengue fever as well as dengue hemorrhagic fever, the antiemetic MCP is used to alleviate the symptoms, including persisting nausea and vomiting

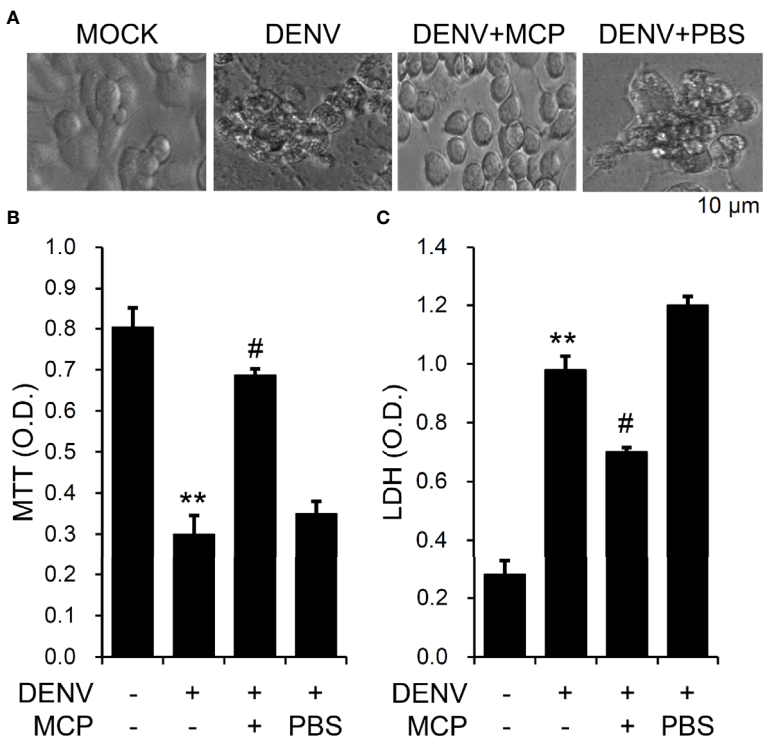

FIGURE 4 | Metoclopramide (MCP) treatment reduces dengue virus (DENV)-induced neurotoxicity *in vitro*. Following pretreatment with MCP, **(A)** cell morphology, **(B)** MTT, and **(C)** lactate dehydrogenase (LDH) cytotoxicity detection assays showed cell growth, viability, and cytotoxicity, respectively, in the DENV-infected cells at 72 h. PBS was used as the control. For all images, representative data were selectively obtained from three individual experiments. All quantitative data are shown as the mean ± SD of three independent experiments. $^{**}p < 0.01$, compared with the untreated cells. $^{\#}p < 0.05$, compared with DENV.

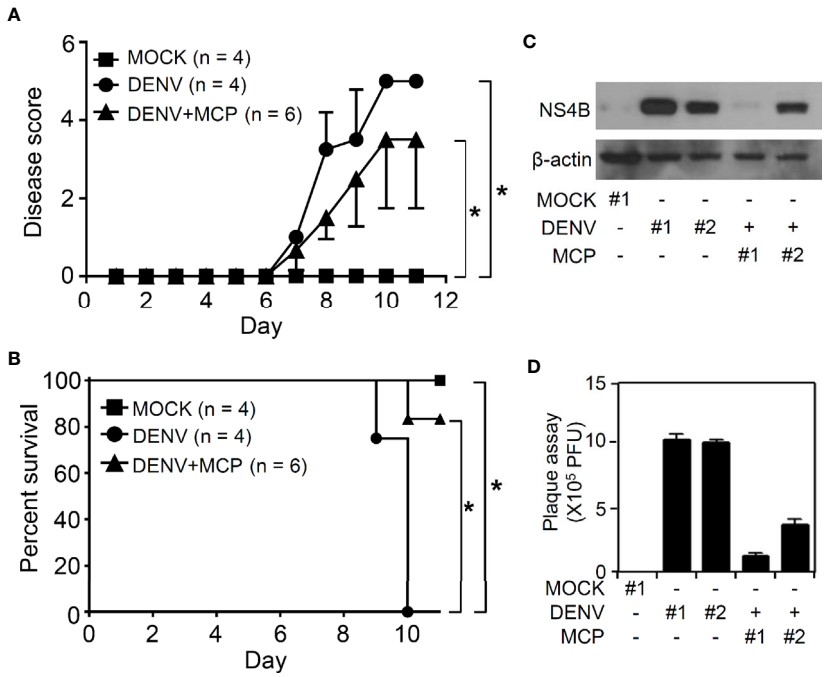

FIGURE 5 | Metoclopramide (MCP) treatment delays the clinical scores in suckling mice during dengue virus (DENV) infection. Seven-day-old ICR suckling mice were inoculated with DENV 2 by concurrent intracranial and intraperitoneal injections with or without MCP (1 mg/kg) cotreatment. Time-kinetic changes in **(A)** the clinical scores and **(B)** the survival rates of mice were measured (MOCK = 4, DENV = 4, DENV+MCP = 6). **(C)** Western blot analysis of viral NS4B protein expression and **(D)** plaque assays of viral replication in the brains of the ICR suckling mice at 9 days post-infection were shown (MOCK = 1, DENV = 2, DENV+MCP = 2). Each bar represented a mouse sample (triplicate analyses). *$p < 0.05$.

(Marra et al., 2011). However, its potential antiviral efficacy through pharmacological targeting of D2R has not been addressed. In this study, repurposing the FDA-approved antiemetic MCP as an alternative D2R antagonist was evaluated for its potential application as an anti-dengue strategy. We provided evidence to determine the antiviral effect of MCP against DENV infection *in vitro* and *in vivo*. By using our previous experimental murine model of CNS impairment accompanied by CNS inflammation (Tsai et al., 2016; Ho et al., 2017; Shen et al., 2019), MCP treatment significantly reduced DENV-induced progressive neuropathic symptoms, including reduced mobility, a hunchback body orientation, limbic seizures, paralysis; and mortality. For MCP's therapeutic advantages, this work also confirmed the possible target and protective roles of MCP in blocking DENV infection as well as DENV-induced neurotoxicity. The potential neuroprotection either by improving neuronal cell survival or by inducing anti-inflammation in CNS needs validation by using an advanced therapeutic protocol.

Similar to PCZ and CPZ, MCP is also a dopamine antagonist and is commonly used to treat nausea and vomiting (Welliver, 2014; Athavale et al., 2020). However, PCZ and CPZ were shown to be effective in treating DENV infection by targeting clathrin-mediated endocytosis as well as D2R (Simanjuntak et al., 2014; Ho et al., 2017). In contrast to PCZ and CPZ, MCP belongs to the benzamide group. Some benzamide derivatives have an inhibitory effect on DENV infection (Welliver, 2014), and an aminobenzamide scaffold can be utilized to inhibit DENV and West Nile virus protease (Aravapalli et al., 2012). There are currently no further reports showing the ability of MCP to inhibit DENV. Based on these rationales, we hypothesize that MCP can retard DENV infection, similar to drugs used for D2R blocking.

According to the D2R expression, we selected the Neuro-2a cell line with a high expression of D2R as a target cell for studying the effect of MCP treatment on DENV infection. The envelope proteins on the virus and proteins on the surface of the cell interact during virus infection. Thus, blocking virus attachment and trafficking into cells has become an attractive strategy to prevent DENV infection (De La Guardia and Lleonart, 2014). Previously, the inhibitory effect of PCZ was shown to avoid DENV infection by targeting D2R and the clathrin-coated vesicle pathway (Simanjuntak et al., 2014). Similarly, CPZ can block DENV infection by targeting D2R (Ho et al., 2017). By using DENV labeled with Alexa 594 fluorescence to assess the ability of MCP to inhibit DENV attachment and entry into cells, we showed that either MCP or a neutralizing antibody against D2R could inhibit DENV binding and entry into Neuro-2a cells. These results indicated the blockade of DENV infection by using the D2R-targeting MCP. HIV replication in macrophages is enhanced through activation of D2R (Gaskill et al., 2009; Gaskill et al., 2014), and signaling of

D2R facilitates JEV infection (Simanjuntak et al., 2017). Repurposing MCP can be used as an antiviral strategy against not only DENV but also HIV and JEV infection.

Previous works identified the induction of neurotoxicity by DENV *in vitro* (Despres et al., 1998; Jan et al., 2000; Ho et al., 2017) and *in vivo* (de Miranda et al., 2012; Velandia-Romero et al., 2012). However, the cytotoxic mechanisms are putatively varied during the infectious processes of viral attachment, internalization, endocytosis, viral protein synthesis, virion assembly, and release. Severe dengue patients may develop symptoms associated with neurological complications, threatening the patient's life (Despres et al., 1998; Solomon et al., 2000). While the expression of dopamine receptors shows a characteristic pattern in neuronal cells, targeting dopamine receptors such as D2R (Simanjuntak et al., 2014; Ho et al., 2017) and D4R (Smith et al., 2014) is believed to have an anti-dengue effect, preventing infection as well as protecting against neurotoxicity in the CNS.

As a potential antiviral approach by repurposing MCP treatment, its immunoregulatory role remains unclear. The IFN-triggered antiviral responses are crucial for eliminating viral replication and spread during DENV infection (Liang et al., 2011; Sprokholt et al., 2017). Also, type 1 IFNs could block DENV viral translation in a protein kinase R-independent pathway to inhibit the infection (Diamond and Harris, 2001). As demonstrated in the experimental animal models, the immunocompromised AG129 mice lacking interferon-α/β and -γ receptors are more susceptible to DENV infection (Shresta et al., 2004; Milligan et al., 2015; Milligan et al., 2017). Our study represented that MCP treatment could reduce DENV infection but does not affect antiviral IFN type I response in Neuro-2a cells *in vitro*, suggesting its main antiviral effect on the blockade of the D2R-mediated viral binding/entry to the host cells. Accordingly, the limitation of the use of MCP-based antiviral therapy is D2R-dependent.

In conclusion, we evaluated the effectiveness of MCP, which is used to prevent nausea and vomiting symptoms in patients with dengue infection, on the blockade of DENV infection through a mechanism involving a D2R-mediated pathway. The results showed that MCP could inhibit DENV infection by interfering with virus binding/entry in a D2R-targeting manner. The results suggest that further research on the effect of this drug against DENV infection should be performed.

DATA AVAILABILITY STATEMENT

The original contributions presented in the study are included in the article/**Supplementary Material**. Further inquiries can be directed to the corresponding author.

ETHICS STATEMENT

The animal study was reviewed and approved by the Institutional Animal Care and User Committee of the National Defense Medical Center (IACUC-18-088).

AUTHOR CONTRIBUTIONS

T-JS, VH, and TN performed most of the experiments and interpreted the results. C-FL participated in the design and supervision of the projects. M-RH and M-KJ conducted mouse experiments. T-JS and C-FL designed the concept of the project and wrote the manuscript. All authors contributed to the article and approved the submitted version.

FUNDING

This work was supported by the grants from the Ministry of Science and Technology (MOST107-2321-B-038-001, 108-2320-B-038-026, and MOST109-2320-B-038-050) and the intramural funding 106TMU-CIT-01-2, Taipei, Taiwan.

ACKNOWLEDGMENTS

We thank the Core Facility Center of Taipei Medical University (TMU) for providing technical support.

SUPPLEMENTARY MATERIAL

The Supplementary Material for this article can be found online at: https://www.frontiersin.org/articles/10.3389/fcimb.2020.606743/full#supplementary-material

REFERENCES

Acosta, E. G., Castilla, V., and Damonte, E. B. (2008). Functional entry of dengue virus into Aedes albopictus mosquito cells is dependent on clathrin-mediated endocytosis. *J. Gen. Virol.* 89 (Pt 2), 474–484. doi: 10.1099/vir.0.83357-0

Aravapalli, S., Lai, H., Teramoto, T., Alliston, K. R., Lushington, G. H., Ferguson, E. L., et al. (2012). Inhibitors of Dengue virus and West Nile virus proteases based on the aminobenzamide scaffold. *Bioorg. Med. Chem.* 20 (13), 4140–4148. doi: 10.1016/j.bmc.2012.04.055

Athavale, A., Athavale, T., and Roberts, D. M. (2020). Antiemetic drugs: what to prescribe and when. *Aust. Prescr.* 43 (2), 49–56. doi: 10.18773/austprescr.2020.011

Botta, L., Rivara, M., Zuliani, V., and Radi, M. (2018). Drug repurposing approaches to fight Dengue virus infection and related diseases. *Front. Biosci. Landmark* 23, 997–1019. doi: 10.2741/4630

Calderon-Pelaez, M. A., Velandia-Romero, M. L., Bastidas-Legarda, L. Y., Beltran, E. O., Camacho-Ortega, S. J., and Castellanos, J. E. (2019). Dengue Virus Infection of Blood-Brain Barrier Cells: Consequences of Severe Disease. *Front. Microbiol.* 10, 1435. doi: 10.3389/fmicb.2019.01435

Cruz-Oliveira, C., Freire, J. M., Conceição, T. M., Higa, L. M., Castanho, M. A. R. B., and Da Poian, A. T. (2015). Receptors and routes of dengue virus entry into the host cells. *FEMS Microbiol. Rev.* 39 (2), 155–170. doi: 10.1093/femsre/fuu004

De La Guardia, C., and Lleonart, R. (2014). Progress in the identification of dengue virus entry/fusion inhibitors. *BioMed. Res. Int.* 2014, 825039. doi: 10.1155/2014/825039

de Miranda, A. S., Rodrigues, D. H., Amaral, D. C., de Lima Campos, R. D., Cisalpino, D., Vilela, M. C., et al. (2012). Dengue-3 encephalitis promotes anxiety-like behavior in mice. *Behav. Brain Res.* 230 (1), 237–242. doi: 10.1016/j.bbr.2012.02.020

Despres, P., Frenkiel, M. P., Ceccaldi, P. E., Duarte Dos Santos, C., and Deubel, V. (1998). Apoptosis in the mouse central nervous system in response to infection with mouse-neurovirulent dengue viruses. *J. Virol.* 72 (1), 823–829. doi: 10.1128/JVI.72.1.823-829.1998

Diamond, M. S., and Harris, E. (2001). Interferon inhibits dengue virus infection by preventing translation of viral RNA through a PKR-independent mechanism. *Virology* 289 (2), 297–311. doi: 10.1006/viro.2001.1114

Ferguson, N. M. (2018). Challenges and opportunities in controlling mosquito-borne infections. *Nature* 559 (7715), 490–497. doi: 10.1038/s41586-018-0318-5

Gaskill, P. J., Calderon, T. M., Luers, A. J., Eugenin, E. A., Javitch, J. A., and Berman, J. W. (2009). Human immunodeficiency virus (HIV) infection of human macrophages is increased by dopamine: a bridge between HIV-associated neurologic disorders and drug abuse. *Am. J. Pathol.* 175 (3), 1148–1159. doi: 10.2353/ajpath.2009.081067

Gaskill, P. J., Yano, H. H., Kalpana, G. V., Javitch, J. A., and Berman, J. W. (2014). Dopamine receptor activation increases HIV entry into primary human macrophages. *PloS One* 9 (9), e108232. doi: 10.1371/journal.pone.0108232

Guzman, M. G., Halstead, S. B., Artsob, H., Buchy, P., Farrar, J., Gubler, D. J., et al. (2010). Dengue: a continuing global threat. *Nat. Rev. Microbiol.* 8 (12supp), S7. doi: 10.1038/nrmicro2460

Guzman, M. G., Gubler, D. J., Izquierdo, A., Martinez, E., and Halstead, S. B. (2016). Dengue infection. *Nat. Rev. Dis. Primers* 2, 16055. doi: 10.1038/nrdp.2016.55

Hadinegoro, S. R. S. (2012). The revised WHO dengue case classification: does the system need to be modified? *Paediatr. Int. Child Health* 32 (sup1), 33–38. doi: 10.1179/2046904712Z.00000000052

Ho, M.-R., Tsai, T.-T., Chen, C.-L., Jhan, M.-K., Tsai, C.-C., Lee, Y.-C., et al. (2017). Blockade of dengue virus infection and viral cytotoxicity in neuronal cells in vitro and in vivo by targeting endocytic pathways. *Sci. Rep.* 7 (1), 6910. doi: 10.1038/s41598-017-07023-z

Ito, K., Haga, T., Lameh, J., and Sadée, W. (1999). Sequestration of dopamine D2 receptors depends on coexpression of G-protein-coupled receptor kinases 2 or 5. *Eur. J. Biochem.* 260 (1), 112–119. doi: 10.1046/j.1432-1327.1999.00125.x

Jan, J. T., Chen, B. H., Ma, S. H., Liu, C.II, Tsai, H. P., Wu, H. C., et al. (2000). Potential dengue virus-triggered apoptotic pathway in human neuroblastoma cells: arachidonic acid, superoxide anion, and NF-kappaB are sequentially involved. *J. Virol.* 74 (18), 8680–8691. doi: 10.1128/jvi.74.18.8680-8691.2000

Joubert, J., Foxen, E. B., and Malan, S. F. (2018). Microwave Optimized Synthesis of N-(adamantan-1-yl)-4-[(adamantan-1-yl)-sulfamoyl]benzamide and Its Derivatives for Anti-Dengue Virus Activity. *Molecules* 23 (7), 1678. doi: 10.3390/molecules23071678

Leong, A. S.-Y., Wong, K. T., Leong, T. Y.-M., Tan, P. H., and Wannakrairot, P. (2007). The pathology of dengue hemorrhagic fever. *Semin. Diagn. Pathol.* 24 (4), 227–236. doi: 10.1053/j.semdp.2007.07.002

Liang, Z., Wu, S., Li, Y., He, L., Wu, M., Jiang, L., et al. (2011). Activation of Toll-like receptor 3 impairs the dengue virus serotype 2 replication through induction of IFN-beta in cultured hepatoma cells. *PloS One* 6 (8), e23346. doi: 10.1371/journal.pone.0023346

Marra, A. R., de Matos, G. F., Janeri, R. D., Machado, P. S., Schvartsman, C., and Dos Santos, O. F. (2011). Managing patients with dengue fever during an epidemic: the importance of a hydration tent and of a multidisciplinary approach. *BMC Res. Notes* 4, 335. doi: 10.1186/1756-0500-4-335

Milligan, G. N., Sarathy, V. V., Infante, E., Li, L., Campbell, G. A., Beatty, P. R., et al. (2015). A Dengue Virus Type 4 Model of Disseminated Lethal Infection in AG129 Mice. *PloS One* 10 (5), e0125476. doi: 10.1371/journal.pone.0125476

Milligan, G. N., Sarathy, V. V., White, M. M., Greenberg, M. B., Campbell, G. A., Pyles, R. B., et al. (2017). A lethal model of disseminated dengue virus type 1 infection in AG129 mice. *J. Gen. Virol.* 98 (10), 2507–2519. doi: 10.1099/jgv.0.000923

Shen, T. J., Jhan, M. K., Kao, J. C., Ho, M. R., Tsai, T. T., Tseng, P. C., et al. (2019). A Murine Model of Dengue Virus-induced Acute Viral Encephalitis-like Disease. *J. Vis. Exp.* 146, e59132. doi: 10.3791/59132

Shresta, S., Kyle, J. L., Snider, H. M., Basavapatna, M., Beatty, P. R., and Harris, E. (2004). Interferon-dependent immunity is essential for resistance to primary dengue virus infection in mice, whereas T- and B-cell-dependent immunity are less critical. *J. Virol.* 78 (6), 2701–2710. doi: 10.1128/jvi.78.6.2701-2710.2004

Simanjuntak, Y., Liang, J.-J., Lee, Y.-L., and Lin, Y.-L. (2014). Repurposing of prochlorperazine for use against dengue virus infection. *J. Infect. Dis.* 211 (3), 394–404. doi: 10.1093/infdis/jiu377

Simanjuntak, Y., Liang, J. J., Lee, Y. L., and Lin, Y. L. (2017). Japanese Encephalitis Virus Exploits Dopamine D2 Receptor-phospholipase C to Target Dopaminergic Human Neuronal Cells. *Front. Microbiol.* 8, 651. doi: 10.3389/fmicb.2017.00651

Smith, J. L., Stein, D. A., Shum, D., Fischer, M. A., Radu, C., Bhinder, B., et al. (2014). Inhibition of dengue virus replication by a class of small-molecule compounds that antagonize dopamine receptor d4 and downstream mitogen-activated protein kinase signaling. *J. Virol.* 88 (10), 5533–5542. doi: 10.1128/JVI.00365-14

Solomon, T., Dung, N. M., Vaughn, D. W., Kneen, R., Raengsakulrach, B., Loan, H. T., et al. (2000). Neurological manifestations of dengue infection. *Lancet* 355 (9209), 1053–1059. doi: 10.1016/S0140-6736(00)02036-5

Sprokholt, J. K., Kaptein, T. M., van Hamme, J. L., Overmars, R. J., Gringhuis, S.II, and Geijtenbeek, T. B. H. (2017). RIG-I-like Receptor Triggering by Dengue Virus Drives Dendritic Cell Immune Activation and TH1 Differentiation. *J. Immunol.* 198 (12), 4764–4771. doi: 10.4049/jimmunol.1602121

Tsai, T. T., Chen, C. L., Lin, Y. S., Chang, C. P., Tsai, C. C., Cheng, Y. L., et al. (2016). Microglia retard dengue virus-induced acute viral encephalitis. *Sci. Rep.* 6, 27670. doi: 10.1038/srep27670

Tuiskunen Bäck, A., and Lundkvist, Å. (2013). Dengue viruses–an overview. *Infect. Ecol. Epidemiol.* 3 (1), 19839. doi: 10.3402/iee.v3i0.19839

van der Schaar, H. M., Rust, M. J., Chen, C., van der Ende-Metselaar, H., Wilschut, J., Zhuang, X., et al. (2008). Dissecting the cell entry pathway of dengue virus by single-particle tracking in living cells. *PloS Pathog.* 4 (12), e1000244. doi: 10.1371/journal.ppat.1000244

Velandia-Romero, M. L., Acosta-Losada, O., and Castellanos, J. E. (2012). In vivo infection by a neuroinvasive neurovirulent dengue virus. *J. Neurovirol.* 18 (5), 374–387. doi: 10.1007/s13365-012-0117-y

Verma, R., Sahu, R., and Holla, V. (2014). Neurological manifestations of dengue infection: a review. *J. Neurol. Sci.* 346 (1–2), 26–34. doi: 10.1016/j.jns.2014.08.044

Welliver, M. (2014). Dopamine antagonists for nausea and vomiting: special considerations. *Gastroenterol. Nurs.* 37 (5), 361–364. doi: 10.1097/SGA.0000000000000068

Welsch, S., Miller, S., Romero-Brey, I., Merz, A., Bleck, C. K., Walther, P., et al. (2009). Composition and three-dimensional architecture of the dengue virus replication and assembly sites. *Cell Host Microbe* 5 (4), 365–375. doi: 10.1016/j.chom.2009.03.007

Yu, I.-M., Zhang, W., Holdaway, H. A., Li, L., Kostyuchenko, V. A., Chipman, P. R., et al. (2008). Structure of the immature dengue virus at low pH primes proteolytic maturation. *Science* 319 (5871), 1834–1837. doi: 10.1126/science.1153264

Zaitseva, E., Yang, S.-T., Melikov, K., Pourmal, S., and Chernomordik, L. V. (2010). Dengue virus ensures its fusion in late endosomes using compartment-specific lipids. *PloS Pathog.* 6 (10), e1001131. doi: 10.1371/journal.ppat.1001131

Conflict of Interest: The authors declare that the research was conducted in the absence of any commercial or financial relationships that could be construed as a potential conflict of interest.

frontiers in Cellular and Infection Microbiology

ORIGINAL RESEARCH
published: 08 March 2021
doi: 10.3389/fcimb.2021.639620

A Comparative Transcriptome Analysis of Human and Porcine Choroid Plexus Cells in Response to *Streptococcus suis* Serotype 2 Infection Points to a Role of Hypoxia

*Alexa N. Lauer[1], Rene Scholtysik[2], Andreas Beineke[3], Christoph Georg Baums[4], Kristin Klose[5], Peter Valentin-Weigand[6], Hiroshi Ishikawa[7], Horst Schroten[1], Ludger Klein-Hitpass[2] and Christian Schwerk[1]**

[1] Pediatric Infectious Diseases, Department of Pediatrics, Medical Faculty Mannheim, University of Heidelberg, Mannheim, Germany, [2] Institute for Cell Biology, University Hospital Essen, Essen, Germany, [3] Institute for Pathology, University of Veterinary Medicine, Hannover, Germany, [4] Faculty of Veterinary Medicine, Institute of Bacteriology and Mycology, Leipzig University, Leipzig, Germany, [5] Faculty of Veterinary Medicine, Institute of Veterinary Pathology, Leipzig University, Leipzig, Germany, [6] Institute for Microbiology, University of Veterinary Medicine, Hannover, Germany, [7] Laboratory of Clinical Regenerative Medicine, Department of Neurosurgery, Faculty of Medicine, University of Tsukuba, Tsukuba, Japan

Streptococcus suis (*S. suis*) is an important opportunistic pathogen, which can cause septicemia and meningitis in pigs and humans. Previous *in vivo* observations in *S. suis*-infected pigs revealed lesions at the choroid plexus (CP). *In vitro* experiments with primary porcine CP epithelial cells (PCPEC) and human CP epithelial papilloma (HIBCPP) cells demonstrated that *S. suis* can invade and traverse the CP epithelium, and that the CP contributes to the inflammatory response *via* cytokine expression. Here, next generation sequencing (RNA-seq) was used to compare global transcriptome profiles of PCPEC and HIBCPP cells challenged with *S. suis* serotype (ST) 2 infected *in vitro*, and of pigs infected *in vivo*. Identified differentially expressed genes (DEGs) were, amongst others, involved in inflammatory responses and hypoxia. The RNA-seq data were validated *via* quantitative PCR of selected DEGs. Employing Gene Set Enrichment Analysis (GSEA), 18, 28, and 21 enriched hallmark gene sets (GSs) were identified for infected HIBCPP cells, PCPEC, and in the CP of pigs suffering from *S. suis* ST2 meningitis, respectively, of which eight GSs overlapped between the three different sample sets. The majority of these GSs are involved in cellular signaling and pathways, immune response, and development, including inflammatory response and hypoxia. In contrast, suppressed GSs observed during *in vitro* and *in vivo S. suis* ST2 infections included those, which were involved in cellular proliferation and metabolic processes. This study suggests that similar cellular processes occur in infected human and porcine CP epithelial cells, especially in terms of inflammatory response.

Keywords: next generation sequencing, *Streptococcus suis*, meningitis, choroid plexus, host-pathogen interaction, blood-cerebrospinal fluid barrier

OPEN ACCESS

Edited by:
Federico Iovino,
Karolinska Institutet (KI), Sweden

Reviewed by:
Yuan Yuan,
Beijing Institute of Microbiology and Epidemiology, China
Barbara Spellerberg,
Ulm University Medical Center, Germany

****Correspondence:***
Christian Schwerk
christian.schwerk@medma.uni-heidelberg.de

Specialty section:
This article was submitted to Bacteria and Host, a section of the journal Frontiers in Cellular and Infection Microbiology

Received: *09 December 2020*
Accepted: *01 February 2021*
Published: *08 March 2021*

Citation:
Lauer AN, Scholtysik R, Beineke A, Baums CG, Klose K, Valentin-Weigand P, Ishikawa H, Schroten H, Klein-Hitpass L and Schwerk C (2021) A Comparative Transcriptome Analysis of Human and Porcine Choroid Plexus Cells in Response to Streptococcus suis Serotype 2 Infection Points to a Role of Hypoxia. Front. Cell. Infect. Microbiol. 11:639620. doi: 10.3389/fcimb.2021.639620

INTRODUCTION

The Gram-positive bacterium *Streptococcus suis* (*S. suis*) is an important opportunistic zoonotic pathogen, of which serotype 2 (ST2) is the most prevalent among invasive isolates from the natural host, the pig, as well as for humans (Goyette-Desjardins et al., 2014). The most common clinical manifestation for pigs and humans is meningitis, but septicemia, endocarditis, arthritis, pneumonia, and peritonitis are also reported. Noteworthy, *S. suis* is considered as a re-emerging pathogen especially in Asian countries (Lun et al., 2007; Dutkiewicz et al., 2017; Dutkiewicz et al., 2018).

Previous observations made in natural and experimentally *in vivo* infected pigs revealed that *S. suis* infections are associated with lesions at the choroid plexus (CP) (Sanford, 1987; Williams and Blakemore, 1990; Beineke et al., 2008). The CP forms an interface between the blood and the central nervous system (CNS), the so-called blood-cerebrospinal fluid barrier (BCSFB). The main barrier property at the CP results from the polarized epithelial cells, which are connected *via* tight junctions and tight junction-associated proteins, such as ZO1 and occludin (Wolburg et al., 2001). Experiments performed *in vitro* using primary porcine CP epithelial cells (PCPEC) or immortal human CP epithelial papilloma (HIBCPP) cells demonstrated that *S. suis* can invade and traverse the CP epithelial cells. As a consequence, challenging the CP with *S. suis* contributes to the immunological response *via* cytokine and chemokine expression and secretion (Tenenbaum et al., 2008; Schwerk et al., 2011; Schwerk et al., 2012).

Some efforts have been made to investigate the response of host cells and organisms to infection with *S. suis*. Previous *in vitro* studies involving infection of different cell types with *S. suis*, such as human brain microvascular endothelial cells (HBMEC) or immune cells, including THP-1 monocytes, J774 macrophages, and dendritic cells, have focused on host-pathogen interaction, the inflammatory response and intracellular signaling of the host cells, or on bacterial survival and their interaction with host cells (Charland et al., 2000; Segura et al., 2002; Segura et al., 2004; Meijerink et al., 2012). Whole transcriptome analyses on host cells after challenge with *S. suis* have been performed using THP-1 monocytes, porcine alveolar macrophages, and primary porcine choroid plexus epithelial cells (PCPEC) (De Greeff et al., 2010; Liu et al., 2011b; Schwerk et al., 2011). Differentially expressed genes (DEGs) identified during these studies belonged to different functional categories. Amongst others, genes involved in immune response and host defense, apoptosis/programmed cell death, and those involved in signal transduction pathways were found to be overrepresented (De Greeff et al., 2010; Liu et al., 2011b; Schwerk et al., 2011).

Approaches to investigate the host response to *S. suis in vivo* have been performed in several organisms, including pigs (Li et al., 2010; Liu et al., 2011a; Gaur et al., 2014; Ye et al., 2017), but also non-porcine species, such as zebrafish and mice (Wu et al., 2010; Rong et al., 2012). Confirming the results of *in vitro* challenged host cells, during these studies genes involved in inflammatory and immune defense responses were identified as DEGs (Li et al., 2010; Liu et al., 2011a; Rong et al., 2012; Ye et al., 2017). Tissues and organs investigated during the porcine *in vivo* studies covered spleen, brain, lung, monocytes, and peritoneal blood, but not specifically the CP. Therefore, the transcriptomic changes at the CP of pigs suffering from meningitis after infection with *S. suis* are unknown, leaving participating target genes and host signaling pathways open for discovery. Furthermore, a comparative analysis of the transcriptional response at the CP, either after infection *in vitro vs. in vivo*, or between human and porcine model systems, has not yet been performed. Due to the function of the CP as entry gate into the CNS during infection with *S. suis*, and its role during inflammatory responses to the pathogen, transcriptome analyses of infected pigs and CP epithelial cell cultures will reveal important differently regulated genes that play a role during these processes and point to the cellular pathways involved.

In this study, we employed next generation sequencing (RNA-seq) to compare changes in global transcriptome profiles caused by *S. suis* SS2 at the CP of infected pigs *in vivo*, as well as in PCPEC and HIBCPP cells infected *in vitro*. Identified DEGs and enriched hallmark gene sets (GSs) point to involvement of cellular signaling, immune and inflammatory responses, and hypoxia, whereas cellular proliferation and metabolic processes are rather suppressed during infection. Additionally, the inflammatory responses appear to involve similar cellular processes in infected human and porcine CP epithelial cells.

MATERIALS AND METHODS

Ethics Statement

In vivo piglet infection experiments, and the subsequent necropsy, were carried out by veterinarians, in compliance with the principles outlined in the European Convention for the Protection of Vertebrate Animals Used for Experimental and Other Scientific Purposes, as well as the German Animal Protection Law (Tierschutzgesetz). The CP tissue samples analyzed in this study originated from two different *in vivo* infection studies. The CP tissue samples from the meningitis-free animals were part of a study, which was approved by the Landesdirektion Sachsen, with the permit number TVV28/16, which includes approval through the registered committee for animal experiments. The experiment analyzing the CP from animals suffering from meningitis were approved by the Committee on Animal Experiments of the Lower Saxonian State Office for Consumer Protection and Food Safety under the permit number 33.12-42,502-04-16/2305A (Rungelrath et al., 2018). The piglets of both studies originated from the same German Landrace herd that is based on the genotyping results of more than 400 *S. suis* isolates free of the *S. suis* pathotype investigated in this study.

In Vivo Porcine Infection Experiments

The CP tissue samples used for the transcriptome analysis were collected from two independent *in vivo* porcine infection experiments using approximately 8-week-old German Landrace pigs. The animals, from which "meningitis-free" samples were obtained, were three 8-week-old male piglets intravenously

infected with 2×10^8 colony forming units (CFU) of *S. suis* ST7 strain 13-00283-02 in the 5th week of life within an unpublished experimental infection. The three piglets, from which "meningitis" samples were obtained, were experimentally infected with *S. suis* ST2 strain 10. Experimental infection was conducted in anesthesia of 8-week-old male piglets *via* intranasal application of 1.5×10^9 CFU following a treatment with 1% acetic acid of the mucosal surface of the nasal cavity as part of a published study carried out by Rungelrath and colleagues (Rungelrath et al., 2018).

In both experiments, the animals were monitored and examined every 8 h post-infection for the onset of disease and were given a clinical score, based on their body temperature, food uptake, and overall behavior (alertness, breathing pattern, mobility). An animal was considered morbid if it presented with a fever of at least 40.2°C. If a high fever persisted (at least 40.5°C), along with apathy and/or anorexia over a 36 h time period, the piglet was euthanized for predefined animal welfare reasons. Additionally, if the piglet presented severe clinical signs, such as opisthotonus, convulsions, inability to rise, or acute polyarthritis, the animal was subject for immediate euthanasia.

Onset of severe disease usually occurred 3 to 5 days post-infection. Once a predefined humane endpoint was reached, the animal was anesthesised through application of 2 mg azaperone (Stresnil®, Firma Yanssen) and 10 mg ketamine hydrochloride (Ursotamin®, Serumwerke Bernburg) per kg body weight intramuscularly and subsequently euthanized *via* the intravenous administration of T61® (200 mg ml^{-1} embutramide, 50 mg ml^{-1} mebezonium, and 5 mg ml^{-1} tetracain; Intervet, Merck, Sharp & Dohme). The "meningitis-free" piglets were euthanized the same way after observation of 23 days following the experimental ST7 infection.

Immediately following the euthanasia of each animal, a necropsy was performed, which has been previously described by Baums and colleagues (Baums et al., 2006). Additionally, the brain was promptly removed and cut between the two brain hemispheres in order to gain access to the lateral ventricles. One of the two CP from the lateral ventricles was removed, briefly rinsed in sterile DPBS, and flash-frozen in liquid nitrogen for subsequent RNA isolation and transcriptome analysis.

Cell Culture

Human choroid plexus papilloma (HIBCPP) cells have been described previously as *in vitro* model of the BCSFB (Schwerk et al., 2012). HIBCPP cells were cultivated in DMEM/F12 (Ham) medium with 4 mM L-glutamine and 15 mM HEPES, supplemented with 100 U/ml penicillin, 100 U/ml streptomycin, and 5 µg/ml insulin (HIBCPP medium) and containing 15% FCS. For infection assays cells were seeded on ThinCert™ cell culture filter membranes (Greiner Bio-One, Frickenhausen, Germany), with a 3 µm pore diameter, a pore density of 2.0×10^6 pores per cm^2, and a membrane diameter of 0.33 cm^2, in the inverted BCSFB model and maintained as previously described (Schwerk et al., 2012; Dinner et al., 2016), with some modifications. Briefly, a maximum of 100,000 cells were seeded on the membrane of inverted cell culture filter inserts, which, when confluent, resulted in approximately 400,000 cells per filter. HIBCPP cells up to passage 38 were used for experiments. The following day filter membranes were flipped, and placed hanging into a 24-well cell culture plate. The cells were supplied with HIBCPP cell culture medium containing 10% FCS that was exchanged every second day. Approximately 3 to 4 days post-seeding TEER values were monitored with an epithelial tissue voltohmmeter (Millipore, Schwalbach, Germany). Once a TEER of at least 70 Ω x cm^2 was reached, cells were transferred to HIBCPP cell medium containing 1% FCS. For infection experiments, filters with a TEER of at least 240 Ω x cm^2 and a maximum of 740 Ω x cm^2 were used, which was reached 1 or 2 days later.

The isolation and culture of primary PCPEC was performed as previously described (Gath et al., 1997; Haselbach et al., 2001) with some modifications. Briefly, CP tissue was collected from the lateral ventricle of freshly slaughtered pigs at the meat-processing center, and subjected to treatment with 0.2% trypsin (Biochrom, Berlin, Germany, 45 min at 4°C, 17 min at 37°C). Following this cold/warm trypsin treatment, 1 volume of pre-warmed FCS was added before the cell suspension (undigested CP tissue was removed) was centrifuged for 10 min at 55 × g at room temperature, and the pellet was resuspended in 10 ml DMEM (1×) with GlutaMAX™ (Gibco Life Technologies, Paisley, UK) with 4.5 g L^{-1} D-Glucose, pyruvate, and phenol red, 2% (v/v) P/S, and 0.05% (v/v) human recombinant insulin solution (Sigma-Aldritch, Steinheim, Germany) (PCPEC medium) containing 10% FCS and 20 µM Cytosine Arabinoside (AraC, Cell Pharm GmbH, Hannover, Germany). Subsequently, 100 µl of the cell suspension was seeded on the membrane of inverted ThinCert™ cell culture filter inserts (Greiner Bio-One, Frickenhausen, Germany), which were pre-coated with mouse laminin. The following day the filters were washed once by flipping and hanging the cell culture filter membranes into a 24-well cell culture plate containing pre-warmed DPBS (containing Ca^{2+} and Mg^{2+}) in order to remove non-adherent cells. Cells were then cultivated for 4 days in PCPEC medium containing 10% FCS and 20 µM AraC, followed by cell culture in AraC-free medium with a medium change every 2 days. Starting 6 days post-seeding, the TEER development was monitored with an epithelial tissue voltohmmeter (Millipore, Schwalbach, Germany). Once the TEER reached approximately 100 Ω x cm^2, the cells were transferred to PCPEC medium without FCS. A confluent primary PCPEC layer on the 24-well cell culture filter membrane consisted of approximately 60,000 cells. For infection experiments filters with a TEER of at least 250 Ω x cm^2 were used.

Measurement of Barrier Integrity

In order to evaluate the barrier development and barrier integrity of HIBCPP cells and PCPEC, the TEER was measured by utilizing a voltohmmeter coupled with a chopstick STX01 electrode (Millipore, Schwalbach, Germany). To calculate the resistance across the cell culture filter membrane area (Ω x cm^2), the measured Ω, from which the blank value was subtracted (cell culture membrane filter not containing any cells) was multiplied by the surface area of the 24-well cell culture filter membrane (approximately 0.336 cm^2).

In order to monitor the paracellular permeability of HIBCPP cells and PCPEC throughout the infection intervals, the permeability for FITC-coupled inulin was determined as previously described (Schwerk et al., 2012).

Bacterial Strains and Cultivation

S. suis ST2 strain 10, kindly provided by Hilde Smith (Lelystad, NL), has been used in various studies for experimental induction of disease including meningitis (Vecht et al., 1992; Smith et al., 1999). *S. suis* ST7 strain 13-00283-02 belongs to sequence type 29 and has recently been characterized (Rieckmann et al., 2018). The genomes of both strains have been sequenced (Bunk et al., 2021). Bacteria were cultivated in liquid Todd Hewitt Broth (THB; Oxoid, Wesel, Germany) in order to prepare bacteria stocks for long-term storage and infection experiments. The medium for long-term preservation at −80°C was composed of bacteria suspended in DMEM/F-12 (1×) medium (containing L-Glutamine, 15 mM HEPES, without phenol red; Gibco/Life Technologies™, Paisley, UK) with an optical density at 600 nm (OD_{600}) of 0.65, containing 20% glycerol (Sigma-Aldrich, Steinheim, Germany).

In order to cultivate bacteria for the infection experiments, long-term storage stock aliquots were added to 10 ml Todd Hewitt Broth (THB) and incubated at 37°C to mid-log phase. Subsequently, bacterial cultures were washed twice with the appropriate medium used during the infection experiment (see above). The bacterial cell suspension was adjusted to an OD_{600} of 0.65, which resulted in approximately 2×10^8 CFU ml^{-1}.

In order to determine the bacterial CFU, which was used for infection of host cells *in vitro*, as well as the CFU throughout the infection time points, the inoculum and an amount, which equaled a multiplicity of infection (MOI) of 10, was serial diluted and plated in duplicate onto Colombia sheep blood agar plates (Oxoid, Wesel, Germany). The sheep blood agar plates were incubated inverted in a humidified incubator at 37°C and 5% CO_2 overnight, and the CFU were counted the following day.

In Vitro Infection Experiments

HIBCPP cells and PCPEC were infected *in vitro* with *S. suis* ST2 strain 10 once the TEER values reached at least 250 $\Omega \times cm^2$. Infection was performed with a MOI of 10. The HIBCPP cells were infected up to 10 h, with time points being in 2 h increments. The primary PCPEC were infected up to 6 h, again, with time increments being in 2 h. Throughout the infection time points, TEER values and paracellular permeability were determined to evaluate barrier integrity.

Cell Viability—Live/Dead Assay

To determine the cell viability of PCPEC and HIBCPP cells live/dead-assays (Invitrogen, Karlsruhe, Germany) were performed according to the manufacturer's instructions. In this assay living cells appear green (intracellular esterase activity), whereas dead cells appear red (loss of plasma membrane integrity allows entry and DNA binding of ethidium homodimer-1). Results were documented by immunofluorescence microscopy.

RNA Isolation

The RNeasy Mini Kit (Qiagen, Hilden, Germany) was used for total RNA isolation from HIBCPP cells and the CP tissue from the *in vivo* porcine experiments. For the HIBCPP cell infection experiments, filters were briefly rinsed with DPBS (with Ca^{2+} and Mg^{2+}), before the cells were processed following the manufacturers protocol "purification of total RNA from animal cells using spin technology." For the CP tissue collected from the *in vivo* porcine infection experiments, 30 mg of fresh-frozen CP tissue was suspended in 600 µl lysis buffer and homogenized using a micro pestle. Subsequently, the homogenized tissue suspension was applied to a QiaShredder column (Qiagen, Hilden, Germany) before RNA was isolated according to the manufacturer's protocol "purification of total RNA from animal tissues." The RNeasy Micro Kit (Qiagen, Hilden, Germany) was used for total RNA isolation from PCPEC. Lysates from four cell culture membranes were pooled. The manufacturer's protocol "purification of total RNA from animal and human cells" was followed. All isolated RNA samples underwent an on-column DNase I treatment (15 min incubation at room temperature), which was integrated during the RNA isolation protocols, as described by the manufacturer (Qiagen, Hilden, Germany). Following the isolation, RNA samples were eluted in RNase-free H_2O and stored at −80°C. The RNA concentration was determined with a spectrophotometer (ND1000, Peqlab Biotechnoloy, Erlangen, Germany).

Semiquantitative RT-PCR and QPCR

Total RNA (0.5 µg RNA from HIBCPP cells and from the CP tissue from the *in vivo* porcine infection experiments; 0.125 µg from PCPEC) was reverse transcribed using random primers included in the AffinityScript QPCR cDNA Synthesis Kit (Agilent Technologies). Semi-quantitative PCR reactions applying defined volumes of the generated cDNA were performed with the Taq DNA Polymerase Kit (Qiagen) following the manufacturers' instructions. PCR reaction mixtures were initially denatured for 2 min at 94°C and subsequently subjected to the indicated cycles of denaturation (94°C, 30 s), annealing (55–60°C, depending on the primers, 30 s), and extension (72°C, 1 min) followed by a final extension step at 72°C for 7 min. PCR products were visualized by gel electrophoresis using 1.5% agarose gels and ethidium bromide staining.

To quantitatively evaluate the expression of selected genes, the Brilliant II SYBR® Green QPCR Master Mix kit (Agilent Technologies) was used according to the manufacturer's instructions. The qPCR was run using the Stratagene Mx3005P system with the MX software using the one plateau pre-melt/RT segment and normal two-step amplification setting, followed by determination of a dissociation curve. The following conditions were applied: initial denaturation (95°C, 10 min) followed by 40 cycles of denaturation (95°C, 30 s), combined annealing and extension (58°C, 60 s), and the denaturation curve (95°C, 60 s; 65°C, 30 s; 95°C, 30 s). Fold-changes were calculated using the $2^{-\Delta\Delta Ct}$ method (Livak and Schmittgen, 2001) and expression of the gene for Glyceraldehyde 3-phosphate dehydrogenase (GAPDH) was used as control.

Primers for RT-PCR and QPCR were designed employing Primer3 software (Rozen and Skaletsky, 2000) and are shown in **Supplementary Tables S1** and **S2**, respectively. The primer sequences were synthesized by Sigma-Aldrich (Steinheim, Germany), delivered in a lypophilic form, and reconstituted in double-distilled water.

RNA-Seq Analyses

RNA samples used for RNA-seq analysis were evaluated for their RNA integrity with the Agilent 2100 Bioanalyzer System (Agilent Technologies, Waldbronn, Germany) in combination with the Agilent Bioanalyzer RNA Nano Chip. RNA integrity numbers were above 9.5 for RNA isolated from HIBCPP cells, above 8.9 for RNA isolated from PCPEC, and above 7.4 for RNA isolated from CP tissues obtained during the *in vivo* porcine infection experiments.

The Ovation® Human FFPE RNA-Seq Multiplex System Kit (NuGen, Illumina, San Diego, CA, USA) was utilized for library preparation from 100 ng of total RNA from the HIBCPP cells for conventional RNA-seq. For the PCPEC and the porcine CP tissues from the *in vivo* infection experiments, the Universal Plus mRNA-Seq kit (NuGen, Illumina, San Diego, CA, USA) was used for the RNA library preparation from 100 ng total RNA.

For transcript fragmentation the Covaris S220 Focused-ultrasonicator, with the Covaris microTUBE, set to 10% duration, 200 cycles per burst, and 140 s was used to generate fragment sizes of approximately 250 bp long. Fragment lengths were analyzed on the Agilent 2100 Bioanalyzer System using the Agilent Bioanalyzer HS DNA chip. Bead-purification steps were carried out with the help of Agencourt AMPure XP SPRI beads in order to remove adapter or primer dimers throughout the various cDNA synthesis, adaptor ligation, or PCR amplification steps. The Qubit system was used in combination with the double stranded DNA high sensitivity assay kit in order to determine the DNA concentration of the prepared libraries before these were pooled. Adaptor ligation introduces specific 8 bp long barcode sequence to each of the individual biological replicates of infected and uninfected samples. With the use of the barcodes, one library pool containing all the biological replicates for each phenotype (infected and uninfected) was generated for sequencing. The library pool was quantified utilizing the NEBNext® Library Quant kit, which is a SYBR Green based qPCR method essential in order to achieve the optimal cluster density on the sequencing flow cell required for an optimal sequencing output.

The sequencing of the pooled HIBCPP cell sample set library was performed using HiSeq 2500 flow cell system (Illumina®, San Diego, CA, USA) in the high-output and paired-end mode. The sequencing of the pooled RNA libraries of the PCPEC samples and the *in vivo* CP samples was carried out on the HiSeq 2500 flow cell system (Illumina®, San Diego, CA, USA) in the rapid-run and paired-end mode, sequencing 100 bp length for each read.

Bioinformatic Processing Post-Sequencing

Subsequently to the sequencing process, the generated raw reads were processed. In a first step the adapter sequences were removed with the help of the Trimmomatic-0.30 software tool, which was designed to identify full and partial adapter sequences from single- and paired-end Illumina NGS data (Bolger et al., 2014). The trimmed sequences were subject to alignment by utilizing the RNA aligner STAR software (Dobin et al., 2013). The sequences generated from the HIBCPP cells were aligned to the human genome 19 and the sequences generated from the porcine samples (PCPEC and CP tissue from the *in vivo* infection experiments) were aligned to the *Sus scrofa* genome 11.1. The aligned sequences of the HIBCPP cell and PCPEC samples were imported into the StrandNGS software and filtered on quality metrics, which included the removal of reads that had more than one match, an alignment score of below 95, mapping quality below 40, and lengths less than 20. This additional filtering step was not carried out on the sequences aligned from the *in vivo* experiment. Instead, these sequences were subject to Universal Molecular Identifiers filtering, which resulted in less than 5% of reads removed. These aligned and filtered reads can be imported to the Integrative Genomics Viewer, which allows visualization of the NGS datasets (Robinson et al., 2011).

Lastly, for the quantification of the RNA sequences, the aligned and filtered reads were imported to the Partek Genomics Suite (PartekGS) software. This software reports the reads per kilobase of exon model per million reads (RPKM), which is a scaling method applied in order to normalize the RNA abundancies for sequencing depth (library size) and gene length (Mortazavi et al., 2008).

RNA-Seq Statistical Data Analysis: DEGs and GSEA

In order to evaluate the differential gene expression and to utilize data analysis platforms for downstream analysis, RPKM values and/or the raw reads were used to generate the Differentially Expressed Genes (DEGs) list and to perform a Gene Set Enrichment Analysis (GSEA). DEGs were identified using the PartekGS software implementing the one-way analysis of variance (ANOVA) test. A step-up method to correct for multiple testing was applied to generate corrected p-values, but due to the low number of replicates, the correction for multiple testing eliminated many potential true-positive targets. For this reason, the identification of DEGs was based on uncorrected p-values. The resulting p-values were exported and further manual filtering steps were carried out in Excel from Microsoft Office. Filters, which were applied in order to generate the final DEG list, included at least 10 (for the PCPEC and *in vivo* samples) or 20 (for the HIBCPP cell samples) raw reads of the transcript in the biological triplicates of one class (uninfected versus infected) and an uncorrected p-value of ≤ 0.05. Additionally, a more stringent list was created which only displayed a list of significant DEGs with a corrected (step-up method) p-value ≤ 0.05 (De and Baron, 2012). The genes resulting in the final DEG list with an uncorrected and corrected p-value ≤ 0.05 were taken into consideration.

A second statistical analysis was applied using the RPKM values, by utilizing the GSEA software, which allows the user to interpret the data on a biological relevant gene set level, and not

on individual genes, when comparing different biological states (Mootha et al., 2003; Subramanian et al., 2005). The GSEA makes use of the Molecular Signature Database (MSigDB), which contains approximately 18,000 gene sets (GSs), categorized into eight major groups (Subramanian et al., 2005; Liberzon et al., 2011; Liberzon et al., 2015). The GSEA was run with the standard settings in the gene set permutation mode, set to 1,000 permutations. In order to select potential interesting candidates, GSs which presented a false discovery rate (FDR) q-value ≤0.25 were considered to be of interest, along with a normalized enrichment score (NES) of approximately ±2.

Accession Numbers

The data generated during RNA-seq was deposited in the Sequence Read Archive (SRA) on the National Center for Biotechnology Information (NCBI) platform. The BioProject accession number for the HIBCPP cell data is PRJNA533919. The BioProject accession number for the PCPEC data is PRJNA533792. The BioProject accession number for the data acquired from the CP tissue which was isolated following the *in vivo* infection experiments and sequenced *via* conventional RNA-seq is PRJNA534398.

Statistics

The significance of the gene fold change from infected samples in comparison to uninfected samples was calculated using the unpaired student's t-test. A result was considered significant if $p \leq 0.05$.

RESULTS

Infection of HIBCPP Cells and PCPEC With *S. suis* ST2

We have previously shown that *S. suis* ST2 invades both HIBCPP cells and PCPEC in a polar fashion from the basolateral side and that the CP contributes to the inflammatory response when challenged with *S. suis* (Tenenbaum et al., 2009; Schwerk et al., 2011; Schwerk et al., 2012). To determine time points following infection of HIBCPP cells and PCPEC, at which the cells demonstrate a transcriptional response, we treated cells grown on inverted cell culture filter inserts with *S. suis* ST2 for different amounts of time and analyzed the expression of selected inflammatory response genes by semi-quantitative RT-PCR (**Figure 1** and data not shown). As shown in **Figure 1A** both HIBCPP cells and PCPEC displayed a strong transcriptional response after 6 h of challenge with *S. suis* ST2. Importantly, the barrier function of both HIBCPP cells and PCPEC stayed intact during this time period as indicated by a stable TEER (**Figure 1B**) and low permeability by FITC-labelled inulin (**Figure 1C**). Furthermore, live/dead assays demonstrated that both cell types remained viable during the infection period (data not shown). Therefore, we selected HIBCPP cells and PCPEC infected with *S. suis* ST2 for 6 h in the inverted cell culture insert model for further transcriptome analyses.

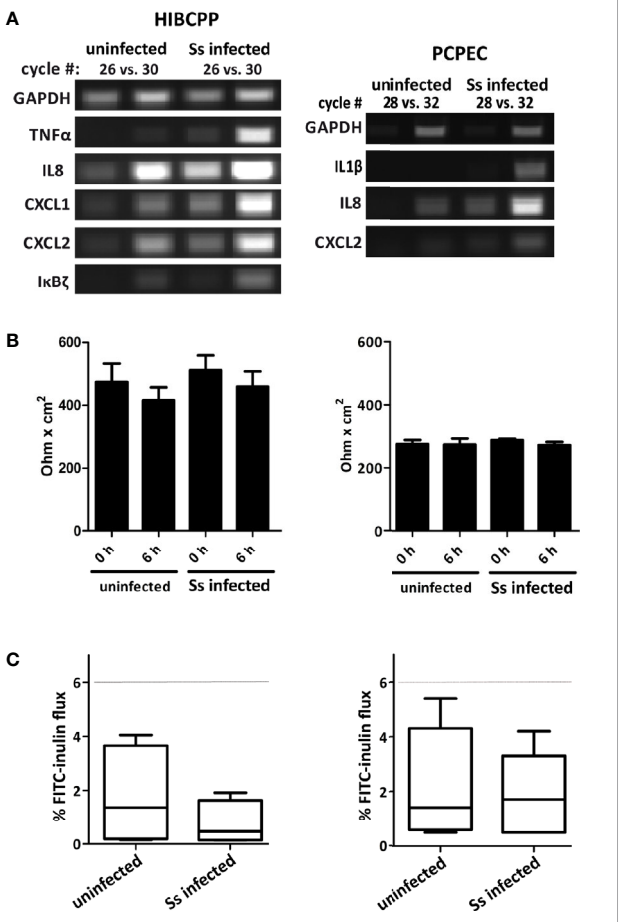

FIGURE 1 | Infection of HIBCPP cells (left) and PCPEC (right) with *S. suis* ST2 (indicated as Ss) causes induction of an inflammatory response. **(A)** HIBCPP cells and PCPEC grown on inverted cell culture filter inserts were treated with *S. suis* ST2 at a MOI of 10 for 6 h and semi-quantitative RT-PCR was performed to determine induction of the genes indicated at the left of the panels. PCR reactions were analyzed after the cycle numbers indicated at the top of the panels. Uninfected HIBCPP cells and PCPEC served as controls **(B)** TEER values of uninfected control cells and of infected HIBCPP cells and PCPEC were measured at the beginning of the experiments (0 h) and after 6 h of infection (6 h). **(C)** The flux of FITC-labelled inulin across uninfected control cells and across infected HIBCPP cells and PCPEC was measured after 6 h of infection and stayed below 6% (dotted lines) under all conditions.

The CP of In Vivo Infected Piglets Suffering From Meningitis Exhibited an Inflammatory Response

In vivo infection experiments with *S. suis* were carried out with 8-week-old piglets. Three meningitis-free control animals intravenously infected with *S. suis* ST7 3 weeks prior euthanasia and three animals suffering from meningitis after intranasal infection with *S. suis* ST2 strain 10 (Rungelrath et al., 2018) were selected for further analysis.

The meningitis-free animals exhibited no clinical signs of central nervous system dysfunction within the entire observation

period. Following the conclusion of the experiment, the animals were euthanized and a necropsy was performed. Part of the necropsy consisted of CSF, swabs, and tissue collections for bacteriological investigations and preserving respective predefined tissues in formalin for histopathological evaluation as described elsewhere (Baums et al., 2006; Rungelrath et al., 2018). No bacterial growth was observed on Columbia blood agar plates used for cultivation of CSF and brain swabs. Furthermore, the absence of fibrinous and purulent inflammations in the brain, meninges and the CP was confirmed for the three animals included in this study. These results are summarized in **Table 1**.

The onset of clinical signs in the animals infected with *S. suis* ST2 occurred 2 to 4 days post-infection, and included high fever, body tremors, convulsions, and ataxia. Due to the severeness and character of these clinical signs these piglets reached the humane endpoint were euthanized. As with the meningitis-free animals, part of the necropsy consisted of CSF, swab and tissue collection and preserving the tissues in formalin for histopathological evaluation. The CSF of all three animals showed a high amount of bacterial CFUs per ml of CSF, which were confirmed *via* MP-PCR (Silva et al., 2006) to be *mrp*+ *epf*+ *sly*+ *cps*2+ *S. suis* (data not shown). The two piglets (5, 34) which exhibited specific central nervous system dysfunctions and piglet 4 with high fever and tremors were found post-mortem to have a fibro-purulent meningitis *via* histopathological evaluation of the brain and CP as summarized in **Table 1**.

RNA isolation was performed from one CP of the lateral ventricles in the selected animals. A semi-quantitative RT-PCR was performed in order to confirm an inflammatory response at the CP of *in vivo S. suis* ST2 infected piglets compared to meningitis-free pigs. As depicted in **Figure 2**, the CP isolated from piglets suffering from meningitis showed a clear inflammatory response by the increased expression (enhanced signal when referencing the GAPDH signal) of the genes encoding IL1β and IL8, as compared to the meningitis-free piglets. The signal for the CXCL2 expression, in contrast, was only enhanced for some piglets suffering from meningitis.

TABLE 1 | Summary of the clinical signs, the specific bacterial loads of CSF, and the histopathological lesions in the brain found in piglets post-infection with *S. suis* ST7 (piglets 17, 24, and 43) and ST2 (piglets 4, 5, and 34).

Animal Number	Symptoms post-infection	Bacterial CFU per ml of CSF	Histopathological findings
Meningitis-free animals[1]			
17	Day 1: 40.4°C fever Day 2: no fever	None	No fibrinous or purulent lesion in the brain, meninges, or CP
24	Day 1: 41.1°C then 40.4°C fever Day 2: 40.7°C fever, which cleared by the end of the day	None	No fibrinous or purulent lesion in the brain, meninges, or CP
43	Day 1: 41.1°C then 41.3°C Day 2: 41.3°C, which cleared by the end of the day Day 14: 40.3°C, which cleared by the end of the day	None	No fibrinous or purulent lesion in the brain, meninges, or CP
Animals suffering from meningitis[2]			
4	42.1°C fever, ataxia, kyphosis, body tremors, abdominally reinforced breathing	3.33×10^7	Moderate multifocal fibro-purulent meningitis and moderate multifocal plexus chorioiditis
5	41°C fever, ataxia, body tremors, convulsions	5.43×10^7	High grade multifocal fibro-purulent meningitis and moderate multifocal plexus chorioiditis
34	41.7°C fever, body tremors, abdominal reinforced breathing, nystagmus, opisthotonus	3.03×10^7	Moderate multifocal fibro-purulent meningitis (no comment on the state of the CP)

[1]*Piglets were euthanized after observation of 23 days following the experimental ST7 infection.*
[2]*Piglets were euthanized for predefined animal welfare reasons if a high fever persisted (at least 40.5°C), along with apathy and/or anorexia over a 36 h time period or if severe clinical signs, such as opisthotonus, convulsions, inability to rise, or acute polyarthritis were presented.*

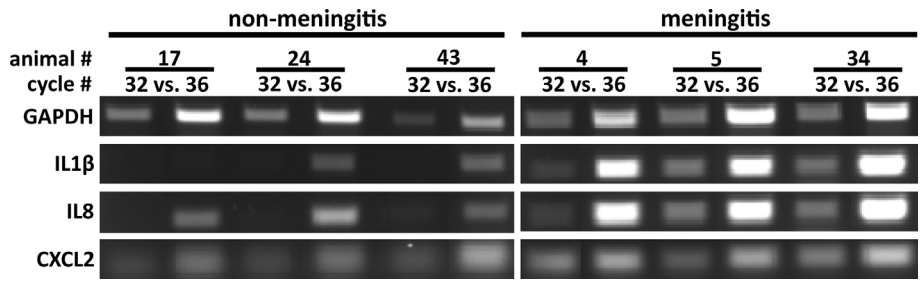

FIGURE 2 | The choroid plexus of *S. suis* ST2 *in vivo* infected piglets shows an inflammatory response in comparison to piglets not suffering from meningitis. Semi-quantitative RT-PCR was performed to determine induction of the genes indicated at the left of the panels and PCR reactions were analyzed after the cycle numbers indicated at the top of the panels. Animals 17, 24, and 43 were meningitis-free, whereas animals 4, 5, and 34 suffered from meningitis.

GAPDH was used as a house-keeping gene, which displayed a non-coherent expression likely due to either the heterogeneous cell population found in the CP tissue or lower RNA integrities compared to RNA from the *in vitro* infection experiments (**Figure 2**).

Bioinformatic Processing of RNA-Seq Data Revealed Efficient Mapping to Exon Gene Regions

The RNA samples from *S. suis* ST2 challenged HIBCPP cells and PCPEC and control cells as well as from CPs isolated from meningitis-free pigs or from pigs suffering from meningitis were subjected to RNA-seq as described in *Materials and Methods*. Following the sequence run, the generated reads were aligned to either the human or the porcine reference genome with the RNA aligner STAR (Dobin et al., 2013) and quantified in PartekGS.

In total, approximately 20 million reads were generated per sample of the HIBCPP cell sample set and for the samples originating from the *in vivo* infection experiments, and approximately 10 million reads were generated for the PCPEC samples.

For the HIBCPP cell samples, approximately 62–74% of the aligned reads fully overlapped to an exon region of the reference genome (data not shown). The aligned reads obtained from the samples of porcine origin (*in vitro* and *in vivo* samples) displayed a higher full exon overlap, of approximately 80%.

The quality assurance for the transcript alignment and mapping post-sequencing displayed values within acceptable ranges (data not shown) for all samples which underwent sequencing and alignment and were statistically analyzed in the next step.

Differentially Expressed Genes (DEGs)

We first determined the magnitude of statistically significant DEGs based on the number of reads detected during the alignment and mapping process. A total of 1,479 significant ($p \leq 0.05$) DEGs were identified following the analysis of *S. suis* ST2 infected versus uninfected HIBCPP cells. A total of 63 DEGs were identified, which exhibited at least a 2-fold up- or down-regulation, of which 32 genes displayed an up-regulation and 31 genes displayed a down-regulation. The results of the uncorrected p-values are presented in **Supplementary Table S3**, while the correction of the p-value yielded no significantly DEGs (data not shown). The highest significant up-regulation observed was a 3.6 fold change for the gene encoding for ZFPL36L1. The strongest down-regulation was observed for the microRNA3648 with an 8-fold change. Interestingly, the majority of the genes only exhibited a 2- to 3-fold differential expression following the 6 h infection period with *S. suis* ST2.

For the *in vitro S. suis* ST2 infected PCPEC samples, a total of 430 genes were identified as significantly differentially regulated with an uncorrected p-value ≤0.05, of which 46 genes exhibited an up-regulation of at least 2-fold, and 4 genes a down-regulation of at least 2-fold. The results of the uncorrected p-values are presented in **Supplementary Table S4**, since the correction of the p-value yielded only one significant gene (ACOD1; $p = 0.025$; data not shown). Interestingly, the *in vitro* infected primary PCPEC displayed a very strong cellular response during the infection with *S. suis* ST2, with a maximum of 134-fold up-regulation for IL1β. A total of 21 genes exhibited an up-regulation of at least 3-fold, with the majority of these genes known to being involved in the inflammatory response and regulation. In contrast, a total of only four genes encoding for VSIG4, DLGAP5, KNL1, and STRC were significantly differentially down-regulated at least 2-fold during *S. suis* ST2 infection. The gene encoding for STRC was the highest significantly down-regulated gene, which exhibited a maximum down-regulation of 3-fold change.

A total of 3,355 DEGs with an uncorrected p-value of ≤0.05 were identified in the CP of pigs suffering from *S. suis* ST2—induced meningitis in relation to meningitis-free pigs. The DEG list of significant genes with a corrected p-value ≤0.05 presented 479 genes, which were at least ±2-fold regulated, of which 171 genes were up-regulated and 308 genes were down-regulated (data not shown). Due to this large number, the significant DEGs with corrected p-values are presented in **Supplementary Table S5**. In total, 30 genes which were significantly differentially regulated exhibited a fold change of at least ±2 with a corrected p-value of ≤0.05. Twelve of the 30 genes displayed an up-regulation and 18 genes displayed a down-regulation. The strongest up-regulation was 11.3-fold for the gene encoding INSM1, whereas the strongest down-regulation was 6.3-fold for the gene encoding for TIMD4. Furthermore, of the 30 genes identified in **Supplementary Table S5**, 13 genes exhibited a fold change ±3.

Only two overlapping significant DEGs were identified in the infected CP epithelial cells, HIBCPP cells and PCPEC, and included transcriptional and immune response regulator (TCIM) and Rho family GTPase 1 (RND1).

Verification of Selected Genes by qPCR

Following the sequencing analysis, the generated data was validated by verifying the expression levels of selected genes by qPCR. The DEG lists presented in *Differentially Expressed Genes (DEGs)* were used in order to select candidate genes for the validation of the sequencing data. Genes, which are implicated during inflammation [IL1β, IL8, C-X-C ligand 2 chemokine (CXCL2), TNFα] and during regulation of the inflammatory response [NFκB inhibitor alpha (NFκBIA), zinc finger CCCH-type containing 12A (ZC3H12A), TCIM] were selected for the verification. Additionally, since hypoxia is implicated during bacterial infections (Schaffer and Taylor, 2015; Zeitouni et al., 2016; Devraj et al., 2017), genes known to play a key role during hypoxia, or are known to have their expression influenced in a hypoxic environment (hypoxia-inducible factor 1 alpha (HIF1α), vascular endothelial growth factor a (VEGFA), MAX interactor 1 (MXI1), dual specificity phosphatase 2 (DUSP2)), were chosen for validation.

Table 2 summarizes the fold change and the corresponding significance (uncorrected p-value of a one-way ANOVA test) of the selected genes during the RNA-seq analysis compared to the relative fold change ($2^{-\Delta\Delta CT}$) between infected versus uninfected samples, along with the S.D., of the qPCR results. Overall, the gene fold change determined following the RNA-seq data analysis could be validated with the qPCR method, and the significances determined following the qPCR analysis largely

TABLE 2 | Summary of the fold changes and uncorrected *p*-values of selected genes from the RNA-seq data and the fold changes of infected samples in relation to uninfected samples.

	HIBCPP cells				PCPEC				*In vivo*			
	RNA-seq		QPCR		RNA-seq		QPCR		RNA-seq		QPCR	
	FC	*p*-value	relative $2^{-\Delta\Delta Ct}$	S.D.	FC	*p*-value	relative $2^{-\Delta\Delta Ct}$	S.D.	FC	*p*-value	relative $2^{-\Delta\Delta Ct}$	S.D.
IL1β	−1.1	0.925	2.0	3.4	134.0	0.041	136.4	83.0	2.8	0.127	4.6	15.3
IL8	3.8	0.386	3.8	7.3	22.6	0.006	20.5	12.8	22.0	0.014	7.6	17.7
CXCL2	4.9	0.258	4.7	5.3	13.8	0.017	19.4	5.5	9.9	0.005	13.0	25.1
TNFα	12.1	0.256	12.0	17.1	70.7	0.006	19.8	2.6	1.1	0.909	1.2	0.3
NFκBIA	4.2	0.266	2.6	3.5	3.9	0.016	3.5	1.2	1.3	0.173	1.7	0.4
ZC3H12A	3.3	0.220	3.1	2.4	2.1	0.004	2.0	1.2	2.9	0.107	1.4	0.6
TCIM	3.1	0.025	2.6	4.6	2.7	0.001	2.7	0.4	2.2	0.114	3.1	1.9
HIF1α	1.1	0.732	0.8	0.3	−1.6	0.306	1.0	0.2	−1.3	0.008	1.0	0.1
VEGFA	2.0	0.075	1.6	0.5	1.6	0.006	1.4	0.3	1.4	0.003	1.4	0.2
MXI1	2.5	0.043	2.8	12.1	1.2	0.008	1.0	0.03	1.1	0.416	1.1	0.1
DUSP2	−2.6	0.015	−4.2	2.2	5.2	0.016	1.3	1.5	8.1	0.004	9.7	1.9

The fold changes and p-values of the RNA-seq data were determined by the software PartekGS. The fold change for the qPCR data was calculated via the $2^{-\Delta\Delta CT}$ method using GAPDH as an internal control, and the relative fold change was determined between infected versus uninfected samples with the S.D. Genes are considered significantly differentially regulated if the p-value ≤0.05. These listed genes were selected for subsequent QPCR validation.
FC, fold change; S.D., standard deviation.

corresponded to the significant fold change determined in the RNA-seq experiment. Genes encoding for the cytokines and chemokines displayed a higher fold change in the PCPEC and in samples from the porcine *in vivo* infection experiments, an observation also made from the DEG lists (*Differentially Expressed Genes (DEGs)*).

Identification of Enriched Individual Genes by GSEA

A GSEA was performed in order to evaluate the data in terms of biologically relevant functions. In addition to attributing enriched genes to pre-defined GSs, GSEA also evaluated the individual genes for their enrichment and how well their expression differentiates in the two phenotypes. **Figure 3** depicts the heat-map generated in the GSEA analysis of the top 50 genes, which were found to be most distinguishing between *S. suis* ST2 infected epithelial cells or animals suffering from meningitis and uninfected epithelial cells or meningitis-free animals. The strongest coherent differential expression between the biological triplicates for each phenotype can be observed for the samples, which originated from the porcine *in vivo* experiments. However, strong coherence was observed for the majority of the biological HIBCPP cells and PCPEC replicates. Furthermore, the majority of the GSEA enriched genes were also identified with the PartekGS software, and can be found in the presented DEG lists in *Differentially Expressed Genes (DEGs)*.

Overall, the majority of the top 50 enriched genes displayed coherent differentiation in all biological replicates for the investigated phenotype. Interestingly, the top enriched genes determined by the GSEA software were also identified through the DEG analysis performed with the PartekGS software.

Identification of Enriched Hallmark GSs by GSEA

The hallmark GS collection consists of 50 GSs, which represent well-defined and coherent biological states, and were created in order to reduce redundancy. Furthermore, these 50 GSs are divided into eight major biological categories of: cellular components, development, immune reaction, cellular metabolism, pathways, cellular proliferation, signaling, and DNA damage (Liberzon et al., 2015).

The GSEA of analyzed HIBCPP cell samples revealed that a total of 18 GSs out of the 50 hallmark GS collection were found to be significantly enriched in 6 h *S. suis* ST2 infected cells. **Table 3** presents these significantly enriched hallmark GSs, which exhibited a FDR q-value of less than or equal to 0.25. The majority of the GSs can be categorized into cell signaling, and include, for e.g., TNFα signaling *via* NFκB, IL2-STAT5, and transforming growth factor beta (TGFβ) signaling. Additionally, five GSs belonging to the immune cellular processes were significantly enriched and include, for e.g., inflammatory response, IL6-JAK/STAT3 signaling, and complement system. Furthermore, the most significantly enriched GS was hypoxia (NES 3.24, q-value 0.000), and is categorized into the cellular pathways, along with apoptosis (NES 1.53, q-value 0.032). The GS epithelial-mesenchymal transition (EMT) was the third significantly enriched GS (NES 1.98, q-value 0.001) and belongs to the category of cellular development.

Table 4 summarizes the enriched GSs of the response of the infected PCPEC. A total of 28 GSs were found to be significantly enriched and displayed a FDR of q ≤ 0.25. The majority of enriched GSs are categorized into the cellular signaling and include the GSs, for e.g., TNFα signaling *via* NFκB, IL2-STAT5, and TGFβ. The category with the second most enriched GSs was found to belong to the immune response and include, for e.g., interferon α, γ, and inflammatory response, IL6-JAK/STAT3 signaling, and complement system. The category containing the third most enriched GSs for the infected or meningitis phenotype was the cellular pathway and included hypoxia, apoptosis, unfolded protein response, and reactive oxygen species pathway. Additionally, the GSs angiogenesis and EMT, which are categorized into cellular development, were found to be enriched.

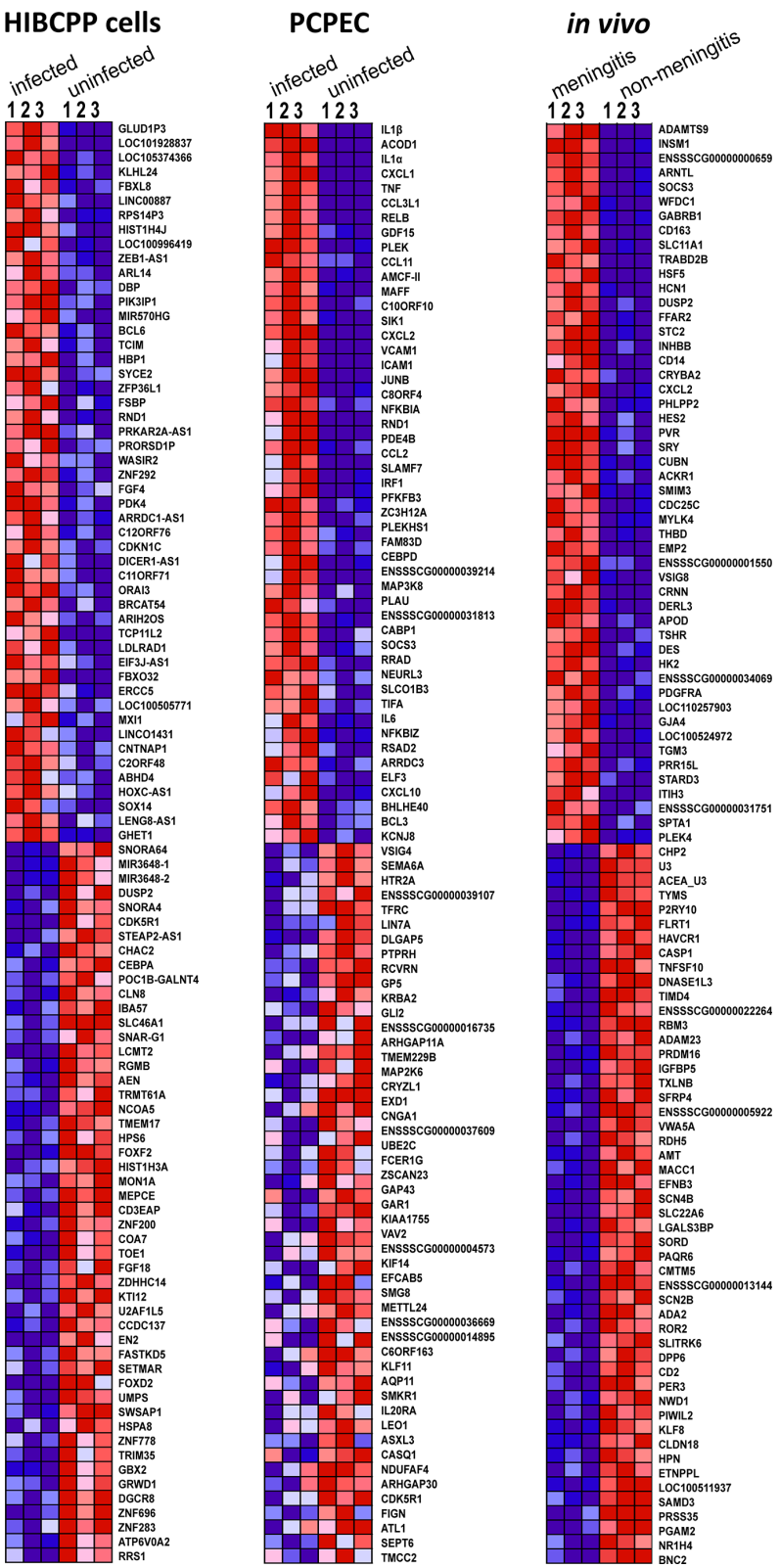

FIGURE 3 | The GSEA generated heat-map depicts a coherent expression of the biological triplicates for all sample sets of the top 50 ranked genes. Dark red indicates high expression, dark blue indicates low expression.

TABLE 3 | GSEA of 18 hallmark GSs, which are significantly enriched in *S. suis* ST2 infected HIBCPP cells.

Hallmark Gene Set Name	Size	NES	FDR q-value
Hypoxia	158	3.24	0.000
TNFα Signaling *via* NFκB	168	2.87	0.000
Epithelial-Mesenchymal transition	112	1.98	0.001
Apical surface	29	1.85	0.002
Glycolysis	171	1.78	0.012
Cholesterol homeostasis	68	1.73	0.012
Inflammatory Response	111	1.69	0.014
IL2-STAT5 Signaling	146	1.60	0.022
Myogenesis	107	1.54	0.030
Apoptosis	126	1.53	0.032
P53 Pathway	177	1.48	0.045
KRAS Signaling_up	124	1.45	0.057
Interferon γ response	159	1.44	0.056
KRAS Signaling_down	70	1.35	0.089
IL6-JAK/STAT3 Signaling	55	1.34	0.090
Allograft rejection	105	1.20	0.210
TGFβ Signaling	48	1.19	0.210
Complement	132	1.19	0.208

The normalized enrichment score (NES) represents the extent of GS enrichment, taking the number of genes ("size"), which compose the GS, into account. The false discovery rate (FDR) is considered significant if q is ≤0.25.
NES, normalized enrichment score; FDR, false discovery rate.

TABLE 4 | GSEA of 28 hallmark GSs, which are significantly enriched in infected primary PCPEC.

Hallmark Gene Set Name	Size	NES	FDR q-value
TNFα signaling *via* NFκB	151	3.12	0.000
Interferon γ response	135	2.49	0.000
Inflammatory response	105	2.48	0.000
Allograft Rejection	108	2.20	0.000
IL6-JAK/STAT3 Signaling	48	2.19	0.000
Hypoxia	146	2.12	0.000
IL2-STAT5 Signaling	129	1.99	0.000
Interferon α response	73	1.90	0.001
Complement	136	1.88	0.001
UV response_up	115	1.87	0.001
Apoptosis	123	1.85	0.002
P53 Pathway	154	1.64	0.016
Coagulation	78	1.54	0.034
Unfolded protein response	93	1.51	0.044
Wnt/β-catenin	31	1.49	0.047
Reactive oxigen species pathway	40	1.47	0.051
Estrogen response_early	136	1.41	0.083
KRAS Signaling_up	127	1.39	0.090
Angiogenesis	23	1.37	0.101
NOTCH Signaling	25	1.36	0.102
KRAS Signaling_down	78	1.28	0.178
TGFβ Signaling	47	1.27	0.177
Xenobiotic Metabolism	129	1.24	0.200
Epithelial-Mesenchymal transition	153	1.24	0.192
Glycolysis	145	1.23	0.195
Cholesterol homeostasis	63	1.23	0.187
Androgen response	86	1.23	0.187
MTORC1 Signaling	162	1.20	0.210

The normalized enrichment score (NES) represents the extent of GS enrichment, taking the number of genes ("size"), which compose the GS, into account. The false discovery rate (FDR) is considered significant if q is ≤0.25.
NES, normalized enrichment score; FDR, false discovery rate.

Table 5 summarizes the enriched GSs of the response of the CP in animals, which suffered from meningitis. In total, 21 GSs were significantly (FDR q ≤ 0.25) enriched. The majority of the GSs belong in the category of cellular signaling, with these GSs being TNFα signaling *via* NFκB, IL2-STAT5, TGFβ. The GS categories for immune system, cellular development, and cellular pathways all displayed an equal amount of enriched GSs. The inflammatory response, IL6-JAK/STAT3 signaling, and coagulation are categorized as immune response. The GSs angiogenesis, myogenesis, and EMT can be categorized under cellular development, and hypoxia, unfolded protein response, and reactive oxygen species pathway are categorized under cellular pathways.

A summary of the significantly enriched GSs designated to the respective cellular processes, as well as the percentage of the designated enriched GSs of the total number of significant GSs, are depicted in **Figure 4**.

GSs which are enriched in uninfected cells or meningitis-free animals in comparison to the infected or diseased state were also evaluated and are summarized in **Table 6**. These GSs display a negative NES score and a FDR q ≤ 0.25. In uninfected HIBCPP cells, the majority of enriched GSs were found to belong to the category of cellular proliferation. Furthermore, an enrichment of GSs belonging to the cellular categories of pathways, DNA damage, and development, was observed.

The uninfected PCPEC displayed the least amount of significant enriched GSs. Most notable was the GS containing genes regulated by the E2F transcription factors, belonging to the cellular proliferation category displayed a significant enrichment.

TABLE 5 | GSEA of the 21 hallmark GSs, which are significantly enriched in animals suffering from meningitis.

Hallmark Gene Set Name	Size	NES	FDR q-value
TNFα signaling *via* NFκB	181	2.77	0.000
Inflammatory response	168	1.98	0.001
IL6-JAK/STAT3 Signaling	69	1.82	0.006
IL2-STAT5 Signaling	174	1.79	0.006
TGFβ Signaling	49	1.73	0.008
Hypoxia	167	1.70	0.008
Estrogen response_early	168	1.58	0.020
Androgen response	89	1.52	0.029
Wnt/β-catenin	36	1.52	0.026
UV response_up	133	1.47	0.036
Myc targets	49	1.40	0.059
Angiogenesis	30	1.36	0.074
Cholesterol homeostasis	66	1.35	0.073
UV response_down	129	1.33	0.078
Coagulation	106	1.33	0.074
Estrogen response_late	167	1.33	0.071
Unfolded protein response	94	1.29	0.089
KRAS Signaling_up	174	1.25	0.118
Reactive oxigen species pathway	40	1.24	0.115
Myogenesis	165	1.19	0.172
Epithelial-Mesenchymal transition	178	1.17	0.186

The normalized enrichment score (NES) represents the extent of GS enrichment, taking the number of genes ("size"), which compose the GS, into account. The false discovery rate (FDR) is considered significant if q is ≤ 0.25.
NES, normalized enrichment score; FDR, false discovery rate.

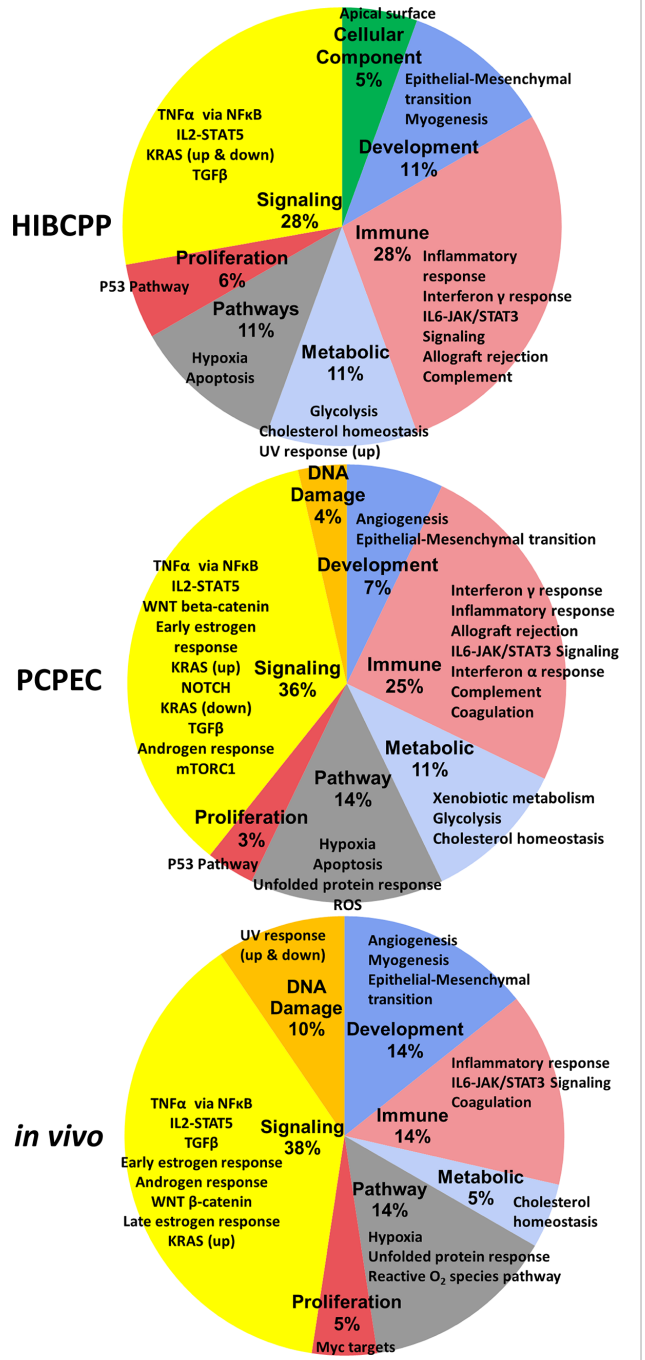

FIGURE 4 | Summary of the enriched GSs of the hallmark GSEA for *S. suis* ST2 infected HIBCPP cells, PCPEC, and pigs. These pie-charts summarize the enriched GSs from **Table 4** to **Table 6**. The percentage, which is listed under the bold labels indicating the cellular process category, is based on the total number of significantly (FDR q ≤ 0.025) enriched GSs for the sample. The outer labels of the pie chart represent the significantly enriched GS for each sample which falls under the respective cellular process category.

The majority of enriched GSs in uninfected cells or meningitis-free pigs are involved in the immune response and cellular metabolism. The interferon α and γ response, as well as the allograft rejection GSs are categorized under immune response, whereas the metabolic processes include oxidative phosphorylation, as well as fatty acid and bile acid metabolism.

TABLE 6 | The hallmark GSs, which are enriched in uninfected cells or meningitis-free animals.

Hallmark Gene Set Name	Size	NES	FDR q-value
uninfected HIBCPP cells			
MYC targets V2	58	−2.29	0.000
MYC targets V1	197	−1.90	0.000
E2F targets	197	−1.86	0.000
Unfolded protein response	109	−1.57	0.020
G2M Checkpoint	195	−1.56	0.016
DNA repair	138	−1.50	0.035
Spermatogenesis	64	−1.42	0.075
uninfected PCPEC			
E2F Targets	150	−1.54	0.128
Pancreas Beta Cells	18	−1.37	0.245
meningitis-free pigs			
Interferon α response	81	−2.57	0.000
Interferon γ response	163	−1.99	0.000
Oxidative phosphorylation	152	−1.72	0.003
E2F Targets	166	−1.62	0.010
DNA Repair	119	−1.40	0.122
Fatty Acid Metabolism	130	−1.38	0.122
Allograft Rejection	173	−1.32	0.186
Bile acid metabolism	97	−1.30	0.202

The normalized enrichment score (NES) represents the extent of GS enrichment, taking the number of genes ("size"), which compose the GS, into account. The false discovery rate (FDR) is considered significant if q is ≤0.25.
NES, normalized enrichment score; FDR, false discovery rate.

DISCUSSION

In this study, the global transcriptome response of *in vitro S. suis*-infected HIBCPP cells and PCPEC, as well as the CP tissue of *in vivo* infected piglets with meningitis, was analyzed *via* RNA-seq. Subsequent to sequencing, the generated data was evaluated on the differential expression of individual genes and was also biologically interpreted by evaluating the enrichment of GSs *via* the GSEA between the infected *versus* uninfected phenotypes.

A previous transcriptome investigation, utilizing microarray technology, of apically *S. suis* ST2 infected PCPEC, which *in vivo* would reflect the state of infection following bacterial translocation into the CNS, revealed that the CP epithelial cells contributed to the inflammatory response *in vitro* (Schwerk et al., 2011). The basolateral infection of PCPEC in this current study, which *in vivo* would reflect the state before bacteria enter the CNS, induced a strong transcriptional response, with the majority of the identified significant DEGs being involved in inflammation as well. Part of the inflammatory response is the upregulation of cytokines and chemokines (including IL1β, TNFα, IL1α, CCL3L1, CXCL8, AMCF-II, CXCL2, CCL2, CCL11, CCL5, and IL6), many of which were also identified in the previous study of apically infected PCPEC (Schwerk et al., 2011). IL1β was found to be the strongest up-regulated gene and is known to be involved in many physiological functions, among others, being a potent inducer of inflammatory signaling expressed by many different cell types, including the CNS

(Hewett et al., 2012). In previous studies evaluating the *S. suis*-dependent cytokine production, IL1β, along with other key inflammatory cytokines, such as IL6 and IL8, was found to be produced by porcine monocytes and polymorphonuclear lymphocytes in a whole-blood system in response to infection, as well as in human THP-1 monocytes (Segura et al., 2002; Segura et al., 2006). Furthermore, utilizing a murine *in vivo S. suis* infection model, the transcription of IL1β, TNFα, and CCL2 in the brain during cerebral inflammation was demonstrated *via in situ* hybridization (Dominguez-Punaro et al., 2007). In addition to the cytokine and chemokine upregulation observed in this present work, the inflammatory response regulators SLAMF7, RELB, NFKBIZ, NFKBIA, and ZC3H12A were identified, further underlining the strong inflammatory response elicited by PCPEC during to infection.

The transcriptome of HIBCPP cells was previously investigated following the *in vitro* infection with *N. meningitidis* from the basolateral cell side and demonstrated a strong inflammatory response, which included the production of cytokines and chemokines (Borkowski et al., 2014). Studies involving infection of other human cells with *S. suis*, such as HBMEC or human immune cells, mainly focused their research on the inflammatory response of host cells, too, or on bacterial survival and interaction with host cells (Charland et al., 2000; Segura et al., 2002; Liu et al., 2011b; Meijerink et al., 2012). Interestingly, in this present study, whereas PCPEC displayed a strong inflammatory response to infection, genes attributed to hypoxia were found to play a more prominent role during infection in HIBCPP cells (including ZFP36L1, MXI1, KLHL24, PNRC1, CDKN1C, and DUSP2).

In addition to the hypoxic response, it was interesting to observe the significant differential regulation of various RNA types, which are known to have a regulatory function and are non-protein coding. These regulatory RNAs included the anti-sense RNAs HLA-F, LIFR, PRKAR2A, ZEB1, and long intergenic non-coding RNAs (LINC) 887, 1431, 2482, as well as microRNAs (MIRs) 22HG and 3648, which are associated with viral inflammation and cancer and cellular proliferation, respectively (Rashid et al., 2017; Razooky et al., 2017; Zhang et al., 2018). This suggests that non-coding RNAs play a role in human CP epithelial cells during infection.

In this study, for the first time the transcriptome of cells found at the CP of pigs was investigated. For this sample set, it is important to consider that the CP tissue obtained from the *in vivo* infected pigs consists of a heterogeneous cell population, such as CP epithelial, endothelial cells, and immune cells located at or recruited to the BCSFB (Strazielle and Ghersi-Egea, 2000). Therefore, the results of the CP tissues samples cannot directly be compared to that of the *in vitro* infection experiments with homogenous PCPEC and HIBCPP epithelial cell populations. However, this data is rich in information, which helps to understand the CP tissue-specific response during *S. suis* infection. Previous studies carried out utilizing *in vivo* porcine *S. suis* infection models investigated the transcriptome of different organs (brain, lung, monocytes, spleen), but not specifically the CP (Li et al., 2010; Liu et al., 2011a). These studies evaluated the transcriptome at pre-defined time points (24 h and 3 days post-infection) of 4- to 5-week-old piglets, as compared to this present study, where the response of 8-week-old pigs was analyzed which developed acute meningitis, finding differentially regulated genes to be predominantly associated with the host's inflammatory response.

The identification of biological pathways, in which multiple DEGs are connected to a common or networked performance, is of high interest in understanding cellular processes. Employing GSEA we identified GSs, which were significantly enriched in uninfected samples in comparison to infected samples. The majority of these GSs can be categorized into cellular metabolism or cellular proliferation. The enrichment of these GSs gives insight into metabolic alterations, which occur at the CP during *S. suis* infection, and is indicative that cellular proliferation is altered or stopped during *S. suis* ST2 infection. One enriched GS, which contains genes regulated by family members of E2F transcription factors, was found to overlap between all of the samples. The E2F transcription factors are important for the regulation of genes involved in DNA replication and the cell division cycle, and in the context of infection, they were previously investigated during viral infections, such as human immunodeficiency virus and adenovirus (Kundu et al., 1997; Bracken et al., 2004; Zheng et al., 2016).

A total of 28 GSs was identified to be significantly enriched in *S. suis*-infected PCPEC. The top enriched GSs are implicated in the immune response, complementing the data obtained in the DEG analysis. In a previous transcriptome study analyzing apically *S. suis*-infected PCPEC cells, Gene Ontology (GO) analysis, which evaluates high through-put data, based on biological processes, molecular functions, and cellular components (Ashburner et al., 2000), also identified many enriched cellular processes to be involved in inflammation, as revealed by the over-represented GO terms for cytokine activity, inflammatory response, defense response, and IκB kinase/NFκB cascade, as well as programmed cell death, which can be induced as a consequence of inflammation (Schwerk et al., 2011).

For the HIBCPP cell samples set, 18 GSs were found to be significantly enriched, with the most significant enrichment being for the GS containing genes in the hypoxia cellular stress response, thereby confirming its corresponding DEG analysis. In addition to the gene enrichment in hypoxia, the GSEA revealed an enrichment of GSs participating in inflammation. A previous GSEA and a GO analysis of *N. meningitidis*-infected HIBCPP cells revealed a predominant inflammatory response, with cytokine and chemokine activity playing a significant role (Borkowski et al., 2014). Additionally, a GS involved in wound healing was identified (Borkowski et al., 2014), which is often associated with epithelial–mesenchymal transition (EMT). The EMT GS was identified in the present study to be the third most enriched GS in infected HIBCPP cells. In a different study investigating the transcriptome of a human monocyte cell line exposed to *S. suis*, GO analysis revealed a cellular response including the participation of intracellular signaling pathways involved in inflammation, such as apoptosis and host defense

and immunity, as well as other cellular processes involving cellular metabolism, gene transcription, and gene translation (Liu et al., 2011b).

The GSEA of the CP isolated from *in vivo*-infected piglets identified 21 significantly enriched GSs. The majority of the GSs displayed involvement in the inflammatory host response, as was also observed with the PCPEC samples. A previous porcine *in vivo* investigation revealed that the brains of *S. suis*-infected piglets displayed gene enrichment also involved in inflammation, and could be categorized into the GO terms of biological processes responding to a stimulus *via* signal transducer activity, cytokine activity and binding, defense response, inflammatory response, immune response, and innate immune response (Liu et al., 2011a). However, it was noted that many GO categories overlapped, due to the same genes being involved in multiple biological processes (Liu et al., 2011a). A further transcriptome study utilizing a zebrafish *S. suis* infection model, underscored the role of inflammation and host defense during infection (Wu et al., 2010).

When comparing the 18, 28, and 21 significantly enriched GSs from *S. suis* ST2 infected HIBCPP cells, PCPEC, and animals suffering from meningitis, respectively, a total of eight GSs were found to overlap (**Figure 5**). These included the five GSs TNFα signaling *via* NFκB, inflammatory response, IL2-STAT5 signaling, IL6-JAK/STAT3 signaling, and TGFβ signaling, which were previously implicated during *S. suis* infection, whereas the three GSs for hypoxia, EMT, and a set of genes up-regulated by KRAS signaling, were not. Activation of the transcription factor NFκB regulates the expression of genes involved in the inflammatory response, including the expression of cytokines and chemokines, such as TNFα (Liu et al., 2017). An increase of TNFα, along with other pro-inflammatory cytokines, was detected in the brain, blood, and kidney of *S. suis*-infected mice, as well as in a porcine *in vivo* infection model, which investigated the brain, mononuclear cells, and lung (Liu et al., 2011a; Nakayama et al., 2011). Furthermore, the virulence associated factor suilysin of *S. suis* was shown to induce the release of TNFα in human monocytes (Lun et al., 2003) and, by utilizing PCPEC, microarray analysis following *S. suis* infection from the apical cell side revealed a strong induction of TNFα and other inflammatory cytokines (Schwerk et al., 2011). Interestingly, the release of TNFα was found to promote the permeability in a human BCSFB *in vitro* model, by inducing cell death (Schwerk et al., 2010). The release of cytokines is known to elicit a downstream cellular signaling cascade. One such signaling cascade is the IL6 induction of JAK/STAT3 signaling, which has been described to influence cell growth and differentiation, and is, therefore, often implicated in cancer when dysregulated (Huynh et al., 2017). Furthermore, as with IL6, IL2 has been described to stimulate the STAT5 signaling cascade, which is known to mainly regulate cellular proliferation and modulate the immune response of T cells (Lin and Leonard, 2000). In the context of *S. suis* infection, STAT3 and STAT5 were found to be up-regulated in the porcine brain *in vivo* (Liu et al., 2011a). However, the roles of these signaling cascades during *S. suis* infection have not been further investigated.

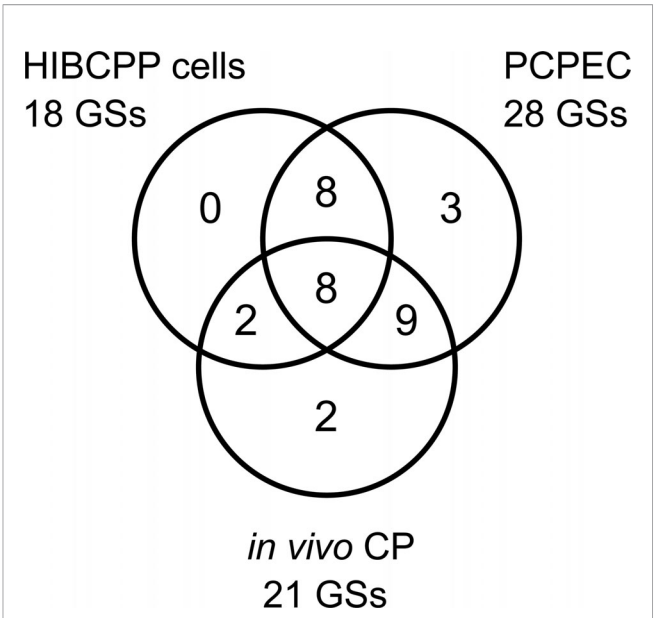

FIGURE 5 | Overlap of the GSEA identified GSs for *S. suis* ST2 infected HIBCPP cells, PCPEC, and the CP of pigs suffering from *S. suis*-induced meningitis. The Venn diagram depicts the number of significantly enriched GSs attributed to each sample set with the number of GSs which were found to overlap between the infected epithelial cells (HIBCPP cells and PCPEC) and the epithelial cells with the *in vivo* CP tissue from meningitis cases, as well as the number of GSs overlapping between all three samples sets analyzed. Eight GSs were found to overlap in the three analyzed samples sets.

Another well described signaling cascade can be induced by the cytokine TGFβ, which was previously found to be upregulated in the porcine spleen and brain of *S. suis in vivo* infected piglets (Li et al., 2010; Liu et al., 2011a). The induction of TGFβ signaling was also implicated during the colonization of *Streptococcus pneumoniae* and *Haemophilus influenzae*, which are other known bacterial meningitis-causative agents, in lung epithelial cells and was accompanied by an inflammatory response (Beisswenger et al., 2009).

To date, hypoxia, EMT, and genes regulated by KRAS signaling have not been directly linked to *S. suis* infection. It should be considered that an enrichment of the KRAS GS in this present study was observed due to overlapping genes found with the GS EMT, which is a cellular program that reverts epithelial cells to mesenchymal cells and is often implicated in cancer, since it promotes metastasis and invasion (Kalluri and Weinberg, 2009). EMT is also often involved in wound healing and tissue regeneration, which occurs following a physical trauma or injury caused by inflammation as a result of, e.g., an infection (Kalluri and Weinberg, 2009; Hofman and Vouret-Craviari, 2012). Furthermore, previous studies, especially in cancer research, have demonstrated that a hypoxic environment is a prerequisite in order for EMT to occur (Cannito et al., 2008).

A hypoxic microenvironment is often associated with infected tissues and elicits a stress response due to oxygen being a necessity in order for animal cells to carry out their normal

physiological functions (Taylor and Colgan, 2017). Hypoxia has been implicated during injury to the CNS, which includes stroke or infection (van der Flier et al., 2003; Mukandala et al., 2016) and affects the global transcription and translation of mRNA molecules by reducing both of these molecular processes, which allows for energy conservation during cellular stress (Koritzinsky and Wouters, 2007). Since the hypoxia GS was the top significantly enriched GS in the infected HIBCPP samples, it could be speculated as a reason for why the HIBCPP cells did not exhibit a strong fold change in the DEG analysis, as compared to the PCPEC post-infection.

Hypoxia stress response can be induced either in a hypoxia-inducible factor (HIF) dependent or independent manner, most notably *via* the NFκB transcription factor, with complex overlaps and cross-talks described between these two pathways (Rius et al., 2008; Schaffer and Taylor, 2015). NFκB activation is known to be associated with the acute phase of hypoxia, as well as cytokine release, most notable being IL1β and TNFα (Mukandala et al., 2016). Additionally, IL1β and TNFα can activate the HIF transcription factor in an oxygen-independent and NFκB-dependent pathway during inflammation (Lin and Simon, 2016). Interestingly, the inflammatory cytokine IL1β was observed to affect BBB permeability by influencing blood vessel plasticity *via* HIF regulation in the angiogenesis program in multiple sclerosis patients (Argaw et al., 2006). A further study investigating the cytokine presence in the CSF of infants who suffered a perinatal hypoxia event, found that infants who displayed an elevated amount of TNFα and IL6 in the CSF, were significantly more likely to suffer from severe neurological abnormalities 12 months post-partum; a phenomenon, which was also observed in survivors of bacterial meningitis and cerebral malaria (John et al., 2008; Perdomo-Celis et al., 2015; Sumanovic-Glamuzina et al., 2017).

Hypoxia does not only induce a cellular stress response, but is also described to modulate cell functions, e.g. of epithelial cells during infection (Schaffer and Taylor, 2015; Taylor and Colgan, 2017). In two previous studies, it was demonstrated that a hypoxic environment during the infection with *Pseudomonas aeruginosa* of lung epithelial cells reduced the host's cellular uptake of the pathogen, thereby diminishing host cell death, as well as causing a decline in the invasion of *Yersinia enterocolitica* into intestinal epithelial cells *in vitro* (Schaible et al., 2013; Zeitouni et al., 2016). Furthermore, hypoxia also negatively affected the virulence factor expression (Schaible et al., 2017). These studies demonstrate that a hypoxic environment was able to aid in containing the infection.

Here, we observed to our knowledge for the first time, that hypoxia-related cellular processes were significantly increased in relation to *S. suis* ST2 infection *in vitro* with human CP epithelial cells and PCPEC, as well as in the *in vivo* infected porcine CP samples. One gene in particular stood out in the enriched hypoxia GS in all three analyzed samples sets. VEGF was found to be one of the top enriched genes in the hypoxia GS of all analyzed samples (data not shown), which is indicative of angiogenesis, and in turn has been implicated in chronic hypoxia response (Mukandala et al., 2016).

The hypoxia transcription factor HIF has been discussed as a potential target for adjunctive therapy options, with already successful candidates against methicillin-sensitive and -resistant *Staphylococcus aureus* strains, in order to improve outcome or potentially replace antimicrobial therapeutics due to a rise in microbial resistance (Zinkernagel et al., 2008; Okumura et al., 2012; Santos and Andrade, 2017). Importantly, HIF therapy would not be solely limited to infections, but could also be applied in the setting of cancer treatment or chronic inflammatory disorders (Santos and Andrade, 2017). By investigating the role of hypoxia in the context of *S. suis* infection, with a focus on the significance of the BCSFB, a long-term aim could be the exploration of alternative therapy options. Those alternative therapy options could potentially limit infection severity, which is often found corresponding to long-term sequelae of survivors, such as full or partial auditory loss frequently associated with *S. suis* infection in humans, or death.

DATA AVAILABILITY STATEMENT

The datasets presented in this study can be found in online repositories. The names of the repository/repositories and accession number(s) can be found below: https://www.ncbi.nlm.nih.gov/, PRJNA533919; https://www.ncbi.nlm.nih.gov/, PRJNA533792; https://www.ncbi.nlm.nih.gov/, PRJNA534398.

ETHICS STATEMENT

In vivo piglet infection experiments, and the subsequent necropsy, were carried out by veterinarians, in compliance with the principles outlined in the European Convention for the Protection of Vertebrate Animals Used for Experimental and Other Scientific Purposes, as well as the German Animal Protection Law (Tierschutzgesetz). The CP tissue samples analyzed in this study originated from two different *in vivo* infection studies. The CP tissue samples from the meningitis-free animals were part of a study, which was approved by the Landesdirektion Sachsen, with the permit number TVV28/16, which includes approval through the registered committee for animal experiments. The experiment analyzing the CP from animals suffering from meningitis were approved by the Committee on Animal Experiments of the Lower Saxonian State Office for Consumer Protection and Food Safety under the permit number 33.12-42,502-04-16/2305A (Rungelrath et al., 2018). The piglets of both studies originated from the same German Landrace herd that is based on the genotyping results of more than 400 S. suis isolates free of the S. suis pathotype investigated in this study.

AUTHOR CONTRIBUTIONS

AL, HS, and CS conceived and coordinated the study. AL performed underlying experiments. AB and KK performed

histology. CB and PV-W coordinated animal experiments. RS and LK-H performed RNA-seq analysis. AL, RS, and LK-H performed the statistics. CB, PV-W, and HI provided resources. AL, CS, and HS drafted the manuscript. All authors contributed to the article and approved the submitted version.

FUNDING

Partial financial support of this research was awarded by the Grimminger-Stiftung für Zoonoseforschung (Grimminger Foundation for Zoonotic Research). The animal experiments were financially supported by a grant of the German Research Foundation (DFG BA 4730/3-1) to CB.

ACKNOWLEDGMENTS

We acknowledge the support of Maren von Köckritz-Blickwede and her group in the ST2 experimental infection of piglets used for collecting *in vivo* samples. We further thank Karoline Rieckmann, Anna Seydel, and Christine Weiße for conducting the ST7 animal experiment.

SUPPLEMENTARY MATERIAL

The Supplementary Material for this article can be found online at: https://www.frontiersin.org/articles/10.3389/fcimb.2021.639620/full#supplementary-material

REFERENCES

Argaw, A. T., Zhang, Y., Snyder, B. J., Zhao, M. L., Kopp, N., Lee, S. C., et al. (2006). IL-1beta regulates blood-brain barrier permeability via reactivation of the hypoxia-angiogenesis program. *J. Immunol.* 177, 5574–5584. doi: 10.4049/jimmunol.177.8.5574

Ashburner, M., Ball, C. A., Blake, J. A., Botstein, D., Butler, H., Cherry, J. M., et al. (2000). Gene ontology: tool for the unification of biology. The Gene Ontology Consortium. *Nat. Genet.* 25, 25–29. doi: 10.1038/75556

Baums, C. G., Kaim, U., Fulde, M., Ramachandran, G., Goethe, R., and Valentin-Weigand, P. (2006). Identification of a novel virulence determinant with serum opacification activity in Streptococcus suis. *Infect. Immun.* 74, 6154–6162. doi: 10.1128/IAI.00359-06

Beineke, A., Bennecke, K., Neis, C., Schroder, C., Waldmann, K. H., Baumgartner, W., et al. (2008). Comparative evaluation of virulence and pathology of Streptococcus suis serotypes 2 and 9 in experimentally infected growers. *Vet. Microbiol.* 128, 423–430. doi: 10.1016/j.vetmic.2007.10.028

Beisswenger, C., Lysenko, E. S., and Weiser, J. N. (2009). Early bacterial colonization induces toll-like receptor-dependent transforming growth factor beta signaling in the epithelium. *Infect. Immun.* 77, 2212–2220. doi: 10.1128/IAI.01224-08

Bolger, A. M., Lohse, M., and Usadel, B. (2014). Trimmomatic: a flexible trimmer for Illumina sequence data. *Bioinformatics* 30, 2114–2120. doi: 10.1093/bioinformatics/btu170

Borkowski, J., Li, L., Steinmann, U., Quednau, N., Stump-Guthier, C., Weiss, C., et al. (2014). Neisseria meningitidis elicits a pro-inflammatory response involving I kappa B zeta in a human blood-cerebrospinal fluid barrier model. *J. Neuroinflamm.* 11, 163. doi: 10.1186/s12974-014-0163-x

Bracken, A. P., Ciro, M., Cocito, A., and Helin, K. (2004). E2F target genes: unraveling the biology. *Trends Biochem. Sci.* 29, 409–417. doi: 10.1016/j.tibs.2004.06.006

Bunk, B., Jakóbczak, B., Florian, V., Dittmar, D., Mäder, U., Jarek, M., et al. (2021). Complete Genome Sequences of Streptococcus suis Pig-Pathogenic Strains 10, 13-00283-02, and 16085/3b. *Microbiol. Resour. Announc.* 10, e01137–e01220. doi: 10.1128/MRA.01137-20

Cannito, S., Novo, E., Compagnone, A., Valfre Di Bonzo, L., Busletta, C., Zamara, E., et al. (2008). Redox mechanisms switch on hypoxia-dependent epithelial-mesenchymal transition in cancer cells. *Carcinogenesis* 29, 2267–2278. doi: 10.1093/carcin/bgn216

Charland, N., Nizet, V., Rubens, C. E., Kim, K. S., Lacouture, S., and Gottschalk, M. (2000). Streptococcus suis serotype 2 interactions with human brain microvascular endothelial cells. *Infect. Immun.* 68, 637–643. doi: 10.1128/iai.68.2.637-643.2000

De, S. K., and Baron, M. (2012). Step-up and step-down methods for testing multiple hypotheses in sequential experiments. *J. Stat. Plann. Inference* 142, 2059–2070. doi: 10.1016/j.jspi.2012.02.005

De Greeff, A., Benga, L., Wichgers Schreur, P. J., Valentin-Weigand, P., Rebel, J. M., and Smith, H. E. (2010). Involvement of NF-kappaB and MAP-kinases in the transcriptional response of alveolar macrophages to Streptococcus suis. *Vet. Microbiol.* 141, 59–67. doi: 10.1016/j.vetmic.2009.07.031

Devraj, G., Beerlage, C., Brune, B., and Kempf, V. A. (2017). Hypoxia and HIF-1 activation in bacterial infections. *Microbes Infect.* 19, 144–156. doi: 10.1016/j.micinf.2016.11.003

Dinner, S., Borkowski, J., Stump-Guthier, C., Ishikawa, H., Tenenbaum, T., Schroten, H., et al. (2016). A Choroid Plexus Epithelial Cell-based Model of the Human Blood-Cerebrospinal Fluid Barrier to Study Bacterial Infection from the Basolateral Side. *J. Vis. Exp.* 111, 54061. doi: 10.3791/54061

Dobin, A., Davis, C. A., Schlesinger, F., Drenkow, J., Zaleski, C., Jha, S., et al. (2013). STAR: ultrafast universal RNA-seq aligner. *Bioinformatics* 29, 15–21. doi: 10.1093/bioinformatics/bts635

Dominguez-Punaro, M. C., Segura, M., Plante, M. M., Lacouture, S., Rivest, S., and Gottschalk, M. (2007). Streptococcus suis serotype 2, an important swine and human pathogen, induces strong systemic and cerebral inflammatory responses in a mouse model of infection. *J. Immunol.* 179, 1842–1854. doi: 10.4049/jimmunol.179.3.1842

Dutkiewicz, J., Sroka, J., Zajac, V., Wasinski, B., Cisak, E., Sawczyn, A., et al. (2017). Streptococcus suis: a re-emerging pathogen associated with occupational exposure to pigs or pork products. Part I - Epidemiology. *Ann. Agric. Environ. Med.* 24, 683–695. doi: 10.26444/aaem/79813

Dutkiewicz, J., Zajac, V., Sroka, J., Wasinski, B., Cisak, E., Sawczyn, A., et al. (2018). Streptococcus suis: a re-emerging pathogen associated with occupational exposure to pigs or pork products. Part II - Pathogenesis. *Ann. Agric. Environ. Med.* 25, 186–203. doi: 10.26444/aaem/85651

Gath, U., Hakvoort, A., Wegener, J., Decker, S., and Galla, H. J. (1997). Porcine choroid plexus cells in culture: expression of polarized phenotype, maintenance of barrier properties and apical secretion of CSF-components. *Eur. J. Cell Biol.* 74, 68–78.

Gaur, U., Xiong, Y. Y., Luo, Q. P., Yuan, F. Y., Wu, H. Y., Qiao, M., et al. (2014). Breed-specific transcriptome response of spleen from six to eight week old piglet after infection with Streptococcus suis type 2. *Mol. Biol. Rep.* 41, 7865–7873. doi: 10.1007/s11033-014-3680-x

Goyette-Desjardins, G., Auger, J. P., Xu, J., Segura, M., and Gottschalk, M. (2014). Streptococcus suis, an important pig pathogen and emerging zoonotic agent-an update on the worldwide distribution based on serotyping and sequence typing. *Emerg. Microbes Infect.* 3, e45. doi: 10.1038/emi.2014.45

Haselbach, M., Wegener, J., Decker, S., Engelbertz, C., and Galla, H. J. (2001). Porcine Choroid plexus epithelial cells in culture: regulation of barrier properties and transport processes. *Microsc. Res. Tech.* 52, 137–152. doi: 10.1002/1097-0029(20010101)52:1<137::AID-JEMT15>3.0.CO;2-J

Hewett, S. J., Jackman, N. A., and Claycomb, R. J. (2012). Interleukin-1beta in Central Nervous System Injury and Repair. *Eur. J. Neurodegener. Dis.* 1, 195–211.

Hofman, P., and Vouret-Craviari, V. (2012). Microbes-induced EMT at the crossroad of inflammation and cancer. *Gut. Microbes* 3, 176–185. doi: 10.4161/gmic.20288

Huynh, J., Etemadi, N., Hollande, F., Ernst, M., and Buchert, M. (2017). The JAK/STAT3 axis: A comprehensive drug target for solid malignancies. *Semin. Cancer Biol.* 45, 13–22. doi: 10.1016/j.semcancer.2017.06.001

John, C. C., Panoskaltsis-Mortari, A., Opoka, R. O., Park, G. S., Orchard, P. J., Jurek, A. M., et al. (2008). Cerebrospinal fluid cytokine levels and cognitive

impairment in cerebral malaria. *Am. J. Trop. Med. Hyg.* 78, 198–205. doi: 10.4269/ajtmh.2008.78.198

Kalluri, R., and Weinberg, R. A. (2009). The basics of epithelial-mesenchymal transition. *J. Clin. Invest.* 119, 1420–1428. doi: 10.1172/JCI39104

Koritzinsky, M., and Wouters, B. G. (2007). Hypoxia and regulation of messenger RNA translation. *Methods Enzymol.* 435, 247–273. doi: 10.1016/S0076-6879(07)35013-1

Kundu, M., Guermah, M., Roeder, R. G., Amini, S., and Khalili, K. (1997). Interaction between cell cycle regulator, E2F-1, and NF-kappaB mediates repression of HIV-1 gene transcription. *J. Biol. Chem.* 272, 29468–29474. doi: 10.1074/jbc.272.47.29468

Li, R., Zhang, A., Chen, B., Teng, L., Wang, Y., Chen, H., et al. (2010). Response of swine spleen to Streptococcus suis infection revealed by transcription analysis. *BMC Genomics* 11, 556. doi: 10.1186/1471-2164-11-556

Liberzon, A., Subramanian, A., Pinchback, R., Thorvaldsdottir, H., Tamayo, P., and Mesirov, J. P. (2011). Molecular signatures database (MSigDB) 3.0. *Bioinformatics* 27, 1739–1740. doi: 10.1093/bioinformatics/btr260

Liberzon, A., Birger, C., Thorvaldsdottir, H., Ghandi, M., Mesirov, J. P., and Tamayo, P. (2015). The Molecular Signatures Database (MSigDB) hallmark gene set collection. *Cell Syst.* 1, 417–425. doi: 10.1016/j.cels.2015.12.004

Lin, J. X., and Leonard, W. J. (2000). The role of Stat5a and Stat5b in signaling by IL-2 family cytokines. *Oncogene* 19, 2566–2576. doi: 10.1038/sj.onc.1203523

Lin, N., and Simon, M. C. (2016). Hypoxia-inducible factors: key regulators of myeloid cells during inflammation. *J. Clin. Invest.* 126, 3661–3671. doi: 10.1172/JCI84426

Liu, M., Fang, L., Tan, C., Long, T., Chen, H., and Xiao, S. (2011a). Understanding Streptococcus suis serotype 2 infection in pigs through a transcriptional approach. *BMC Genomics* 12, 253. doi: 10.1186/1471-2164-12-253

Liu, M., Tan, C., Fang, L., Xiao, S., and Chen, H. (2011b). Microarray analyses of THP-1 cells infected with Streptococcus suis serotype 2. *Vet. Microbiol.* 150, 126–131. doi: 10.1016/j.vetmic.2010.12.014

Liu, T., Zhang, L., Joo, D., and Sun, S. C. (2017). NF-kappaB signaling in inflammation. *Signal Transd. Targ. Ther.* 2, 17023. doi: 10.1038/sigtrans.2017.23

Livak, K. J., and Schmittgen, T. D. (2001). Analysis of relative gene expression data using real-time quantitative PCR and the 2(-Delta Delta C(T)) Method. *Methods* 25, 402–408. doi: 10.1006/meth.2001.1262

Lun, S., Perez-Casal, J., Connor, W., and Willson, P. J. (2003). Role of suilysin in pathogenesis of Streptococcus suis capsular serotype 2. *Microb. Pathog.* 34, 27–37. doi: 10.1016/s0882-4010(02)00192-4

Lun, Z. R., Wang, Q. P., Chen, X. G., Li, A. X., and Zhu, X. Q. (2007). Streptococcus suis: an emerging zoonotic pathogen. *Lancet Infect. Dis.* 7, 201–209. doi: 10.1016/S1473-3099(07)70001-4

Meijerink, M., Ferrando, M. L., Lammers, G., Taverne, N., Smith, H. E., and Wells, J. M. (2012). Immunomodulatory effects of Streptococcus suis capsule type on human dendritic cell responses, phagocytosis and intracellular survival. *PloS One* 7, e35849. doi: 10.1371/journal.pone.0035849

Mootha, V. K., Lindgren, C. M., Eriksson, K. F., Subramanian, A., Sihag, S., Lehar, J., et al. (2003). PGC-1alpha-responsive genes involved in oxidative phosphorylation are coordinately downregulated in human diabetes. *Nat. Genet.* 34, 267–273. doi: 10.1038/ng1180

Mortazavi, A., Williams, B. A., Mccue, K., Schaeffer, L., and Wold, B. (2008). Mapping and quantifying mammalian transcriptomes by RNA-Seq. *Nat. Methods* 5, 621–628. doi: 10.1038/nmeth.1226

Mukandala, G., Tynan, R., Lanigan, S., and O'connor, J. J. (2016). The Effects of Hypoxia and Inflammation on Synaptic Signaling in the CNS. *Brain Sci.* 6, 6. doi: 10.3390/brainsci6010006

Nakayama, T., Takeuchi, D., Akeda, Y., and Oishi, K. (2011). Streptococcus suis infection induces [corrected] bacterial accumulation in the kidney. *Microb. Pathog.* 50, 87–93. doi: 10.1016/j.micpath.2010.11.005

Okumura, C. Y., Hollands, A., Tran, D. N., Olson, J., Dahesh, S., Von Kockritz-Blickwede, M., et al. (2012). A new pharmacological agent (AKB-4924) stabilizes hypoxia inducible factor-1 (HIF-1) and increases skin innate defenses against bacterial infection. *J. Mol. Med. (Berl)* 90, 1079–1089. doi: 10.1007/s00109-012-0882-3

Perdomo-Celis, F., Torres, M. A., Ostos, H., Gutierrez-Achury, J., Molano, V., Duran, L. F., et al. (2015). Patterns of Local and Systemic Cytokines in Bacterial Meningitis and its Relation with Severity and Long-Term Sequelae. *Biomark Insights* 10, 125–131. doi: 10.4137/BMI.S35005

Rashid, F., Awan, H. M., Shah, A., Chen, L., and Shan, G. (2017). Induction of miR-3648 Upon ER Stress and Its Regulatory Role in Cell Proliferation. *Int. J. Mol. Sci.* 18, 1375. doi: 10.3390/ijms18071375

Razooky, B. S., Obermayer, B., O'may, J. B., and Tarakhovsky, A. (2017). Viral Infection Identifies Micropeptides Differentially Regulated in smORF-Containing lncRNAs. *Genes (Basel)* 8, 206. doi: 10.3390/genes8080206

Rieckmann, K., Seydel, A., Szewczyk, K., Klimke, K., Rungelrath, V., and Baums, C. G. (2018). Streptococcus suis cps7: an emerging virulent sequence type (ST29) shows a distinct, IgM-determined pattern of bacterial survival in blood of piglets during the early adaptive immune response after weaning. *Vet. Res.* 49, 48. doi: 10.1186/s13567-018-0544-8

Rius, J., Guma, M., Schachtrup, C., Akassoglou, K., Zinkernagel, A. S., Nizet, V., et al. (2008). NF-kappaB links innate immunity to the hypoxic response through transcriptional regulation of HIF-1alpha. *Nature* 453, 807–811. doi: 10.1038/nature06905

Robinson, J. T., Thorvaldsdottir, H., Winckler, W., Guttman, M., Lander, E. S., Getz, G., et al. (2011). Integrative genomics viewer. *Nat. Biotechnol.* 29, 24–26. doi: 10.1038/nbt.1754

Rong, J., Zhang, W., Wang, X., Fan, H., Lu, C., and Yao, H. (2012). Identification of candidate susceptibility and resistance genes of mice infected with Streptococcus suis type 2. *PLoS One* 7, e32150. doi: 10.1371/journal.pone.0032150

Rozen, S., and Skaletsky, H. (2000). Primer3 on the WWW for general users and for biologist programmers. *Methods Mol. Biol.* 132, 365–386. doi: 10.1385/1-59259-192-2:365

Rungelrath, V., Weisse, C., Schutze, N., Muller, U., Meurer, M., Rohde, M., et al. (2018). IgM cleavage by Streptococcus suis reduces IgM bound to the bacterial surface and is a novel complement evasion mechanism. *Virulence* 9, 1314–1337. doi: 10.1080/21505594.2018.1496778

Sanford, S. E. (1987). Gross and histopathological findings in unusual lesions caused by Streptococcus suis in pigs. II. Central nervous system lesions. *Can. J. Vet. Res.* 51, 486–489.

Santos, S., and Andrade, D. R. J. (2017). HIF-1alpha and infectious diseases: a new frontier for the development of new therapies. *Rev. Inst. Med. Trop. Sao Paulo* 59, e92. doi: 10.1590/S1678-9946201759092

Schaffer, K., and Taylor, C. T. (2015). The impact of hypoxia on bacterial infection. *FEBS J.* 282, 2260–2266. doi: 10.1111/febs.13270

Schaible, B., Mcclean, S., Selfridge, A., Broquet, A., Asehnoune, K., Taylor, C. T., et al. (2013). Hypoxia modulates infection of epithelial cells by Pseudomonas aeruginosa. *PLoS One* 8, e56491. doi: 10.1371/journal.pone.0056491

Schaible, B., Rodriguez, J., Garcia, A., Von Kriegsheim, A., Mcclean, S., Hickey, C., et al. (2017). Hypoxia Reduces the Pathogenicity of Pseudomonas aeruginosa by Decreasing the Expression of Multiple Virulence Factors. *J. Infect. Dis.* 215, 1459–1467. doi: 10.1093/infdis/jix139

Schwerk, C., Rybarczyk, K., Essmann, F., Seibt, A., Molleken, M. L., Zeni, P., et al. (2010). TNFalpha induces choroid plexus epithelial cell barrier alterations by apoptotic and nonapoptotic mechanisms. *J. BioMed. Biotechnol.* 2010, 307231. doi: 10.1155/2010/307231

Schwerk, C., Adam, R., Borkowski, J., Schneider, H., Klenk, M., Zink, S., et al. (2011). In vitro transcriptome analysis of porcine choroid plexus epithelial cells in response to Streptococcus suis: release of pro-inflammatory cytokines and chemokines. *Microbes Infect.* 13, 953–962. doi: 10.1016/j.micinf.2011.05.012

Schwerk, C., Papandreou, T., Schuhmann, D., Nickol, L., Borkowski, J., Steinmann, U., et al. (2012). Polar Invasion and Translocation of Neisseria meningitidis and Streptococcus suis in a Novel Human Model of the Blood-Cerebrospinal Fluid Barrier. *PLoS One* 7, e30069. doi: 10.1371/journal.pone.0030069

Segura, M., Vadeboncoeur, N., and Gottschalk, M. (2002). CD14-dependent and -independent cytokine and chemokine production by human THP-1 monocytes stimulated by Streptococcus suis capsular type 2. *Clin. Exp. Immunol.* 127, 243–254. doi: 10.1046/j.1365-2249.2002.01768.x

Segura, M., Gottschalk, M., and Olivier, M. (2004). Encapsulated Streptococcus suis inhibits activation of signaling pathways involved in phagocytosis. *Infect. Immun.* 72, 5322–5330. doi: 10.1128/IAI.72.9.5322-5330.2004

Segura, M., Vanier, G., Al-Numani, D., Lacouture, S., Olivier, M., and Gottschalk, M. (2006). Proinflammatory cytokine and chemokine modulation by Streptococcus suis in a whole-blood culture system. *FEMS Immunol. Med. Microbiol.* 47, 92–106. doi: 10.1111/j.1574-695X.2006.00067.x

Silva, L. M., Baums, C. G., Rehm, T., Wisselink, H. J., Goethe, R., and Valentin-Weigand, P. (2006). Virulence-associated gene profiling of Streptococcus suis isolates by PCR. *Vet. Microbiol.* 115, 117–127. doi: 10.1016/j.vetmic.2005.12.013

Smith, H. E., Damman, M., Van Der Velde, J., Wagenaar, F., Wisselink, H. J., Stockhofe-Zurwieden, N., et al. (1999). Identification and characterization of the cps locus of Streptococcus suis serotype 2: the capsule protects against phagocytosis and is an important virulence factor. *Infect. Immun.* 67, 1750–1756. doi: 10.1128/IAI.67.4.1750-1756

Strazielle, N., and Ghersi-Egea, J. F. (2000). Choroid plexus in the central nervous system: biology and physiopathology. *J. Neuropathol. Exp. Neurol.* 59, 561–574. doi: 10.1093/jnen/59.7.561

Subramanian, A., Tamayo, P., Mootha, V. K., Mukherjee, S., Ebert, B. L., Gillette, M. A., et al. (2005). Gene set enrichment analysis: a knowledge-based approach for interpreting genome-wide expression profiles. *Proc. Natl. Acad. Sci. U. S. A.* 102, 15545–15550. doi: 10.1073/pnas.0506580102

Sumanovic-Glamuzina, D., Culo, F., Culo, M. I., Konjevoda, P., and Jerkovic-Raguz, M. (2017). A comparison of blood and cerebrospinal fluid cytokines (IL-1beta, IL-6, IL-18, TNF-alpha) in neonates with perinatal hypoxia. *Bosn. J. Basic Med. Sci.* 17, 203–210. doi: 10.17305/bjbms.2017.1381

Taylor, C. T., and Colgan, S. P. (2017). Regulation of immunity and inflammation by hypoxia in immunological niches. *Nat. Rev. Immunol.* 17, 774–785. doi: 10.1038/nri.2017.103

Tenenbaum, T., Matalon, D., Adam, R., Seibt, A., Wewer, C., Schwerk, C., et al. (2008). Dexamethasone prevents alteration of tight junction-associated proteins and barrier function in porcine choroid plexus epithelial cells after infection with Streptococcus suis in vitro. *Brain Res.* 1229, 1–17. doi: 10.1016/j.brainres.2008.06.118

Tenenbaum, T., Papandreou, T., Gellrich, D., Friedrichs, U., Seibt, A., Adam, R., et al. (2009). Polar bacterial invasion and translocation of Streptococcus suis across the blood-cerebrospinal fluid barrier in vitro. *Cell Microbiol.* 11, 323–336. doi: 10.1111/j.1462-5822.2008.01255.x

van der Flier, M., Geelen, S. P., Kimpen, J. L., Hoepelman, I. M., and Tuomanen, E. I. (2003). Reprogramming the host response in bacterial meningitis: how best to improve outcome? *Clin. Microbiol. Rev.* 16, 415–429. doi: 10.1128/cmr.16.3.415-429.2003

Vecht, U., Wisselink, H. J., Van Dijk, J. E., and Smith, H. E. (1992). Virulence of Streptococcus suis type 2 strains in newborn germfree pigs depends on phenotype. *Infect. Immun.* 60, 550–556. doi: 10.1128/IAI.60.2.550-556.1992

Williams, A. E., and Blakemore, W. F. (1990). Pathogenesis of meningitis caused by Streptococcus suis type 2. *J. Infect. Dis.* 162, 474–481. doi: 10.1093/infdis/162.2.474

Wolburg, H., Wolburg-Buchholz, K., Liebner, S., and Engelhardt, B. (2001). Claudin-1, claudin-2 and claudin-11 are present in tight junctions of choroid plexus epithelium of the mouse. *Neurosci. Lett.* 307, 77–80. doi: 10.1016/s0304-3940(01)01927-9

Wu, Z., Zhang, W., Lu, Y., and Lu, C. (2010). Transcriptome profiling of zebrafish infected with Streptococcus suis. *Microb. Pathog.* 48, 178–187. doi: 10.1016/j.micpath.2010.02.007

Ye, M. H., Bao, H., Meng, Y., Guan, L. L., Stothard, P., and Plastow, G. (2017). Comparative transcriptomic analysis of porcine peripheral blood reveals differentially expressed genes from the cytokine-cytokine receptor interaction pathway related to health status. *Genome* 60, 1021–1028. doi: 10.1139/gen-2017-0074

Zeitouni, N. E., Chotikatum, S., Von Kockritz-Blickwede, M., and Naim, H. Y. (2016). The impact of hypoxia on intestinal epithelial cell functions: consequences for invasion by bacterial pathogens. *Mol. Cell Pediatr.* 3, 14. doi: 10.1186/s40348-016-0041-y

Zhang, D. Y., Zou, X. J., Cao, C. H., Zhang, T., Lei, L., Qi, X. L., et al. (2018). Identification and Functional Characterization of Long Non-coding RNA MIR22HG as a Tumor Suppressor for Hepatocellular Carcinoma. *Theranostics* 8, 3751–3765. doi: 10.7150/thno.22493

Zheng, Y., Stamminger, T., and Hearing, P. (2016). E2F/Rb Family Proteins Mediate Interferon Induced Repression of Adenovirus Immediate Early Transcription to Promote Persistent Viral Infection. *PLoS Pathog.* 12, e1005415. doi: 10.1371/journal.ppat.1005415

Zinkernagel, A. S., Peyssonnaux, C., Johnson, R. S., and Nizet, V. (2008). Pharmacologic augmentation of hypoxia-inducible factor-1alpha with mimosine boosts the bactericidal capacity of phagocytes. *J. Infect. Dis.* 197, 214–217. doi: 10.1086/524843

Conflict of Interest: The authors declare that the research was conducted in the absence of any commercial or financial relationships that could be construed as a potential conflict of interest.

frontiers in Cellular and Infection Microbiology

ORIGINAL RESEARCH
published: 15 March 2021
doi: 10.3389/fcimb.2021.641261

OPEN ACCESS

Edited by:
Tatiana Barichello, University of Texas Health Science Center at Houston, United States

Reviewed by:
Jaqueline Generoso, Universidade do Extremo Sul Catarinense, Brazil
Charles T. Spencer, The University of Texas at El Paso, United States
Tejaswini Doifode, Carilion Clinic, United States

***Correspondence:**
Ana Tereza Ribeiro de Vasconcelos
atrv@lncc.br
Renato Santana de Aguiar
santanarnt@ufmg.br

†These authors have contributed equally to this work and share first authorship

‡These authors have contributed equally to this work and share last authorship

Specialty section:
This article was submitted to Virus and Host, a section of the journal Frontiers in Cellular and Infection Microbiology

Received: *13 December 2020*
Accepted: *28 January 2021*
Published: *15 March 2021*

Citation:
Geddes VEV, Brustolini OJB, Cavalcante LTdF, Moreira FRR, de Castro FL, Guimarães APdC, Gerber AL, Figueiredo CM, Diniz LP, Neto EdA, Tanuri A, Souza RP, Assunção-Miranda I, Alves-Leon SV, Romão LF, de Souza JPBM, de Vasconcelos ATR and de Aguiar RS (2021) Common Dysregulation of Innate Immunity Pathways in Human Primary Astrocytes Infected With Chikungunya, Mayaro, Oropouche, and Zika Viruses. Front. Cell. Infect. Microbiol. 11:641261. doi: 10.3389/fcimb.2021.641261

Common Dysregulation of Innate Immunity Pathways in Human Primary Astrocytes Infected With Chikungunya, Mayaro, Oropouche, and Zika Viruses

Victor Emmanuel Viana Geddes[1,2†], Otávio José Bernardes Brustolini[3†], Liliane Tavares de Faria Cavalcante[1], Filipe Romero Rebello Moreira[1], Fernando Luz de Castro[1], Ana Paula de Campos Guimarães[3], Alexandra Lehmkuhl Gerber[3], Camila Menezes Figueiredo[4], Luan Pereira Diniz[5], Eurico de Arruda Neto[6], Amilcar Tanuri[1], Renan Pedra Souza[2], Iranaia Assunção-Miranda[4], Soniza Vieira Alves-Leon[7], Luciana Ferreira Romão[5], Jorge Paes Barreto Marcondes de Souza[7], Ana Tereza Ribeiro de Vasconcelos[3‡] and Renato Santana de Aguiar[1,2*‡]*

[1] Laboratório de Virologia Molecular, Departamento de Genética, Instituto de Biologia, Universidade Federal do Rio de Janeiro, Rio de Janeiro, Brazil, [2] Laboratório de Biologia Integrativa, Departamento de Genética Ecologia e Evolução, Instituto de Ciências Biológicas, Universidade Federal de Minas Gerais, Belo Horizonte, Brazil, [3] Laboratório de Bioinformática, Laboratório Nacional de Computação Científica, Ministério de Ciência Tecnologia e Comunicações, Petrópolis, Brazil, [4] Instituto de Microbiologia Paulo de Goes, Universidade Federal do Rio de Janeiro, Rio de Janeiro, Brazil, [5] Instituto de Ciências Biomédicas, Universidade Federal do Rio de Janeiro, Rio de Janeiro, Brazil, [6] Departamento de Biologia Celular e Molecular, Faculdade de Medicina de Ribeirão Preto, Universidade de São Paulo, Ribeirão Preto, Brazil, [7] Hospital Universitário Clementino Fraga Filho, Universidade Federal do Rio de Janeiro, Rio de Janeiro, Brazil

Arboviruses pose a major threat throughout the world and represent a great burden in tropical countries of South America. Although generally associated with moderate febrile illness, in more severe cases they can lead to neurological outcomes, such as encephalitis, Guillain-Barré syndrome, and Congenital Syndromes. In this context astrocytes play a central role in production of inflammatory cytokines, regulation of extracellular matrix, and control of glutamate driven neurotoxicity in the central nervous system. Here, we presented a comprehensive genome-wide transcriptome analysis of human primary astrocytes infected with Chikungunya, Mayaro, Oropouche, or Zika viruses. Analyses of differentially expressed genes (DEGs), pathway enrichment, and interactomes have shown that Alphaviruses up-regulated genes related to elastic fiber formation and N-glycosylation of glycoproteins, with down-regulation of cell cycle and DNA stability and chromosome maintenance genes. In contrast, Oropouche virus up-regulated cell cycle and DNA maintenance and condensation pathways while down-regulated extracellular matrix, collagen metabolism, glutamate and ion transporters pathways. Zika virus infection only up-regulated eukaryotic translation machinery while down-regulated interferon pathways. Reactome and integration analysis revealed a common signature in down-regulation of innate immune response, antiviral response,

and inflammatory cytokines associated to interferon pathway for all arboviruses tested. Validation of interferon stimulated genes by reverse transcriptase quantitative polymerase chain reaction (RT-qPCR) corroborated our transcriptome findings. Altogether, our results showed a co-evolution in the mechanisms involved in the escape of arboviruses to antiviral immune response mediated by the interferon (IFN) pathway.

Keywords: Chikungunya, Mayaro, Oropouche, Zika, innate immunity, astrocytes

INTRODUCTION

Arthropod-borne viruses (*i.e.* arboviruses) comprehend a large group of viruses belonging to different families that are transmitted mainly by the bite of infected mosquitoes or ticks during the blood meal. As many of them are the etiological agents of relevant human pathologies, they pose a special threat in vulnerable countries around the world. Tropical countries of South America, such as Brazil, are specially in risk for arboviruses outbreaks due to the suitable warm weather, abundance of insect vectors, deforestation, high population concentration near forest areas, social-economical disparities, and overburden of the public healthcare system (Peña-García et al., 2017; Figueiredo, 2019; Medeiros and Vasconcelos, 2019). Many endemic outbreaks along the history, as well the recent introduction of arboviruses in Brazil, have risen the alarm of scientific and medical communities concerning the risk of new outbreaks, co-circulation of those viruses, and increasing of more severe cases (Metsky et al., 2017; Zanotto and Leite, 2018; Lorenz et al., 2019; Gutierrez et al., 2020). Viruses members of *Alphavirus*, *Orthobunyavirus*, and *Flavivirus* genus (*Togaviridae*, *Peribunyaviridae*, and *Flaviviridae* viral families, respectively) present a higher incidence in Brazil and has been associated to a plethora of clinically relevant outcomes, such as mild to debilitating fever, hemorrhagic fever, arthritis, microcephaly, and neurological disorders (Figueiredo, 2015; Santiago et al., 2015; Burt et al., 2017; Azeredo et al., 2018; Vernal et al., 2019; Brito Ferreira et al., 2020; Diagne et al., 2020; Gutierrez et al., 2020).

Alphaviruses as Chikungunya Virus (CHIKV) and Mayaro Virus (MAYV) circulate in Brazil, with many cases reported from Northern to Southeastern regions of the country (Carvalho et al., 2019; Lorenz et al., 2019; Naveca et al., 2019; Vasconcellos et al., 2019). They are enveloped viruses with single positive RNA (+) strand genome, flanked by 5' and 3' UTRs (untranslated regions). The genome is ~11.5 kb long and composed by two ORFs (open reading frame): the first one encodes the non-structural proteins nsP1-4 that plays a role in viral replication and host factors interaction and modulation, followed by a second ORF that encodes the structural proteins C (capsid), E3, E2, E1 (envelope glycoproteins) (Acosta-Ampudia et al., 2018; Frolov and Frolova, 2019; Levi and Vignuzzi, 2019). CHIKV are mainly transmitted by mosquito vectors from genera *Aedes* and MAYV is more restricted to sylvatic species of *Sabethes* and *Haemagogus*, reflecting on the epidemic pattern of CHIKV and in local MAYV circulation. Those alphaviruses cause a febrile illness, with common symptoms such as nausea, headache, rash, myalgia, and polyarthralgia. The arthralgia can persist for months after the acute infection, characterizing the main chronic incapacitating symptom of those infections. However, both viruses have been associated with more severe neurological manifestations, such as meningo-encephalitis, Guillain-Barré syndrome, acute disseminated encephalomyelitis (ADEM), and severe myelitis, with increasing reports of neuro-CHIKV in endemic areas such as Brazil (Bandeira et al., 2016; Balavoine et al., 2017; Khatri et al., 2018; Maria et al., 2018; Simon et al., 2018; Hameed and Khan, 2019; Silva et al., 2020).

Oropouche Virus (OROV) is an *Orthobunyavirus* responsible for many outbreaks, in Brazil and other South America countries (Elliott, 2014; De Regge, 2017). OROV genome is composed of three single strand negative RNAs (–) flanked by 5' and 3' UTRs: namely the S (small) RNA, a 961 nt long RNA that encodes the nucleocapsid protein N and the non-structural protein NSs; a 4.5 kb long M (medium) RNA that encodes the viral envelope glycoproteins Gn and Gc, and the non-structural protein NSm; and a 6.9 kb long L (large) RNA that encodes the viral RNA-dependent RNA polymerase (RdRp) (Travassos da Rosa et al., 2017; Sakkas et al., 2018). The midge *Culicoides paraensis* has been considered the main urban vector of OROV, although it was already isolated from other mosquitoes' vectors, including species from the genera *Aedes* and *Culex*. OROV is the causative agent of Oropouche Fever, a mild febrile illness that shares common symptoms with other arboviral fevers as moderate to high fever, headache, nausea and diarrhea, vomiting, dizziness, and myalgia. Photophobia is also a particular common symptom and, in some cases, OROV has been associated with neurological meningo-encephalitis outcomes (Bastos et al., 2012; Santos et al., 2014; Vernal et al., 2019).

Zika Virus (ZIKV) has raised global attention in the past few years as a potential threat to humans, mainly to pregnant women, due to the infection could promote severe neurological disorders and congenital fetal malformations in Brazil (Duffy et al., 2009). Those clinical outcomes were first described in the last outbreaks, in French Polynesia (2013) and with the arrival and spread of ZIKV throughout the Americas (2014) (Cao-Lormeau et al., 2016; Schuler-Faccini et al., 2016). ZIKV is a flavivirus with a genome composed of a single positive strand RNA of ~11 kb, flanked by 5' and 3' UTR regions coding a precursor polyprotein that is processed by viral and cellular protease to generate three structural proteins C (capsid), prM, and E (envelope) and seven non-structural proteins NS1, NS2A, NS2B, NS3, NS4A, NS4B, and NS5. The epidemics in South America between 2014 and 2016 brought light to the severe neurological manifestations of ZIKV infection, named

Congenital Zika Syndrome (CZS), that affects the nervous system and multiple organs of the developing fetus of infected pregnant women. The CZS comprehend a myriad of clinical neurological manifestations including microcephaly, hydrocephaly and lissencephaly as well as ventricular calcifications and arthrogryposis (congenital joints contracture) (Liang et al., 2019). In adults, ZIKV infection can also be associated with encephalitis, ADEM, and Guillain-Barré Syndrome (Bautista, 2019).

Despite all the description of neurological associated manifestations of arboviruses, the neurotropism of viruses such as MAYV and OROV is still elusive. CHIKV and ZIKV can infect central nervous system (CNS) cells such as: neurons, astrocytes, and microglia (Klein et al., 2019). Astrocytes play a pivotal role in the CNS and are highly associated with encephalitis caused by those viruses (Soung and Klein, 2018). Astrocytes are responsible for the maintenance of the Blood-Brain Barrier (BBB) interacting with the brain microvascular endothelial cells (BMECs) (Cardoso et al., 2010), secretion of proinflammatory cytokines (Voet et al., 2019), recruitment of T cells upon brain injury or infection (Zhang et al., 2008), regulation of synapses, and regulation of glutamate uptake (Olsen et al., 2015). Viral infections can induce apoptosis in neuronal cells and dysregulate astrocyte functions increasing the BBB permeability and neuroinvasion by up-regulating metalloproteinases expression (Wang et al., 2008; Ju et al., 2009; Yang et al., 2012), promoting injury derived from long-term astrocytic inflammatory response (Garber et al., 2018), and neurotoxicity by accumulation of extracellular glutamate (Cisneros and Ghorpade, 2012), which all together contributes to the encephalitis process.

Here, we present a comparative transcriptome study of human primary astrocytes cells infected with CHIKV, MAYV, OROV, or ZIKV describing the specific genes and pathways modulated by each virus and the integration of common pathways by system biology strategy. Human primary astrocytes were highly permissive to all viruses with consequent down-modulation of IFN and interferon-stimulated genes (ISGs) pathways as a viral escape strategy to the innate antiviral immune response.

MATERIALS AND METHODS

Primary Human Astrocyte Isolation

Adult primary human astrocytes were isolated from surgically resected anterior temporal lobe tissue, from patients selected for surgical treatment of temporal lobe epilepsy associated with hippocampal sclerosis. The selected patients were evaluated by video-electroencephalography monitoring with a 132-channel Nihon-Kohden® apparatus, and the ictal onset zone was concordant with neuroimaging and semiology data. The pathological tissue targeted in surgery for these cases is the gliotic hippocampus, and the anterior temporal lobe resection is used merely as a surgical pathway to the diseased area. All patients gave written consent to the study, and the procedures were in agreement with the Brazilian Ministry of Health Ethics Committee (Certification of Presentation for Ethical Approval, *CAAE*, submission number 69409617.9.0000.5258, decision number 2.792.114). As previously described (Sebollela et al., 2012), only healthy cortical tissue was used to produce astrocyte cultures. Experimental protocols were performed as described previously (Diniz et al., 2012; Dezonne et al., 2017). Briefly, tissues were washed in Dulbecco's Modified Eagle's Mediu (DMEM), mechanically dissociated, chopped into small (<2 mm3) pieces with a sterile scalpel, and incubated in 10 ml of 0.25% trypsin solution at 37°C for 10 min. After centrifugation for 10 min, the cell pellet was resuspended in DMEM/F-12 growth medium supplemented with 10% Fetal Calf Serum (FCS) and plated onto tissue culture plates in a humidified 5% CO_2, 95% air atmosphere at 37°C for 2 h in order to achieve adherence of microglial cells. The non-adherent astrocytes were transferred to other culture plates, previously coated with poly-L-lysine. Adherent astrocytes were allowed to grow by replacing the medium once a week. New passages of cells were generated by harvesting confluent astrocyte cultures using trypsin-EDTA (Ethylenediamine tetraacetic acid) solution (0.25% trypsin with EDTA; *Thermo Fisher Scientific*). Human astrocytes from up to the seventh passage and from two different donors were used in the study.

Cell Lines, Viruses, and Infections

Vero cells (*ATCC*, *CCL-81*) were maintained in DMEM (*Gibco*) and primary astrocytes were maintained in DMEM/F12 (*Gibco*), both supplemented with 10% v/v Fetal Bovine Serum (FBS) (*Gibco*) and 1% v/v of penicillin-streptomycin (10.000 U/ml-10.000 μg/ml) (*Gibco*). DMEM/F12 was also supplemented with 1% v/v of glutamine (200 mM, *Gibco*), 0.6% g/v of glucose (*Sigma-Aldrich*), and 0.13% g/v of sodium bicarbonate (*Sigma-Aldrich*). All cells were incubated at 37°C and 5% CO_2. CHIKV isolate BHI3745/H804709 (GenBank accession #KP164570.1), MAYV strain 4675 (*ATCC 66*, GenBank accession #MK070492.1), OROV strain BeAn19991 (GenBank accession #KP052852.1, #KP052851.1, #KP052850.1), and ZIKV strain PE/243 (GenBank accession #KX197192.1) were used to perform infection. Viral stocks used here are expressed as Plaque Forming Units/ml (CHIKV, 1.6×10^8 PFU/ml; MAYV, 7×10^7 PFU/ml; OROV, 2×10^6 PFU/ml; and ZIKV, 2.6×10^6 PFU/ml) and were propagated by serial passages in Vero cells by routine methods using DMEM. Astrocyte infections were performed at multiplicity of infection (MOI) 1 (2×10^5 cells/well) for all four viruses in 12-well plate during 1 h at 37°C and 5% CO_2 in medium without FBS, under biosafety level 3 conditions at a Biosafety Level-3 laboratory at Federal University of Rio de Janeiro. For each infection, uninfected cells from the same donor were used in a pairwise experiment. Virus titration was performed by plaque assay in Vero cells plated at 3×10^5 cells/well in 12-well plates 1 day prior to infection. After 1 h incubation with the virus, cells medium was replenished by DMEM supplemented with 1% v/v FBS, 1% v/v antibiotics, and 1% v/v carboxymethyl cellulose (CMC) (*Sigma-Aldrich*), and incubated at 37°C and 5% CO_2 during 2 days for CHKV and MAYV, and 5 days for OROV and ZIKV. Cells were fixed with

4% formaldehyde for 20 min at room temperature, washed in Phosphate Buffered Saline (PBS) (*Gibco*), and stained with 20% v/v ethanol-violet crystal solution for 15 min for visual counting. Astrocytes viability assay upon virus infection was evaluated by CellTiter-Blue (*Promega*) according to manufacturer's instructions. The fluorescence was measured at SpectraMax Paradigm Multi-Mode Detection Platform (*Molecular Devices*).

Flow Cytometry, Immunofluorescence, and Antibodies

Virus infectivity was evaluated using specific antibodies against viral proteins as follows. Briefly, astrocytes (2×10^5 cells/sample) were fixed with 4% paraformaldehyde for 20 min and permeabilized in 1% v/v Triton X-100 PBS solution. Blocking was performed in 5% v/v Donkey Serum (*Sigma-Aldrich)* PBS solution for 1h at 37°C. Primary antibodies for each virus were diluted as follows: for CHIKV was used 1:50 of mouse monoclonal J31F (*Thermo Fisher Scientific*), for MAYV was used 1:300 of mouse monoclonal anti-alphavirus E1 antibody (MAB8754, *Sigma-Aldrich*), for OROV was used 1:300 of mouse polyclonal anti-OROV antibody, and for ZIKV was used 1:300 of mouse monoclonal anti-NS1 antibody (Abcam, ab218546), all diluted in blocking solution at 37°C for 30 min. Cells were then washed thrice in PBS and incubated with 2 µg/ml *Donkey anti-mouse AlexaFluor 488* secondary antibody (*Thermo Fisher Scientific*) at 37°C for 30 min. After incubation with the secondary antibody, cells were washed and resuspended in PBS. Flow cytometry was performed using Accuri C6 cytometer (*BD Biosciences*). At least 10,000 gated events were counted per experimental replica at Fluorescein isothiocyanate (FITC) channel. Astrocytes specific markers were confirmed by immunofluorescence. For that, cells were fixed and permeabilized as described above, followed by blocking in PBS 3% Bovine Serum Albumin (BSA) (*Sigma-Aldrich*) and 5% Normal Goat Serum (NGS) (*Thermo Fisher Scientific*) for 1 h and followed by overnight incubation at 4°C with the primary antibodies. Primary antibodies were diluted in block solution as follows: 1:500 of rabbit anti-GFAP (Glial Fibrillary Acidic Protein) (*Dako, Glostrup, DK*), 1:200 of mouse anti-GS (Glutamine Synthetase) (*Merck-Milipore*), 1:200 of rabbit anti-GLAST(Glutamate Aspartate Transporter 1) (*Abcam*), and 1:200 of rabbit anti-GLT1 (Glutamate Transporter 1) (*Abcam*). Cells were washed with PBS and incubated for 2 h with 1:400 dilution of goat anti-rabbit or anti-mouse IgG *AlexaFluor 488*, or 1:1,000 dilution of goat anti-rabbit IgG *AlexaFluor 546* secondary antibodies (*Thermo Fisher Scientific*). Nuclei was stained with 4',6-Diamidino-2-Phenylindole, Dihydrochloride (DAPI) (*Sigma-Aldrich*). Cells were mounted with mounting medium (DakoCytomation) and imaged under a confocal microscope (Leica TCS SPE).

RNA Isolation, Quality Assessment, and RNA-Seq

Astrocytes were plated at 2×10^5 cells/well and infected at MOI 1 with either CHIKV, MAYV, OROV, or ZIKV. Eighteen h post-infection (hpi) for CHIKV, MAYV, and OROV or 48 hpi for ZIKV, cells were washed with PBS, trypsinized, centrifuged, and the pellet were used for RNA extraction. Six replicates of non-infected astrocytes and three replicates of infected astrocytes were used for each virus. Total cellular RNA was isolated using *RNeasy Mini kit* (*Qiagen*) according to manufacturer's instructions. RNA quantification was performed using *Qubit RNA HS Assay kit* and *Qubit 3 Fluorometer* (*Thermo Fisher Scientific*). Genomic DNA contamination was avoided by DNase treatment (TURBO DNA-free Kit, *Thermo Fisher Scientific*) before RNA-Seq and RT-qPCR validation. Only samples with *RNA integrity number* (RIN) ≥ 9 were used, as verified by *RNA 6000 Pico Kit* and *2100 Bioanalyzer* (*Agilent Technologies*). Ribossomal RNA was depleted using *Ribo-Zero Gold* (*Illumina*) and 200 ng of total RNA for each sample were used for library preparation with TruSeq Stranded Total RNA Library Prep (*Illumina*) according to manufacturer's instructions. RNA-seq were performed in 2 × 9 samples using *NextSeq 500/550 High Output v2 Kit (150 cycles)* (*Illumina*) in a NextSeq 550 platform (*Illumina*).

RNA-Seq Statistical Analysis

The RNA sequence files (fastq) were applied to the software BBDuk2 (https://jgi.doe.gov/data-and-tools/bbtools/bb-tools-user-guide/bbduk-guide) to trim low quality-related sequences (bellow Q30) and remove Illumina adapter-contaminant tags. The FASTQC (https://www.bioinformatics.babraham.ac.uk/projects/fastqc) reports the overall quality of the sequencing. The aligner HiSat2 (Kim et al., 2015) mapped the filtered reads to the human genome assembly GRCh38.p12 presented at the Ensembl database (https://www.ensembl.org/Homo_sapiens). The R/Bioconductor package Rsubread using the function of feature counts (Liao et al., 2019) performed the counting table of the mapped reads for the following statistical analysis. The R/Bioconductor package DESeq2 (Love et al., 2014) conducts the differential gene expression (DGE) test. It is also applied to the R/Bioconductor package apeglm (Zhu et al., 2019) to shrink log-fold change. The criteria of the adjusted p-value (corrected by false discovery rate—FDR) below 0.05 and log2 fold change (FC) above the absolute value of 1.0 was followed to classify genes as differentially expressed. The GOstats (Falcon and Gentleman, 2007) performed the Gene Ontology (GO) enrichment analysis. The package Pathview (Luo and Brouwer, 2013) visualizes the KEGG pathways and shows the associated genes. The ReactomePA package (Yu and He, 2016) leads the Reactome database analysis applying enrichment and allowing to create graphics. All the results and additional information about the RNAseq analysis were stored in the relational database PostgreSQL 12. The data can be easily accessed at the site: http://biotools.labinfo.lncc.br/astrocitovirus_data. The dataset used in our study is publicly available in SRA-NCBI (www.ncbi.nlm.nih.gov/sra), SRA accession PRJNA662366.

RT-qPCR Validation

Cells were seeded (2×10^5 cells/sample) and infected at MOI 1 as described above. The RNA was extracted and treated as described above at the indicated times points post infection and cDNA was produced using High Capacity cDNA Reverse Transcription Kit (*Thermo Fisher Scientific*) and 500 ng of RNA. Quantitative PCR was performed in three biological replicates

per condition using 20 ng of RNA input and *SYBR Green PCR Master Mix* (*Applied Biosystems*) on 7500 Fast Real-Time PCR System (*Thermo Fisher Scientific*) according to manufacturer's instructions. Hypoxanthine Phosphoribosyltransferase 1 (*HPRT1*) gene was used as normalization and pre-designed *PrimeTime* primers (*Integrated DNA Technologies*) were used for selected target genes according to manufacturer's instruction (for primers sequences see **Table S1**). Normalized gene expression was compared between experimental and mock non-infected conditions using Mann-Whitney test. Fold change and p-value for each comparison are presented using volcano plots.

RESULTS

Human Primary Astrocytes Are Permissive to Different Arboviruses Infection

In order to investigate the neuropathogenesis of arboviruses, we infected human cortical primary astrocytes (hAST) with CHIKV, MAYV, OROV, or ZIKV due to those cells multiple roles in maintaining the homeostasis of CNS and respond to infections. We confirmed the expression of classical astrocytes markers such as: glial protein (GFAP), glutamine synthetase (GS), and glutamate transporters (GLT1 and GLAST); which corroborates the same previously demonstrated astrocytic phenotype derived from induced pluripotent stem cells (iPSC) (**Figure 1A**) (Sebollela et al., 2012; Diniz et al., 2014; Garcia et al., 2014; Dezonne et al., 2017; Eugenio et al., 2018; da Silva et al., 2019). No cytopathic effects were observed in response to CHIKV, MAYV, and OROV until 48 h post infection (hpi) and until 72 h post ZIKV infection (**Figure 1B**). We also assured that at least 80% of cells were infected in that time span at MOI 1, as demonstrated by flow cytometry using antibodies against each virus protein (**Figure 1C**). Flaviviruses as ZIKV presents a slow replication rate compared to alphaviruses such as CHIKV and MAYV, taking more time to reach the same levels of replication. Even in the earliest time point (i.e., 6 hpi for CHIKV, MAYV, and OROV, and 24 hpi for ZIKV) 80% of cells were infected with all viruses tested, reinforcing that hAST is highly susceptible to different arboviruses infections, including MAYV and OROV, which have never been described before. To assure that infections were productive in astrocytes cells, we quantified the viral titer derived from the supernatant of infected cells. All arboviruses were able to produce infectious particles as evaluated by plaque assay (**Figure 1D**). Alphaviruses infection were more productive in those cells, followed by Orthobunyavirus and Flavivirus, respectively. CHIKV produced the highest titer: 1.52×10^6 PFU/ml as soon as 6 hpi, peaking 1.24×10^7 PFU/ml at 18 hpi; followed by MAYV and OROV, respectively. Again, ZIKV took additional 24 h to reach the same levels of virus production compared to the other viruses, confirming its lower replication rate in hAST compared with CHIKV, MAYV, and OROV (**Figure 1D**). With exception of ZIKV (Hamel et al., 2017; Kozak et al., 2017; Meertens et al., 2017; Chen et al., 2018;

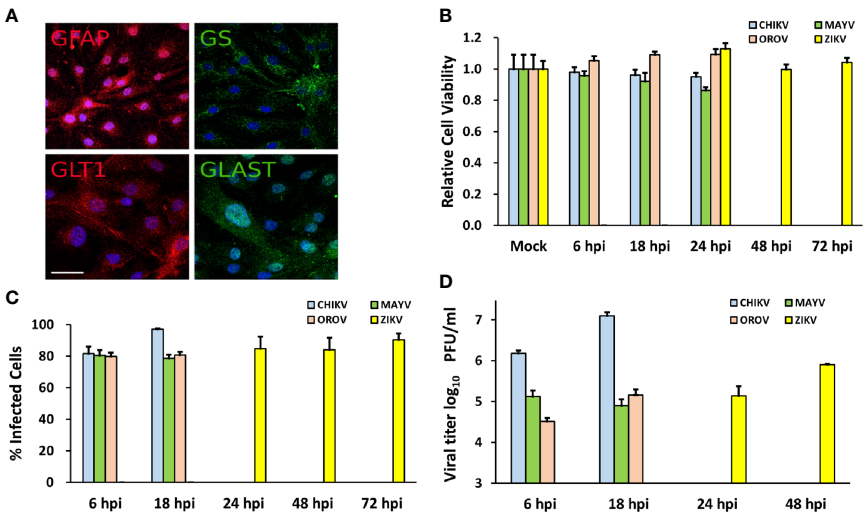

FIGURE 1 | Human primary astrocytes are permissive to CHIKV, MAYV, OROV, and ZIKV infection. Human primary astrocytes were isolated from brain surgery and infected with CHIKV, MAYV, OROV, or ZIKV at MOI 1 in different time points. **(A)** Immunofluorescence microscopy showing astrocytes specific cell markers: GFAP, Glial Fibrillary Acidic Protein, and GLT1, Glutamate Transporter 1 (both in red); GS, Glutamine Synthetase, and GLAST, Glutamate Aspartate Transporter 1 (both in green). Nuclei are stained with DAPI (cyan). Scale bar = 50 µm. **(B)** Cell viability post infection was measured at indicated time points. All infected cells were normalized by mock (uninfected) cells. **(C)** Virus infectivity was measured by flow cytometry using primary antibodies for virus proteins: CHIKV (J31F, anti-E1 antibody); MAYV (anti-alphavirus E1 antibody); OROV (anti-OROV serum), and ZIKV (anti-NS1 antibody) and plotted as percentage of infected cells in gated population. 10.000 events were recorded. **(D)** Viral production measured by plaque assay from the supernatants of infected cells. Viral titers were plotted as $\log_{10}$ Plaque Forming Units/ml. All the experiments were performed on three replicates from two independent experiments presented here as media and standard deviation (SD).

Stefanik et al., 2018; Sher et al., 2019), this is the first study to demonstrate the capacity of CHIKV, MAYV, and OROV to infect hAST, corroborating their potential as agents of neuro-associated outcomes.

Alphaviruses (CHIKV and MAYV) Replicate Better in Human Astrocytes Cells and Modulate a Higher Number of Cellular Genes

To analyze host cellular genes and pathways modulated upon infection, we performed a transcriptome-wide sequencing of uninfected (n = 6) and infected hAST with each virus (n = 3). Transcriptome analyses were performed at 18 hpi for CHIKV, MAYV, and OROV and 48 hpi for ZIKV, following the infection peak and absence of cytopathic effect for each virus (**Figures 1B, C**). We found an increasing number of RNA-seq reads that mapped on CHIKV and MAYV genomes compared with OROV and ZIKV suggesting that alphaviruses present higher replication rates in hAST (**Figure 2A**). As a reflection of higher titers of viral replication for alphaviruses, we found an increasing number of cellular genes dysregulated by CHIKV and MAYV compared with OROV and ZIKV (**Figure 2B** and **Table S2**).

Briefly, we found 3578, 4104, 2056, and 133 up-regulated genes for CHIKV, MAYV, OROV, and ZIKV infected cells, respectively, in contrast with 4883, 6388, 2802, and 415 down-regulated genes ($p \leq 0.05$ and at least 1 $\log_2$FC dysregulation over uninfected cells) (**Figures 2C–F**). Those results reflect an increasing impact in the modulation of differentially expressed genes (DEGs) that corroborates with the crescent genus-dependent viral replication as follows: flavivirus, orthobunyavirus, and alphaviruses. Altogether, the four viruses interfere with astrocyte gene expression down-regulating a higher number of genes compared with up-regulated genes (**Figures 2C–F** and **Table S2**).

CHIKV Interferes With Extracellular Matrix, N-Glycosylation, Translation, Cell Cycle, and Interferon Pathways

Our reactome analysis showed that CHIKV infected astrocytes presented an enrichment of up-regulated DEGs in pathways related to protein translation, post-translational modification of glycoproteins (N-linked glycosylation and metabolism of aminoacid), remodeling of extracellular matrix, protein translation, and targeting to endoplasmic reticulum (ER) membrane (**Figure 3A** and **Table S3**). The most significant genes associated with those pathways were: extracellular matrix/elastic fiber formation, as fibronectin 1 (*FN1*), fibulin (EGF Containing Fibulin Extracellular Matrix Protein 1, *EFEMP1*; Fibulin 1, *FBLN*), and elastin (Elastin Microfibril Interfacer 2, *EMILIN2*); amino acid activation, including aminoacyl-tRNA synthetases (Seryl-tRNA Synthetase, *SARS*; Bifunctional Aminoacyll-tRNA Synthetase, *EPRS*; Glycyl-tRNA Synthetase 1, *GARS*; Alanyl-tRNA Synthetase 1, *AARS*; Tyrosyl-Trna Synthetase 1, *YARS*); ER associated translation (Translocation Associated Membrane Protein 1, *TRAM1*; Protein Disulfide Isomerase Family A Member 3, *PDIA3*; Calreticulin, *CALR*; KDEL Endoplasmic Reticulum Protein Retention Receptor 1, *KDELR1*); and glycosylation (LEM Domain Containing 3, *MAN1*; Beta-1,4-Mannosyl-Glycoprotein 4-Beta-N-Acetylglucosaminyltransferase, *MGAT3*; Dolichyl-Diphosphooligosaccharide–Protein Glycosyltransferase Non-Catalytic Subunit, *DDOST*; Alpha-1,3-Mannosyl-Glycoprotein 2-Beta-N-Acetylglucosaminyltransferase, *MGAT1*). Translation factors are usually modulated by RNA viruses to promote viral protein production (Au and Jan, 2014). Indeed, the glycosylation of virus envelope proteins are crucial to increase CHIKV virulence and the up-regulation of genes related to asparagine N-linked glycosylation reinforces this hypothesis (Acharya et al., 2015; Lancaster et al., 2016). Cytoskeleton tubulin isoforms predominantly found in differentiated neurologic cells (Tubulin Alpha 1a, *TUBA1A*) and transmembrane vesicular protein involved in traffic (Transmembrane P24 Trafficking Protein 10, *TMED10*) were highly induced by CHIKV (**Figure 3A**), showing the importance of glycosylation pathways not only for envelope proteins, but also in virus assembly and budding.

CHIKV down-regulated pathways in astrocytes included: chromosome stability, DNA repair and maintenance; and cell cycle (in special, nucleosome assembly and prometaphase directed steps) (**Figure 4A** and **Table S4**). It is known that viruses always interfere with cell cycle to increase their own replication, promoting virus translation and avoiding apoptosis (Bressy et al., 2019; Caller et al., 2019). In fact, our reactome analysis of down-regulated pathways showed a consistent relationship within cell cycle controlling genes, indicating a possible G2 arrest phenotype (**Figure 4A**). Among the down-regulated genes were: genes from the cell division processes, as centrosome, centromere, and tubulin associated genes (Centrosomal Protein, *CEPs*; Centromere Protein, *CENPs*; and Tubulin, *TUBs*); cell cycle (Cell Division Cycle, *CDCs*); and chromosome stability, such as histones (*HISTs*) and DNA polymerase subunits *(POLs)* (**Figure 4A**). This goes in agreement with previous reports of CHIKV interfering with cell cycle in other cell models (Saxena et al., 2013; Thio et al., 2013). The *Aurora Kinase B* (*AURKB*), a chromosome segregation and cytokinesis promoting gene, was the most down-regulated gene in CHIKV infected cells (**Figure 4A**). Although the role of *AURKB* depletion has been controversially described for flaviviruses (Madejón et al., 2015; Pérez-Olais et al., 2019), its impact remains elusive for alphaviruses; nonetheless, it could be speculated as a reinforcer of G2 arrest.

MAYV Dysregulates the Same Profile of CHIKV Associated Pathways, With Prominent Down-Modulation of Interferon Response Genes

MAYV infection led to an enrichment and up-regulation of elastic fiber formation and N-glycosylation pathways, as in CHIKV infection; carbohydrates metabolism, platelet degranulation, and extracellular matrix organization (**Figure 3B**). The gene interactome modulated by MAYV is highly heterogeneous compared with CHIKV. Nonetheless, many

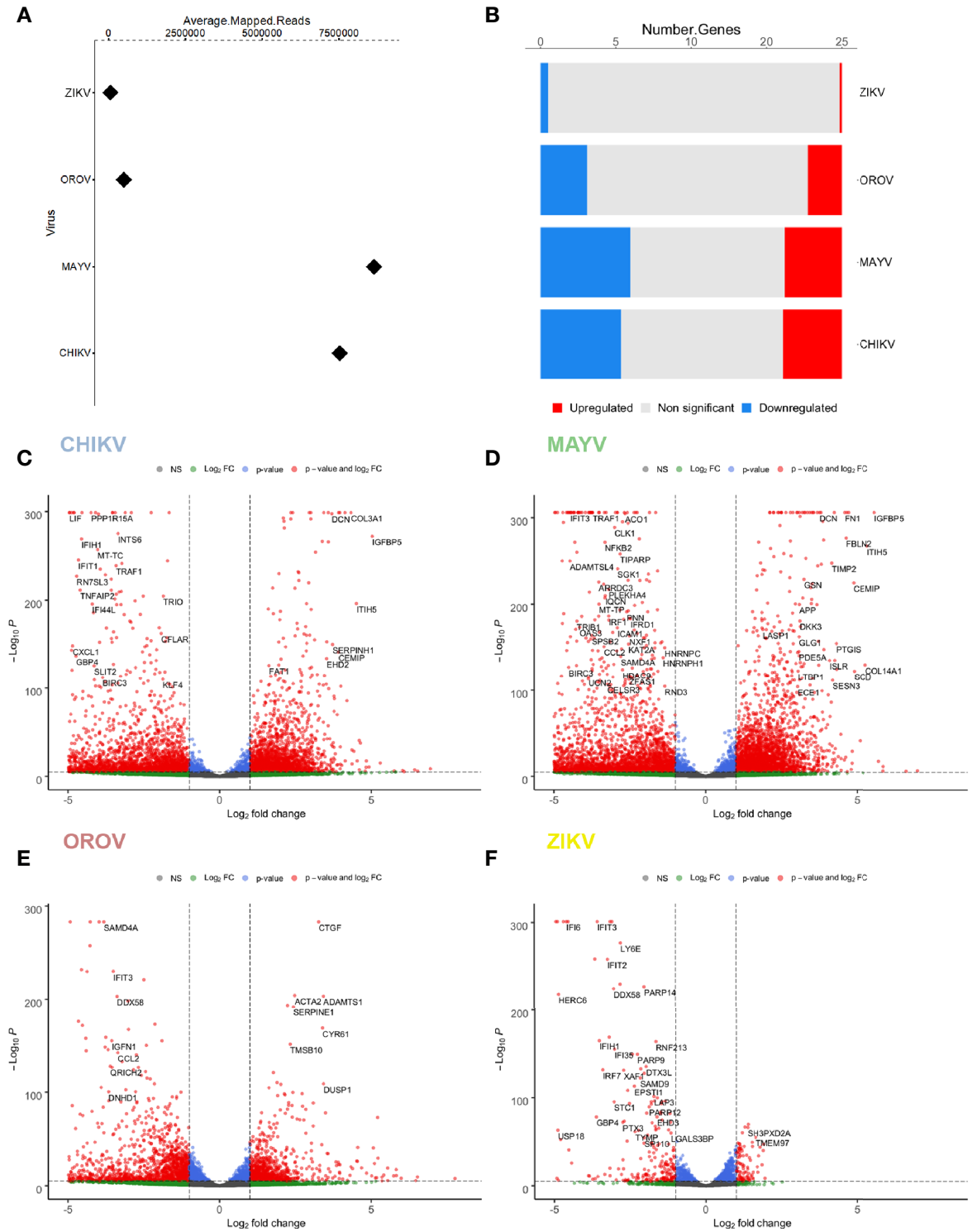

FIGURE 2 | Differentially expressed genes (DEGs) signature for CHIKV, MAYV, OROV, and ZIKV in human primary astrocytes. Signature of DEGs detected in RNA-Seq of infected (n = 3) over uninfected (n=6) cells. **(A)** Relative abundance (average of mapped reads) of viral RNA in hAST infected with CHIKV, MAYV, OROV, and ZIKV. **(B)** Number of up- and down-regulated genes for CHIKV, MAYV, OROV, and ZIKV with statistical significance ($p \leq 0.05$ and at least 1 $\log_2$FC dysregulation over uninfected cells). Volcano plots for the differentially expressed genes (DEGs) for CHIKV **(C)**, MAYV **(D)**, OROV **(E)**, and ZIKV **(F)**. RNA-seq from triplicates were performed from CHIKV, MAYV, and OROV infected cells 18 hpi and ZIKV infected cells 48 hpi. X-axis represents the $\log_2$ Fold Change of DEG relative to uninfected cells and Y-axis depicts significance. Hpi, hours post infection.

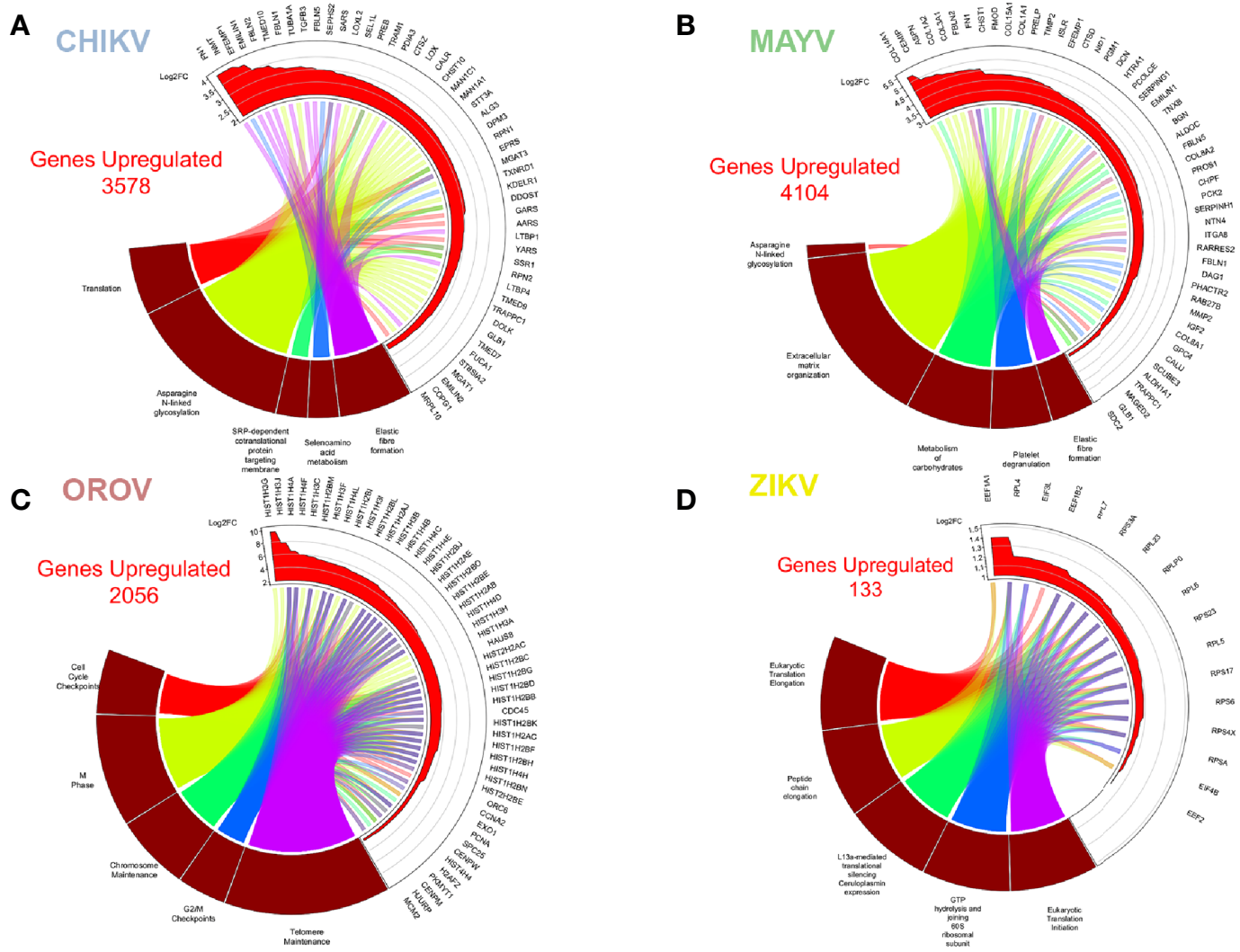

FIGURE 3 | Enriched up-regulated pathways in CHIKV, MAYV, OROV, and ZIKV infected astrocytes. Cell pathways with up-regulated genes in **(A)** CHIKV (18 hpi), **(B)** MAYV (18 hpi), **(C)** OROV (18 hpi), and **(D)** ZIKV (48 hpi) infected cells. Circus plot of Gene Set Enrichment Analysis (GSEA) of the five up-regulated most significantly enriched Reactome pathways (dark red sectors at the bottom of the circus plot) with the 50 associated DEGs. The 20 most significant up-regulated pathways are depicted. In the upper sector of the circus plot the genes were ordered by modulus of log2 Fold Change relative to uninfected cells.

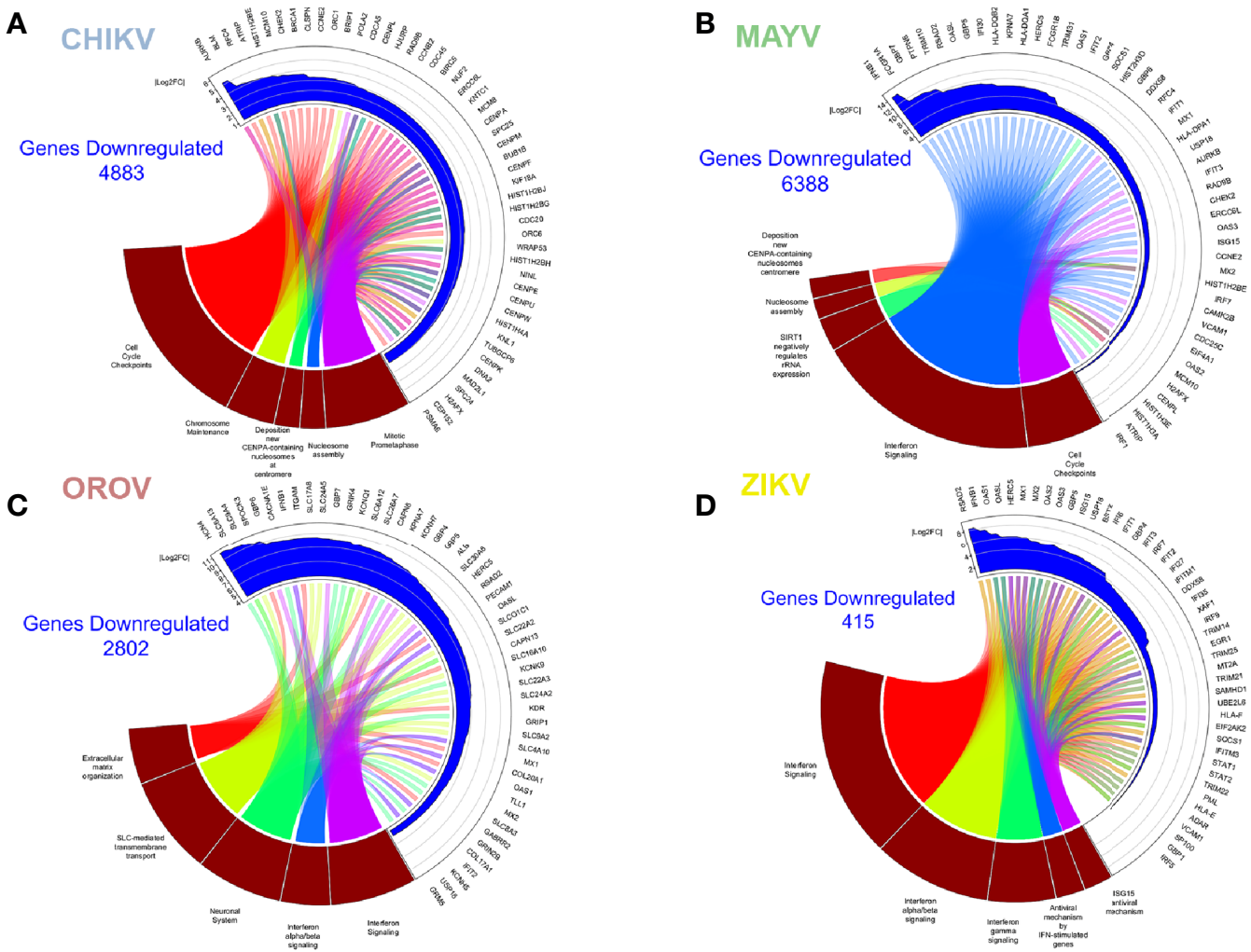

FIGURE 4 | Enriched down-regulated pathways in CHIKV, MAYV, OROV, and ZIKV infected astrocytes. Cell pathways with down-regulated genes in **(A)** CHIKV (18 hpi), **(B)** MAYV (18 hpi), **(C)** OROV (18 hpi), and **(D)** ZIKV (48 hpi) infected cells. Circus plot of Gene Set Enrichment Analysis (GSEA) of the five down-regulated most significantly enriched Reactome pathways (dark red sectors at the bottom of the circus plot) with the 50 associated DEGs. The 20 most significant down-regulated pathways are depicted. In the upper sector of the circus plot the genes were ordered by modulus of log2 Fold Change relative to uninfected cells.

genes related to elastic fiber/extracellular matrix pathways as integrins (*ITGA8*), fibronectin (*FN1*, also highly up-regulated in CHIKV infection), collagens (*COLs*), and metalloproteinases (*MMP2*) were up-regulated by MAYV (**Figure 3B**). Metalloproteinases are involved in extracellular matrix degradation and are associated with neurological outcomes in viral infections (Savarin et al., 2011; Shukla et al., 2016; Xing et al., 2017; Barkhash et al., 2018; Song et al., 2018; Chopra et al., 2019).

MAYV shares common down-modulated pathways with CHIKV, such as as Type-I interferon signaling (**Table S2**), nucleossome assembly and formation, and cell cycle (**Figure 4B** and **Table S4**). Reactome analysis showed two main clusters: (i) one related to interferon signaling and innate immunity, and (ii) another one related to pathways associated to cell cycle arrest, and repression of DNA replication and cell division (**Figure 4B**). MAYV and CHIKV, both alphaviruses, down-regulated common genes related to cell cycle and chromosome stability, such as *CENPs*, *HISTs*, and *CDCs* (**Figures 4A, B**). Indeed, interferon (*IFNB1*), interferon stimulated genes—ISGs (Interferon Induced Protein With Tetratricopeptide Repeats, *IFITs*; Radical S-Adenosyl Methionine Domain Containing 2, *RSAD2*; MX Dynamin Like GTPase 1, *MX1*; 2'-5'-Oligoadenylate Synthetase, *OASs*; Tripartite Motif Containing, *TRIMs*) and agonists of interferon response (DExD/H-Box Helicase 58, *DDX58*; Interferon Regulatory Factor 7, *IRF7*; Interferon Regulatory Factor 1, *IRF1*) were represented among the most down-regulated genes by MAYV, with higher fold change values, up to 12 (*IFNB1*) (**Figure 4B**).

OROV Infection Interferes With Ion Transport, Neuronal Synapses Regulation and Type-I Interferon Pathways, Contributing to Neuropathogenesis

OROV infection in human astrocytes, contrasting with alphaviruses infection, up-regulated pathways related to cell cycle, cell division, DNA maintenance and replication, and extracellular matrix remodeling (**Figure 3C** and **Table S3**). The opposite direction of pathways regulated by Alphavirus and Orthobunyavirus demonstrates the complexity and diversity in host factors modulation and may represent different strategies of virus replication. The pathway reactome corroborates the overall tendency in OROV infection, up-regulating pathways related to DNA condensation (mainly through the core H2, H3, and H4 histones), cell cycle checkpoints and G2 arrest, and telomere maintenance (**Figure 3C** and **Table S3**). Some proteins from related orthobunyaviruses were already demonstrated to have nuclear localization, interfering with cell cycle and hampering global cellular transcription through histone modification (Copeland et al., 2013; Gouzil et al., 2017). The genes in the reactome corroborated this hypothesis, as many histones, *CENPs*, and other G2/M step related proteins were up-regulated. The G2/M arrest could increase the availability of capped-mRNAs, which serves as primer donors for bunyaviruses translation: a process named cap-snatching. Corroborating our findings, and in contrast with bunyaviruses, alphaviruses can cap their own RNAs using nsP activities (Hopkins and Cherry, 2013) (**Figure 3C**).

Overall, the pathways found down-regulated by OROV in astrocytes corroborate the dysregulation of interferon response; highlighting genes with antiviral activities (*RSAD2*, also known as viperin; *OASL*; *OAS1*; *MX1/2*; *IFIT2*). However, unlike alphaviruses, OROV infection also down-regulated extracellular matrix remodeling genes [such as SPARC (Osteonectin), Cwcv And Kazal Like Domains Proteoglycan 3, *SPOCK3*, and Integrin Subunit Alpha M, *ITGAM*] and collagen metabolism pathways (Collagen Type XVII Alpha 1 Chain, *COL17A1*, and Collagen Type XX Alpha 1 Chain, *COL20A1*) (**Figure 4C** and **Table S4**). Moreover, OROV infection also down-modulates ion channels, transmembrane solute carriers, and synapses regulation pathways that play crucial roles in astrocytes functions. Genes related to potassium channels (Potassium Voltage-Gated Channel, *KCNs*, and Hyperpolarization Activated Cyclic Nucleotide Gated Potassium Channel 4, *HCN4*) and solute transporters from the family of Solute Carrier (*SLCs*) were the most representative clusters (**Figure 4C**) down-modulated by OROV. Recently, it was demonstrated that K^+ channels are up-regulated and therefore required for endosomal trafficking and high infectivity of bunyaviruses, corroborating our findings (Hover et al., 2016; Hover et al., 2018). SLC family of transporters includes Excitatory Amino Acid Transporter 1 (*EAAT1*, also known as*SLC1A3*/*GLAST*) and Excitatory Amino Acid Transporter 2 (*EAAT2*, also known as *SLC1A2*/*GLT1*), both glutamate transporters whose dysfunction have been implicated in increasing neurotoxicity driven by accumulation of extracellular glutamate (Legay et al., 2003; Wang et al., 2003; Moidunny et al., 2016). Those pathways, together with down-regulation of Type-I interferon signaling, could increase the neuropathological manifestations of OROV infection.

ZIKV Up-Regulated Eukaryotic and Viral Translation Pathways, and Down-Regulated Type-I Interferon Signaling Proteins

ZIKV infection modulated the least number of genes (133 up- and 415 down-regulated, respectively) compared with the other viruses. This observation is in agreement with the lower replication rates expected for flaviviruses compared with alphaviruses or orthobunyaviruses (**Figures 1B–D**). However, it is important to note that Asian derived strains (as the Brazilian one used here) have usually lower virulence and replication kinetics compared to African strains (Simonin et al., 2016; Hamel et al., 2017). Nonetheless, the most enriched up-regulated pathways upon ZIKV infection were viral mRNA translation, translation elongation, aminoacid synthesis, ribosomal assembly, and cap-dependent translation (**Figure 3D** and **Table S3**); all related to host translation machinery. All up-regulated genes were either eukaryotic initiation (*EIFs*) or elongation factors (*EEFs*), and ribosomal proteins (*RPSs*and *RPLs*) (**Figure 3D**). Most of the pathways down-regulated by ZIKV in astrocytes were related to interferon-induced antiviral

innate immune response (**Figure 4D** and **Table S4**). The clusterization of the pathways classified them into type I and II interferon signaling, and antiviral interferon-responsive genes (**Figure 4D**). Transcriptional factors related to interferon pathways were also down-modulated (*IRFs* and Signal Transducer And Activator of Transcription, *STATs*), reinforcing the relevance of ISGs in controlling ZIKV infection. As demonstrated by other cellular models, most genes down-regulated by ZIKV were ISGs: *RSAD2*, *IFITs*, Guanylate Binding Protein (*GBPs*), *MXs*, and *OASs* (**Figure 4D**). Cytoplasmatic RNA sensor (*DDX58*, also known as Retinoic Acid Inducible Gene I, *RIG-I*) and classical interferon induced antiviral genes that direct block virus replication at several steps (SAM And HD Domain Containing Deoxynucleoside Triphosphate Triphosphohydrolase 1, *SAMHD1*: RNA virus replication; *TRIMs*: virus uncoating; and Bone Marrow Stromal Cell Antigen 2, *BST2*: virus budding, respectively) were also down-modulated by ZIKV infection. All this scenario suggests that ZIKV establishes stable infection in astrocytes counteracting and down-modulating interferon pathway at several steps.

Viral Infection Leads to an Overall Down-Regulation of Innate Immunity Genes in Astrocytes

We performed RNA-seq integration to identify common pathways modulated by the four viruses. Only 9 up-regulated and 171 down-regulated DEGs were co-modulated by CHIKV, OROV, MAYV, and ZIKA (**Figures 5A, B**, respectively and **Table S5**). As expected, CHIKV and MAYV shared a higher number of up- (2,450) and down- (2,528) regulated genes among themselves compared with other viruses analyzed, suggesting a signature for alphaviruses (**Figures 5A, B**). Gene ontology analysis of the 171 common down-regulated genes indicated that most of those genes belongs to pathways related to virus

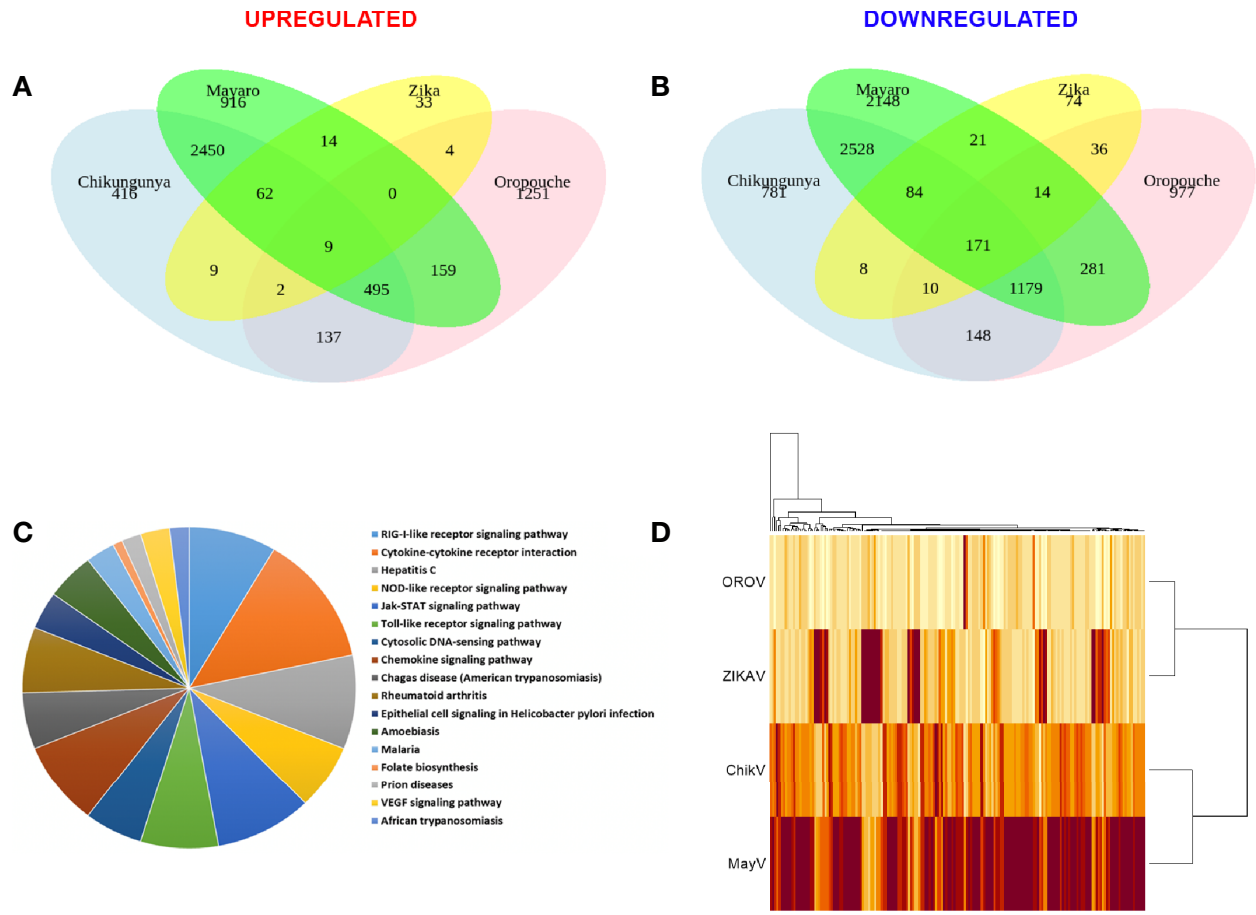

FIGURE 5 | Common differentially expressed genes (DEGs) signature for CHIKV, MAYV, OROV, and ZIKV in human primary astrocytes. Signature of DEGs detected in RNA-Seq of infected (n = 3) over mock uninfected (n = 6) hAST cells. Venn diagram showing the quantity of common and exclusive up-regulated **(A)** and down-regulated **(B)** genes found in the RNA-Seq dataset. Only DEGs with at least 1 $\log_2$ Fold Change and an adjusted P value ≤ 0.05 are shown. **(C)** Gene ontology by biological processes of 171 common down-regulated genes by all viruses (CHIKV, MAYV, OROV, and ZIKV). **(D)** Heatmap of the common up-regulated (9) and down-regulated (171) genes among all viruses here included. Dendrogram of Euclidian hierarchical clusterization among the four viruses are shown. Color scale represents baseMean (estimative of abundance) of up-regulated and down-regulated genes (light yellow represents lower and brown represents higher abundance).

RNA sensing (*RIG-1*), interferon signaling (including ISGs), cytokines and chemokine signaling, JAK-STAT (Janus Kinase-STAT), and Toll receptors signaling, suggesting a global modulation of innate immune response and inflammatory response in primary astrocytes infected by RNA viruses (**Figure 5C** and **Table S5**). The alphaviruses CHIKV and MAYV also cluster together when analyzing only the common dysregulated genes for all viruses, as expected (**Figure 5D**). Deeper analysis of the virus RNA sensing and interferon signaling pathways down-modulated by the four viruses identified antiviral genes triggered by interferon stimulation (ISGs), such as: *ISG15*, *MX1-2*, *DDX58*, CT And RLD Domain Containing E3 Ubiquitin Protein Ligase 5 (*HERC5*), *OAS*, Interferon Induced Protein With Tetratricopeptide Repeats (*IFIT*), Adenosine Deaminase RNA Specific (*ADAR*), *SAMHD1*, Interferon Induced Transmembrane Protein 1 (IFITM1), and *TRIMs*; all those already described for other RNA and DNA viruses infections.

We performed RT-qPCR of 16 common genes dysregulated for all viruses in order to validate our RNA-seq data (**Figure 6**). We selected genes belonging to cytoskeleton and motility (Actin Alpha 2, *ACTA2*) (Rockey et al., 2019), autophagy (Decidual Protein Induced By Progesterone, DEPP1), L-serine synthesis (Phosphoserine Aminotransferase 1, *PSAT1*) (Jiang et al., 2020), inflammatory response (Interleukin 7 Receptor, *IL7R*, and Major Histocompatibility Complex, Class II, DO Beta, *HLA-DOB*) (Inchley et al., 2013; Alsadeq et al., 2018), axonal guidance and neuropathology (Semaphorin 3A, *SEMA3A*) (Niclou et al., 2003; Yang et al., 2019), interferon induction (*DDX58*, Interferon Induced With Helicase C Domain 1, *IFIH1*, *TRIM25*, and *IRF7*), and interferon responsive/agonist genes with antiviral activity (*IFIT1*, *IFIT2*, *MX1*, *MX2*, *ISG15*, and *RSAD2*) (García-Sastre, 2017; Schoggins, 2019).

Overall, the majority of genes tested by RT-qPCR confirmed the dysregulation in expression found in our RNA-Seq data. To validate our findings, we also perform a kinetics of DEGs during virus infection at increasing time points. Most of the tested genes presented an increasing time-dependent down-regulation in later time points for each virus infection (6 and 18 hpi for CHIKV, MAYV, and OROV; 24 and 48 hpi for ZIKV) (**Figures 6A–D**, respectively). The only exceptions found were *DDX58*, *IFIT*, and *IFIH1*, that were down-modulated at early times of OROV infection and lose significance at later points. *PSAT1* and *ACTA2* were up-regulated in response to all viral infections, with higher induction in cells infected with CHIKV and MAYV at 18 hpi. Those genes are related to cell cytoskeleton and invasion, suggesting the virus dependence of intracellular trafficking to sustain replication. ISGs and immune response genes such as *IFIT1*, *IFIT2*, *IFIH1*, *MX1*, *MX2*, and *RSAD2* were highly down-regulated in response to all viruses at later time points of infection, confirming our transcriptome data. The intracellular virus RNA sensor *DDX58* (*RIG-I*) was down-regulated by all viruses, regardless the virus family, showing the central importance of this pathway in recognize viruses in infected cells and stimulate IFN and ISGs. Taken together, those results corroborate our transcriptome analysis showing that viruses from different families, such as CHIKV, MAYV, OROV, and ZIKV, interfere with antiviral and interferon mediated immune response to stablish an efficient and persistent infection in human primary astrocytic cells.

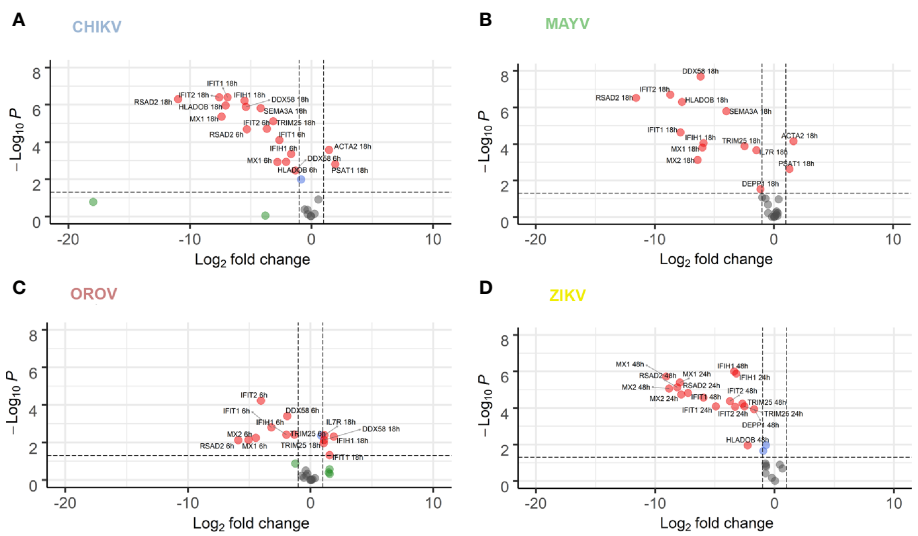

FIGURE 6 | RT-qPCR validation of 16 selected DEGs co-modulated by CHIKV, MAYV, OROV, and ZIKV. hAST cells were infected with MOI 1 of CHIKV **(A)**, MAYV **(B)**, OROV **(C)** at 6 and 18 hpi and ZIKV **(D)** at 24 and 48 hpi and RT-qPCR was performed at indicated time points and compared to uninfected cells (n = 3 for each time point and condition). Data denotes p-values (y-axis) and mean fold change (x-axis) of infected cells relative to uninfected cells for 16 DEGs selected from commonly modulated genes in RNA-Seq dataset. Gene expression was normalized by endogenous *HPRT1* levels. Red dots represent DEGs with at least 1 log2 Fold Change and P value ≤ 0.05. Blue dots represent DEGs with only P value ≤ 0.05. Green dots represent DEGs with at least 1 log2 Fold Change. Grey dots represent non-significant DEGs.

DISCUSSION

Arboviruses from *Togaviridae*, *Peribunyaviridae*, and *Flaviviridae* families account for the most epidemics and public health system burden in tropical countries, mainly in South and Central Americas. Although the most common manifestations of acute infection involve self-limiting febrile illness with mild to moderate symptoms, in some cases those viruses can invade CNS and generate severe neurological disorders, some of them with mimicking phenotypes of inflammatory autoimmune nervous system diseases. Even so, the mechanisms of neuropathogenesis and host interaction remain poorly understood for most of them. Here, we presented a comprehensive genome-wide transcriptome analysis of human primary astrocytes infected with CHIKV, MAYV, OROV, or ZIKV.

The capacity to infect and sustain productive infection in astrocytes was previously demonstrated for ZIKV (Hamel et al., 2017; Kozak et al., 2017; Meertens et al., 2017; Chen et al., 2018; Stefanik et al., 2018; Sher et al., 2019). However, to date there was no report of the same capacity for CHIKV, MAYV, and OROV in human cells. Those viruses were not only capable of infecting but demonstrated a more prominent viral production than ZIKV (**Figures 1C, D**, and **2A**). Those findings demonstrated that arthritogenic alphaviruses and OROV have also neurotropic potential like already described for encephalic alphaviruses (Ronca et al., 2016) and encephalic orthobunyaviruses (Evans and Peterson, 2019). Our RNA-Seq data showed an greater number of DEGs and different cellular pathways modulated by viruses presenting higher viremia since the beginning of infection (CHIK, MAYV e OROV), compared with lower replication rates of ZIKV in human primary astrocytes. Indeed, viruses from the same family, such as CHIKV and MAYV (*Togaviridae*), dysregulate a higher number of common genes and cellular pathways compared to OROV and ZIKV that belong to *Peribunyaviridae* and *Flaviviridae* families, respectively. Those results suggest that the virus genome RNA polarity (positive or negative) and replication strategy could differentially interfere with cellular pathways. However, the integration analysis showed a common signature of DEGs by those different viruses, reflecting the down-regulation of antiviral innate immune response and interferon pathway. This observation suggests that to stablish an efficient and productive infection in human primary astrocytes, viruses from different families need to counteract the cellular and immune response against the virus replication (**Figure 5**). *DDHX58* (*RIG-I*), a cytosolic dsRNA-sensing protein, was consistently down-regulated among all viruses. Besides, *IFN-β* was the second most commonly down-regulated gene to all viral infections (**Table S5**). Transcription factors that control interferon induction such as IRFs, mainly IRF-7, was also consistently down-regulated. Since the upstream RIG-I along with IRFs were down-regulated, it is reasonable to estimate the suppression in *IFN-β* and ISGs expression (**Figure 5** and **Table S5**). However, other RNA-Seq studies in mice (Wilson et al., 2017) and in human cohort (Soares-Schanoski et al., 2019) showed that CHIKV infection led to a global up-regulation in innate immunity and pro-inflammatory genes. The same was observed in neuroprogenitors cells infected with ZIKV (Lima et al., 2019). In case of ZIKV, though induced in neuroprogenitor cells, interferon, innate immunity, and inflammation were repressed in microglia (Tiwari et al., 2017) and dendritic cells (Sun et al., 2017), indicating cell type-specific dynamic in regulation of antiviral response. Aside of cell or tissue specific responses, another hypothesis that could explain contradictory innate immunity regulation among the datasets is the time-dependent effect on gene expression. In general, previous studies showed an induction of IFN pathways triggered by RIG-I recognition of virus double strand RNA structures at early points of RNA viruses infection, followed by antiviral and ISGs stimulation. Our results showed a common down-regulation of this pathway in later steps of CHIKV, MAYV, OROV, and ZIKV infection, possibly as a viral escape response to innate immune antiviral genes, allowing their replication in human astrocytic cells. A recent study using Vesicular Stomatitis Virus (VSV) as model proposed that a social evolution dictates the innate immunity evasion (Domingo-Calap et al., 2019). According to this model, IFN suppression is a costly mechanism, but it is evolutionary necessary to establish an efficient and productive infection. Due to high infectivity (about 80% of cell population) in astrocytes in a relative short time span (**Figure 1B**), it is likely that innate immunity suppression is occurring in early moments after infection. Among the various ISGs found, *IFITs* and *MXs* were also consistently down-regulated (**Figure 6**). From those, *RSAD2*, also known as Viperin, is a well characterized antiviral protein that already was demonstrated to restrict ZIKV (Panayiotou et al., 2018) and CHIKV (Teng et al., 2012), but its antiviral activity against MAYV and OROV was never described. Interestingly, in opposition to our results, in another study was demonstrated that *RSAD2* as wells as IFN response is induced upon ZIKV infection in mice astrocytes (Lindqvist et al., 2016); however, *RSAD2* regulation and its capacity to restrict viral replication in human astrocytes remain to be investigated.

Eukaryotic translation factors and ribosomal proteins were up-regulated upon ZIKV (**Figure 3D**), which reflects the viral recruitment of host translation machinery for viral protein synthesis (Walsh et al., 2013; Li, 2019). CHIKV and MAYV both up-regulated N-glycosylation machinery (**Figures 3A, B**), which, coupled with the up-regulation of translation machinery, suggests a multiple-step retargeting of host cell machinery towards viral protein synthesis and maturation (Acharya et al., 2015; Lancaster et al., 2016). Moreover, metalloproteinases, collagen and integrin genes were found up-regulated by CHIKV and MAYV infection but down-regulated in response to OROV infection (**Figure 4C**), suggesting opposite regulation of extracellular matrix and adhesion proteins between the two viral families. Regulation of CNS extracellular matrix by astrocytes is fundamental to neurogenesis, neuronal migration, and formation of new synapses (Cope and Gould, 2019); therefore, any unbalancing in the processes could lead to neuropathological effects.

Another interesting divergent regulation was observed between alphaviruses and OROV. Cyclin Dependent Kinase 1 (*CDK1*) and cyclins (*CCNs*) A, B, and E were down-regulated in CHIKV and

MAYV infection, while they were up-regulated in OROV infection (**Table S2**). Those results suggest a G1 cell cycle arrest induced by alphaviruses, and a G2/M arrest for OROV. G1 arrest was already described to be beneficial to viral production (Lundberg et al., 2018; Wang et al., 2018), which corroborates the overall recruitment of host translation and glycoprotein processing machineries in order to favor alphavirus production. Rift Valley Fever Virus (RVFV), a bunyavirus from *Phleboviridae* family, induces G2 cell cycle arrest for optimal cap-snatching and viral replication (Hopkins et al., 2013). It is possible that OROV induces the same cell cycle arrest in G2, what should be further investigated, since cap-snatching was never proved for OROV, but it is common for other bunyaviruses. OROV infection also down-regulated many membrane transporters and ion channels (**Figure 4C**). From those, *SLC1A2/EAAT2* (see **Table S2**) is implicated in glutamate uptake, suggesting that its down-regulation lead to accumulation of extracellular glutamate, which is often associated to neurotoxicity (Legay et al., 2003; Wang et al., 2003; Moidunny et al., 2016). We previously demonstrated the down-regulation of this gene in OROV infected HuH-7 cells and its possible association with upregulation of *miR-217* (Geddes et al., 2018). Taken together, that suggests that *EAAT2* might be a regulated target in OROV infected cells that could explain the neuropathogeny associated to the virus.

In this study, we provided an integrated genome-wide transcriptome analysis of human primary astrocytes, crucial cells responsible for a variety of functions in the CNS, infected with the emergent and clinically alarming human pathogens CHIKV, MAYV, OROV, and ZIKV. To our knowledge, this is the first study to present a transcriptome for MAYV and OROV, as well as first to present CHIKV transcriptome in cells from CNS. This work shed a light upon the mechanisms and viral-host interactions in the neuropathologies associated to those widespread human arboviruses regarding nervous system outcomes.

DATA AVAILABILITY STATEMENT

The datasets presented in this study can be found in online repositories. The names of the repository/repositories and accession number(s) can be found in the article/ **Supplementary Material**.

AUTHOR CONTRIBUTIONS

Conceptualization, VG and RA. Methodology, VG, OB, LR, JS, AV, and RA. Validation, VG, OB, and LC. Formal analysis, OB, FM, and RS. Investigation, VG, LC, FC, AG, AL, CF, and LD. Resources, CF, EN, AT, IA-M, SA-L, LR, JS, AV, and RA. Data curation, OB. Writing—original draft, VG, OB, and RA. Writing—review and editing, VG, OB, LC, FC, RS, IA-M, SA-L, LR, JS, AV, and RA. Visualization, VG, OB, AV, and RA. Supervision, AV and RA. Project Administration, AV and RA. Funding Acquisition, AV and RA. All authors contributed to the article and approved the submitted version.

FUNDING

This research was supported by FINEP (grant no. 01.16.0078.00) and the European Union's Horizon 2020 research and innovation program through the ZIKAlliance project (grant agreement no. 734548). VG is supported by CAPES under the grant number: 1545985. RA is supported by CNPQ 312688/2017-2, 439119/2018-9; FAPERJ 202.922/2018. AV is supported by CNPq (303170/2017-4) and FAPERJ (26/202.903/20). LC is supported by RABICO/CAPES Project 88887.333817/2019-00. IA-M is supported by CNPq (436933/2018-7) and FAPERJ (203.225/2017).

SUPPLEMENTARY MATERIAL

The Supplementary Material for this article can be found online at: https://www.frontiersin.org/articles/10.3389/fcimb.2021.641261/full#supplementary-material

Supplementary Table 1 | Oligonucleotides used in this study.

Supplementary Table 2 | All DEGs found in transcriptome for each virus.

Supplementary Table 3 | 50 most up-regulated genes for each virus used in Circoplot.

Supplementary Table 4 | 50 most down-regulated genes for each virus used in Circoplot.

Supplementary Table 5 | Common DEG among CHIKV, MAYV, OROV, and ZIKV.

REFERENCES

Acharya, D., Paul, A. M., Anderson, J. F., Huang, F., and Bai, F. (2015). Loss of Glycosaminoglycan Receptor Binding after Mosquito Cell Passage Reduces Chikungunya Virus Infectivity. *PLoS Negl. Trop. Dis.* 9, e0004139. doi: 10.1371/journal.pntd.0004139

Acosta-Ampudia, Y., Monsalve, D. M., Rodríguez, Y., Pacheco, Y., Anaya, J.-M., and Ramírez-Santana, C. (2018). Mayaro: an emerging viral threat? *Emerg. Microbes Infect.* 7, 163. doi: 10.1038/s41426-018-0163-5

Alsadeq, A., Lenk, L., Vadakumchery, A., Cousins, A., Vokuhl, C., Khadour, A., et al. (2018). IL7R is associated with CNS infiltration and relapse in pediatric B-cell precursor acute lymphoblastic leukemia. *Blood* 132, 1614–1617. doi: 10.1182/blood-2018-04-844209

Au, H. H. T., and Jan, E. (2014). Novel viral translation strategies. Wiley Interdiscip. *Rev. RNA* 5, 779–801. doi: 10.1002/wrna.1246

Azeredo, E. L., Dos Santos, F. B., Barbosa, L. S., Souza, T. M. A., Badolato-Corrêa, J., Sánchez-Arcila, J. C., et al. (2018). Clinical and Laboratory Profile of Zika and Dengue Infected Patients: Lessons Learned From the Co-circulation of Dengue, Zika and Chikungunya in Brazil. *PLoS Curr.* 10. ecurrents.outbreaks.0bf6aeb4d30824de63c4d5d745b217f5. doi: 10.1371/currents.outbreaks.0bf6aeb4d30824de63c4d5d745b217f5

Balavoine, S., Pircher, M., Hoen, B., Herrmann-Storck, C., Najioullah, F., Madeux, B., et al. (2017). Guillain-Barré Syndrome and Chikungunya: Description of All Cases Diagnosed during the 2014 Outbreak in the French West Indies. *Am. J. Trop. Med. Hyg.* 97, 356–360. doi: 10.4269/ajtmh.15-0753

Bandeira, A. C., Campos, G. S., Sardi, S. I., Rocha, V. F. D., and Rocha, G. C. M. (2016). Neonatal encephalitis due to Chikungunya vertical transmission: First report in Brazil. *IDCases* 5, 57–59. doi: 10.1016/j.idcr.2016.07.008

Barkhash, A. V., Yurchenko, A. A., Yudin, N. S., Ignatieva, E. V., Kozlova, I. V., Borishchuk, I. A., et al. (2018). A matrix metalloproteinase 9 (MMP9) gene

single nucleotide polymorphism is associated with predisposition to tick-borne encephalitis virus-induced severe central nervous system disease. Ticks Tick. *Borne. Dis.* 9, 763–767. doi: 10.1016/j.ttbdis.2018.02.010

Bastos, M., de, S., Figueiredo, L. T. M., Naveca, F. G., Monte, R. L., Lessa, N., et al. (2012). Identification of Oropouche Orthobunyavirus in the cerebrospinal fluid of three patients in the Amazonas, Brazil. *Am. J. Trop. Med. Hyg.* 86, 732–735. doi: 10.4269/ajtmh.2012.11-0485

Bautista, L. E. (2019). Zika virus infection and risk of Guillain-Barré syndrome: A meta-analysis. *J. Neurol. Sci.* 403, 99–105. doi: 10.1016/j.jns.2019.06.019

Bressy, C., Droby, G. N., Maldonado, B. D., Steuerwald, N., and Grdzelishvili, V. Z. (2019). Cell Cycle Arrest in G(2)/M Phase Enhances Replication of Interferon-Sensitive Cytoplasmic RNA Viruses via Inhibition of Antiviral Gene Expression. *J. Virol.* 93 (4), e01885–18. doi: 10.1128/JVI.01885-18

Brito Ferreira, M. L., Militão de Albuquerque, M., de, F. P., de Brito, C. A. A., de Oliveira França, R. F., Porto Moreira, Á. J., et al. (2020). Neurological disease in adults with Zika and chikungunya virus infection in Northeast Brazil: a prospective observational study. *Lancet Neurol.* 19, 826–839. doi: 10.1016/S1474-4422(20)30232-5

Burt, F. J., Chen, W., Miner, J. J., Lenschow, D. J., Merits, A., Schnettler, E., et al. (2017). Chikungunya virus: an update on the biology and pathogenesis of this emerging pathogen. *Lancet Infect. Dis.* 17, e107–e117. doi: 10.1016/S1473-3099(16)30385-1

Caller, L. G., Davies, C. T. R., Antrobus, R., Lehner, P. J., Weekes, M. P., and Crump, C. M. (2019). Temporal Proteomic Analysis of BK Polyomavirus Infection Reveals Virus-Induced G(2) Arrest and Highly Effective Evasion of Innate Immune Sensing. *J. Virol.* 93 (16), e00595–19. doi: 10.1128/JVI.00595-19

Cao-Lormeau, V.-M., Blake, A., Mons, S., Lastère, S., Roche, C., Vanhomwegen, J., et al. (2016). Guillain-Barré Syndrome outbreak associated with Zika virus infection in French Polynesia: a case-control study. *Lancet (London England)* 387, 1531–1539. doi: 10.1016/S0140-6736(16)00562-6

Cardoso, F. L., Brites, D., and Brito, M. A. (2010). Looking at the blood-brain barrier: molecular anatomy and possible investigation approaches. *Brain Res. Rev.* 64, 328–363. doi: 10.1016/j.brainresrev.2010.05.003

Carvalho, F. R., Medeiros, T., Vianna, R. A., de, O., Douglass-Jaimes, G., Nunes, P. C. G., et al. (2019). Simultaneous circulation of arboviruses and other congenital infections in pregnant women in Rio de Janeiro, Brazil. *Acta Trop.* 192, 49–54. doi: 10.1016/j.actatropica.2019.01.020

Chen, J., Yang, Y.-F., Yang, Y., Zou, P., Chen, J., He, Y., et al. (2018). AXL promotes Zika virus infection in astrocytes by antagonizing type I interferon signalling. *Nat. Microbiol.* 3, 302–309. doi: 10.1038/s41564-017-0092-4

Chopra, S., Overall, C. M., and Dufour, A. (2019). Matrix metalloproteinases in the CNS: interferons get nervous. *Cell. Mol. Life Sci.* 76, 3083–3095. doi: 10.1007/s00018-019-03171-9

Cisneros, I. E., and Ghorpade, A. (2012). HIV-1, methamphetamine and astrocyte glutamate regulation: combined excitotoxic implications for neuro-AIDS. *Curr. HIV Res.* 10, 392–406. doi: 10.2174/157016212802138832

Cope, E. C., and Gould, E. (2019). Adult Neurogenesis, Glia, and the Extracellular Matrix. *Cell Stem Cell* 24, 690–705. doi: 10.1016/j.stem.2019.03.023

Copeland, A. M., Altamura, L. A., Van Deusen, N. M., and Schmaljohn, C. S. (2013). Nuclear relocalization of polyadenylate binding protein during rift valley fever virus infection involves expression of the NSs gene. *J. Virol.* 87, 11659–11669. doi: 10.1128/JVI.01434-13

da Silva, V. D., de Faria, B. M., Colombo, E., Ascari, L., Freitas, G. P. A., Flores, L. S., et al. (2019). Design, synthesis, structural characterization and in vitro evaluation of new 1,4-disubstituted-1,2,3-triazole derivatives against glioblastoma cells. *Bioorg. Chem.* 83, 87–97. doi: 10.1016/j.bioorg.2018.10.003

De Regge, N. (2017). Akabane, Aino and Schmallenberg virus-where do we stand and what do we know about the role of domestic ruminant hosts and Culicoides vectors in virus transmission and overwintering? *Curr. Opin. Virol.* 27, 15–30. doi: 10.1016/j.coviro.2017.10.004

Dezonne, R. S., Sartore, R. C., Nascimento, J. M., Saia-Cereda, V. M., Romão, L. F., Alves-Leon, S. V., et al. (2017). Derivation of Functional Human Astrocytes from Cerebral Organoids. *Sci. Rep.* 7, 45091. doi: 10.1038/srep45091

Diagne, C. T., Bengue, M., Choumet, V., Hamel, R., Pompon, J., and Missé, D. (2020). Mayaro Virus Pathogenesis and Transmission Mechanisms. Pathog. *(Basel Switzerland)* 9, 738. doi: 10.3390/pathogens9090738

Diniz, L. P., Almeida, J. C., Tortelli, V., Vargas Lopes, C., Setti-Perdigão, P., Stipursky, J., et al. (2012). Astrocyte-induced synaptogenesis is mediated by transforming growth factor β signaling through modulation of D-serine levels in cerebral cortex neurons. *J. Biol. Chem.* 287, 41432–41445. doi: 10.1074/jbc.M112.380824

Diniz, L. P., Tortelli, V., Garcia, M. N., Araújo, A. P. B., Melo, H. M., Silva, G. S. S., et al. (2014). Astrocyte transforming growth factor beta 1 promotes inhibitory synapse formation via CaM kinase II signaling. *Glia* 62, 1917–1931. doi: 10.1002/glia.22713

Domingo-Calap, P., Segredo-Otero, E., Durán-Moreno, M., and Sanjuán, R. (2019). Social evolution of innate immunity evasion in a virus. *Nat. Microbiol.* 4, 1006–1013. doi: 10.1038/s41564-019-0379-8

Duffy, M. R., Chen, T.-H., Hancock, W. T., Powers, A. M., Kool, J. L., Lanciotti, R. S., et al. (2009). Zika virus outbreak on Yap Island, Federated States of Micronesia. *N. Engl. J. Med.* 360, 2536–2543. doi: 10.1056/NEJMoa0805715

Elliott, R. M. (2014). Orthobunyaviruses: recent genetic and structural insights. *Nat. Rev. Microbiol.* 12, 673–685. doi: 10.1038/nrmicro3332

Eugenio, M., Campanati, L., Müller, N., Romão, L. F., de Souza, J., Alves-Leon, S., et al. (2018). Silver/silver chloride nanoparticles inhibit the proliferation of human glioblastoma cells. *Cytotechnology* 70, 1607–1618. doi: 10.1007/s10616-018-0253-1

Evans, A. B., and Peterson, K. E. (2019). Throw out the Map: Neuropathogenesis of the Globally Expanding California Serogroup of Orthobunyaviruses. *Viruses* 11 (9), 794. doi: 10.3390/v11090794

Falcon, S., and Gentleman, R. (2007). Using GOstats to test gene lists for GO term association. *Bioinformatics* 23, 257–258. doi: 10.1093/bioinformatics/btl567

Figueiredo, L. T. M. (2015). The recent arbovirus disease epidemic in Brazil. Rev. *Soc Bras. Med. Trop.* 48, 233–234. doi: 10.1590/0037-8682-0179-2015

Figueiredo, L. T. M. (2019). Human Urban Arboviruses Can Infect Wild Animals and Jump to Sylvatic Maintenance Cycles in South America. *Front. Cell. Infect. Microbiol.* 9, 259. doi: 10.3389/fcimb.2019.00259

Frolov, I., and Frolova, E. I. (2019). Molecular Virology of Chikungunya Virus. *Curr. Top. Microbiol. Immunol.* 1–31. doi: 10.1007/82_2018_146

Garber, C., Vasek, M. J., Vollmer, L. L., Sun, T., Jiang, X., and Klein, R. S. (2018). Astrocytes decrease adult neurogenesis during virus-induced memory dysfunction via IL-1. *Nat. Immunol.* 19, 151–161. doi: 10.1038/s41590-017-0021-y

Garcia, C., Dubois, L. G., Xavier, A. L., Geraldo, L. H., da Fonseca, A. C. C., Correia, A. H., et al. (2014). The orthotopic xenotransplant of human glioblastoma successfully recapitulates glioblastoma-microenvironment interactions in a non-immunosuppressed mouse model. *BMC Cancer* 14, 923. doi: 10.1186/1471-2407-14-923

García-Sastre, A. (2017). Ten Strategies of Interferon Evasion by Viruses. *Cell Host Microbe* 22, 176–184. doi: 10.1016/j.chom.2017.07.012

Geddes, V. E. V., de Oliveira, A. S., Tanuri, A., Arruda, E., Ribeiro-Alves, M., and Aguiar, R. S. (2018). MicroRNA and cellular targets profiling reveal miR-217 and miR-576-3p as proviral factors during Oropouche infection. *PLoS Negl. Trop. Dis.* 12, e0006508. doi: 10.1371/journal.pntd.0006508

Gouzil, J., Fablet, A., Lara, E., Caignard, G., Cochet, M., Kundlacz, C., et al. (2017). Nonstructural Protein NSs of Schmallenberg Virus Is Targeted to the Nucleolus and Induces Nucleolar Disorganization. *J. Virol.* 91 (1), e01263–16. doi: 10.1128/JVI.01263-16

Gutierrez, B., Wise, E. L., Pullan, S. T., Logue, C. H., Bowden, T. A., Escalera-Zamudio, M., et al. (2020). Evolutionary Dynamics of Oropouche Virus in South America. *J. Virol.* 94, e01127–e01119. doi: 10.1128/JVI.01127-19

Hameed, S., and Khan, S. (2019). Rare variant of Guillain-Barré syndrome after chikungunya viral fever. *BMJ Case Rep.* 12 (4), e228845. doi: 10.1136/bcr-2018-228845

Hamel, R., Ferraris, P., Wichit, S., Diop, F., Talignani, L., Pompon, J., et al. (2017). African and Asian Zika virus strains differentially induce early antiviral responses in primary human astrocytes. *Infect. Genet. Evol. J. Mol. Epidemiol. Evol. Genet. Infect. Dis.* 49, 134–137. doi: 10.1016/j.meegid.2017.01.015

Hopkins, K., and Cherry, S. (2013). Bunyaviral cap-snatching vs. decapping: recycling cell cycle mRNAs. *Cell Cycle* 12, 3711–3712. doi: 10.4161/cc.26878

Hopkins, K. C., McLane, L. M., Maqbool, T., Panda, D., Gordesky-Gold, B., and Cherry, S. (2013). A genome-wide RNAi screen reveals that mRNA decapping restricts bunyaviral replication by limiting the pools of dcp2-accessible targets for cap-snatching. *Genes Dev.* 27, 1511–1525. doi: 10.1101/gad.215384.113

Hover, S., King, B., Hall, B., Loundras, E.-A., Taqi, H., Daly, J., et al. (2016). Modulation of Potassium Channels Inhibits Bunyavirus Infection. *J. Biol. Chem.* 291, 3411–3422. doi: 10.1074/jbc.M115.692673

Hover, S., Foster, B., Fontana, J., Kohl, A., Goldstein, S. A. N., Barr, J. N., et al. (2018). Bunyavirus requirement for endosomal K+ reveals new roles of cellular ion channels during infection. *PLoS Pathog.* 14, e1006845. doi: 10.1371/journal.ppat.1006845

Inchley, C. S., Osterholt, H. C. D., Sonerud, T., Fjærli, H. O., and Nakstad, B. (2013). Downregulation of IL7R, CCR7, and TLR4 in the cord blood of children with respiratory syncytial virus disease. *J. Infect. Dis.* 208, 1431–1435. doi: 10.1093/infdis/jit336

Jiang, J., Zhang, L., Chen, H., Lei, Y., Zhang, T., Wang, Y., et al. (2020). Regorafenib induces lethal autophagy arrest by stabilizing PSAT1 in glioblastoma. *Autophagy* 16, 106–122. doi: 10.1080/15548627.2019.1598752

Ju, S. M., Song, H. Y., Lee, J. A., Lee, S. J., Choi, S. Y., and Park, J. (2009). Extracellular HIV-1 Tat up-regulates expression of matrix metalloproteinase-9 via a MAPK-NF-kappaB dependent pathway in human astrocytes. *Exp. Mol. Med.* 41, 86–93. doi: 10.3858/emm.2009.41.2.011

Khatri, H., Shah, H., Roy, D., and Tripathi, K. M. (2018). A Case Report on Chikungunya Virus-Associated Encephalomyelitis. *Case Rep. Infect. Dis.* 2018, 8904753. doi: 10.1155/2018/8904753

Kim, D., Langmead, B., and Salzberg, S. L. (2015). HISAT: a fast spliced aligner with low memory requirements. *Nat. Methods* 12, 357–360. doi: 10.1038/nmeth.3317

Klein, R. S., Garber, C., Funk, K. E., Salimi, H., Soung, A., Kanmogne, M., et al. (2019). Neuroinflammation During RNA Viral Infections. *Annu. Rev. Immunol.* 37, 73–95. doi: 10.1146/annurev-immunol-042718-041417

Kozak, R. A., Majer, A., Biondi, M. J., Medina, S. J., Goneau, L. W., Sajesh, B. V., et al. (2017). MicroRNA and mRNA Dysregulation in Astrocytes Infected with Zika Virus. *Viruses* 9 (10), 297. doi: 10.3390/v9100297

Lancaster, C., Pristatsky, P., Hoang, V. M., Casimiro, D. R., Schwartz, R. M., Rustandi, R., et al. (2016). Characterization of N-glycosylation profiles from mammalian and insect cell derived chikungunya VLP. *J. Chromatogr. B Anal. Technol. Biomed. Life Sci.* 1032, 218–223. doi: 10.1016/j.jchromb.2016.04.025

Legay, V., Deleage, C., Beaulieux, F., Giraudon, P., Aymard, M., and Lina, B. (2003). Impaired glutamate uptake and EAAT2 downregulation in an enterovirus chronically infected human glial cell line. *Eur. J. Neurosci.* 17, 1820–1828. doi: 10.1046/j.1460-9568.2003.02621.x

Levi, L. I., and Vignuzzi, M. (2019). Arthritogenic Alphaviruses: A Worldwide Emerging Threat? *Microorganisms* 7 (5), 133. doi: 10.3390/microorganisms7050133

Li, S. (2019). Regulation of Ribosomal Proteins on Viral Infection. *Cells* 8 (5), 508. doi: 10.3390/cells8050508

Liang, B., Guida, J. P., Costa Do Nascimento, M. L., and Mysorekar, I. U. (2019). Host and viral mechanisms of congenital Zika syndrome. *Virulence* 10, 768–775. doi: 10.1080/21505594.2019.1656503

Liao, Y., Smyth, G. K., and Shi, W. (2019). The R package Rsubread is easier, faster, cheaper and better for alignment and quantification of RNA sequencing reads. *Nucleic Acids Res.* 47, e47. doi: 10.1093/nar/gkz114

Lima, M. C., de Mendonça, L. R., Rezende, A. M., Carrera, R. M., Aníbal-Silva, C. E., Demers, M., et al. (2019). The Transcriptional and Protein Profile From Human Infected Neuroprogenitor Cells Is Strongly Correlated to Zika Virus Microcephaly Cytokines Phenotype Evidencing a Persistent Inflammation in the CNS. *Front. Immunol.* 10, 1928. doi: 10.3389/fimmu.2019.01928

Lindqvist, R., Mundt, F., Gilthorpe, J. D., Wölfel, S., Gekara, N. O., Kröger, A., et al. (2016). Fast type I interferon response protects astrocytes from flavivirus infection and virus-induced cytopathic effects. *J. Neuroinflamm.* 13, 277. doi: 10.1186/s12974-016-0748-7

Lorenz, C., Freitas Ribeiro, A., and Chiaravalloti-Neto, F. (2019). Mayaro virus distribution in South America. *Acta Trop.* 198, 105093. doi: 10.1016/j.actatropica.2019.105093

Love, M. I., Huber, W., and Anders, S. (2014). Moderated estimation of fold change and dispersion for RNA-seq data with DESeq2. *Genome Biol.* 15, 550. doi: 10.1186/s13059-014-0550-8

Lundberg, L., Fontenot, J., Lin, S.-C., Pinkham, C., Carey, B. D., Campbell, C. E., et al. (2018). Venezuelan Equine Encephalitis Virus Capsid Implicated in Infection-Induced Cell Cycle Delay in vitro. *Front. Microbiol.* 9, 3126. doi: 10.3389/fmicb.2018.03126

Luo, W., and Brouwer, C. (2013). Pathview: an R/Bioconductor package for pathway-based data integration and visualization. *Bioinformatics* 29, 1830–1831. doi: 10.1093/bioinformatics/btt285

Madejón, A., Sheldon, J., Francisco-Recuero, I., Perales, C., Domínguez-Beato, M., Lasa, M., et al. (2015). Hepatitis C virus-mediated Aurora B kinase inhibition modulates inflammatory pathway and viral infectivity. *J. Hepatol.* 63, 312–319. doi: 10.1016/j.jhep.2015.02.036

Maria, A., Vallamkonda, N., Shukla, A., Bhatt, A., and Sachdev, N. (2018). Encephalitic presentation of Neonatal Chikungunya: A Case Series. *Indian Pediatr.* 55, 671–674. doi: 10.1007/s13312-018-1356-7

Medeiros, D. B. A., and Vasconcelos, P. F. C. (2019). Is the brazilian diverse environment is a crib for the emergence and maintenance of exotic arboviruses? *An. Acad. Bras. Cienc.* 91, e20190407. doi: 10.1590/0001-3765201920190407

Meertens, L., Labeau, A., Dejarnac, O., Cipriani, S., Sinigaglia, L., Bonnet-Madin, L., et al. (2017). Axl Mediates ZIKA Virus Entry in Human Glial Cells and Modulates Innate Immune Responses. *Cell Rep.* 18, 324–333. doi: 10.1016/j.celrep.2016.12.045

Metsky, H. C., Matranga, C. B., Wohl, S., Schaffner, S. F., Freije, C. A., Winnicki, S. M., et al. (2017). Zika virus evolution and spread in the Americas. *Nature* 546, 411–415. doi: 10.1038/nature22402

Moidunny, S., Matos, M., Wesseling, E., Banerjee, S., Volsky, D. J., Cunha, R. A., et al. (2016). Oncostatin M promotes excitotoxicity by inhibiting glutamate uptake in astrocytes: implications in HIV-associated neurotoxicity. *J. Neuroinflamm.* 13, 144. doi: 10.1186/s12974-016-0613-8

Naveca, F. G., Claro, I., Giovanetti, M., de Jesus, J. G., Xavier, J., Iani, F. C., et al. (2019). Genomic, epidemiological and digital surveillance of Chikungunya virus in the Brazilian Amazon. *PLoS Negl. Trop. Dis.* 13, e0007065–e0007065. doi: 10.1371/journal.pntd.0007065

Niclou, S. P., Franssen, E. H. P., Ehlert, E. M. E., Taniguchi, M., and Verhaagen, J. (2003). Meningeal cell-derived semaphorin 3A inhibits neurite outgrowth. *Mol. Cell. Neurosci.* 24, 902–912. doi: 10.1016/S1044-7431(03)00243-4

Olsen, M. L., Khakh, B. S., Skatchkov, S. N., Zhou, M., Lee, C. J., and Rouach, N. (2015). New Insights on Astrocyte Ion Channels: Critical for Homeostasis and Neuron-Glia Signaling. *J. Neurosci.* 35, 13827–13835. doi: 10.1523/JNEUROSCI.2603-15.2015

Panayiotou, C., Lindqvist, R., Kurhade, C., Vonderstein, K., Pasto, J., Edlund, K., et al. (2018). Viperin Restricts Zika Virus and Tick-Borne Encephalitis Virus Replication by Targeting NS3 for Proteasomal Degradation. *J. Virol.* 92 (7), e02054–17. doi: 10.1128/JVI.02054-17

Peña-García, V. H., McCracken, M. K., and Christofferson, R. C. (2017). Examining the potential for South American arboviruses to spread beyond the New World. Curr. Clin. *Microbiol. Rep.* 4, 208–217. doi: 10.1007/s40588-017-0076-4

Pérez-Olais, J. H., Ruiz-Jiménez, F., Calderón-Garcia, E. J., De Jesús-González, L. A., Hernández-Rivas, R., and Del Angel, R. M. (2019). The activity of Aurora kinase B is required for dengue virus release. *Virus Res.* 274, 197777. doi: 10.1016/j.virusres.2019.197777

Rockey, D. C., Du, Q., Weymouth, N. D., and Shi, Z. (2019). Smooth Muscle α-Actin Deficiency Leads to Decreased Liver Fibrosis via Impaired Cytoskeletal Signaling in Hepatic Stellate Cells. *Am. J. Pathol.* 189, 2209–2220. doi: 10.1016/j.ajpath.2019.07.019

Ronca, S. E., Dineley, K. T., and Paessler, S. (2016). Neurological Sequelae Resulting from Encephalitic Alphavirus Infection. *Front. Microbiol.* 7, 959. doi: 10.3389/fmicb.2016.00959

Sakkas, H., Bozidis, P., Franks, A., and Papadopoulou, C. (2018). Oropouche Fever: A Review. *Viruses* 10 (4), 175. doi: 10.3390/v10040175

Santiago, F. W., Halsey, E. S., Siles, C., Vilcarromero, S., Guevara, C., Silvas, J. A., et al. (2015). Long-Term Arthralgia after Mayaro Virus Infection Correlates with Sustained Pro-inflammatory Cytokine Response. *PLoS Negl. Trop. Dis.* 9, e0004104–e0004104. doi: 10.1371/journal.pntd.0004104

Santos, R. I., Bueno-Júnior, L. S., Ruggiero, R. N., Almeida, M. F., Silva, M. L., Paula, F. E., et al. (2014). Spread of Oropouche virus into the central nervous system in mouse. *Viruses* 6, 3827–3836. doi: 10.3390/v6103827

Savarin, C., Stohlman, S. A., Rietsch, A. M., Butchi, N., Ransohoff, R. M., and Bergmann, C. C. (2011). MMP9 deficiency does not decrease blood-brain barrier disruption, but increases astrocyte MMP3 expression during viral encephalomyelitis. *Glia* 59, 1770–1781. doi: 10.1002/glia.21222

Saxena, T., Tandon, B., Sharma, S., Chameettachal, S., Ray, P., Ray, A. R., et al. (2013). Combined miRNA and mRNA signature identifies key molecular players and pathways involved in chikungunya virus infection in human cells. *PLoS One* 8, e79886. doi: 10.1371/journal.pone.0079886

Schoggins, J. W. (2019). Interferon-Stimulated Genes: What Do They All Do? Annu. Rev. *Virol* 6, 567–584. doi: 10.1146/annurev-virology-092818-015756

Schuler-Faccini, L., Ribeiro, E. M., Feitosa, I. M. L., Horovitz, D. D. G., Cavalcanti, D. P., Pessoa, A., et al. (2016). Possible Association Between Zika Virus Infection and Microcephaly - Brazil. *MMWR Morb. Mortal. Wkly. Rep.* 65, 59–62. doi: 10.15585/mmwr.mm6503e2

Sebollela, A., Freitas-Correa, L., Oliveira, F. F., Paula-Lima, A. C., Saraiva, L. M., Martins, S. M., et al. (2012). Amyloid-β oligomers induce differential gene expression in adult human brain slices. *J. Biol. Chem.* 287, 7436–7445. doi: 10.1074/jbc.M111.298471

Sher, A. A., Glover, K. K. M., and Coombs, K. M. (2019). Zika Virus Infection Disrupts Astrocytic Proteins Involved in Synapse Control and Axon Guidance. *Front. Microbiol.* 10, 596. doi: 10.3389/fmicb.2019.00596

Shukla, V., Shakya, A. K., Shukla, M., Kumari, N., Krishnani, N., Dhole, T. N., et al. (2016). Circulating levels of matrix metalloproteinases and tissue inhibitors of matrix metalloproteinases during Japanese encephalitis virus infection. *Virusdisease* 27, 63–76. doi: 10.1007/s13337-015-0301-9

Silva, V. P., Costa, D. S., Carvalho, V.C.C.V.L., Garcês, T. C. C. S., Barros, E. L. T., Oliveira, J. S., et al. (2020). Peripheral polyneuropathy associated with Chikungunya virus infection. *J. Neurovirol.* 26, 122–126. doi: 10.1007/s13365-019-00782-7

Simon, F., Barnay, J.-L., and Lannuzel, A. (2018). The wide spectrum of neurological consequences of chikungunya disease. *Rev. Med. Virol.* 28, e1999. doi: 10.1002/rmv.1999

Simonin, Y., Loustalot, F., Desmetz, C., Foulongne, V., Constant, O., Fournier-Wirth, C., et al. (2016). Zika Virus Strains Potentially Display Different Infectious Profiles in Human Neural Cells. *EBioMedicine* 12, 161–169. doi: 10.1016/j.ebiom.2016.09.020

Soares-Schanoski, A., Baptista Cruz, N., de Castro-Jorge, L. A., de Carvalho, R. V. H., Santos, C. A., Dos, Rós, N., et al. (2019). Systems analysis of subjects acutely infected with the Chikungunya virus. *PLoS Pathog.* 15, e1007880. doi: 10.1371/journal.ppat.1007880

Song, J., Hu, Y., Li, H., Huang, X., Zheng, H., Hu, Y., et al. (2018). miR-1303 regulates BBB permeability and promotes CNS lesions following CA16 infections by directly targeting MMP9. Emerg. *Microbes Infect.* 7, 155. doi: 10.1038/s41426-018-0157-3

Soung, A., and Klein, R. S. (2018). Viral Encephalitis and Neurologic Diseases: Focus on Astrocytes. *Trends Mol. Med.* 24, 950–962. doi: 10.1016/j.molmed.2018.09.001

Stefanik, M., Formanova, P., Bily, T., Vancova, M., Eyer, L., Palus, M., et al. (2018). Characterisation of Zika virus infection in primary human astrocytes. *BMC Neurosci.* 19, 5. doi: 10.1186/s12868-018-0407-2

Sun, X., Hua, S., Chen, H.-R., Ouyang, Z., Einkauf, K., Tse, S., et al. (2017). Transcriptional Changes during Naturally Acquired Zika Virus Infection Render Dendritic Cells Highly Conducive to Viral Replication. *Cell Rep.* 21, 3471–3482. doi: 10.1016/j.celrep.2017.11.087

Teng, T.-S., Foo, S.-S., Simamarta, D., Lum, F.-M., Teo, T.-H., Lulla, A., et al. (2012). Viperin restricts chikungunya virus replication and pathology. *J. Clin. Invest.* 122, 4447–4460. doi: 10.1172/JCI63120

Thio, C. L.-P., Yusof, R., Abdul-Rahman, P. S. A., and Karsani, S. A. (2013). Differential proteome analysis of chikungunya virus infection on host cells. *PLoS One* 8, e61444. doi: 10.1371/journal.pone.0061444

Tiwari, S. K., Dang, J., Qin, Y., Lichinchi, G., Bansal, V., and Rana, T. M. (2017). Zika virus infection reprograms global transcription of host cells to allow sustained infection. *Emerg. Microbes Infect.* 6, e24. doi: 10.1038/emi.2017.9

Travassos da Rosa, J. F., de Souza, W. M., Pinheiro, F., de, P., Figueiredo, M. L., Cardoso, J. F., et al. (2017). Oropouche Virus: Clinical, Epidemiological, and Molecular Aspects of a Neglected Orthobunyavirus. *Am. J. Trop. Med. Hyg.* 96, 1019–1030. doi: 10.4269/ajtmh.16-0672

Vasconcellos, A. F., Silva, J. M. F., de Oliveira, A. S., Prado, P. S., Nagata, T., and Resende, R. O. (2019). Genome sequences of chikungunya virus isolates circulating in midwestern Brazil. *Arch. Virol.* 164, 1205–1208. doi: 10.1007/s00705-019-04174-4

Vernal, S., Martini, C. C. R., and da Fonseca, B. A. L. (2019). Oropouche Virus-Associated Aseptic Meningoencephalitis, Southeastern Brazil. *Emerg. Infect. Dis.* 25, 380–382. doi: 10.3201/eid2502.181189

Voet, S., Srinivasan, S., Lamkanfi, M., and van Loo, G. (2019). Inflammasomes in neuroinflammatory and neurodegenerative diseases. *EMBO Mol. Med.* 11 (6), e10248. doi: 10.15252/emmm.201810248

Walsh, D., Mathews, M. B., and Mohr, I. (2013). Tinkering with translation: protein synthesis in virus-infected cells. *Cold Spring Harb. Perspect. Biol.* 5, a012351. doi: 10.1101/cshperspect.a012351

Wang, Z., Pekarskaya, O., Bencheikh, M., Chao, W., Gelbard, H. A., Ghorpade, A., et al. (2003). Reduced expression of glutamate transporter EAAT2 and impaired glutamate transport in human primary astrocytes exposed to HIV-1 or gp120. *Virology* 312, 60–73. doi: 10.1016/S0042-6822(03)00181-8

Wang, P., Dai, J., Bai, F., Kong, K.-F., Wong, S. J., Montgomery, R. R., et al. (2008). Matrix metalloproteinase 9 facilitates West Nile virus entry into the brain. *J. Virol.* 82, 8978–8985. doi: 10.1128/JVI.00314-08

Wang, Z., Wang, Y., Wang, S., Meng, X., Song, F., Huo, W., et al. (2018). Coxsackievirus A6 Induces Cell Cycle Arrest in G0/G1 Phase for Viral Production. *Front. Cell. Infect. Microbiol.* 8, 279. doi: 10.3389/fcimb.2018.00279

Wilson, J. A. C., Prow, N. A., Schroder, W. A., Ellis, J. J., Cumming, H. E., Gearing, L. J., et al. (2017). RNA-Seq analysis of chikungunya virus infection and identification of granzyme A as a major promoter of arthritic inflammation. *PLoS Pathog.* 13, e1006155. doi: 10.1371/journal.ppat.1006155

Xing, Y., Shepherd, N., Lan, J., Li, W., Rane, S., Gupta, S. K., et al. (2017). MMPs/TIMPs imbalances in the peripheral blood and cerebrospinal fluid are associated with the pathogenesis of HIV-1-associated neurocognitive disorders. *Brain Behav. Immun.* 65, 161–172. doi: 10.1016/j.bbi.2017.04.024

Yang, C.-M., Lin, C.-C., Lee, I.-T., Lin, Y.-H., Yang, C. M., Chen, W.-J., et al. (2012). Japanese encephalitis virus induces matrix metalloproteinase-9 expression via a ROS/c-Src/PDGFR/PI3K/Akt/MAPKs-dependent AP-1 pathway in rat brain astrocytes. *J. Neuroinflamm.* 9, 12. doi: 10.1186/1742-2094-9-12

Yang, M., Wang, X., Fan, Y., Chen, Y., Sun, D., Xu, X., et al. (2019). Semaphorin 3A Contributes to Secondary Blood-Brain Barrier Damage After Traumatic Brain Injury. *Front. Cell. Neurosci.* 13, 117. doi: 10.3389/fncel.2019.00117

Yu, G., and He, Q.-Y. (2016). ReactomePA: an R/Bioconductor package for reactome pathway analysis and visualization. *Mol. Biosyst.* 12, 477–479. doi: 10.1039/C5MB00663E

Zanotto, P. M. A., and Leite, L. C. C. (2018). The Challenges Imposed by Dengue, Zika, and Chikungunya to Brazil. *Front. Immunol.* 9, 1964. doi: 10.3389/fimmu.2018.01964

Zhang, B., Chan, Y. K., Lu, B., Diamond, M. S., and Klein, R. S. (2008). CXCR3 mediates region-specific antiviral T cell trafficking within the central nervous system during West Nile virus encephalitis. *J. Immunol.* 180, 2641–2649. doi: 10.4049/jimmunol.180.4.2641

Zhu, A., Ibrahim, J. G., and Love, M. I. (2019). Heavy-tailed prior distributions for sequence count data: removing the noise and preserving large differences. *Bioinformatics* 35, 2084–2092. doi: 10.1093/bioinformatics/bty895

Conflict of Interest: The authors declare that the research was conducted in the absence of any commercial or financial relationships that could be construed as a potential conflict of interest.

frontiers in Cellular and Infection Microbiology

ORIGINAL RESEARCH
published: 18 March 2021
doi: 10.3389/fcimb.2021.645778

Targeted Transcriptomic Analysis of C57BL/6 and BALB/c Mice During Progressive Chronic *Toxoplasma gondii* Infection Reveals Changes in Host and Parasite Gene Expression Relating to Neuropathology and Resolution

Kristina V. Bergersen[1], *Ashli Barnes*[1], *Danielle Worth*[1], *Clement David*[1,2] *and Emma H. Wilson*[1*]

[1] Division of Biomedical Sciences, School of Medicine, University of California, Riverside, Riverside, CA, United States, [2] NanoString Technologies, Seattle, WA, United States

OPEN ACCESS

Edited by:
Federico Iovino,
Karolinska Institutet (KI), Sweden

Reviewed by:
Dong-Hui Zhou,
Fujian Agriculture and Forestry University, China
Joseph Stone Doggett,
VA Portland Health Care System, United States

***Correspondence:**
Emma H. Wilson
emmaw@ucr.edu

Specialty section:
This article was submitted to Parasite and Host, a section of the journal Frontiers in Cellular and Infection Microbiology

Received: 24 December 2020
Accepted: 23 February 2021
Published: 18 March 2021

Citation:
Bergersen KV, Barnes A, Worth D, David C and Wilson EH (2021) Targeted Transcriptomic Analysis of C57BL/6 and BALB/c Mice During Progressive Chronic Toxoplasma gondii Infection Reveals Changes in Host and Parasite Gene Expression Relating to Neuropathology and Resolution. Front. Cell. Infect. Microbiol. 11:645778. doi: 10.3389/fcimb.2021.645778

Toxoplasma gondii is a resilient parasite that infects a multitude of warm-blooded hosts and results in a lifelong chronic infection requiring continuous responses by the host. Chronic infection is characterized by a balanced immune response and neuropathology that are driven by changes in gene expression. Previous research pertaining to these processes has been conducted in various mouse models, and much knowledge of infection-induced gene expression changes has been acquired through the use of high throughput sequencing techniques in different mouse strains and post-mortem human studies. However, lack of infection time course data poses a prominent missing link in the understanding of chronic infection, and there is still much that is unknown regarding changes in genes specifically relating to neuropathology and resulting repair mechanisms as infection progresses throughout the different stages of chronicity. In this paper, we present a targeted approach to gene expression analysis during *T. gondii* infection through the use of NanoString nCounter gene expression assays. Wild type C57BL/6 and BALB/c background mice were infected, and transcriptional changes in the brain were evaluated at 14, 28, and 56 days post infection. Results demonstrate a dramatic shift in both previously demonstrated and novel gene expression relating to neuropathology and resolution in C57BL/6 mice. In addition, comparison between BALB/c and C57BL/6 mice demonstrate initial differences in gene expression that evolve over the course of infection and indicate decreased neuropathology and enhanced repair in BALB/c mice. In conclusion, these studies provide a targeted approach to gene expression analysis in the

brain during infection and provide elaboration on previously identified transcriptional changes and also offer insights into further understanding the complexities of chronic *T. gondii* infection.

Keywords: Toxoplasma, neuropathology, chronic infection, neurons, inflammation

INTRODUCTION

Toxoplasma gondii is a resilient parasite that infects ~ 10% of the population older than 6 years in the United States alone and more than 60% of populations in other countries worldwide (Prevention, 2018). Following a period of systemic infection and inflammation, the parasite is sequestered within neurons in the brain creating a lifelong infection. A requirement for continuous peripheral inflammation including CD4 and CD8 T cells is required to prevent uncontrolled parasite replication and potentially fatal pathology (Gazzinelli et al., 1992). Despite the presence of parasites and inflammation, infection is subclinical. However, infection in the immunocompromised can result in reactivation of the parasite, leading to Toxoplasmic encephalitis.

Previous data have reported broad transcriptomic changes in the brain of *T. gondii*-infected mice at both acute and chronic time points (Tanaka et al., 2013; Schneider et al., 2019; Hu et al., 2020; Li S. et al., 2020). However, these studies often focus on one specific time point in chronic infection, and they fail to explore transcriptomic changes that occur over the course of infection that are important to determine directional change. The parasite itself goes through genetic changes in order to convert from a fast-replicating tachyzoite during acute systemic infection to a cyst-forming bradyzoite during the early stage of chronic infection after crossing the blood brain barrier (Lachenmaier et al., 2011; Feustel et al., 2012; Hong et al., 2017; Radke et al., 2018). At this early chronic stage, CNS-resident cells begin actively recruiting peripheral immune cells in response to the presence of the parasite, which is still transitioning from tachyzoite to bradyzoite to cyst. As infection progresses and reaches the mid-chronic stage, cyst numbers stabilize as the majority of parasites in the brain are now slow-replicating bradyzoites. At this point in chronicity, both innate and adaptive peripheral immune cells have been in the brain for some time and are constantly maintaining the balance between pro- and anti-inflammatory cytokine production. In addition, subtle neuropathology is commonly seen as noted by changes in morphology and function of both infected and non-infected neurons and changes in glia (David et al., 2016; Graham et al., 2020). Control of infection is maintained for the lifetime of the host and pathology at this stage can vary depending on the genetics of the parasite as well as the background of the host (Liesenfeld et al., 1996; Denkers, 1999; Lee and Kasper, 2004; Lilue et al., 2013; Mukhopadhyay et al., 2020). These changes in parasite phenotype, host immune response, and neuropathology have yet to be fully explored in the context of progressive chronic infection.

The lifelong presence of cysts within neurons and continuous neuroinflammation gives ample opportunity for *T. gondii* infection to initiate significant changes in the brain. Indeed, many studies have demonstrated significant alterations in rodent behavior including attraction to cat urine postulated to be parasite manipulation to maximize the chances of return to the definitive host (Berdoy et al., 2000; Vyas et al., 2007; Boillat et al., 2020). Additionally, infected mice also show significant changes in behavior in an elevated plus maze (David et al., 2016). Such changes may be related to direct and indirect modulation of neurotransmitters including imbalances in excitatory and inhibitory signaling and the production of dopamine (Webster and McConkey, 2010; Prandovszky et al., 2011; Brooks et al., 2015; David et al., 2016; Ngô et al., 2017). However, the presence of the parasite is hard to unlink from the degree of neuroinflammation and any changes in host behavior is likely as much to do with cytokine signaling as the presence of the parasite (Boillat et al., 2020).

To address the complex interplay of infection, inflammation and neurochemistry, there have been several studies investigating transcriptional changes related to chronic CNS Toxoplasma infection. RNAseq analysis of *in vitro* cultured neurons, astrocytes, fibroblasts and skeletal muscle cells tested infection-induced changes in cell -specific transcriptomes and indicated a host-cell dependent genetic basis for spontaneous cyst formation in neurons and skeletal muscle cells (Swierzy et al., 2017). A comprehensive transcriptomic and proteomic study of human brain tissue including those congenitally infected suggests *T. gondii* infection alters neurodevelopment, plasticity, and disease association in various neural and immune networks (Ngô et al., 2017). Although not as clinically relevant, murine studies are robust and have recently underlined the dominance of immune changes in the brain following infection with oocysts of the Prugniaud strain revealing activated pathways of metabolism and biosynthesis at both acute and chronic stages of infection (Jia et al., 2013; Hu et al., 2020).

As with all infections, host genetic background plays an important role in disease and despite the ability of Toxoplasma to establish itself in almost all mammalian hosts, it has been known for some time that the development of disease is highly dependent on mouse strain, recently reviewed by Mukhopadhyay (Blackwell et al., 1993; Johnson et al., 2002; Resende et al., 2008; Mukhopadhyay et al., 2020). Indeed, continuous culturing of Toxoplasma strains *in vivo* rely upon resistant and susceptible strains of mice to maintain virulence and cyst formation, something vitally important to maintain life cycle competency (Goerner et al., 2020). Thus, in the common lab strains of mice, C57Bl/6 are susceptible to disease with greater parasite burden and inflammation while BALB/c mice are resistant to encephalitis dependent on MHC presentation of the antigen GRA6 (Jia et al., 2013; Tanaka et al., 2013; Ngô et al., 2017; Hu et al., 2020;

Li S. et al., 2020). These striking differences may provide an opportunity to model disease processes in the brain however little direct comparisons of the kinetics of this host response have been conducted.

In this study, we utilize a targeted approach to analysis gene expression and investigate >1500 genes associated with neurological and immunological processes by direct counting of RNA transcripts without the need for amplification *via* NanoString technology (Geiss et al., 2008). We determine the changes in these host genes over time in parallel with changes in *T. gondii* developmental-specific genes. In addition, we compare side-by-side gene expression changes between susceptible (C57BL/6) and resistant (BALB/c) mouse strains to address possible pathological versus repair signatures of neuroinflammation. Results demonstrate a dramatic shift in both previously demonstrated and novel gene expression relating to neuropathology, inflammation, and neuroinflammation as chronic infection progresses and reveals possible pathways of inflammation resolution.

MATERIALS AND METHODS

Animals and Infections

Animals. All research was conducted in accordance with the Animal Welfare Act, and all efforts were made to minimize suffering. All protocols were approved by the Institutional Animal Care and Use Committee (IACUC) of the University of California, Riverside. Female WT C57BL/6 and BALB/c mice were obtained from Jackson Laboratories and were maintained in a pathogen-free environment in accordance with IACUC protocols at the University of California Riverside.

Infections. The ME49 strain of *T. gondii* was maintained in cyst form by continuous passaging in SW and CBA background mice. Female 6-8 week old WT C57BL/6 and WT BALB/c mice were infected with 10 ME49 cysts per mouse in 200µl of sterile 1x PBS solution *via* intraperitoneal (IP) injection. Naïve controls received 200µl of sterile 1x PBS solution *via* intraperitoneal (IP) injection. This infection protocol regularly leads to ~3000 cysts in the brains of infected mice by 4 weeks post infection (Goerner et al., 2020).

DNA Extraction and Parasite Burden Quantification

Parasite burden in brain was quantified as previously described (Goerner et al., 2020). Briefly, DNA from naïve and 2, 4, and 8-week infected half brains of C57BL/6 (n=4/group) and BALB/c (n=5/group) mice was extracted and purified using a High Pure PCR Template Prep Kit (Roche). DNA concentration of each sample was determined via NanoDrop, and all DNA was normalized to 12.5ng/µl before amplification. Parasite burden was measured by amplifying the B1 gene of *T. gondii* by RT PCR.

RNA Extraction

RNA from brain lysate of naïve, 2 week infected, 4 week infected, and 8 week infected C57BL/6 and BALB/c mice (n=3 for all groups) was collected using Trizol extraction method. At each time point, mice were sacrificed and perfused intracardially with 20mL of sterile 1x PBS. Whole brain was dissected and homogenized in 1mL Trizol. Phase separation was completed by adding 200µl of chloroform and incubating at room temperature for 2-3 minutes. Samples were centrifuged at 12,000xg for 15 minutes at 4°C, and upper aqueous phase was collected followed by RNA precipitation using 500µl isopropyl alcohol. Samples were incubated at room temperature for 10 minutes followed by centrifugation. RNA pellet was washed with 1mL of 75% ethanol twice. All supernatant was discarded and RNA pellet was dissolved in 100µl of nuclease free water. RNA concentration for each sample was determined using a NanoDrop 2000, and RNA samples normalized to a concentration of 10ng/µL in molecular grade water.

NanoString nCounter Gene Expression Assays and Analysis

Gene Expression Assays. nCounter gene expression assays (NanoString Technologies) were performed for each of the following NanoString panels: Neuropathology, Neuroinflammation, and Inflammation+CustomizedPLUS covering a total of 1530 targeted genes including 10 parasite-specific genes: *ROP18, GDA1/CD39, ADF, GRA12, SRS22A, TUBA1, SRS35A, SRS44, BAG1*, and *LDH2* (Geiss et al., 2008). *T. gondii* genes included in custom PLUS codeset were selected based on the percent expression in tachyzoite and bradyzoite growth stages (90% expression in one stage and 0% in other stage) using previous studies differentiating growth stages and ToxoDB (Goerner et al., 2020). Briefly, panel codeset probes were hybridized with 150ng of total RNA per brain over 18hr at 65C according to NanoString protocol. Inclusion of a customized PLUS codeset in the Inflammation panel required additional Reporter and Capture Plus codesets to be added during the hybridization reaction (NanoString User Manual C0019-08). Hybridized RNA was then diluted in molecular grade water and loaded into nCounter SPRINT cartridge (NanoString), placed into nCounter SPRINT Profiler, and quantified. RNA-conjugated probes were counted *via* NanoString Sprint Profiler technology.

nSolver and Advanced Analysis

Results from each panel were merged into one data file for comparative analysis, normalized in nSolver following best practices, and analyzed using nSolver and Advanced Analysis software according to previously published protocols (Danaher et al., 2017). nSolver-generated heat maps were created using normalized (merged) data and agglomerative clustering, a bottom-up form of hierarchical clustering (NanoString User Manual C0019-08). For Advanced Analysis, normalized merged data was used (NanoString User Manual 10030-03). Differential expression (DE) analysis was performed to identify specific targets that exhibit significantly increased or decreased expression in response to naïve control values or, in the case of BALB/c C57BL/6 comparison, to C57BL/6 control values at each time point. Gene set analysis was run to determine the change in direction of regulation within each pre-defined gene set relative

to naïve controls. Global significance scores, a summary T-statistic used to measure change (NanoString User Manual 10030-03) were calculated, and the directed global significance scores were expressed *via* heatmap. Cell type profiling module analysis was conducted to determine the relative abundance in classically activated cell types during infection using genes assigned to each cell type: T cells (*CD3e, CD6, CD3g, TRAT1*, and *CD3d*), CD8+ T cells (*CD8a*), macrophages (*CD68* and *CD84*), and microglia (*GPR84, LRRC25, IRF8, NCF1, TNF, TLR2*, and *TNF.1*). NanoString cell type profiling is a validated method to measure relative abundance of up to 24 different immune cell types, with high concordance to flow cytometry (Danaher et al., 2017). Pathway analysis was also conducted to determine overall changes in pathways based on the first principal component of the targets within a pathway as annotated by NanoString (NanoString User Manual 10030-03). Direction of pathway change (up- or downregulated) was determined by cross referencing the pathway score with the corresponding volcano plot for that pathway. Summary pathway score plot colors are based on calculated scores and are represented as downregulation (blue) to upregulation (orange). Statistical significance was determined using R software. All data are available on Gene Expression Omnibus (GEO).

Separate Statistical Analyses

Normalized Log_2 scores for *T. gondii*-specific genes were used in fold changes analysis of tachyzoite-associated genes and bradyzoite-associated genes compared to naïve controls in Prism. In addition, results from cell type profiling modules were placed into Prism and evaluated at each time point. Violin plots were created in a similar fashion by analyzing normalized Log_2 scores of specific probes to show the rounded distribution of data. Statistical significance was determined by 2-tailed, unpaired Student's *t*-test and One-Way ANOVA with multiple comparisons (p-value < 0.05).

RESULTS

Chronic *Toxoplasma gondii* Infection Stimulates a Dramatic Shift in Gene Expression as Infection Progresses From Early to Late Chronic Stages

To determine broad transcriptomic changes that occur over the course of infection, RNA from infected C57BL/6 mouse brains was harvested at day 14, 28 and 56 days post infection (dpi) representing time points associated with transitionary, stable and late chronic infection respectively. RNA was hybridized with NanoString panel-specific codesets using two panels of genes specific for inflammation and neuropathology, and RNA-conjugated probes were counted *via* NanoString Sprint Profiler technology. Resulting gene expression changes compared to calculated control z-scores are demonstrated in **Figure 1**. Merged data analysis of NanoString neuropathology, neuroinflammation, inflammation, and a Toxoplasma-specific custom codeset probes using basic nSolver software demonstrate dramatic shifts in gene expression (**Figure 1A**). The majority of genes relating to neuropathology, neuroinflammation, and inflammation switch completely from low expression (blue) compared to control z-scores in an uninfected state to high expression (orange) by late chronic infection, signifying an 8-10 fold change in expression. This significant switch is seen almost in entirety by the mid-chronic stage of infection when cysts are prevalent in the brain. Contrastingly, a multitude of gene expression changes are still occurring at the early chronic stage correlating with tachyzoite entry and active cyst formation (Dupont et al., 2012; Cabral et al., 2016; Mendez and Koshy, 2017). Biological replicates in each time point generally exhibit close clustering with 14dpi showing the greatest variation in line with a transitioning state between acute and chronic infection (**Figure 1B**).

Consistent with a powerful infection in an otherwise immune privileged site, differential expression analysis reveals that at all timepoints, the majority of genes significantly altered by infection are upregulated as compared to naïve controls (**Figures 1C–E**; **Supplementary Table 1**). At 14dpi, the majority of genes that experience changes in expression undergo significant upregulation despite CNS infection not being fully established. At this early stage, many genes exhibit fold changes up to 7-fold (*CCL5, CD74*) and this only increases at later chronic timepoints, reaching up to 8-fold change at 28dpi and up to 10-fold change at 56dpi.

Comparison of genes that are significantly altered as determined by differential expression analysis reveals both conserved gene expression changes across all timepoints as well as time point-specific changes (**Figure 1E**). At 28dpi (light green), there are 202 genes that have significant changes in expression (22% of total) that are specific to this mid-chronic stage of infection. This number is significantly greater than the stage-specific changes seen at 14dpi (dark blue; 4 genes = 0.4%) and 56dpi (dark purple; 11 genes = 1.2%). There are no shared differentially expressed genes (DEGs) between the early (14dpi) and late (56dpi) chronic stages and very few shared genes (light blue, 4 genes = 0.4%) between the early (14dpi) and mid- (28dpi) chronic stages of infection. Consistent with establishment of infection, mid- (28dpi) and late (56dpi) chronic stages share a far greater number of DEGs (light purple, 237 genes = 26% of total), signifying a similar infection phenotype between later stages of infection as chronicity is firmly established and maintained. Of all genes expressed above background levels included in the merged analysis, 454 genes (grey, 49.8% of total) are significantly altered at all timepoints.

Toxoplasma gondii Stage-Specific Gene Expression Correlates With Host Gene Changes

Toxoplasma goes through several phases of development and in the intermediate mammalian host, two stages dominate: i) a fast-replicating tachyzoite responsible for dissemination, cell lysis, and acute pathologies and ii) the bradyzoite that replicates slowly, and forms cysts in neurons (Montoya and Liesenfeld, 2004). How these classical Toxoplasma signatures change in relation to the host transcriptome over the course of *in vivo* infection has not been explored in depth. The broad significant

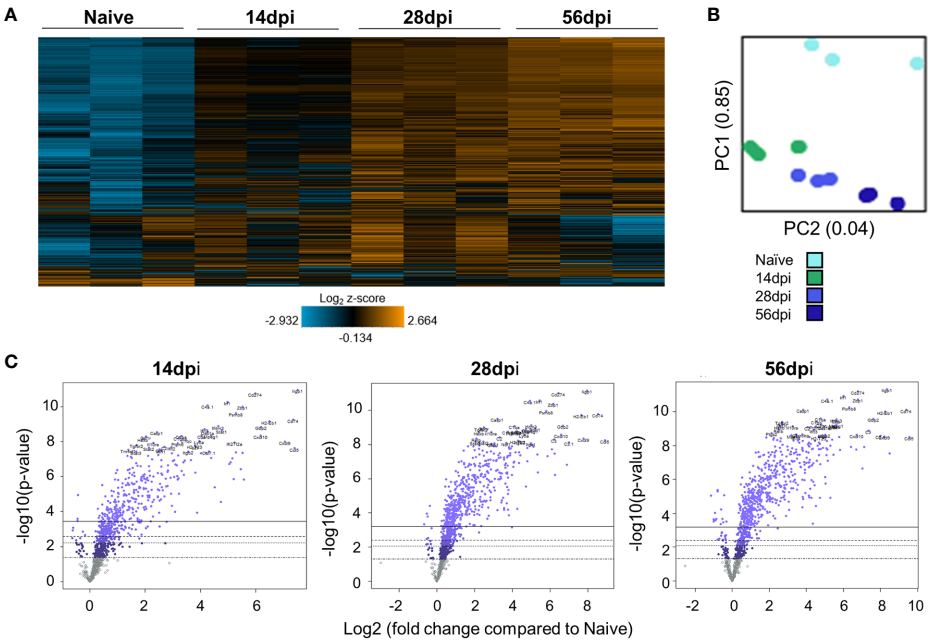

D

14dpi	28dpi	56dpi
IIGP1 (7.50)	*IIGP1* (7.96)	*IIGP1* (8.35)
CD274 (5.97)	*CD274* (6.45)	*CD274* (6.79)
IRF1 (4.98)	*IRF1* (5.46)	*IRF1* (6.00)
C4A.1 (4.26)	*C4A.1* (4.93)	*ZBP1* (6.80)
ZBP1 (5.52)	*ZBP1* (6.17)	*C4A.1* (5.13)
PSMB8 (5.28)	*PSMB8* (5.81)	*PSMB8* (6.32)
CD74 (7.35)	*CD74* (8.54)	*CD74* (9.40)
H2-EB1 (6.49)	*H2-EB1* (7.67)	*CASP1* (3.84)
IFITM3 (4.64)	*CASP1* (3.23)	*H2-EB1* (8.26)
GBP2 (6.19)	*IFITM3* (5.00)	C1QA (4.77)

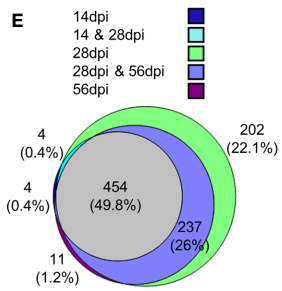

FIGURE 1 | Chronic *T. gondii* infection stimulates a dramatic shift in gene expression as infection progresses from early to late chronic stages. **(A)** Heat map of all genes from merged Neuropathology, Neuroinflammation, and InflammationPLUSCustomCodeset panels. Gene expression depicted from low expression (blue) to high expression (orange). Heat map generated from normalized gene expression data using nSolver software. **(B)** PCA plot of biological replicates at all time points. Numbers on axes represent percentage of variation in that component. **(C)** Differential expression analysis results of 14 dpi, 28 dpi, and 56 dpi compared to Naïve control values demonstrates the majority of genes as upregulated. Top 25 genes most significantly upregulated identified based on fold change (x-axis) vs. p-value (y-axis). Four adjusted p-value cutoffs in each plot are as follows from bottom (dashed line) to top (solid line): <0.50, <0.10, <0.05, <0.01. **(D)** Table of 10 most significantly upregulated genes at each time point (from C.) Numbers in parentheses represent fold-change of gene. **(E)** Overlap between differentially expressed genes plotted in **(C)**. Numbers and percentages in diagram based on genes significantly upregulated with adjusted p-value cutoff <0.05.

changes in host genes following infection may represent a triggering of inflammation cascades and neurological remodeling that is independent of infection, or they could be closely tied to the development of the parasite niche in the brain. To determine the relationship between host and parasite genetic changes, Toxoplasma stage-specific genes were selected based on their stage specificity and frequency of expression in RNAseq data sets of Me49 bradyzoites, tachyzoites, and late-stage bradyzoites as seen in ToxoDB and in recent publications (Goerner et al., 2020). These genes were incorporated into the NanoString analysis *via* the use of custom codesets, and changes in expression of these genes were analyzed at each time point. To further elucidate *T. gondii* stage-specific gene expression changes across the course of infection, fold changes of tachyzoite-associated genes and bradyzoite-associated genes compared to naïve controls were analyzed *via* OneWay ANOVA for significance. Normalized parasite gene counts for each sample at each time point were used to determine fold change. To verify normal progression of infection, parasite B1 amplification was conducted (**Supplementary Figure 1**). Visualization of parasite-specific gene expression changes correlates with development of chronic and sustained infection (**Figures 2A–C**; **Supplementary Figure 1**).

Most tachyzoite associated genes (top 5 genes in heat map) are expressed at or around background levels in the brain and remain so for the duration of infection (**Figure 2A**). *ROP18,*

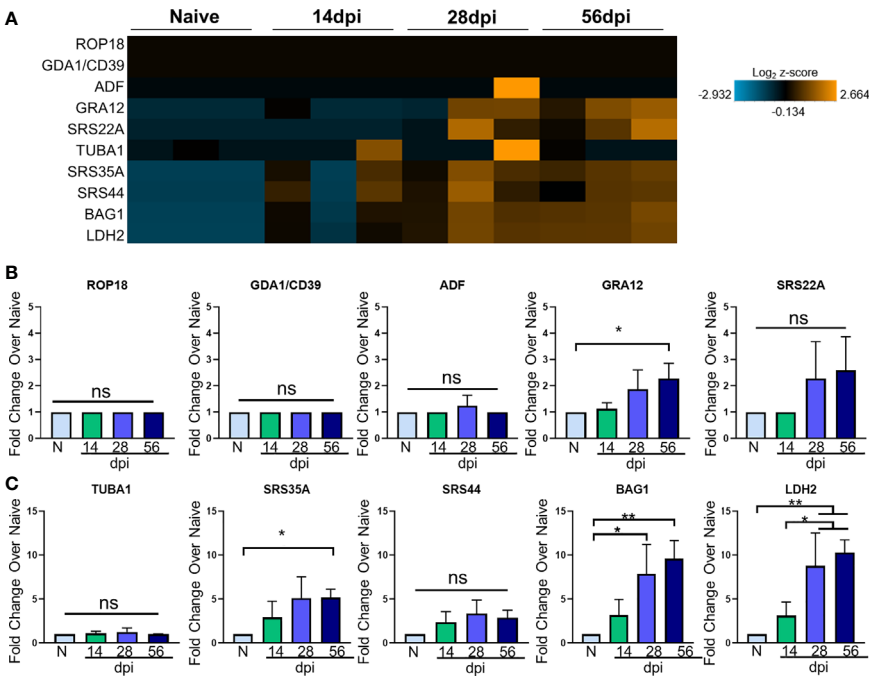

FIGURE 2 | T. gondii stage-specific gene expression correlates with host gene changes. **(A)** Heat map of *T. gondii*-specific genes from merged Neuropathology, Neuroinflammation, and InflammationPLUSCustomCodeset panels. Gene expression depicted from low expression (blue) to high expression (orange). Heat map generated from normalized gene expression data using nSolver software and Background Thresholding to account for lower parasite gene counts. **(B, C)** Fold change compared with naive of tachyzoite genes **(B)** and bradyzoite genes **(C)** from normalized gene counts. Significance determined by One-Way ANOVA using Multiple Comparisons (*p-value <0.05, **p-value <0.01.). ns, not significant.

GDA1/CD39, and *ADF* are constitutively expressed across all developmental stages according to ToxoDB but are never detectable above background here and may indicate limitations in sensitivity compared to the abundance of host genetic material (**Figures 2A, B**). These are all genes constitutively expressed in varying stages of Me49 strain development, and their expression is not altered at any point during chronic infection (**Figure 2B**). Therefore, although C57BL/6 mice are susceptible to infection exhibiting increasing parasite burden over time, the stable expression of *ROP18, GDA1/CD39*, and *ADF* in this study suggest that even at 56dpi, there are not classical indicators of parasite reactivation and bradyzoite genes continue to dominate.

The genes *GRA12* (Krishnamurthy and Saeij, 2018) and *SRS22A* (Michelin et al., 2009) help with formation of the parasitophorous vacuole (PV) membrane that protects the parasite during both acute and chronic infection, and *GRA12* is one of the genes that orchestrates cyst formation in the transition from tachyzoite to bradyzoite and is seen in the 99th percentile in both tachyzoites and bradyzoites (Guevara et al., 2019). Our data show *GRA12* increasing by 2.5-fold at 56 days post infection, signifying the presence of non-replicating parasites in the brain while *SRS22A* remains unchanged compared to naïve controls (**Figure 2B**).

In addition to tachyzoite associated genes, early- and late-stage bradyzoite genes were selected for this analysis based on ToxoDB expression values. *SRS35A*, also known as *SAG4*, is a surface protein expressed above the 95th percentile in both early and late-stage bradyzoites (Zhou and Wang, 2017). *SRS44*, also known as *CST1*, is a cyst wall component that is expressed above the 89th percentile in both bradyzoite stages and maintains the integrity of the cyst during chronic infection (Tomita et al., 2013). The bradyzoite-specific antigen *BAG1*, also thought to aid in cyst formation (Zhang Y.W. et al., 1999), is expressed at the 91st and 100th percentile in early and late stage bradyzoites respectively. *LDH2*, one of the main controllers of bradyzoite differentiation (Abdelbaset et al., 2017) is expressed between the early and late bradyzoite stages of growth.

All of these genes increase in percentile of expression in early- and/or late-stage bradyzoite stages of growth compared to tachyzoites. In contrast to the lack of tachyzoite genes, kinetics of these selected bradyzoite genes follow a pattern of increasing expression from 14dpi to 56dpi (**Figures 2A, C**). Fold change analysis of bradyzoite associated genes reveal significant increases of the bradyzoite specific *SRS35A, BAG1* and *LDH2* as infection progresses (**Figures 2A, C**). *SRS35A* shows a 5-fold change compared to naïve controls at 56 days post infection. *SRS44* experiences an increasing trend but does not reach significance. *BAG1* demonstrates between a 5-10-fold increase in expression at 28 and 56 days post infection, supporting the presence of bradyzoites in the brain at these later chronic stages. *LDH2* shows an approximately 10-fold increase at 28 and 56 days post infection. Expression of *LDH2* at the mid- and late-chronic stage is also significantly higher compared to expression at 14dpi.

Thus, several ToxoDB-identified constitutively expressed tachyzoite genes were unchanged between the early and late chronic stages of infection based on their expression at or below background levels. However, by 28dpi a significant pattern of Toxoplasma gene expression has been established dominated by late-stage bradyzoite specific genes (Hong et al., 2017; Garfoot et al., 2019; Goerner et al., 2020). Interestingly, this pattern remains mostly unchanged 4 weeks later at 56dpi with the exception of *GRA12* that may support renewed cyst formation at this later stage (Watts et al., 2015). Taken together, the kinetics of parasite-specific gene expression in the C57BL/6 mouse indicate an established chronic infection, minimal tachyzoite replication and a predominantly late-stage bradyzoite phenotype.

Kinetics of Chronic Infection Demonstrates Classical Immune Cell Activation and Increases in IFNγ Signaling-Related Genes

Regulation of inflammation is especially important in the CNS during chronic infection, and a balanced host immune response is vital for survival. The role of T cells in protection against Toxoplasmic encephalitis has been known for some time however, the accumulation of innate immune cells, resident CNS cells and subsets of all of these are still not fully documented (Landrith et al., 2015; Khan et al., 2019). In contrast to RNA-seq, the direct counting of transcripts (Geiss et al., 2008) allows cell type profiling analysis of immune cells based on the counts of particular cell-specific transcripts (Danaher et al., 2017). Results of cell type profiling demonstrate significant changes in abundance of canonical cell types involved in the *T. gondii* immune response (**Figure 3A**). As would be expected all T cells and specifically CD8+ T cells significantly increase in abundance over naive and 14dpi as infection progresses (Hu et al., 2020) (**Figure 3A**). In addition, macrophages and resident microglia also increase in abundance and activation. The increase in these innate immune cell types follows the same pattern as T cells, with macrophages demonstrating the largest increase over time. Both macrophages and microglia exhibit significant increases over naïve at all time points and level off after 28dpi.

To examine the overall directional change of specific infection-associated pathways, gene set analysis (GSA) was performed and directed global significance scores were analyzed. As seen in **Figure 3B**, classical inflammatory

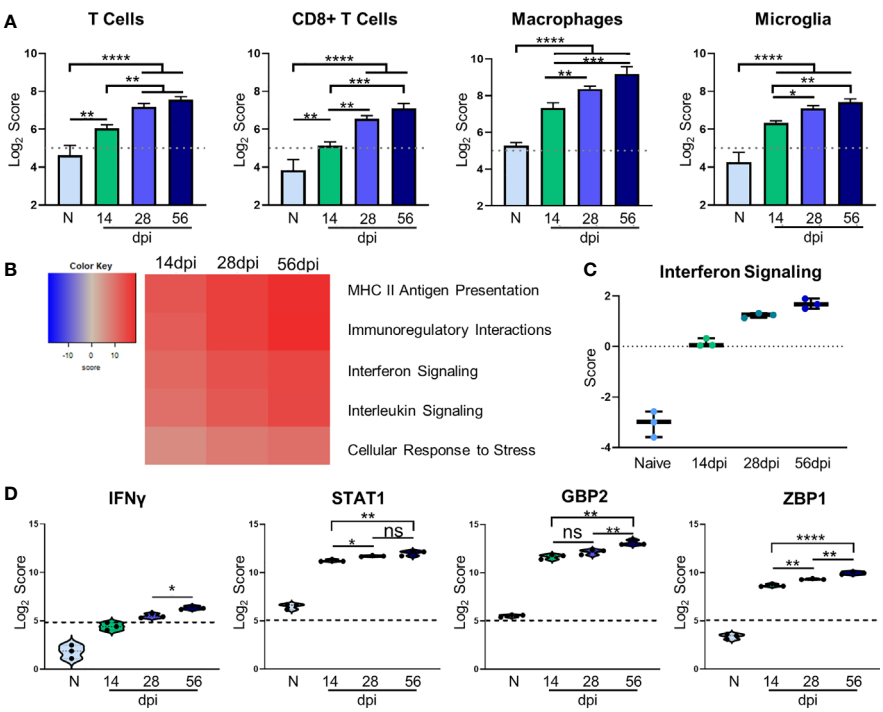

FIGURE 3 | Kinetics of chronic infection demonstrates classical immune cell activation and increases in IFNγ signaling-related genes. Cell-type profiling, global significance analysis, pathway scoring, and individual gene results of merged Neuropathology, Neuroinflammation, and InflammationPLUSCustomCodeset panels. **(A)** $\log_2$ score plots of infiltrating immune cell types T cells, CD8+ T cells, macrophages, and resident microglia compared to naïve time point control (*p-value < 0.05, **p-value < 0.01, ***p-value < 0.001, ****p-value < 0.0001). All cell types checked for expression above background level of 5 (shown by dashed line). **(B)** Heatmap of directed global significance scores compared to naïve controls based on direction of gene set pathway change. Red denotes gene sets whose genes exhibit extensive over-expression with the covariate, blue denotes gene sets with extensive under-expression. **(C)** Pathway analysis results of Interferon Signaling. Pathway checked for expression compared to background score of 0 (shown by dashed line). **(D)** $\log_2$ score plots of specific genes relating to IFNγ signaling, specifically *IFNγ*, *STAT1*, *GBP2*, and *ZBP1* compared to naïve time point control (*p-value < 0.05, **p-value < 0.01, ***p-value < 0.001, ****p-value < 0.0001). All genes checked for expression above background level of 5 (shown by dashed line). ns, not significant.

response pathways follow a trend of steady upregulation across all time points supporting the need for a maintained robust immune response. Our pathway analysis results show an anticipated initial increase in IFN signaling during the early chronic stage of infection that consistently increases over time (**Figure 3C**). Downstream IFNγ-dependent mechanisms such as *STAT1* signaling and parasite-killing genes *GBP1* and *ZBP2* are vital to prevent parasite reactivation in the brain (Virreira Winter et al., 2011; Kravets et al., 2012; Hidano et al., 2016; Pittman et al., 2016). To address the kinetics of *IFNγ, STAT1, GBP2*, and *ZBP2* Log_2 scores of transcript numbers were plotted for each time point (**Figure 3D**). *IFNγ* expression serves as a reassuring control of previously known infection-induced brain changes, results demonstrate low *IFNγ* at 14dpi consistent with lower numbers of T cells at this early stage in the brain (**Figure 3D**, left). This increases as chronicity progresses and reaches peak significance at 56dpi compared to the mid-chronic stage. Despite this conservative *IFNγ* expression, it is highly effective with large increases in IFNγ-dependent signaling including *STAT1*. Corresponding to increased IFNγ-dependent signaling, *STAT1* expression is increased 2-fold in the brain at 14dpi and continues to increase as infection progresses through the mid-chronic stage, levelling off between 28 and 56dpi (**Figure 3D**, second from left). *GBP2* and *ZBP1* expression are also increased at 14dpi compared to naïve controls, but while *GBP2* remains constant until the late stage of infection, *ZBP2* is significantly increased at each time point (**Figure 3D**, right). The differences in timing of expression of these genes suggests stage-specific, IFNγ-dependent mechanisms of parasite control. Taken together, these results demonstrate classical activation of immune cells and infection-associated pathways that supports previous research as well as previously unknown kinetics of IFNγ-dependent signaling mechanisms.

Kinetic Analysis Reveals Progressive Neuropathological Changes and Previously Unexplored Attempts at Repair During Chronic *Toxoplasma gondii* Infection

Changes in neurochemistry in the infected brain have previously been reported including alterations in the excitatory and inhibitory neurotransmitters (Xiao et al., 2013; Brooks et al., 2015; David et al., 2016; Barbosa et al., 2020) that suggest that even in the absence of clinical pathology, there are underlying changes in neuronal structure and connectivity that would be described as pathological. To determine the full extent of genetic changes related to neuropathology, we analyzed a group of genes with known roles in transmitter function, neural connectivity and function, and neural maintenance and repair *via* GSA and pathway analyses. GSA results demonstrate upregulation of most of the Neuropathology panel pathways at each time point while a handful of pathways (namely, Vesicle Trafficking, Neural Connectivity, Transmitter Synthesis and Storage, Transmitter Release, and Carbohydrate Metabolism) experience noticeable downregulation (**Figure 4A**). To confirm worsening of neuropathology *via* the activation of CNS-resident immune cells and decreases in neuronal function, Log_2 scores of the astrocyte activation gene *GFAP* and the inhibitory neurotransmitter GABA signaling gene *GABRA1* were analyzed (**Figure 4B**). Astrocytic *GFAP* increases in expression initially during the early chronic stage of infection, remains steady between 14 and 28dpi, and then experiences a significant increase in expression by 56dpi (**Figure 4B**, top). Over the course of chronic infection, *GABRA1* remains at levels comparable to naïve controls until 56dpi where it demonstrates a significant decrease (**Figure 4B**, bottom).

As neurons are the primary CNS-resident cell type infected by *T. gondii*, and these cells undergo changes in morphology and function during infection, the pathway of neural connectivity was examined more thoroughly *via* pathway analysis and corresponding volcano plots. Pathway analysis supports GSA results and shows a steady decrease in neural connectivity across all timepoints (**Figure 4C**). Volcano plots of the genes driving the neural connectivity score show increases in significantly downregulated genes as infection progresses corresponding with the lower GSA score at each time point (**Figure 4C**). One gene that drives this downregulation at all time points is *Glrb*, a receptor that functions as a neurotransmitter-gated ion channel (Handford et al., 1996; Ridderbusch et al., 2019). *Slc9a6*, a gene that encodes the protein NHE6 which plays a role in dendritic spine growth (Park et al., 2006; Gao et al., 2019), becomes highly downregulated at the later time points (**Figure 4C**). *Slc17a6* which aids in glutamate uptake (Takamori et al., 2001; Serrano-Saiz et al., 2020) drives downregulation of neural connectivity at 14dpi (**Figure 4C**). In addition to supporting previous findings and in contrast to immune scoring, this data suggests a continuous progression of neuropathology specifically in the areas of neurotransmitter production and function (**Supplementary Table 1**).

GSA and pathway analyses also reveal an increase in pathways associated with myelination (**Figures 4A, D**). The myelination pathway experiences consistent upregulation as infection progresses through chronicity (**Figures 4A, D**). It is well known that myelination of neuronal axons is a critical process not only for neuronal signaling, but also for continued supply of required metabolites to neurons for their survival and function and the process of re-myelination has been seen in various instances of CNS injury and disease (Saab and Nave, 2017; Wang F. et al., 2018). Throughout all stages of infection, the increase in the myelination pathway is driven by the genes *Hexb*, *Tgfb1*, and *Cxcr4* (**Figure 4D**). These results demonstrate an increase in genes associated with myelination and support increased attempts at repair of neuropathology.

Kinetics of *Toxoplasma gondii* Infection Reveals Significant Alteration of Novel Genes

In addition to changes in expression of canonical *T. gondii* infection-associated genes, differential expression analysis also identified significant changes in several genes previously not associated with this parasitic infection. Of the 25 most significantly upregulated genes from all time points compared to Naïve controls, 4 of these genes were determined to be novel in

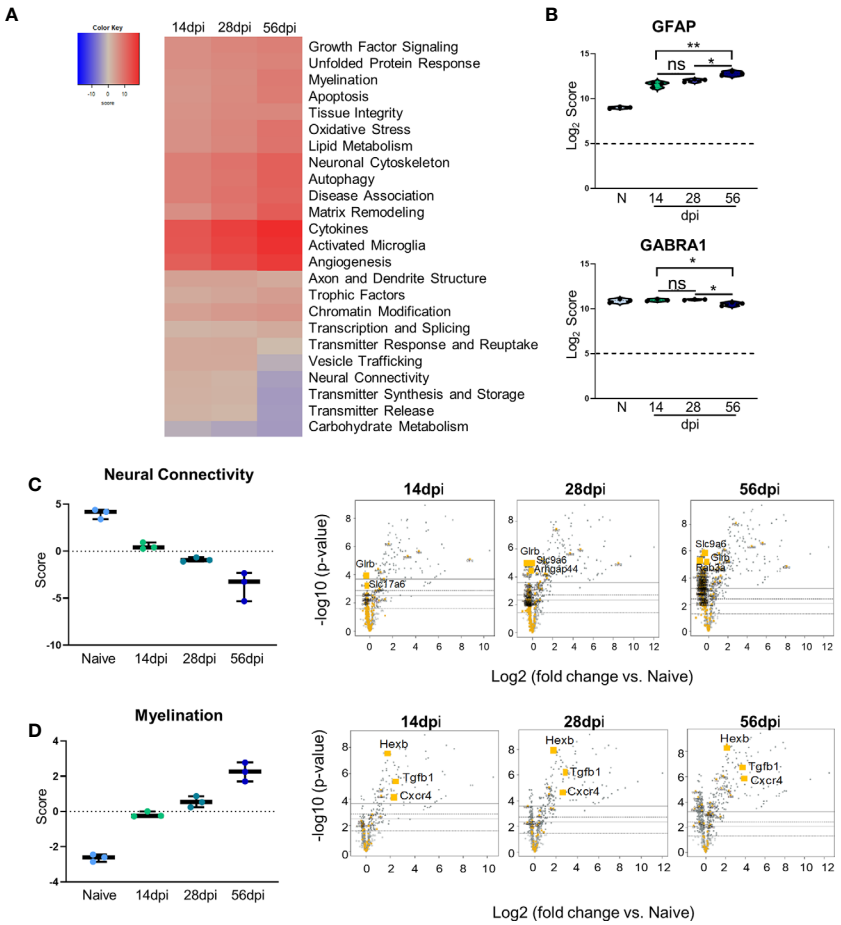

FIGURE 4 | Kinetics of chronic infection reveals progressive neuropathological changes and previously unexplored attempts at repair/maintenance during chronic *T. gondii* infection. Global significance analysis, individual gene, and pathway scoring results of Neuropathology Panel. **(A)** Heatmap of directed global significance scores compared to naïve controls based on direction of gene set pathway change. Red denotes gene sets whose genes exhibit extensive over-expression with the covariate, blue denotes gene sets with extensive under-expression. **(B)** $\log_2$ score plots of specific genes relating to neuropathology, specifically *GFAP* and *GABRA1* compared to naïve time point control (*p-value < 0.05, **p-value < 0.01). All genes checked for expression above background level of 5 (shown by dashed line). **(C, D)** Pathway analysis and volcano plot results of neural connectivity **(C)** and myelination **(D)** pathways significantly affected during *T. gondii* infection based on analysis. Volcano plot of directed global significance scores for neural connectivity and myelination gene sets. Genes within the selected gene set are highlighted in orange. Top three genes driving directional change identified based on fold change (x-axis) vs. p-value (y-axis). Four adjusted p-value cutoffs in each plot are as follows from bottom (dashed line) to top (solid line): <0.50, <0.10, <0.05, <0.01. ns, not significant.

the context of *T. gondii* infection, and their Log_2 scores were analyzed further (**Figure 5A**).

C4A gene expression increases compared to naïve controls beginning at the early stage of chronic infection, and while this expression does not change significantly between 14dpi and 28dpi or 28dpi and 56dpi, expression increases by approximately 1.5 fold overall between the early and late chronic stages (**Figure 5A**). This gene is primarily known for activation of the complement pathway along with *C3A* and *C5A* (Liesmaa et al., 2018; Melbourne et al., 2018; Prasad et al., 2018; Ji et al., 2019). *CTSS* is a member of the peptidase C1 family that encodes for cathepsin S which is expressed by neurons in the CNS (Ji et al., 2018). Similar to *C4A*, *CTSS* expression experiences >1.5 fold change over the course of infection, but this gene is also significantly increased at each chronic time point (**Figure 5A**). *IFITM3*, commonly known for its anti-viral functions, experiences a similar pattern of upregulation as *CTSS*, and over the course of chronic infection is upregulated >1.5 fold overall (**Figure 5A**). *PSMB8* expression increases 2-fold overall and follows the trend of a step-wise increase between each time point (**Figure 5A**). This gene has the greatest fold change in expression compared to naïve controls.

While the majority of novel differentially expressed genes are upregulated over the course of infection, a handful of previously unreported genes are significantly downregulated compared to naïve controls (**Figure 5B**). One such gene is *ATF2*, activating transcription factor 2, which is required to regulate the transcription of the pro-inflammatory cytokine TNFα (Falvo et al., 2000; Tsytsykova and Goldfeld, 2002). *ATF2* decreases significantly from 28dpi to 56dpi after an initial decrease at 14dpi (**Figure 5B**). *NRG3* belongs to the NRG gene family and is the

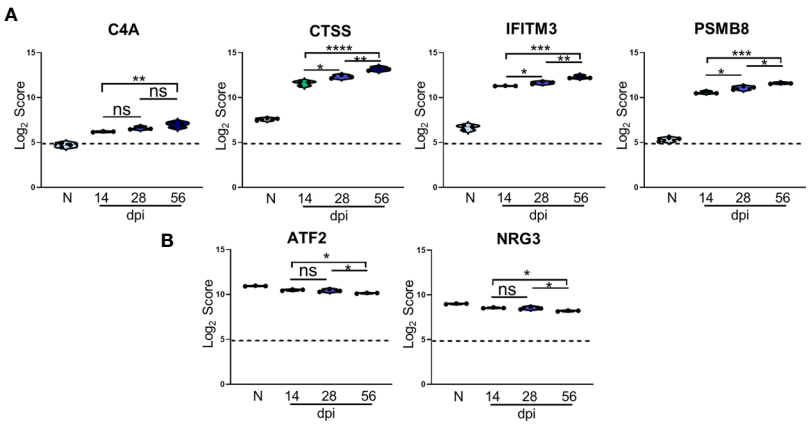

FIGURE 5 | Kinetics of *T. gondii* infection reveals significant alteration of novel genes. **(A, B)** $\log_2$ score plots of specific novel genes from merged Neuropathology, Neuroinflammation, and InflammationPLUSCustomCodeset panels compared to naïve time point control. **(A)** Violin plot results of most highly upregulated non-canonical genes *C4A*, *CTSS*, *IFITM3*, and *PSMB8* as determined by differential expression analysis. **(B)** Results of most highly downregulated non-canonical genes *ATF2* and *NRG3* as determined by differential expression analysis. All genes shown are expressed above background threshold of 5 (shown by dashed line) and are significantly altered during infection based on differential expression analysis statistics (p-value<0.01). All graphs shown as fold change over background. Significance between timepoints determined by One-Way ANOVA using Multiple Comparisons (*p-value <0.05, **p-value <0.01, ***p-value < 0.001, ****p-value < 0.0001). ns, not significant.

second most common form of NRG found in the adult brain (Paterson et al., 2017). *NRG3* experiences a similar decrease in expression as *ATF2* over the course of chronicity (**Figure 5B**). Taken together, the consistent pattern of change in these newly analyzed genes over the course of infection point to additional targets for understanding the complexity of chronic infection.

BALB/c Mice Exhibit Differences in Timing and Expression of Genes, Immune Cell Recruitment, and Pathway Activation Compared With C57BL/6 Mice Suggesting Decreased Neuropathology and Enhanced Repair

Host genetics influence the outcome of Toxoplasma infection even if they do not prevent chronic infection. Thus, C57BL/6 mice are considered susceptible with high cyst burden that levels off around 30 days post infection (Burke et al., 1994) while BALB/c mice, another commonly used mouse strain, are more resistant (**Supplementary Figure 1**) (Mukhopadhyay et al., 2020). While the increased resistance to infection in BALB/c mice has previously been linked to enhanced immune response specifically *via* MHC gene expression (Brown et al., 1995), less is known regarding how neuropathology signatures differ between resistant BALB/c mice and the more susceptible C57BL/6 model over the course of chronic infection.

To compare neuropathology and neuroinflammatory signatures in BALB/c and C57BL/6 mice during chronic infection, NanoString analysis was conducted on BALB/c mouse brain RNA using the same time points of infection as before. Results of merged BALB/c vs. C57BL/6 analysis demonstrate initial differences in gene expression between naïve mice (**Figure 6A**) consistent with previous analysis (Sellers et al., 2011; Yuan et al., 2020). In contrast to B6 mice which generally show a continued increase in gene change over the course of infection, BALB/c mice exhibit the largest change at 14dpi which then returns to patterns similar to naïve at chronic infection. (**Figure 6A**). Principal component analysis (PCA) shows little variation between biological replicates and no divergent point between BALB/c and C57Bl/6 instead gene expression in these different hosts at all time points remain separated. Based on PC1 and PC2 clustering of day 28 and day 56 post infection on the BALB/c background are almost identical (**Figure 6B**). When comparing DEGs between naïve C57BL/6 and BALB/c mice, there is an initial difference in gene expression (**Figure 6C**). While most DEGs (582) are conserved between the 2 strains, the majority of BALB/c genes are downregulated compared to naïve C57BL/6 mice, and there are notably less DEGs that are specific to BALB/c mice (24 BALB/c compared to 230 C57BL/6). At each infection time point, there are between 350-420 genes that remain shared between the 2 mouse strains suggesting conserved gene expression changes relating to neuropathology and neuroinflammation across different mouse species (**Figure 6D**). However, despite this shared number of altered genes, there is a much higher number of DEGs in C57BL/6 mice (368, 543, and 436 genes respectively) compared to BALB/c mice (94, 31, and 27 genes) at each time point. It is important to note that BALB/c mice also have lower numbers of DEGs overall at each time point compared to C57BL/6 mice (**Supplementary Table 2**). The underlying genetic difference between these two strains of mice is observed in the expression of MHC II (*H2-Ea-ps*) and dominates the genes that are upregulated in BALB/c mice (**Figure 6D**). It is not apparent in baseline differences as little MHC II expression occurs in a naïve brain. The overall downregulation of genes following infection of BALB/c mice is dominated by *Mpeg1*

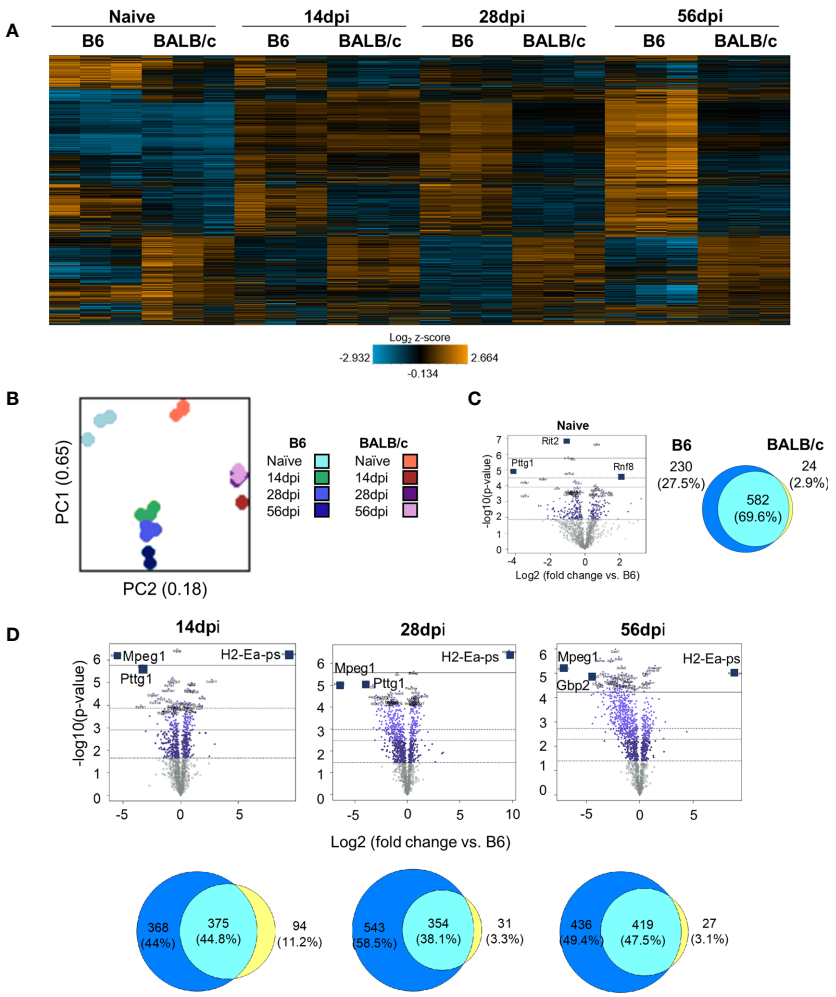

FIGURE 6 | BALB/c mice exhibit differences in timing and expression of genes compared to B6 mice during chronic infection. **(A)** Heat map of all genes from B6vsBALB/c merged Neuropathology, Neuroinflammation, and InflammationPLUSCustomCodeset panels. Gene expression depicted from low expression (blue) to high expression (orange). Heat map generated from normalized gene expression data using Basic nSolver software. **(B)** PCA plot of B6 and BALB/c biological replicates at all time points. Numbers on axes represent percentage of variation in that component. **(C, D)** BALB/c differential expression analysis results and overlap between differentially expressed genes of Naïve **(C)** and infection timepoints **(D)** (14dpi, 28dpi, and 56dpi) compared to B6 control values. Top 3 genes identified based on fold change (x-axis) vs. p-value (y-axis). 4 adjusted p-value cutoffs in each plot are as follows from bottom (dashed line) to top (solid line): <0.50, <0.10, <0.05, <0.01. Numbers and percentages in Venn diagrams based on genes significantly upregulated with adjusted p-value cutoff <0.05.

and *Pttg1* (**Figure 6D**). These genes are primarily responsible for innate immune responses and apoptosis *via* the p53 pathway (Zhang X. et al., 1999; Bernal et al., 2002; Bai et al., 2018; McCormack et al., 2020; Ni et al., 2020).

Based on the differences in differential gene expression between BALB/c mice and C57BL/6 mice, cell type profiling and pathway analyses were conducted to determine effects of cell composition and pathway activation on differences in BALB/c vs. C57BL/6 neuropathology signatures. Cell type profiling demonstrates notable differences in cell composition in the brain across chronic infection between these strains (**Figure 7A**). At each stage, BALB/c mice demonstrate drastically different cell composition overall compared to those of C57BL/6 mice at the same infection stage after comparison to control "Tumor Infiltrating Leukocyte" (TIL) expression as well as other cell types. While not all cell types are consistently up- or downregulated in BALB/c mice at each time point, CD4+ and CD8+ T cells show patterns of decreased and increased amounts respectively (**Figure 7A**) corresponding with previous research demonstrating decreased importance of CD4+ T cells and increased dependence on CD8+ T cell activity in BALB/c chronic infection (Parker et al., 1991; Deckert-Schlüter et al., 1994; Harris et al., 2010). In addition, there are significantly elevated macrophages at 56dpi in BALB/c mice compared to C57BL/6 mice. Notably, total TILs are predominantly downregulated in BALB/c at 28 and 56dpi suggesting less absolute numbers of immune cells and therefore immune cell recruitment overall while TILs are relatively comparable at 14dpi

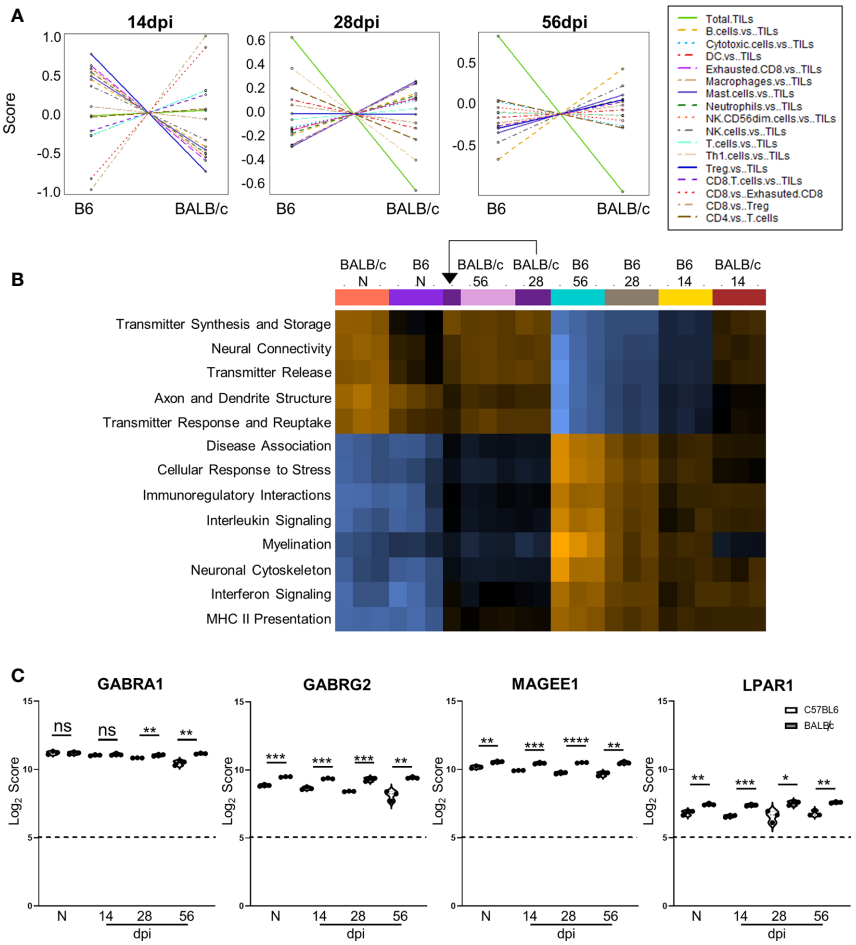

FIGURE 7 | Differences in cell recruitment, pathway activation, and specific regulatory genes demonstrate enhanced control of infection in BALB/c mice. **(A)** Cell type summary plots of recruited cells shown in BALB/c mice vs. B6 mice per time point. **(B)** Pathway score summary plot of BALB/c Vs. B6 mice depicted from downregulation (blue) to upregulation (orange). Summary plot generated by clustering pathways based on similar scores. Samples are arranged in plot according to similarity of pathway score profiles. **(C)** $\log_2$ score plots of specific genes relating to neuronal health and repair, specifically *GABRA1*, *GABRG2*, *MAGEE1*, and *LPAR1* compared to naïve time point control (* = p-value < 0.05, ** = p-value < 0.01, *** = p-value < 0.001, **** = p-value < 0.0001). All genes checked for expression above background level of 5 (shown by dashed line). Gene selection significance determined *via* differential expression analysis statistics (p-value<0.05). All graphs shown as fold change over background Significance between mouse strains at each time point determined by Unpaired Two-Tailed Student's t-Test (* = p-value <0.05, ** = p-value <0.01, *** = p-value < 0.001, **** = p-value < 0.0001). ns, not significant..

between the mouse strains. This is consistent with increased control of parasite replication in BALB/c (**Supplementary Figure 1**).

To compare pathway score profiles between mouse strains, the heatmap of overall pathway scores was analyzed. This summary plot clusters pathways together based on similar expression patterns and arranges samples based on similarity of pathway expression profiles. When evaluating pathway activation associated with neuropathology, BALB/c mice demonstrate downregulation of neuropathological and inflammatory pathways such as "Disease Association," "Cellular Stress Response," "Interleukin Signaling," "Interferon Signaling," and "MHC II Presentation" when compared to the same C57BL/6 time points (**Figure 7B**). In addition to decreased neuropathology and inflammatory pathway activation, BALB/c mice also demonstrate upregulation of pathways associated with neurological health and function such as "Transmitter Synthesis and Storage," "Neural Connectivity," "Transmitter Release," "Axon and Dendrite Structure," and "Transmitter Response and Reuptake" at later chronic time points compared to C57BL/6 mice. While pathway activation patterns are comparable between BALB/c and B6 mice at Naïve and 14dpi, there is a switch in up- and downregulated pathways associated with neuropathology, inflammation, and neurological health at later chronic time points.

To determine if the contrasting pathway activation between BALB/c and C57BL/6 mice are driven by differences in neurological DEGs at each time point, Log_2 scores for specific neurological signaling (*GABRA1* and *GABRG2*) and repair (*MAGEE1* and *LPAR1*) genes were compared between BALB/c

and C57BL/6 mice (**Figure 7C**). *GABRA1* expression is comparable at both naïve and 14dpi timepoints and significantly increases compared to C57BL/6 mice at both 28 and 56dpi (**Figure 3C**). In contrast, neuronal signaling *GABRG2* expression is significantly elevated in BALB/c mice at all time points (**Figure 7C**). Neuronal signaling and repair genes *MAGEE1* and *LPAR1* also follow similar patterns of expression at each time point and are significantly elevated in BALB/c mice at each stage of infection (**Figure 7C**). Taken together, these results collectively demonstrate differences in timing and expression of genes, immune cell recruitment, and pathway activation in resistant BALB/c mice compared to B6 mice indicating decreased neuropathology and enhanced repair.

DISCUSSION

In this study, we utilized a targeted approach to analysis of gene expression and investigated >1500 genes associated with neurological and immunological processes by direct counting of RNA transcripts without the need for amplification *via* NanoString technology (Geiss et al., 2008). We determined the changes in these host genes over time in parallel with changes in *T. gondii* developmental-specific genes. While much is known about changes in gene expression at specific stages of infection *via* commonly used sequencing techniques like RNAseq, there is a gap in knowledge regarding how gene expression fluctuates as infection progresses through chronicity and how these changes relate to development of the parasite (Montoya and Liesenfeld, 2004; Jia et al., 2013; Ngô et al., 2017). In addition, we compared gene expression changes between susceptible and resistant mouse strains with specific focus on differences in neuropathology and neuroinflammatory signatures. Results demonstrate a dramatic shift in both previously demonstrated and novel gene expression relating to neuropathology and neuroinflammation as chronic infection progresses and reveals possible pathways of inflammation resolution.

The establishment and maintenance of chronic infection involves complex changes as infection progresses from parasite entry and formation of cysts early during infection to long-term control of encysted parasites *via* immune cell recruitment and cytokine production leading to subtle worsening of neuropathology as infection progresses through the mid- and late chronic stages (Liesenfeld et al., 1996; Denkers, 1999; Lee and Kasper, 2004; Lachenmaier et al., 2011; Feustel et al., 2012; Lilue et al., 2013; Hong et al., 2017; Radke et al., 2018; Graham et al., 2020; Mukhopadhyay et al., 2020). Our chosen timepoints represent each of these stages to capture as much directional change in gene expression as possible. Initial results demonstrate that despite the establishment of chronic infection seen by stabilization of Toxoplasma genes by 28dpi, there continue to be changes in overall gene expression relating to neuropathology, neuroinflammation, and inflammation at varying stages of chronicity. The multitude of signature changes suggests an initial activation of neuropathology and neuroinflammation phenotypes by 14dpi. This switch becomes more pronounced as chronicity progresses even while immune parameters between 4 and 8 weeks post infection steady. 454 DEGs remain shared between time points indicating conserved transcriptomic changes as chronic infection progresses, with fewer specific genes for each time point.

Previous analyses of parasite genes at different developmental stages have established some developmental specific gene signatures of the parasite as it transitions from disseminating tachyzoite to cyst-forming bradyzoite (Hong et al., 2017; Radke et al., 2018; Garfoot et al., 2019; Goerner et al., 2020; Krishnan et al., 2020; Waldman et al., 2020). Evaluating selected genes whose expression corresponds with either constitutive, tachyzoite, or immature/mature bradyzoite phenotypes using ToxoDB, we identified gene expression during chronic infection that supports the phenotype of maturing cysts and little reactivation to tachyzoite replication even in a susceptible mouse model. The genes were selected based on their percentile of expression in each growth stage of *T. gondii*, for example, *BAG1* is expressed at the 91st and 100th percentile in ME49 early and late-stage bradyzoites but only at the 15th percentile in tachyzoites making it a bradyzoite associated gene. The variability between biological replicates is greater during analysis of Toxoplasma specific genes (**Supplementary Figure 2**). This likely reflects the non-homogeneous pattern of cyst location in the brain as well as technical limitations due to overabundance of host material compared to parasite. Our results show that the constitutively expressed tachyzoite genes *ROP18, GDA1/CD39*, and *ADF* remain lowly expressed throughout the course of chronic infection. The transitional gene *GRA12* is upregulated at 56dpi indicating possible continued cyst formation in line with a general low level increase in cyst numbers overtime (Sinai et al., 2016). Even though neuropathology scores worsen in the C57BL/6 strain, these data do not suggest that significant parasite reactivation is the cause. Most bradyzoite-specific genes such as *SRS35A, BAG1*, and *LDH2* accumulate over time and remain dominant as infection progresses with increased presence of late-stage bradyzoites and support a maturation of cysts in the brain (Watts et al., 2015; Garfoot et al., 2019; Goerner et al., 2020).

Our results confirm previous research demonstrating immune response and canonical T cell activation while also showing accumulation of macrophages and continued proliferation and activation of CNS microglia. While cell type profiling and pathway analyses used in this study identify the most significantly changed cell types and broad pathway changes, other cell types and more specific pathways can be excluded or overlooked due to low probe counts. In the future, additional genes relating to cell types and pathways of interest such as neurons and astrocytes could be added and analyzed. We confirm classical immune pathway activation that demonstrates possible stabilization over time. Recent work has demonstrated similar increases in these pathways between the acute and chronic stage of infection after infection with *T. gondii* oocysts following GO analysis of RNAseq (Hu et al., 2020). In addition, we provide new in-depth analysis of *IFNγ* expression and downstream IFNγ-signaling genes *STAT1, GBP2*, and *ZBP1* in

the context of chronic infection in the brain. Specifically, the differences in timing of expression of these genes suggests stage-specific, IFNγ-dependent mechanisms of parasite control.

While our results offer further insight into the kinetics of expression for genes previously associated with chronic *T. gondii* infection, our analysis also reveals novel genes associated with neuropathology and neuroinflammation that have not been explored. Specifically, results demonstrate significant upregulation of the genes *C4A, CTSS, IFITM3* and *PSMB8* and downregulation of *ATF2* and *NRG3* across all stages of chronic infection. *C4A* works in conjunction with *C3A* and *C5A* to activate the complement cascade and together, these genes trigger the degranulation of mast cells and basophils and increase vascular permeability in the context of the inflammatory immune response. In addition, *C4A* has been associated with roles in schizophrenia (Liesmaa et al., 2018; Melbourne et al., 2018; Prasad et al., 2018; Ji et al., 2019). While complement activation has been previously demonstrated in the brain during Toxoplasma infection, the common functions of *C4A* point toward a possible role in increasing vascular permeability gradually during chronic infection for the continued infiltration of peripheral immune cells into the brain (Xiao et al., 2016; Huang et al., 2019). Interestingly, BALB/c mice experience significantly less expression of *C4A* at each infection time point compared to C57BL/6 mice which is an indication that there is decreased vascular permeability in these mice compared to B6. *CTSS* encodes for cathepsin S that is expressed by neurons and is required for elastase activity in alveolar macrophages (Ji et al., 2018; Doherty et al., 2019). It has also been demonstrated that *CTSS* participates in both the production of pro-inflammatory cytokines interleukin 6 (IL-6), interleukin 8 (IL-8), tumor necrosis factor-α (TNF-α), and interleukin-1β (IL-1β) during ocular inflammation (Klinngam et al., 2018) as well as the degradation of antigenic proteins to peptides during antigen presentation (Hughes et al., 2016; Klinngam et al., 2018). The pattern of *CTSS* expression at each stage of chronic infection suggests a potential role for this gene in pro-inflammatory cytokine production, neuronal function, and continued antigen presentation as part of the immune response to *T. gondii* infection. There are no known functions of *IFITM3* during *T. gondii* infection, but is important for anti-viral effector functions *via* inhibition of viral protein synthesis and shuttling incoming virus particles to lysosomes for degradation (Lee et al., 2018; Appourchaux et al., 2019; Bedford et al., 2019; Kenney et al., 2019; Spence et al., 2019). *IFTIM3* plays a role in viral infections through IFN signaling, indicating possible novel anti-parasitic functions of this gene during *T. gondii* infection. *PSMB8* is involved in the degradation of cytoplasmic antigen processing to generate MHC I binding proteins *via* stimulation by IFNγ production, provides instructions to make one subunit of immunoproteasomes responsible for helping in response to infections, and also regulates glioma cell migration proliferation and apoptosis (Agarwal et al., 2010; Basler et al., 2018a; Basler et al., 2018b; Yang et al., 2018). While previous work on PSMB8 has produced minimal data in relation to Toxoplasma infection (Agarwal et al., 2010), further research specifically relating to chronic infection could elaborate on anti-parasitic functions in the CNS. In addition to regulating TNFα production, *ATF2* is a cAMP-or activator protein-dependent transcription factor that regulates the transcription of various genes involved in anti-apoptosis, cell growth, and DNA damage response (Falvo et al., 2000; Tsytsykova and Goldfeld, 2002; Watson et al., 2017; Meijer et al., 2020). While the effect of *T. gondii* infection on the transcription of TNFα has been studied in the past, the specific role of *ATF2* in the context of chronic *T. gondii* infection in the CNS has not been elucidated, and this gene may play a vital role in regulating TNFα production specifically in the brain or by CNS-resident cells (Leng et al., 2009). *NRG3* is well-known for aiding in the development and survival of neurons and oligodendrocytes in the brain in addition to aiding in excitatory and inhibitory synapse formation and controlling glutamate release by neurons (Müller et al., 2018; Wang Y. N. et al., 2018). While it has not been explored previously in *T. gondii* infection, the significant decrease in *NRG3* may be partly responsible for some infection-induced neuropathology such as increases in extracellular glutamate concentration and excess neuronal firing.

Our results demonstrate a progressive worsening of neuropathology and increased attempted repair of this pathology *via* upregulated angiogenesis genes as infection becomes more chronic in a susceptible mouse model. While most of these directional changes are not as dramatic as those associated with the immune response (**Figure 3**), these changes support previous research demonstrating neuropathology caused by infection (Cabral et al., 2016; David et al., 2016; Ngô et al., 2017), and a small group of pathways such as Cytokines, Activated Microglia, and Angiogenesis experience drastic changes as infection progresses to the late chronic stage. It is important to note that this worsening neuropathology is unlikely to be caused by reactivation of cysts in the brain even at the late stage of infection as seen by the low expression of tachyzoite genes and instead suggests more indirect neurological consequences of infection. However, the limitations in sensitivity of measuring parasite genes in samples dominated by host material means that we cannot rule out low level cyst activation despite a consistent late-stage bradyzoite phenotype over the duration of infection. Analysis results of astrocytic activation marker *GFAP* and neuronal signaling gene *GABRA1* support this idea of progressive worsening neuropathology. While the initial increase in astrocytic *GFAP* is expected as part of the initial response to CNS infection, what isn't expected is the significant increase in expression that takes place in the late stage of infection after chronicity has been well established. *GABRA1*, along with *GABRB3*, is vital for the formation of $GABA_A$ receptors and plays a pivotal role in GABAergic signaling that protects neurons in the brain from over-signaling, which can often lead to diseases such as epilepsy (McKernan et al., 1991; Tozuka et al., 2005). The significant drop in *GABRA1* expression during the mid- and late chronic stage could be a major target for treatment of infection-induced neuropathology and chronic infection in the future. In addition to supporting previous findings, our data also suggests a continuous progression of neuropathology specifically in the areas of transmitter production, function, and response, areas that were previously lacking in the context of chronic infection. However, while our results indicate progressive neuropathology as seen *via* decreased overall neural connectivity, we also see increases in genes and pathways such

as myelination that suggest enhanced attempts at repairing and resolving this neuropathology.

Neuroprotective and repair mechanisms in other non-infectious models of CNS injury include remyelination to increase conductivity between previously damaged neurons, synaptic pruning by microglia to limit over-signaling, regeneration of axons, and various others. Recent work by the Harris lab indicates a role for local release of the DAMP IL-33 either by oligodendrocytes or astrocytes that is then required for protection against Toxoplasma (Still et al., 2020). Such innate sensing mechanisms may be needed not just for parasite recognition but also as a trigger to activate neural repair during late infection. The process of myelination has been explored extensively in the context of other models of CNS disease and injury (Gonsette, 2010; Kapitein and Hoogenraad, 2015; Felten et al., 2016; Li et al., 2017; Pałasz et al., 2017; Saab and Nave, 2017; Wang F. et al., 2018; Avila et al., 2020). The myelination pathway in this analysis is driven by several genes that are also associated with immune modulation. Throughout all stages of infection in the susceptible C57BL/6 strain, the increase in the myelination pathway is driven by the genes *Hexb, Tgfb1*, and *Cxcr4*. *Hexb* encodes enzymes in lysosomes that break down toxic substances and act as recycling centers (Mahuran, 1999; Ogawa et al., 2018). *Tgfb1* has been shown to promote remyelination in the adult CNS in addition to its classical pro-inflammatory role (Hamaguchi et al., 2019; Mota et al., 2020). *Cxcr4* is a known regulator of remyelination in other models of infection and CNS inflammation (Carbajal et al., 2011; Tian et al., 2018; Beigi Boroujeni et al., 2020). The steady increase in myelination genes throughout the kinetics of chronic *T. gondii* infection demonstrates a possible role of myelination in maintaining neuronal signaling and function to prohibit worsening of neuropathology as well as the possibility of remyelination to heal pathology or reorganize neuronal circuits (David et al., 2016). Thus, further experiments need to be conducted to determine if there is an increase in myelin or attempts at remyelination during infection which are now warranted following this data.

In contrast, the use of resistant BALB/c mice in these experiments reveals enhanced repair and resolution during infection allowing for insights into the role of neurological repair mechanisms in the context of resistance to chronic Toxoplasma infection. BALB/c mice exhibit differences in pathway activation of neuropathology and neurological health and function. Specifically, BALB/c mice experience downregulation in neuropathological and inflammatory pathways and upregulation in neurological transmitter function and neuronal structure compared to C57BL/6. This indicates that BALB/c mice may have differences in specific neurological genes that aid in maintaining neurological signaling and repairing damage done by infection. The differentially expressed neuronal signaling genes *GABRA1* and *GABRG2* and the repair genes *MAGEE1* and *LPAR1* were analyzed in BALB/c mice to answer this question. *GABRA1* and *GABRG2* are both critical for the formation of $GABA_A$ receptors that regulate neuronal signaling (McKernan et al., 1991; Tozuka et al., 2005; Li X. et al., 2020), and these receptors are significantly upregulated in BALB/c mice compared to C57BL/6 mice indicating possible enhanced GABAergic signaling in BALB/c mice brains enabling better control of neuropathology caused by infection. *MAGEE1*, also known as melanoma-associated antigen E1 (MAGE Family Member E1) or *DAMAGE*, is plays roles in neuronal signaling and functions in tissue growth and repair (Albrecht and Froehner, 2004). *LPAR1* induces downstream signaling cascades that are essential for normal brain development and function of the nervous system and functions as intrinsic axon growth modulators for neurons after injury (Fink et al., 2017; Plastira et al., 2019). Both of these genes are also significantly upregulated in BALB/c mice at all chronic time points suggesting enhanced neuronal signaling, DNA repair, and regulation of regrowth of neurons during infection.

It is known that host background is a factor in resistance to *T. gondii* infection. While increased resistance to infection in BALB/c mice has previously been linked to enhanced immune response, less is known regarding how neuropathology signatures differ between resistant BALB/c mice and the more susceptible C57BL/6 model over the course of chronic infection. Results of merged BALB/c vs. C57BL/6 analysis demonstrate differences in gene expression at each stage of chronic infection. BALB/c mice exhibit their largest change in gene expression at 14dpi which then plateaus by 56dpi while the opposite is true for C57BL/6 mice. This indicates that BALB/c mice may experience pathological changes in the brain early during infection which are then at least partially rescued as indicated by the plateauing of gene expression at the later chronic stages. While 350-420 neuropathology and neuroinflammation genes are conserved between the mouse species during infection, BALB/c mice exhibit more downregulated DEGs compared to C57BL/6 mice. This indicates a definitive difference in neuropathology signatures between BALB/c and C57BL/6 mice that indicates less neuropathology in the resistant BALB/c strain.

In conclusion, the results of absolute RNA counts of inflammatory and neuropathology genes support previously published whole genome RNAseq data sets while demonstrating novel gene expression relating to neuropathology and neuroinflammation as chronic Toxoplasma infection progresses. It reveals possible pathways of resolution through the use of a targeted transcriptomic approach in a susceptible and resistant mouse model of infection. The use of this technology presents an additional analysis tool in the *T. gondii* scientific field with the possibility for more strategic analysis in the future. These results also open a doorway to a multitude of potential gene candidates that can be explored to elucidate possible therapeutic targets and to further the vital understanding of the kinetics of chronic infection in the brain.

DATA AVAILABILITY STATEMENT

The data presented in the study are deposited in the Gene Expression Omnibus (GEO) repository (link: https://www.ncbi.nlm.nih.gov/geo/), accession numbers GSE166828 (reference SuperSeries), GSE166825, GSE166826, GSE166827 (SubSeries).

ETHICS STATEMENT

The animal study was reviewed and approved by the Institutional Animal Care and Use Committee (IACUC) University of California Riverside.

AUTHOR CONTRIBUTIONS

KB, DW, and EW designed and conducted the experiments. KB, AB, CD, and EW analyzed the data, and KB and EW wrote the manuscript. All authors contributed to the article and approved the submitted version.

FUNDING

The authors received generous support from the following sources: NIH grants RNS072298 and RAI124682 (EW). EW also received support from UCR Graduate Division. CD is employed by Nanostring.

ACKNOWLEDGMENTS

The authors would like to thank the members of the University of California Riverside's Center for Glial Neuronal Interactions (CGNI) and the Genomics and School of Medicine Research COREs for all advice and use of equipment. We are also thankful for the Bioinformatics team at NanoString Technologies for aiding in customization and the useful advice. Last, we sincerely appreciate the work conducted by UCR's IACUC and the animal husbandry provided by Leslie Karpinski and Linda McCloud.

SUPPLEMENTARY MATERIAL

The Supplementary Material for this article can be found online at: https://www.frontiersin.org/articles/10.3389/fcimb.2021.645778/full#supplementary-material

REFERENCES

Abdelbaset, A. E., Fox, B. A., Karram, M. H., Abd Ellah, M. R., Bzik, D. J., and Igarashi, M. (2017). Lactate dehydrogenase in Toxoplasma gondii controls virulence, bradyzoite differentiation, and chronic infection. *PloS One* 12, e0173745–e0173745. doi: 10.1371/journal.pone.0173745

Agarwal, A. K., Xing, C., DeMartino, G. N., Mizrachi, D., Hernandez, M. D., Sousa, A. B., et al. (2010). PSMB8 encoding the β5i proteasome subunit is mutated in joint contractures, muscle atrophy, microcytic anemia, and panniculitis-induced lipodystrophy syndrome. *Am. J. Hum. Genet.* 87, 866–872. doi: 10.1016/j.ajhg.2010.10.031

Albrecht, D. E., and Froehner, S. C. (2004). DAMAGE, a novel alpha-dystrobrevin-associated MAGE protein in dystrophin complexes. *J. Biol. Chem.* 279, 7014–7023. doi: 10.1074/jbc.M312205200

Appourchaux, R., Delpeuch, M., Zhong, L., Burlaud-Gaillard, J., Tartour, K., Savidis, G., et al. (2019). Functional Mapping of Regions Involved in the Negative Imprinting of Virion Particle Infectivity and in Target Cell Protection by Interferon-Induced Transmembrane Protein 3 against HIV-1. *J. Virol.* 93, e01716–18. doi: 10.1128/JVI.01716-18

Avila, J., Sousa, M. M., and Sayas, C. L. (2020). Editorial: Shaping the Brain by Neuronal Cytoskeleton: From Development to Disease and Degeneration. *Front. Cell. Neurosci.* 14, 12. doi: 10.3389/fncel.2020.00012

Bai, F., McCormack, R. M., Hower, S., Plano, G. V., Lichtenheld, M. G., and Munson, G. P. (2018). Perforin-2 Breaches the Envelope of Phagocytosed Bacteria Allowing Antimicrobial Effectors Access to Intracellular Targets. *J. Immunol.* 201, 2710–2720. doi: 10.4049/jimmunol.1800365

Barbosa, J. L., Béla, S. R., Ricci, M. F., Noviello, M. L. M., Cartelle, C. T., Pinheiro, B. V., et al. (2020). Spontaneous T. gondii neuronal encystment induces structural neuritic network impairment associated with changes of tyrosine hydroxilase expression. *Neurosci. Lett.* 718, 134721. doi: 10.1016/j.neulet.2019.134721

Basler, M., Lindstrom, M. M., LaStant, J. J., Bradshaw, J. M., Owens, T. D., Schmidt, C., et al. (2018a). Co-inhibition of immunoproteasome subunits LMP2 and LMP7 is required to block autoimmunity. *EMBO Rep.* 19, e46512. doi: 10.15252/embr.201846512

Basler, M., Mundt, S., and Groettrup, M. (2018b). The immunoproteasome subunit LMP7 is required in the murine thymus for filling up a hole in the T cell repertoire. *Eur. J. Immunol.* 48, 419–429. doi: 10.1002/eji.201747282

Bedford, J. G., O'Keeffe, M., Reading, P. C., and Wakim, L. M. (2019). Rapid interferon independent expression of IFITM3 following T cell activation protects cells from influenza virus infection. *PloS One* 14, e0210132. doi: 10.1371/journal.pone.0210132

Beigi Boroujeni, F., Pasbakhsh, P., Mortezaee, K., Pirhajati, V., Alizadeh, R., Aryanpour, R., et al. (2020). Intranasal delivery of SDF-1α-preconditioned bone marrow mesenchymal cells improves remyelination in the cuprizone-induced mouse model of multiple sclerosis. *Cell Biol. Int.* 44, 499–511. doi: 10.1002/cbin.11250

Berdoy, M., Webster, J. P., and Macdonald, D. W. (2000). Fatal attraction in rats infected with Toxoplasma gondii. *Proc. Biol. Sci.* 267, 1591–1594. doi: 10.1098/rspb.2000.1182

Bernal, J. A., Luna, R., Espina, A., Lázaro, I., Ramos-Morales, F., Romero, F., et al. (2002). Human securin interacts with p53 and modulates p53-mediated transcriptional activity and apoptosis. *Nat. Genet.* 32, 306–311. doi: 10.1038/ng997

Blackwell, J. M., Roberts, C. W., and Alexander, J. (1993). Influence of genes within the MHC on mortality and brain cyst development in mice infected with Toxoplasma gondii: kinetics of immune regulation in BALB H-2 congenic mice. *Parasite Immunol.* 15, 317–324. doi: 10.1111/j.1365-3024.1993.tb00616.x

Boillat, M., Hammoudi, P. M., Dogga, S. K., Pagès, S., Goubran, M., Rodriguez, I., et al. (2020). Neuroinflammation-Associated Aspecific Manipulation of Mouse Predator Fear by Toxoplasma gondii. *Cell Rep.* 30, 320–334.e6. doi: 10.1016/j.celrep.2019.12.019

Brooks, J. M., Carrillo, G. L., Su, J., Lindsay, D. S., Fox, M. A., and Blader, I. J. (2015). Toxoplasma gondii Infections Alter GABAergic Synapses and Signaling in the Central Nervous System. *mBio* 6, e01428–e01415. doi: 10.1128/mBio.01428-15

Brown, C. R., Hunter, C. A., Estes, R. G., Beckmann, E., Forman, J., David, C., et al. (1995). Definitive identification of a gene that confers resistance against Toxoplasma cyst burden and encephalitis. *Immunology* 85, 419–428.

Burke, J. M., Roberts, C. W., Hunter, C. A., Murray, M., and Alexander, J. (1994). Temporal differences in the expression of mRNA for IL-10 and IFN-gamma in the brains and spleens of C57BL/10 mice infected with Toxoplasma gondii. *Parasite Immunol.* 16, 305–314. doi: 10.1111/j.1365-3024.1994.tb00353.x

Cabral, C. M., Tuladhar, S., Dietrich, H. K., Nguyen, E., MacDonald, W. R., Trivedi, T., et al. (2016). Neurons are the Primary Target Cell for the Brain-Tropic Intracellular Parasite Toxoplasma gondii. *PloS Pathog.* 12, e1005447–e1005447. doi: 10.1371/journal.ppat.1005447

Carbajal, K. S., Miranda, J. L., Tsukamoto, M. R., and Lane, T. E. (2011). CXCR4 signaling regulates remyelination by endogenous oligodendrocyte progenitor cells in a viral model of demyelination. *Glia* 59, 1813–1821. doi: 10.1002/glia.21225

Danaher, P., Warren, S., Dennis, L., D'Amico, L., White, A., Disis, M. L., et al. (2017). Gene expression markers of Tumor Infiltrating Leukocytes. *J. Immunother. Cancer* 5, 18. doi: 10.1186/s40425-017-0215-8

David, C. N., Frias, E. S., Szu, J. I., Vieira, P. A., Hubbard, J. A., Lovelace, J., et al. (2016). GLT-1-Dependent Disruption of CNS Glutamate Homeostasis and Neuronal Function by the Protozoan Parasite Toxoplasma gondii. *PloS Pathog.* 12, e1005643. doi: 10.1371/journal.ppat.1005643

Deckert-Schlüter, M., Schlüter, D., Schmidt, D., Schwendemann, G., Wiestler, O. D., and Hof, H. (1994). Toxoplasma encephalitis in congenic B10 and BALB mice: impact of genetic factors on the immune response. *Infect. Immun.* 62, 221–228. doi: 10.1128/IAI.62.1.221-228.1994

Denkers, E. Y. (1999). T lymphocyte-dependent effector mechanisms of immunity to Toxoplasma gondii. *Microbes Infect.* 1, 699–708. doi: 10.1016/S1286-4579(99)80071-9

Doherty, D. F., Nath, S., Poon, J., Foronjy, R. F., Ohlmeyer, M., Dabo, A. J., et al. (2019). Protein Phosphatase 2A Reduces Cigarette Smoke-induced Cathepsin S and Loss of Lung Function. *Am. J. Respir. Crit. Care Med.* 200, 51–62. doi: 10.1164/rccm.201808-1518OC

Dupont, C. D., Christian, D. A., and Hunter, C. A. (2012). Immune response and immunopathology during toxoplasmosis. *Semin. Immunopathol.* 34, 793–813. doi: 10.1007/s00281-012-0339-3

Falvo, J. V., Uglialoro, A. M., Brinkman, B. M., Merika, M., Parekh, B. S., Tsai, E. Y., et al. (2000). Stimulus-specific assembly of enhancer complexes on the tumor necrosis factor alpha gene promoter. *Mol. Cell Biol.* 20, 2239–2247. doi: 10.1128/MCB.20.6.2239-2247.2000

Felten, D. L., O'Banion, M. K., and Maida, M. S. (2016). "1 - Neurons and Their Properties," in *Netter"s Atlas of Neuroscience (Third Edition)*. Eds. D. L. Felten, M. K. O'Banion and M. S. Maida (Philadelphia: Elsevier), 1–42.

Feustel, S. M., Meissner, M., and Liesenfeld, O. (2012). Toxoplasma gondii and the blood-brain barrier. *Virulence* 3, 182–192. doi: 10.4161/viru.19004

Fink, K. L., López-Giráldez, F., Kim, I. J., Strittmatter, S. M., and Cafferty, W. B. J. (2017). Identification of Intrinsic Axon Growth Modulators for Intact CNS Neurons after Injury. *Cell Rep.* 18, 2687–2701. doi: 10.1016/j.celrep.2017.02.058

Gao, A. Y. L., Ilie, A., Chang, P. K. Y., Orlowski, J., and McKinney, R. A. (2019). A Christianson syndrome-linked deletion mutation (Δ287ES288) in SLC9A6 impairs hippocampal neuronal plasticity. *Neurobiol. Dis.* 130, 104490. doi: 10.1016/j.nbd.2019.104490

Garfoot, A. L., Wilson, G. M., Coon, J. J., and Knoll, L. J. (2019). Proteomic and transcriptomic analyses of early and late-chronic Toxoplasma gondii infection shows novel and stage specific transcripts. *BMC Genomics* 20, 859. doi: 10.1186/s12864-019-6213-0

Gazzinelli, R., Xu, Y., Hieny, S., Cheever, A., and Sher, A. (1992). Simultaneous depletion of CD4+ and CD8+ T lymphocytes is required to reactivate chronic infection with Toxoplasma gondii. *J. Immunol.* 149, 175.

Geiss, G. K., Bumgarner, R. E., Birditt, B., Dahl, T., Dowidar, N., Dunaway, D. L., et al. (2008). Direct multiplexed measurement of gene expression with color-coded probe pairs. *Nat. Biotechnol.* 26, 317–325. doi: 10.1038/nbt1385

Goerner, A. L., Vizcarra, E. A., Hong, D. D., Bergersen, K. V., Alvarez, C. A., Talavera, M. A., et al. (2020). An ex vivo model of Toxoplasma recrudescence. *bioRxiv*. 2020. 05.18.101931. doi: 10.1101/2020.05.18.101931

Gonsette, R. E. (2010). Endogenous neuroprotection in multiple sclerosis. *Acta Neurol. Belg.* 110, 26–35.

Graham, A. K., Fong, C., Naqvi, A., and Lu, J. Q. (2020). Toxoplasmosis of the central nervous system: Manifestations vary with immune responses. *J. Neurol. Sci.* 420, 117223. doi: 10.1016/j.jns.2020.117223

Guevara, R. B., Fox, B. A., Falla, A., and Bzik, D. J. (2019). Toxoplasma gondii Intravacuolar-Network-Associated Dense Granule Proteins Regulate Maturation of the Cyst Matrix and Cyst Wall. *mSphere* 4, e00487–19. doi: 10.1128/mSphere.00487-19

Hamaguchi, M., Muramatsu, R., Fujimura, H., Mochizuki, H., Kataoka, H., and Yamashita, T. (2019). Circulating transforming growth factor-β1 facilitates remyelination in the adult central nervous system. *eLife* 8, e41869. doi: 10.7554/eLife.41869

Handford, C. A., Lynch, J. W., Baker, E., Webb, G. C., Ford, J. H., Sutherland, G. R., et al. (1996). The human glycine receptor beta subunit: primary structure, functional characterisation and chromosomal localisation of the human and murine genes. *Brain Res. Mol. Brain Res.* 35, 211–219. doi: 10.1016/0169-328X(95)00218-H

Harris, T. H., Wilson, E. H., Tait, E. D., Buckley, M., Shapira, S., Caamano, J., et al. (2010). NF-kappaB1 contributes to T cell-mediated control of Toxoplasma gondii in the CNS. *J. Neuroimmunol.* 222, 19–28. doi: 10.1016/j.jneuroim.2009.12.009

Hidano, S., Randall, L. M., Dawson, L., Dietrich, H. K., Konradt, C., Klover, P. J., et al. (2016). STAT1 Signaling in Astrocytes Is Essential for Control of Infection in the Central Nervous System. *mBio* 7, e01881–e01816. doi: 10.1128/mBio.01881-16

Hong, D.-P., Radke, J. B., and White, M. W. (2017). Opposing Transcriptional Mechanisms Regulate Toxoplasma Development. *mSphere* 2, e00347–e00316. doi: 10.1128/mSphere.00347-16

Hu, R. S., He, J. J., Elsheikha, H. M., Zou, Y., Ehsan, M., Ma, Q. N., et al. (2020). Transcriptomic Profiling of Mouse Brain During Acute and Chronic Infections by Toxoplasma gondii Oocysts. *Front. Microbiol.* 11, 570903. doi: 10.3389/fmicb.2020.570903

Huang, W. Y., Wang, Y. P., Mahmmod, Y. S., Wang, J. J., Liu, T. H., Zheng, Y. X., et al. (2019). A Double-Edged Sword: Complement Component 3 in Toxoplasma gondii Infection. *Proteomics* 19, e1800271. doi: 10.1002/pmic.201800271

Hughes, C. S., Colhoun, L. M., Bains, B. K., Kilgour, J. D., Burden, R. E., Burrows, J. F., et al. (2016). Extracellular cathepsin S and intracellular caspase 1 activation are surrogate biomarkers of particulate-induced lysosomal disruption in macrophages. *Part Fibre Toxicol.* 13, 19. doi: 10.1186/s12989-016-0129-5

Ji, C., Tang, M., Harrison, J., Paciorkowski, A., and Johnson, G. V. W. (2018). Nuclear transglutaminase 2 directly regulates expression of cathepsin S in rat cortical neurons. *Eur. J. Neurosci.* 48, 3043–3051. doi: 10.1111/ejn.14159

Ji, R. N., Zhang, L. L., Zhao, M. F., He, H. F., Bai, W., Duan, R. X., et al. (2019). Decreased serum complement component 4 levels in patients with schizophrenia. *Psychiatr. Genet.* 29, 127–129. doi: 10.1097/YPG.0000000000000226

Jia, B., Lu, H., Liu, Q., Yin, J., Jiang, N., and Chen, Q. (2013). Genome-wide comparative analysis revealed significant transcriptome changes in mice after Toxoplasma gondii infection. *Parasit. Vectors* 6, 161–161. doi: 10.1186/1756-3305-6-161

Johnson, J., Suzuki, Y., Mack, D., Mui, E., Estes, R., David, C., et al. (2002). Genetic analysis of influences on survival following Toxoplasma gondii infection. *Int. J. Parasitol.* 32, 179–185. doi: 10.1016/S0020-7519(01)00321-6

Kapitein, L. C., and Hoogenraad, C. C. (2015). Building the Neuronal Microtubule Cytoskeleton. *Neuron* 87, 492–506. doi: 10.1016/j.neuron.2015.05.046

Kenney, A. D., McMichael, T. M., Imas, A., Chesarino, N. M., Zhang, L., Dorn, L. E., et al. (2019). IFITM3 protects the heart during influenza virus infection. *Proc. Natl. Acad. Sci. U. S. A.* 116, 18607–18612. doi: 10.1073/pnas.1900784116

Khan, I. A., Hwang, S., and Moretto, M. (2019). Toxoplasma gondii: CD8 T Cells Cry for CD4 Help. *Front. Cell Infect. Microbiol.* 9, 136. doi: 10.3389/fcimb.2019.00136

Klinngam, W., Fu, R., Janga, S. R., Edman, M. C., and Hamm-Alvarez, S. F. (2018). Cathepsin S Alters the Expression of Pro-Inflammatory Cytokines and MMP-9, Partially through Protease-Activated Receptor-2, in Human Corneal Epithelial Cells. *Int. J. Mol. Sci.* 19, 3530. doi: 10.3390/ijms19113530

Kravets, E., Degrandi, D., Weidtkamp-Peters, S., Ries, B., Konermann, C., Felekyan, S., et al. (2012). The GTPase activity of murine guanylate-binding protein 2 (mGBP2) controls the intracellular localization and recruitment to the parasitophorous vacuole of Toxoplasma gondii. *J. Biol. Chem.* 287, 27452–27466. doi: 10.1074/jbc.M112.379636

Krishnamurthy, S., and Saeij, J. P. J. (2018). Toxoplasma Does Not Secrete the GRA16 and GRA24 Effectors Beyond the Parasitophorous Vacuole Membrane of Tissue Cysts. *Front. Cell. Infect. Microbiol.* 8, 366–366. doi: 10.3389/fcimb.2018.00366

Krishnan, A., Kloehn, J., Lunghi, M., Chiappino-Pepe, A., Waldman, B. S., Nicolas, D., et al. (2020). Functional and Computational Genomics Reveal Unprecedented Flexibility in Stage-Specific Toxoplasma Metabolism. *Cell Host Microbe* 27, 290–306.e11. doi: 10.1016/j.chom.2020.01.002

Lachenmaier, S. M., Deli, M. A., Meissner, M., and Liesenfeld, O. (2011). Intracellular transport of Toxoplasma gondii through the blood-brain barrier. *J. Neuroimmunol.* 232, 119–130. doi: 10.1016/j.jneuroim.2010.10.029

Landrith, T. A., Harris, T. H., and Wilson, E. H. (2015). Characteristics and critical function of CD8+ T cells in the Toxoplasma-infected brain. *Semin. Immunopathol.* 37, 261–270. doi: 10.1007/s00281-015-0487-3

Lee, Y. H., and Kasper, L. H. (2004). Immune responses of different mouse strains after challenge with equivalent lethal doses of Toxoplasma gondii. *Parasite* 11, 89–97. doi: 10.1051/parasite/200411189

Lee, W. J., Fu, R. M., Liang, C., and Sloan, R. D. (2018). IFITM proteins inhibit HIV-1 protein synthesis. *Sci. Rep.* 8, 14551. doi: 10.1038/s41598-018-32785-5

Leng, J., Butcher, B. A., Egan, C. E., Abi Abdallah, D. S., and Denkers, E. Y. (2009). Toxoplasma gondii prevents chromatin remodeling initiated by TLR-triggered macrophage activation. *J. Immunol. (Baltimore Md. 1950)* 182, 489–497. doi: 10.4049/jimmunol.182.1.489

Li, S., Hafeez, A., Noorulla, F., Geng, X., Shao, G., Ren, C., et al. (2017). Preconditioning in neuroprotection: From hypoxia to ischemia. *Prog. Neurobiol.* 157, 79–91. doi: 10.1016/j.pneurobio.2017.01.001

Li, S., He, B., Yang, C., Yang, J., Wang, L., Duan, X., et al. (2020). Comparative transcriptome analysis of normal and CD44-deleted mouse brain under chronic infection with Toxoplasma gondii. *Acta Trop.* 210, 105589. doi: 10.1016/j.actatropica.2020.105589

Li, X., Guo, S., Liu, K., Zhang, C., Chang, H., Yang, W., et al. (2020). GABRG2 Deletion Linked to Genetic Epilepsy with Febrile Seizures Plus Affects the Expression of GABA(A) Receptor Subunits and Other Genes at Different Temperatures. *Neuroscience* 438, 116–136. doi: 10.1016/j.neuroscience.2020.04.049

Liesenfeld, O., Kosek, J., Remington, J. S., and Suzuki, Y. (1996). Association of CD4+ T cell-dependent, interferon-gamma-mediated necrosis of the small intestine with genetic susceptibility of mice to peroral infection with Toxoplasma gondii. *J. Exp. Med.* 184, 597–607. doi: 10.1084/jem.184.2.597

Liesmaa, I., Paakkanen, R., Järvinen, A., Valtonen, V., and Lokki, M. L. (2018). Clinical features of patients with homozygous complement C4A or C4B deficiency. *PloS One* 13, e0199305. doi: 10.1371/journal.pone.0199305

Lilue, J., Müller, U. B., Steinfeldt, T., and Howard, J. C. (2013). Reciprocal virulence and resistance polymorphism in the relationship between Toxoplasma gondii and the house mouse. *Elife* 2, e01298. doi: 10.7554/eLife.01298

Mahuran, D. J. (1999). Biochemical consequences of mutations causing the GM2 gangliosidoses. *Biochim. Biophys. Acta* 1455, 105–138. doi: 10.1016/S0925-4439(99)00074-5

McCormack, R., Hunte, R., Podack, E. R., Plano, G. V., and Shembade, N. (2020). An Essential Role for Perforin-2 in Type I IFN Signaling. *J. Immunol.* 204, 2242–2256. doi: 10.4049/jimmunol.1901013

McKernan, R. M., Quirk, K., Prince, R., Cox, P. A., Gillard, N. P., Ragan, C. I., et al. (1991). GABAA receptor subtypes immunopurified from rat brain with alpha subunit-specific antibodies have unique pharmacological properties. *Neuron* 7, 667–676. doi: 10.1016/0896-6273(91)90379-E

Meijer, B. J., Giugliano, F. P., Baan, B., van der Meer, J. H. M., Meisner, S., van Roest, M., et al. (2020). ATF2 and ATF7 Are Critical Mediators of Intestinal Epithelial Repair. *Cell. Mol. Gastroenterol. Hepatol.* 10, 23–42. doi: 10.1016/j.jcmgh.2020.01.005

Melbourne, J. K., Rosen, C., Feiner, B., and Sharma, R. P. (2018). C4A mRNA expression in PBMCs predicts the presence and severity of delusions in schizophrenia and bipolar disorder with psychosis. *Schizophr. Res.* 197, 321–327. doi: 10.1016/j.schres.2018.01.018

Mendez, O. A., and Koshy, A. A. (2017). Toxoplasma gondii: Entry, association, and physiological influence on the central nervous system. *PloS Pathog.* 13, e1006351–e1006351. doi: 10.1371/journal.ppat.1006351

Michelin, A., Bittame, A., Bordat, Y., Travier, L., Mercier, C., Dubremetz, J.-F., et al. (2009). GRA12, a Toxoplasma dense granule protein associated with the intravacuolar membranous nanotubular network. *Int. J. Parasitol.* 39, 299–306. doi: 10.1016/j.ijpara.2008.07.011

Montoya, J. G., and Liesenfeld, O. (2004). Toxoplasmosis. *Lancet* 363, 1965–1976. doi: 10.1016/S0140-6736(04)16412-X

Mota, M., Porrini, V., Parrella, E., Benarese, M., Bellucci, A., Rhein, S., et al. (2020). Neuroprotective epi-drugs quench the inflammatory response and microglial/macrophage activation in a mouse model of permanent brain ischemia. *J. Neuroinflamm.* 17, 361. doi: 10.1186/s12974-020-02028-4

Mukhopadhyay, D., Arranz-Solís, D., and Saeij, J. P. J. (2020). Influence of the Host and Parasite Strain on the Immune Response During Toxoplasma Infection. *Front. Cell Infect. Microbiol.* 10, 580425. doi: 10.3389/fcimb.2020.580425

Müller, T., Braud, S., Jüttner, R., Voigt, B. C., Paulick, K., Sheean, M. E., et al. (2018). Neuregulin 3 promotes excitatory synapse formation on hippocampal interneurons. *EMBO J.* 37, e98858. doi: 10.15252/embj.201798858

Ngô, H. M., Zhou, Y., Lorenzi, H., Wang, K., Kim, T.-K., Zhou, Y., et al. (2017). Toxoplasma Modulates Signature Pathways of Human Epilepsy, Neurodegeneration & Cancer. *Sci. Rep.* 7, 11496. doi: 10.1038/s41598-017-10675-6

Ni, T., Jiao, F., Yu, X., Aden, S., Ginger, L., Williams, S. I., et al. (2020). Structure and mechanism of bactericidal mammalian perforin-2, an ancient agent of innate immunity. *Sci. Adv.* 6, eaax8286. doi: 10.1126/sciadv.aax8286

Ogawa, Y., Irisa, M., Sano, T., Yanagi, Y., Furusawa, E., Saito, T., et al. (2018). Improvement in dysmyelination by the inhibition of microglial activation in a mouse model of Sandhoff disease. *Neuroreport* 29, 962–967. doi: 10.1097/WNR.0000000000001060

Pałasz, E., Bąk, A., Gąsiorowska, A., and Niewiadomska, G. (2017). The role of trophic factors and inflammatory processes in physical activity-induced neuroprotection in Parkinson's disease. *Postepy Hig. Med. Dosw (Online)* 71, 713–726. doi: 10.5604/01.3001.0010.3850

Park, M., Salgado, J. M., Ostroff, L., Helton, T. D., Robinson, C. G., Harris, K. M., et al. (2006). Plasticity-induced growth of dendritic spines by exocytic trafficking from recycling endosomes. *Neuron* 52, 817–830. doi: 10.1016/j.neuron.2006.09.040

Parker, S. J., Roberts, C. W., and Alexander, J. (1991). CD8+ T cells are the major lymphocyte subpopulation involved in the protective immune response to Toxoplasma gondii in mice. *Clin. Exp. Immunol.* 84, 207–212. doi: 10.1111/j.1365-2249.1991.tb08150.x

Paterson, C., Wang, Y., Hyde, T. M., Weinberger, D. R., Kleinman, J. E., and Law, A. J. (2017). Temporal, Diagnostic, and Tissue-Specific Regulation of NRG3 Isoform Expression in Human Brain Development and Affective Disorders. *Am. J. Psychiatry* 174, 256–265. doi: 10.1176/appi.ajp.2016.16060721

Pittman, K. J., Cervantes, P. W., and Knoll, L. J. (2016). Z-DNA Binding Protein Mediates Host Control of Toxoplasma gondii Infection. *Infect. Immun.* 84, 3063–3070. doi: 10.1128/IAI.00511-16

Plastira, I., Joshi, L., Bernhart, E., Schoene, J., Specker, E., Nazare, M., et al. (2019). Small-Molecule Lysophosphatidic Acid Receptor 5 (LPAR5) Antagonists: Versatile Pharmacological Tools to Regulate Inflammatory Signaling in BV-2 Microglia Cells. *Front. Cell Neurosci.* 13, 531. doi: 10.3389/fncel.2019.00531

Prandovszky, E., Gaskell, E., Martin, H., Dubey, J. P., Webster, J. P., and McConkey, G. A. (2011). The neurotropic parasite Toxoplasma gondii increases dopamine metabolism. *PloS One* 6, e23866–e23866. doi: 10.1371/journal.pone.0023866

Prasad, K. M., Chowdari, K. V., D'Aiuto, L. A., Iyengar, S., Stanley, J. A., and Nimgaonkar, V. L. (2018). Neuropil contraction in relation to Complement C4 gene copy numbers in independent cohorts of adolescent-onset and young adult-onset schizophrenia patients-a pilot study. *Transl. Psychiatry* 8, 134. doi: 10.1038/s41398-018-0181-z

Prevention, C. f. D. C. a (2018). Parasites - Toxoplasmosis (Toxoplasma infection).

Radke, J. B., Worth, D., Hong, D., Huang, S., Sullivan, W. J.Jr., Wilson, E. H., et al. (2018). Transcriptional repression by ApiAP2 factors is central to chronic toxoplasmosis. *PloS Pathog.* 14, e1007035. doi: 10.1371/journal.ppat.1007035

Resende, M. G., Fux, B., Caetano, B. C., Mendes, E. A., Silva, N. M., Ferreira, A. M., et al. (2008). The role of MHC haplotypes H2d/H2b in mouse resistance/susceptibility to cyst formation is influenced by the lineage of infective Toxoplasma gondii strain. *An. Acad. Bras. Cienc.* 80, 85–99. doi: 10.1590/S0001-37652008000100005

Ridderbusch, I. C., Richter, J., Yang, Y., Hoefler, M., Weber, H., Reif, A., et al. (2019). Association of rs7688285 allelic variation coding for GLRB with fear reactivity and exposure-based therapy in patients with panic disorder and agoraphobia. *Eur. Neuropsychopharmacol.* 29, 1138–1151. doi: 10.1016/j.euroneuro.2019.07.133

Saab, A. S., and Nave, K. A. (2017). Myelin dynamics: protecting and shaping neuronal functions. *Curr. Opin. Neurobiol.* 47, 104–112. doi: 10.1016/j.conb.2017.09.013

Schneider, C. A., Figueroa Velez, D. X., Azevedo, R., Hoover, E. M., Tran, C. J., Lo, C., et al. (2019). Imaging the dynamic recruitment of monocytes to the blood-brain barrier and specific brain regions during Toxoplasma gondii infection. *Proc. Natl. Acad. Sci. U. S. A.* 116, 24796–24807. doi: 10.1073/pnas.1915778116

Sellers, R. S., Clifford, C. B., Treuting, P. M., and Brayton, C. (2011). Immunological Variation Between Inbred Laboratory Mouse Strains: Points to Consider in Phenotyping Genetically Immunomodified Mice. *Vet. Pathol.* 49, 32–43. doi: 10.1177/0300985811429314

Serrano-Saiz, E., Vogt, M. C., Levy, S., Wang, Y., Kaczmarczyk, K. K., Mei, X., et al. (2020). SLC17A6/7/8 Vesicular Glutamate Transporter Homologs in Nematodes. *Genetics* 214, 163–178. doi: 10.1534/genetics.119.302855

Sinai, A. P., Watts, E. A., Dhara, A., Murphy, R. D., Gentry, M. S., and Patwardhan, A. (2016). Reexamining Chronic Toxoplasma gondii Infection: Surprising Activity for a "Dormant" Parasite. *Curr. Clin. Microbiol. Rep.* 3, 175–185. doi: 10.1007/s40588-016-0045-3

Spence, J. S., He, R., Hoffmann, H. H., Das, T., Thinon, E., Rice, C. M., et al. (2019). IFITM3 directly engages and shuttles incoming virus particles to lysosomes. *Nat. Chem. Biol.* 15, 259–268. doi: 10.1038/s41589-018-0213-2

Still, K. M., Batista, S. J., O'Brien, C. A., Oyesola, O. O., Früh, S. P., Webb, L. M., et al. (2020). Astrocytes promote a protective immune response to brain Toxoplasma gondii infection via IL-33-ST2 signaling. *PloS Pathog.* 16, e1009027. doi: 10.1371/journal.ppat.1009027

Swierzy, I., Händel, U., Kaever, A., Jarek, M., Scharfe, M., Schlüter, D., et al. (2017). Divergent co-Transcriptomes of different host cells infected with Toxoplasma gondii reveal cell type-specific host-parasite interactions. *Sci. Rep.* 7, 7229. doi: 10.1038/s41598-017-07838-w

Takamori, S., Rhee, J. S., Rosenmund, C., and Jahn, R. (2001). Identification of differentiation-associated brain-specific phosphate transporter as a second vesicular glutamate transporter (VGLUT2). *J. Neurosci.* 21, Rc182. doi: 10.1523/JNEUROSCI.21-22-j0002.2001

Tanaka, S., Nishimura, M., Ihara, F., Yamagishi, J., Suzuki, Y., and Nishikawa, Y. (2013). Transcriptome analysis of mouse brain infected with Toxoplasma gondii. *Infect. Immun.* 81, 3609–3619. doi: 10.1128/IAI.00439-13

Tian, Y., Yin, H., Deng, X., Tang, B., Ren, X., and Jiang, T. (2018). CXCL12 induces migration of oligodendrocyte precursor cells through the CXCR4–activated MEK/ERK and PI3K/AKT pathways. *Mol. Med. Rep.* 18, 4374–4380. doi: 10.3892/mmr.2018.9444

Tomita, T., Bzik, D. J., Ma, Y. F., Fox, B. A., Markillie, L. M., Taylor, R. C., et al. (2013). The Toxoplasma gondii cyst wall protein CST1 is critical for cyst wall integrity and promotes bradyzoite persistence. *PloS Pathog.* 9, e1003823–e1003823. doi: 10.1371/journal.ppat.1003823

Tozuka, Y., Fukuda, S., Namba, T., Seki, T., and Hisatsune, T. (2005). GABAergic excitation promotes neuronal differentiation in adult hippocampal progenitor cells. *Neuron* 47, 803–815. doi: 10.1016/j.neuron.2005.08.023

Tsytsykova, A. V., and Goldfeld, A. E. (2002). Inducer-specific enhanceosome formation controls tumor necrosis factor alpha gene expression in T lymphocytes. *Mol. Cell Biol.* 22, 2620–2631. doi: 10.1128/MCB.22.8.2620-2631.2002

Virreira Winter, S., Niedelman, W., Jensen, K. D., Rosowski, E. E., Julien, L., Spooner, E., et al. (2011). Determinants of GBP recruitment to Toxoplasma gondii vacuoles and the parasitic factors that control it. *PloS One* 6, e24434. doi: 10.1371/journal.pone.0024434

Vyas, A., Kim, S.-K., Giacomini, N., Boothroyd, J. C., and Sapolsky, R. M. (2007). Behavioral changes induced by Toxoplasma infection of rodents are highly specific to aversion of cat odors. *Proc. Natl. Acad. Sci. U. S. A.* 104, 6442–6447. doi: 10.1073/pnas.0608310104

Waldman, B. S., Schwarz, D., Wadsworth, M. H.2nd2nd, Saeij, J. P., Shalek, A. K., and Lourido, S. (2020). Identification of a Master Regulator of Differentiation in Toxoplasma. *Cell* 180, 359–372.e16. doi: 10.1016/j.cell.2019.12.013

Wang, F., Yang, Y. J., Yang, N., Chen, X. J., Huang, N. X., Zhang, J., et al. (2018a). Enhancing Oligodendrocyte Myelination Rescues Synaptic Loss and Improves Functional Recovery after Chronic Hypoxia. *Neuron* 99, 689–701.e5. doi: 10.1016/j.neuron.2018.07.017

Wang, Y. N., Figueiredo, D., Sun, X. D., Dong, Z. Q., Chen, W. B., Cui, W. P., et al. (2018b). Controlling of glutamate release by neuregulin3 via inhibiting the assembly of the SNARE complex. *Proc. Natl. Acad. Sci. U. S. A.* 115, 2508–2513. doi: 10.1073/pnas.1716322115

Watson, G., Ronai, Z. E. A., and Lau, E. (2017). ATF2, a paradigm of the multifaceted regulation of transcription factors in biology and disease. *Pharmacol. Res.* 119, 347–357. doi: 10.1016/j.phrs.2017.02.004

Watts, E., Zhao, Y., Dhara, A., Eller, B., Patwardhan, A., and Sinai, A. P. (2015). Novel Approaches Reveal that Toxoplasma gondii Bradyzoites within Tissue Cysts Are Dynamic and Replicating Entities In Vivo. *mBio* 6, e01155–e01115. doi: 10.1128/mBio.01155-15

Webster, J. P., and McConkey, G. A. (2010). Toxoplasma gondii-altered host behaviour: clues as to mechanism of action. *Folia Parasitol. (Praha)* 57, 95–104. doi: 10.14411/fp.2010.012

Xiao, J., Li, Y., Jones-Brando, L., and Yolken, R. H. (2013). Abnormalities of neurotransmitter and neuropeptide systems in human neuroepithelioma cells infected by three Toxoplasma strains. *J. Neural Transm. (Vienna)* 120, 1631–1639. doi: 10.1007/s00702-013-1064-3

Xiao, J., Li, Y., Gressitt, K. L., He, H., Kannan, G., Schultz, T. L., et al. (2016). Cerebral complement C1q activation in chronic Toxoplasma infection. *Brain Behav. Immun.* 58, 52–56. doi: 10.1016/j.bbi.2016.04.009

Yang, B. Y., Song, J. W., Sun, H. Z., Xing, J. C., Yang, Z. H., Wei, C. Y., et al. (2018). PSMB8 regulates glioma cell migration, proliferation, and apoptosis through modulating ERK1/2 and PI3K/AKT signaling pathways. *BioMed. Pharmacother.* 100, 205–212. doi: 10.1016/j.biopha.2018.01.170

Yuan, R., Musters, C. J. M., Zhu, Y., Evans, T. R., Sun, Y., Chesler, E. J., et al. (2020). Genetic differences and longevity-related phenotypes influence lifespan and lifespan variation in a sex-specific manner in mice. *Aging Cell* 19, e13263. doi: 10.1111/acel.13263

Zhang, X., Horwitz, G. A., Prezant, T. R., Valentini, A., Nakashima, M., Bronstein, M. D., et al. (1999). Structure, expression, and function of human pituitary tumor-transforming gene (PTTG). *Mol. Endocrinol.* 13, 156–166. doi: 10.1210/mend.13.1.0225

Zhang, Y. W., Kim, K., Ma, Y. F., Wittner, M., Tanowitz, H. B., and Weiss, L. M. (1999). Disruption of the Toxoplasma gondii bradyzoite-specific gene BAG1 decreases in vivo cyst formation. *Mol. Microbiol.* 31, 691–701. doi: 10.1046/j.1365-2958.1999.01210.x

Zhou, J., and Wang, L. (2017). SAG4 DNA and Peptide Vaccination Provides Partial Protection against T. gondii Infection in BALB/c Mice. *Front. Microbiol.* 8, 1733–1733. doi: 10.3389/fmicb.2017.01733

Conflict of Interest: CD is an employee of NanoString.

The remaining authors declare that the research was conducted in the absence of any commercial or financial relationships that could be construed as a potential conflict of interest.

frontiers in Cellular and Infection Microbiology

ORIGINAL RESEARCH
published: 04 May 2021
doi: 10.3389/fcimb.2021.672720

CX_3CL1 Recruits NK Cells Into the Central Nervous System and Aggravates Brain Injury of Mice Caused by *Angiostrongylus cantonensis* Infection

Rong Zhang[1], Tingting Miao[2], Min Qin[2], Chengsi Zhao[2], Wei Wang[2], Chengcheng Zhang[2], Xinjian Liu[2], Ying Chen[3], Ailing Chen[3] and Yong Wang[2]**

[1] Experimental Teaching Center of Basic Medicine, Nanjing Medical University, Nanjing, China, [2] Department of Pathogen Biology, Key Laboratory of Pathogen Biology of Jiangsu Province, Nanjing Medical University, Nanjing, China, [3] Translational Medicine Laboratory, Research Institute for Reproductive Health and Genetic Diseases, The Affiliated Wuxi Maternity and Child Health Care Hospital of Nanjing Medical University, Wuxi, China

OPEN ACCESS

Edited by:
Tatiana Barichello,
University of Texas Health Science Center at Houston, United States

Reviewed by:
Diego Luis Costa,
University of São Paulo, Brazil
Saikat Majumder,
University of Pittsburgh, United States

***Correspondence:**
Ailing Chen
chenailing@njmu.edu.cn
Yong Wang
yongwsh@njmu.edu

Specialty section:
This article was submitted to Parasite and Host, a section of the journal Frontiers in Cellular and Infection Microbiology

Received: 26 February 2021
Accepted: 20 April 2021
Published: 04 May 2021

Citation:
Zhang R, Miao T, Qin M, Zhao C, Wang W, Zhang C, Liu X, Chen Y, Chen A and Wang Y (2021) CX_3CL1 Recruits NK Cells Into the Central Nervous System and Aggravates Brain Injury of Mice Caused by Angiostrongylus cantonensis Infection. Front. Cell. Infect. Microbiol. 11:672720. doi: 10.3389/fcimb.2021.672720

Background: *Angiostrongylus cantonensis* (*A. cantonensis*), is a food-borne zoonotic parasite that can cause central nervous system (CNS) injury characterized by eosinophilic meningitis. However, the pathogenesis of angiostrongylosis remains elusive. Natural killer cells (NK cells) are unique innate lymphocytes important in early defense against pathogens. The aim of this study was to investigate the role of NK cells in *A. cantonensis* infection and to elucidate the key factors that recruit NK cells into the CNS.

Methods: Mouse model of *A. cantonensis* infection was established by intragastric administration of third-stage larvae. The expression of cytokines and chemokines at gene and protein levels was analyzed by qRT-PCR and ELISA. Distribution of NK cells was observed by immunohistochemistry and flow cytometry. NK cell-mediated cytotoxicity against YAC-1 cells was detected by LDH release assay. The ability of NK cells to secrete cytokines was determined by intracellular flow cytometry and ELISA. Depletion and adoptive transfer of NK cells *in vivo* was induced by tail vein injection of anti-asialo GM1 rabbit serum and purified splenic NK cells, respectively. CX_3CL1 neutralization experiment was performed by intraperitoneal injection of anti-CX_3CL1 rat IgG.

Results: The infiltration of NK cells in the CNS of *A. cantonensis*-infected mice was observed from 14 dpi and reached the peak on 18 and 22 dpi. Compared with uninfected splenic NK cells, the CNS-infiltrated NK cells of infected mice showed enhanced cytotoxicity and increased IFN-γ and TNF-α production ability. Depletion of NK cells alleviated brain injury, whereas adoptive transfer of NK cells exacerbated brain damage in *A. cantonensis*-infected mice. The expression of CX_3CL1 in the brain tissue and its receptor CX_3CR1 on the CNS-infiltrated NK cells were both elevated after *A. cantonensis* infection. CX_3CL1 neutralization reduced the percentage and absolute number of the CNS-infiltrated NK cells and relieved brain damage caused by *A. cantonensis* infection.

Conclusions: Our results demonstrate that the up-regulated CX_3CL1 in the brain tissue recruits NK cells into the CNS and aggravates brain damage caused by *A. cantonensis* infection. The findings improve the understanding of the pathogenesis of angiostrongyliasis and expand the therapeutic intervention in CNS disease.

Keywords: CX_3CL1, NK cells, *Angiostrongylus cantonensis*, infection, brain injury, central nervous system

INTRODUCTION

Angiostrongylus cantonensis (*A. cantonensis*), is a food-borne zoonotic parasite that can cause damage to the central nervous system (CNS) (Wang et al., 2012). With the development of global logistics transportation and climate warming, *A. cantonensis* has spread from its traditional endemic regions of Southeast Asia and the Pacific islands to the American continent, Europe, Africa and Australia (Gelis et al., 2011; Iwanowicz et al., 2015; Liu et al., 2018; Rael et al., 2018; Barbosa et al., 2020; Federspiel et al., 2020). Angiostrongyliasis has become a potentially fatal globally emerging infectious disease.

Humans and mouse are both non-permissive hosts of *A. cantonensis* and become infected *via* ingestion of raw or undercooked intermediate hosts including snails or slugs, or vegetables or water contaminated by the infective third-stage larvae (Barratt et al., 2016). After penetrating the intestinal wall, the larvae migrate in the body with the flow of blood, and finally settle in the CNS. These larvae in non-permissive hosts cannot develop into adults, but can survive in the form of larvae for a long time (Lv et al., 2017). Most patients when infected with *A. cantonensis* develop eosinophilic meningitis and common clinical symptoms include headache, fever, neck stiffness, paresthesia and vomiting (Martins et al., 2015). However, the pathogenesis of angiostrongyliasis is not fully understood. Mechanical damage to the CNS caused by the larvae' movements, inflammation and immune response induced by the larval secretion and excreta, may be involved (Gosnell and Kramer, 2013; Martins et al, 2015; Mengying et al., 2017).

Natural killer cells (NK cells) are a special type of lymphocyte critical to the innate immune system. They are able to rapidly kill target cells by cytotoxicity without antigen presentation and regulate immune response by secreting various cytokines and chemokines (Vivier et al., 2011). NK cells are one of the earliest cell types to arrive at target organs of inflammation. It was reported that NK cells could migrate to the CNS under several pathological conditions, such as brain ischemia, traumatic injury, or infections (Hao et al., 2010; Gan et al., 2014; Zhang et al., 2014; Li et al., 2020). However, very little is known about whether NK cells are involved in the brain injury caused by *A. cantonensis* infection. NK cells derived from bone marrow and migrate through the blood to the spleen, liver, lung and many other organs (Abel et al., 2018). They can respond to a large array of chemokines and be recruited to distinct sites during physiological and pathological conditions. For example, CCL2 attracts $CCR2^+$ NK cells to the liver during murine cytomegalovirus (MCMV) infection (Hokeness et al., 2005), CX_3CL1 recruit CX_3CR1^+ NK cells into the CNS of experimental autoimmune encephalomyelitis (EAE) mice (Huang et al., 2006), CXCL10 attracts $CXCR3^+$ NK cells accumulate into the ischemic brain tissues (Zhang et al., 2014), CCL3/CCL4/CCL5 attracts $CCR5^+$ NK cells to the synovial fluid of rheumatoid arthritis (RA) patients (Parolini et al., 2007). The mechanism of recruitment of NK cells across the blood-brain barrier (BBB) into the CNS needs to be studied.

The aim of this study was to investigate the role of NK cells in the brain injury caused by *A. cantonensis* infection and to elucidate the key factors that recruit NK cells into the CNS. Our findings will be helpful to further understand the pathogenesis of angiostrongyliasis and expand therapeutic intervention in CNS disease.

MATERIALS AND METHODS

Animal Experiments

A total of 300 female BALB/c mice (6–8 weeks old and weighing 18-20 g) were purchased from the Animal Core Facility of Nanjing Medical University (China), maintained in a specific pathogen-free environment, and provided unlimited access to food and water. All experiments were performed in strict compliance with the institutional guidelines and were approved by the Institutional Animal Care and Use Committee of Nanjing Medical University (Approval No. IACUC-1812040). Each mouse was infected with 20 *A. cantonensis* third-stage larvae (L3) by intragastric administration. L3 were isolated from *A. cantonensis*-infected Biomphalaria glabrata using the method described previously (Mengying et al., 2017). The mice were euthanized on 10, 14, 18, 22, and 26 days post-infection (dpi).

Experimental Grouping

The experiment was grouped according to different objectives.

To detect the effect of *A. cantonensis* infection on mice and the percentage and absolute number of NK cells, the mice were divided into five groups according to the time of infection with twelve mice per group: 0, 10, 14, 18 and 22 dpi.

When detecting the phenotypic and functional changes of NK cells, cells were isolated from mice on 18 dpi and divided into three groups with three to four mice per group: splenic NK cells of uninfected mice (uninfected sNK), splenic NK cells of infected mice (infected sNK) and brain NK cells of infected mice (infected bNK).

In the experiment of NK cell depletion, NK cell adoptive transfer and CX_3CL1 neutralization, the mice were euthanatized on 18 dpi and divided into four groups with twelve mice per group: uninfected group, infected group, NK depleted/NK

transferred/CX_3CL1 neutralized group and depleted/transferred/isotype control group.

Neurological Impairment Evaluation

Longa's score, Clark's general score and Clark's focal score were used to evaluate the neurological impairment of mice infected with *A. cantonensis*. Longa's score is based on a five-point scale, where 0 point indicates no neurologic deficit, 1 point (failure to extend forepaw fully) a mild focal neurologic deficit, 2 point (circling to one side) a moderate focal neurologic deficit, 3 point (falling to one side) a severe focal deficit, and animals with 4 point cannot walk spontaneously or lose consciousness (Clark et al., 1997). Clark's general score includes hair, ears, eyes, posture, autonomous movement, and epileptic seizures. Clark's focal score comprises of body symmetry, gait, climbing, rotation test, forelimb symmetry and beard reactivity (Longa et al., 1989). Clark's general score and Clark's focal score are between 0 and 28. The higher the score, the more serious the neurological impairment is. The mice were scored by two technicians using a blind method.

Histopathological Examination

Mice were perfused transcardially with 0.9% sodium chloride followed by 4% paraformaldehyde after anesthetized with 2% pentobarbital sodium (Sigma-Aldrich, USA). Brain samples were collected, fixed in 10% neutral formalin, embedded in paraffin, and cut into 3 μm-thick sections. Brain sections were then de-paraffinized in xylene, rehydrated *via* graded alcohols and stained with hematoxylin and eosin (H&E) (Biosharp, Wuhan, China). The sections were observed and photographed under a light microscope (Leica, Heidelberg, Germany).

For immunohistochemistry (IHC) analysis, brain sections were subjected to antigen retrieval by boiling the slices in citrate buffer (pH 6.0) with high heat for 15 min. Then sections were treated with 3% H_2O_2 for 10 min to remove endogenous peroxidase, blocked with 5% rabbit serum at room temperature for 20 min, and incubated with rabbit anti-mouse CD49b monoclonal antibody (mAb) (Abcam, Cambridge, UK) at 4°C overnight. After being washed in PBS, the sections were incubated with an HRP-conjugated secondary antibody (DAKO, Glostrup, Denmark) at room temperature for 15 min and then stained with 3, 3'-diaminobenzidine (DAB) for 10 min. Haematoxylin was used for cell nuclei detection. The sections were visualized and digitally scanned with a light microscope.

Quantitative Reverse Transcription PCR (qRT-PCR)

Total RNA was extracted from mouse brains and NK cells using TRIzol Reagent (Thermo Fisher Scientific, USA) and reverse-transcribed to cDNA using a PimerScript™ RT Master Mix (TaKaRa, Kusatsu, Japan). qRT-PCR was performed on the LightCycler480® Real-Time PCR System (Roche, Reinach, Switzerland) with the RealUniversal Color PreMix (SYBR Green) (Tiangen, Beijing, China), in accordance with the manufacturer's instructions. The primer sequences were shown in **Table S1**. The mRNA levels of these genes were measured by the Ct value (threshold cycle), and the relative expression levels were calculated with the $2^{-\Delta\Delta Ct}$ method.

Detection of Cytokine Expression in Brain Tissue

Each brain tissue was added into 4 mL tissue lysate (RayBiotech, USA) and 20 μL protease inhibitor (Merck, Germany) and homogenized in a gentle MACS separator (MiltenyiBiotec, Bergisch Gladbach, Germany). The total protein concentration in each sample was detected by BCA Protein Assay Kit (Tiangen, Beijing, China) according to the manufacturer's instructions. And then, the levels of cytokines (IL-1β, IL-6 and TNF-α) and chemokines (CCL1, CCL2, CCL3, CCL4, CCL5, CXCL10 and CX_3CL1 in brain tissue homogenate samples were determined with commercial ELISA Kits (MultiSciences, Hangzhou, China) according to the manufacturer's manuals.

Cell Isolation

Blood was collected by eyeball bleeding and gathered in tubes with 1% heparin sodium (Sigma-Aldrich, USA). The mice were anesthetized and perfused as described previously. And then, the brain, spleen, tibia, and femur were collected from the mice respectively.

Brain tissues were homogenized in grinders and filtered through a 70-μm cell strainer. And then cell pellets were resuspended in 30% Percoll (GE Healthcare, Pittsburgh, USA) and centrifuged against 70% Percoll. The cells between the 30–70% Percoll interfaces were collected as the brain mononuclear cells. Spleen was grinded with a syringe core and filtered through a nylon membrane. Erythrocytes were lysed and removed using Red Cell Lysis Buffer (Beyotime, Shanghai, China). Blood was double diluted and layered on the Ficoll-Paque (GE Healthcare, Pittsburgh, USA). After centrifugation, peripheral blood mononuclear cells (PBMCs) were distributed between plasma and Ficoll-Paque. PBMCs were transferred and resuspended in PBS. The tibia and femur bones were used to prepare bone marrow cells. The medullary cavity was washed repeatedly with RPMI-1640 (Gibco B, Gaithersburg, MD, USA) by syringe and bone marrow cells were collected and separated from erythrocytes.

NK cells were purified from brain mononuclear cells and splenic lymphocytes using a magnetic cell sorting system (MACS) incorporating anti-mice CD49 MicroBeads (MiltenyiBiotec, Bergisch Gladbach, Germany), following the manufacturer's instructions. The purity of $CD3^-CD49^+$ NK cells after sorting was over 90% detected by FCM (**Figure S1**).

Flow Cytometry (FCM)

Cells isolated from the brain, spleen, peripheral blood, and bone marrow were prepared to single cell suspension and resuspended in FCM buffer (0.5% BSA in PBS). For Cell surface marker detection, cells were incubated with TruStain FcX™ anti- CD16/32 (Biolegend, San Diego, USA) to block Fc-receptor for 5 min at 4 °C and then stained with the following specific antibodies: anti-CD45-percp-cy5.5, anti-CD3-FITC, anti-CD49b-APC, anti-CD122-PE, anti-CD69-PE, anti-NKp46-PE, anti-NKG2D-PE, anti-NKG2A-PE, anti-CD107a-PE mAbs or isotype controls (Biolegend, San Diego, USA) for 30 min at 4 °C. Cells were then detected on a Verse flow cytometer (BD Biosciences, San Jose, CA, USA). Data analysis was performed using FlowJo software (TreeStar, Ashland, USA). Gating strategy for the

mouse $CD45^+CD3^-CD49b^+$ NK cell population was shown in **Figure S2**.

For intracellular cytokine analysis, cells were cultured at a density of 2×10^6/ml densities in 12-well plates and stimulated with 2 μL/mL Leukocyte Activation Cocktail plus GolgiPlug (BD Biosciences, San Jose, CA, USA) for 5 h. Cells were collected and stained with anti-CD45-percp-cy5.5, anti-CD3-FITC, anti-CD49b-APC mAbs for 30 min at 4 °C. After washing, cells were fixed and permeabilized using Cytofix/Cytoperm™ Fixation/Permeabilization Kit (BD Biosciences, San Jose, CA, USA) according to the manufacturer's instructions. And then cells were incubated with anti-TNF-α-PE, anti- IFN-γ-BV421 mAbs or isotype controls (Biolegend, San Diego, USA) for 30 min at 4 °C. Cells were detected and data were analyzed as described previously.

NK Cell Cytotoxicity Assays

NK cell-mediated cytotoxicity was determined using the Cytotoxicity Detection Kit^{PLUS} (Roche, Reinach, Switzerland) based on the measurement of LDH released from damaged cells according to the manufacturer's manual. Purified NK cells (as effector cells) were incubated with YAC-1 cells (as target cells) at various effector cell/target cell ratios (1:1, 5:1, 10:1, 20:1) in 96-well plates for 3.5 h. All test samples were prepared in triplicate. Reaction mixture and stop solution were added into each well in turn. The absorbance of the samples was measured at 490 nm by an ELISA reader. The percentage of NK cell-mediated cytotoxicity was calculated by ODs using the following equation: Cytotoxicity (%) = (effector/target cell mix - effector cell control - low control)/(high control - low control) × 100.

Detection of NK Cells Cytokine Secretion

Freshly purified NK cells were cultured in 24-well plates at a density of 1×10^6/mL in the presence of 1 ng/mL IL-12 (PeproTech, Rocky Hill, NJ, USA). After 24 h of incubation, the culture supernatants were harvested. The concentrations of TNF-α and IFN- γ in supernatants were detected using Mouse TNF-α or IFN- γ High Sensitivity ELISA Kits (MultiSciences, Hangzhou, China) according to the instructions of the manufacturer.

Depletion of NK Cells

5-7 Ganglio-N-tetraosylceramide (asialo GM1) is a glycolipid expressed on NK cells in mice, rats, and humans. Depletion of NK cells *in vivo* in infected mice was induced by tail vein injection of anti-asialo GM1 rabbit serum (Wako Pure Chemical Industries, Japan) according to the instructions from manufacturer and other researchers (Nishikado et al., 2011; Golic et al., 2016). Injection time and dose were shown in **Table 1**. Normal rabbit serum (Abbkine, CA, USA) were given to the infected mice at the same time as control. To evaluate the effect of NK cell depletion, the mice were euthanatized at 18 dpi and the percentage and absolute number of NK cells in brain and spleen were analyzed by FCM.

TABLE 1 | Injection time and dose of anti-asialo GM1.

Injection	1st	2nd	3rd	4th
Days post-infection	0	5	10	15
Dose (μL per mouse)	20	20	20	20

Adoptive Transfer of NK Cells

The splenic NK cells from normal mice were purified using MACS and were suspended in PBS. The NK cells (1×10^6/mouse in 200 μL PBS) were transferred to the infected mice by tail vein injection on 12 dpi according to the protocols published by other investigators (Voynova et al., 2015). The respective diluents were injected to the control mice simultaneously. To evaluate the effect of adoptive transfer, the mice were euthanatized at 18 dpi and the percentage and absolute number of NK cells in brain and spleen were analyzed by FCM.

In Vivo CX_3CL1 Neutralization Experiment

To neutralize CX_3CL1 *in vivo*, *A. cantonensis*-infected mice were injected intraperitoneally with anti-CX_3CL1 rat IgG (R&D Systems, MN, USA) or isotype anti-rat IgG (R&D Systems, MN, USA) (4 μg/mouse) once a day from 10 dpi to 17 dpi according to the instructions from manufacturer and other researchers (Mills et al., 2012; Okuma et al., 2017). The mice were euthanatized and detected at 18 dpi to evaluate the effect of CX_3CL1 neutralization.

Statistical Analysis

Statistical analyses were performed using GraphPad Prism 5.0 (GraphPad Software, San Diego, USA). Survival curve comparison was determined using Log-rank Test. Comparison of the neurological impairment scores was performed using non-parametric test. The difference between two groups was compared using independent-samples T test. Multiple comparison procedures were carried out with one-way analysis of variance (ANOVA). The correlation between the percentage and absolute number of NK cells in different tissues was analyzed by linear correlation. The data are presented as the mean ± standard deviation (SD). A P value < 0.05 was considered statistically significant.

RESULTS

NK Cells Infiltrate Into the CNS of Mice Infected With *A. cantonensis*

We constructed a mouse model of *A. cantonensis* infection by intragastric administration of third-stage larvae. To evaluate the pathological damage caused by *A. cantonensis* infection, the survival rate, body weight, neurological function, histological changes and cytokine levels in brain tissue were detected on 0, 10, 14, 18 and 22 dpi. As shown in **Figure S3**, infected mice showed decreased survival rate, reduced body weight, increased neurological dysfunction, aggravated tissue damage, and elevated levels of inflammatory cytokines (IL-1β, IL-6 and TNF-α) on 18 and 22 dpi, compared with that of 0 dpi.

And then, we prepared the brain tissue sections with H&E staining. We observed that the meninges were damaged and more and more inflammatory cells infiltrated under the meninges from 14 to 22 dpi (**Figure 1A**). In order to detect

the presence of NK cells in these infiltrating inflammatory cells, we performed IHC staining on brain tissue sections using anti-CD49b mAb as NK cell marker. **Figures 1B, C** showed that almost no NK cell was observed in the CNS on 0 dpi and 10 dpi. On 14 dpi, a small number of NK cells staining brown appeared under the meninges indicating that NK cells began to infiltrate into the CNS. On 18 dpi, more NK cells appeared in the CNS and the number of CNS-infiltrated NK cells peaked on 22 dpi. To monitor NK cells quantitatively, brain mononuclear cells were isolated and analyzed by FCM. As shown in **Figures 1D–F**, few NK cells were detected in the brain tissue at 0 dpi and 10 dpi. From 14 dpi to 22 dpi, the percentage and absolute number of CNS-infiltrated NK cells increased gradually with the extension of infection time. The highest percentage of CNS-infiltrated NK cells appeared on 22 dpi (22 dpi *vs* 0 dpi: 17.47 ± 6.11% *vs* 0.45 ± 0.12%, $P < 0.001$) and the maximum number of CNS-infiltrated NK cells were found on 18 dpi (18 dpi *vs* 0 dpi: $1.92 \pm 0.43 \times 10^5$ *vs* 696.90 ± 617.20 cells/mouse, $P < 0.001$).

We further analyzed the distribution of NK cells in the spleen, peripheral blood and bone marrow of *A. cantonensis*-infected mice. The results showed that the percentage and absolute number of NK cells in splenic lymphocytes decreased on 14, 18 and 22 dpi (**Figures 2A, C, D**). So did the absolute number of NK cells in PBMCs from 10 dpi to 22 dpi (**Figures 2B, E, F**). Furthermore, the percentage and absolute number of sNK (NK cells in spleen) were negatively correlated with those of bNK (NK cells in brain) (r =–;0.79, $P < 0.01$; r =–0.85, $P < 0.01$) (**Figures 2G, H**). The percentage and absolute number of pbNK (NK cells in PBMCs) and bNK were also negatively correlated, but there was no statistical significance (**Figures 2I, J**). However, the percentage of total NK cells (bmNK, $CD122^+$), NK precursor cells (NKP, $CD49b^-CD122^+$) and mature NK cells (mature NK,

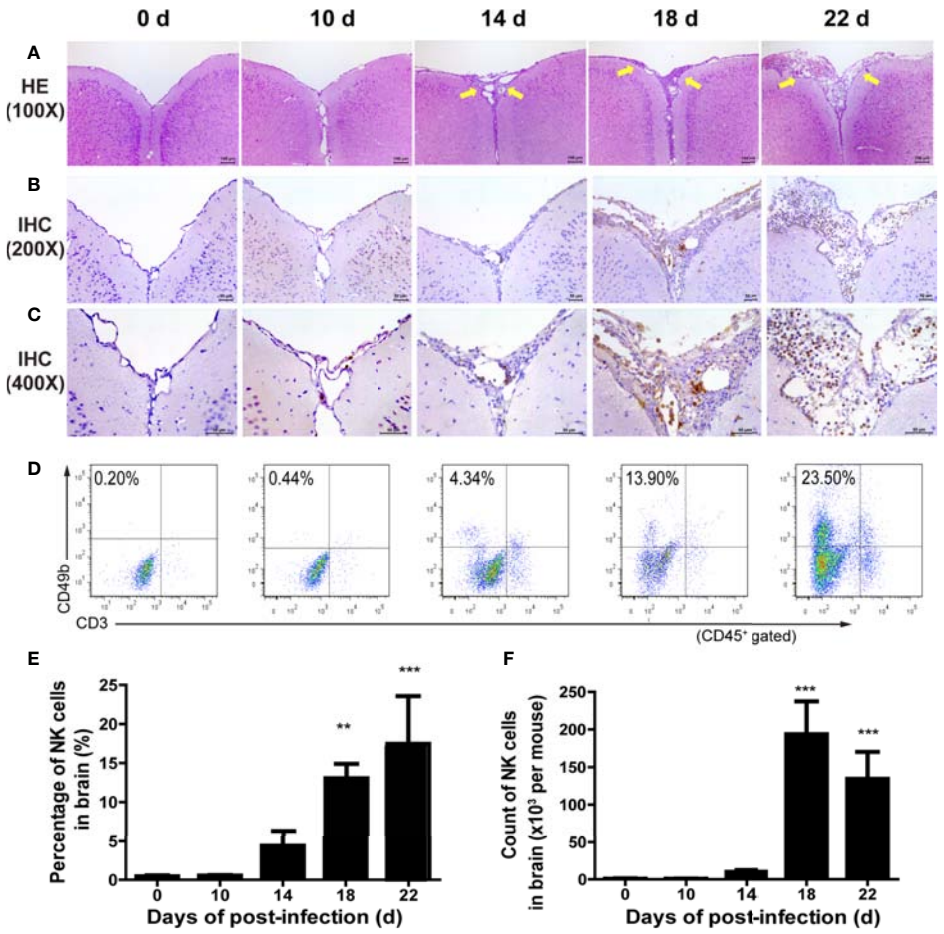

FIGURE 1 | NK cells infiltrated into the CNS after *A. cantonensis* infection. **(A)** Representative histopathological sections of brain tissue in infected mice with H&E staining. The meninges of infected mice were damaged and inflammatory cells infiltrated under the meninges (yellow arrow) from 14 to 22 dpi. Images are shown at 100 × magnification (Scale bar, 100 μm). **(B, C)** Representative histopathological sections of brain tissue in infected mice with IHC staining. Brain sections were incubated with rabbit anti-mouse CD49b monoclonal antibody and stained with DAB. From 14 dpi to 22 dpi, more and more NK cells (stained brown) appeared under the meninges. Images are shown at 200 × and 400×magnification (Scale bar, 100 μm). **(D–F)** The percentage and absolute number of NK cells in brain mononuclear cells of infected mice. NK cells in brain mononuclear cells were detected by FCM. Data shown represent analysis from two independent experiments with three mice per group. Significance was determined by one-way ANOVA. $^{**}P < 0.01$; $^{***}P < 0.001$, compared with that of 0 dpi.

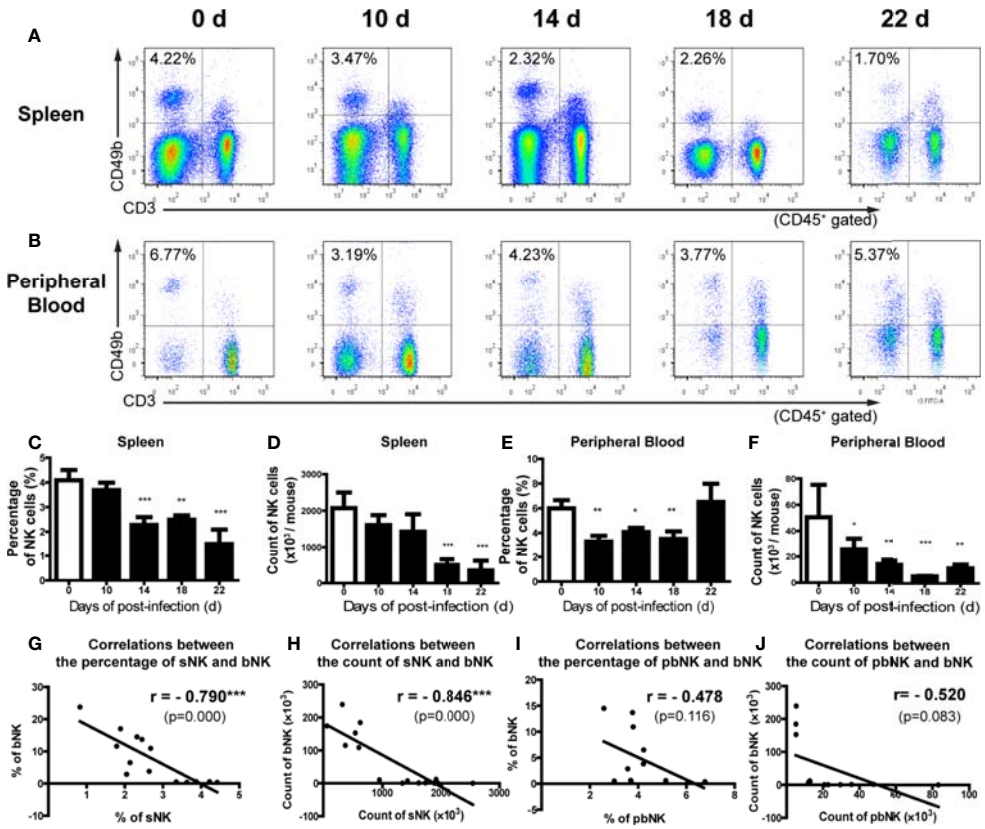

FIGURE 2 | The percentage and absolute number of NK cells in spleen and peripheral blood decreased after *A. cantonensis* infection. **(A, C, D)** The percentage and absolute number of NK cells in splenic lymphocytes of infected mice. **(B, E, F)** The percentage and absolute number of NK cells peripheral blood mononuclear cells of infected mice. NK cells in the splenic lymphocytes and peripheral blood mononuclear cells were detected by FCM. **(G, H)** The correlation between the percentage and absolute number of NK cells in spleen and brain. **(I, J)** The correlation between the percentage and absolute number of NK cells in peripheral blood and brain. Data are expressed as the means ± SD. Data shown represent analysis from two independent experiments with three mice per group. Multiple comparisons of the percentage and count of NK cells at different time-points of infection were performed by one-way ANOVA. The correlation between the percentage and absolute number of NK cells in different tissues was analyzed by linear correlation. $^{*}P < 0.05$; $^{**}P < 0.01$; $^{***}P < 0.001$, compared with that of 0 dpi. sNK, NK cells in spleen; bNK, NK cells in brain; pbNK, NK cells in peripheral blood.

$CD49b^{+}CD122^{+}$) in bone marrow all significantly increased on 18 and 22 dpi (**Figures 3A–D**). And the ratio of NKP to mature NK in bone marrow was up-regulated (**Figure 3E**). In addition, the percentage of total NK cells in bone marrow was positively correlated with that of bNK (r = 0.87, $P < 0.001$) (**Figure 3F**). Our results also showed that the percentage of T cells in splenic lymphocytes increased (22 dpi *vs* 0 dpi: 48.62 ± 6.65% *vs* 33.61 ± 2.23%, $P < 0.01$), while the absolute number of splenic T cells decreased with the extension of infection time (22 dpi *vs* 0 dpi: 9.77 ± 4.22 × 10^6 *vs* 16.97 ± 2.74 × 10^6 cells/mouse, $P < 0.05$) (**Figure S4**).

CNS-Infiltrated NK Cells of *A. cantonensis*-Infected Mice Have Elevated Cytotoxicity and Secretory Ability

We further detected the phenotypic and functional changes of NK cells after *A. cantonensis* infection. We measured the expression of activation marker CD69, activated receptor NKp46 and NKG2D, and inhibitory receptor NKG2A on NK cells by FCM. **Figure 4** revealed that infected bNK and infected sNK expressed lower levels of CD69, NKp46 and NKG2D, but higher levels of NKG2A, compared with uninfected sNK. Although the phenotypic changes of infected bNK were greater than those of infected sNK, there was no statistical difference between them.

Then we detected NK cell-mediated cytotoxicity against YAC-1 cells by LDH release assay. As shown in **Figure 5A**, infected bNK and infected sNK had enhanced cytotoxicity, compared with uninfected sNK (infected bNK *vs* infected sNK *vs* uninfected sNK: 19.37% *vs* 10.59% *vs* 8.35%, as Effect cells: Target cells = 20:1). Furthermore, the expression of CD107a, a surface marker of NK cell degranulation, on infected bNK and infected sNK was up-regulated compared with that of uninfected sNK (**Figures 5B, C**).

The ability of NK cells to secrete cytokines was determined by two methods: ELISA (secretory levels) and FCM (intracellular levels). Firstly, we detected the concentrations of TNF-α and IFN-γ in the culture supernatant of NK cells after IL-12

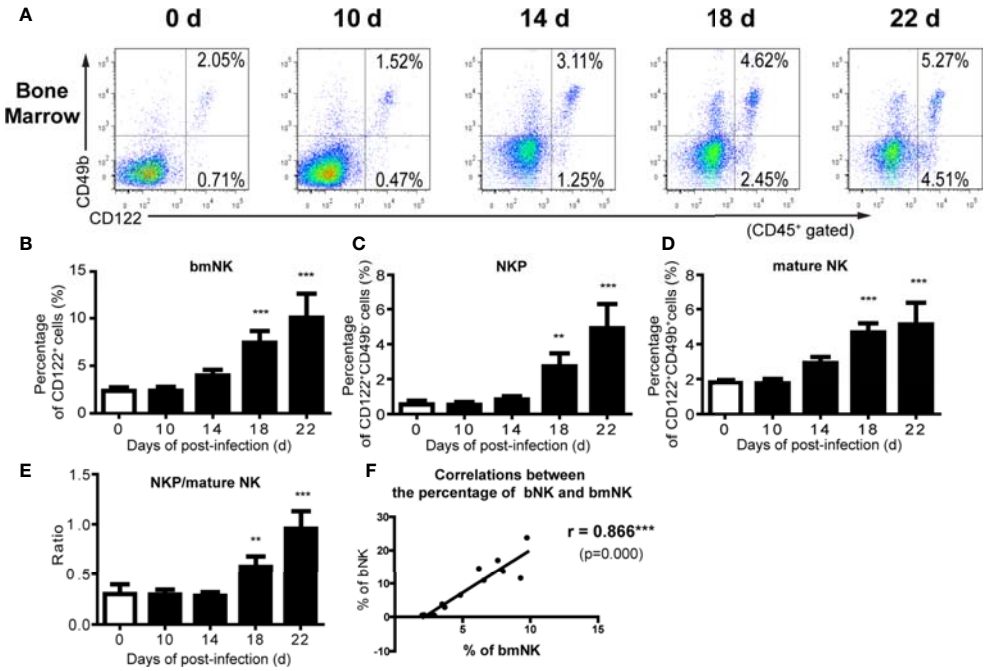

FIGURE 3 | The percentage of NK cells in bone marrow increased after *A. cantonensis* infection. **(A–D)** The percentage of NK cells in bone marrow lymphocytes of *A. cantonensis*-infected mice. NK cells in bone marrow ($CD122^+$) were divided into NK precursor cells ($CD122^+CD49b^-$) and mature NK cells ($CD122^+$ $CD49b^+$) detected by FCM. **(E)** The ratio of NK precursor cells to mature NK cells in bone marrow. **(F)** The correlation between the percentage of NK cells in bone marrow and brain. Data are expressed as the means ± SD. Data shown represent analysis from two independent experiments with three mice per group. Multiple comparisons of the percentage of NK cells at different time-points of infection were performed by one-way ANOVA. The ratio of different time points was analyzed by nonparametric test. The correlation between the percentage and number of NK cells in different tissues was analyzed by linear correlation. $^{**}P < 0.01$; $^{***}P < 0.001$, compared with that of 0 dpi. bmNK, NK cells in bone marrow; NKP, NK precursor cells; mature NK, mature NK cells.

stimulation using ELISA. The levels of TNF-α and IFN- γ secreted by infected bNK and infected sNK were significantly higher than those of uninfected sNK (**Figure 5D**). Subsequently, purified NK cells were stimulated and measured for intracellular cytokine by FCM. The percentage of IFN-γ^+ cells in infected bNK was higher than that of uninfected sNK, while the percentage of TNF-α^+ or IFN-γ^+ cells in infected sNK did not change (**Figures 5E, F**).

NK Cells Aggravate Brain Injury of Mice Caused by *A. cantonensis* Infection

We designed NK cell depletion and adoptive transfer experiments to elucidate the role of NK cells in brain injury induced by *A. cantonensis* infection. Firstly, NK cells were depleted by tail vein injection of anti-asialo GM1 serum to infected mice. The percentage and absolute number of NK cells in brain and spleen of infected mice significantly decreased after NK cell depletion (**Figures 6A–D, J**). Survival rate of the NK-depleted mice increased ($P < 0.01$), body weight elevated (NK-depleted *vs* infected: 17.35 ± 1.38 g *vs* 15.61 ± 1.10 g, $P < 0.05$), neurological impairment score decreased slightly, brain tissue inflammation alleviated, and the expression levels of inflammatory cytokines in brain tissue reduced (NK-depleted *vs* infected: IL-1β 25.88 ± 2.38 pg/mg *vs* 30.75 ± 2.83 pg/mg, IL-6 12.88 ± 1.23 pg/mg *vs* 15.08 ± 1.13 pg/mg, TNF-α 57.17 ± 4.20 pg/mg *vs* 64.68 ± 4.34 pg/mg, $P < 0.05$), compared with the infected mice (**Figures 6E–P**).

And then, purified splenic NK cells were transferred to infected mice by tail vein injection. The percentage of NK cells in brain and spleen of infected mice increased significantly after adoptive transferring NK cells (**Figures 7A–D, J**). Compared with the infected mice, survival rate, body weight and neurological impairment score of the NK-transferred mice did not change significantly, but brain tissue inflammation aggravated, and the expression levels of inflammatory cytokines in brain tissue elevated (NK-transferred *vs* infected: IL-1β 36.36 ± 1.89 pg/mg *vs* 30.75 ± 2.83 pg/mg, $P < 0.05$; IL-6 18.08 ± 0.55 pg/mg *vs* 15.08 ± 1.13 pg/mg, $P < 0.01$; TNF-α 76.84 ± 1.21 pg/mg *vs* 64.68 ± 4.34 pg/mg, $P < 0.01$) (**Figures 7E–P**).

CX_3CL1 Recruits NK Cells Into the CNS of Mice After *A. cantonensis* Infection

To elucidate the key factors that recruited NK cells into the CNS of *A. cantonensis*-infected mice, we detected the expression of various chemokines in brain tissue. As shown in **Figures 8A–N**, the expression levels of CCL3, CCL5, CXCL10 and CX_3CL1 in the brain tissue of infected mice was elevated with the extension of infection time. Among them, CX_3CL1 showed the most

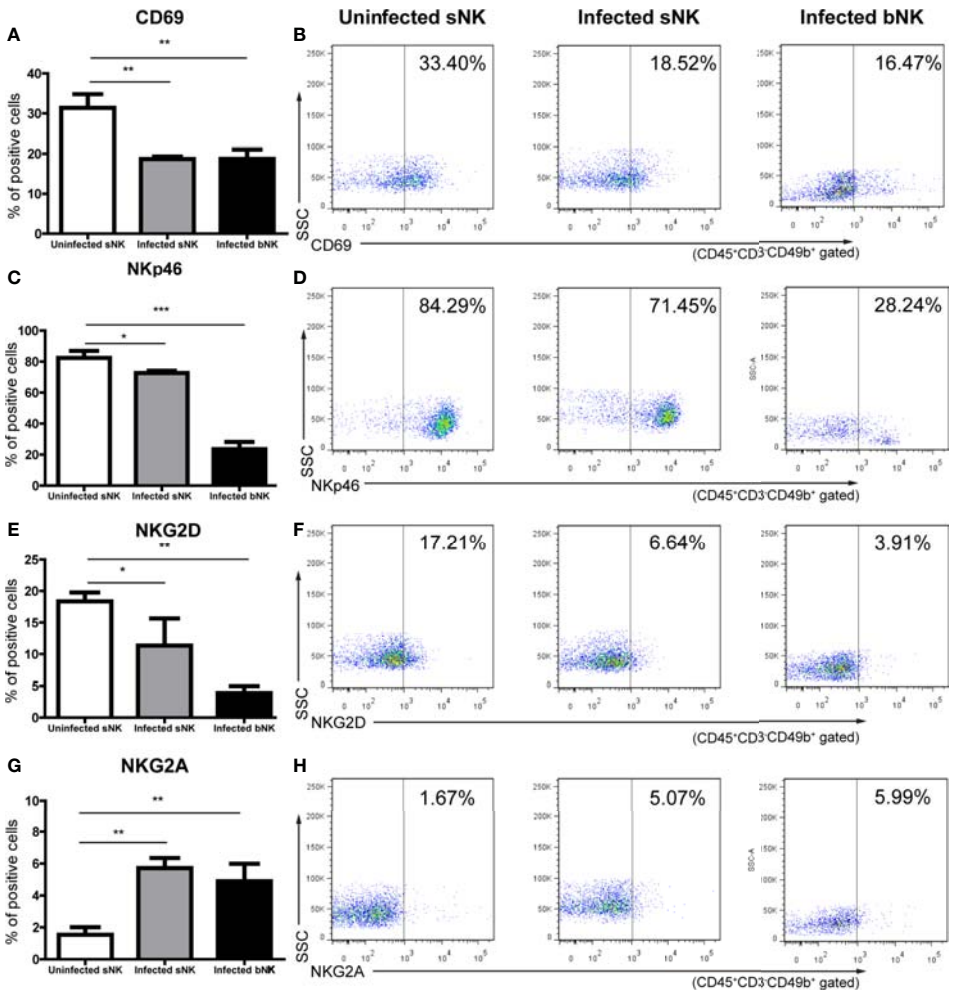

FIGURE 4 | The phenotypes of NK cells changed after *A. cantonensis* infection. The expression of activation marker CD69 **(A, B)**, activated receptor NKp46 **(C, D)** and NKG2D **(E, F)**, and inhibitory receptor NKG2A **(G, H)** on the surface of sNK and bNK were detected by FCM. Gating strategy for the mouse $CD45^+CD3^-CD49b^+$ NK cell population was shown in **Figure S2**. Representative dot plots stained with isotype controls was shown in **Figure S5**. Data are expressed as the means ± SD. Data shown represent analysis from two independent experiments with three mice per group. Multiple comparisons of phenotypes between uninfected sNK, infected sNK and infected bNK were performed by ANOVA. $^*P < 0.05$; $^{**}P < 0.01$; $^{***}P < 0.001$. sNK, NK cells in spleen; bNK, NK cells in brain.

significant change. The gene and protein expression levels of CX_3CL1 were both significantly increased on 18 dpi compared with those of 0 dpi (18 dpi *vs* 0 dpi: mRNA 138.00 ± 13.3 *vs* 1.11 ± 0.59, protein 441.40 ± 118.70 *vs* 112.60 ± 13.38 pg/mg, $P < 0.001$). And then, we analyzed the expression of chemokine receptors on NK cells. The gene expression levels of CCR1(the receptor of CCL5), CCR8 (the receptor of CCL1) and CX_3CR1 (the receptor of CX_3CL1) on infected bNK was significantly elevated, compared with that of uninfected sNK or infected sNK (**Figures 8O–V**). Taken together, the expression of CX_3CL1 in the brain tissue and its receptor CX_3CR1 on the CNS-infiltrated NK cells were both upregulated after *A. cantonensis* infection.

To determine if CX_3CL1 activity is important for the recruitment of NK cells into the CNS, *A. cantonensis*-infected mice were given daily intraperitoneal injections of anti-CX_3CL1 IgG (neutralizing antibody) or an isotype control antibody starting at 10 dpi (before the increase of CX_3CL1 in brain tissue of infected mice shown in **Figures 8G, N**) and euthanatized at 18 dpi. After CX_3CL1 neutralization, the percentage and absolute number of NK cells in brain of infected mice significantly decreased (CX_3CL1 neutralized *vs* infected: 5.38 ± 1.49% *vs* 12.90 ± 1.91%, $P < 0.001$; $9.88 \pm 5.78 \times 10^3$ *vs* $1.96 \pm 0.24 \times 10^5$ cells/mouse, $P < 0.001$), while the percentage and absolute number of NK cells in spleen significantly increased (CX3CL1 neutralized *vs* infected: 3.32 ± 0.43% *vs* 2.22 ± 0.32%, $P < 0.05$; $1.73 \pm 0.16 \times 10^6$ *vs* $0.52 \pm 0.05 \times 10^6$ cells/mouse, $P < 0.001$) (**Figures 9A–D, J**). The CX_3CL1 neutralized mice showed elevated survival rate ($P < 0.05$), increased body weight (CX_3CL1 neutralized *vs* infected: 17.13 ± 1.26 g *vs* 15.22 ± 0.75 g, $P < 0.01$), slightly decreased neurological impairment score, alleviated brain tissue inflammation, and reduced expression levels of inflammatory cytokines (CX_3CL1 neutralized *vs* infected: IL-1β 21.36 ± 0.77 pg/mg *vs* 28.37 ± 1.58 pg/mg, $P < 0.05$;

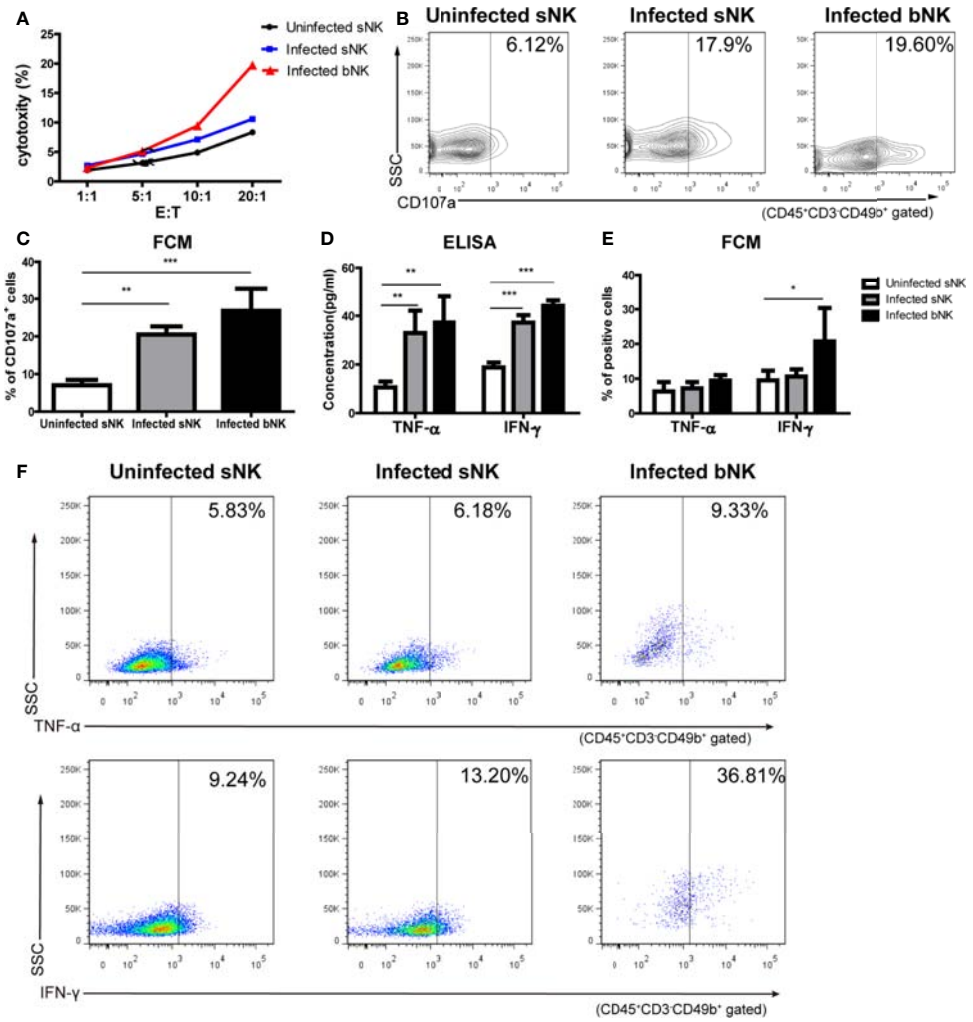

FIGURE 5 | The cytotoxicity and secretory ability of NK cells elevated after *A. cantonensis* infection. **(A)** NK cell-mediated cytotoxicity against YAC-1 cells. Purified sNK and bNK (as effector cells) were incubated with YAC-1 cells (as target cells) at various effector cell/target cell ratios (E:T = 1:1, 5:1, 10:1, 20:1). NK cell-mediated cytotoxicity was detected by LDH release assay. **(B, C)** The expression of CD107a on NK cells. Splenic lymphocytes and brain mononuclear cells were isolated and detected by FCM. Gating strategy for the mouse $CD45^+CD3^-CD49b^+$ NK cell population was shown in **Figure S2**. **(D)** The concentrations of TNF-α and IFN-γ in the culture supernatants of NK cells. Purified sNK and bNK were stimulated with IL-12 and the concentrations of TNF-α and IFN-γ in the culture supernatants were detected using ELISA. **(E, F)** The expression of intracellular cytokine TNF-α and IFN-γ in NK cells. Splenic lymphocytes and brain mononuclear cells were isolated and stimulated with Leukocyte Activation Cocktail. The percentage of $TNF\text{-}\alpha^+$ cells and $IFN\text{-}\gamma^+$ cells in $CD45^+CD3^-CD49b^+$ NK cells was detected by FCM. Data are expressed as the means ± SD. Data shown represent analysis from two independent experiments with four mice per group. Multiple comparisons were performed by one-way ANOVA. $^*P < 0.05$; $^{**}P < 0.01$; $^{***}P < 0.001$. sNK, NK cells in spleen; bNK, NK cells in brain.

IL-6 12.97 ± 0.19 pg/mg *vs* 15.45 ± 0.95 pg/mg, $P < 0.01$; TNF-α 60.76 ± 4.28 pg/mg *vs* 79.41 ± 11.15 pg/mg, $P < 0.05$), compared to the infected mice (**Figures 9E–P**).

DISCUSSION

Angiostrongylosis, a food-borne parasitic disease, is caused by the larvae of *A. cantonensis* in the host's central nervous system (Martins et al., 2015). NK cells are important innate immune effector cells. They can be swiftly mobilized by danger signals and are among the earliest arrivals at target organs against pathogen infection (Cruzmunoz and Veillette, 2010). However, the role of NK cells in the CNS damage caused by *A. cantonensis* infection remains elusive. Our previous work has reported that NK cells in the spleen and peripheral blood showed quantitative reduction and functional changes in an *A. cantonensis*-infected mice model (Chen et al., 2014). In the current study, we focused on the NK cells in the CNS. We found a large number of NK cells infiltrated into the CNS of mice after *A. cantonensis* infection and these CNS-infiltrated NK cells had elevated cytotoxicity and secretory ability. Moreover, we demonstrated that the increased expression

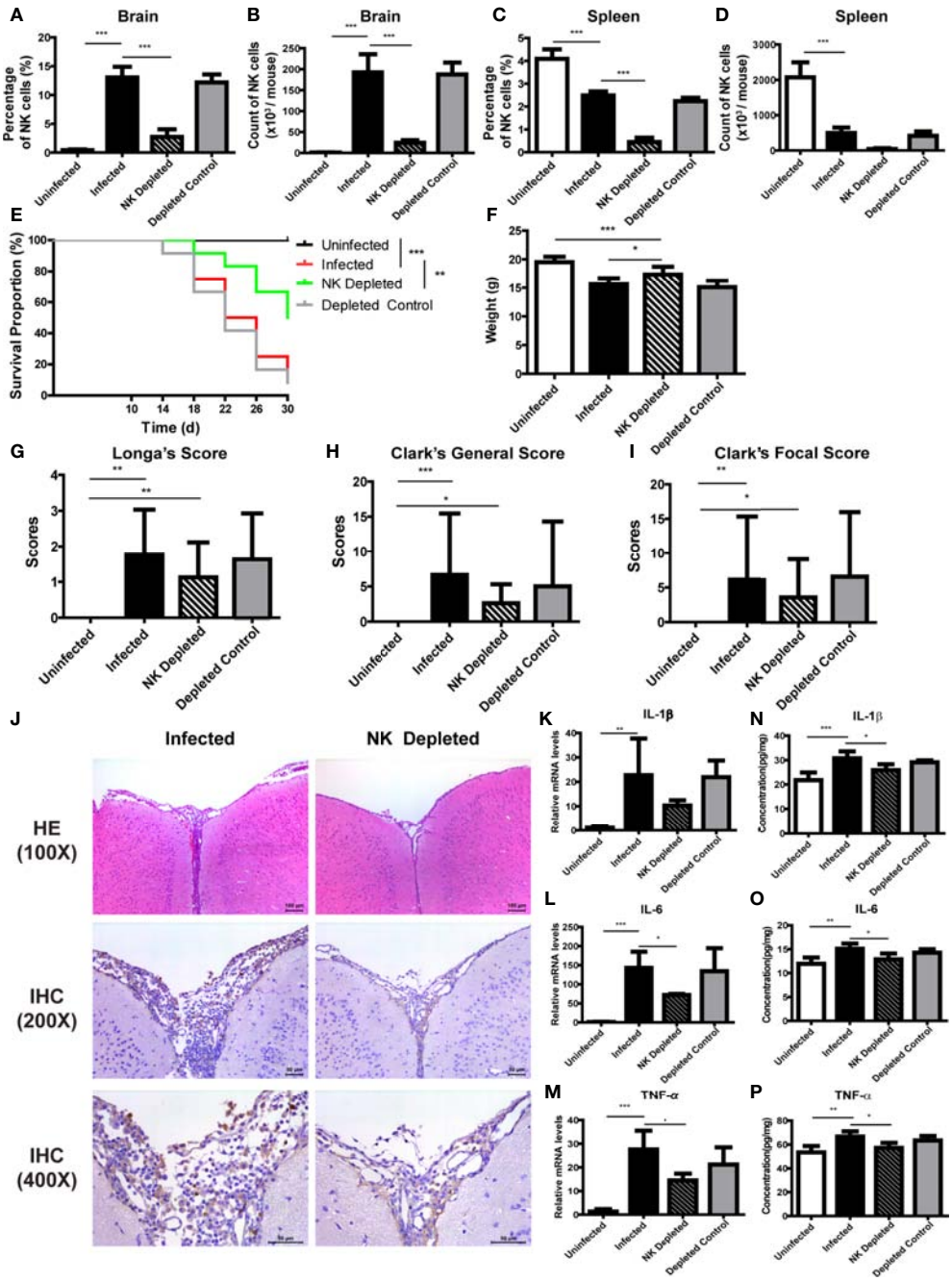

FIGURE 6 | Depletion of NK cells alleviated brain injury in *A. cantonensis*-infected mice. Depletion of NK cells in infected mice was induced by tail vein injection of anti-asialo GM1 rabbit serum. The percentage and absolute number of NK cells in brain **(A, B)** and spleen **(C, D)** were detected by FCM to evaluate NK cell depleting efficiency. After NK cell depletion, the survival rate of infected mice increased **(E)**, body weight elevated **(F)**, while neurological impairment scores did not have significant changes **(G–I)**. Representative histopathological sections of brain tissue with H&E and IHC staining showed alleviated inflammation and fewer infiltrating NK cells in the brain of NK-depleted mice **(J)**. Images are shown at 100 ×, 200 × and 400 × magnification (Scale bar, 50-100 μm). The gene **(K–M)** and protein levels **(N–P)** of inflammatory cytokines IL-1β, IL-6 and TNF-α in brain tissue reduced after NK cell depletion measured by qRT-PCR and ELISA. Data are expressed as the means ± SD. Data shown represent analysis from two independent experiments with three to twelve mice per group. Survival curve comparison was determined by Log-rank Test. Comparison of the neurological impairment scores was compared by non-parametric test. Multiple comparisons of the percentage and absolute number of NK cells, body weight and expression of cytokines were performed using one-way ANOVA. $^{*}P < 0.05$; $^{**}P < 0.01$; $^{***}P < 0.001$. Uninfected, normal mice; Infected, mice infected with *A. cantonensis*; NK Depleted, infected mice depleted NK cells by injection of anti-asialo GM1 rabbit serum; Depleted Control, infected mice given normal rabbit serum as control.

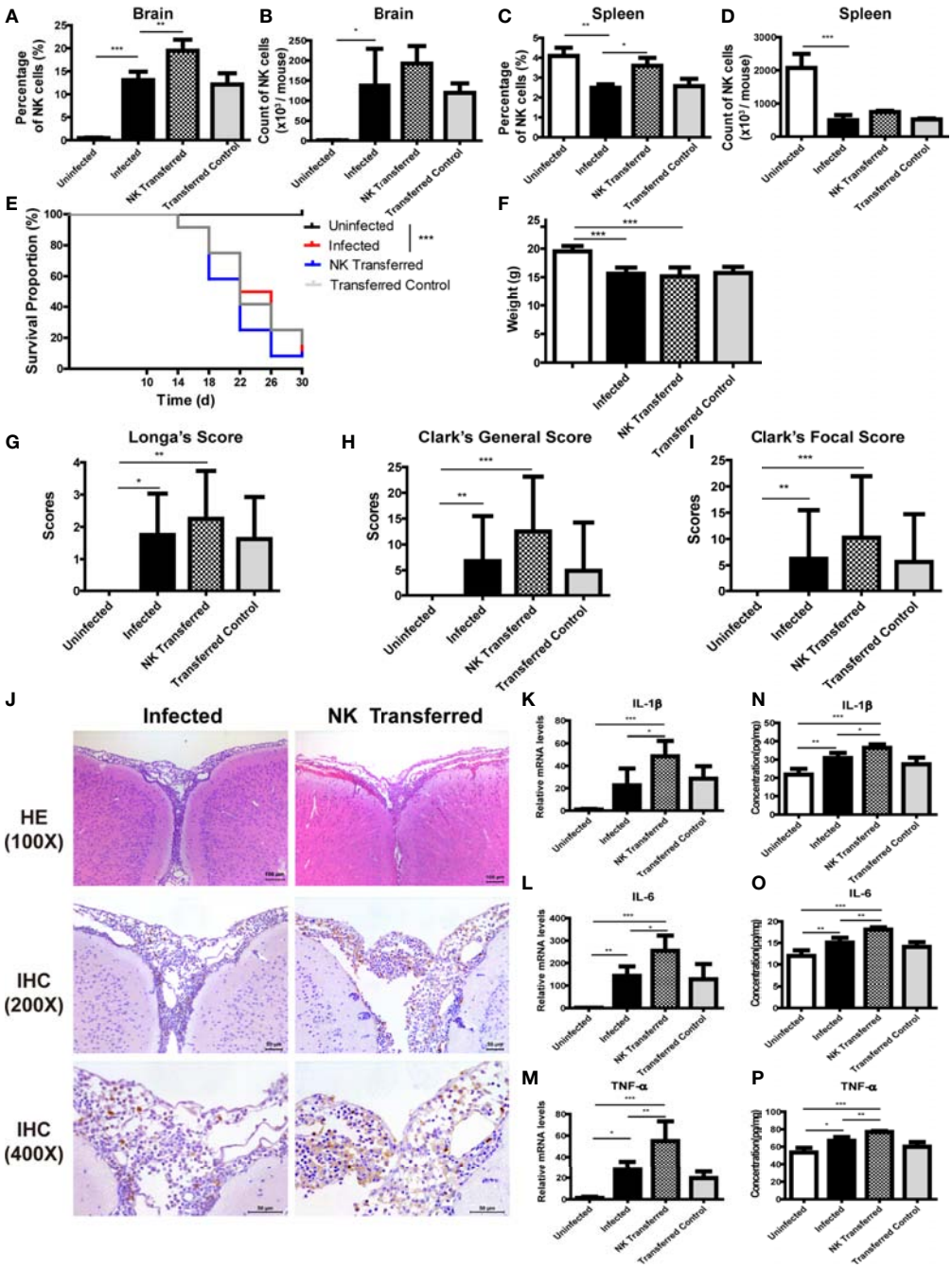

FIGURE 7 | Adoptive transfer of NK cells exacerbated brain damage in *A. cantonensis*-infected mice. Purified splenic NK cells from normal mice were transferred to infected mice by tail vein injection. The percentage and absolute number of NK cells in brain **(A, B)** and spleen **(C, D)** were detected by FCM to evaluate NK cell adoptive transferring efficiency. After adoptive transferring NK cells, the survival rate of infected mice **(E)**, body weight **(F)** and neurological impairment score **(G–I)** did not change significantly. Representative histopathological sections of brain tissue with H&E and IHC staining showed aggravated inflammation and more infiltrating NK cells in the brain of NK- transferred mice **(J)**. Images are shown at 100 ×, 200 × and 400 × magnification (Scale bar, 50-100 μm). The gene **(K–M)** and protein levels **(N–P)** of inflammatory cytokines IL-1β, IL-6 and TNF-α in brain tissue elevated after NK cell adoptive transferring measured by qRT-PCR and ELISA. Data are expressed as the means ± SD. Data shown represent analysis from two independent experiments with three to twelve mice per group. Survival curve comparison was determined by Log-rank Test. Comparison of the neurological impairment scores was compared by non-parametric test. Multiple comparisons of the percentage and absolute number of NK cells, body weight and expression of cytokines were performed using one-way ANOVA. $^{*}P < 0.05$; $^{**}P < 0.01$; $^{***}P < 0.001$. Uninfected, normal mice; Infected, mice infected with *A. cantonensis*; NK Transferred, infected mice transferred NK cells by tail vein injection; Transferred Control, infected mice injected with PBS as control.

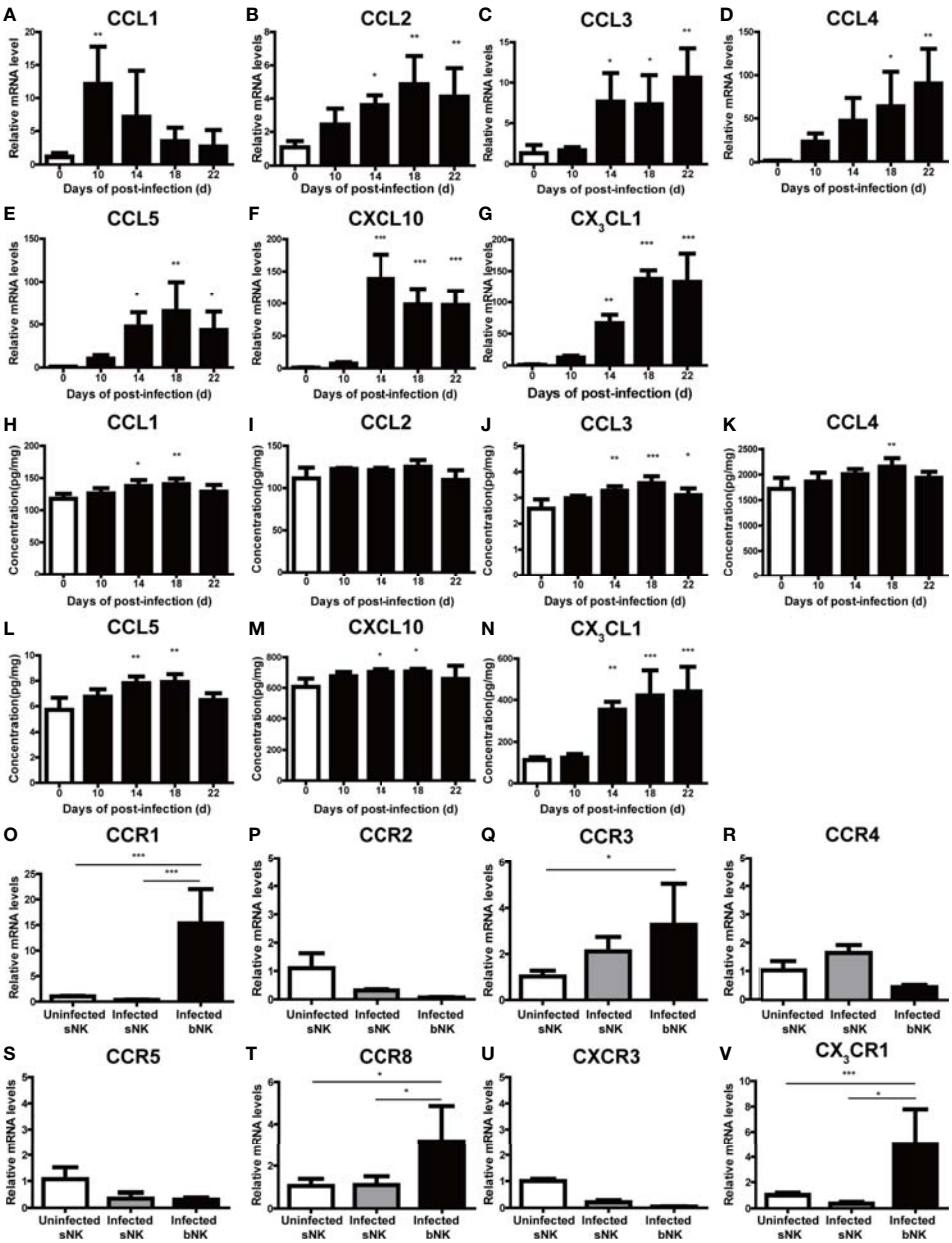

FIGURE 8 | The expression of CX_3CL1 in the brain tissue and CX_3CR1 on the CNS-infiltrated NK cells were elevated after *A. cantonensis* infection. The gene **(A–G)** and protein levels **(H–N)** of various chemokines (CCL1, CCL2, CCL3, CCL4, CCL5, CXCL10 and CX_3CL1) in brain tissue were measured by qRT-PCR and ELISA. **(O–V)** The gene expression levels of chemokine receptors (CCR1, CCR2, CCR3, CCR4, CCR5, CCR8, CXCR3 and CX_3CR1) on NK cells were detected by qRT-PCR. Multiple comparisons were performed by ANOVA. $^*P < 0.05$; $^{**}P < 0.01$; $^{***}P < 0.001$. sNK, NK cells in spleen; bNK, NK cells in brain.

of CX_3CL1 in the brain tissue recruited NK cells into the CNS and aggravated brain injury of mice caused by *A. cantonensis* infection.

Mice and humans are both non-permissive hosts of *A. cantonensis*, and the pathogenic process is comparatively similar (Ouyang et al., 2012). Consistent with other reports (Guo et al., 2008; Wang et al., 2015; Chen et al., 2016), we successfully constructed a mouse model infected with *A. cantonensis* and observed serious neurological damage from 18 dpi to 22 dpi. What is noteworthy in this study is that we confirmed that NK cells infiltrated into the CNS after *A. cantonensis* infection. The results of IHC and FCM showed that NK cells began to appear in the brain tissues at 14 dpi. The percentage and absolute number of NK cells increased gradually with the extension of infection time until 22 dpi. The CNS, including the brain and spinal cord, is considered as an immune privileged organ because of the low permeability of the BBB. However, it is conceivable that peripherally activated

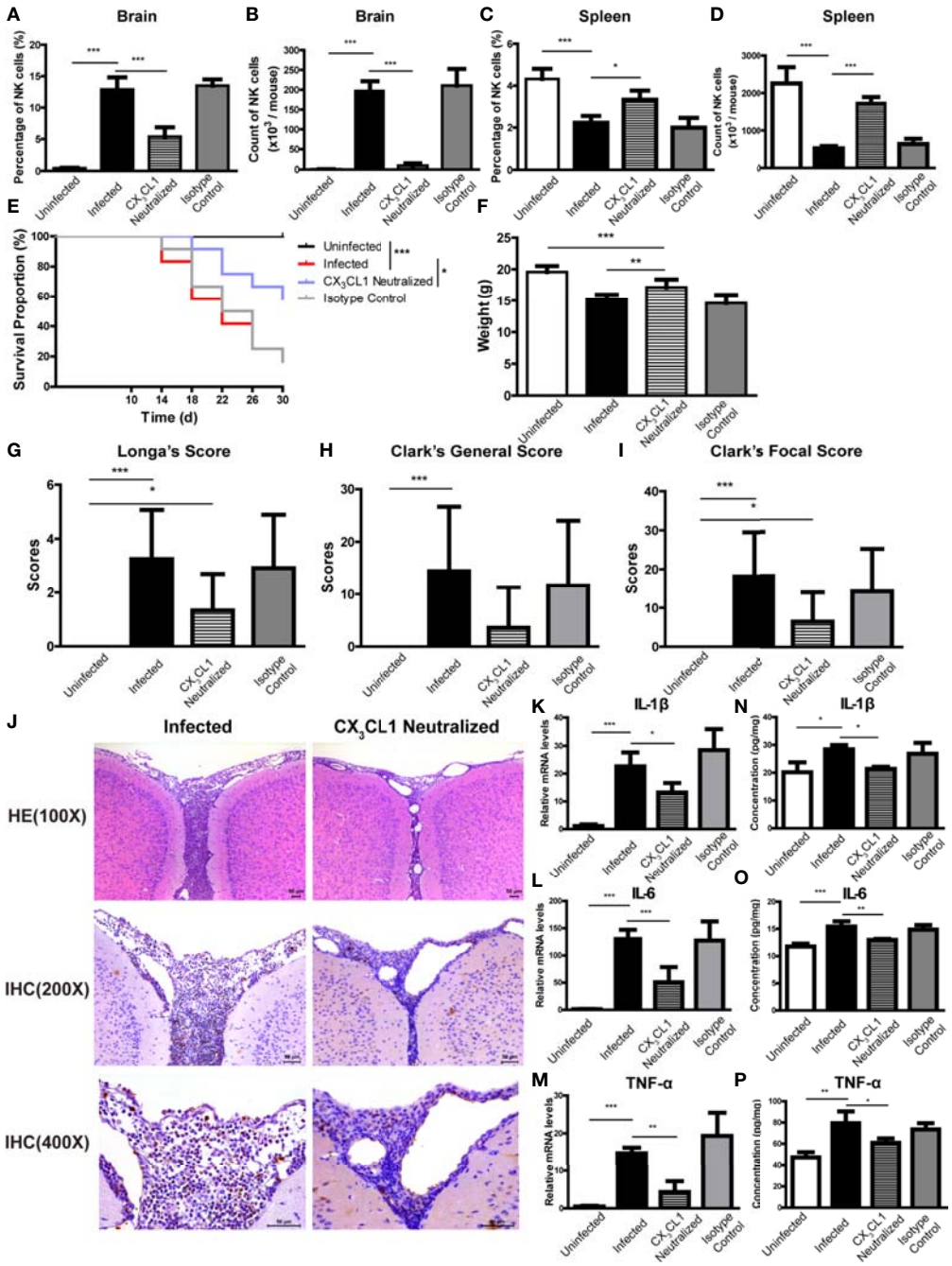

FIGURE 9 | CX_3CL1 neutralization reduced the infiltration of NK cells into CNS and relieved brain damage caused by *A. cantonensis* infection. Infected mice were given daily intraperitoneal injections of anti-CX_3CL1 IgG or isotype control IgG from 10 dpi to 17 dpi and euthanatized at 18 dpi. After CX_3CL1 neutralization, the percentage and absolute number of NK cells in brain **(A, B)** of infected mice significantly decreased, while the percentage and absolute number of NK cells in spleen **(C, D)** significantly increased detected by FCM. The CX_3CL1 neutralized mice showed elevated survival rate **(E)**, increased body weight **(F)**, slightly decreased neurological impairment score **(G–I)**, compared with the infected mice. Representative histopathological sections of brain tissue with H&E and IHC staining showed alleviated inflammation and fewer infiltrating NK cells in the brain of CX_3CL1 neutralized mice **(J)**. Images are shown at 100 ×, 200 × and 400 × magnification (Scale bar, 50-100 μm). The gene **(K–M)** and protein levels **(N–P)** of inflammatory cytokines IL-1β, IL-6 and TNF-α in brain tissue reduced after CX_3CL1 neutralization measured by qRT-PCR and ELISA. Data are expressed as the means ± SD. Data shown represent analysis from two independent experiments with three to twelve mice per group. Survival curve comparison was determined by Log-rank Test. Comparison of the neurological impairment scores was compared by non-parametric test. Multiple comparisons of the percentage and absolute number of NK cells, body weight and expression of cytokines were performed using one-way ANOVA. $^*P < 0.05$; $^{**}P < 0.01$; $^{***}P < 0.001$. Uninfected, normal mice; Infected, mice infected with *A. cantonensis*; CX_3CL1 Neutralized, infected mice inject with anti-CX_3CL1 IgG; Isotype Control, infected mice given isotype control IgG.

lymphocytes, including NK cells, might also be able to penetrate the BBB and infiltrate into the CNS under several pathological conditions. In human ischemic brain tissue and a permanent middle cerebral artery occlusion (pMCAO) mouse model, infiltration of NK cells into the ischemic infarct region are observed (Gan et al., 2014; Zhang et al., 2014; Li et al., 2020). NK cells are activated in the periphery and then migrated into the CNS of EAE mice (Hao et al., 2010). NK cells can be detected in mouse CNS tissues during a variety of infections, including Semliki Forest virus (SFV) (Alsharifi et al., 2006), murine coronavirus (Hayashi et al., 2009) and *L. monocytogenes* (Trifilo et al., 2004). NK cells are also recruited to the CNS in glioma-bearing mice and constitute approximately 50% of all leukocytes in the CNS (Alizadeh et al., 2010). We further examined the distribution of NK cells in the spleen, peripheral blood and bone marrow of *A. cantonensis*-infected mice. The results showed that the percentage and absolute number of NK cells in spleen and in peripheral blood both decreased, consistent with our previous study (Chen et al., 2014), while the percentage of NK cells in bone marrow increased after *A. cantonensis* infection. In addition, the percentage and absolute number of splenic NK cells were negatively correlated with those of brain NK cells, while the percentage of NK cells in bone marrow was positively correlated with brain NK cells. It was suggested that the CNS-infiltrated NK cells probably were related with the increased hematopoiesis of bone marrow and migration of peripheral NK cells after *A. cantonensis* infection.

To identify the characteristics of the CNS-infiltrated NK cells, we detected the phenotype and function of NK cells after *A. cantonensis* infection. The results showed that the expression of activation molecule CD69, activating receptor NKp46 and NKG2D on the CNS-infiltrated NK cells of infected mice was decreased compared with the splenic NK cells of uninfected mice, while the expression of inhibitory receptor NKG2A increased. Consistent phenotypic changes were observed in the splenic NK cells of infected mice. CD69, as an early activation marker on NK cells, is also a novel immune regulator, which can inhibit the cytotoxicity of NK cells by inducing the production of TGF-β. It was demonstrated that the administration of anti-CD69 mAbs can activate resting NK cells, resulting in a substantial increase in both NK-cell cytolytic activity and IFN-γ production (Esplugues et al., 2005). NK cells express an array of inhibitory and activating receptors recognizing self-ligands or microbial molecules on infected and tumor cells. Coordinated acquisition of these inhibitory and activating signals regulates the effector functions of NK cells (Vivier et al., 2011). Some studies have reported the phenotypic changes in the CNS-infiltrated NK cells under pathological conditions. In the EAE mice, the CNS-infiltrated NK cells upregulate the inhibitory receptor NKG2A and kill reactive $CD4^+$T cells (Hao et al., 2010). In a mouse model of cerebral ischemia, NK cells in the ischemic hemisphere have increased expression of NKG2D, an activation receptor, while similar expression of NKG2A, an inhibitory receptor. Of note, expression of the MHC-Ib molecule Qa1, the ligand for NKG2A, decreased significantly on ischemic neurons (Gan et al., 2014). NK cell-mediated neuronal damage is associated with the loss of self-identity for ischemic neuron-modulated NK cell tolerance and the activation of NK cells. The down-regulation of CD69 and activating receptors and up-regulation of inhibitory receptors on NK cells following *A. cantonensis* infection might imply the changes of their effector functions.

NK cells have a variety of biological functions, with the most important role being cytotoxicity (Abel et al., 2018). In our study, we found that the CNS-infiltrated NK cells of infected mice had an enhanced cytotoxicity against YAC-1 cells with higher expression of CD107a. CD107a, also known as Lysosome associated membrane protein-1 (LAMP-1), is a marker for degranulation of NK cells and its expression correlates with NK cell-mediated lysis of target cells (Alter et al., 2004; Aktas et al., 2009). NK cells can also produce a variety of cytokines in response to activation signaling to regulate immune response. Our results showed that compare with the splenic NK cells of uninfected mice, the CNS-infiltrated NK cells of infected mice produced higher levels of TNF-α and IFN-γ, which are both proinflammatory cytokines and involved in mediating anti-pathogen immune responses (Schoenborn and Wilson, 2007; Zou et al., 2010). Taken together, the CNS-infiltrated NK cells in *A. cantonensis*-infected mice showed stronger activity with enhanced cytotoxicity and elevated production of TNF-α and IFN-γ. There are no NK cells in the steady-state CNS, but NK cells might migrate into the CNS under certain pathological conditions. After homing to the inflamed CNS, NK cells become receptive to an array of cellular components that they have not encountered in the periphery. These include astrocytes, microglia, neurons and other cells, which release numerous soluble factors with diversified and perhaps coordinated effects on NK cells (Shi et al., 2011). The fate and function of NK cells are determined by focal environmental factors (Li et al., 2020). The exact cellular and molecular interactions that shape the phenotype and function of NK cells in the CNS still need to be determined.

We then investigated the role of NK cells in the brain damage caused by *A. cantonensis* infection using NK cell depletion and adoptive transfer experiments. We found that after NK depletion, the survival rate and body weight increased, nerve injury and brain inflammation decreased in *A. cantonensis*-infected mice. On the contrary, the inflammation in brain aggravated after adoptive transfer of NK cells. These results indicated that the CNS-infiltrated NK cells might exacerbated the brain injury after *A. cantonensis* infection. Many studies have reported that NK cells can rapidly accumulated into the CNS under pathological conditions (Alsharifi et al., 2006; Hayashi et al., 2009; Hao et al., 2010; Gan et al., 2014; Li et al., 2020). However, the role of NK cells in brain injury diseases remains is complex and sometimes paradoxical. Li et al. (2020) identified, NK cells infiltrate into the CNS during early stages of intracerebral hemorrhage (ICH), express up-regulated CD69 and perforin and exacerbate brain edema *via* cytotoxicity toward cerebral endothelial cells and recruitment of neutrophils. Gan et al. (2014) reported NK cells with the increased expression of NKG2D and IFN-γmediate exacerbation of brain infarction after ischemia *via* the disruption of NK cell tolerance, augmenting local inflammation and neuronal hyperactivity. Alsharifi et al. (2006)

found that NK cells exert both disease-exacerbating and protective effects in the CNS of SFV-infected in mice. The cytolytic activity of NK cells is detrimental, while IFN-γ production is beneficial for recovery from SFV infection. However, Hao et al. (2010) demonstrated that the CNS-resident NK cells have a protective role in the brain of EAE mice, as they inhibit the activation of autoimmune T cells through the killing of activated microglia. Jiang et al. (2017) disclosed that acetylcholine-producing NK cells attenuate CNS inflammation of EAE model *via* modulation of infiltrating monocytes/macrophages. NK cells play different roles in brain injury, which may be related to the initial factors of the primary disease, the time of immune response, and the overall inflammatory process (Gan et al., 2014).

NK cells originate from bone marrow, are mainly distributed in peripheral blood and spleen, and some lymphatic tissues (Abel et al., 2018). However, the distribution of NK cells is not static because these cells can recirculate between organs. NK cells can respond to a large array of chemokines and be recruited to distinct sites in several pathological circumstances (Shi et al., 2011). The detailed trafficking patterns of NK cells are not very well characterized. Nevertheless, it appears that chemokines produced by cells that are unique to specific organs may have a role in orchestrating NK cell migration to each organ (Shi et al., 2011). It was reported that NK cells might be recruited to the CNS by chemokines such as CX_3CL1 produced by neurons (Gan et al., 2014; Hertwig et al., 2016) and CCL2 and CXCL10 produced by microglia, astrocytes or infiltrating inflammatory cells (Hao et al., 2011; Zhang et al., 2014). We examined the expression levels of various chemokines (CCL1, CCL2, CCL3, CCL4, CCL5, CXCL10 and CX_3CL1) in brain tissue and their corresponding receptors on NK cells of *A. cantonensis*-infected mice. The upregulation of CX_3CL1 in the brain tissue and its receptor CX_3CR1 on the CNS-infiltrated NK cells of infected mice indicated that CX_3CL1 might be involved in the recruitment of NK cells into the CNS after *A. cantonensis* infection.

CX_3CL1, also known as fractalkine (in human) and neurotactin (in mouse), is a large cytokine protein of 373 amino acids and is the only member of the CX_3C chemokine family (Poniatowski et al., 2017). CX_3CL1 have two forms: membrane-bound and soluble type. Soluble CX_3CL1 potently chemoattracts T cells, monocytes, NK cells and other lymphocytes, while the membrane-bound CX_3CL1 promotes strong adhesion of leukocytes to activated endothelial cells, where it is primarily expressed (Lee et al., 2018). CX_3CL1 discloses its biological properties through interaction with one dedicated chemokine receptor CX_3CR1 (Sheridan and Murphy, 2013). Some studies have reported the CX_3CL1/CX_3CR1 signal mediates NK cell migration from the periphery to the CNS. Huang et al. (2006) firstly reported that chemokine CX_3CL1 selectively recruits NK cells to the CNS and modify experimental autoimmune encephalomyelitis. Hertwig et al. (2016) showed that mature NK cells are mobilized from the periphery and accumulate in the inflamed CNS of EAE mice in a CX_3CR1-dependent way and contributes to control autoimmune neuroinflammation. Gan Y (Gan et al., 2014) demonstrated that ischemic neurons are the major source of CX_3CL1 in the brain and the neuron-derived CX_3CL1 recruits CX_3CR1-expressing NK cells to the infarct sites, determining the sizes of brain lesions in a mouse model of cerebral ischemia. In our study, we found that the neutralization of CX_3CL1 reduced the percentage and absolute number of NK cells in the CNS of *A. cantonensis*-infected mice, whereas increased the percentage and absolute number of the splenic NK cells. NK cells are a special heterogeneous population. The NK cells in different tissues and organs have divergent phenotypic and functional features, and are recruited by different chemokines (Shi et al., 2011). CX_3CL1 neutralization only reduced the migration of brain NK cells in *A. cantonensis*-infected mice but did not inhibit the recruitment of splenic NK cells. After the neutralization of CX_3CL1, infected mice had elevated survival rate, increased body weight, slightly decreased neurological impairment score, alleviated brain tissue inflammation, and reduced expression levels of inflammatory cytokines. These results suggest that CX_3CL1 plays an important role in the recruitment of NK cells into the CNS and the progression of brain injury caused by *A. cantonensis* infection. We hypothesize that *A. cantonensis* larvae enter the brain tissue and induce mechanical damage and inflammatory response. Worm antigen and excretory-secretory antigens stimulate neurons to produce CX_3CL1, which recruits CX_3CR1^+ NK cells in peripheral blood across the damaged BBB into the CNS. The inflammatory environment in the brain shapes NK cell new features with enhanced cytotoxicity and increased cytokine secretion ability, which causing immunopathologic damage while clearing pathogens, and eventually exacerbate brain injury.

Currently, the treatment for angiostrongyliasis includes supportive treatment and corticosteroid therapy (Graeff-Teixeira et al., 2018). The use of anthelmintic drugs, such as albendazole and mebendazole, to kill worms remains controversial. The dead worm lysis in the CNS might cause severe inflammatory response and further damage (Lv et al., 2017). Meanwhile, Patients under the treatment of high-dose corticosteroids would experience immune suppression (Cowie, 2017). Therefore, it is urgent to develop new therapeutic interventions for angiostrongyliasis. Recently, the selective blockage of disease-relevant chemokines/chemokines receptors has become a new treatment strategy and has been proved to be effective in various diseases (Miao et al., 2020). Three chemokine antagonists have been approved: Maraviroc (a CCR5 antagonist) for anti-HIV treatment (Xu et al., 2014), Plerixafor (a CXCR4 antagonist) for the treatment of multiple myeloma or non-Hodgkin's lymphoma (Uy et al., 2008), and Mogamulizumab (a CCR4 antagonist) for the treatment of mycosis fungoides or Sézary syndrome (Sato et al., 2018). Moreover, clinical trials are ongoing to evaluate many potent candidates. For example, E6011 is a novel humanized anti-CX_3CL1 monoclonal antibody being developed as a therapeutic target for Crohn's disease, RA, and primary biliary cholangitis (Tabuchi et al., 2019). We speculated that selective blockage of NK cell infiltration into the CNS may help to alleviate the brain injury caused by *A. cantonensis* infection or other pathogens, which need to be further investigated in our future work.

In conclusion, our study demonstrates that NK cells infiltrate into the CNS of *A. cantonensis*-infected mice. These CNS-

infiltrated NK cells display enhanced cytotoxicity and secretory ability. The up-regulated CX_3CL1 in the brain tissue recruits NK cells into the CNS and aggravates brain damage caused by *A. cantonensis* infection. Our findings not only enrich the understanding of the pathogenesis of angiostrongylosis but also provide a clue to novel potential therapeutic strategies against CNS disease.

DATA AVAILABILITY STATEMENT

The original contributions presented in the study are included in the article/**Supplementary Material**. Further inquiries can be directed to the corresponding authors.

ETHICS STATEMENT

The animal study was reviewed and approved by the Institutional Animal Care and Use Committee of Nanjing Medical University.

AUTHOR CONTRIBUTIONS

AC conceived the project and designed the experiments. YW designed the experiments, supervised the project, and was involved in all aspects of the submission. RZ performed most of the experiments, analyzed data, and wrote the manuscript. TM was responsible for the infection and feeding of animals, performed cell isolation and detection by FCM. MQ and CSZ performed detection of cytokine by qRT-PCR and ELISA. WW and CCZ participated in neurological impairment evaluation and NK cell cytotoxicity assays. XL and YC performed histopathological examination and data analysis. All authors contributed to the article and approved the submitted version.

FUNDING

This work was supported by the National Natural Science Foundation of China (No. 81501371), the Post doctorate Foundation of China (2019M651963), the Post doctorate Foundation of Jiangsu Province (2018Z093), Jiangsu Provincial Medical Youth Talent of the Project of Invigorating Health Care through Science, Technology and Education (QNRC2016165), and the Foundation of top notch young and middle-aged medical and health talents in Wuxi (BJ2020079). This work was also supported, in part, by the National Basic Research Program of China (973 Program) (No. 2010CB530004).

ACKNOWLEDGMENTS

We thank Professor Xi Sun, Sun Yat-sen University, Guangzhou, China, for providing us with the *A. cantonensis*-infected snails. We thank Associate Professor Haiwei Wu, Brown University, Center for International Health Research, Rhode Island Hospital, USA, for her advice on writing.

SUPPLEMENTARY MATERIAL

The Supplementary Material for this article can be found online at: https://www.frontiersin.org/articles/10.3389/fcimb.2021.672720/full#supplementary-material

Supplementary Table 1 | Primer sequences used for qRT-PCR.

Supplementary Figure 1 | Representative flow cytometry plots of NK cell purity before and after magnetic cell sorting. NK cells were purified from brain mononuclear cells and splenic lymphocytes using a magnetic cell sorting system (MACS) incorporating anti-mice CD49 MicroBeads. The purity of $CD3^-CD49^+$ NK cells in brain and spleen after sorting was over 90% detected by FCM. sNK; NK cells in spleen; bNK, NK cells in brain.

Supplementary Figure 2 | Gating strategy for the mouse $CD45^+CD3^-CD49b^+$ NK cell population by FCM. **(A)** NK cells in spleen of uninfected mice. **(B)** NK cells in spleen of infected mice. **(C)** NK cells in brain of infected mice. Firstly, R1 was gated according to cell size presented by FSC and SSC. Next, $CD45^+$ cells in R1 were gated as R2 representing lymphocytes. Then, $CD3^-CD49b^+$ cells in R2 were gated as R3 and identified as the mouse NK cell population. sNK; NK cells in spleen; bNK, NK cells in brain.

Supplementary Figure 3 | Construction of a mouse model of *A. cantonensis* infection. Mice were infected with 20 *A. cantonensis* third-stage larvae by intragastric administration and detected at 0, 10, 14, 18 and 22 dpi, respectively. **(A, B)** Survival rate and body weight of mice at different infection time points. **(C)** Representative images of infected mice with neurologic deficit symptoms including erect hair, arched back, falling to one side when walking, blindness. **(D–F)** Neurological impairment scores of infected mice evaluated by Longa's score, Clark's general score and Clark's focal score. **(G)** Representative images of brain tissue in infected mice. The brains tissue of infected mice displayed obvious hemorrhage and fourth-stage larvae (blue arrow) from 14 to 22 dpi. **(H–N)** Expression of inflammatory cytokines IL-1β, IL-6 and TNF-α in brain at different infection time points detected by qRT-PCR and ELISA. Data are expressed as the means ± SD. Data shown represent analysis from two independent experiments with four to twelve mice per group. Survival curve comparison was determined by Log-rank Test. Comparison of body weight was carried by independent-samples T test. Comparison of the neurological impairment scores was compared by non-parametric test. Multiple comparisons of gene and protein levels of cytokines at different infection time-points were performed using one-way ANOVA. $^*P < 0.05$; $^{**}P < 0.01$; $^{***}P < 0.001$.

Supplementary Figure 4 | The percentage and absolute number of splenic T cells in *A. cantonensis*-infected mice. **(A)** The percentage T cells in splenic lymphocytes. **(B)** The absolute number of splenic T cells. Splenic T cells were identified as $CD3^+CD49b^-$ cells and detected by FCM. Data are expressed as the means ± SD. Data shown represent analysis from two independent experiments with three mice per group. Multiple comparisons of the percentage and count of T cells at different time-points of infection were performed by one-way ANOVA. $^*P < 0.05$; $^{**}P < 0.01$, compared with that of 0 dpi.

Supplementary Figure 5 | Representative dot plots stained with isotype controls of anti-NKG2D-PE **(A)** and anti-NKG2A-PE **(B)**. The cells isolated from the brain and spleen were stained with anti-NKG2D-PE, anti-NKG2A-PE or their isotype controls and detected by FCM.

REFERENCES

Abel, A. M., Yang, C., Thakar, M. S., and Malarkannan, S. (2018). Natural Killer Cells: Development, Maturation, and Clinical Utilization. *Front. Immunol.* 9, 1869. doi: 10.3389/fimmu.2018.01869

Aktas, E., Kucuksezer, U. C., Bilgic, S., Erten, G., and Deniz, G. (2009). Relationship Between CD107a Expression and Cytotoxic Activity. *Cell. Immunol.* 254, 149–154. doi: 10.1016/j.cellimm.2008.08.007

Alizadeh, D., Zhang, L., Brown, C. E., Farrukh, O., Jensen, M. C., and Badie, B. (2010). Induction of Anti-Glioma Natural Killer Cell Response Following Multiple Low-Dose Intracerebral CpG Therapy. *Clin. Cancer Res.* 16, 3399–3408. doi: 10.1158/1078-0432.ccr-09-3087

Alsharifi, M., Lobigs, M., Simon, M. M., Kersten, A., Muller, K., Koskinen, A., et al. (2006). NK Cell-Mediated Immunopathology During an Acute Viral Infection of the CNS. *Eur. J. Immunol.* 36, 887–896. doi: 10.1002/eji.200535342

Alter, G., Malenfant, J. M., and Altfeld, M. (2004). CD107a as a Functional Marker for the Identification of Natural Killer Cell Activity. *J. Immunol. Methods* 294, 15–22. doi: 10.1016/j.jim.2004.08.008

Barbosa, T. A., Thiengo, S. C., Fernandez, M. A., Graeff-Teixeira, C., Morassutti, A. L., Mourão, F. R. P., et al. (2020). Infection by Angiostrongylus Cantonensis in Both Humans and the Snail Achatina (Lissachatina) Fulica in the City of Macapá, in the Amazon Region of Brazil. *Mem. Inst. Oswaldo Cruz* 115, e200115. doi: 10.1590/0074-02760200115

Barratt, J., Chan, D., Sandaradura, I., Malik, R., Spielman, D., Lee, R., et al. (2016). Angiostrongylus Cantonensis: A Review of its Distribution, Molecular Biology and Clinical Significance as a Human Pathogen. *Parasitology* 143, 1087–1118. doi: 10.1017/s0031182016000652

Chen, A. L., Qiu, X. Y., Wang, W., Zhou, C. L., Zeng, X., Liu, X. J., et al. (2014). The Quantitative and Functional Changes of NK Cells in Mice Infected With Angiostrongylus Cantonensis. *Parasitol. Res.* 113, 2087–2094. doi: 10.1007/s00436-014-3858-0

Chen, A. L., Sun, X., Wang, W., Liu, J. F., Zeng, X., Qiu, J. F., et al. (2016). Activation of the Hypothalamic-Pituitary-Adrenal (HPA) Axis Contributes to the Immunosuppression of Mice Infected With Angiostrongylus Cantonensis. *J. Neuroinflammation* 13, 266. doi: 10.1186/s12974-016-0743-z

Clark, W. M., Lessov, N. S., Dixon, M. P., and Eckenstein, F. (1997). Monofilament Intraluminal Middle Cerebral Artery Occlusion in the Mouse. *Neurol. Res.* 19, 641–648. doi: 10.1080/01616412.1997.11740874

Cowie, R. H. (2017). Angiostrongylus Cantonensis: Agent of a Sometimes Fatal Globally Emerging Infectious Disease (Rat Lungworm Disease). *ACS Chem. Neurosci.* 8, 2102–2104. doi: 10.1021/acschemneuro.7b00335

Cruzmunoz, M. E., and Veillette, A. (2010). Do NK Cells Always Need a License to Kill? *Nat. Immunol.* 11, 279–280. doi: 10.1038/ni0410-279

Esplugues, E., Vegaramos, J., Cartoixà, D., Vazquez, B. N., Salaet, I., Engel, P., et al. (2005). Induction of Tumor NK-cell Immunity by anti-CD69 Antibody Therapy. *Blood* 105, 4399–4406. doi: 10.1182/blood-2004-10-3854

Federspiel, F., Skovmand, S., and Skarphedinsson, S. (2020). Eosinophilic Meningitis Due to Angiostrongylus Cantonensis in Europe. *Int. J. Infect. Dis.* 93, 28–39. doi: 10.1016/j.ijid.2020.01.012

Gan, Y., Liu, Q., Wu, W., Yin, J. X., Bai, X. F., Shen, R., et al. (2014). Ischemic Neurons Recruit Natural Killer Cells That Accelerate Brain Infarction. *Proc. Natl. Acad. Sci. U.S.A.* 111, 2704. doi: 10.1182/blood-2004-10-3854

Gelis, S., Spratt, D. M., and Raidal, S. R. (2011). Neuroangiostrongyliasis and Other Parasites in Tawny Frogmouths (Podargus Strigoides) in South-Eastern Queensland. *Aust. Vet. J.* 89, 47–50. doi: 10.1111/j.1751-0813.2010.00660.x

Golic, M., Haase, N., Herse, F., Wehner, A., Vercruysse, L., Pijnenborg, R., et al. (2016). Natural Killer Cell Reduction and Uteroplacental Vasculopathy. *Hypertension* 68, 964. doi: 10.1161/HYPERTENSIONAHA.116.07800

Gosnell, W. L., and Kramer, K. J. (2013). The Role of Eosinophils in Angiostrongyliasis: Multiple Roles for a Versatile Cell? *Hawaii J. Med. Public Health* 72, 49–51.

Graeff-Teixeira, C., Morassutti, A. L., and Jones, M. K. (2018). Diagnosing and Understanding Angiostrongyliasis, A Zoonotic Cause of Meningitis. *ACS Chem. Neurosci.* 9, 393–394. doi: 10.1021/acschemneuro.8b00018

Guo, P. J., Zhan, X. M., Gan, M., Pan, Z. H., Yu, Y. J., Zhang, M. C., et al. (2008). Pathological Change in the Brain of Mice Infected With Angiostrongylus Cantonensis. *Chin. J. Parasit. Parasit. Dis.* 26, 353–355. (in Chinese).

Hao, J., Campagnolo, D., Liu, R., Piao, W., Shi, S., Hu, B., et al. (2011). Interleukin-2/interleukin-2 Antibody Therapy Induces Target Organ Natural Killer Cells That Inhibit Central Nervous System Inflammation. *Ann. Neurol.* 69, 721–734. doi: 10.1002/ana.22339

Hao, J., Liu, R., Piao, W., Zhou, Q., Vollmer, T. L., Campagnolo, D. I., et al. (2010). Central Nervous System (CNS)-Resident Natural Killer Cells Suppress Th17 Responses and CNS Autoimmune Pathology. *J. Exp. Med.* 207, 1907–1921. doi: 10.1084/jem.20092749

Hayashi, T., Nagai, S., Fujii, H., Baba, Y., Ikeda, E., Kawase, T., et al. (2009). Critical Roles of NK and CD8+ T Cells in Central Nervous System Listeriosis. *J. Immunol.* 182, 6360–6368. doi: 10.4049/jimmunol.0803798

Hertwig, L., Hamann, I., Romero-Suarez, S., Millward, J. M., Pietrek, R., Chanvillard, C., et al. (2016). CX_3CR1-Dependent Recruitment of Mature NK Cells Into the Central Nervous System Contributes to Control Autoimmune Neuroinflammation. *Eur. J. Immunol.* 46, 1984–1996. doi: 10.1002/eji.201546194

Hokeness, K. L., Kuziel, W. A., Biron, C. A., and Salazar-Mather, T. P. (2005). Monocyte Chemoattractant Protein-1 and CCR2 Interactions are Required for IFN-alpha/beta-induced Inflammatory Responses and Antiviral Defense in Liver. *J. Immunol. (Baltimore Md 1950)* 174, 1549–1556. doi: 10.4049/jimmunol.174.3.1549

Huang, D., Shi, F. D., Jung, S., Pien, G. C., Wang, J., Salazar-Mather, T. P., et al. (2006). The Neuronal Chemokine CX_3CL1/fractalkine Selectively Recruits NK Cells That Modify Experimental Autoimmune Encephalomyelitis Within the Central Nervous System. *FASEB J.* 20, 896–905. doi: 10.1096/fj.05-5465com

Iwanowicz, D. D., Sanders, L. R., Schill, W. B., Xayavong, M. V., da Silva, A. J., Qvarnstrom, Y., et al. (2015). Spread of the Rat Lungworm (Angiostrongylus Cantonensis) in Giant African Land Snails (Lissachatina Fulica) in Florida, USA. *J. Wildl. Dis.* 51, 749–753. doi: 10.7589/2014-06-160

Jiang, W., Li, D., Han, R., Zhang, C., Jin, W. N., Wood, K., et al. (2017). Acetylcholine-Producing NK Cells Attenuate CNS Inflammation Via Modulation of Infiltrating Monocytes/Macrophages. *Proc. Natl. Acad. Sci. U.S.A.* 114, E6202–e6211. doi: 10.1073/pnas.1705491114

Lee, M., Lee, Y., Song, J., Lee, J., and Chang, S. Y. (2018). Tissue-Specific Role of CX(3)CR1 Expressing Immune Cells and Their Relationships With Human Disease. *Immune Netw.* 18, e5. doi: 10.4110/in.2018.18.e5

Li, Z., Li, M., Shi, S. X., Yao, N., Cheng, X., Guo, A., et al. (2020). Brain Transforms Natural Killer Cells That Exacerbate Brain Edema After Intracerebral Hemorrhage. *J. Exp. Med.* 217, e20200213. doi: 10.1084/jem.20200213

Liu, E. W., Schwartz, B. S., Hysmith, N. D., DeVincenzo, J. P., Larson, D. T., Maves, R. C., et al. (2018). Rat Lungworm Infection Associated With Central Nervous System Disease - Eight U.S. States, January 2011-January 2017. *MMWR Morb. Mortal. Wkly. Rep.* 67, 825–828. doi: 10.15585/mmwr.mm6730a4

Longa, E. Z., Weinstein, P. R., Carlson, S., and Cummins, R. (1989). Reversible Middle Cerebral Artery Occlusion Without Craniectomy in Rats. *Stroke* 20, 84–91. doi: 10.1161/01.str.20.1.84

Lv, S., Zhou, X. N., and Andrews, J. R. (2017). Eosinophilic Meningitis Caused by Angiostrongylus Cantonensis. *ACS Chem. Neurosci.* 8, 1815–1816. doi: 10.1021/acschemneuro.7b00233

Martins, Y. C., Tanowitz, H. B., and Kazacos, K. R. (2015). Central Nervous System Manifestations of Angiostrongylus Cantonensis Infection. *Acta Trop.* 141, 46–53. doi: 10.1016/j.actatropica.2014.10.002

Mengying, Z., Yiyue, X., Tong, P., Yue, H., Limpanont, Y., Ping, H., et al. (2017). Apoptosis and Necroptosis of Mouse Hippocampal and Parenchymal Astrocytes, Microglia and Neurons Caused by Angiostrongylus Cantonensis Infection. *Parasit. Vectors* 10, 611. doi: 10.1186/s13071-017-2565-y

Miao, M., De Clercq, E., and Li, G. (2020). Clinical Significance of Chemokine Receptor Antagonists. *Expert Opin. Drug Metab. Toxicol.* 16, 11–30. doi: 10.1080/17425255.2020.1711884

Mills, J. H., Alabanza, L. M., Mahamed, D. A., and Bynoe, M. S. (2012). Extracellular Adenosine Signaling Induces CX_3CL1 Expression in the Brain to Promote Experimental Autoimmune Encephalomyelitis. *J. Neuroinflammation* 9, 193. doi: 10.1186/1742-2094-9-193

Nishikado, H., Mukai, K., Kawano, Y., Minegishi, Y., and Karasuyama, H. (2011). NK Cell-Depleting Anti-Asialo GM1 Antibody Exhibits a Lethal Off-Target Effect on Basophils In Vivo. *J. Immunol.* 186, 5766–5771. doi: 10.4049/jimmunol.1100370

Okuma, A., Hanyu, A., Watanabe, S., and Hara, E. (2017). p16(Ink4a) and p21 (Cip1/Waf1) Promote Tumour Growth by Enhancing Myeloid-Derived Suppressor Cells Chemotaxis. *Nat. Commun.* 8, 2050. doi: 10.1038/s41467-017-02281-x

Ouyang, L., Wei, J., Wu, Z., Zeng, X., Li, Y., Jia, Y., et al. (2012). Differences of Larval Development and Pathological Changes in Permissive and Nonpermissive Rodent Hosts for Angiostrongylus Cantonensis Infection. *Parasitol. Res.* 111, 1547–1557. doi: 10.1007/s00436-012-2995-6

Parolini, S., Santoro, A., Marcenaro, E., Luini, W., Massardi, L., Facchetti, F., et al. (2007). The Role of Chemerin in the Colocalization of NK and Dendritic Cell Subsets Into Inflamed Tissues. *Blood* 109, 3625–3632. doi: 10.1182/blood-2006-08-038844

Poniatowski, Ł. A., Wojdasiewicz, P., Krawczyk, M., Szukiewicz, D., Gasik, R., Kubaszewski, Ł., et al. (2017). Analysis of the Role of CX_3CL1 (Fractalkine) and Its Receptor CX_3CR1 in Traumatic Brain and Spinal Cord Injury: Insight Into Recent Advances in Actions of Neurochemokine Agents. *Mol. Neurobiol.* 54, 2167–2188. doi: 10.1007/s12035-016-9787-4

Rael, R. C., Peterson, A. C., Ghersi-Chavez, B., Riegel, C., Lesen, A. E., and Blum, M. J. (2018). Rat Lungworm Infection in Rodents Across Post-Katrina New Orleans, Louisiana, USA. *Emerg. Infect. Dis.* 24, 2176–2183. doi: 10.3201/eid2412.180056

Sato, T., Coler-Reilly, A. L. G., Yagishita, N., Araya, N., Inoue, E., Furuta, R., et al. (2018). Mogamulizumab (Anti-CCR4) in HTLV-1-Associated Myelopathy. *N. Engl. J. Med.* 378, 529–538. doi: 10.1056/NEJMoa1704827

Schoenborn, J. R., and Wilson, C. B. (2007). Regulation of Interferon-Gamma During Innate and Adaptive Immune Responses. *Adv. Immunol.* 96, 41. doi: 10.1016/S0065-2776(07)96002-2

Sheridan, G. K., and Murphy, K. J. (2013). Neuron-Glia Crosstalk in Health and Disease: Fractalkine and CX_3CR1 Take Centre Stage. *Open Biol.* 3, 130181. doi: 10.1098/rsob.130181

Shi, F. D., Ljunggren, H. G., Cava, A. L., and Kaer, L. V. (2011). Organ-Specific Features of Natural Killer Cells. *Nat. Rev. Immunol.* 11, 658–671. doi: 10.1016/S0065-2776(07)96002-2

Tabuchi, H., Katsurabara, T., Mori, M., Aoyama, M., Obara, T., Yasuda, N., et al. (2019). Pharmacokinetics, Pharmacodynamics, and Safety of E6011, a Novel Humanized Antifractalkine (CX_3CL1) Monoclonal Antibody: A Randomized, Double-Blind, Placebo-Controlled Single-Ascending-Dose Study. *J. Clin. Pharmacol.* 59, 688–701. doi: 10.1002/jcph.1361

Trifilo, M. J., Montalto-Morrison, C., Stiles, L. N., Hurst, K. R., Hardison, J. L., Manning, J. E., et al. (2004). CXC Chemokine Ligand 10 Controls Viral Infection in the Central Nervous System: Evidence for a Role in Innate Immune Response Through Recruitment and Activation of Natural Killer Cells. *J. Virol.* 78, 585–594. doi: 10.1128/jvi.78.2.585-594.2004

Uy, G. L., Rettig, M. P., and Cashen, A. F. (2008). Plerixafor, a CXCR4 Antagonist for the Mobilization of Hematopoietic Stem Cells. *Expert Opin. Biol. Ther.* 8, 1797–1804. doi: 10.1517/14712598.8.11.1797

Vivier, E., Raulet, D. H., Moretta, A., Caligiuri, M. A., Zitvogel, L., Lanier, L. L., et al. (2011). Innate or Adaptive Immunity? The Example of Natural Killer Cells. *Science* 331, 44–49. doi: 10.1126/science.1198687

Voynova, E., Qi, C. F., Scott, B., and Bolland, S. (2015). Cutting Edge: Induction of Inflammatory Disease by Adoptive Transfer of an Atypical NK Cell Subset. *J. Immunol.* 195, 806–809. doi: 10.4049/jimmunol.1500540

Wang, L. C., Jung, S. M., Chen, K. Y., Wang, T. Y., and Li, C. H. (2015). Temporal-Spatial Pathological Changes in the Brains of Permissive and Non-Permissive Hosts Experimentally Infected With Angiostrongylus Cantonensis. *Exp. Parasitol.* 157, 177–184. doi: 10.1016/j.exppara.2015.08.006

Wang, Q. P., Wu, Z. D., Wei, J., Owen, R. L., and Lun, Z. R. (2012). Human Angiostrongylus Cantonensis: an Update. *Eur. J. Clin. Microbiol. Infect. Dis.* 31, 389–395. doi: 10.1007/s10096-011-1328-5

Xu, G. G., Guo, J., and Wu, Y. (2014). Chemokine Receptor CCR5 Antagonist Maraviroc: Medicinal Chemistry and Clinical Applications. *Curr. Top. Med. Chem.* 14, 1504–1514. doi: 10.2174/1568026614666140827143745

Zhang, Y., Gao, Z., Wang, D., Zhang, T., Sun, B., Mu, L., et al. (2014). Accumulation of Natural Killer Cells in Ischemic Brain Tissues and the Chemotactic Effect of IP-10. *J. Neuroinflammation* 11, 1186. doi: 10.1186/1742-2094-11-79

Zou, Y., Chen, T., Han, M., Wang, H., Yan, W., Song, G., et al. (2010). Increased Killing of Liver NK Cells by Fas/Fas Ligand and NKG2D/NKG2D Ligand Contributes to Hepatocyte Necrosis in Virus-Induced Liver Failure. *J. Immunol. (Baltimore Md 1950)* 184, 466–475. doi: 10.4049/jimmunol.0900687

Conflict of Interest: The authors declare that the research was conducted in the absence of any commercial or financial relationships that could be construed as a potential conflict of interest.

frontiers in Cellular and Infection Microbiology

ORIGINAL RESEARCH
published: 31 August 2021
doi: 10.3389/fcimb.2021.701820

Brain Microvascular Endothelial Cell-Derived HMGB1 Facilitates Monocyte Adhesion and Transmigration to Promote JEV Neuroinvasion

Song-Song Zou[1,2,3,4], *Qing-Cui Zou*[1,2,3,4], *Wen-Jing Xiong*[1,2,3,4], *Ning-Yi Cui*[1,2,3,4], *Ke Wang*[1,2,3,4], *Hao-Xuan Liu*[1,2,3,4], *Wen-Juan Lou*[1,2,3,4], *Doaa Higazy*[1,2,3,4], *Ya-Ge Zhang*[1,2,3,4] *and Min Cui*[1,2,3,4]*

[1] State Key Laboratory of Agricultural Microbiology, College of Veterinary Medicine, Huazhong Agricultural University, Wuhan, China, [2] Key Laboratory of Preventive Veterinary Medicine in Hubei Province, The Cooperative Innovation Center for Sustainable Pig Production, Wuhan, China, [3] Key Laboratory of Development of Veterinary Diagnostic Products, Ministry of Agriculture of the People's Republic of China, Wuhan, China, [4] International Research Center for Animal Disease, Ministry of Science and Technology of the People's Republic of China, Wuhan, China

OPEN ACCESS

Edited by:
Tatiana Barichello,
University of Texas Health Science Center at Houston, United States

Reviewed by:
Charles T. Spencer,
The University of Texas at El Paso, United States
Jaqueline Generoso,
Universidade do Extremo Sul Catarinense, Brazil

***Correspondence:**
Min Cui
cuimin@mail.hzau.edu.cn

Specialty section:
This article was submitted to Virus and Host, a section of the journal Frontiers in Cellular and Infection Microbiology

Received: 28 April 2021
Accepted: 10 August 2021
Published: 31 August 2021

Citation:
Zou S-S, Zou Q-C, Xiong W-J, Cui N-Y, Wang K, Liu H-X, Lou W-J, Higazy D, Zhang Y-G and Cui M (2021) Brain Microvascular Endothelial Cell-Derived HMGB1 Facilitates Monocyte Adhesion and Transmigration to Promote JEV Neuroinvasion. Front. Cell. Infect. Microbiol. 11:701820. doi: 10.3389/fcimb.2021.701820

Infection with Japanese encephalitis virus (JEV) induces high morbidity and mortality, including potentially permanent neurological sequelae. However, the mechanisms by which viruses cross the blood-brain barrier (BBB) and invade into the central nervous system (CNS) remain unclear. Here, we show that extracellular HMGB1 facilitates immune cell transmigration. Furthermore, the migration of immune cells into the CNS dramatically increases during JEV infection which may enhance viral clearance, but paradoxically expedite the onset of Japanese encephalitis (JE). In this study, brain microvascular endothelial cells (BMECs) were utilized for the detection of HMGB1 release, and leucocyte, adhesion, and the integrity of the BBB *in vitro*. Genetically modified JEV-expressing EGFP (EGFP-JEV) and the BBB model were established to trace JEV-infected immune cell transmigration, which mimics the process of viral neuroinfection. We find that JEV causes HMGB1 release from BMECs while increasing adhesion molecules. Recombinant HMGB1 enhances leukocyte-endothelium adhesion, facilitating JEV-infected monocyte transmigration across endothelia. Thus, JEV successfully utilizes infected monocytes to spread into the brain, expanding inside of the brain, and leading to the acceleration of JE onset, which was facilitated by HMGB1. HMGB1-promoted monocyte transmigration may represent the mechanism of JEV neuroinvasion, revealing potential therapeutic targets.

Keywords: transmigration, adhesion, monocyte, HMGB1, Japanese encephalitis virus (JEV), neuroinvasion

INTRODUCTION

Japanese encephalitis virus (JEV) is a mosquito-borne, positive-sense single-stranded RNA virus (Misra and Kalita, 2010). JEV is an epidemic virus in the southern and eastern regions of Asia (Solomon et al., 2000; Misra and Kalita, 2010). The overall incidence of Japanese encephalitis (JE) is about 1.8 per 100,000. Approximately 20% of JE patients succumb to infection, and 50% of the survivors present with permanent neuropsychiatric sequelae (Solomon et al., 2000; Misra and Kalita, 2010). Numerous neurotropic pathogens affect blood-brain barrier (BBB) integrity, such as West Nile virus (WNV) and dengue virus (DENV) (Spindler and Hsu, 2012; Koyuncu et al., 2013). Pathologically, it has been suggested that impairment of the BBB is conclusively correlated with neuroinflammation. During JEV infection, dramatic BBB damage occurs, which is associated with Guillain-Barre syndrome (Wang et al., 2020). Currently, there are no effective therapeutics against JE (Misra and Kalita, 2010). Therefore, it is essential to investigate the pathways and mechanisms of JEV neuroinvasion.

As a dynamic interface of the central nervous system (CNS), the BBB is composed of closely packed fenestrated BMECs, supported by pericytes, astrocyte end-feet, neurons, and the extracellular matrix (Spindler and Hsu, 2012; Obermeier et al., 2013). The BBB manages transport and metabolism as a physical and physiological barrier, restricting the infiltration of immune cells into the brain (Obermeier et al., 2013; Li et al., 2015). The Transwell monolayer model mimics the BBB *in vitro*, and the integrity of the model can be reflected by the resistance measurement (TEER, transendothelial electrical resistance) *in vitro* (Eigenmann et al., 2013; Chen et al., 2014). During JEV infection, highly expressed proinflammatory cytokines and chemokines contribute to pathogenesis (Li et al., 2015). Increasing evidence suggests that recruitment and transmigration of leukocytes from the bloodstream to the CNS are involved in encephalitis (Man et al., 2007; Lim et al., 2011; Terry et al., 2012). Besides, cell adhesion molecules and their ligands promote immune cell trafficking, which has been confirmed by specific blockade assays or gene-deficient animal models (Miner and Diamond, 2016; Varatharaj and Galea, 2017).

There are several possible routes by which viruses invade the CNS: infection of BMECs, spread from the olfactory bulb, and immune cells acting as "Trojan horses" (Koyuncu et al., 2013; Suthar et al., 2013; Miner and Diamond, 2016). Infiltrated leukocytes present a paradoxical character in different diseases, especially monocytes, which can act as virus carriers disseminating the virus in the tissues or act as virus cleaner *via* activating immune responses. Nonetheless, the appearance of infected monocytes might act as an indicator of the severity of CNS disease (Charlier et al., 2009; Terry et al., 2012). Many viral infection models have shown that monocytes are well-suited viral vectors and exhibit the ability of transmigration as "Trojan horses" for viruses such as HIV-1, WNV, and ZIKV (Koyuncu et al., 2013; Ayala-Nunez et al., 2019; de Carvalho et al., 2019).

High-mobility group box 1 (HMGB1) is the most extensively studied HMG protein; normally located in the nucleus as a DNA chaperone (Romani et al., 1979; Muller et al., 2001; Stros, 2010). HMGB1 can actively translocate and be released from cells responding to stimuli (Kang et al., 2014; Hosakote et al., 2016). HMGB1 participates in cell recruitment, adhesion and migration as an adhesion molecule and a chemoattractant, and it is a damage-associated molecular pattern (DAMP) protein that initiates the immune response (Scaffidi et al., 2002; Rouhiainen et al., 2004; Kang et al., 2014). It has been confirmed that extracellular HMGB1 contributes to monocyte migration (Rouhiainen et al., 2004; Kang et al., 2014). Furthermore, extracellular HMGB1 initiates inflammatory pathways, leading to the production of multiple inflammatory factors (Scaffidi et al., 2002; Hosakote et al., 2016; Rayavara et al., 2018), which may damage the BBB.

In this study, JEV infection led to human brain microvascular endothelial cells (HBMECs) producing abundant HMGB1, which promoted JEV-infected monocytes transmigration, acting as "Trojan horses", resulting in JEV neuroinvasion. These data provide insights into the correlation of leucocytes transmigration and JEV dissemination and may assist in JE treatment.

MATERIALS AND METHODS

Mice and Virus

C57BL/6 mice were supplied by the Laboratory Animal Center of Huazhong Agricultural University, Wuhan, China. All work was performed following the Committee for Protection, Supervision, and the Control of Experiments on Animals guidelines of Huazhong Agricultural University. The JEV-P3 strain was employed in our previous research (Li et al., 2015) and 15 μl (5×10^4 PFU) of viral inoculum was injected into the brains of 1-day suckling mice. After euthanization, the mouse (symptoms exhibition) brain was removed. Homogenized brains were suspended in Dulbecco's modified Eagle's medium (DMEM) at a concentration of 10% (wt/vol). After centrifugation, the debris was discarded and the supernatant was stored at −80°C until use. The baby hamster kidney fibroblast cell line (BHK-21) was used for viral titration by plaque assay.

Viral Infection

Female C57BL/6 mice aged 6–8 weeks were classified into two groups: the control group ($n = 6$), which was injected with 50 μl of DMEM. In the JEV-infected group ($n = 6$), the mice were injected in the footpad with 10^5 PFU or infected *via* intravenous injection (i.v.) with 5×10^6 PFU of JEV. Mouse tissues were collected for tissue sectioning and RNA extraction.

Abbreviations: BBB, blood-brain barrier; BMEC, brain microvascular endothelial cell; CNS, central nervous system; HBMEC, human brain microvascular endothelial cell; HMGB1, high mobility group box 1; ICAM-1, intercellular adhesion molecule-1; ICAM-2, intercellular adhesion molecule-2; JE, Japanese encephalitis; JEV, Japanese encephalitis virus; LFA-1, lymphocyte function-associated antigen-1; rHMGB1, recombinant HMGB1; TEER, transendothelial electrical resistance; VLA-4, very late antigen-4; VCAM-1, vascular cell adhesion molecule-1.

Primary splenocytes and BMECs (HBMECs and bEnd.3 cells) were exposed to JEV at an MOI of 1 and incubated in DMEM at 37°C with 5% CO_2 for 2 h. The cells were washed with PBS and then grown in culture medium. Virus-free cells were served as control.

Cell Culture and Coculture

HBMECs were maintained in our laboratory and grown in DMEM containing 10% fetal bovine serum (FBS, Gibco, Grand Island, NY, USA) and endothelial cell growth supplement containing nonessential amino acids (Sigma, Ronkonkoma, NY, USA), minimum essential medium (Sigma, USA) vitamins, sodium pyruvate (Sigma, USA), 100 U/ml penicillin, and 100 mg/ml streptomycin sulfate at 37°C with 5% CO_2. BHK-21 cells and bEnd.3 cells were maintained in our laboratory and grown in DMEM containing 10% FBS (Gibco, USA), 100 U/ml penicillin, and 100 mg/ml streptomycin sulfate at 37°C with 5% CO_2. C6/36 cells were obtained from the Wuhan Institute of Virology, Chinese Academy of Sciences, cultured at 28°C with 5% CO_2, using the same culture medium was used for the BHK-21 cells.

Primary splenocytes and peripheral blood mononuclear cells (PBMCs) were collected from healthy adult mice. After spinning down the red blood cells, cells were cultured at a density of 1×10^6 cells/ml in DMEM containing 10% FBS, 100 U/ml penicillin, and 100 mg/ml streptomycin sulfate.

Primary splenocytes and PBMCs were treated with rHMGB1 (100 ng/ml, Sino Biological, Beijing, China) or infected with JEV (MOI = 1) and cultured at 37°C with 5% CO_2. And RNA samples were collected at indicated times.

Primary splenocytes (treated or untreated) were incubated with the BMEC monolayer (JEV-infected or uninfected) in a 12-well plate for 2 h at 37°C with 5% CO_2. Then the samples were collected for analysis at the indicated times. JEV-free or rHMGB1-free cells were served as control.

Western Blotting

Cells were lysed in RIPA buffer containing protease inhibitor cocktail, homogenized, and centrifuged at 12,000×*g* and 4°C for 5 min. The protein concentration was determined by a BCA protein assay kit (Beyotime, Shanghai, China). Protein samples were separated by SDS-PAGE with 12% polyacrylamide gel. The proteins were transferred to polyvinylidene difluoride membranes (Bio-Rad, Richmond, CA, USA). Then, the proteins on the membranes were blocked for 2 h at room temperature in Tris-buffered saline with Tween 20 (TBST) containing 5% nonfat dry milk. The membranes were incubated overnight at 4°C with JEV-E protein monoclonal antibody (preserved in the laboratory) and the following antibodies: anti-ICAM-2, anti-beta-catenin, and anti-E-selectin (Proteintech, Wuhan, China); anti-HMGB1 (Novus Biologicals, Centennial, CO, USA); anti-VE-cadherin and anti-VCAM-1 (Abcam, Cambridge, MA, USA); and anti-Lamin A/C and anti-beta-actin (ABclonal, Wuhan, China). The membranes were washed with TBST and then incubated with horseradish peroxidase-conjugated (HRP) secondary antibodies. Enhanced chemiluminescence reagents (Bio-Rad, USA) were utilized to visualize the HRP-induced signal.

Injection of Immune Cells Into the Brain

Purified $CD3^+$ T cells, $CD19^+$ B cells, and $Ly6C^+$ monocytes were infected with JEV (MOI = 1) in DMEM for 2 h. The cells were then washed with PBS and incubated with JEV antiserum. Then, 1×10^5 cells (virus-infected or uninfected) were injected into normal mouse brains. The JE onset time data were registered, and the JE mouse brains were removed for virus detection.

Immunofluorescence

Ketamine-xylazine and PBS were used for the anesthetization and perfusion of symptomatic mice. The collected tissues were immediately fixed with 4% paraformaldehyde in an aseptic environment. All fixed tissues were embedded in paraffin for sectioning. In addition, the antigen was thermally retrieved in 0.01 M sodium citrate solution buffer.

Tissue sections were blocked in 5% BSA sealing fluid for 30 min at room temperature and incubated with anti-JEV-E protein monoclonal antibody overnight at 4°C. The sections were washed with PBS, incubated with the Alexa Fluor 488 labeled secondary antibody (Invitrogen, Grand Island, NY, USA) for 1 h, and nuclei were stained with 4′,6-diamidino-2-phenylindole (DAPI) for 3 min at room temperature. The tissue sections were sealed with glycerin. A fluorescence microscope was used to observe the sealed sections.

Highly express GFP-LFA-1 (ICAM-1 ligand) yeast cells were used to detect the ICAM-1 in the JEV-infected bEnd.3 cells (Zhang et al., 2018). The amount of the fluorescence (GFP) yeast cell represents the expression of ICAM-1 in the BMEC monolayer.

BBB Monolayer Transwell Model

The BBB monolayer Transwell model (12-well, 3.0 μm pore size, Corning, NY, USA) was adopted in this study. Two hundred microliters of rat tail collagen (50 μg/ml, Sigma, USA) was used to enclose the upper Transwell chamber at room temperature for 1 h. After washed with PBS, 500 μl of DMEM (without phenol red, Sigma, USA) was added to the upper chamber for pre-equilibration at 37°C for 1 h. BMECs (5×10^5 bEnd.3 cells) were cultured in the upper chamber with a total volume of 500 μl of culture medium (without phenol red, Sigma, USA) at 37°C and 5% CO_2 for approximately 24 h. Monolayer leakage was monitored for 4 h, and FITC-dextran (10 kD and 70 kD, Sigma-Aldrich, USA) was added for the permeability measurement of the BBB monolayer model.

Electric Cell-Substrate Impedance Sensing (ECIS)

Electrode plates were equilibrated in 500 μl DMEM overnight at 37°C. Then, 350 μl of bEnd.3 cells was added to each well at a density of 2×10^6/ml. Until the impedance stabilization, real-time impedance changes were measured (Applied BioPhysics, Troy, NY, USA).

Cell Transmigration

Virus was added to the upper Transwell chamber to infect the bEnd.3 cells (MOI = 1) for 2 h in DMEM (without phenol red, Sigma, USA). In addition, primary splenocytes were infected

with virus or treated with rHMGB1 (100 ng/ml). After washing by PBS, the Transwell chamber was refreshed with new culture medium. The treated splenocytes (5×10^5 cells) were added to the upper chamber and cocultured with the monolayer of infected bEnd.3 cells for 24 h at 37°C and 5% CO_2. Then, the transmigrated cells were collected in the lower chamber and analyzed by flow cytometry.

Transendothelial electrical resistance (TEER; ohm.cm^2) (Millicell, ERS-2,Millipore, Billerica, MA), a criterion used to evaluate the permeability of monolayer models *in vitro*, was monitored and recorded at the indicated times (0 h, 6 h, 12 h, 18 h, and 24 h).

Flow Cytometry and Quantitative Real-Time PCR Analysis

Splenocytes were stained with the combination of mAbs conjugated with FITC, PE, PE-Cy7, APC-Cy7, PB, and APC. For cell surface marker staining, splenocyte suspensions were incubated with the appropriate Abs, anti-CD3, anti-CD11b, anti-Ly6C, and anti-CD19 in PBS buffer (pH = 7.4) containing 0.2% BSA (BioSharp, China), at 4°C for 30 min. PBS was provided for double washing (400×*g*, 5 min, 4°C), and cell suspension. Cell identification and separation were achieved by flow cytometry with FACS Calibur (BD Biosciences, Billerica, MA, USA) system or Beckman CytoFlex (Beckman Coulter, Carlsbad, CA, USA), and CytExport 2.0 CellQuest Pro software were used for data analysis. The EGFP-JEV is utilized is to intracellular JEV detection.

Total RNA was extracted with TRIzol reagent (Invitrogen, USA). One microgram of RNA was used to synthesize cDNA with a ReverTra Ace RT-PCR RT kit (Toyobo, Osaka, Japan) following the manufacturer's instructions. SYBR Green (Invitrogen, USA) was employed for quantitative real-time PCR using StepOne Plus and StepOne Software v2.2.2 (Applied Biosystems, Foster City, CA, USA). The relative expression of the JEV-C gene was normalized to the level of the beta-actin. The pcDNA3.0-HA/JEV-C gene plasmid served as a template for generating a standard curve to quantify JEV copy numbers. The real-time PCR primers were listed in **Supplementary Table S1**.

Statistical Analysis

All experiments were repeated at least three times. The data are expressed as the means ± SEM. The data were analyzed by Student's *t*-test or one-way analysis of variance followed by Tukey's *post-hoc* tests. Graphs were plotted and analyzed using GraphPad Prism software (v7.0; GraphPad, La Jolla, CA, USA).

RESULTS

JEV Infection Caused HMGB1 Cytoplasmic Translocation and Secretion From HBMEC

HBMECs were infected with JEV at an MOI of 1, and the expression of JEV-E protein was measured by Western blotting. JEV replicated in HBMECs (**Figure 1A**), and abundant intracellular JEV-E protein was observed at 24 and 48 h (**Figure 1B**). JEV infection caused a dramatic increase in HMGB1 expression at both the mRNA and protein levels (**Figures 1C, D**). In addition, HMGB1 was upregulated in mouse BMECs (bEnd.3 cell line) during JEV infection (**Figure S1A**). These results demonstrate that JEV infection induced upregulation of HMGB1 expression in BMECs.

The biological functions of HMGB1 are dominated by its expression and subcellular localization (Deng et al., 2019). Thus, the cellular distribution and release of HMGB1 were determined. HMGB1 was mainly located in the nucleus of uninfected HBMECs and expressed at a low level, but its expression was significantly increased in the cytoplasm of JEV-infected HBMECs at 24 h (**Figure S1B**), suggesting the translocation of HMGB1 from the nucleus to the cytoplasm. To confirm this translocation, the protein was extracted separately from the nucleus and cytoplasm, and the HMGB1 level was detected (**Figure 1E**). The results showed a significant increase of HMGB1 in the cytoplasm after JEV infection, reaching a peak at 12 h and then gradually declining from 24 h to 48 h. The expression of HMGB1 in the nucleus was increased at 6 h. Accumulation of HMGB1 in the cytoplasm may actively initiate HMGB1 secretion. The detection of secreted HMGB1 revealed approximately 2- and 3.5-fold increase in HMGB1 released from JEV-infected cells at 24 and 48 h, respectively (**Figure 1F**).

Taken together, these data suggested that JEV induces the upregulation and translocation of HMGB1, which is subsequently released from cells.

JEV Infection Induced the Activation of BMECs and an Increase in the Expression of Adhesion Molecules

BMECs are critical to the formation of the BBB and the maintenance of its barrier function. High expression of adhesion molecules and integrin ligands is necessary for circulating cell adhesion to the BBB endothelium, which may facilitate cell infiltration into the CNS. In this study, yeast cells that highly express GFP-LFA-1 (ICAM-1 ligand) were used to detect ICAM-1 expression and LFA-1-ICAM-1-mediated interactions between yeast cells and JEV-activated endothelial cells (Zhang et al., 2018). The JEV-infected bEnd.3 monolayer accommodated more GFP$^+$ LFA-1 yeast cells than the control monolayer (**Figures 2A, B**), which suggested that JEV induced upregulation of ICAM-1 in the bEnd.3 cells. Western blotting confirmed the increase in adhesion molecules on endothelial cells following infection, including VCAM-1, ICAM-2, E-selectin, VE-cadherin, and beta-catenin (**Figures 2C, D**). Since HMGB1 is released from BMECs, which may affect circulating immune cells, rHMGB1 was used to treat the isolated splenocytes *in vitro*, and the expression of adhesion molecules was measured. As expected, treatment with rHMGB1 (100 ng/ml) upregulated LFA-1 and VLA-4 on mouse splenocytes (**Figures 2E, F**), which act as receptors of ICAM-1 and VCAM-1.

In addition, the expression of ICAM-1 and VCAM-1 in HBMECs was increased after JEV infection (**Figures S2A, B**). With the treatment of rHMGB1, an upregulation was also

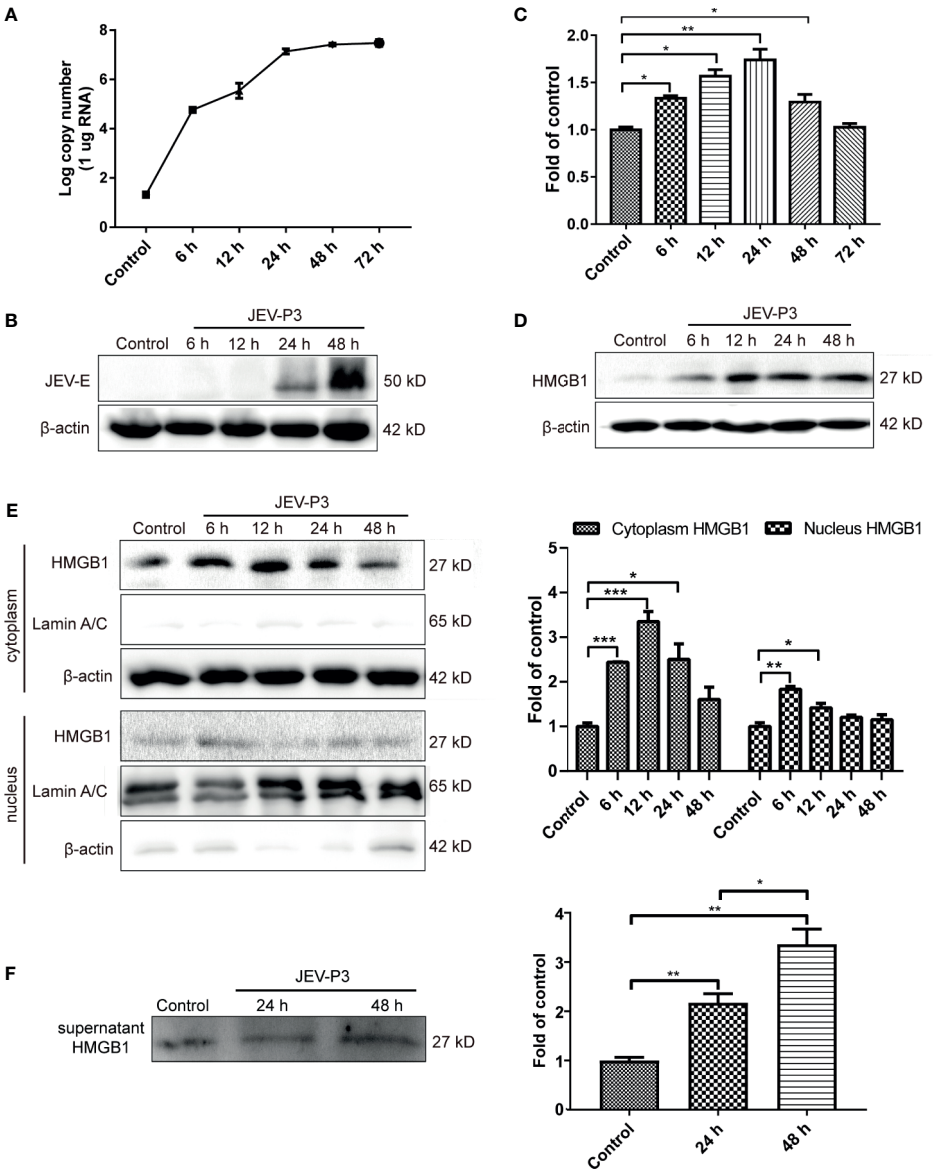

FIGURE 1 | JEV-induced fluctuation of HMGB1 in HBMECs. HBMECs were infected with JEV-P3 at an MOI of 1, and total cell protein and RNA samples were collected at the indicated times to measure JEV replication in HBMECs by real-time PCR **(A)** and Western blotting using an anti-JEV-E protein monoclonal antibody **(B)**. HMGB1 expression was measured by real-time PCR **(C)** and Western blot **(D)** at the indicated times during JEV infection. JEV free cells were served as control. **(E)** Total cytoplasmic and nuclear proteins were extracted from JEV-infected HBMECs at 0 h (Control), 6 h, 12 h, 24 h, and 48 h postinfection. HMGB1 protein expression was measured by Western blotting, with beta-actin as the internal control for protein integrity and Lamin A/C was assessed in the nuclear extract, and quantitatively analyzed as the fold change relative to the control. **(F)** HBMEC culture supernatant was collected at indicated times after virus infection (24 h, and 48 h). Supernatant HMGB1 was measured by Western blotting and quantitatively analyzed as the fold change relative to the control (JEV-free cell culture supernatant). The experiments are repeated at least three times. The data are expressed as the means ± SEM. *$p < 0.05$, **$p < 0.01$, and ***$p < 0.001$.

observed in the expression of LFA-1 (CD11a and CD18) and VLA-4 (CD49d and CD29) in human THP-1 cells (**Figures S2C, D**). Furthermore, upregulation of ICAM-1 and VCAM-1 was found in JEV-infected mouse brains (**Figures S3A, B**) and was coupled with an increase of LFA-1 and VLA-4 expression in the PBMCs (**Figures S3C, D**).

All these results suggested that JEV infection upregulated adhesion molecules on BMECs and that HMGB1 also induced an increase in integrin ligands on circulating immune cells, which may contribute to immune cells binding to the BBB endothelium.

Extracellular HMGB1 Promoted the Adhesion of Immune Cells to the Endothelium

Leukocyte-endothelium adhesion is indispensable for the infiltration of cells into the CNS. bEnd.3 monolayers were

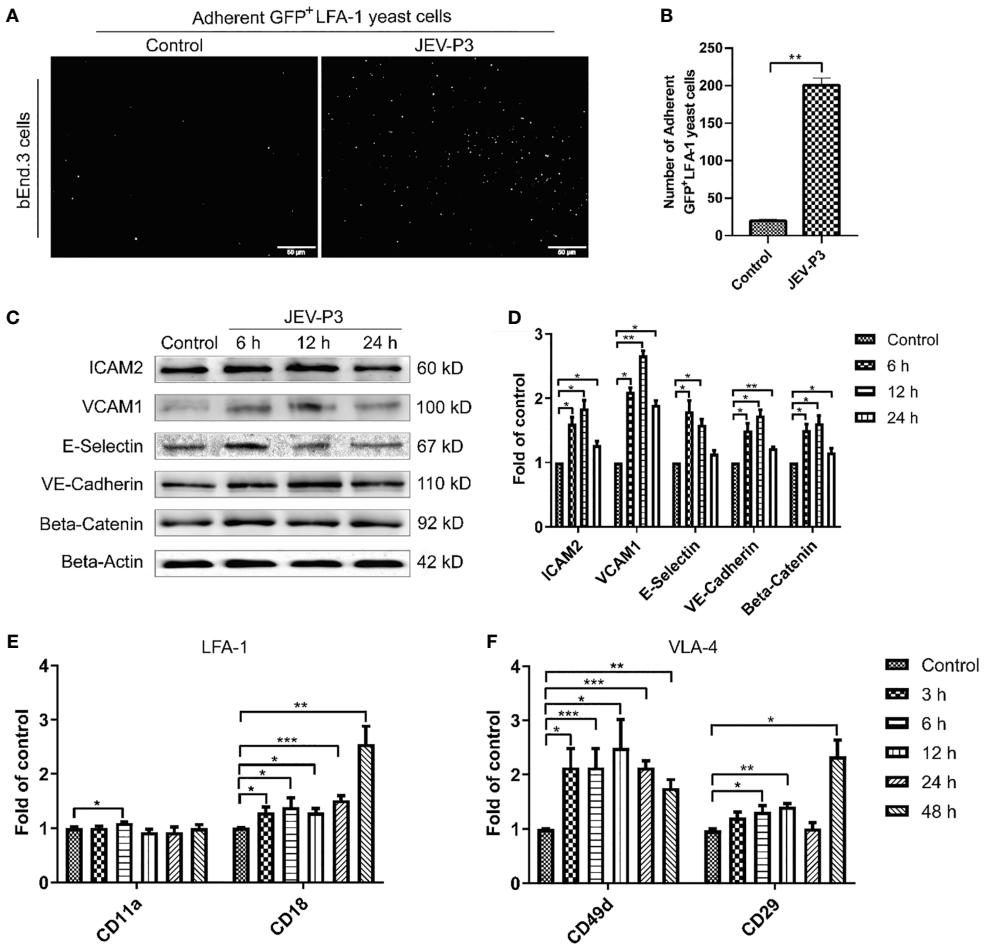

FIGURE 2 | JEV infection upregulated adhesion molecules expression in bEnd.3 cells, and rHMGB1 increased the expression of integrin ligands in splenocytes. **(A)** ICAM-1 expression level was detected in the JEV-infected bEnd.3 cells at 6 h. Representative images showing the binding of highly expressed GFP$^+$ LFA-1 yeast cells. **(B)** Statistical analysis of fluorescence was performed, and the result represents the expression levels of ICAM-1 in bEnd.3 cells. **(C)** Detection of ICAM-2, VCAM-1, E-selectin (CD62E), VE-cadherin, and beta-catenin expression levels in JEV-infected bEnd.3 cells were determined by Western blotting. Protein samples were collected at 0 h (Control), 6 h, 12 h, and 24 h. **(D)** The protein expressions reported in panel **(C)** were normalized to that of beta-actin and quantitatively analyzed as the fold change relative to the control. The expression levels of LFA-1 (CD11a and CD18) **(E)** and VLA-4 (CD49d and CD29) **(F)** in rHMGB1-treated (100 ng/ml) mouse splenocytes, determined by real-time PCR at 0 h (Control), 3 h, 6 h, 12 h, 24 h, 48 h. Untreated cells were served as control. The scale bar for **(A)** is 50 μm. The experiments were repeated at least three times. The data are expressed as the means ± SEM. $^*p < 0.05$, $^{**}p < 0.01$, and $^{***}p < 0.001$.

primed with live JEV-P3 or UV-deactivated JEV-P3. More GFP$^+$ splenocytes, isolated from GFP-transgenic mice, were bound to the JEV-infected monolayer group compared with the control (uninfected monolayer) and UV-deactivated virus groups (**Figures 3A, B**). Moreover, HMGB1 was overexpressed in 293T cells (data not shown). The supernatant from these HMGB1-overexpressing 293T cells was collected to treat THP-1 cells. More supernatant HMGB1-treated THP-1 cells were adherent to the virus-infected HBMECs compared with the untreated THP-1 cells (**Figure S4A**). To investigate whether HMGB1 stimulate immune cell adherence to the BBB endothelium, mouse splenocytes were treated with only rHMGB1 and then added to a bEnd.3 monolayer. After 2 h of incubation, the cells were gently washed and subjected to flow cytometry analysis. The results showed that rHMGB1 treatment led to more Ly6C$^+$CD11b$^+$ monocytes binding to the monolayer, but there were no significant effects on CD3$^+$ T cells or CD19$^+$ B cells (**Figures 3C, D**). Additionally, rHMGB1 treatment stimulated more CD3$^+$ T cells and Ly6C$^+$CD11b$^+$ monocytes adhering to the JEV-primed endothelial monolayer (**Figures 3C, D**). Furthermore, CD3$^+$ T cells and CD11b$^+$ monocytes were sorted from the JEV-infected mice at 3 dpi and then added to a BMEC monolayer. JEV infection dramatically enhanced the adherence of CD11b$^+$ monocytes but not CD3$^+$ T cells to the BMECs (**Figures 3E, F**). These results indicated that the upregulation of adhesion molecules triggered by JEV and the extracellular HMGB1 can promote monocyte binding to the BBB, which may potentiate monocyte crossing the BBB.

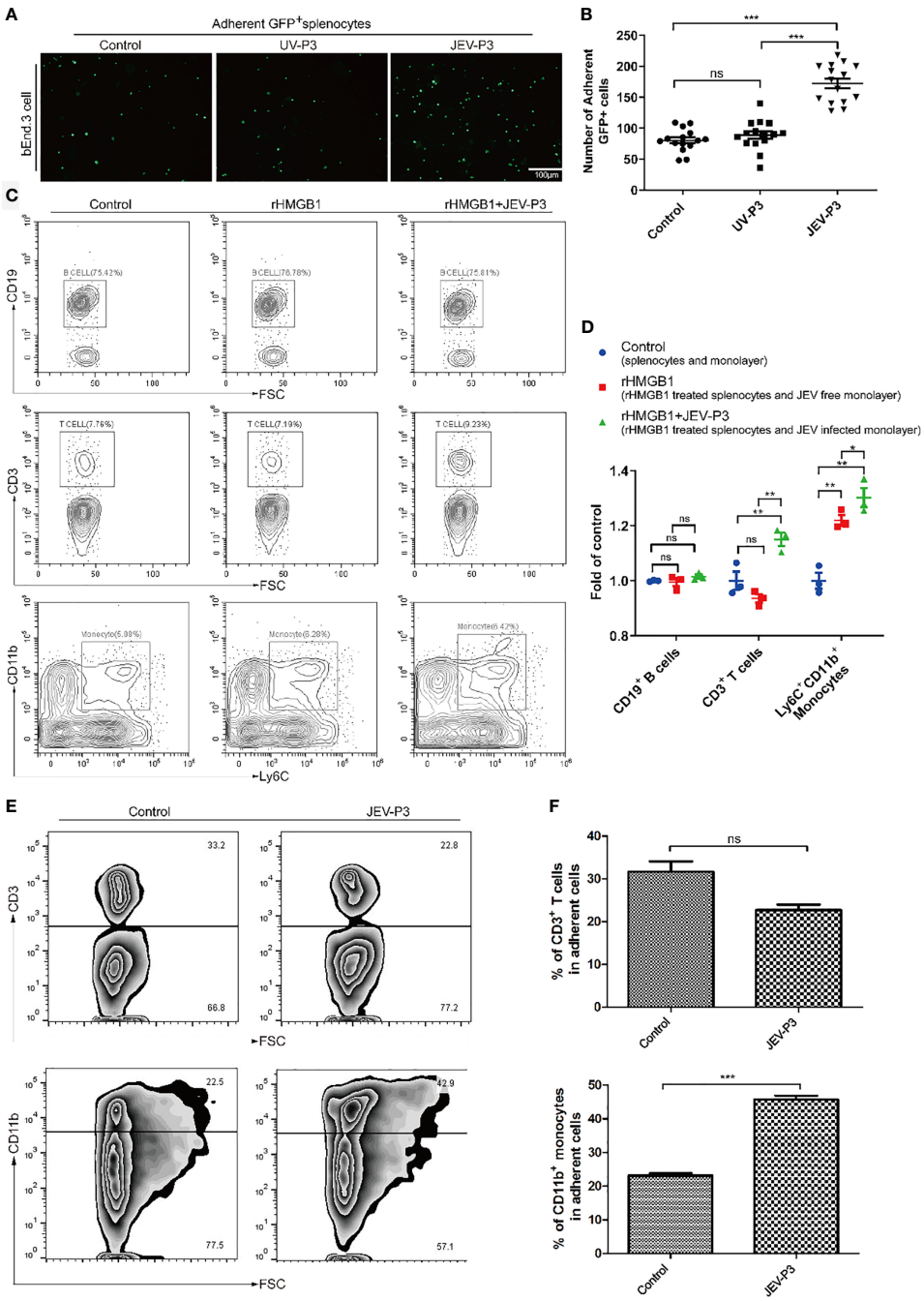

FIGURE 3 | HMGB1 promoted immune cell adhesion to the BMEC monolayer. **(A)** GFP$^+$ splenocytes were incubated with JEV-P3/UV-P3-infected bEnd.3 cell monolayers for 2 h; the GFP$^+$ splenocytes were obtained from transgenic mice. After washing with PBS, the cells were fixed with 4% paraformaldehyde and then observed by fluorescence microscopy. The fluorescence represents the number of adherent splenocytes. JEV free monolayers were served as control. **(B)** Statistical analysis of the GFP$^+$ splenocytes binding to the bEnd.3 cell monolayer of **(A)**. **(C)** Mouse splenocytes were treated with rHMGB1 (100 ng/ml) for 2 h. Then, splenocytes (rHMGB1 treated or untreated) were incubated with the bEnd.3 cell monolayers (JEV infected or uninfected) for 2 h. After gentle washing with PBS, the adherent splenocytes were collected, and the amount of CD19$^+$ B cells, CD3$^+$ T cells, and Ly6C$^+$CD11b$^+$ monocytes was analyzed by flow cytometry. Untreated splenocytes and uninfected monolayers were served as control. **(D)** Statistical analysis of the binding splenocytes to the bEnd.3 cell monolayer as reported in **(C)**. **(E)** Purified CD3$^+$ T cells and CD11b monocytes (obtained from JEV-infected mice, tail vein injection **(F)**, 3 dpi) were inoculated onto the virus-infected bEnd.3 cell monolayer and incubated for 2 h. After washing with PBS, the bound cells were detected by flow cytometry. The right panels show the results of the statistical analysis of CD3$^+$ T cells and CD11b monocytes binding to the bEnd.3 cell monolayer of **(E)**. JEV free bEnd.3 cell monolayers were served as control. The scale bar for **(A)** is 100 μm. These experiments were repeated at least three times. The data are expressed as the means ± SEM. $p > 0.05$ (ns, no significant difference), $^*p < 0.05$, $^{**}p < 0.01$, and $^{***}p < 0.001$.

Extracellular HMGB1 Facilitated Transendothelial Migration of JEV-Infected Monocytes

Notably, JEV infection did not have a significant effect on the integrity of the endothelium *in vitro*, and there was no difference between the virus and the UV-inactivated virus treatments (**Figure 4A**). However, treatment with JEV-infected mouse brain supernatant (10%) led to a loss of integrity in the BMEC monolayer (**Figure 4A**), which suggested that JEV does not disrupt the BBB, but the subsequent inflammatory reactions may result in BBB damage.

To further elucidate the role of extracellular HMGB1 in leucocyte migration during JEV infection, a Transwell insert was covered with bEnd.3 cells (**Figure S5A**). The cells formed a tight monolayer, as expected, reaching the standard level of confluence. Few FITC-dextran (10 kD and 70 kD) was detected in the lower chamber compared with the upper chamber, indicating robust membrane impermeability (**Figure S5B**). The integrity of the BBB, evaluated by TEER, remained stable over 24 h (>200 ohm.cm^2) in the control monolayers (**Figure 4B**). Quantification of the TEER showed that the exposure to rHMGB1 exacerbated the destruction of the

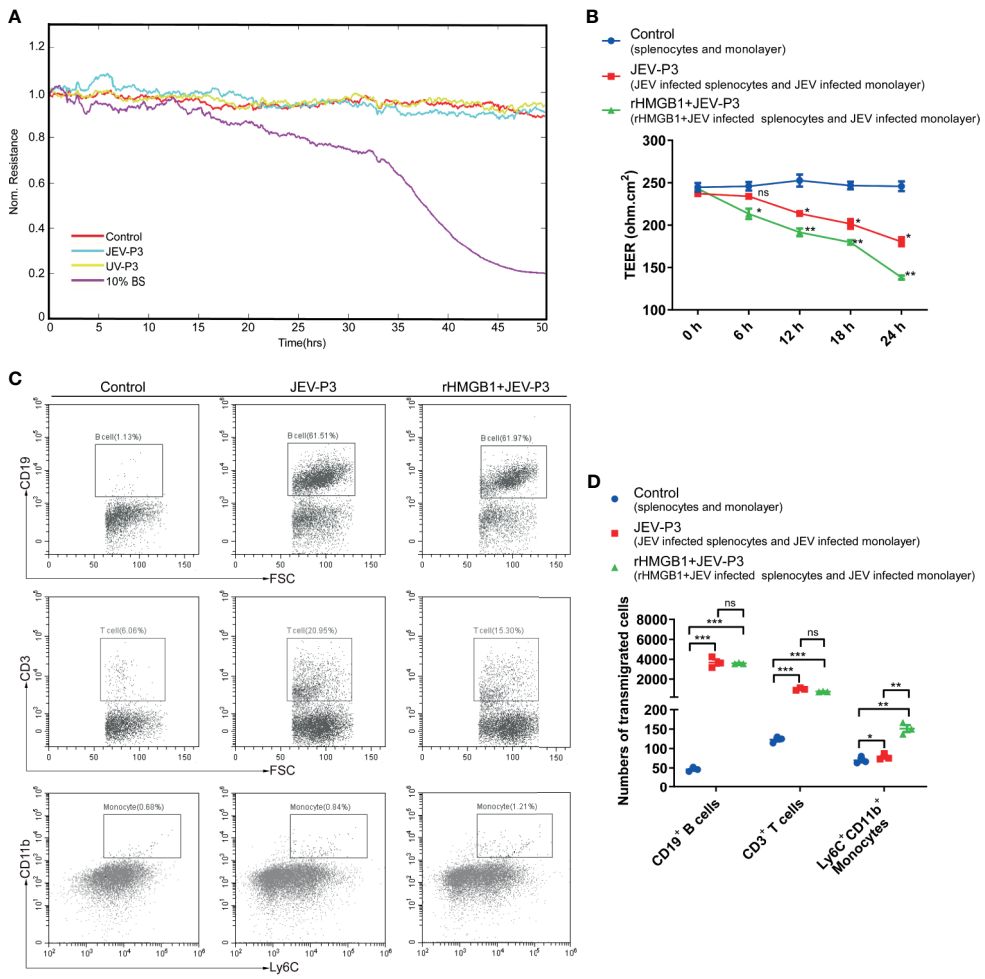

FIGURE 4 | HMGB1 facilitated immune cell transmigration during infection. **(A)** Real-time measurement of the JEV-P3/UV-P3 effect on the tight junction between bEnd.3 cells *in vitro*. The electrical resistance value represents the tight junction integrity of the bEnd.3 cells. TEER was measured at 4 kHz. bEnd.3 cells were exposed to JEV-P3, UV-P3, and 10% BS (the supernatant of JEV-infected mouse brain). Each line represents experimental repeats as measured in three wells of cells. Increased resistance is positively correlated with the barrier function of bEnd.3 cells. **(B)** bEnd.3 cells were cultured in the collagen-covered upper Transwell chamber in culture medium (without phenol red) for 24 h. Then, the permeability and TEER of the BMEC monolayer models were measured. Mouse splenocytes (5×10^5) were added to the upper chamber and cocultured with the monolayer for 24 h. Then, the transmigrated cells in the lower chamber were collected and counted by flow cytometry. The TEER value of control (splenocytes cocultured with monolayer), JEV-P3 (JEV infected splenocytes cocultured with JEV infected monolayer) and rHMGB1+JEV-P3 (rHMGB1 was added in the cocultured system of JEV infected splenocytes and JEV infected monolayer) models were measured at the indicated times (0 h, 6 h, 12 h, 18 h, and 24 h). **(C)** After splenocytes were cocultured with the bEnd.3 cell monolayer for 24 h, the transmigrated cells (obtained from the lower chamber), including $CD19^+$ B cells, $CD3^+$ T cells, and $Ly6C^+CD11b^+$ monocytes, were collected and analyzed by flow cytometry. rHMGB1 free and JEV free groups were served as control. **(D)** Statistics of transmigration cells in the lower chamber of panel **(C)**. The experiments were repeated at least three times. The data are expressed as the means ± SEM. $p > 0.05$ (ns, no significant difference), $^*p < 0.05$, $^{**}p < 0.01$, and $^{***}p < 0.001$.

monolayer during JEV infection compared with the effect on the virus-infected cells (**Figure 4B**). To confirm that HMGB1 promotes leucocyte migration, the Transwell model was used for a transmigration assay. Flow cytometry analysis indicated that JEV infection triggered the transmigration of $Ly6C^+CD11b^+$ monocytes, $CD3^+$ T cells, and $CD19^+$ B cells (**Figures 4C, D**), accompanied by a decrease in the TEER (**Figure 4B**). Moreover, rHMGB1 led to significantly more $Ly6C^+CD11b^+$ monocyte transmigration upon JEV infection but had no effects on $CD3^+$ T cells and $CD19^+$ B cells compared with the effect on the virus-infected cells (**Figures 4C, D**). These results indicated that HMGB1 can exacerbate BBB fluctuation and monocyte transmigration during JEV infection.

To discover which cells act as virus carriers, JEV with an EGFP tag (EGFP-JEV) was applied to visualize cell transmigration. There was an increased percentage of EGFP-positive $Ly6C^+CD11b^+$ monocytes, $CD3^+$ T cells, and $CD19^+$ B cells that transmigrated, compared with the control cells (**Figures 5A–C**). Furthermore, there were significantly more transmigrated JEV-positive ($EGFP^+Ly6C^+CD11b^+$) monocytes than transmigrated JEV-positive T cells ($EGFP^+CD3^+$) or B cells ($EGFP^+CD19^+$) (**Figure 5D**).

These data suggested that extracellular HMGB1 promotes cell transmigration, especially monocytes, which serve as "Trojan horses" during JEV neuroinvasion.

JEV-Infected Immune Cells Disseminate JEV to the was Brain Correlated With JE in Mouse

Mouse splenocytes were isolated and subjected to JEV infection. Real-time PCR showed that JEV replication reached a peak at 24 h (**Figure 6A**). The purified $Ly6C^+$ monocytes, $CD3^+$ T cells, and $CD19^+$ B cells were exposed to JEV and assessed by Western blot. The findings showed the ability of the virus to replicate in the purified cells (**Figure 6B**). The results in **Figure 5** indicated monocyte could carry JEV across the BBB *in vitro*. To study virus-infected leucocyte and virus CNS dissemination, virus-infected cells were incubated with the anti-JEV serum to neutralize nonspecifically adhering viruses. Thus, 1×10^5 cells were intracranially injected into the brain to simulate cell-associated JEV dissemination *in vivo*. As expected, the injection of virus-infected cells caused mouse disease symptoms (emaciation, seizures, motion disorders, and paralysis), same as that in the group injected with the virus *via*

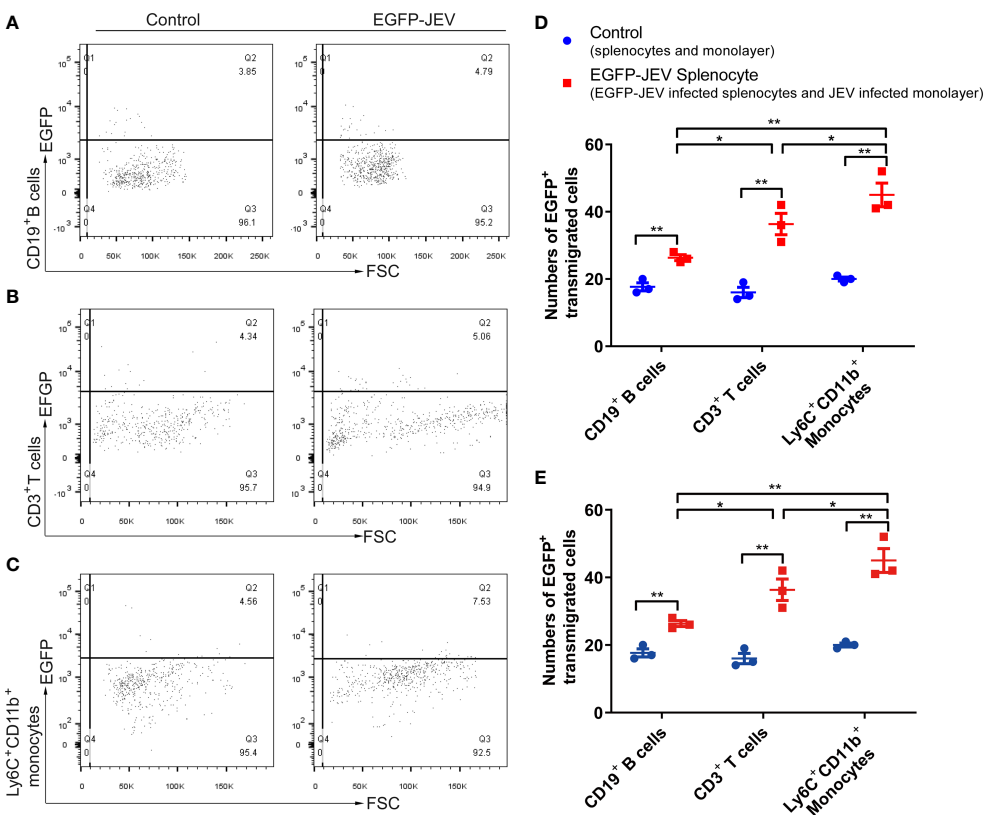

FIGURE 5 | Virus-carrying splenocyte transmigration *in vitro*. **(A–C)** JEV-infected bEnd.3 cell monolayers were cocultured with EGFP-JEV-infected splenocytes (5×10^5) for 24 h, and the transmigrated cells (lower chamber) were collected and measured by flow cytometry. An enhanced sensitivity measure at 488 nm was performed for the detection of intracellular EGFP-JEV in $CD19^+$ B cells, $CD3^+$ T cells, and $Ly6C^+CD11b^+$ monocytes by flow cytometry. EGFP-JEV free cells were the nonspecific control. **(D, E)** The statistical analysis of EGFP-positive cells in the transmigrated cells in the lower chamber reported in **(A–C)**. The experiments were repeated at least three times. The data are expressed as the means ± SEM. $p > 0.05$ (ns, no significant difference), $^*p < 0.05$ and $^{**}p < 0.01$.

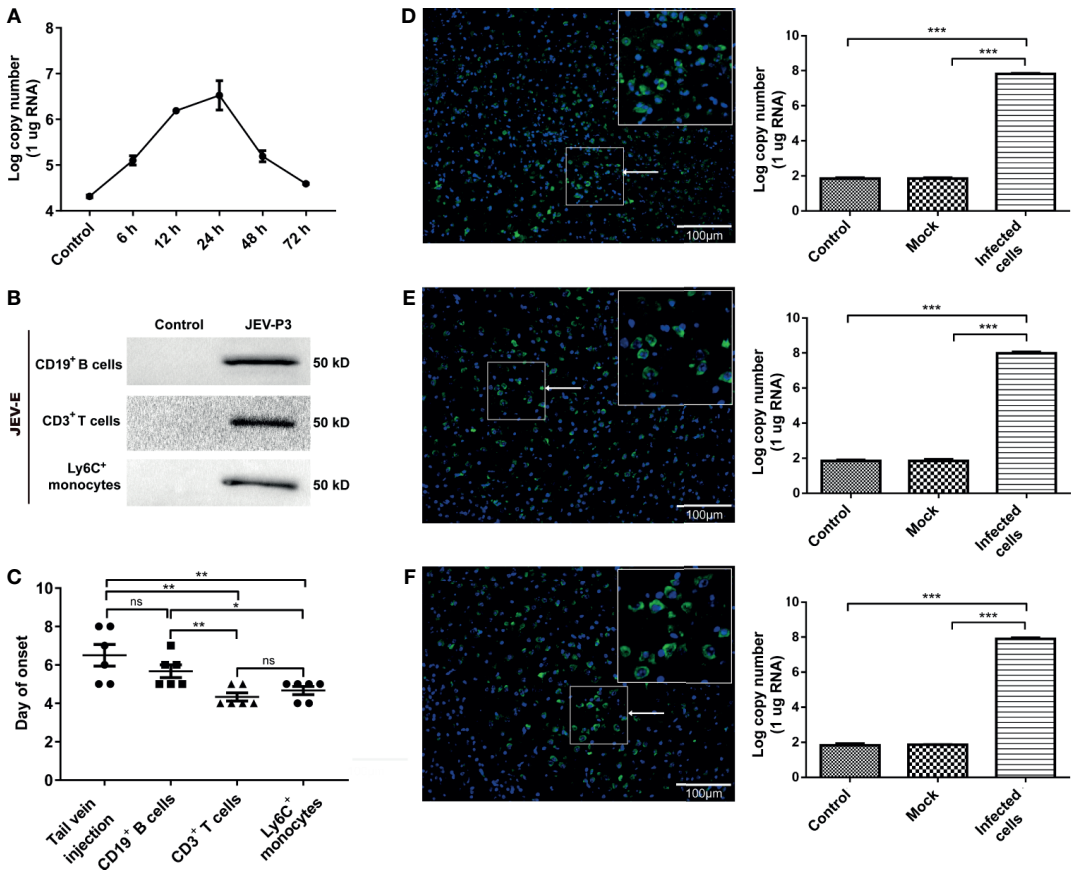

FIGURE 6 | JEV-infected immune cells facilitating virus dissemination in the CNS were affiliated with JE in mice. **(A)** The replication of JEV in mouse splenocytes from 0 h (Control) to 72 h was measured by real-time PCR. **(B)** Purified $CD3^+$ T cells, $CD19^+$ B cells, and $Ly6^+$ monocytes were exposed to JEV-P3, which was detected by Western blotting using an anti-JEV-E protein antibody. JEV free cells were served as control. **(C)** The statistical analysis of JE onset after JEV-infected $CD19^+$ B cells, $CD3^+$ T cells, and $Ly6C^+$ monocytes were injected into healthy adult mice brains, compared with the JE onset in the tail vein injection group. After the intracranial injection of PBS (Control), JEV-infected (Infected cells) or uninfected (Mock) $Ly6C^+$ monocytes **(D)**, $CD3^+$ T cells **(E)**, and $CD19^+$ B cells. **(F)** Immunofluorescence images of the JE mice brains, which showed cells stained for DNA (blue, DAPI) and JEV (green, JEV-E protein). JEV replication in mouse brains was measured by real-time PCR. The scale bar for **(D–F)** is 100 μm. The experiments were repeated at least three times. The data are expressed as the means ± SEM. $p > 0.05$ (ns, no significant difference), $^*p < 0.05$, $^{**}p < 0.01$, and $^{***}p < 0.001$.

the tail vein. Furthermore, the initial appearance of JE was earlier in the mice with the intracranial injection of JEV-infected $Ly6C^+$ monocytes and $CD3^+$ T cells than in the mice injected with JEV-infected $CD19^+$ B cells (**Figure 6C**). All types of virus-infected cells induced JE in mice and caused greater virus replication in the brain compared with the control (PBS injection) and mock groups (virus-free cell injection) (**Figures 6D–F**). Moreover, the onset time of JE was positively associated with the quantity of JEV-infected immune cells injected (data not shown). These data indicated that cell-associated JEV promotes viral dissemination, and eventually leads to neurological disease.

The natural route of infection was also mimicked by JEV injection in the footpad of C57BL/6 mice. Tissue samples were collected from mouse cerebrum, olfactory bulb, and spinal cord after infection, and the viral loads were determined by real-time PCR and immunofluorescence. The results showed that there was a higher number of the JEV particles in the cerebrum than in the olfactory bulb or spinal cord (**Figures S6A–C**). These results suggested that CNS dissemination of JEV presumably occurs through the blood.

Together, these data indicated that JEV-infected immune cells, especially monocytes, serves as "Trojan horses" carrying JEV to the brain and contribute to JE onset in mouse.

DISCUSSION

HMGB1 is a DNA-binding, intracellular transcription-regulating protein (Kang et al., 2014). Cell activation or necrosis induces HMGB1 translocation to the cytoplasm and its release into the extracellular space (Hosakote et al., 2016), which has been described as a DAMP factor that initiates inflammatory responses and regarded as a cell migration mediator (Lotze and Tracey, 2005; Kang et al., 2014). In this study, we demonstrated that JEV infection triggered HMGB1 release

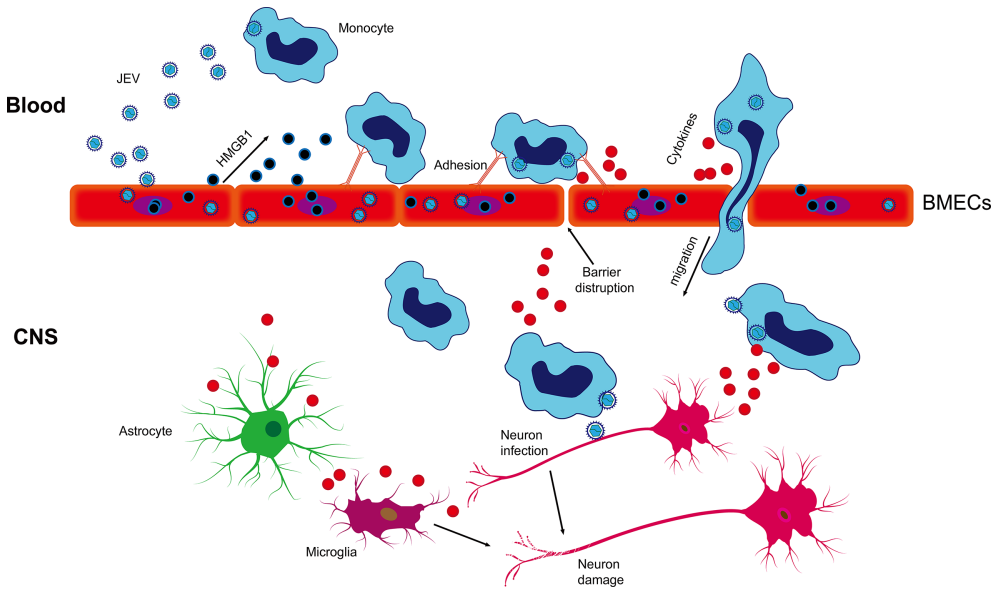

FIGURE 7 | Schematic description of BMEC-derived HMGB1 contributing to JEV-infected monocyte transendothelial migration. JEV induced HMGB1 release from BMECs and upregulated the expression of adhesion molecules, which showed enhanced leukocyte-endothelium adhesion accompanied by promoted JEV-infected monocyte transendothelial migration and BBB fluctuation. JEV-infected monocytes acted as "Trojan horses," inducing a positive effect on JE and glia activation and subsequently expanding neuronal infection, causing uncontrolled inflammatory cytokine production and neuronal damage, resulting in the appearance of JE symptoms.

from BMECs. BMEC-derived HMGB1 promoted immune cells binding to the BBB endothelium and transmigrating into the CNS as "Trojan horses". Therefore, HMGB1, as a mediator of intercellular adhesion and transmigration, promotes virus neuroinvasion and contributes to the pathogenesis of JEV, which was associated with JEV-infected monocytes.

Previous studies have reported that viral infection induces the translocation and secretion of HMGB1 (Wang et al., 2006; Hosakote et al., 2016). Additionally, HMGB1 is important to cell migration, particularly monocyte transmigration (Rouhiainen et al., 2004; Kang et al., 2014). This investigation primarily illustrated that JEV infection induced the release of HMGB1 from BMECs. JEV infection also induced the initiation of cell activation and upregulated the expression of adhesion molecules, such as ICAM-1 and VCAM-1. In addition, HMGB1 upregulated the expression of LFA-1 and VLA-4 in immune cells. Increase in adhesion molecules and HMGB1 level facilitates leukocyte binding to virus-infected monolayers and can promote immune cell CNS transmigration (Ley and Reutershan, 2006; Lai et al., 2012; Ayala-Nunez et al., 2019). However, the interaction between virus-infected leukocytes and BBB homeostasis remains unclear. Our results from a previous study revealed that JEV itself is not the leading cause of the tight junction loss between endothelial cells during early infection. In contrast, supernatant of JE brain, containing proinflammatory factors, dramatically destroyed the integrity of the BBB monolayer *in vitro*, supporting the idea that a systemic inflammatory response disrupts the BBB (Li et al., 2015; Mustafa et al., 2019).

It has been shown that during HIV/WNV infection, as the virus carriers, immune cells (T cells, monocytes) are recruited to the BBB surface for CNS infiltration (Terry et al., 2012; Koyuncu et al., 2013). Similarly, monocytes also act as JEV carriers and transmigrate to the CNS, causing neuroinfection. It has been suggested that extracellular HMGB1 may activate immune cells to produce inflammatory cytokines (Rayavara et al., 2018). Moreover, previous evidence has shown that HMGB1 is directly associated with the breakdown of the BBB *in vitro* (Festoff et al., 2016). Monocyte migration is probably different from that of T cells in response to HMGB1, which showed a distinct difference in transmigration efficiency in our model. Furthermore, our data suggested that HMGB1 accelerates the breakdown of the BBB and immune cell infiltration during JEV infection, which was reflected by a decrease in the TEERs and an increase in the amount of migrating cells. All the results from our study suggest that HMGB1 facilitates the endothelial adhesion and transmigration of monocytes during JEV infection, including specific and nonspecific binding and migration cells. However, neither the BBB monolayer model nor the *in vitro* Transwell model could fully represent the intact BBB *in vivo* (Helms et al., 2016). More comprehensive *in vivo* or *in vitro* BBB models are being developed or sought for the study of JEV-infected monocytes with HMGB1-mediated effects in the early stage of viral neuroinvasion.

Neurotropic viruses may spread through multiple pathways to achieve CNS invasion, including endothelial cell infection and the "Trojan horses". The intracranial injection of virus-infected cells is performed to link that cell-associated JEV could promote viral dissemination in the brain. However, direct evidence of cell migration *in vivo* is still lacking, and further *in vivo* studies using JEV infection models to explore the mechanism of natural

infection are necessary. It has been reported that virus-infected monocytes acting as Trojan horse-like carriers contribute to virus dissemination in the CNS, enhancing viral persistence (O'Connor et al., 2018; Ayala-Nunez et al., 2019). Notably, it has been suggested that the migration of T cells into the CNS may be regulated by the transmigration of monocytes (Savarin et al., 2010; Man et al., 2012; Netland and Bevan, 2013). Therefore, monocytes may act as an important mediator in viral spread towards neural tissues, and further study is needed to evaluate the relative contribution of monocytes to JEV neuroinvasion.

In summary, our results suggest that JEV infection induces the release of HMGB1 from BMECs, enhancing virus-associated leucocyte adhesion and transendothelial migration and promoting viral dissemination, leading to neuroinfection and neuroinflammation (**Figure 7**). Our findings have important implications for the current understanding of JEV-host interactions by highlighting that HMGB1 and monocyte transmigration can be specifically targeted for the treatment of JE.

DATA AVAILABILITY STATEMENT

The original contributions presented in the study are included in the article/**Supplementary Material**. Further inquiries can be directed to the corresponding author.

ETHICS STATEMENT

The animal study was reviewed and approved by Research Ethics Committee of the College of Veterinary Medicine, Huazhong Agricultural University, Hubei, Wuhan, China.

AUTHOR CONTRIBUTIONS

MC and S-SZ designed the investigation. S-SZ, N-YC, Q-CZ, and W-JX performed the experiments. S-SZ, W-JX, KW, and N-YC analyzed the data. MC and S-SZ organized the data. S-SZ and MC wrote the paper. All authors contributed to the article and approved the submitted version.

FUNDING

This work was financially supported by the National Program on Key Research Project of China (2016YFD0500406), the Fundamental Research Fund for the Central University (2662018PY016), Natural Science Foundation of Hubei Province (2019CFA010), and the funds of the State Key Laboratory of Agricultural Microbiology.

ACKNOWLEDGMENTS

The authors thank Dr. Bo Zhang (Wuhan Institute of Virology, Chinese Academy of Sciences, China) for permission to use EGFP-JEV. The authors also thank Dr. Zhe Hu (Huazhong Agricultural University) for using the confocal microscopy (Nikon, Japan).

SUPPLEMENTARY MATERIAL

The Supplementary Material for this article can be found online at: https://www.frontiersin.org/articles/10.3389/fcimb.2021.701820/full#supplementary-material

REFERENCES

Ayala-Nunez, N. V., Follain, G., Delalande, F., Hirschler, A., Partiot, E., Hale, G. L., et al. (2019). Zika Virus Enhances Monocyte Adhesion and Transmigration Favoring Viral Dissemination to Neural Cells. *Nat. Commun.* 10 (1), 4430. doi: 10.1038/s41467-019-12408-x

Charlier, C., Nielsen, K., Daou, S., Brigitte, M., Chretien, F., and Dromer, F. (2009). Evidence of a Role for Monocytes in Dissemination and Brain Invasion by Cryptococcus Neoformans. *Infect. Immun.* 77 (1), 120–127. doi: 10.1128/IAI.01065-08

Chen, C. J., Ou, Y. C., Li, J. R., Chang, C. Y., Pan, H. C., Lai, C. Y., et al. (2014). Infection of Pericytes *In Vitro* by Japanese Encephalitis Virus Disrupts the Integrity of the Endothelial Barrier. *J. Virol.* 88 (2), 1150–1161. doi: 10.1128/JVI.02738-13

de Carvalho, G. C., Borget, M. Y., Bernier, S., Garneau, D., da Silva Duarte, A. J., and Dumais, N. (2019). RAGE and CCR7 Mediate the Transmigration of Zika-Infected Monocytes Through the Blood-Brain Barrier. *Immunobiology* 224 (6), 792–803. doi: 10.1016/j.imbio.2019.08.007

Deng, M., Scott, M. J., Fan, J., and Billiar, T. R. (2019). Location is the Key to Function: HMGB1 in Sepsis and Trauma-Induced Inflammation. *J. Leukoc. Biol.* 106 (1), 161–169. doi: 10.1002/JLB.3MIR1218-497R

Eigenmann, D. E., Xue, G., Kim, K. S., Moses, A. V., Hamburger, M., and Oufir, M. (2013). Comparative Study of Four Immortalized Human Brain Capillary Endothelial Cell Lines, hCMEC/D3, hBMEC, TY10, and BB19, and Optimization of Culture Conditions, for an *In Vitro* Blood-Brain Barrier Model for Drug Permeability Studies. *Fluids Barriers CNS* 10 (1), 33. doi: 10.1186/2045-8118-10-33

Festoff, B. W., Sajja, R. K., van Dreden, P., and Cucullo, L. (2016). HMGB1 and Thrombin Mediate the Blood-Brain Barrier Dysfunction Acting as Biomarkers of Neuroinflammation and Progression to Neurodegeneration in Alzheimer's Disease. *J. Neuroinflamm.* 13 (1), 194. doi: 10.1186/s12974-016-0670-z

Helms, H. C., Abbott, N. J., Burek, M., Cecchelli, R., Couraud, P. O., Deli, M. A., et al. (2016). In Vitro Models of the Blood-Brain Barrier: An Overview of Commonly Used Brain Endothelial Cell Culture Models and Guidelines for Their Use. *J. Cereb. Blood Flow. Metab.* 36 (5), 862–890. doi: 10.1177/0271678X16630991

Hosakote, Y. M., Brasier, A. R., Casola, A., Garofalo, R. P., and Kurosky, A. (2016). Respiratory Syncytial Virus Infection Triggers Epithelial HMGB1 Release as a Damage-Associated Molecular Pattern Promoting a Monocytic Inflammatory Response. *J. Virol.* 90 (21), 9618–9631. doi: 10.1128/JVI.01279-16

Kang, R., Chen, R., Zhang, Q., Hou, W., Wu, S., Cao, L., et al. (2014). HMGB1 in Health and Disease. *Mol. Aspects Med.* 40, 1–116. doi: 10.1016/j.mam.2014.05.001

Koyuncu, O. O., Hogue, I. B., and Enquist, L. W. (2013). Virus Infections in the Nervous System. *Cell Host Microbe* 13 (4), 379–393. doi: 10.1016/j.chom.2013.03.010

Lai, C. Y., Ou, Y. C., Chang, C. Y., Pan, H. C., Chang, C. J., Liao, S. L., et al. (2012). Endothelial Japanese Encephalitis Virus Infection Enhances Migration and Adhesion of Leukocytes to Brain Microvascular Endothelia *via* MEK-Dependent Expression of ICAM1 and the CINC and RANTES Chemokines. *J. Neurochem.* 123 (2), 250–261. doi: 10.1111/j.1471-4159.2012.07889.x

Ley, K., and Reutershan, J. (2006). Leucocyte-Endothelial Interactions in Health and Disease. *Handb. Exp. Pharmacol.* 176 Pt 2), 97–133. doi: 10.1007/3-540-36028-X_4

Lim, J. K., Obara, C. J., Rivollier, A., Pletnev, A. G., Kelsall, B. L., and Murphy, P. M. (2011). Chemokine Receptor Ccr2 is Critical for Monocyte Accumulation

and Survival in West Nile Virus Encephalitis. *J. Immunol.* 186 (1), 471–478. doi: 10.4049/jimmunol.1003003

Li, F., Wang, Y., Yu, L., Cao, S., Wang, K., Yuan, J., et al. (2015). Viral Infection of the Central Nervous System and Neuroinflammation Precede Blood-Brain Barrier Disruption During Japanese Encephalitis Virus Infection. *J. Virol.* 89 (10), 5602–5614. doi: 10.1128/JVI.00143-15

Lotze, M. T., and Tracey, K. J. (2005). High-Mobility Group Box 1 Protein (HMGB1): Nuclear Weapon in the Immune Arsenal. *Nat. Rev. Immunol.* 5 (4), 331–342. doi: 10.1038/nri1594

Man, S., Tucky, B., Cotleur, A., Drazba, J., Takeshita, Y., and Ransohoff, R. M. (2012). CXCL12-Induced Monocyte-Endothelial Interactions Promote Lymphocyte Transmigration Across an *In Vitro* Blood-Brain Barrier. *Sci. Transl. Med.* 4 (119), 119ra114. doi: 10.1126/scitranslmed.3003197

Man, S., Ubogu, E. E., and Ransohoff, R. M. (2007). Inflammatory Cell Migration Into the Central Nervous System: A Few New Twists on an Old Tale. *Brain Pathol.* 17 (2), 243–250. doi: 10.1111/j.1750-3639.2007.00067.x

Miner, J. J., and Diamond, M. S. (2016). Mechanisms of Restriction of Viral Neuroinvasion at the Blood-Brain Barrier. *Curr. Opin. Immunol.* 38, 18–23. doi: 10.1016/j.coi.2015.10.008

Misra, U. K., and Kalita, J. (2010). Overview: Japanese Encephalitis. *Prog. Neurobiol.* 91 (2), 108–120. doi: 10.1016/j.pneurobio.2010.01.008

Muller, S., Scaffidi, P., Degryse, B., Bonaldi, T., Ronfani, L., Agresti, A., et al. (2001). New EMBO Members' Review: The Double Life of HMGB1 Chromatin Protein: Architectural Factor and Extracellular Signal. *EMBO J.* 20 (16), 4337–4340. doi: 10.1093/emboj/20.16.4337

Mustafa, Y. M., Meuren, L. M., Coelho, S. V. A., and de Arruda, L. B. (2019). Pathways Exploited by Flaviviruses to Counteract the Blood-Brain Barrier and Invade the Central Nervous System. *Front. Microbiol.* 10, 525. doi: 10.3389/fmicb.2019.00525

Netland, J., and Bevan, M. J. (2013). CD8 and CD4 T Cells in West Nile Virus Immunity and Pathogenesis. *Viruses* 5 (10), 2573–2584. doi: 10.3390/v5102573

O'Connor, M. A., Tisoncik-Go, J., Lewis, T. B., Miller, C. J., Bratt, D., Moats, C. R., et al. (2018). Early Cellular Innate Immune Responses Drive Zika Viral Persistence and Tissue Tropism in Pigtail Macaques. *Nat. Commun.* 9 (1), 3371. doi: 10.1038/s41467-018-05826-w

Obermeier, B., Daneman, R., and Ransohoff, R. M. (2013). Development, Maintenance and Disruption of the Blood-Brain Barrier. *Nat. Med.* 19 (12), 1584–1596. doi: 10.1038/nm.3407

Rayavara, K., Kurosky, A., Stafford, S. J., Garg, N. J., Brasier, A. R., Garofalo, R. P., et al. (2018). Proinflammatory Effects of Respiratory Syncytial Virus–Induced Epithelial HMGB1 on Human Innate Immune Cell Activation. *J. Immunol.* 201 (9), 2753–2766. doi: 10.4049/jimmunol.1800558

Romani, M., Rodman, T. C., Vidali, G., and Bustin, M. (1979). Serological Analysis of Species Specificity in the High Mobility Group Chromosomal Proteins. *J. Biol. Chem.* 254 (8), 2918–2922. doi: 10.1016/S0021-9258(17)30161-8

Rouhiainen, A., Kuja-Panula, J., Wilkman, E., Pakkanen, J., Stenfors, J., Tuominen, R. K., et al. (2004). Regulation of Monocyte Migration by Amphoterin (HMGB1). *Blood* 104 (4), 1174–1182. doi: 10.1182/blood-2003-10-3536

Savarin, C., Stohlman, S. A., Atkinson, R., Ransohoff, R. M., and Bergmann, C. C. (2010). Monocytes Regulate T Cell Migration Through the Glia Limitans During Acute Viral Encephalitis. *J. Virol.* 84 (10), 4878–4888. doi: 10.1128/JVI.00051-10

Scaffidi, P., Misteli, T., and Bianchi, M. E. (2002). Release of Chromatin Protein HMGB1 by Necrotic Cells Triggers Inflammation. *Nature* 418 (6894), 191–195. doi: 10.1038/nature00858

Solomon, T., Dung, N. M., Kneen, R., Gainsborough, M., Vaughn, D. W., and Khanh, V. T. (2000). Japanese Encephalitis. *J. Neurol. Neurosurg. Psychiatry* 68 (4), 405–415. doi: 10.1136/jnnp.68.4.405

Spindler, K. R., and Hsu, T. H. (2012). Viral Disruption of the Blood-Brain Barrier. *Trends Microbiol.* 20 (6), 282–290. doi: 10.1016/j.tim.2012.03.009

Stros, M. (2010). HMGB Proteins: Interactions With DNA and Chromatin. *Biochim. Biophys. Acta* 1799 (1-2), 101–113. doi: 10.1016/j.bbagrm.2009.09.008

Suthar, M. S., Diamond, M. S., and Gale, M.Jr (2013). West Nile Virus Infection and Immunity. *Nat. Rev. Microbiol.* 11 (2), 115–128. doi: 10.1038/nrmicro2950

Terry, R. L., Getts, D. R., Deffrasnes, C., van Vreden, C., Campbell, I. L., and King, N. J. (2012). Inflammatory Monocytes and the Pathogenesis of Viral Encephalitis. *J. Neuroinflamm.* 9, 270. doi: 10.1186/1742-2094-9-270

Varatharaj, A., and Galea, I. (2017). The Blood-Brain Barrier in Systemic Inflammation. *Brain Behav. Immun.* 60, 1–12. doi: 10.1016/j.bbi.2016.03.010

Wang, G., Li, H., Yang, X., Guo, T., Wang, L., Zhao, Z., et al. (2020). Guillain-Barre Syndrome Associated With JEV Infection. *N Engl. J. Med.* 383 (12), 1188–1190. doi: 10.1056/NEJMc1916977

Wang, H., Ward, M. F., Fan, X. G., Sama, A. E., and Li, W. (2006). Potential Role of High Mobility Group Box 1 in Viral Infectious Diseases. *Viral Immunol.* 19 (1), 3–9. doi: 10.1089/vim.2006.19.3

Zhang, Q., Hu, S., Wang, K., Cui, M., Li, X., Wang, M., et al. (2018). Engineering a Yeast Double-Molecule Carrier for Drug Screening. *Artif. Cells Nanomed Biotechnol.* 46 (sup2), 386–396. doi: 10.1080/21691401.2018.1457539

Conflict of Interest: The authors declare that the research was conducted in the absence of any commercial or financial relationships that could be construed as a potential conflict of interest.

Publisher's Note: All claims expressed in this article are solely those of the authors and do not necessarily represent those of their affiliated organizations, or those of the publisher, the editors and the reviewers. Any product that may be evaluated in this article, or claim that may be made by its manufacturer, is not guaranteed or endorsed by the publisher.

Advantages of publishing in Frontiers

OPEN ACCESS
Articles are free to read for greatest visibility and readership

FAST PUBLICATION
Around 90 days from submission to decision

HIGH QUALITY PEER-REVIEW
Rigorous, collaborative, and constructive peer-review

TRANSPARENT PEER-REVIEW
Editors and reviewers acknowledged by name on published articles

Frontiers
Avenue du Tribunal-Fédéral 34
1005 Lausanne | Switzerland

Visit us: www.frontiersin.org
Contact us: frontiersin.org/about/contact

REPRODUCIBILITY OF RESEARCH
Support open data and methods to enhance research reproducibility

DIGITAL PUBLISHING
Articles designed for optimal readership across devices

FOLLOW US
@frontiersin

IMPACT METRICS
Advanced article metrics track visibility across digital media

EXTENSIVE PROMOTION
Marketing and promotion of impactful research

LOOP RESEARCH NETWORK
Our network increases your article's readership